

**Synthesis, Characterisation and Properties of  
Benzenepolycarboxylate Metal-organic  
Frameworks**



Newcastle X-Ray Crystallography

**James Holcroft**

A Thesis Submitted for the Degree of Doctor of  
Philosophy

September 2012

## **Acknowledgements**

Firstly I would like to thank my supervisor Bill Clegg for giving me the opportunity to do this PhD and for the invaluable help and advice given throughout.

I would also like to thank the past and present members of X-ray Crystallography that I have worked with, in particular; Ulrich Baisch, Luca Russo and Ross Harrington for their help with various aspects of crystallography and synthesis developments.

Further thanks are extended to Northern Carbon Research Laboratories in particular; Mark Thomas; for allowing me to use both the TGAs and have time on the IGA for thermostability and gas adsorption studies, Jon Bell and Jayne Armstrong for running the adsorption isotherms of compound 17 and their tireless efforts in the data analysis.

Many thanks go to the personnel at the Diamond Light Source (beamline I19) for their help during the long hours at the synchrotron facility used to collect numerous samples presented in this thesis.

Finally, the most important thanks go to my outstanding family who have supported and helped me throughout my academic career, without them and my dog Jerry this would not have been possible.

## Abstract

Metal-organic frameworks (MOFs) are coordination polymers that extend in one, two or three dimensions, forming networks. These materials need to be strongly bonding metal centres linked by organic ligands to form a geometrically well-defined structure. MOFs are of interest due to our ability to identify some of the principles that govern the design and assembly of the target framework. The careful selection of MOF building blocks such that their properties are retained by the framework can yield unique materials with a host of physical characteristics and applications. The nature of the organic linkers often leads to voids present in the structure; these are usually occupied by guest molecules such as solvent, which need to be removed or exchanged for the MOF to be activated. The design of frameworks that are robust and withstand the desolvation can lead to porous compounds with the ability to adsorb other guest molecules, giving a platform for numerous scientific and industrial applications.

This thesis describes the synthesis, the structural characterisation and the study of thermostability and gas adsorption characteristics of MOFs. The structures of compounds of some transition metal ions [Mn(II), Co(II), Ni(II), Cu(II), Zn(II) and Cd(II)] and some other metals with symmetrical benzenepolycarboxylates (terephthalic, trimesic, pyromellitic and mellitic acid) are described. A detailed adsorption study of one particular compound is presented.

The compounds presented were prepared using a variety of methods: solvothermal, hydrothermal, ionothermal, vapour diffusion and solvent diffusion using specially adapted reaction vessels. Single-crystal X-ray crystallographic techniques were used for structure determination and characterisation, utilising in-house and synchrotron facilities. Further analysis was carried out using elemental analysis and powder X-ray diffraction to determine overall 'bulk' sample purity. Thermogravimetric analysis and hot-stage microscopy were used to assess the thermal stability of selected compounds, producing the temperature profile needed for Intelligent Gravimetric Analysis which determined the pore characteristics and potential applications of the compounds.

A total of forty-four metal-benzenepolycarboxylate complexes are presented, mostly with transition metals. Nine complexes containing the 1,4-

benzenedicarboxylate ligand (terephthalate) (**1-9**) are reported. This ligand formed complexes with zinc (**3,5,6,8**), cobalt (**2,4**), nickel (**1**), cadmium (**7**) and copper (**9**). The structures of the compounds include one-dimensional chains (**1,2**), two-dimensional sheets (**3-6**) and three-dimensional coordinated frameworks (**7-9**).

Twelve complexes containing the 1,3,5-benzenetricarboxylate ligand (trimesate) (**10-21**) are reported. This ligand formed complexes with zinc (**11,12,17**), cobalt (**14,18**), nickel (**13**), cadmium (**15,16**) and manganese (**19,10,21**). The structures of the compounds include two-dimensional sheets (**10-12,16**) and three-dimensional coordinated frameworks (**17-21**).

Fifteen complexes containing the 1,2,4,5-benzenetetracarboxylate ligand (pyromellitate) (**22-36**) are reported. This ligand formed complexes with zinc (**32,33,36**), cobalt (**22,25,34,35**), nickel (**26**), cadmium (**27,28,31**), copper (**23,24,29**) and the alkali metal potassium (**34**). The structures of the compounds include two-dimensional sheets (**22-27**) and three-dimensional coordinated frameworks (**28-36**).

Eight complexes containing the fully substituted 1,2,3,4,5,6-benzenehexacarboxylate ligand (mellitate) (**37-44**) are reported. This ligand formed complexes with cobalt (**41**), nickel (**37,38**), cadmium (**42,43**), copper (**39,40,44**). The structures of the compounds include one-dimensional chains (**37**), two-dimensional sheets (**39,41,42**) and three-dimensional coordinated frameworks (**38,40,43,44**).

The adsorption characteristics of the porous MOF NEW105 (compound **17**) were studied. N<sub>2</sub> and CO<sub>2</sub> adsorption at low temperatures gave a pore volume that was much lower than the value calculated from the crystallographic data. Virial analysis of the CO<sub>2</sub> isotherm confirmed interactions that are equivalent to ultra-nanoporous materials, indicating that the structure has undergone a structural rearrangement. Further kinetic analysis of gas adsorption isotherms of CO<sub>2</sub>, N<sub>2</sub> and O<sub>2</sub> showed the new nanoporous material was capable of kinetic molecular sieving of gases, a process observed only once before in MOFs. The Adsorption studies were carried out by Northern Carbon Research Laboratories; M. Thomas, J. Bell and J. Armstrong.



## Table of Contents

<b>Chapter One: Supramolecular Chemistry of Porous Materials</b>	<b>1</b>
Introduction	1
Porous Materials	1
Inorganic Materials	3
Zeolites	3
Activated Carbon	4
Coordination Polymers	6
Metal-organic Frameworks	6
Metal Centers and Geometries	7
Organic linkers	11
Nitrogen Donor Linkers	12
Oxygen Donor Linkers	13
Supramolecular Chemistry of Benzenepolycarboxylate based MOFs	15
Hydrogen Bonding	17
Aromatic Interactions	22
Secondary Building Units	23
Framework Topologies and Motifs	24
Two-dimensional Coordination Polymers	25
Three-dimensional Coordination Polymers	27
Porosity	30
Interpenetration and Catenation	31
Synthesis	32
Characterisation	34
Adsorption	35
Applications	37
References	44
 <b>Chapter Two: A Brief Summary of Single-Crystal X-ray</b>	 <b>53</b>
<b>Crystallography</b>	<b>53</b>
Introduction	53
Crystallographic Principles	54
Diffraction	56
Sample Selection	56
Data Collection	57
Data Reduction	58
Structure Solution	58
The Patterson Synthesis	59
Direct Methods	59
Structure Refinement	62
Final Results	63
References	

<b>Chapter Three: Research Objectives</b>	<b>64</b>
Overall Objectives	64
Specific Objectives	64
Synthesis of Metal-organic Frameworks	64
Characterisation of Metal-organic Frameworks	65
Adsorption studies	65
<b>Chapter Four: Experimental</b>	<b>66</b>
Introduction	66
Synthetic Techniques	66
Vapour Diffusion	66
Direct Addition	67
H-Cells	68
Hydrothermal/Solvothermal Synthesis	69
Ionothermal Synthesis	70
Silica Gels	72
Analytical Techniques	75
Single-Crystal X-ray Crystallography	75
Thermogravimetric Analysis	76
Hot-stage Analysis	77
Powder X-ray Diffraction	77
Elemental Analysis	77
Gas Adsorption	78
References	80
<b>Chapter Five: Crystal Structures of Transition Metal and 1,4-benzenedicarboxylic acid Compounds</b>	<b>81</b>
Introduction	81
Compound 1	82
Compound 2	88
Compound 3	93
Compound 4	100
Compound 5	108
Compound 6	117
Compound 7	122
Compound 8	130
Compound 9	138
Conclusion	144
References	146

## **Chapter Six: Crystal Structures of Transition Metal and**

### **1,3,5-benzenetricarboxylic acid Compounds 147**

Introduction	
Compound 10	147
Compound 11	148
Compound 12	155
Compound 13	163
Compound 14	169
Compound 15	176
Compound 16	184
Compound 17	194
Compound 18	204
Compound 19	227
Compound 20	236
Compound 21	246
Conclusion	256
References	267
	271

## **Chapter Seven: Crystal Structures of Transition Metal and**

### **1,2,4,5-benzenetetracarboxylic acid Compounds 273**

Introduction	
Compound 22	273
Compound 23	274
Compound 24	282
Compound 25	291
Compound 26	299
Compound 27	308
Compound 28	316
Compound 29	323
Compound 30	330
Compound 31	338
Compound 32	346
Compound 33	354
Compound 34	365
Compound 35	375
Compound 36	385
Conclusion	396
References	404
	408

<b>Chapter Eight: Crystal Structures of Transition Metal and</b>	<b>409</b>
<b>1,2,3,4,5,6-benzenehexacarboxylic acid Compounds</b>	<b>410</b>
Introduction	419
Compound 37	429
Compound 38	437
Compound 39	445
Compound 40	455
Compound 41	465
Compound 42	473
Compound 43	480
Compound 44	484
Conclusion	
References	<b>485</b>

<b>Chapter Nine: Future Work</b>	<b>CD</b>
----------------------------------	-----------

## **Appendix 1**

## Chapter One – Supramolecular Chemistry of Porous Materials

### Introduction

The last decade has seen enormous research efforts in the synthesis and studies of porous framework materials. This field of research continues to expand rapidly, affording various architectures constructed from a variety of molecular building blocks with a host of different interactions between them. A major portion of work deals with the chemical and physical functionalization of these frameworks through crystal engineering, structure design or control<sup>1-3</sup> and characterizing porous properties by ability for storage, separation and exchange of guest molecules in order to design and produce the next generation of functional porous materials.<sup>4</sup>

### Porous Materials

The vast array of porous materials encompasses classically known materials such as inorganic and carbon based materials; in the case of microporous inorganic solids the two largest subgroups are aluminosilicates and aluminophosphates. These materials up until the 1990s were the main groups of porous materials; only recently coordination polymers as a group of porous materials have taken up an important place in the porous material area.

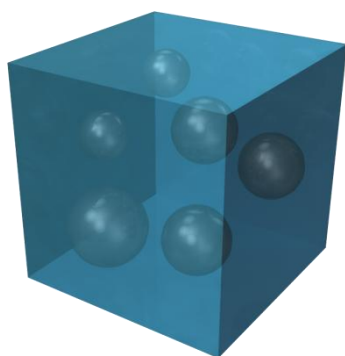
The porosity of these materials measures the amount of void present in the material and is measured as the ratio of volume of pores to the volume of solid in the material.<sup>4</sup> These pores may vary in geometry and are therefore classified according to the size by the International Union of Pure and Applied Chemistry as shown in Table 1.0.<sup>5</sup>

Classification	Width
Ultramicroporosity	Less than 0.5 nm
Microporosity	0.5 – 1.4 nm
Super Microporosity	1.4 – 2 nm
Mesoporosity	2 – 50 nm
Macroporosity	More than 50 nm

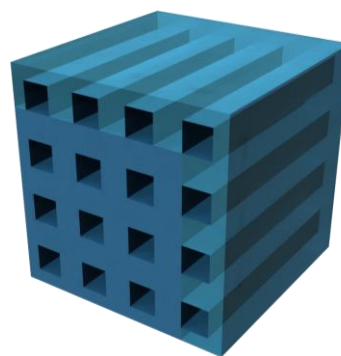
**Table 1.0: Pore size classification<sup>5</sup>**

The accessibility of these pores is crucial to the functional properties of the material. Based on special dimensions there are four types of porous structures:<sup>6</sup>

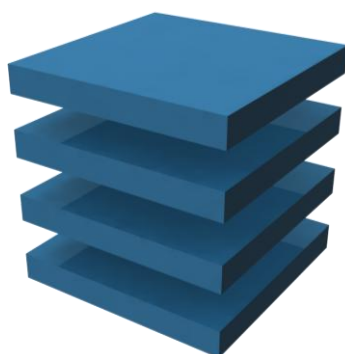
- 0D Cavities (Closed pore): Nanosized pores that are isolated and do not connect with the surface of the material.
- 1D Space (Channels): These pores are seen in a variety of compounds and are useful transport channels from the surface to the inner porosity.
- 2D Space (Layers): These pores cut through the structure creating layers joined together by Van der Waals forces or interactions with guest molecules.
- 3D Space (Intersecting channels): The material contains 3D intersecting channels constructed from several 1D channels running in different directions.



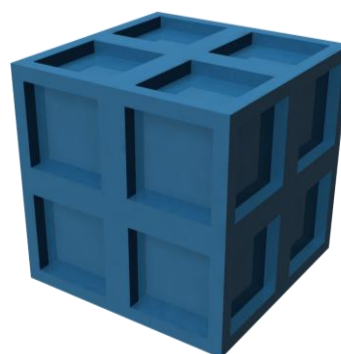
0D Cavities (Closed pore)



1D Space (Channels)



2D Space (Layers)



3D Space (Intersecting channels)

**Figure 1.0: Pore Types adapted from Kitagawa et al.<sup>6</sup>**

### **Inorganic Materials – Zeolites**

Microporous inorganic solids such as aluminosilicates are commonly known as zeolites. These are 3D crystalline materials with general formula  $M^{n+}_n[(AlO_2)_x(SiO_2)_y]^{x-}.wH_2O$ .<sup>7,8</sup> These structures create a 3D network based on

aluminium cations and silicates, with  $\text{SiO}_4$  tetrahedra linked at their corners producing tetrahedrally disposed Si–O bonds caused by the  $\text{sp}^3$  hybridization of silicon.<sup>8-10</sup> The structures of zeolites can be compared based on secondary building units (SBU), which are structural features that are due to the vertex condensation of tetrahedra e.g. Sodalite and Faujasite have double six-ring units within their structures.<sup>11</sup>

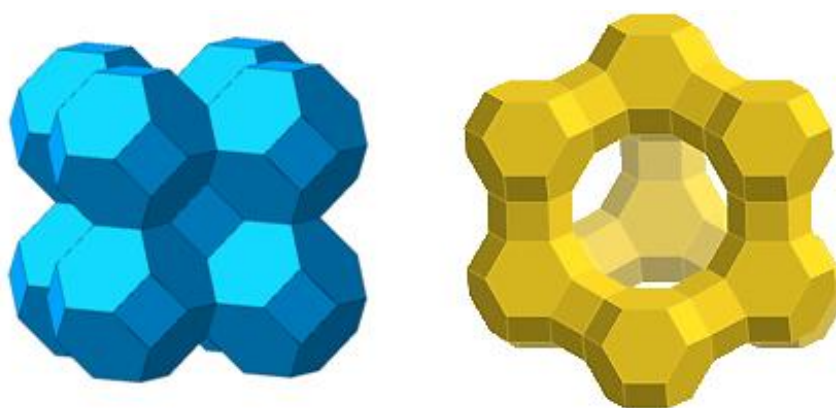


**Figure 1.01: Sodalite and Faujasite structures reproduced from Venuto et al.<sup>8</sup>**

Naturally occurring zeolites such as Faujasite, Sodalite and Chabazite have been known for around 250 years and are generally negatively charged due to the substitution of  $\text{Al}^{3+}$  at the silicon sites. The charge is balanced by guest molecules in the cavities that consist of water and group 1 and 2 metals. These impurities limit the applications of naturally occurring zeolites and need to be removed using desolvation and/or thermal decomposition to yield  $\text{H}^+$  ions allowing access to the pores of the structure.<sup>9</sup>

Synthetic zeolites were first observed in 1862<sup>12</sup> and major further developments were made in the 1940's by Barrer and Milton.<sup>13-15</sup> Synthetic zeolites such as  $(\text{AlPO}_4)$  consist of  $\text{Al}^{3+}$  and  $\text{P}^{5+}$  tetrahedra linked via corner-sharing oxygen atoms to build a neutral 3D network.<sup>16</sup> These materials have been used for a variety of applications. The first industrial application of zeolites was the fluid catalytic cracking of heavy petroleum distillates using a synthetic aluminosilicate zeolite ( $\text{La}^{3+}$  substituted Faujasite). The catalytic function of zeolites is dependent on the Brønsted or Lewis acidic sites along with the maximum pore size that determines the size range of substrates that can be used.<sup>17-20</sup>

Zeolites are commonly used in the industrial processes of ion exchange and gas separation. Chabazite was one of the first natural zeolites to exhibit ion exchange capabilities, selectively taking up alkali metals  $\text{Cs}^+ > \text{K}^+ > \text{Na}^+ > \text{Li}^+$  and alkaline

earths  $\text{Ba}^{2+} > \text{Sr}^{2+} > \text{Ca}^{2+} > \text{Mg}^{2+}$ .<sup>21,22</sup> It was also used in the gas separation of  $\text{O}_2$  from  $\text{N}_2$  using pressure swing adsorption, the large rigid cavities of zeolites also making them ideal for separation based on size, as only certain molecules can enter the zeolite pores, making them highly selective.<sup>23</sup>

### Activated Carbon

The activated carbon materials are a form of carbon that has been processed to have a high open porosity and a high specific surface area with a disordered structure. These materials are produced from carbonaceous sources such as coal, wood and nutshells.

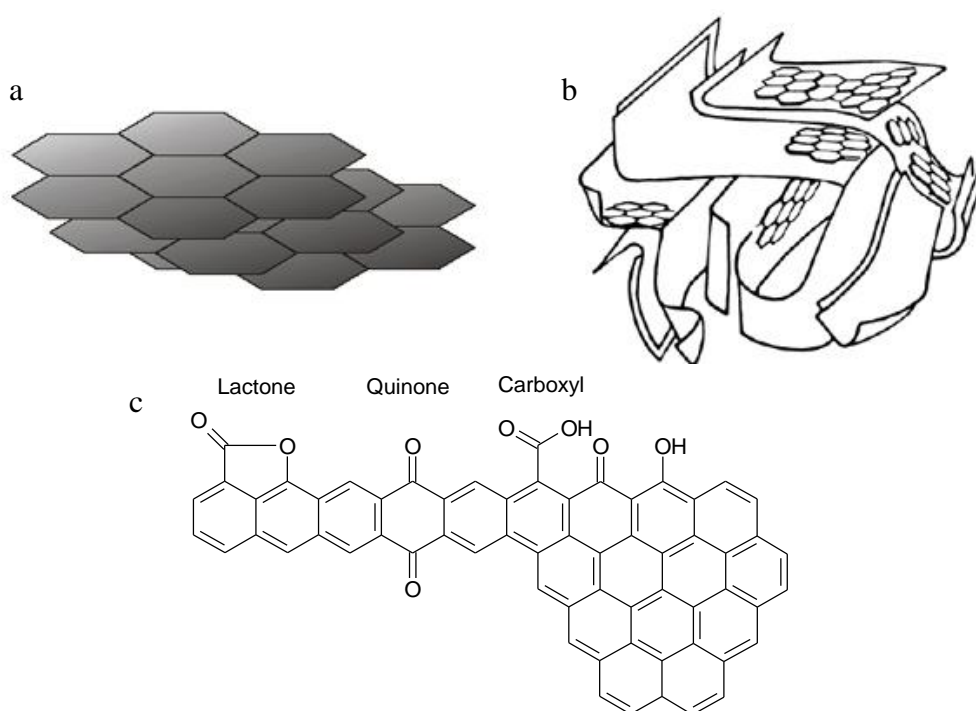


**Figure 1.02: a) Layers of carbon polymers, b) Schematic structure of activated carbon and c) Common carbon surface groups.**<sup>24,26</sup>

The structure of activated carbon is a complex interpenetrating network of pores passing through defective hexagonal carbon layers. Functional groups and heteroatoms are incorporated into this network and are bonded to the surface of the carbon during activation.<sup>24</sup> The surface may also contain oxygen functional groups such as carboxylic, lactone, quinones and hydroquinones, along with nitrogen functional groups including pyridine, ammonium or cyano groups. These functional groups have significant effect on the adsorption properties of the materials.<sup>25,26</sup>



The activated carbon materials are prepared in a three-step manufacturing process: dehydration, carbonisation and activation. After the source material has been dehydrated it undergoes a process known as carbonisation, this involves the production of char via the rearrangement of carbon atoms into graphene layers at 700 °C in an inert atmosphere.

Activation of this material results in the porous structure of the char improving, increasing both pore volume and accessibility. The activation process can be either chemical or physical. Physical activation is the gasification of the char material using steam or carbon dioxide at temperatures ranging from 800 to 1100 °C. Chemical activation uses  $\text{ZnCl}_2$ ,  $\text{H}_3\text{PO}_4$  and  $\text{KOH}$  in a series of mixing and heating reactions using an activating kiln at 500 – 900 °C.

Applications for the activated carbon materials include a variety of liquid phase applications (80 %) and gas phase applications (20 %).<sup>27</sup> Liquid phase applications include major industrial processes such as chemical and pharmaceutical purification, portable water treatment and metal recovery. Gas phase applications encompass gas separation and purification in cigarette filters, air purification systems and dechlorination processes.<sup>28</sup>

## **Coordination Polymers**

The chemistry of coordination polymers since their discovery has advanced significantly, showing how crystal engineering has become a paradigm for the design of supramolecular structures. The research by Wells on the overall structure of solids, particularly inorganic materials, forms the foundation of coordination polymers.<sup>29,30</sup> Wells' research defined structures in terms of topology, reducing structures down to nodes and linkers; the resulting structures can be characterized as discrete (zero dimensional) and infinite (1D, 2D and 3D) periodic nets. However it was the work by Hoskins and Robson in 1989 and 1990 building upon Wells' research that facilitated the rapid growth of the field of coordination polymers.<sup>31,32</sup> They adapted Wells' research into an area of coordination polymers known as metal-organic frameworks; here the "node-linker" approach has been extremely successful, extensively developing the area of crystal engineering for structure design and architecture control.<sup>1-3,33-37</sup> Considering the extensive array of publications, a complete review of all coordination polymer structures is beyond the limitations of this report; instead emphasis is focussed on the properties and applications of metal-organic frameworks.

## **Metal-organic Frameworks**

Metal-organic frameworks (MOFs) are coordination polymers that extend into two-dimensional or three-dimensional networks. These materials need to be strong bonding metal centres linked by organic ligands to form a geometrically well-defined structure.<sup>38</sup> MOFs are of interest due to the ability to identify some of the principles that govern the design and assembly of the target framework. This process of reticular synthesis is almost unheard of in coordination polymer chemistry outside of MOF literature.<sup>39</sup> The careful selection of MOF building blocks such that their properties are retained by the framework can yield unique materials with a host of physical and optical characteristics and applications. The nature of the linkers often leads to voids present in the structure; these are usually occupied by guest molecules, which interact with the framework and need to be removed or exchanged for the MOF to be activated. The design of frameworks that are robust and withstand the desolvation can lead to porous compounds with the ability to adsorb guest molecules, giving a platform for numerous applications.

## **Metal Centres and Geometries**

Metal-organic frameworks predominantly contain transition metal or lanthanide ions as the “nodes” of the structure. Transition metals are often utilized as a versatile coordination node, due to their ability to form multiple geometries and the wide range of lability of the coordination bonds formed.<sup>40</sup> Coordination numbers can range from two to seven depending on the oxidation state of the metal used, this generates various possibilities of geometries such as linear, tetrahedral, square-planar, square-pyramidal, trigonal-bipyramidal, trigonal-prismatic, octahedral and their corresponding distorted forms.<sup>6</sup> (figure 1.03)

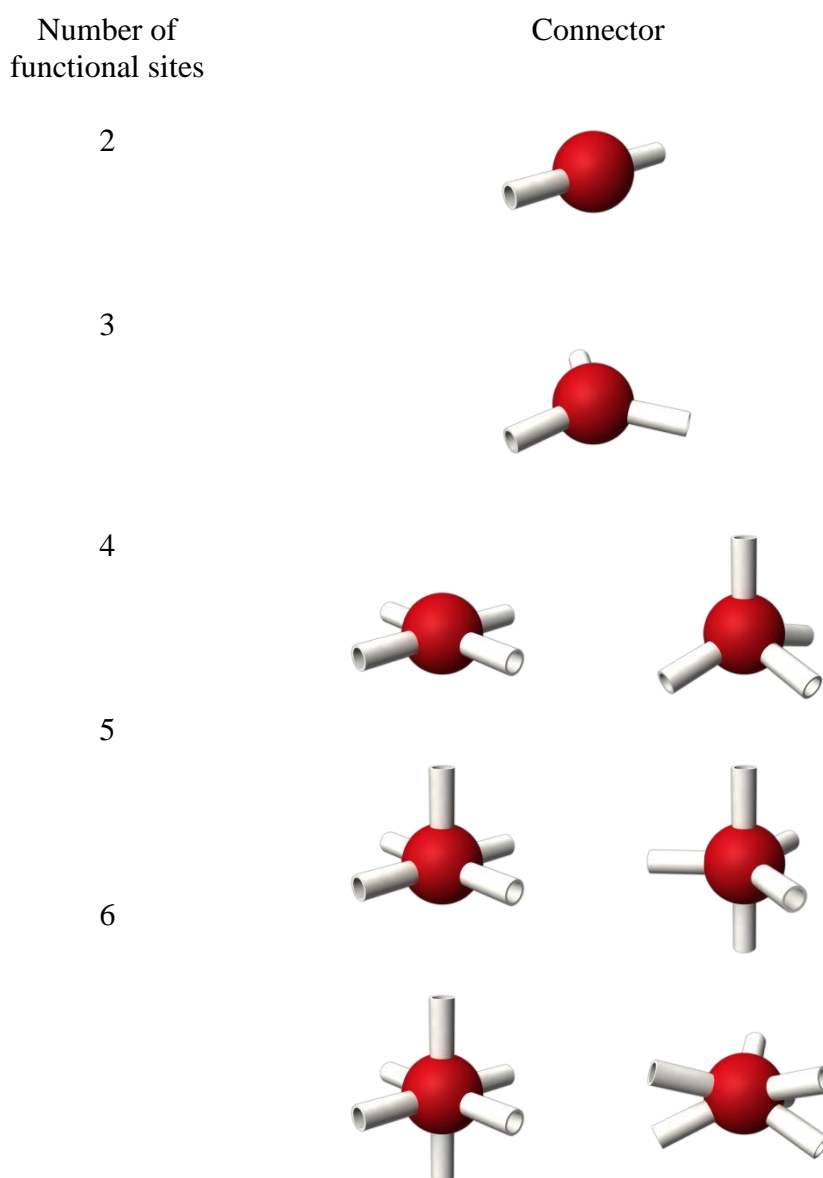


**Figure 1.03: Coordination polymer possible node geometries adapted from Kitagawa et al.<sup>6</sup>**

The most commonly used transition metals are cobalt, nickel, copper, manganese and zinc. These have variable valencies which results in the following commonly observed geometries.

- Copper – Electron configuration of zero-valent metal is  $[\text{Ar}]3d^{10}4s^1$ . Copper nodes are often in distorted octahedral and square-planar geometries. The distortion occurs mainly due to Jahn-Teller distortion commonly resulting in octahedral geometries having four short bonds and two longer bonds as the  $d_z^2$  orbital is filled whilst the  $d_{x^2-y^2}$  orbital is only partially filled.
- Cobalt – Electron configuration of the zero-valent metal is  $[\text{Ar}]3d^74s^2$ . There is a range of common coordination numbers for  $\text{Co}^{2+}$ . Geometries of cobalt(II) nodes are generally octahedral and tetrahedral; within this thesis structures that contain cobalt(II) present in both forms are presented.
- Nickel – Electron configuration of the zero-valent metal is  $[\text{Ar}]3d^84s^1$ . The most prevalent nickel geometries are octahedral and square-planar with consistent bond lengths.
- Manganese – Electron configuration of the zero-valent metal is  $[\text{Ar}]3d^54s^2$ . Manganese(II) compounds take on a range of coordination modes and geometries in metal-organic frameworks, the most common of which is octahedral.
- Zinc – Electron configuration of the zero-valent metal is  $[\text{Ar}]3d^{10}4s^2$ . Zinc(II) compounds often take up octahedral or tetrahedral geometries

Although varying valency of the transition metals may seem to expand the number of potential structures to be produced with diminishing ability to predict structural architecture, this problem can be solved by carefully changing reaction conditions to favour a particular coordination number and geometry.<sup>6,36,38,41,42</sup>

Recently the generation of frameworks with new and unusual network topologies has seen the emergence of lanthanides as metal centres.<sup>43</sup> Lanthanide metal ions commonly have the oxidation state +3 and possess large ionic radii. Therefore binding is non-directional and electrostatic with steric factors often directing the coordination geometries of resulting frameworks. Coordination numbers usually range between seven and ten giving rise to the unusual topologies seen in the figures 1.04 and 1.05.

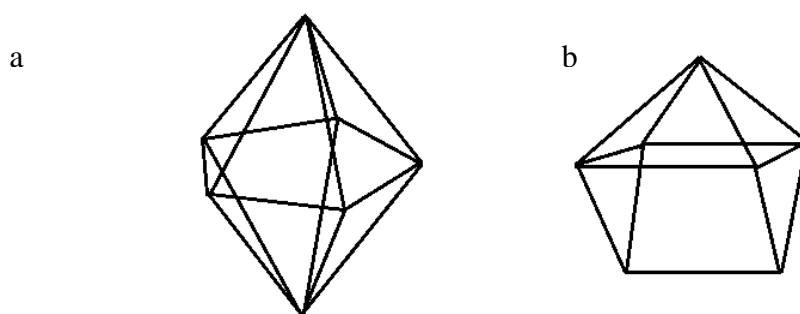


**Figure 1.04:** Seven-coordinate metal centres can adopt a) pentagonal bipyramidal or b) capped trigonal prismatic geometry.

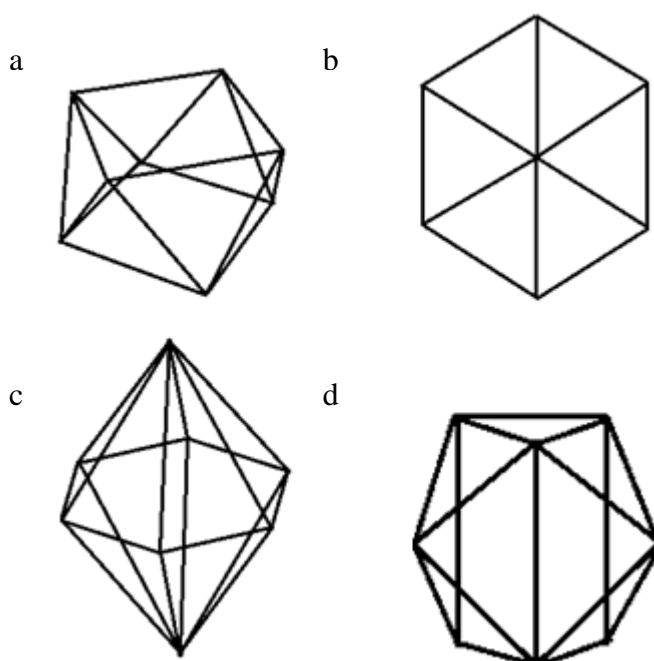


**Figure 1.05:** Eight-coordinate metal centres can adopt a) square antiprismatic, b) cubic, c) hexagonal bipyramidal or d) bicapped trigonal prismatic geometry

The higher coordination geometries of nine for  $[\text{Ln}(\text{H}_2\text{O})_9]^{3+}$  and ten for  $[\text{Ln}(\text{NO}_3)_5]^{2-}$  are very rarely seen in framework materials primarily due to the steric hindrance of ligands when the framework is formed.<sup>44</sup>

The use of ligands to control the coordination geometries of lanthanide frameworks has the added advantage of enabling coordinatively unsaturated lanthanide centres to be formed by the removal of solvent molecules or chemically labile ligands. This allows the framework to utilize vacant sites for chemical adsorption, sensors and heterogeneous catalysis.<sup>45,46</sup>

The luminescent properties of lanthanide frameworks containing trivalent cations has been prevalent from early examples of lanthanide MOFs reported by Schröder *et al.* and later frameworks that contained chromophores to improve the absorption and transmittance of light to the cation.<sup>47,48</sup> These luminescent properties may be harnessed to produce “smart” materials, where the framework is capable of sensing guest molecules producing an “on/off” mode between desolvated and solvated states. Recently a mixed lanthanide (Eu, Tb) framework reported by De Lill *et al.*<sup>49</sup> shows enhanced luminescence of the  $\text{Eu}^{3+}$  yielding the potential for the material as a light-emitting diode.<sup>49</sup>

Mixed transition metal frameworks and transition metal/alkali metal frameworks also have been reported, showing a variety of interesting properties. An extensive report by Chen *et al.*<sup>50</sup> shows a mixed metal framework composed of zinc/copper metal nodes forming the compound  $\text{Zn}_3(\text{BDC})_3[\text{Cu}(\text{Pyen})].(\text{DMF})_5(\text{H}_2\text{O})_5$  where  $\text{H}_2\text{BDC}$  = 1, 4-benzene dicarboxylic acid and  $\text{H}_2\text{Pyen}$  = 5-methyl-4-oxo-1,4-dihydropyridine-3-carbaldehyde. This material contains two types of pores, regular  $5.6 \times 12.0$  Å channels running along the crystallographic *c*-axis and irregular microporous channels running along the crystallographic *b*-axis. The unusual arrangement of copper and zinc within the material enables the copper to coordinate through only four of the six possible coordination sites, forming two vacant metal sites ideal for hydrogen bonding. This results in the compound displaying kinetic isotope molecular sieving of  $\text{H}_2$  and  $\text{D}_2$  an application rarely seen within MOF chemistry.<sup>50</sup>

## Organic Linkers

The organic linkers used to connect the metal nodes in coordination polymers are usually multidentate organic molecules. The binding strength, directionality and chemical functionality of the linkers enables the tailoring of MOF structures to possess desirable surface chemistry by ligand design and post-synthetic modifications.

The conventional multidentate organic linkers used in MOF synthesis contain nitrogen and oxygen donor atoms with popular functionalities of pyridyl and carboxylate groups (figure 1.06, 1.07). These linkers are selected for their rigidity and thermal stability; this aids the production of frameworks of a predicted geometry that are less susceptible to collapse upon desolvation.<sup>6,33,36,51</sup>

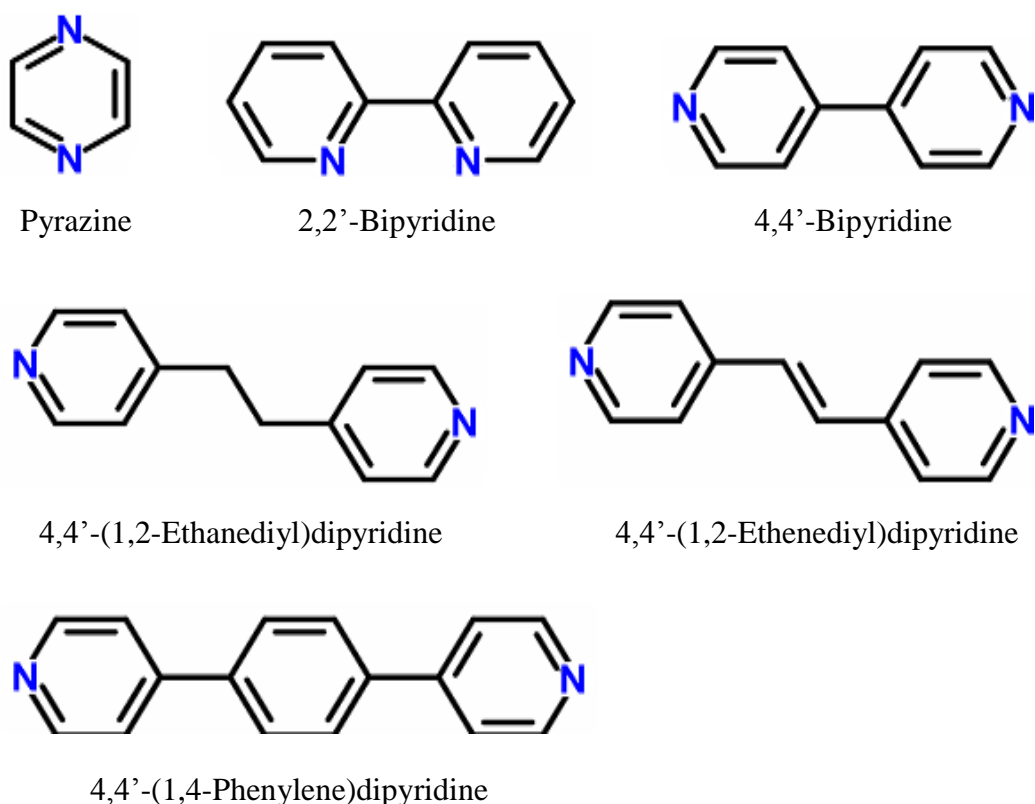


**Figure 1.06: N-donor linkers – neutral organic linkers**

## Nitrogen Donor Linkers – Neutral Organic Linkers

The wide variety of nitrogen-based bidentate ligands as shown in figure 1.06 is testament to their prolific use in metal-organic framework synthesis. The predominant attribute of linkers with pyridine functionality is their ability to act as borderline Lewis bases in terms of hard-soft acid-base theory, making them a suitable linker for first row transition metals in the 2+ state which are also classed as borderline.<sup>52,53</sup>

The most frequently used neutral organic ligands for framework construction are 4,4'-bipyridine and pyrazine for their ability to produce three-dimensional coordinated frameworks unlike the majority of neutral linkers, which tend to form one- or two-dimensional frameworks as they adopt T-shaped secondary building units (SBU).<sup>2,54,55</sup>

The compound 4,4'-bipyridine has the ability to bind to almost all metal ions in the periodic table as it is both a  $\sigma$ -donor and a  $\pi$ -acceptor. The nitrogen's lone pair of electrons can be donated to the metal ion to form a dative covalent  $\sigma$ -bond, whilst the d-orbitals of the metal ion overlap the  $\pi^*$ -orbitals of the bipyridine resulting in a reinforcement of the  $\sigma$ -bond.<sup>56</sup> This coordination chemistry has resulted in 4,4'-bipyridines use in a vast array of metal-organic frameworks including highly stable porous compounds, that remain rigid and porous upon desolvation and show interesting reversible guest exchange properties.<sup>57-59</sup> The frameworks based on 4,4'-bipyridine have become a focal point for gas adsorption and have been extensively studied, resulting in 4,4'-bipyridine becoming a prominent example of a prototypical ligand. The various tailored derivatives of 4,4'-bipyridine use different length spaces to form a diverse array of architectures including one-dimensional chains,<sup>60</sup> two-dimensional grids<sup>61</sup> and three-dimensional frameworks with various metal connectors.<sup>62,63</sup>



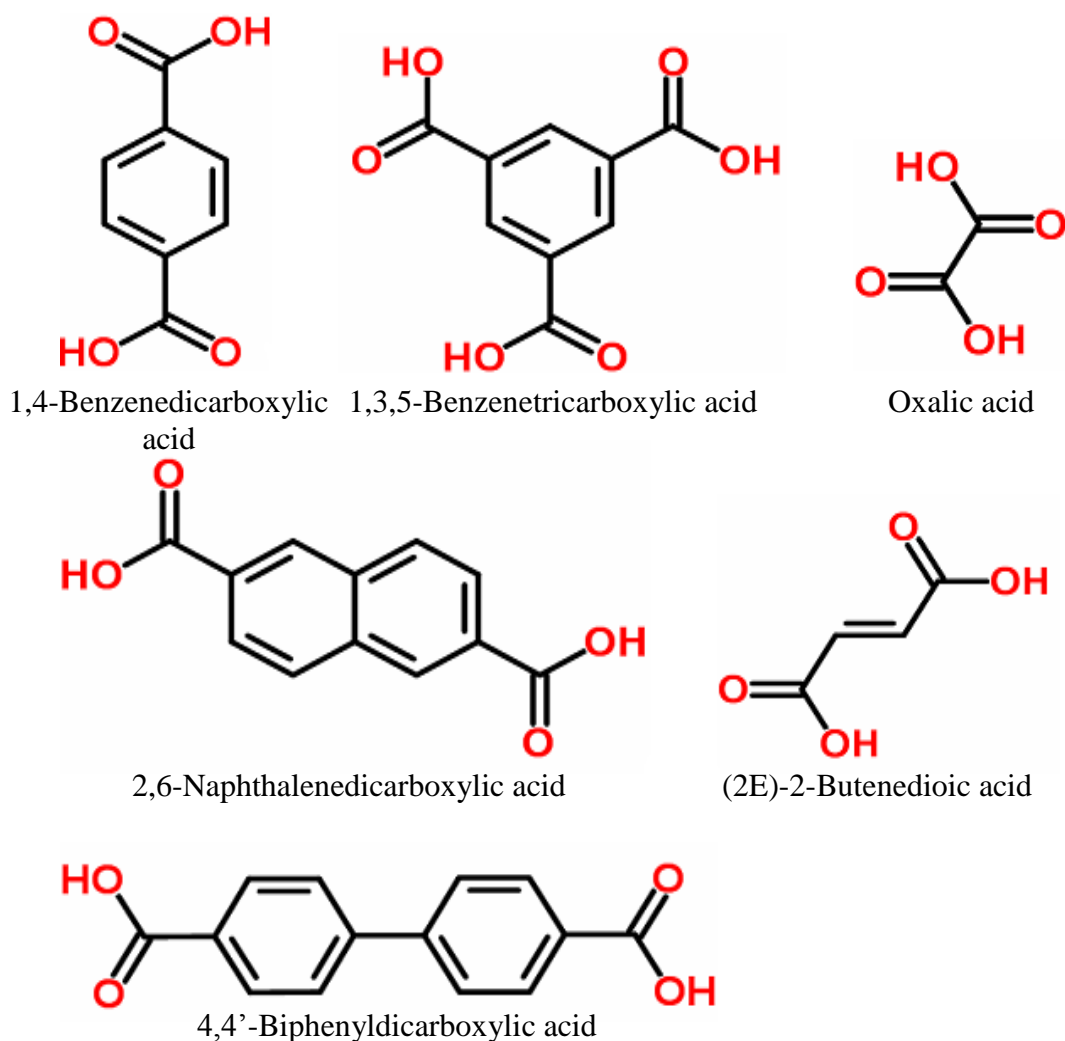


**Figure 1.07: O-donor linkers – anionic organic linkers**

### Oxygen Donor Linkers – Anionic Organic Ligands

A wide range of anionic ligands such as aliphatic, oxalate and polycarboxylates (figure 1.07) have been used in the construction of coordination polymers. The carboxylate group is the most predominantly used functional group for the construction of metal-organic frameworks with di-,<sup>1,64</sup> tri-,<sup>1,65-68</sup> tetra-<sup>66,69-71</sup> and hexacarboxylate<sup>73-75</sup> molecules being typical linkers. When compared to bidentate N-donor linkers the ability of the planar  $sp^2$  hybridised carboxylate groups to chelate metal ions in different ways (figure 1.08) and rotation around the C-C bond gives polycarboxylates more flexibility and offers the potential to generate a wider variety of coordination modes and polymer framework structures.

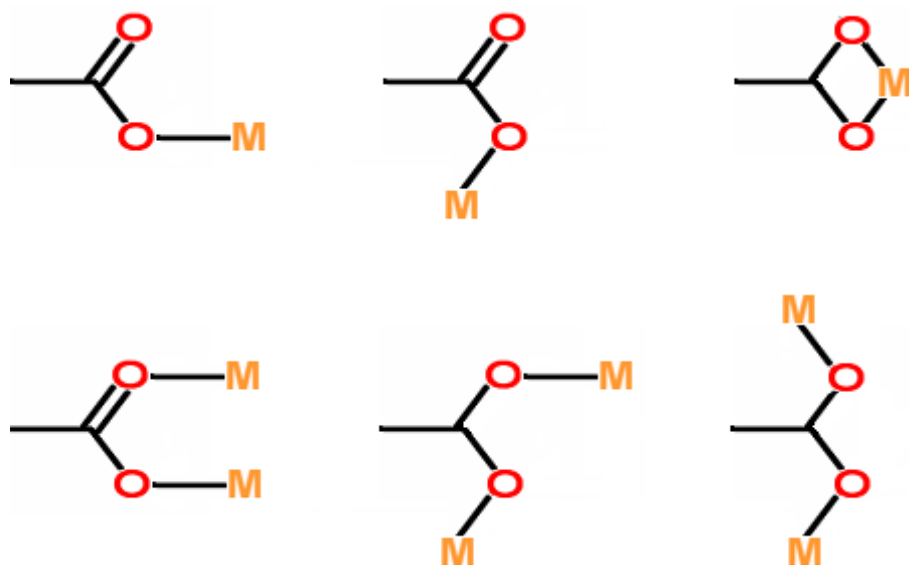


**Figure 1.08: Modes of coordination of the carboxylate ion.**

Considering the large number of papers published and the vast array of different linkers and subsequent coordination polymers, a complete review of all reported structures and properties is outside the scope of this perspective. Instead emphasis is placed on the supramolecular chemistry and the investigations of properties and potential applications of metal-organic frameworks constructed with benzenepolycarboxylate linkers such as those used in the synthesis of structures presented in this thesis.

### Supramolecular Chemistry of Benzenepolycarboxylate-based MOFs

The systematic study of specific compounds and interactions provides the knowledge required for understanding and designing supramolecular systems of growing complexity. The research in this thesis is concerned with four members of the benzenepolycarboxylic acid series, terephthalic acid (1,4-benzenedicarboxylic acid), trimesic acid (1,3,5-benzenetricarboxylic acid), pyromellitic acid (1,2,4,5-benzenetetracarboxylic acid) and mellitic acid (1,2,3,4,5,6-benzenehexacarboxylic acid) (figure 1.09). It explores the architecture and supramolecular structures resulting from reactions of the four ligands with transition metal and lanthanide salts.

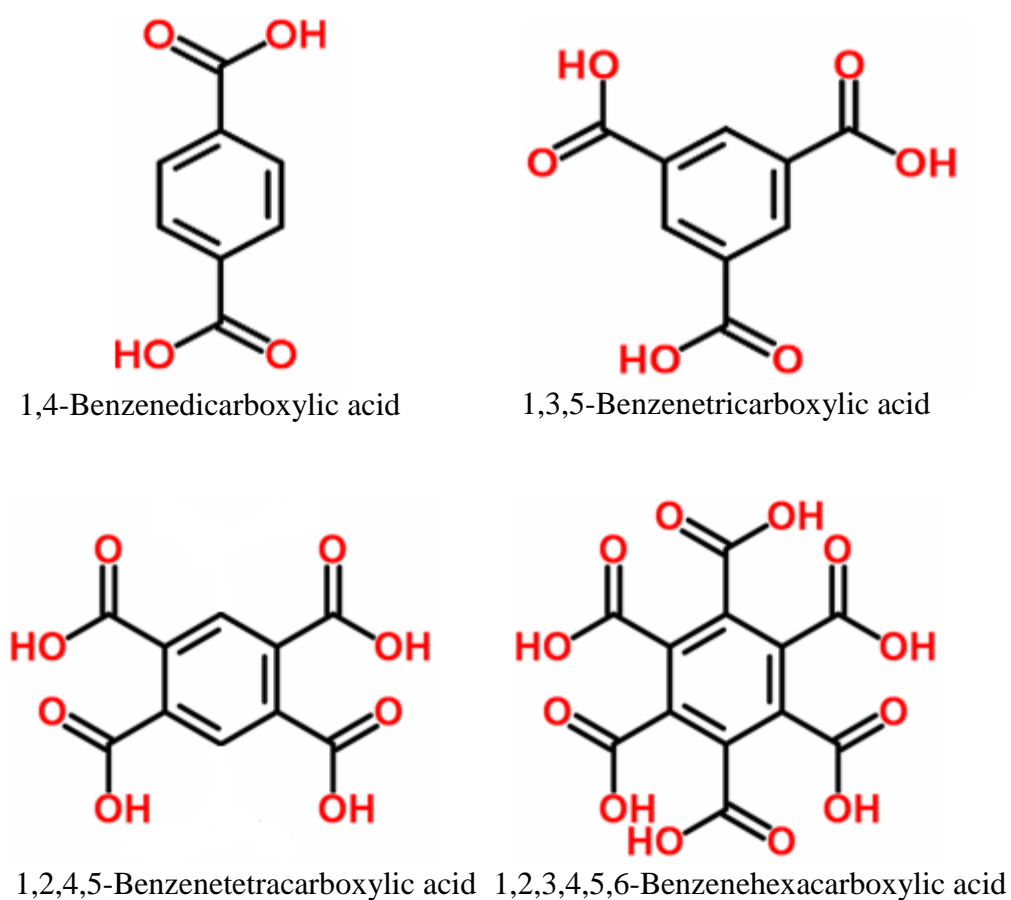


**Figure 1.09: Benzenepolycarboxylates commonly used for MOF synthesis**

The benzenepolycarboxylic acid linkers are considered useful building blocks for coordination polymers due to the rigid core structure of the benzene ring and the flexibility in the orientation of the carboxylate groups relative to the benzene plane. The carboxylate groups on benzenepolycarboxylate ligands can be deprotonated in various degrees, providing different anionic multidentate ligands with the same core structure. Upon deprotonation carboxylate groups bind to metal ions through dative covalent bonds forming a strong C-O-M bond. This also helps balance the overall charge of the framework, reducing the probability of additional cations in the pores of the framework material.

The high interest and importance of benzenepolycarboxylate ligands in supramolecular chemistry is apparent by the many related structures deposited in the CSD at the start of this thesis;<sup>76</sup>

- Terephthalic acid – 453 structures
- Trimesic acid – 407 structures
- Pyromellitic acid – 423 structures
- Mellitic acid – 23 structures

Although metal carboxylate interactions are present in nearly all the structures in the CSD search and presented in this thesis, they often appear with a multitude of weaker and less favourable interactions that can influence the structure of the final product. These bonding interactions form the supramolecular chemistry of coordination polymers and are classified into four types shown in figure 1.10;

- a) Coordination bond
- b) Coordination bond and hydrogen bond
- c) Coordination bond and other interaction (metal-metal bond,  $\pi$ - $\pi$  or  $\pi$ - $\sigma$ )
- d) Coordination bond and mixture of interactions

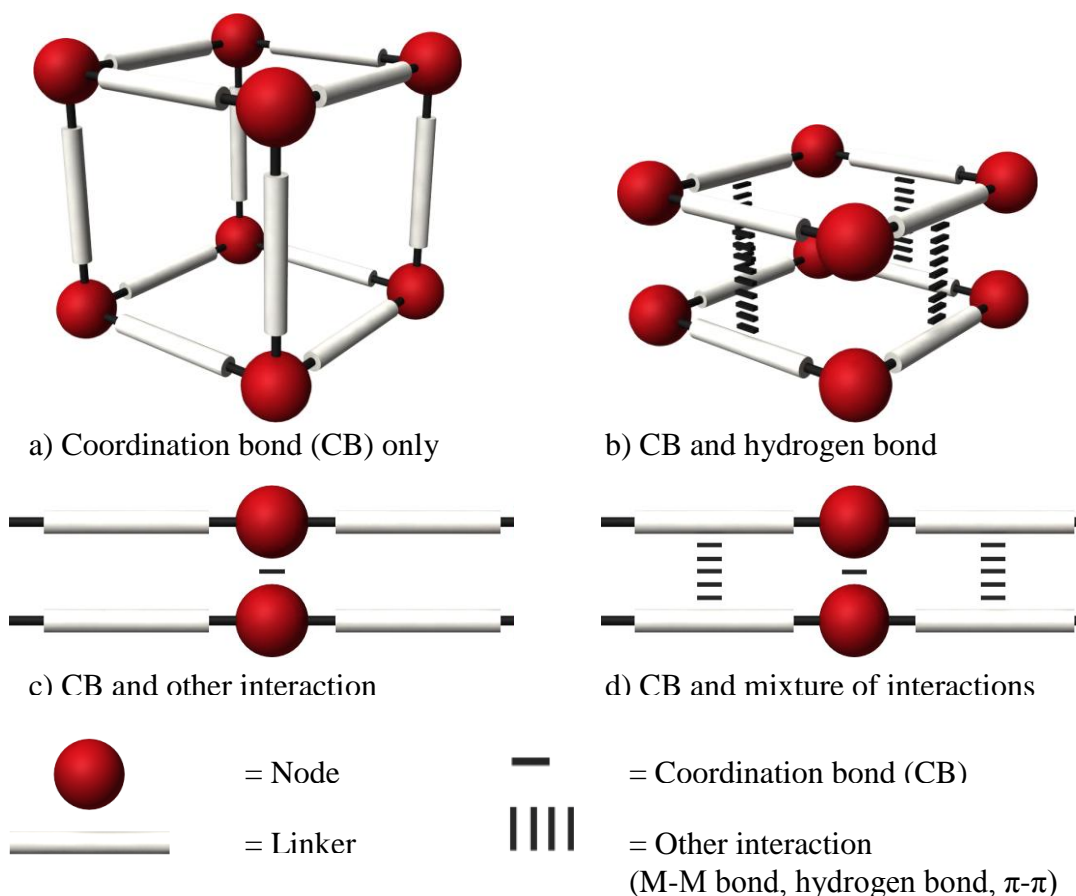


**Figure 1.10: Combinations of interactions used in the construction of MOFs adapted from Kitagawa et al.<sup>6</sup>**

The combination of different interactions within one supramolecular structure has been the subject of many reviews in the field, particularly the combination of hydrogen bonding,  $\pi$ - $\pi$  stacking and metal ligand interactions.<sup>77-82</sup>

### Hydrogen Bonding

Hydrogen bonds are extremely useful in crystal engineering as they display a wide range of interaction energies and directionality. They can be classified as strong, medium and weak depending on their interaction energy.<sup>77</sup>

Strong hydrogen bonds have donor (D) and acceptor (A) distances in the range 2.2 – 2.5 Å with bond energies between 60 and 120 kJmol<sup>-1</sup>. The bond angle is almost linear, ranging only between 175 and 180° with almost equal D-H and H...A distances, which is optimal for electrostatic and charge transfer energy.<sup>83,84</sup>

Medium hydrogen bonds are the most commonly occurring for hydrogen atoms attached to electronegative atoms such as oxygen and nitrogen. They have D...A

distances ranging from 2.5 to 3.2 Å with energies of 16 – 60 kJmol<sup>-1</sup>. The D-H...A bond angle often lies between 130 and 180°; this can lead to the formation of three-centre (bifurcated) or four-centre (trifurcated) hydrogen bonds when acceptors with more than one lone pair or multi-hydrogen donor are present.<sup>85</sup> These systems have longer distances, and angles ranging from 90 to 140 °; however, multi-centre hydrogen bonds tend to be more stable than single-centre linear hydrogen bonds.

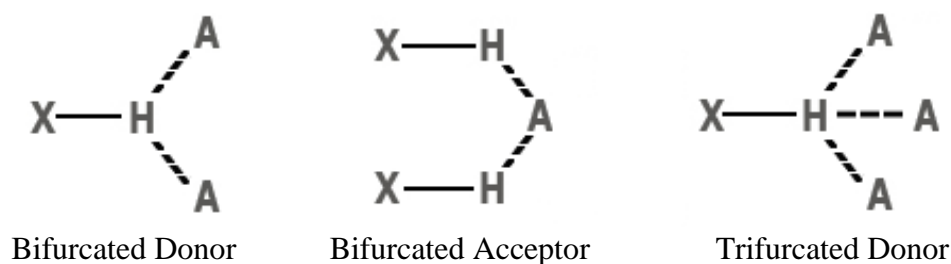


**Figure 1.11: Multi-centre hydrogen bonding interactions.**

Weak hydrogen bonds have been recognised to be of growing importance in directing supramolecular architecture and to allow for the recovery of “mistakes” in the process of topology formation.<sup>86-88</sup> They occur when in the presence of weak donors such as an acidic C-H attached to an electronegative atom, or in the presence of a weak acceptor. They tend to have large D...A distances ranging from 3.2 to 4.0 Å with bond energies less than 12 kJmol<sup>-1</sup>.

Indeed the important role of hydrogen bonding in the orientation of molecules for crystal engineering is observed throughout the benzenepolycarboxylate series. Most carboxylic acids exist as dimers held together by hydrogen bonds.<sup>89</sup>

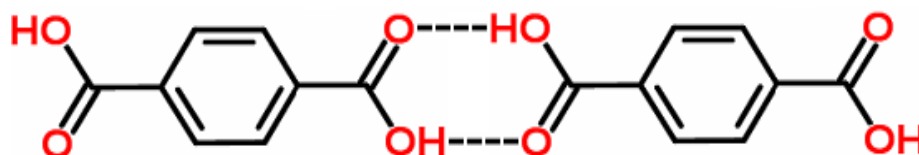


**Figure 1.12: Hydrogen bonding between carboxylic acids.**

The hydrogen bond dimer results in terephthalic acid and isophthalic acid forming linear and non-linear 1D chains respectively. The more substituted benzenepolycarboxylate ligands have a tendency to form more long-range ordered 2D structures.

Trimesic acid crystallizes into a two-dimensional lattice, in which six trimesic acid molecules are hydrogen bonded together to form a porous cyclic hexamer held together by additional aromatic interactions to form the ‘chicken-wire’ motif as depicted in figure 1.13.<sup>90</sup>

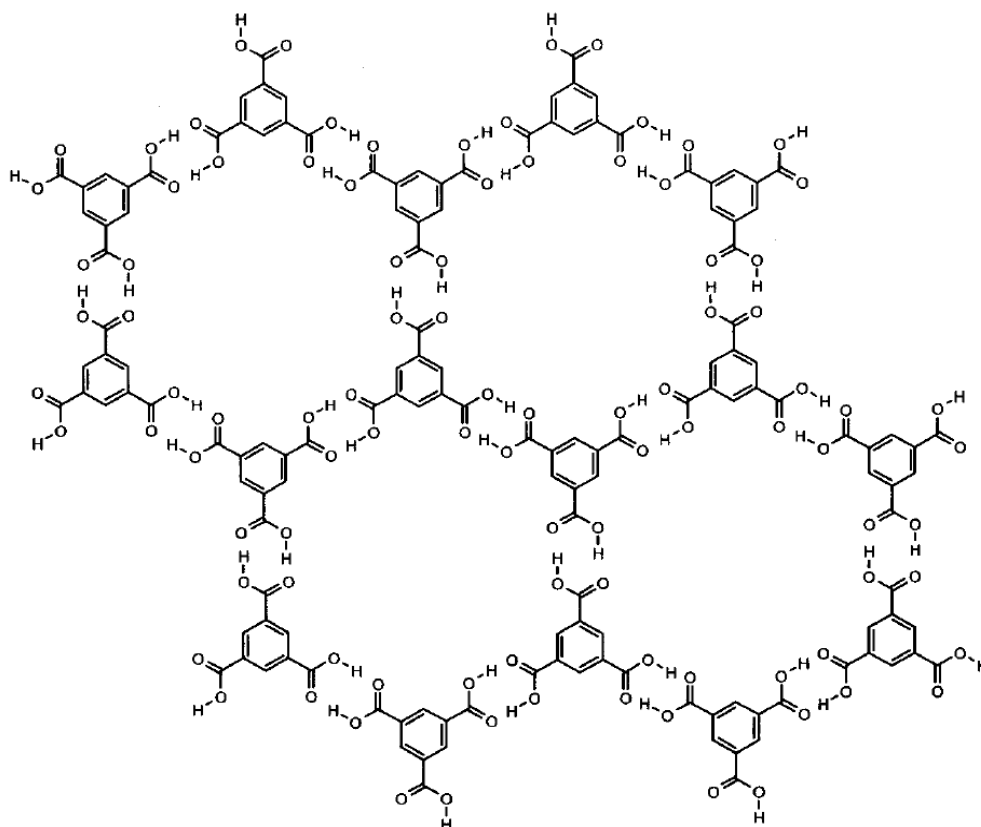


**Figure 1.13: Trimesic acid ‘Chicken-wire’ motif reproduced from Reisner et al.<sup>90</sup>**

This sheet-like structure and the linear chains of terephthalic acid can be transferred to framework materials, where the replacement of hydrogen bonds at some or all the sites with metal ion coordination can be used in crystal engineering to produce coordinated frameworks that maintain the ‘chicken-wire’ structure. This replacement of bonding is well presented by Du *et al.*<sup>91</sup> with fully deprotonated trimesic acid binding to  $\text{Cd}^{2+}$  cations to form a ‘chicken-wire’ two-dimensional sheet. The extent and reproducibility of this replacement is also shown with the formation of a zinc analogue (figure 1.14) reported by Yaghi *et al.*<sup>92</sup>

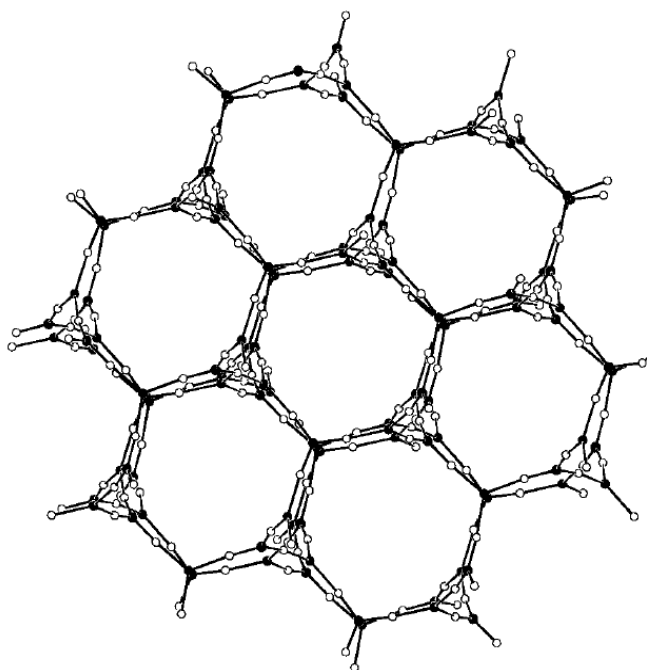


**Figure 1.14: Zinc-trimesate framework reproduced from Yaghi et al.<sup>92</sup>**

Pyromellitic acid also exhibits a well ordered two-dimensional sheet structure (figure 1.15). However, the pyromellitic acid ligands have a tendency to twist into either plane to form a three-dimensional hydrogen bonding network. The replacement of the hydrogen bonding within these structures is common in the literature and can have diverse effects.<sup>93</sup>

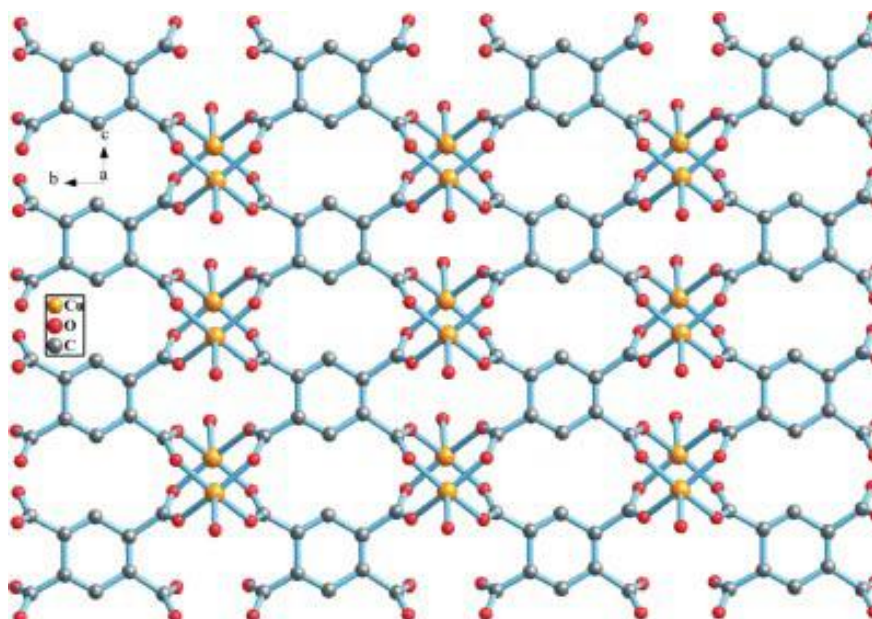


**Figure 1.15: Two-dimensional sheet of copper-pyromellitate framework reproduced from Liang et al.<sup>93</sup>**



These hydrogen bonding motifs are often the most energetically favourable orientations of the benzenepolycarboxylate ligands and form the primary contribution to the templating of the ligands' architectural structure; however, some weak non-bonded interactions are clearly observed in the recurrence of some characteristic packing and layering of motifs. The carboxylic dimer interaction is a good example, where the carboxylic acid groups can form 2 different stacking arrangements to form weak hydrogen bonds (figure 1.16). This and similar features that occur in the packing of carboxylic acid linkers are extensively reviewed by Leiserowitz *et al.*<sup>94</sup>

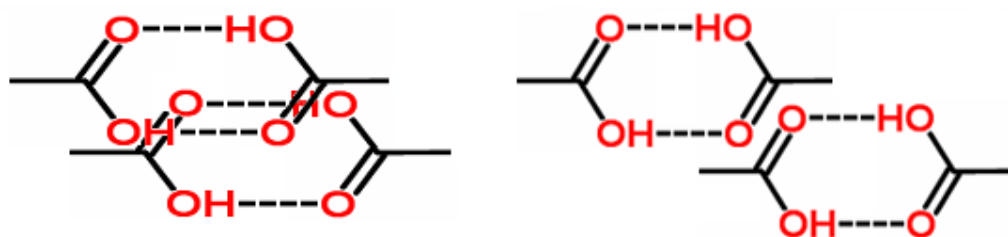


**Figure 1.16: Two possible overlaps of the carboxylic acid dimer.**

Terephthalic acid is a prime example of how architecture can be dictated by these factors, as two crystalline forms are observed.<sup>95,96</sup> The crystalline form in Figure 1.17 shows the packing reliance upon aromatic interactions, with  $\pi$ - $\pi$  stacking being prevalent throughout benzenepolycarboxylate structures.

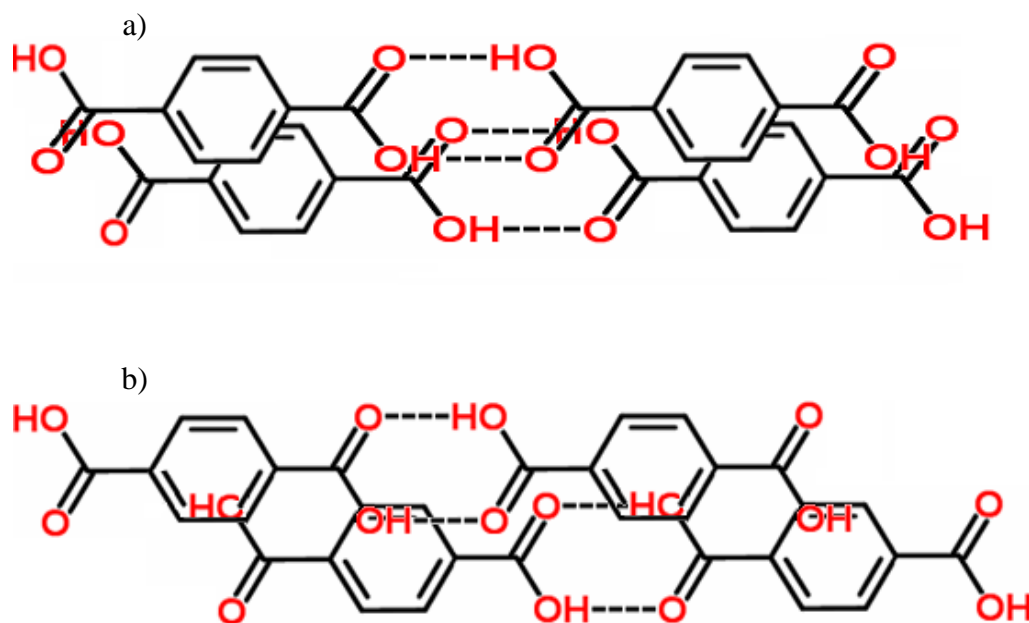


**Figure 1.17: Weak CH-O bonding and  $\pi$ - $\pi$  stacking forming a) parallel and b) staggered stacking of terephthalic acid.**<sup>95,96</sup>

## Aromatic Interactions

It is unusual for linkers in coordination polymers not to contain aromatic rings. Aromatic rings in frameworks help maintain the structural integrity of the complex and direct the geometry of the framework as seen in the previous example of terephthalic acid crystal packing motifs.<sup>95,96</sup>

$\pi$ - $\pi$  interactions have energy values in the range 1 – 50 kJmol<sup>-1</sup> and are weakly directional. They exist in two forms: face-to-face and edge-to-face (figure 1.18). The face-to-face ( $\pi$ - $\pi$  stacking) involves parallel rings approximately 3.5 Å apart with a slight offset caused by the repulsive nature of the  $\pi$  system overlap.<sup>97,98</sup> Edge-to-face interactions ( $\sigma$ - $\pi$  bonding) are considered as weak hydrogen bonds between a C-H of one ring and the  $\pi$  electron cloud of an adjacent ring. This style of interaction generates the herringbone packing shown in the crystal structures of benzene.<sup>98,99</sup>

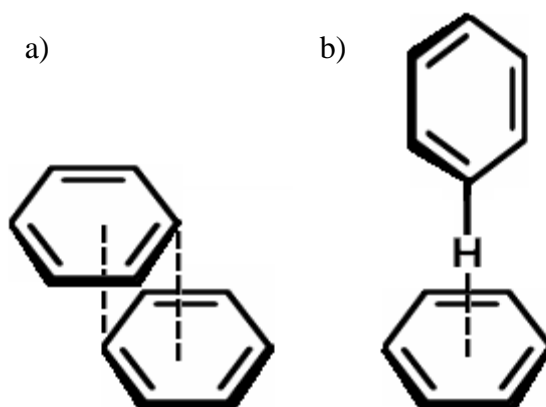


**Figure 1.18: Aromatic stacking interactions a)  $\pi$ - $\pi$  stacking and b)  $\sigma$ - $\pi$  bonding.**

Many one-dimensional linear coordination polymers use hydrogen bonds between the linkers and ‘free’ solvent molecules to form two-dimensional sheets; these in turn are often linked by favourable aromatic interactions using molecules such as pyridine and aromatic linkers to form close-packed networks.<sup>79-82</sup>

Functional groups coupled by one or more of these interactions are defined as ‘supramolecular synthons’; metal-organic frameworks also use discrete aggregates with well-defined geometries to add control and stability to the structures formed. These are usually defined as secondary building units (SBUs).

## Secondary Building Units

Secondary building units (SBUs) are polynuclear clusters constructed from two or more metal ions connected together through multidentate linkers. SBUs can have unusual metal sites with special coordination numbers and geometries as the metal ions are ‘locked’ into position by the linkers. Specific SBUs can be generated *in situ* under correct chemical conditions and are sufficiently rigid to produce extended porous frameworks with high stability. These frameworks are uncharged, removing the need for counter-ions in the pores, and thus allowing them to be used in adsorption and separation studies. Additional features are often present in the form of removable terminal ligands, allowing for an open metal site to be formed and studied.<sup>1,39,92,100,101</sup>

Discrete di-, tri- and tetranuclear metal carboxylate clusters are targets for SBU formation with the square ‘paddlewheel’, trigonal prismatic oxo-centred trimer and octahedral zinc acetate clusters being the most typical SBUs used in MOF synthesis.<sup>102-105</sup> The coordination mode of the carboxylate linkers in these SBUs is crucial to predicting the topology of the resulting network; an example of a series of frameworks utilizing SBUs for topology generation is the IR-MOF series reported by Yaghi *et al.* (figure 1.19), with a variety of different organic linkers between the terminal carboxylate groups.<sup>100</sup>

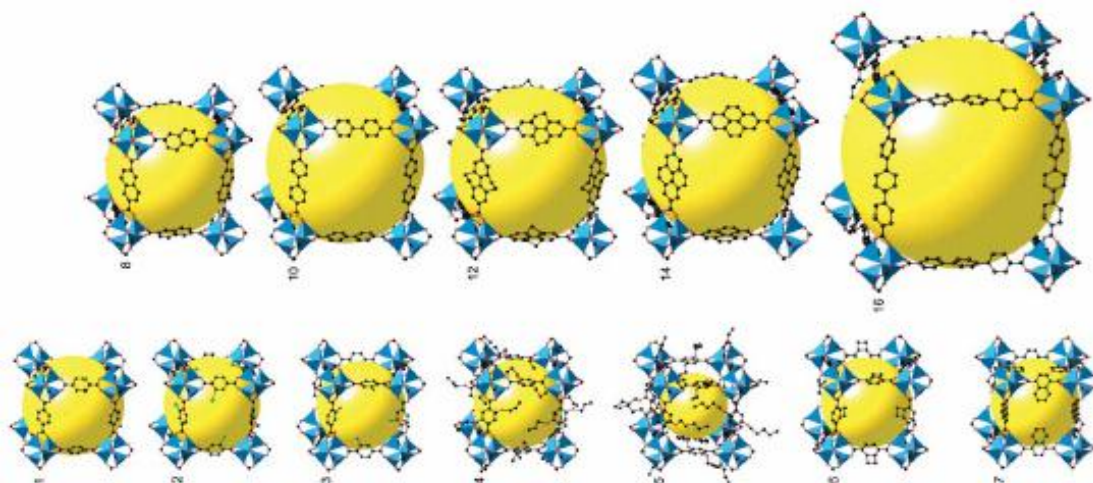


**Figure 1.19: IR-MOF series reproduced from Yaghi et al.<sup>100</sup>**

The IR-MOF series shows that the same structure topology can be retained by using a zinc carboxylate cluster connected by 1,4-benzenedicarboxylate linkers (MOF-1); the series is then extended by using organic linkers based on the 1,4-dicarboxylate

configuration.<sup>100</sup> This series highlights the impact of SBUs on topology design with tuneable pore size and porosity by using longer linkers to increase the spacing between vertices, giving a net void gain proportional to linker length but controlling topology using rigid node geometries.

### Framework Topologies and Motifs

The variety of motifs observed for MOFs is driven by the shape of the molecular building blocks formed from combinations of the connectors and linkers mentioned in the previous section. Figure 1.20 shows representative motifs of frameworks constructed from connectors and linear linkers.

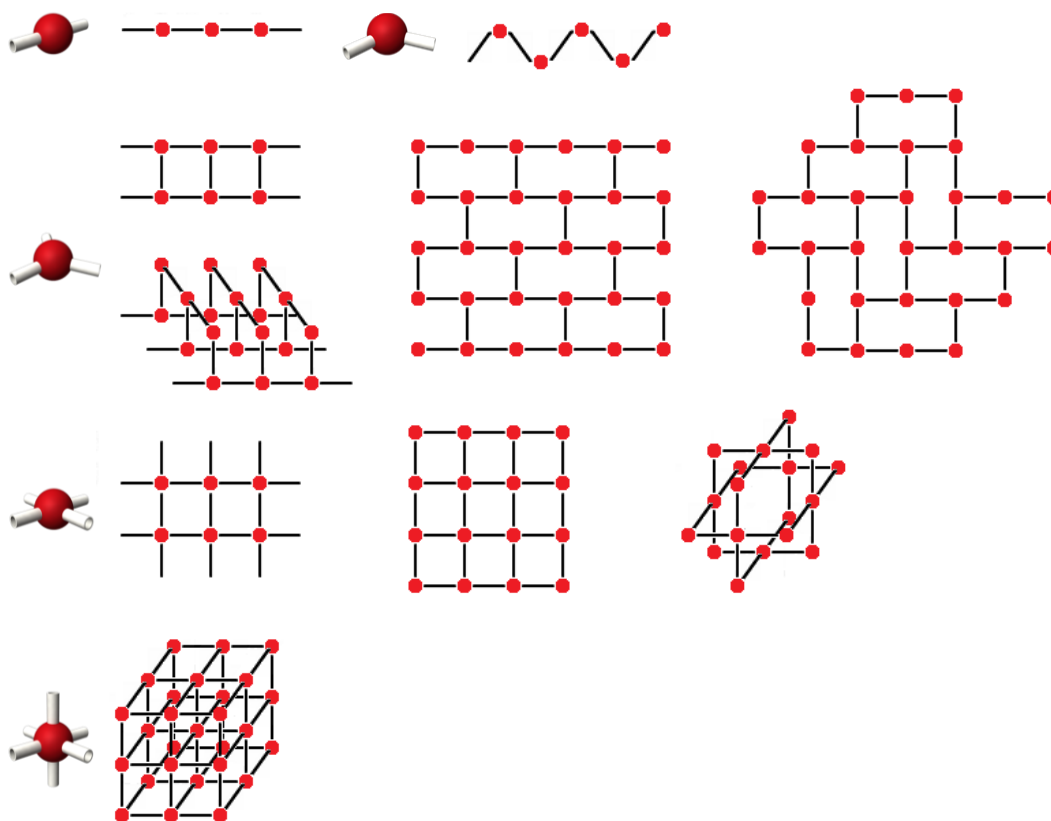


**Figure 1.20: Structural frameworks constructed using different linear linkers adapted from Kitagawa et al.<sup>6</sup>**

### One-dimensional Coordination Polymers

One-dimensional coordination polymers, both linear and zigzag, are widely known and observed for most linkers used in framework construction. These structures tend to pack efficiently and eschew open frameworks or cavities; in the case of benzenepolycarboxylate compounds the 1D polymeric metal-organic chains are

further expanded to 2D or 3D supramolecular frameworks via multiple hydrogen bonds.<sup>89,106</sup> Research undertaken by Pombeiro *et al.*<sup>106</sup> shows terephthalic acid, isophthalic acid and trimesic acid 1D chains are stabilized by intercalating water clusters such as water trimers, octamers and disordered water-nitrates that allow structures to close pack with short hydrogen bonds.<sup>106-109</sup>

## Two-dimensional Coordination Polymers

Square grid networks are a commonly reported example of two-dimensional metal-organic frameworks. They consist of molecular building units with metal:ligand ratios of 1:2 and utilize bidentate linkers. Square grid networks were first reported using cyano linkers<sup>110,111</sup> but since have been expanded in both chemical type and cavity size to include pyrazines,<sup>112</sup> bipyridine analogues<sup>113,114</sup> and benzenepolycarboxylates.<sup>115</sup> These motifs have cavities within the plane of the structure and are of interest in the interpenetration or enclathration of organic molecules for catalysis.

Two-dimensional motifs are often built from T-shaped molecular building blocks that generate unique structural motifs such as the brick-wall,<sup>116</sup> herringbone<sup>57,117,118</sup> and bilayer.<sup>57,119</sup> (figure 1.21)

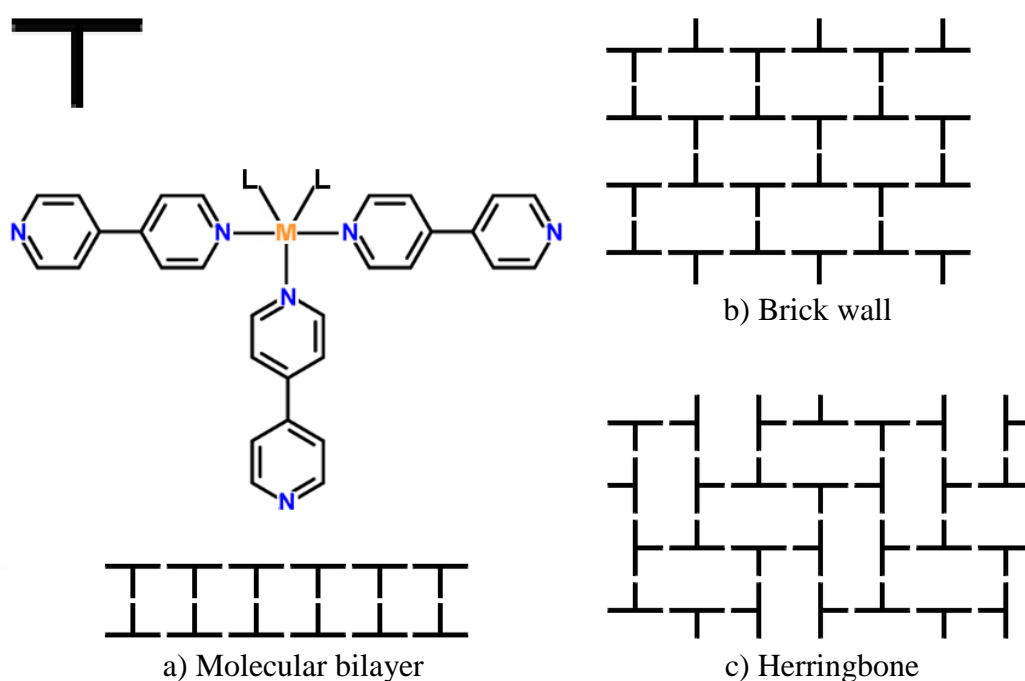


**Figure 1.21: T-shaped linker and structural motifs.**

To create T-shaped building blocks *mer*-substituted octahedral metal centres or tri-substituted square planar metal centres are required. Ligands such as  $\text{NO}_3^-$ ,  $\text{H}_2\text{O}$  and

CH<sub>3</sub>OH are utilized to block four coordination sites of the heptacoordinate metal centres such as Cd(II) and Co(II), thus leaving three coordination sites to be bridged by bidentate linkers to form a T-shaped module.

The brick architecture (figure 1.21 (b)) is observed as the product of the reaction between Ni(II), a macrocycle containing hydroxyl pendants, and trimesic acid.<sup>120</sup> The T-shaped geometry results from the Ni(II) macrocycle binding two fully deprotonated trimesic acid linkers in the *trans* position, and each trimesic acid linker binding three Ni(II) macrocycles through C<sub>1</sub> symmetry, resulting in the compound [Ni(C<sub>12</sub>H<sub>30</sub>N<sub>6</sub>O<sub>2</sub>)<sub>3</sub>]<sub>3</sub>[C<sub>9</sub>H<sub>3</sub>O<sub>6</sub>]<sub>2</sub>·18H<sub>2</sub>O. The aromatic rings in the layers run parallel with a slight offset of 25.3°, leaving channels running parallel to the *a*-axis filled with guest molecules.

The herringbone architecture (figure 1.21 (c)) has been observed by several groups.<sup>57,117,118</sup> In these structures the coordination sphere is very similar to that of the brick architectures; they contain heptacoordinate M(II) nodes with two terminal bidentate nitrate ligands and coordination by three anion ligands.

Bilayer architectures are widely known and are often observed as the product from reacting metal nitrates and 4,4'-bipyridine or terephthalic acid; however, these reactions can also produce the square grid and herringbone architectures. The reaction of Co(NO<sub>3</sub>)<sub>2</sub> and 4,4'-bipyridine in the presence of water produces the bilayer product [Co(C<sub>10</sub>H<sub>8</sub>N<sub>2</sub>)<sub>1.5</sub>(NO<sub>3</sub>)<sub>2</sub>]; this packs by interdigitation, allowing channels to run through the structure.<sup>121</sup> This is of particular relevance due to the stability of the structure upon desolvation and its representation as one of the first 'metal-organic zeolites' reported.

The topology of brick and herringbone motifs are both examples of (6,3) nets and can be related to honeycomb (6,3) nets. Honeycomb networks are uncommon in metal-organic frameworks, usually occurring only in those that contain trigonal nodes such as trimesic acid, but they remain a source of great interest due to the potential applications of the porous structures predicted.<sup>122</sup>

### Three-dimensional Coordination Polymers

Two of the simplest examples of three-dimensional networks are generated by self assembly of tetrahedral or octahedral nodes. Tetrahedral nodes are predisposed to form diamondoid architectures; in contrast octahedral nodes are expected to afford octahedral networks.<sup>1,2</sup>

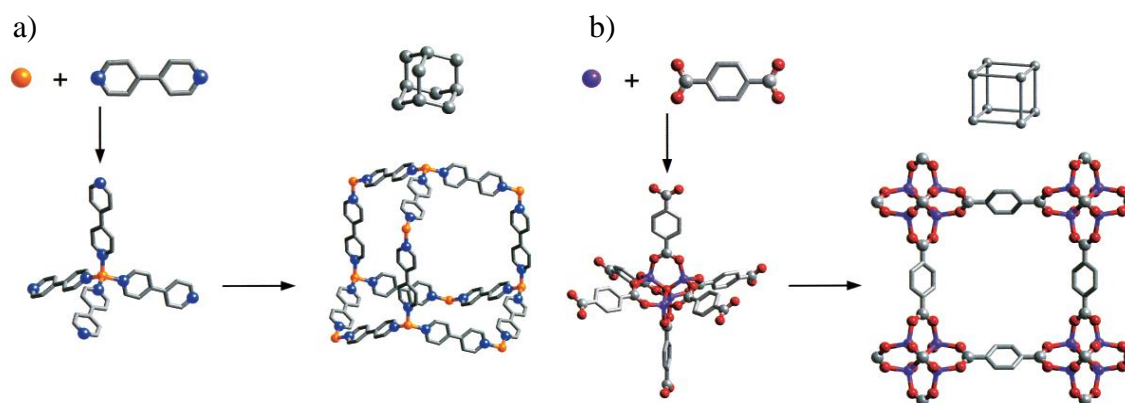


**Figure 1.22: Framework motifs formed from a) tetrahedral b) octahedral nodes reproduced from Eddaoudi et al.<sup>1</sup>**

One of the first diamondoid metal-organic frameworks reported was  $[\text{Cu}(\text{C}_{10}\text{H}_8\text{N}_2)_2(\text{PF}_6)]$ .<sup>123</sup> This copper-4,4'-bipyridine MOF contains anions in the cavities generated by the diamondoid network; the intermetallic separations of 11.16 Å are sufficient to enable both the inclusion of counter-ions and to facilitate 4-fold interpenetration.<sup>123</sup> A subsequently reported silver(I) and 4,4'-bipyridine structure  $[\text{Ag}(\text{C}_{10}\text{H}_8\text{N}_2)_2(\text{CF}_3\text{SO}_3)]$  also shows metal...metal distances of 11.6 Å; this structure also exhibits the 4-fold interpenetration observed by Zaworotko *et al.*<sup>123</sup>. Subsequent studies on diamondoid metal-organic frameworks also display varying levels of interpenetration.<sup>124-126</sup>

Octahedral networks have been known for centuries in the form of iron-cyano compounds used in pigments; however, the first synthetic metal-organic octahedral network  $[\text{Ag}(\text{pyrazine})_3](\text{SbF}_6)$  was reported only in 1995.<sup>127</sup> This structure forms a square grid topology which is not susceptible to interpenetration due to the linkers blocking the walls of the channels. This structure and the copper analogue show high capacities for methane adsorption with high stability for guest loss, leading to reversible gas exchange. The nature of octahedral geometries

producing non-interpenetrated grid structures has led to significant research using benzenepolycarboxylic acid linkers such as 1,4-benzenedicarboxylate<sup>1</sup> and 1,3-benzenedicarboxylate.<sup>128</sup>

The  $\text{Zn}_4\text{O}(\text{1,3-benzenedicarboxylate})_3$  structure reported by Yaghi *et al.*<sup>128</sup> shows remarkable stability after guest loss, with crystallinity remaining intact up to 300 °C. The geometry of the compound is octahedral; however, it is produced from a tetrahedral building unit. As all six edges of the tetrahedral SBU are linked by spacer ligands it adopts the octahedral geometry instead of the diamondoid architecture. The reported structure  $\text{Cu}_{24}(\text{1,3-benzenedicarboxylate})_{24}(\text{DMF})_{14}(\text{H}_2\text{O})_{10}(\text{H}_2\text{O})_{50}(\text{DMF})_6(\text{C}_2\text{H}_5\text{OH})_6$  - (MOP1)<sup>129</sup> also displays this property. The structure of MOP1 consists of twelve disordered tetrahedral paddlewheel units linked by 1,3-benzenedicarboxylate linkers to form a large ‘cuboctahedron’. This large porous polyhedron has both square and triangular pores accessible upon desolvation. The structure shows remarkable thermostability upon desolvation with the structure remaining stable until 300 °C comparable to the  $\text{Zn}_4\text{O}(\text{1,3-benzenedicarboxylate})_3$  structure.<sup>129</sup>

The ability of tetrahedral SBUs to form octahedral networks is frequently observed in MOFs synthesised using benzenepolycarboxylate linkers. The most common of these building units that results in octahedral geometry is the distorted tetrahedral ‘four blade’ paddlewheel. A review by Reiger *et al.*<sup>102</sup> highlights the multitude of compounds using paddlewheel building units and their corresponding geometries, such as octahedral, square grid and ‘honeycomb’ networks.

One of the most significant paddlewheel structures is  $[\text{Cu}_3(\text{C}_9\text{H}_3\text{O}_6)(\text{H}_2\text{O})_2]_n$  – (HKUST1).<sup>130</sup> The framework is composed of dimeric cupric tetracarboxylate units; each copper is of tetrahedral geometry but completes a pseudooctahedral coordination sphere with an axial  $\text{Cu}\cdots\text{Cu}$  interaction (figure 1.23)



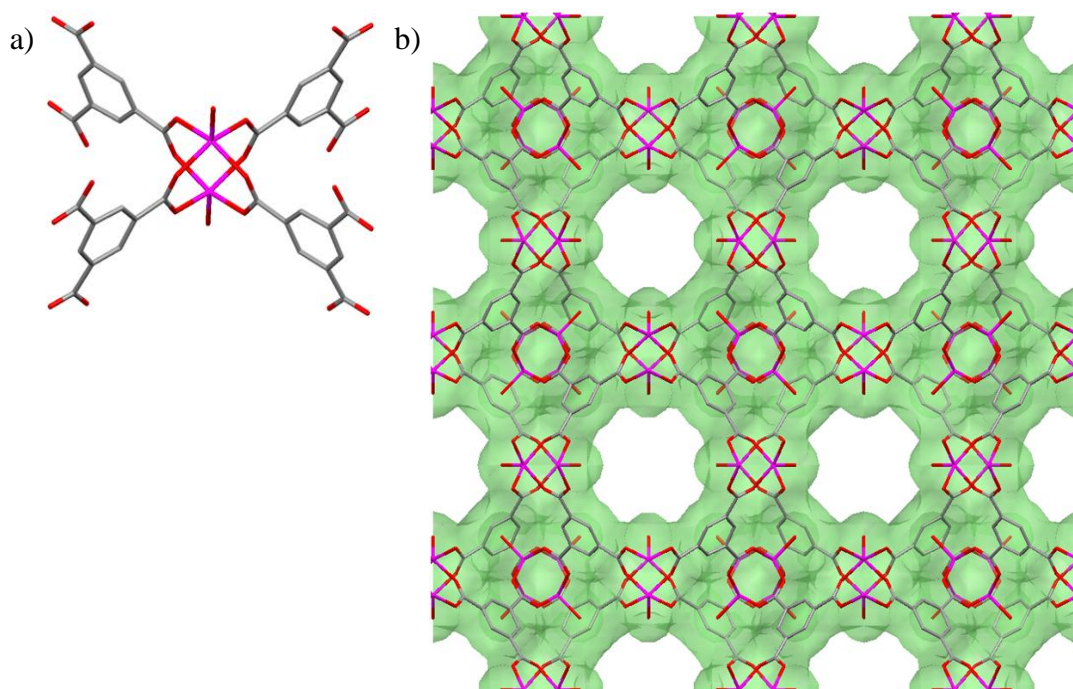


**Figure 1.23: a) Dimeric copper(II) tetracarboxylate building unit b) Packing of HKUST1 viewed down the [100] axis adapted from Williams et al.<sup>130</sup>**

The view down the [100] axis of the cubic cell (figure 1.23 (b)) shows pores 7 Å in diameter; these nanochannels are intersected by triangular pores along the [111] cell body diagonal to provide an extensive three-dimensional network of pores that equate to 67 % solvent-accessible volume. The pore size, volume, accessibility and lability of axial ligands gives rise to a host of applications in gas storage and catalysis, making structures and topologies of this nature a prime target in crystal engineering.<sup>130</sup>

## Porosity

The pores of metal-organic frameworks contain guest molecules; these are residual molecules from the synthesis such as solvent, templating or deprotonating agents. The role of these molecules on architectural design and topology of the final product is still uncertain. There are two predominant theories;<sup>1,6</sup>

- The guest molecules have no effect on the structure and only occur in pores to prevent a vacuum.
- The framework forms around the guest molecule, and pore size and shape are determined by the interactions between the framework material and guest molecules.

A significant amount of current research focuses on the second theory and aims to utilize solvent interactions in crystal engineering and architecture design; unfortunately the exact role of guest molecules and templating agents has yet to be determined.

A major consideration to be made on solvent and template choice is, for MOFs to be used for applications, that the guest molecules need to be removed and/or exchanged to activate the framework. A significant proportion of MOFs fail to withstand the desolvation process and collapse; this can be attributed to a number of reasons such as ion imbalances, coordinated guest molecules, low thermostability, unstable linkers or trapped guest molecules. Research resulting from these issues now focuses on neutral charged ‘open’ frameworks that contain volatile or labile guests.<sup>1,2,4,6,100</sup>

The stability of the framework upon desolvation is investigated using thermogravimetric analysis. This technique also provides crucial information of the thermostability of the framework by determining the temperatures at which guest and labile ligands are removed from the framework and ultimately the terminal temperature at which the structure collapses. It must be noted that instances of MOFs reforming after collapsing upon solvent addition or undergoing a structural change to produce an active product such as microporous MOFs are known, and are presented in this thesis.

After guest removal, the ability of the framework to adsorb molecules largely depends on the pore size and potential pore volume. The question of ‘is bigger better’ was well illustrated by the IR-MOF series (figure 1.19). This series shows

that the systematic lengthening of the linker to increase pore diameter and volume also increases the total volume of hydrogen adsorbed; however, the pressure needed also increases significantly. This is predominantly caused by the loss of favourable interactions between the host and the guest.<sup>100</sup> New framework materials now seek to capitalise on host-guest interactions using nanopores that undergo monolayer adsorption, using a larger number of smaller pores not a small number of larger pores. Research is also looking to ‘smart’ materials that will allow the kinetic ‘trapping’ of guest molecules using bare metal sites or flexible ligands as a new generation of gas storage and separation materials.<sup>1,4</sup>

### **Interpenetration and Catenation**

Interpenetration and catenation occur when long linkers are used in the framework synthesis and are extremely detrimental to the porosity of the framework.

Interpenetration is widely encountered and mitigates against the production of extremely porous materials, where the voids constructed by one framework are occupied by one or more independent frameworks. The structures can only be disentangled by the destruction of internal bonds in an attempt to form the non-interpenetrating porous framework; however, this may not be required as a detailed review on interpenetrated structures shows new research on microporous materials and the special abilities these interpenetrated structures have to offer.<sup>131</sup>

Catenation is the formation of ring, chain and cage structures that block the pores; currently only negative impacts on adsorption uptake and applications have been observed.<sup>132</sup>

These are often cited as the major obstacles that must be overcome in the production of porous MOFs; with both interpenetration and catenation being dependent on network topology and linker choice they play a large role in crystal engineering and MOF synthesis.

## Synthesis

One aim in MOF synthesis is to obtain high quality single crystals for structural analysis. The main difficulty in the synthesis is the insolubility of the ligands used and their subsequent high reactivity, resulting in an immediate reaction that produces amorphous material. A variety of methods have been designed to overcome these problems; they generally involve the slow introduction of the reagents to one another or the vapour diffusion of deprotonating agents such as amines to ‘activate’ the ligands. The selection of polar solvent and/or base is essential, with care taken to avoid competitive coordination with the linkers for available metal sites. This has resulted in exploratory synthesis methods to perfect several ideal synthetic conditions for specific SBU formation. However, with the need for robust MOFs increasing, new methods and synthesis conditions have been discovered in an attempt to ‘by-pass’ the time-consuming slow addition methods.

Solvothermal techniques have been found to be the most convenient solution to the problem of slow reaction times, allowing the direct addition of the reagents into sealed Teflon-lined bombs for high-temperature and high-pressure synthesis. This allows the reagents to surpass the activation energies of the reagents. Solvothermal synthesis also allows for the use of a multitude of mixed solvent systems that can be used to ‘tune’ the solvent-ligand exchange and control the polarity of the system with relative ease. These reactions are often only hours – days long, a stark contrast to the time line of weeks – months of previous systems; this allows for batch processing and rapid modifications to the synthesis protocols to produce desired frameworks on a bulk scale.

Ionothermal synthesis is an adaptation of the solvothermal technique, using ionic liquids as a reaction medium. Ionic liquids have unique solubility properties and have the ability to function as reaction media, templating agent or charge compensating groups. They also display high thermostability, ionic conductivity and negligible vapour pressure, making them ideal for the use as a solvent in Teflon-lined bomb reactions.<sup>133-135</sup> The systematic variation in the composition of the ionic liquids allows novel structures that previously were unobtainable to be realised using the ‘tailoring’ of the ionic liquid by varying alkyl chain length and counter-ion.<sup>133,136</sup> Increasing the alkyl chain length up to eight carbon atoms reduces the melting point of the ionic liquid stepwise; after this point it begins to rise again due to the changes in efficiency of ion packing as the free rotation volume decreases.<sup>136,137</sup> The effect of

alkyl chain length on crystal formation and coordination modes of nodes and linkers was demonstrated by Kwon *et al.* (table 1.01 and figure 1.24)<sup>133</sup>

Compound	Ionic Liquid	Connectivity mode of BTC <sup>3-</sup>	Coordination geometries of Zn
[Zn <sub>3</sub> (BTC) <sub>2</sub> (H <sub>2</sub> O) <sub>2</sub> ].2H <sub>2</sub> O	[EMI]Br	A	6, 4
[EMI][Zn(BTC)]	[EMI]Br	F	4
[PMI][Zn(BTC)]	[PMI]Br	H	3
[AMI][Zn <sub>2</sub> (BTC)(OH)Br]	[AMI]Br	D	5, 4

**Table 1.01: Factors affecting reaction system and resulting frameworks reproduced from Kwon *et al.*<sup>133</sup>**

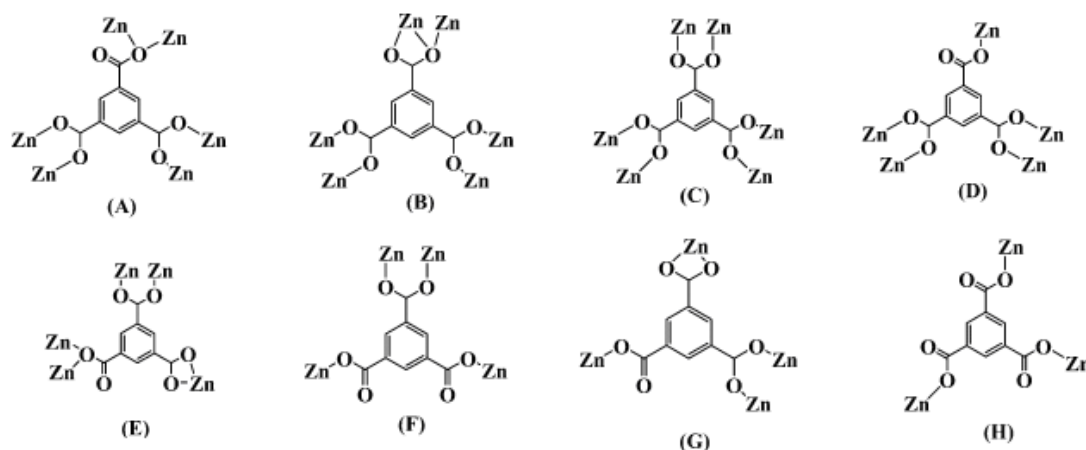


**Figure 1.24: Connectivity modes of BTC<sup>3-</sup> with Zn(II) nodes reproduced from Kwon *et al.*<sup>133</sup>**

Additional research by Kwon *et al.*<sup>134</sup> demonstrates the thermodynamic and kinetic products of 1-methyl-3-propylimidazolium halide [PMI], 1-methyl-3-butyylimidazolium halide [BMI] and 1-methyl-3-ethylimidazolium halide [EMI]. The [EMI] ionic liquid favours small cavity MOF formation and [PMI]/[BMI] favour frameworks with larger pores; this is a direct result of [PMI] and [BMI] undergoing compression tension on the formation of smaller pore lattices, making the larger pore structures thermodynamically more favourable and allowing alkyl chain length to determine the pore size and topology of the framework. The kinetically favourable products are formed only when the halide is adjusted to a more nucleophilic/basic halide ( $\text{Cl}^- > \text{Br}^- > \text{I}^-$ ) thereby fully deprotonating the trimesic acid linker ( $\text{BTC}^{3-}$ ).

This then directly prevents the formation of larger pore structures that require the HBTC<sup>2-</sup> linker to form the correct secondary building unit, thus forcing the [PMI] and [BMI] into their corresponding small pore structures, often with detrimental consequences on framework stability.<sup>134</sup>

The use of both slow diffusion techniques and high throughput methods enables a wide variety of structures to be produced under a multitude of reaction conditions. This can be used to elude the influence of guest and templating molecules on framework synthesis and topology, allowing them to be eventually used in crystal engineering and architecture design and synthesis with greater accuracy.

### **Characterisation**

The primary tool employed in the characterisation of MOFs is single-crystal X-ray crystallography. This can give an insight into the relative positions of atoms and ions, giving a geometrical representation of the framework including pore size, void availability and potential chemical active sites. Powder X-ray diffraction and elemental analysis can be used to assess the bulk purity of framework samples, and play an important role in determining structural change of microcrystalline materials that are often the result of desolvation.

Thermogravimetric analysis is used to give a thermal profile of the framework, including temperature of desolvation (activation of the framework) and terminal temperature at which the framework decomposes.

Porous frameworks are analyzed further using adsorption isotherms of various gases and vapours. Basic characterisation of the pores and the frameworks potential is carried out using the adsorption of nitrogen at 77 K and carbon dioxide at 195 K and 273 K. This determines the calculated pore volume that can be compared to the theoretical pore volume calculated from crystallographic data; the correlation of these values is indicative of sample purity and can also show early indications of sample stability after desolvation.

### **Adsorption**

There are many applications for metal-organic frameworks; these applications rely upon the ability of the materials to adsorb gases and vapours. The process of adsorption is defined as the increase in concentration of a dissolved substance at the interface of a liquid phase, due to the effects of surface forces.<sup>138</sup>

There are two types of adsorption:

- Chemisorption
- Physisorption

Chemisorption involves the adsorbate forming chemical bonds, usually covalent, to the surface of the pores of the adsorbent. The adsorbate forms monolayers due to the nature of the interactions and is heavily dependant on the surface area of the adsorbent. The process of chemisorption is usually a dissociative process as bonds within the molecules of the adsorbate are broken in order to form chemical bonds with the adsorbent.

Metal-organic frameworks have a tendency to adsorb via physisorption; a non- dissociative process that usually leaves the electronic structure of both the adsorbate and adsorbent unaffected. This occurs as the adsorbate interacts with the surface of the adsorbent through a series of long range and relatively weak interactions, similar to those involved in the condensation of gas to liquid with the  $-\Delta H_{\text{phys}} \leq 35 \text{ J mol}^{-1}$ . These long range interactions are associated with the redistribution of electrons within the adsorbate and adsorbent separately and are often reversible.<sup>139, 140</sup>

The adsorption of a guest molecule onto the adsorbent depends on a multitude of factors such as pore size, topology and importantly host-guest interactions. Figure 1.25 shows the ability of physisorption to become chemisorption as the energy of the system increases, overcoming the  $E_{\text{diss}}^{\text{a}}$  resulting in severe implications upon the structure of the adsorbent and the ability to remove the adsorbate from the lattice.<sup>140</sup>

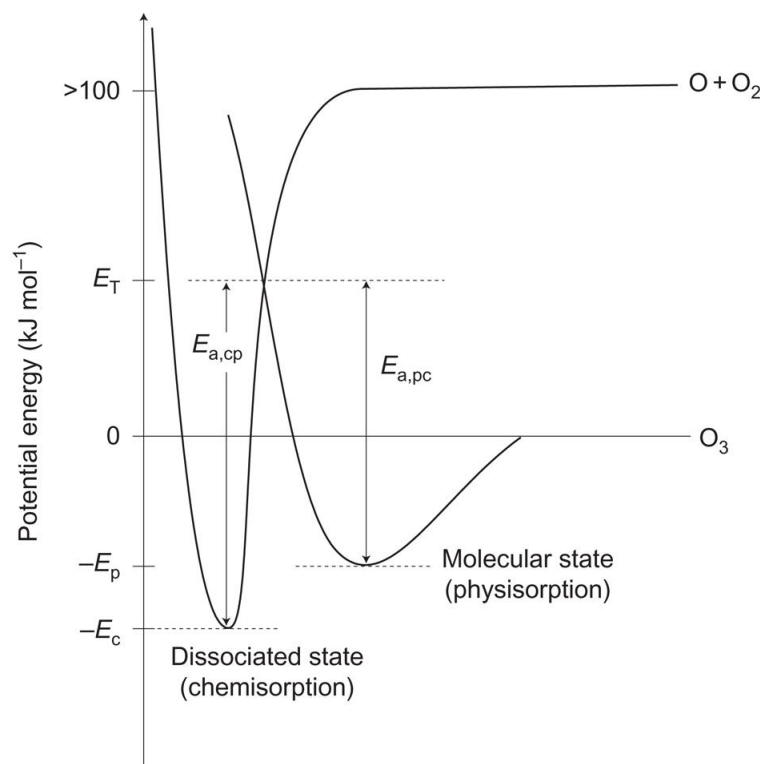


**Figure 1.25: Potential energy diagram for dissociative adsorption reproduced from Atkins et al.<sup>140</sup>**

The nature of adsorption can be described by the adsorption isotherms. These display the relationship between adsorption concentration and pressure at constant temperature.<sup>139</sup> There are five types of isotherms classified by Teller *et al.* (figure 1.26):<sup>139</sup>

- Type I – Indicative of adsorbents with microporous structures (0.7-1.4 nm).
- Type II – Correlates to adsorption of gases by non porous materials.
- Type III – Indicative of macroporous structures ( $\geq 50$  nm) with weak adsorbate to adsorbent interactions.
- Type IV – Correlates to adsorption on mesoporous materials (2–50 nm).
- Type V – Isotherm produced from mesoporous materials with weak interactions.
- Type VI – Theoretical Isotherm of adsorption on a homogeneous non porous surface.



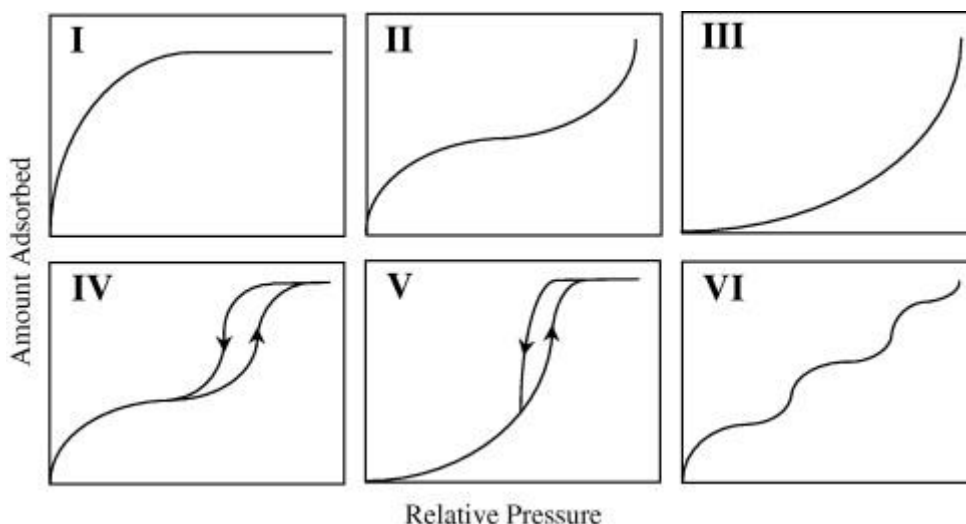


**Figure 1.26: Adsorption classification isotherms reproduced from Barnes et al.<sup>139</sup>**

Porous metal-organic frameworks tend to produce type I isotherms, where at relatively low pressures a large concentration of adsorbate is adsorbed before it plateaus as the total available pore volume is reached. Kinks in the type I isotherm are sometimes observed due to changes in the lattice, this normally occurs in flexible frameworks.<sup>141</sup>

The differences in isotherms II, III and IV are due to the adsorbent and adsorbate interactions. The isotherms can yield information on pore volume, surface area and enthalpies of adsorption; for example type II isotherms show strong interactions within a non-porous material, where as isotherms IV and V show the complete filling of the initial layers occurring at low pressures with additional layers adsorbed upon more pressure indicating a large pore volume also capable of forming strong long range interactions.<sup>139, 141</sup>

Isotherms are measured using Intelligent Gravimetric Analysis (IGA) in conjunction with thermogravimetric analysis that determines the critical temperature of the structure to help determine potential applications of the material.

## Applications

The development and expansion of the metal-organic field has been one driven by potential applications, with many potential applications proposed and fulfilled using a host of materials. Applications for MOFs include the storage of separation of gases/vapours, catalysis, sensing and biomedical applications such as drug delivery.

Porous materials are already utilized for a wide range of applications in important industrial processes, such as zeolites and activated carbons, which are used within the gas separation and catalysis industries. The crucial properties of MOFs having uniform, crystalline structures with the ability to rationally design the framework lattice makes them a highly desirable material for many applications.

### **Gas and Vapour Storage**

The storage of gases and vapours in solids is becoming an evermore important field, where metal-organic frameworks have already proved useful; with applications and potential applications in; the storage of gases for fuels, such as hydrocarbons and hydrogen, for environmentally important gases such as sulphur dioxide and carbon dioxide and the storage of biomedically important gases such as nitric oxide for medicinal purposes.<sup>142</sup> Since the discovery of metal-organic frameworks extensive studies have been carried out on gas adsorption properties regarding the storage of hydrogen for use as a fuel.<sup>101</sup>

The use of MOFs in hydrogen storage is of importance as current methods including; metal hydrides, high pressure gas storage and liquefied hydrogen do not satisfy the current requirements for the use of hydrogen as a fuel, and have excessive safety issues associated with them.<sup>143,144</sup> Several examples of hydrogen adsorption on metal-organic frameworks have been reported<sup>145-148</sup> showing a trend between capacity and surface area; the larger the surface area the material has, the higher the capacity for hydrogen adsorption.<sup>148,149</sup> However at higher pressures the total pore volume of the material determines the hydrogen capacity and not the surface area, which along with enthalpy of adsorption plays a significant role at the lower pressures.<sup>50,150,153</sup> This has resulted in MOFs being targeted and retrosynthetically designed for high capacity adsorption of hydrogen with focus on materials with large total surface areas with relatively small pores to create favourable interactions between the hydrogen molecules and the adsorbent.<sup>151-153</sup>

The enhancing of hydrogen adsorption capacity by exploiting hydrogen...surface interactions enables the increase of adsorption nearer to ambient conditions, with the inclusion of hydrophobic surfaces or open metal centres.<sup>149,154,155</sup> The Kubas coordination<sup>156</sup> shows the first complex with a hydrogen molecule coordinated side-on ( $\eta^2$ ) to the metal, since this complex was reported several compounds have shown the enhancement of hydrogen storage upon the

production of open metal centres.<sup>156-160</sup> The binding strength of the Kubas coordination is midway between physisorption and metal-hydride interactions, ideal for hydrogen adsorption materials.<sup>160</sup> The reversibility of this hydrogen binding is also a key feature of the Kubas complexes; with the alteration of the benzyl ligands increasing the reversibility of the coordination whilst keeping the hydrogen-hydrogen bond intact,<sup>161</sup> paving the way for potential materials for hydrogen storage.<sup>101, 153</sup> Hydrogen adsorption has also been shown to increase with the use of flexible microporous frameworks, with the bipyridine frameworks reported by Thomas *et al.* showing hysteresis in the desorption of hydrogen as a result of ligand flexibility.<sup>162</sup> Second and third generation compounds were produced by Kitagawa *et al.*<sup>163</sup> displaying induced-fit properties; [Cu<sub>2</sub>(pyrazine-2,3-dicarboxylate)<sub>2</sub>(4,4'-bipyridine)] and breathing pore properties; [Zn(benzenedicarboxylate)(water)]. These compounds upon adsorption undergo drastic structural changes to accommodate the adsorbant.<sup>163</sup>

Although extensive research and a wide variety of compounds have been produced that show promises as potential hydrogen storage devices, for them to be used as fuel stores they require low temperatures and high pressures. For MOFs to be considered as practical fuel stores they would be required to operate at close to ambient conditions. The storage of methane has also been a forefront of adsorption research within MOFs.<sup>144,164</sup> The high capacity framework IRMOF-6 reported by Yaghi *et al.*<sup>42</sup> showed extremely high affinity for methane at near ambient temperatures, this coupled with additional frameworks adsorbing the hydrocarbons; acetylene and light alkanes<sup>165,166</sup> suggests metal-organic frameworks are a promising material for these applications.

Metal-organic frameworks are also being progressively used in the sequestration of carbon dioxide. Carbon dioxide is a green house gas and is a prominent pollutant, currently there are considerable efforts being employed to reduce the amount present in the atmosphere. Multiple frameworks have been reported with high affinities for carbon dioxide<sup>167-169</sup> with significant not to the flexible framework reported by Férey *et al.*<sup>168</sup> that undergoes structural changes upon carbon dioxide adsorption.

### **Separation of Gases and Vapours**

In recent years there has been significant public and scientific concern over the risks of industrial gas emissions, that may contribute to damage to the environment and

public health. Two dominant technologies applied at an industrial level are adsorption processes and membrane separations; with meso-macroporous activated carbons used in water treatment<sup>170,171</sup> and nanoporous activated carbons used for gas removal of sulphur dioxide and nitric oxide along with volatile organic carbons.<sup>172,173</sup> The tailoring ability of metal-organic frameworks for specific applications has resulted in them becoming tools for several different types of separation. Processes involving adsorptive separation using MOFs include xylene separation, acetylene production from mixed gases, volatile organic compound removal, desulphurisation of methane and hydrogen along with many others.<sup>144,166,167,174</sup>

The adsorptive separation of gases or vapours falls under either bulk separation of a large proportion of the gas sample or purification of a small quantity of impurity from a stream of gas or vapour. The separation by adsorption of gases or vapours can occur in three ways:<sup>175</sup>

- Size exclusion
- Kinetic separation based on size and shape differences
- Surface interactions

The separation of gases based on steric effects is known as molecular sieving and involves selective adsorption based on ion size and shape of the adsorbates; molecules of specific sizes can enter the MOF whilst the rest of the gas passes around the material, separating part of the gaseous mixture. Examples of this separation include *n*-paraffin recovery and the separation of xylene isomers.<sup>176</sup>

The separation of gases and vapours by kinetics of the adsorbates occurs with the adsorption of a mixture of adsorbates, these pass through the adsorbent at different rates depending on the respective interactions with the adsorbent. Examples of separation using this method include nitrogen generation from air<sup>177</sup> and quantum molecular sieving of H<sub>2</sub> and D<sub>2</sub> that occurs in microporous materials at low temperatures.<sup>177</sup>

Separations based on surface interactions occurs when the surface of the adsorbent preferentially adsorbs a particular adsorbent over others in the mixture, this is due to the favourable interactions between the adsorbate and the adsorbent. Examples of this separation are observed in the filtering of carbon dioxide and

methane, as carbon dioxide can form strong interactions with the surfaces of the pores.<sup>178</sup>

## Catalysis

Heterogeneous catalysis was one of the first explored applications for metal-organic frameworks.<sup>179</sup> This was due to the similarities between porous MOFs and zeolites that were being used in catalytic cracking in a extremely lucrative multibillion dollar industry.<sup>9</sup> Although crystalline MOFs share a portion of the catalytically important features of zeolites such as large internal surface areas and regular arrays of pores; they differ significantly in thermal stability with much lower terminal temperatures, limiting their uses in reactions with challenging conditions. The advantage of MOFs is their ability to be ‘tuned’ to reactions with the inclusion of organic molecules making them tailorable for specific reactions of delicate molecules, giving them an edge over zeolites.

Recently the field of MOFs as catalysts has expanded rapidly as the formation of synthetic chemistry to provide predictable structures for this field is now in place. Many applications have been demonstrated with examples of framework-stabilisation of short lived catalysts,<sup>180</sup> coupling of catalysis to chemical separation,<sup>181</sup> post synthetic inclusion of catalytic metal sites<sup>182,183</sup> and size selective catalysis.<sup>181-184</sup>

One of the earliest examples of a MOF-based catalyst was a two-dimensional cadmium-bipyridine framework reported by Fujita *et al.* in 1994, used for the catalysis of aldehydes in cyanosilylation.<sup>179</sup> The investigation focused on size and shape selectivity with the aldehydes required to reach the active sites within the framework.<sup>179</sup> Further examples were reported by Xamena *et al.*<sup>185</sup> focussing on two-dimensional, square grid frameworks containing Pd(II) nodes that catalyse a range of reactions such as; Suzuki C-C coupling, olefin hydrogenation and alcohol oxidation.<sup>185</sup> The previous examples are defined as opportunistic catalysts, with trial and error catalytic investigations, a second generation of materials with designed frameworks such as HKUST-1<sup>130</sup> and MOF-199<sup>186</sup>, that contain large cavities with labile water ligands coordinated to the metal nodes, allowing the formation of open metal sites upon desolvation. These compounds were shown to have Lewis acid sites that can catalyse the cyanosilylation of benzaldehyde or acetone; further investigations on the reactions of  $\alpha$ -pinene oxide,  $\alpha$ -bromoacetate rearrangement and

the cyclisation of citronellal compounds confirmed the lewis acid catalytic nature of the compounds.<sup>187</sup>

### **Sensing**

The application of MOFs as sensors has recently been expanded with optical and magnetic changes observed within compounds upon adsorption. This property is often coupled with the addition of components with luminescent properties that are then included into the framework to enhance the materials ability to act as a optical gas or vapour sensor. This process is reported by Chen *et al.*<sup>188</sup> with MOF-76 that has the capability of detecting small molecules with luminescent changes corresponding to respective anions in methanol solutions; this compound is particularly sensitive to fluoride anions.<sup>188</sup> Wong *et al.*<sup>189</sup> also reported a microporous framework that shows reversible sensing of anions controlled by a molecular sieve property,<sup>189</sup> additional research by Yeom *et al.*<sup>190</sup> produced a gas preconcentrator with IRMOF-1 that emits an enhanced electrical signal from contact with toxic gases.<sup>190</sup>

### **Biomedical**

The use of MOFs in biological applications requires the materials to have low toxicity levels that are determined from the toxicity of the linkers and metal nodes individually. Based on this only biologically friendly linkers and metals can be used such as Ca, Mg, Zn, Fe or Ti that have acceptable LD<sub>50</sub> ranges. The toxicity concerning the linkers often leads to the targeting of naturally occurring materials such as polycarboxylates or highly polar compounds that have fast excretion times within the body, including 1-methylimidazole, terephthalic and trimesic acid.

This has resulted in bioactive MOFs with sufficient pore volumes to encapsulate the bioactive molecules and deliver them to the site of action. One such series of compounds were reported by Li *et al.* that included amino acid zinc MOFs with therapeutic activities.<sup>191</sup> Other examples of peptide and norfloxacin based MOFs have been reported; however none have been evaluated for controlled release of the active molecules.<sup>192,193</sup>

The incorporation of the biomolecule as a linker with a non-toxic metal has produced a bioactive MOF; BIOMIL-1, based on nicotinic acid and iron nodes.<sup>194</sup> This framework has a 71 % drug content and releases the drug through degrading of

the framework in a phosphate solution at 37°C.<sup>194</sup> This rapid release and instability limits the compounds practical applications; however a second generation of carboxylate derivatives show higher stabilities and slower drug release rates, whilst maintaining the vasodilating and antilipemic properties.

The use of MOFs as adsorbents for nitric oxide has been reported in the structures; HKUST-1<sup>130</sup>, CPO-27<sup>195</sup>, MIL-100<sup>196</sup> and MIL-101<sup>196</sup> that exhibit a high uptake of NO. The bioactivity and delivery of the adsorbed NO has been concentrated on three *in-vitro* experiments to investigate antithrombosis, blood vessel relaxation and antibacterial properties of the NO-loaded MOFs. HKUST-1<sup>130</sup> showed that even with low concentrations of NO within its framework, it remained the most active compound for the treatment of thrombosis with respect to the frameworks listed; whilst CPO-27<sup>195</sup> materials with highest NO load capacities had an optimum application in vasodilatory treatments.<sup>195</sup>

## References:

- 1 M. Eddaoudi, D.B. Moler, H. Li, B. Chen, T. M. Reineke, M. O'Keefe, O. M. Yaghi, *Acc. Chem. Res.*, **2001**, 34, 319.
- 2 B. Moulton, M. J. Zaworotko, *Chem. Rev.*, **2001**, 101, 1629.
- 3 M. J. Zaworotko, *Chem. Commun.*, **2001**, 1.
- 4 F. Rouquerol, J. Rouquerol, K. Sing, *Adsorption by Powders and Porous solids*; Academic Press, **1999**.
- 5 K. Sing, D. H. Everett, R. A. W. Haul, L. Moscou, R. A. Pierotti, J. Rouquerol, T. Siemieniewska, *Pure Appl. Chem.*, **1985**, 574, 603.
- 6 S. Kitagawa, R. Kitaura, S. Noro, *Angew. Chem. Int. Ed.*, **2004**, 43, 2334.
- 7 D. W. Breck, *Zeolite Molecular Sieves; Structure, Chemistry and Use*, Wiley, New York, **1974**.
- 8 P. B. Venuto, *Microporous Mater.*, **1994**, 2, 297.
- 9 J. Weitkamp, *Solid State Ionics*, **2000**, 131, 175.
- 10 O. D. Friedrichs, A. W. M. Dress, D. H. Huson, J. Klinowski, A. L. Mackay, *Nature*, **1999**, 400, 644
- 11 C. P. Greg, F. I. Pashni, A. F. Gualtieri, P. Norby, J. C. Hanson, D. R. Corbin, *J. Am. Chem. Soc.*, **1997**, 119, 1981.
- 12 H. de Sainte Claire Deville, C. R. Hebd, *Seanes Acad. Sci.*, **1862**, 54, 324.
- 13 R. M. Barrer, *J. Chem. Soc.*, **1948**, 127.
- 14 R. M. Barrer, *J. Chem. Soc.*, **1948**, 2158.
- 15 J. A. Rabo, M. W. Scoanover, *Appl. Catal. A: Gen.*, **2001**, 222, 261.
- 16 J. V. Smith, *Chem. Rev.*, **1988**, 88, 149.
- 17 F. G. Dwyer in W. R. Moser, Ed., *Catalysis of Organic Reactions*; Marcel Dekker, New York, **1981**, 39.
- 18 J. Scherzer, A. J. Gruia, *Hydrocracking Science and Technology*; Marcel Dekker, New York, **1996**. 305.
- 19 M. E. Davis, *Nature*, **2002**, 417, 813.
- 20 N. Y. Chem, W. E. Garwood, F. G. Dwyer, *Shape Selective Catalysis in Industrial Applications*; Marcel Dekker, New York, **1989**, 203.
- 21 R. T. Pabalan, F. P. Bertetti, *Natural Zeolites: Occurrence, Properties, Applications*, D. L. Bish, D. W. Ming, Mineralogical Society of America, Washington D. C., USA, **2001**.
- 22 L. L. Jr. Ames, *Am. Mineral*, **1961**, 46, 1120.



- 23 T. R. Gaffney, *Current Opinion in Solid State and Materials Science* **1**, **1995**, 69.
- 24 P. N. Cheremisinoff, F. Ellerbusch, Ed., *Carbon Adsorption Handbook*; Ann Arbor Science Publishers, Inc. Michigan, **1978**.
- 25 J. S. Mattson, H. B. Mark, *Activated Carbon*; Marcel Dekker, New York, **1988**.
- 26 N. N. Avgal, A. V. Kiselev, *Chemistry and Physics of Carbon*: Wlater, P. L. Jr., Ed., Marcel Dekker, New York, **1970**, 6, 2.
- 27 R. C. Bansal, D. B. Donnet, F. Stoeki, *Active Carbon*; Marcel Dekker, New York, **1988**.
- 28 J. Goin, V. V. Schuller-Goetzburg, Y. Sakuma, *Chemical Economics Handbook*, SRI International, California, **1989**, 731:20001P.
- 29 A. F. Wells, *Structural Inorganic Chemistry*, 5<sup>th</sup> Ed.; Oxford University Press, Oxford, **1984**.
- 30 A. F. Wells, *Three dimensional Nets and Polyhedra*; Wiley, New York, **1977**.
- 31 B. F. Hoskins, R. Robson, *J. Am. Chem. Soc.*, **1989**, 111, 5982.
- 32 B. F. Hoskins, R. Robson, *J. Am. Chem. Soc.*, **1990**, 112, 1546.
- 33 M. Munkata, L. P. Wu, T. Kuroda-Sowa, *Adv. Inorg. Chem.*, **1999**, 46, 173.
- 34 A. J. Blake, N. R. Brooks, N. R. Champness, M. Crew, L. R. Hanton, P. Hubberstey, S. Parsons, M. Schröder, *J. Chem. Soc. Dalton Trans.*, **1999**, 2813.
- 35 N. S. Oxtoby, A. J. Blake, N. R. Champness, C. Wilson, *Proc. Natl. Acad. Sci USA*, **2002**, 99, 4905.
- 36 M. Eddaoudi, J. Kim, D. Vodak, A. Sudik, J. Wachter, M. O'Keeffe, O. M. Yaghi, *Proc. Natl. Acad. Sci USA*, **2002**, 99, 4900.
- 37 L. Tei, V. Lippolis, A. J. Blake, P. A. Cooke, M. Schröder, *Chem. Commun.*, **1998**, 2633.
- 38 J. L. C. Roswell, O. M. Yaghi, *Micro. and Meso. Mater.*, **2004**, 73, 3.
- 39 O. M. Yaghi, M. O'Keeffe, N. W. Ockwig, H. K. Chae, M. Eddaoudi, J. Kim, *Nature*, **2003**, 423, 705.
- 40 S. L. James, *Chem. Soc. Rev.*, **2003**, 32, 276.
- 41 S. Kitagawa, M. Munakata, *Trends Inorg. Chem.*, **1993**, 3, 437.
- 42 M. Eddaoudi, J. Kim, N. Rosi, D. Vodak, J. Wachter, M. O'Keeffe, O. M. Yaghi, *Science*, **2002**, 295, 469.
- 43 M. D. Allendorf, C. A. Bauer, R. K. Bhaktaa, R. J. T. Houka, *Chem. Soc. Rev.*, **2009**, 38, 1330.
- 44 J. W. Cheng, S. T. Zheng, G. Y. Yang, *Dalton Trans.*, **2007**, 4059.

- 45 L. Pan, K. M. Adams, H. E. Hernandez, X. Whang, C. Zheng, Y. Hattori, K. Kaneko, *J. Am. Chem. Soc.*, **2003**, 125, 3062.
- 46 T. M. Reinke, M. Eddaoudi, M. Fehr, D. Kelley, O. M. Yaghi, *J. Am. Chem. Soc.*, **1999**, 121, 1651.
- 47 D. Long, A. J. Blake, N. R. Champness, C. Wilson, M. Schröder, *Angew. Chem. Int. Ed.*, **2001**, 40, 13, 2444.
- 48 F. J. Steemes, W. Verboom, D. N. Reinhout, E. B. van der Tol, J. W. Verhaven, *J. Am. Chem. Soc.*, **1995**, 117, 37, 9408.
- 49 D. T. de Lill, A. de Bettencourt-Dias, C. L. Cahill, *Inorg. Chem.*, **2007**, 46, 10, 3960.
- 50 B. Chen, X. Zhao, A. Putkham, K. Hong, E. B. Lobkovsky, E. J. Hurtado, A. J. Fletcher, K. M. Thomas, *J. Am. Chem. Soc.*, **2008**, 130, 20, 6411.
- 51 M. J. Rosseinsky, *Micro. and Meso. Mater.*, **2004**, 73, 15.
- 52 R. G. Pearson, *J. Am. Chem. Soc.*, **1963**, 85, 3533.
- 53 T. L. Ho, *Chem. Rev.*, **1975**, 75, 1.
- 54 P. J. Hagerman, D. Hagerman, J. Zubieta, *Angew. Chem.*, **1999**, 111, 2789.
- 55 S. Kitagawa, M. Kondo, *Bull. Chem. Soc. Jpn.*, **1998**, 71, 1739.
- 56 F. Vögle, *Supramolecular Chemistry*; Wiley, Chichester, **1991**.
- 57 C. J. Kepert, M. J. Rosseinsky, *Chem. Commun.*, **1999**, 4, 375.
- 58 A. J. Fletcher, E. J. Cussen, T. J. Prior, M. J. Rosseinsky, C. J. Kepert, K. M. Thomas, *J. Am. Chem. Soc.*, **2001**, 123, 41, 1001.
- 59 S. Noro, S. Kitagawa, M. Kondo, K. Seki, *Angew. Chem. Int. Ed.*, **2000**, 39, 12, 2081.
- 60 M. Kondo, M. Shimamura, S. I. Noro, T. Yoshitomi, S. Minakoshi, S. Kitagawa, *Chem. Lett.*, **1999**, 285.
- 61 G. de Monno, D. Armentano, T. Poerio, M. Julve, J. A. Real, *J. Chem. Soc., Dalton Trans.*, **1999**, 1813.
- 62 C. Janiak, L. Uehlin, H. P. Wu, P. Klüfers, H. Piotrowski, T. G. Scharmann, *J. Chem. Soc. Dalton Trans.*, **1999**, 3121.
- 63 H. P. Wu, C. Janiak, L. Uehlin, P. Klüfers, P. Mayer, *Chem. Commun.*, **1998**, 2637.
- 64 H. X. Zhang, B. S. Kang, A. W. Xu, Z. N. Chen, Z. Y. Zhou, A. S. C. Chan, K. B. Yu, C. Ren, *J. Chem. Soc. Dalton Trans.*, **2001**, 2559.
- 65 H. J. Choi, T. S. Lee, M. P. Suh, *J. Inclusion Chem. Macro-cyclic Chem.*, **2001**, 41, 155.
- 66 S. O. H. Gutschke, D. J. Price, A. K. Powell, P. T. Wood, *Angew. Chem.*, **2001**, 113, 1974.

- 67 O. M. Yaghi, H. Li, T. L. Groy, *J. Am. Chem. Soc.*, **1996**, 118, 9096.
- 68 T. J. Prior, M. J. Rosseinsky, *Chem. Commun.*, **2001**, 495.
- 69 M. Kumagai, C. J. Kepert, M. Kurmoo, *Inorg. Chem.*, **2002**, 41, 3410.
- 70 R. Cao, Q. Shi, D. Sun, M. Hong, W. Bi, Y. Zhao, *Inorg. Chem.*, **2002**, 41, 6161.
- 71 N. Snejko, E. Gutierrez-Puebla, J. L. Martinez, M. A. Monge, C. Ruiz-Valero, *Chem. Mater.*, **2002**, 14, 1879.
- 72 L. J. Zhang, J. Q. Xu, Z. Shi, W. Xu, T. G. Wang, *J. Chem. Soc. Dalton Trans.*, **2003**, 1148.
- 73 S. S. Y. Chui, A. Siu, X. Feng, Z. Y. Zheng, T. C. W. Mak, I. D. Williams, *Inorg. Chem. Commun.*, **2001**, 4, 467.
- 74 H. Endres, A. Knieszner, *Acta. Crystallogr. Sect. C*, **1984**, 40, 770.
- 75 H. Kumagai, Y. Oka, M. Akita-Tanaka, K. Inoue, *Inorg. Chem. Acta*, **2002**, 332, 176.
- 76 F. H. Allen, *Acta. Crystallogr.*, **2002**, B58, 380.
- 77 L. J. Prins, D. N. Reinhoudt, P. Timmerman, *Angew. Chem. Int. Ed.*, **2001**, 40, 2382.
- 78 C. B. Aakeröy, A. M. Beatty, *Aust. J. Chem.*, **2001**, 54, 409.
- 79 J. Lu, T. Paliwala, S. C. Lim, C. Yu, T. Niu, A. J. Jacobson, *Inorg. Chem.*, **1997**, 36, 923.
- 80 N. Moliner, M. C. Murioz, J. A. Real, *Inorg. Chem. Commun.*, **1999**, 2, 25.
- 81 S. Noro, M. Kondo, T. Ishii, S. Kitagawa, H. Matasuzaka, *J. Chem. Soc. Dalton Trans.*, **1999**, 1569.
- 82 A. J. Blake, S. J. Hill, P. Hubberstey, W. S. Li, *J. Chem. Soc. Dalton Trans.*, **1997**, 913.
- 83 P. A. Kollman, L. A. Allen, *Chem. Rev.*, **1972**, 72, 283.
- 84 P. Schuster, G. Zundel, C. Sandorfy, *The Hydrogen Bond; Recent Developments in Theory and Experiments: Volume 1-3*, North Holland, Amsterdam, **1976**.
- 85 R. Taylor, O. Kenard, W. Versichel, *J. Am. Chem. Soc.*, **1984**, 106, 244.
- 86 M. C. Wahl, M. Sundaralingam, *Trends Biochem. Sci.*, **1997**, 22, 97.
- 87 M. Nishio, *Cryst. Eng. Comm.*, **2004**, 6, 130.
- 88 G. R. Desiraju, *Acc. Chem. Res.*, **1991**, 24, 290.
- 89 M. C. Etter, *J. Phys. Chem.*, **1991**, 95, 12, 4601.
- 90 F. H. Herstein, M. Kapon, G. M. Reisner, *J. Inclusion Phenom.*, **1987**, 5, 211.
- 91 S. Xia, S. Hu, J. J. Zhang, X. Wu, Z. Fu, W. Du, *Inorg. Chem. Commun.*, **2004**, 7, 271.
- 92 O. M. Yaghi, C. E. Davis, G. Li, H. Li, *J. Am. Chem. Soc.*, **1997**, 119, 2861.
- 93 D. Sun, R. Cao, W. Bi, J. Weng, M. Hong, Y. Liang, *Inorg. Chim. Acta.*, **2002**, 332, 176.
- 94 L. Leiserowitz, *Acta. Crystallogr.*, **1976**, B32, 775.

- 95 A. Domenicano, G. Schultz, I. Hargittai, M. Colapietro, G. Portalone, P. George, C. W. Brock, *Struct. Chem.*, **1990**, 1, 107.
- 96 M. Bailey, C. J. Brown, *Acta. Crystallogr.*, **1976**, 22, 387.
- 97 C. A. Hunter, J. K. M. Saunders, *J. Am. Chem. Soc.*, **1991**, 112, 5525.
- 98 C. Janiak, *Dalton*, **2000**, 21, 3885.
- 99 J. D. Dunitz, A. Gavezzotti, *Angew. Chem. Int. Ed.*, **2005**, 44, 12, 1766.
- 100 M. Eddaoudi, J. Kim, N. Rossi, D. Vodak, J. Watcher, M. O'Keeffe, O. M. Yaghi, *Science*, **2002**, 295, 469.
- 101 M. Eddaoudi, H. Li, O. M. Yaghi, *J. Am. Chem. Soc.*, **2000**, 122, 1391.
- 102 S. Vagin, A. K. Ott, B. Rieger, *Chemie Ingenieur Technik*, **2007**, 79, 6, 767.
- 103 W. Clegg, I. R. Little, B. P. Straoghan, *J. Chem. Soc. Dalton Trans.*, **1986**, 1283.
- 104 W. Clegg, I. R. Little, B. P. Straoghan, *Chem. Commun.*, **1985**, 73.
- 105 N. P. Kuz'mina, L. I. Martgnenko, Z. A. Tu, C. T. Nguet, S. I. Troyanov, A. N. Rykov, Y. M. Korenev, *J. Inorg. Chem.*, **1994**, 39, 512.
- 106 A. M. Kirillov, Y. Y. Karabach, M. Haukka, M. F. C. Guedesda Silva, J. Sanchiz, M. N. Kopylovich, A. J. L. Pombeiro, *Inorg. Chem.*, **2008**, 47, 162.
- 107 V. Shivaiah, S. K. Das, *Inorg. Chem.*, **2005**, 44, 8846.
- 108 S. K. Ghosh, P. K. Bharadwaj, *Inorg. Chim. Acta.*, **2006**, 359, 1685.
- 109 A. Y. Robin, J. L. S. Doimeados, A. Neels, T. V. Slenters, K. M. Fromm, *Inorg. Chim. Acta.*, **2007**, 360, 212.
- 110 S. Nishikiori, T. Iwamoto, *Inorg. Chem.*, **1986**, 25, 788.
- 111 T. Miyoshi, T. Iwamoto, Y. Sasaki, *Inorg. Chim. Acta.*, **1972**, 6, 59.
- 112 R. Groeneman, L. R. MacGillvray, J. L. Atwood, *Chem. Commun.*, **1998**, 2735.
- 113 R. W. Gable, B. F. Hoskins, R. Robson, *Chem. Commun.*, **1990**, 1677.
- 114 D. Hagrman, R. P. Hammond, R. Haushalter, J. Zubieta, *Chem. Mater.*, **1998**, 10, 2091.
- 115 K. Biradha, M. J. Zaworotko, *Cryst. Eng.*, **1998**, 1, 67.
- 116 M. Fujita, Y. J. Kwon, O. Sasaki, K. Yamaguti, K. Ogura, *J. Am. Chem. Soc.*, **1995**, 117, 7287.
- 117 M. A. Withersby, A. J. Blake, N. R. Champness, P. A. Cooke, P. Hubberstey, M. Schröder, *New J. Chem.*, **1999**, 23, 573.
- 118 R. Masse, J. F. Nicoud, M. Bagieu-Beucher, C. Bourgogne, *Chem. Phys.*, **1999**, 245, 365.

- 119 S. Noro, R. Kitaura, M. Kondo, S. Kitagawa, T. Ishii, H. Matasuzaka, M. Yamashita, *J. Am. Chem. Soc.*, **2002**, 124, 2568.
- 120 H. J. Choi, M. P. Suh, *J. Am. Chem. Soc.*, **1998**, 120, 10622.
- 121 S. Kitagawa, M. Kondo, *Bull. Chem. Soc. Jpn.*, **1998**, 71, 1739.
- 122 A. F. Wells, *Three Dimensional Nets and Polyhedra*; New York, **1977**.
- 123 L. R. MacGillivray, S. Subramanian, M. J. Zaworotko, *Chem. Commun.*, **1994**, 1325.
- 124 S. Lopez, M. Kahraman, M. Harmata, S. Keller, *Inorg. Chem.*, **1997**, 36, 6138.
- 125 O. R. Evans, Z. Y. Wang, R. G. Xiang, B. M. Foxman, W. B. Lin, *Inorg. Chem.*, **1999**, 38, 2969.
- 126 K. A. Hirsch, D. Venkataraman, S. R. Wilson, J. S. Moore, S. Lee, *Chem. Commun.*, **1995**, 2199.
- 127 L. Carlucci, G. Ciani, D. M. Proserpio, A. Sironi, *Angew. Chem. Int. Ed. Engl.*, **1995**, 34, 1895.
- 128 H. Li, M. Eddaoudi, M. O'Keeffe, O. M. Yaghi, *Nature*, **1999**, 402, 276.
- 129 M. Eddaoudi, J. Kim, J. Wachter, H. K. Chae, M. O'Keeffe, O. M. Yaghi, *J. Am. Chem. Soc.*, **2001**, 123, 4368.
- 130 S. S. Y. Chui, S. Lo, J. P. H. Charmant, A. G. Orpen, I. D. Williams, *Science*, **1999**, 283, 1148.
- 131 S. R. Batten, R. Robson, *Angew. Chem. Int. Ed.*, **1998**, 37, 1460.
- 132 H. Frost, R. Q. Snurr, *J. Phys. Chem. C.*, **2007**, 111, 18794.
- 133 L. Xu, E. Y. Choi, Y. U. Kwon, *Inorg. Chem.*, **2007**, 46, 10670.
- 134 L. Xu, S. Yan, E. Y. Choi, J. Y. Lee, Y. U. Kwon, *Chem. Commun.*, **2009**, 3431.
- 135 K. E. Gutowski, G. A. Broker, H. D. Willaver, J. G. Huddleston, R. P. Swatloski, J. D. Holbrey, R. D. Rogers, *J. Am. Chem. Soc.*, **2003**, 125, 6632.
- 136 E. R. Parnham, R. E. Morris, *Acc. Chem. Res.*, **2007**, 40, 1005.
- 137 A. S. Larsen, J. D. Holbrey, F. S. Tham, C. A. Reed, *J. Am. Chem. Soc.*, **2000**, 122, 7264.
- 138 S. Brunaur, L. S. Deming, W. E. Deming, E. Teller, *Theory of the Van der Waals Adsorption of gases*, **1940**, 1723.
- 139 G. Attard, C. Barnes, *Surfaces*; Oxford University Press, New York, **1998**.
- 140 P. Atkins, J. D. Paula, *Atkins Physical Chemistry*, 7<sup>th</sup> Ed., Oxford University Press, Oxford, **2002**.
- 141 A. J. Fletcher, K. M. Thomas, M. J. Rosseinsky, *J. Sol. Struct. Chem.*, **2005**, 178, 2491.
- 142 R. E. Morris, P. S. Wheatley, *Angew. Chem. Int. Ed.*, **2008**, 47, 4966.

- 143 L. Schlapback, *MRS Bull.*, **2002**, 27, 675.
- 144 M. Kondo, T. Okubo, A. Asami, S. Noro, T. Yoshitomi, S. Kitagawa, T. Ishii, H. Matasuzaka, K. Seki, *Angew. Chem. Int. Ed.*, **1999**, 38, 140.
- 145 L. Pan, M. B. Sander, X. Huang, J. Li, M. Smith, E. Bittner, B. Bockrath, J. K. Johnson, *J. Am. Chem. Soc.*, **2004**, 126, 1308.
- 146 M. Dinca, A. F. Yu, J. R. Long, *J. Am. Chem. Soc.*, **2006**, 128, 8904.
- 147 J. L. C. Roswell, A. R. Millward, K. S. Park, O. M. Yaghi, *J. Am. Chem. Soc.*, **2004**, 126, 5666.
- 148 B. Panella, M. Hirscher, H. Putter, U. Müller, *Adv. Funct. Mater.*, **2006**, 16, 520.
- 149 S. S. Kaye, J. R. Long, *J. Am. Chem. Soc.*, **2005**, 127, 6506.
- 150 D. J. Collins, H. C. Zhou, *J. Mater. Chem.*, **2007**, 17, 3154.
- 151 P. D. C. Dietzel, B. Panella, M. Hirscher, R. Blom, H. Fjellvag, *Chem. Commun.*, **2006**, 959.
- 152 J. G. Vitillo, L. Regili, S. Chavan, G. Richardi, G. Spoto, P. D. C. Dietzel, S. Bordiga, A. Zecchina, *J. Am. Chem. Soc.*, **2008**, 130, 8386.
- 153 K. M. Thomas, *Dalton Trans.*, **2009**, 1487.
- 154 P. M. Foster, J. Eckert, J. Cheng, S. Park, G. Férey, A. Cheetham, *J. Am. Chem. Soc.*, **2003**, 125, 1309.
- 155 J. L. C. Roswell, O. M. Yaghi, *Angew. Chem. Int. Ed.*, **2005**, 44, 4670.
- 156 G. J. Kubas, R. R. Ryan, B. I. Swanson, P. J. Vergamini, H. J. Wasserman, *J. Am. Chem. Soc.*, **1984**, 106, 451.
- 157 G. J. Kubas, *Chem. Rev.*, **2007**, 107, 4152.
- 158 G. J. Kubas, *Proc. Natl. Acad. Sci. USA*, **2007**, 104, 6901.
- 159 M. Dinca, J. R. Long, *Angew. Chem. Int. Ed.*, **2008**, 47, 6766.
- 160 T. K. A. Hoang, D. M. Antonelli, *Adv. Mater.*, **2009**, 21, 1787.
- 161 S. Dutta, B. R. Jagirdar, M. Nethaji, *Inorg. Chem.*, **2008**, 47, 548.
- 162 X. Zhao, B. Xiao, A. J. Fletcher, K. M. Thomas, D. Bradshaw, M. J. Rosseinsky, *Science*, **2004**, 306, 1012.
- 163 K. Uemura, R. Matsuda, S. Kitagawa, *J. Solid State Chem.*, **2005**, 178, 2420.
- 164 W. Mori, F. Yoshida, H. Nakayama, S. Takamizawa, M. Kishita, *Chem. Lett.*, **1997**, 1219.
- 165 R. Matsuda, R. Kitaura, S. Kitagawa, Y. Kubota, R. V. Belosludar, T. C. Kobayashi, H. Sakamoto, T. Chiba, M. Takata, Y. Kawazoe, Y. Mita, *Nature*, **2005**, 238.

- 166 U. Müller, M. Schubert, F. Teich, H. Puetter, K. Schierle-Arnt, J. Pastré, *J. Mater. Chem.*, **2006**, 16, 626.
- 167 H. Li, M. Eddaoudi, T. L. Groy, O. M. Yaghi, *J. Am. Chem. Soc.*, **1998**, 120, 8571.
- 168 C. Serne, F. Millenge, C. Thouvenot, M. Nogues, G. Marsolier, D. Louer, G. Fèrey, *J. Am. Chem. Soc.*, **2002**, 124, 13519.
- 169 S. Surble, C. Serre, C. Mellot-Draznieks, F. Millange, G. Fèrey, *Chem. Commun.*, **2006**, 284.
- 170 G. Cini, *Bioresour Technol.*, **2006**, 97, 9, 1061.
- 171 I. Tan, A. L. Ahmad, B. H. Hammed, *Bioresour Technol.*, **2009**, 100, 3, 1494.
- 172 H. Tamon, M. Okazaki, *Carbon*, **1996**, 34, 6, 741.
- 173 Y. A. Alhamed, H. S. Bamufleh, *Fuel*, **2009**, 88, 1, 87.
- 174 S. Kitagawa, M. Kondo, *Bull. Chem. Soc. Jpn.*, **1998**, 71, 1739.
- 175 J. R. Li, R. J. Kuppler, H. C. Zhou, *Chem. Soc. Rev.*, **2009**, 38, 1477.
- 176 Z. Y. Gu, D. Q. Jiang, H. F. Wang, X. Y. Chui, X. P. Yan, *J. Phys. Chem. C*, **2010**, 114, 311.
- 177 B. Chen, X. Zhao, A. Putkham, K. Hong, E. B. Lobkovshy, E. J. Hurtado, A. J. Fletcher, K. M. Thomas, *J. Am. Chem. Soc.*, **2008**, 130, 6411.
- 178 V. Finsy, L. Ma, L. Alaerts, D. E. de Vos, G. V. Baron, J. F. M. Denayer, *Microporous and Mesoporous Materials*, **2009**, 120, 221.
- 179 M. Fujika, Y. J. Kwon, S. Washizu, K. Ogura, *J. Am. Chem. Soc.*, **1994**, 116, 1151.
- 180 S. H. Cho, B. Ma, S. T. Nguyen, J. T. Hupp, T. E. Albrecht-Schmitt, *Chem. Commun.*, **2006**, 2563.
- 181 A. L. Nuzhdin, D. N. Dybtsev, K. P. Bryliakov, E. P. Talsi, V. P. Fedin, *J. Am. Chem. Soc.*, **2007**, 129, 12958.
- 182 C. D. Wu, A. Hu, L. Zhang, W. Lin, *J. Am. Chem. Soc.*, **2005**, 127, 8940.
- 183 O. K. Farha, K. L. Mulfort, J. T. Hupp, *Inorg. Chem.*, **2008**, 47, 10223.
- 184 S. Horike, M. Dinca, K. Tamaki, J. R. Long, *J. Am. Chem. Soc.*, **2008**, 130, 5854.
- 185 F. X. L. Xamea, A. Abad, A. Corma, H. Garcia, *J. Catal.*, **2007**, 250, 294.
- 186 D. J. Tranchemontagne, J. R. Hunt, O. M. Yaghi, *Tetrahedra*, **2008**, 64, 8553.
- 187 L. Alaerts, E. Séguin, H. Poleman, F. Thibault-Starzyk, P. A. Jacobs, D. E. de Vos, *Chem.-Eur. J.*, **2006**, 12, 7353.
- 188 B. Chen, L. Wang, F. Zapata, G. Qion, E. B. Lobkovsky, *J. Am. Chem. Soc.*, **2008**, 130, 6718.
- 189 K. L. Wong, G. L. Law, Y. Y. Yang, W. T. Wong, *Adv. Mater.*, **2006**, 18, 8, 1051.

- 190 J. Yeom, I. Oh, C. Field, A. Radadia, Z. Ni, B. Bae, J. Han, R. I. Masel, M. A. Shannon, *Micro. Electro. Mech. Sys.*, **2008**, IEE 21<sup>st</sup> International Conference, **2008**, 232.
- 191 Y. Xie, Z. Yu, X. Huang, Z. Wang, L. Niu, M. Teng, J. Li, *Chem.-Eur. J.*, **2007**, 13, 9, 399
- 192 S. G. Srivatsana, M. Parvezb, S. Vermaa, *J. Inorg. Biochem.*, **2003**, 97, 340.
- 193 A. Manton, L. Massüger, P. Rabu, C. Palivan, L. B. McCusker, A. Taubert, *J. Am. Chem. Soc.*, **2008**, 130, 2517.
- 194 S. R. Miller, D. Heurtaux, T. Baati, P. Horcajada, J. M. Grenèche, C. Serre, *Chem. Commun.*, **2010**, 46, 4525.
- 195 P. D. C. Dietzel, Y. Morita, R. Blom, H. Fjellvag, *Angew. Chem. Int. Ed.*, **2005**, 44, 6358.
- 196 P. Horcajada, S. Surblé, C. Serre, D. Y. Hong, Y. K. Seo, J. S. Chang, J. M. Grenèche, I. Margiolaki, G. Ferëy, *Chem. Commun.*, **2007**, 2020.



## **Chapter Two - A Brief Summary of Single-Crystal X-Ray Crystallography**

### **Introduction**

Single-crystal X-ray diffraction is possibly the most powerful and key structural analytical technique used in current chemistry. One of the fundamental aims of chemists is the structure determination of molecular and non-molecular materials. X-ray diffraction allows the determination of the relative positions of atoms or ions, giving a geometrical representation of the material with bond lengths, torsion angles and non-bonded distances quantified. Structural analysis by X-ray diffraction is only a small branch of crystallography, with many texts<sup>1-6</sup> covering the breadth of the subject in great detail, hence a brief overview of the subject is presented here.

### **Crystallographic Principles**

The principle behind single-crystal X-ray analysis is that electrons in atoms diffract X-ray radiation. In the laboratory, sources of X-rays are generated via electronic bombardment of an anode of a chosen element. The majority of electrons are not stopped by a single collision, causing the production of X-rays, photoelectrons and Auger electrons.

Each element has a characteristic X-ray emission spectrum, composed of a white emission band, formed when the electrons bombarding the element reach certain critical energies and remove electrons out of the atomic orbitals of the target element. This vacancy is filled by the descent of another electron from a higher shell, and this decrease in potential energy appears as radiation. Monochromatic X-rays can be selected from this complex emission spectrum as the energies of the shells are very well defined.<sup>7</sup>

Laboratory sources of X-rays are generally 'X-ray tubes', an evacuated chamber made with glass or a ceramic material with a chosen metal such as copper ( $\lambda = 1.54184 \text{ \AA}$ ) or molybdenum ( $\lambda = 0.71073 \text{ \AA}$ ) as the target anode. The radiation source selected for an experiment depends on the type of crystal.

Molybdenum radiation is usually selected when heavy (high atomic number) atoms are present, as it results in smaller absorption effects. Its shorter wavelength enables higher angle reflections as detectable reciprocal space volume is limited by  $2/\lambda$ .

Copper radiation has a longer wavelength; this reduces the overlap of reflections for crystals with large unit cells. Copper radiation has high efficient diffraction due to a higher flux of incident photons for the same voltage setting as molybdenum, hence maximising diffraction intensities; this makes copper radiation especially useful for small crystals.

For microcrystalline or low quality crystals a more powerful source of X-rays can be used at a synchrotron facility. Synchrotron radiation is electromagnetic radiation with wavelengths varying from X-ray to infrared. The radiation is produced by electrons that are injected into a storage ring and accelerated to near to the speed of light; these are passed through a series of magnets, changing their direction and causing radiation to be emitted. A single wavelength of this radiation is selected using a monochromator.

## Diffraction

When a crystal is placed in a beam of monochromatic X-ray radiation, some of the radiation is diffracted by electron density within the crystal. This crystal has a given motif, the unit cell, which is repeated by translation in three dimensions. This extended order coupled with X-rays diffracting from each atom within each unit cell led W. L. Bragg to formulate Bragg's law. When Bragg's law is applied in three dimensions it shows that every diffracted beam from a crystal can be regarded geometrically as a reflection from parallel planes passing through the lattice points. (figure 2.01)

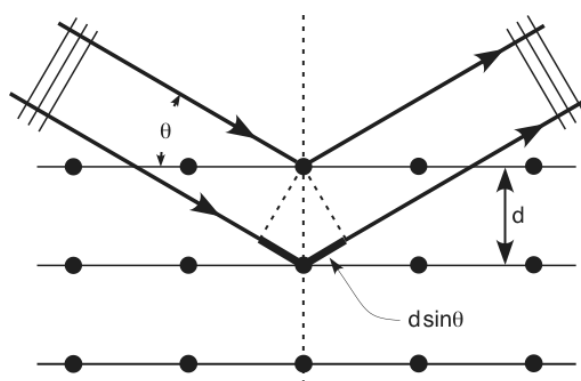


**Figure 2.01: Bragg reflections of X-rays by lattice planes within the crystal**

The angles of incidence and reflection must be equal and the incoming and outgoing beams along with the normal to the reflecting planes must all lie in the same plane.

Diffracted X-rays can add constructively or destructively. For constructive interference to occur the individual scattered beams must be in phase i.e. all radiation scattered from adjacent planes will be in phase for certain angles if the difference in path length is an integer number of wavelengths. By knowing wavelength and the angle of diffraction,  $d_{hkl}$  values can be determined using the Bragg equation, thus giving information about lattice geometry.

$$n\lambda = 2d_{hkl}\sin\theta$$

- $\lambda$  = wavelength of radiation (Å)
- $n$  = order of diffraction
- $d_{hkl}$  = lattice plane spacing (Å)
- $\theta$  = angle between the incident X-rays and the lattice plane

The value of  $n$  can always be set to one by considering planes with smaller spacing such as:  $n = 2$  for planes  $hkl$  is equivalent to  $n = 1$  for planes  $2h2k2l$  which have exactly half the spacing. Taking this into consideration, rearrangement of the Bragg equation gives:

$$\sin\theta = \left(\frac{\lambda}{2}\right) \times \left(\frac{1}{d}\right)$$

This shows that the diffraction angle of  $\theta$  is directly related to  $1/d_{hkl}$ , such that the X-ray diffraction pattern is proportional to  $\sin\theta$  and  $1/d_{hkl}$  for a set of lattice planes. This reciprocal lattice construct allows the visualisation of the relationship of the crystal lattice and its diffraction pattern. A set of vector end points, one representing each reflection in the diffraction pattern, defines a lattice with dimensions that are inversely related to the crystal lattice, and is known as the reciprocal lattice, describing the geometry of the diffraction pattern.

## **Sample Selection**

In order to obtain a high quality diffraction pattern that will enable structure determination, it is essential to select a high quality single crystal with no obvious defects.

The quality of the crystal can be initially checked using a microscope with crossed polars. As the crystal is rotated the crystal should extinguish light every  $90^\circ$ . A crystal will fail to extinguish light when it is not single or when it is twinned with misaligned unit cells.

When selecting a crystal the following considerations of size need to be made. If the crystal is too large it will not be uniformly immersed in the X-ray beam, which can generate errors when recording diffraction. However, if the crystal is too small, it may not be possible to get a structure solution due to lack of high angle data. Diffraction intensities are proportional to crystal size, larger crystals have larger volumes and hence more electrons giving greater scattering. The absorption of X-rays also increases exponentially with crystal size and can become significant when heavy atoms are present in a large crystal.

## **Data Collection**

Data for the structures presented in this thesis have been collected using a Bruker AXS SMART CCD area detector, an Oxford Diffraction Gemini Diffractometer, or at the UK synchrotron Diamond Light Source (beamline I19).

The crystalline sample is exposed to a series of short exposures covering small sections of the complete diffraction pattern. These data are then autoindexed to determine unit cell and lattice type. If the unit cell is reasonable the full data collection is performed, with exposure time and radiation type depending on the quality of diffraction. The reflection intensities are extracted using profile fitting routines and the unit cell is refined again using the complete data set.

## Data Reduction

The data collection generates thousands of reflections, each with Miller indices  $h, k, l$  and their integrated intensities  $I_{hkl}$ ; each intensity ( $I$ ) has an associated standard uncertainty (s.u.),  $\sigma(I)$ . This uncertainty is a measure of the precision and reliability of the measurement.

To solve the structure from the collected data the structure factor amplitudes  $|F_{hkl}|$  are required. The structure factor amplitudes can be calculated as they are proportional to the square root of measured intensity.

$$I_{hkl} \propto |F_{hkl}|^2 \qquad |F_{hkl}| \propto \sqrt{I_{hkl}}$$

The conversion of intensities into structure amplitudes is known as data reduction; however, corrections must be applied to the data before converting. These corrections account for Lorentz ( $L(\theta)$ ) and polarisation ( $p(\theta)$ ) effects caused by measuring diffraction from certain planes longer than others, a consequence of crystal rotation and the partial polarization of incident X-rays by the monochromator along with further partial polarization during diffraction by the crystal. Absorption effects ( $A(\theta)$ ) must also be accounted for, as X-ray intensity is reduced as it passes through the crystal; this is dependent on the elements within the crystal and the path lengths of the X-rays for each individual reflection.

Correction factors for the radiation damage ( $d(t)$ ) and decay of the sample, although rare in the samples presented in this thesis, were applied for data collected at synchrotron sources. When the corrections are made  $|F_{hkl}|$  is obtained by the following equation:

$$I_{hkl} = cL(\theta)p(\theta)A(\theta)E(\theta)d(t)m|F_{hkl}|^2$$

## Structure Solution

In order for the crystal structure to be solved and atomic positions defined the electron density distribution in the unit cell is needed. The X-ray diffraction pattern obtained is a Fourier transform of the crystal structure; to recombine the data in the Fourier transform both intensities and phases of the diffracted radiation are needed.

$$\rho(xyz) = \frac{1}{V_c} \sum_h \sum_k \sum_l |F_{hkl}| \cos 2\pi (hx + ky + lz - \alpha_{hkl})$$

$\rho(xyz)$  = electron density at point  $x, y, z$  in the unit cell

$V_c$  = volume of unit cell

$|F_{hkl}|$  = structure factor amplitude for reflection with indices  $h, k, l$

$\alpha$  = phase angle for reflection with indices  $h, k, l$ .

The data reduction generates a list of reflections with Miller indices  $h, k, l$  and their associated structure factor amplitudes and standard uncertainty values. However, the relative phases are lost and are required to calculate the electron density and solve the structure. This is commonly known in crystallography as ‘the phase problem’. There are a multitude of methods to overcome this problem; presented in this thesis are two of the most frequently used in crystallography.

## The Patterson Synthesis

The Patterson synthesis uses a method of ignoring the phase problem by setting the phases of all reflections to zero, resulting in the following equation:

$$P(uvw) = \frac{1}{V_c} \sum_h \sum_k \sum_l |F_{hkl}|^2 \cos 2\pi (hu + kv + lw)$$

$P(uvw)$  = Patterson function in vector space  $u, v, w$

$V_c$  = volume of unit cell

$|F_{hkl}|$  = structure factor amplitude at  $h, k, l$

The Patterson synthesis produces a vector map which shows the separation of pairs of atoms in the unit cell. For every pair of atoms at positions  $(x_1, y_1, z_1)$  and  $(x_2, y_2, z_2)$  there are peaks in the Patterson map at  $(x_1 - x_2, y_1 - y_2, z_1 - z_2)$  and  $(x_2 - x_1, y_2 - y_1, z_2 - z_1)$ .

For a unit cell containing  $n$  atoms, there will be  $n^2$  possible peaks in the vector map, including  $n$  peaks from vectors of atoms to themselves with zero length at the origin.

The height of the peaks is proportional to the product of the atomic numbers that give that vector, thus the largest peak at the origin can be used to scale the other peaks. Due to the prominence of heavy atom to heavy atom vectors the Patterson synthesis is most effective for structures containing a few heavy atoms in the asymmetric unit. By locating the heavy atoms a trial solution can be used as an initial phase model.

### **Direct Methods**

Direct methods attempt to assign phases using the assumptions that electron density can only be positive and it concentrates in spherical sites around atoms with zero density elsewhere. This imposes restrictions on the relative values of combinations of phase angles for sets of reflections with related indices. The mathematical analysis of probable relationships between structure factors enables approximate phases to be calculated. The approximate phases can be used to produce an approximate electron density map for a trial solution.

Although the basic assumption in direct methods is that all atoms are equal, direct methods can still be used for structures with heavy atoms. This versatility has resulted in direct methods becoming the preferred method for structure solution in small molecule crystallography.

The structures presented in this thesis were solved using the program XS within the commercial Bruker AXS package SHELXTL.<sup>8</sup>

### **Structure Refinement**

The initial trial structure solution often does not locate all the atomic positions of the structure. To locate the remaining atoms Fourier synthesis methods are used. Observed structure factors  $|F_o|$  are obtained from the data reduction, and using the initial solutions by Patterson or Direct methods we obtain calculated structure factors  $|F_c|$  and calculated phases  $\alpha_c$ . The differences between  $|F_o|$  and  $|F_c|$ , together with the calculated phases  $\alpha_c$ , are used in a Fourier transform to produce a difference electron density map. This map contains peaks that correspond to missing atoms and holes where atoms are wrongly assigned or misplaced. This information is then used in a

revised structure model, allowing a new  $|F_c|$  and  $\alpha_c$  to be calculated, producing a further difference electron map. This process is repeated several times until all non-hydrogen atoms are present in the structure. Once this is achieved the model cannot be improved further using Fourier transform synthesis methods, therefore least squares refinement methods are used. The least squares refinement involves the adjustment of the scale factor and the positional and displacement parameters of the atoms in the model, together with a few other parameters.

The program used for the refinement of all the structures in this thesis was XL its implementation in the commercial Bruker AXS package SHELXTL.<sup>9,10</sup> This program obtains the best agreement between the observed and calculated structure factors using the function:

$$\sum w(F_o^2 - F_c^2)^2$$

$w$  = weight of a reflection based on its perceived reliability (a function of the standard uncertainties)

$F_o$  = observed structure factor amplitude

$F_c$  = calculated structure factor amplitude.

The  $F^2$  values are used as they are calculated from the observed intensities enabling all the observed data including weak reflections with apparent negative intensity to be used in the refinement.

In some cases it is necessary to apply constraints or restraints in a least squares refinement. These are usually geometric in nature in order to compensate for disorder in the structure. A constraint will reduce the number of parameters being refined as it assigns an exact parameter to a value or imposes an exact relationship between two or more parameters. Examples of constraints used in structures presented in this thesis include the introduction of hydrogen atoms in positions with ideal geometry, riding on their parent carbon or other atoms. It was occasionally necessary that perfect hexagonal geometry was imposed on poorly defined benzene or pyridine rings using the SHELX AFIX 66 command; this is an exact mathematical condition.



A restraint such as restricting chemically equivalent bond lengths or angles to be similar increases the effective number of observations without affecting the number of parameters to be refined. Each restraint has associated uncertainty that determines the weight and reliability in refinement; this is more of an observation to be approximately satisfied rather than a fixed constraint. Examples of restraints used in structures presented within this thesis include restraining geometries of solvent molecules such as water along with the displacement parameters of ‘non-positive-definite’ (NPD) atoms. NPD atoms occur as atoms are modelled anisotropically as displacement ellipsoids; when the magnitudes of the displacement parameters do not correspond to a physical ellipsoid but to another quadratic surface they lose physical significance. Restraints used to prevent non-positive-definite behaviour were ISOR, DELU and SIMU, each restraining the displacement parameters in different ways. The ISOR command restrains the displacement parameters to be approximately isotropic, and is a ‘soft’ restraint with a large standard uncertainty. DELU restrains the displacement parameters of two atoms in the direction of their common bond; this is usually a relatively ‘hard’ restraint with a small standard uncertainty. The SIMU command restrains the displacement parameters for spacially close atoms (especially in cases of disorder) to be approximately equal.

Hydrogen atoms are often not detected accurately in the difference electron density map due to their low scattering ability. Therefore hydrogen atoms are usually constrained to give them a fixed bond length and tying their atomic displacement parameters to the atoms to which they are bonded. Alternatively the SADI distance restraint may be applied to make chemical equivalent distances equal; this was used for O-H distances and  $H_A \cdots H_B$  distances in water molecules.

In the least-squares refinement, it is necessary to weight each observed reflection depending upon its reliability. This is based upon an estimate of the precision of the reflection amplitude and is used for refinement on  $F^2$ .

$$w = \frac{1}{\sigma^2(F_o^2)}$$

The quality of the final structure can be assessed by the comparison between observed and calculated structure amplitudes. The most common method used for the comparison

is that of the residual index, known as the R-factor. Structures refined using the  $F^2$  amplitudes in the program XL have the following definitions of R-factor and weighted R-factor.

$$R_1 = \frac{\sum |F_0| - |F_c|}{\sum |F_0|} \qquad wR_2 = \left[ \frac{\sum w(F_0^2 - F_c^2)^2}{\sum w(F_0^2)^2} \right]^{\frac{1}{2}}$$

The R-factor, in general, gives a good indication of the quality of the structure with a lower number suggesting a better fit of data. However, a true indication of a good quality model is a featureless final difference map, together with small standard uncertainty values for the parameters calculated by the least squares refinement.

A number of non-centrosymmetric and chiral space groups are presented within this thesis, these include compounds **12-14**, **34**, **39** and **44**. The compounds were refined to include the Flack parameter that determines if the correct chirality or polarity of these structures has been selected and has a physical value range between  $0.0 \leq x \leq 1$ ; the correct handedness has been assigned when  $0.0 \leq x \leq 0.5$ , the structure represents the inverted model when  $0.5 \leq x \leq 1$  and the structure may be twinned by inversion if  $x = 0.5$ .<sup>11</sup>

These unusual space groups include  $P2_1/m$  (**12**),  $C_2/m$  (**30**) and  $Pnma$  (**18**); looking at the statistics in the CSD<sup>12</sup> space groups that contain pure mirrors and pure rotations are less common due to molecular packing constraint; however they are more common if the mirror is part of the molecules in the structure or all the atoms lie in the mirrors as is the case with these structures.

## Final Results

The results of the least squares refinement provide tables of atomic coordinates, bond lengths, angles, torsion angles and anisotropic displacement parameters for each atom with potential hydrogen bonds produced when the refinement is complete. These tables are produced for each structure presented in this thesis and can be found in the appendix.

## References:

- 1 W. Clegg, *Crystal Structure Determination*; Oxford Chemistry Primer, 60, Oxford University Press, **1998**.
- 2 W. Clegg, A. J. Blake, R. O. Gould, P. Main, *Crystal Structure Analysis Principles and Practice*; IUCr, Oxford University Press, **2001**.
- 3 C. Hammond, *The Basics of Crystallography and Diffraction*, 2<sup>nd</sup> Ed.; IUCr, Oxford University Press, **2001**.
- 4 J. P. Glusker, M. Lewis, M. Rossi, *Crystal Structure Analysis for Chemists and Biologists*; VCH Publishers, UK, **1994**.
- 5 J. P. Glusker, K. N. Trueblood, *Crystal Structure Analysis; A Primer*, Oxford University Press, **1985**.
- 6 C. Giacovazzo, H. L. Monaco, G. Artioli, D. Viterbo, G. Ferraris, G. Gilli, G. Zanotti, M. Catti, *Fundamentals of Crystallography*, 2<sup>nd</sup> Ed.; IUCr, Oxford University Press, **2002**.
- 7 G. H. Stout, L. H. Jensen, *X-ray Structure Determination, A Practical Guide*; J. Wiley & Sons, New York, **1989**.
- 8 G. M. Sheldrick, *Acta. Crystallogr. A*, **2008**, 64, 112.
- 9 Bruker AXS, Madison, USA, **1998**.
- 10 G. M. Sheldrick, *SHELXTL VERSION 5.1*, Bruker AXS, Madison, USA, **1998**.
- 11 H. D. Flack, G. Bernardinelli, *J. Appl. Cryst.* **2000**, 33, 1143
- 12 F. H. Allen, *Acta. Crystallogr.*, **2002**, B58, 380

## **Chapter Three - Research Objectives**

### **Overall Objectives**

The overall objectives of this research are to synthesize new metal-organic frameworks, using a multitude of techniques, to investigate the supramolecular chemistry of the frameworks formed and the influence of solvents and templating agents on structure formation and function.

### **Specific Objectives**

#### **Synthesis of Metal-organic Frameworks**

- The synthesis of new metal-organic frameworks using transition metals as nodes and benzenepolycarboxylate linkers.
- The use of solvo/hydrothermal techniques to produce a wide range of compounds with varying reaction conditions to investigate the influence of solvent on topology and pore formation.
- The synthesis of new ionic liquids with varying alkyl chain lengths and counter-ions, to test their suitability as solvent and templating media for MOF production with a investigation of interactions of ionic liquids and frameworks produced to determine the true effect of both counter-ion and alkyl chain length on topology formation and the potential size and accessibility of pores.
- The use of slow diffusion techniques to gain high quality crystals for X-ray diffraction studies, and to gain further understanding of the topologic effects of volatile bases, both on the coordination geometry of the metal nodes and the templating effects of the bases on pore formation.
- To derive reaction conditions that form reproducible structures that can be scaled up to batch formation for further analysis.

## **Characterisation of Metal-organic Frameworks**

- The formation of good quality single crystals for analysis by X-ray crystallography, and the subsequent structure determination and characterization.
- Characterisation of framework topologies and motifs with investigations into molecular driving forces such as SBU formation, solvent templating and deprotonation effects.
- The characterisation of bulk sample by elemental analysis and X-ray powder diffraction studies.
- Thermal stability properties investigated to determine potential porosity, desolvation temperatures and terminal temperature using thermogravimetric analysis.
- Crystal analysis using a 'Hot-stage' microscope to investigate phase changes of the structure and varying temperatures to determine crystal stability.
- Pore structure characterisation using intelligent gravimetric analysis to determine pore volume, size and accessibility.

## **Adsorption Studies**

- The investigation into potential applications and pore characteristics using intelligent gravimetric analysis.
- Nitrogen adsorption studies at 77K.
- Carbon dioxide adsorption studies at 195 and 273K to calculate pore volume and surface area.
- Isotherm analysis of adsorptions to determine further potential gas and vapour analysis such as hydrogen, methane and ethanol.

## **Chapter Four - Experimental**

### **Introduction**

Metal-organic frameworks have a tendency to form powders rather than single crystals due to their low solubility on formation. To fully characterise these materials single crystal X-ray diffraction must be used, therefore single crystals of the product must be obtained from the reaction mixture as the nature of the product prevents recrystallisation of the powders. Synthetic techniques have to be adapted to enable crystallization to occur, and the experimental conditions needed for the synthesis of MOFs presented in this thesis are outlined in the following pages.

In addition to single crystal X-ray crystallography other analytical techniques such as X-ray powder diffraction, elemental analysis, thermogravimetric analysis, hot-stage microscopic thermal analysis and intelligent gravimetric analysis were used to complete the characterisation of the materials produced.

### **Synthetic Techniques**

#### **Vapour Diffusion**

The use of vapour diffusion to obtain single crystals of coordination polymers is well established in the literature.<sup>1-3</sup> The slow diffusion of an anti-solvent through the vapour phase into the reaction mixture reduces the solubility of the product, encouraging crystallisation.

This technique has been widely adapted for experimental reactions with a solution of metal and ligand placed into a small sample vial. The speed of the reaction is controlled by covering this vial with Whatman Laboratory Sealing Film before placing the vial into a larger sample vial containing a volatile base; the reaction vessel is then fully sealed and left until crystallisation is complete (Figure 4.01).

This method is effective as the base diffuses slowly through the air into the reaction solution; this then gradually deprotonates the ligand, controlling the reaction speed. The base must be volatile but also have stabilising effects for crystallisation, thus

volatile amines such as trimethylamine, triethylamine, pyridine and ammonia were used through the course of this research. It was quickly found that trimethylamine and triethylamine were highly reactive and the exposure volume was dramatically reduced to encourage slow crystal formation; this produced results that highlight the templating nature of these bases and their influence on crystal production. Pyridine was also used extensively with the highly competitive ligand used to direct topology formation.

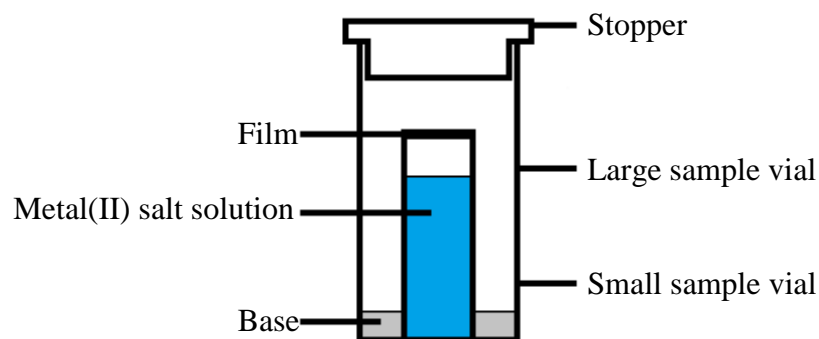


**Figure 4.01: Diagram of vapour diffusion apparatus.**

Typical reactions involved the benzenepolycarboxylic acid (0.05 mmol – 0.17 mmol) and the metal(II) salt (0.17 mmol – 0.33 mmol) dissolved in 10 ml of solvent (ethanol, methanol, DMF, water or dioxane). Each small vial had 0.5 ml of metal(II) salt solution and 0.5 ml of ligand solution added, this was then sealed and placed into the centre of a larger sample vial. Only 0.1 ml to 0.5 ml of amine was added to the vessel before the system was sealed and left to crystallise. Each metal(II) salt was combined with every ligand used in each solvent with each base; this formed an extensive array of crystallisations, approximately 360 for each concentration. The synthesis procedure for each product is listed with its characterisation in the corresponding results chapter.

#### **Direct Addition – Solvent Layering**

The ligand is dissolved in a solution containing a base for deprotonation, and then is added to the reaction vessel. The metal(II) salt is dissolved in a different solvent of lower density than the solvent used for the ligand. A buffer solution such as 'bank' solvent or NUJOL is placed on top of the ligand solution before the metal(II) solution is

pipetted slowly onto the top. This enables the reagents to slowly diffuse through the buffer solution to react together in the middle. This approach has added advantages other than slow addition; it also controls the templating solvent in which the framework is formed and can be used as a variant to alter topology of the resulting frameworks. (Figure 4.02)

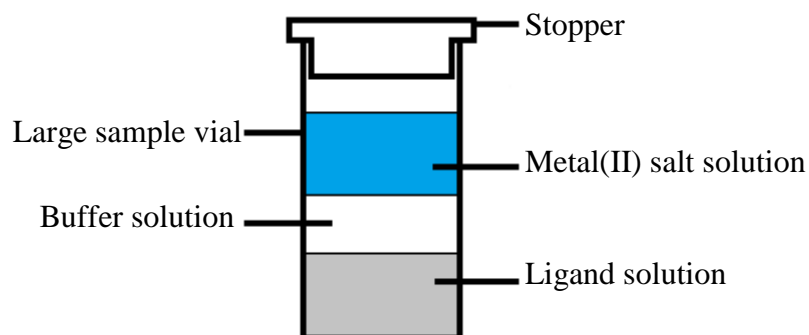


**Figure 4.02: Diagram of layering apparatus.**

### H-Cells

The H-cell apparatus separates solutions of reagents with a buffer solvent of lower density. This synthesis method works on the same principle as solvent layering; however, both the reagent solutions need to diffuse up into the buffer solution to react, slowing the reaction further in order to form better quality crystals. (Figure 4.03)

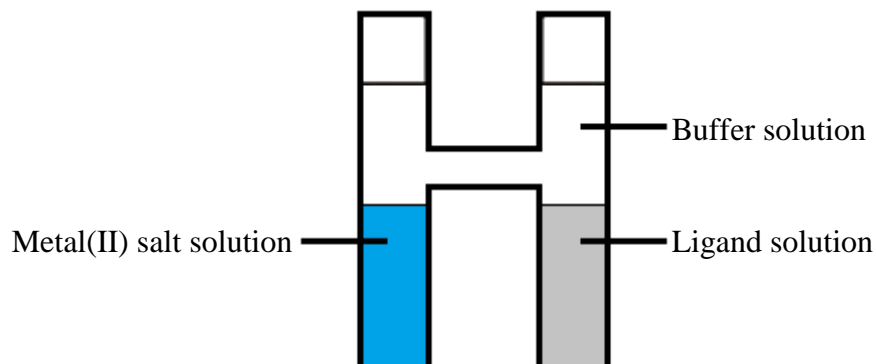


**Figure 4.03: Diagram of H-Cell apparatus**



The reaction conditions for H-cell synthesis usually involved metal(II) salts (0.33 mmol) dissolved in 10 ml DMF or ethanol and benzenepolycarboxylate ligand (0.17 mmol) dissolved in 10 ml DMF or ethanol. Only 3 ml of each solution was added to its corresponding side, the top of the H-cell was then filled with 5 ml of methanol or water and left to allow crystallisation to occur. Although this method produced some of the best quality crystals reported in this thesis along with several unique products, the time taken for crystal production averaged in the 4-6 month region.

### Hydrothermal/Solvothermal Synthesis

This method enables the direct addition of reagents and solvents in a one-chamber reaction vessel (Teflon-lined Parr bomb (figure 4.04)). The reaction vessel is then heated at a constant rate for a set amount of time before cooling at controlled rates. This process allows for unusual product formation due to the increased temperature and pressure of the system. The higher pressure helps keep solvents in liquid form at high temperatures, an organic solvent has a specific vapour pressure at a given temperature. Vapour pressure increases with increasing temperature, allowing pressure to control the range over which the solvent is in the liquid phase. This is a particularly useful technique for reagents with low solubility and aids in keeping the insoluble products from forming amorphous powders, allowing them to crystallise slowly in the cooling phase of the reaction.

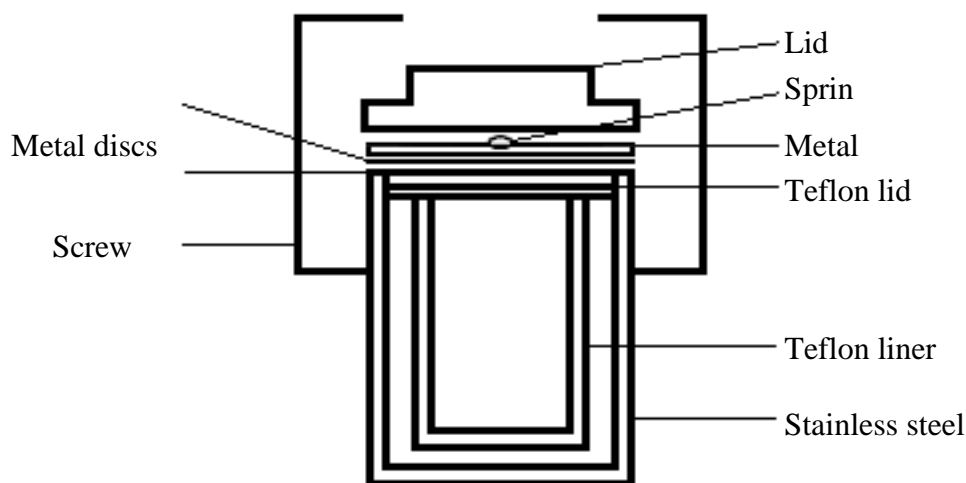


**Figure: 4.04: Schematic diagram of the Teflon-lined Parr bomb.**

Reactions carried out using solvothermal synthesis utilize the ability to use mixed solvent systems in order to have both solvent and anti-solvent present in the reaction vessel. The most common solvent system used in this thesis was DMF (4 ml), ethanol (4 ml) and water (3 ml). In this system the DMF is used both to dissolve the reagents and also to deprotonate the benzenepolycarboxylate ligands as it degrades into its amine form at high temperatures and pressures; the water by contrast is used as an anti-solvent for the crystallization process. Various alterations and ‘tuning’ occurred throughout the research to investigate the role of the solvent on structure and topology formation to gain further information on its role as a templating agent. Reactions mainly used metal(II) salts (0.33mmol – 1 mmol) and benzenepolycarboxylates (0.17 mmol – 0.5 mmol) added into the Teflon vessel before the solvents were added. This was then sealed and heated to 80 °C for 1 – 3 days before cooling at a rate of 0.1 °C per minute.

This has been by far the most successful method of framework production, allowing for fast accurate synthesis and tunable systems that shed light on the role of solvent in product formation. Crystals produced via hydro/solvothermal synthesis are usually good quality single crystals ranging in size from micro- to macro-crystalline.

### **Ionothermal Synthesis**

This synthesis method is a modification of solvothermal synthesis and uses the Teflon-lined Parr bomb (figure 4.04). Ionic liquids have unique solubility properties and have the ability to function as reaction media, templating agent or charge compensating groups. They also display high thermostability, ionic conductivity and negligible vapour pressure, making them ideal for use as a solvent in Teflon-lined bomb reactions.<sup>4-6</sup>

The most commonly used ionic liquid in the synthesis of MOFs is 1-ethyl-3-methylimidazolium bromide due to its thermodynamic and kinetic properties lying on the boundary between templated and template-free MOFs, allowing for the synthesis of a variety of possible MOFs<sup>4-6</sup> (Figure 4.05).

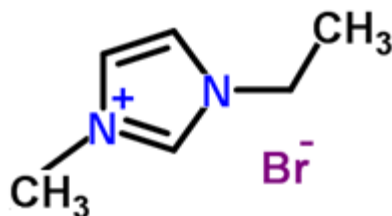


**Figure 4.05: Chemical structure of 1-Ethyl-3-methylimidazolium bromide.**

The systematic variation in the composition of the ionic liquids allows novel structures that previously were unobtainable to be realised using the ‘tailoring’ of the ionic liquid by varying alkyl chain length and counter-ion.<sup>4,7</sup> Ionic liquids were synthesized using the method outlined by Morris et al.<sup>8</sup>

#### **Synthesis of 1-Ethyl-3-methylimidazolium bromide (EMIBr)**

Under inert conditions degassed ethyl bromide (0.79 mol) was added to redistilled *N*-methylimidazole (0.68 mol) with constant stirring. This was refluxed at 40 °C for 3 hours and allowed to cool to room temperature. Ethyl acetate was added and the product precipitated of solution. The product was filtered and washed with ethyl acetate 4 times before drying under vacuum for 12 hours to give the desired product.

#### **Synthesis of 1-Propyl-3-methylimidazolium bromide (PrMIBr)**

Under inert conditions degassed propyl bromide (0.93 mol) was added to redistilled *N*-methylimidazole (0.68 mol) with constant stirring. This was refluxed at 50 °C for 3 hours and allowed to cool to room temperature, producing a colourless oil. The product was washed with ethyl acetate 4 times before drying under vacuum for 12 hours to give the desired product.

#### **Synthesis of 1-Butyl-3-methylimidazolium bromide (BMIBr)**

Under inert conditions degassed butyl bromide (0.21 mol) was added to redistilled *N*-methylimidazole (0.14 mol) with constant stirring. This was refluxed at 50 °C for 5 hours and allowed to cool to room temperature, producing a pale yellow oil. The product

was washed with ethyl acetate 4 times before drying under vacuum for 12 hours to give the desired product.

### **Synthesis of 1,1'-Dimethyl-3,3'-hexamethyldiimidazolium dibromide**

Under inert conditions degassed 1,6-dibromohexane (0.17 mol) was added to redistilled *N*-methylimidazole (0.38 mol) with constant stirring. This was refluxed at 25 °C for 5 hours, producing a yellow solid. The product was washed with ethyl acetate 6 times before drying under vacuum for 12 hours to give the desired slightly off-white product.

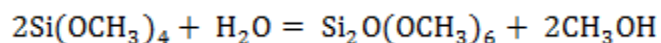
For the reactions using ionic liquids a mixture of metal(II) salt 1.5mmol, benzenepolycarboxylate 1mmol and alkylbromide (ionic liquid) 1g was placed into a Teflon-lined Parr bomb. This was heated in a programmable oven to 180°C for 7 days before cooling to room temperature at a rate of 0.1°C per minute.

These reactions are very time consuming and often lead to impure products with a mixture of different types of crystals; however, products were obtained that clearly show how the different ionic liquids template the pores and hence topology of the structure.

### **Silica Gels**

Silica gels are extremely useful for crystal growth; they provide an inert medium in which reagents slowly diffuse and form products. The reaction occurs in near-ambient conditions, reducing the equilibrium defects. As the crystal grows the gel gently yields, enabling the even crystal growth in all directions. This method can also be adapted to form a reaction medium whereby the gel is impregnated with a base so that as the ligand diffuses through it becomes activated; this limits both the base and activated ligand contact with the metal(II) solution.

The gels were synthesised using the hydrolysis of tetramethoxysilane to give silica gel and water.<sup>9-11</sup>



Tetramethoxysilane is insoluble in water, so heavy stirring was required to mix the two layers. The mixture was left to stand for 5 minutes before being added to the reaction vessel (figure 4.06 and 4.07) and left to solidify. The gelling process took about 24 hours and a further 12 hours was allowed to help the gel settle. The density of the gel is dependent on the volume of tetramethoxysilane used; a 5 -10 % volume mixture was recommended for the best possible crystal growth.<sup>9,12</sup>

This was confirmed by reacting copper(II) chloride hexahydrate (0.33 mmol) and pyromellitic acid (0.17 mmol) in 4 ml ethanol with 1ml pyridine through various density gels. (Table 4.01)

<b>Tetramethoxysilane %</b>	<b>Crystal growth</b>
2	No crystals, gel failed to solidify
4	Large number of small crystals
6	Few large crystals
8	Few large crystals
10	Only two large crystals
12	Crystals inter-growing
14	Small crystals in clusters
16	Few small crystals
18	Gel dried out, precipitate formed
20	Gel dried out, precipitate formed

**Table 4.01: Crystal growth with varying gel density.**

Two types of gel apparatus were used in this research, the U-Tube (figure 4.06) and sample tube (figure 4.07). The U-tube design allows both metal(II) salt and polycarboxylate to be placed in the same side, with a deprotonating agent in the other. Both solutions need to diffuse through the gel in order for the ligand to be activated; this was observed at the point FP where first precipitation was observed (figure 4.06). However, the majority of the crystals formed in the left well (X) where they had sufficient space to grow, producing good quality single crystals suitable for X-ray diffraction analysis.

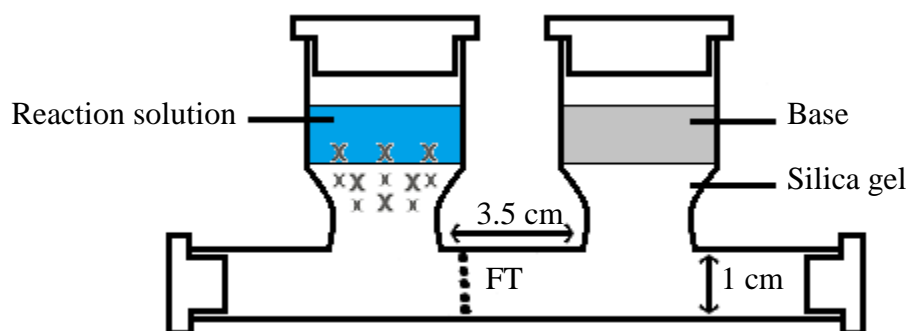


**Figure 4.06: Diagram of U-Tube apparatus.**

The sample tube design (figure 4.07) uses a 10 % gel and can be impregnated with both base and acid. A layer of metal(II) salt solution (0.33 mmol) in 5 ml methanol is layered on top and slowly diffuses down. The advantage of this method is that crystals tend to form on the surface, making them easily accessible.

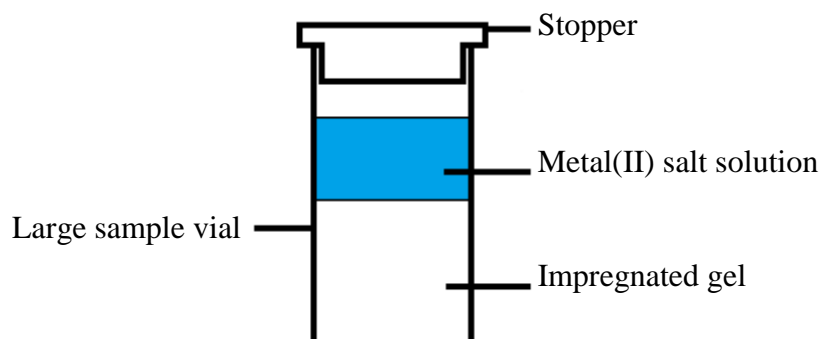


**Figure 4.07: Diagram of gel sample tube apparatus.**

## **Analytical Techniques**

### **Single-crystal X-ray Crystallography**

Single-crystal X-ray crystallography was used as the primary analytical method for the research in this thesis. For a brief summary of the theory and methodology of single-crystal crystallography see Chapter 2: The Theory of Single Crystal X-ray Crystallography.

The diffractometers used to collect the data to solve the structures presented in this thesis were the Nonius KappaCCD and the Oxford Diffraction Gemini (figure 4.08). Crystalline samples that proved to be too small or poorly diffracting for laboratory-based diffractometers were analysed at a synchrotron. Two synchrotrons were used to collect data for structures for this thesis: the Advanced Light Source (beamline 11.13.1) at Berkley, California, and the Diamond Light Source (beamline I19), Oxfordshire.

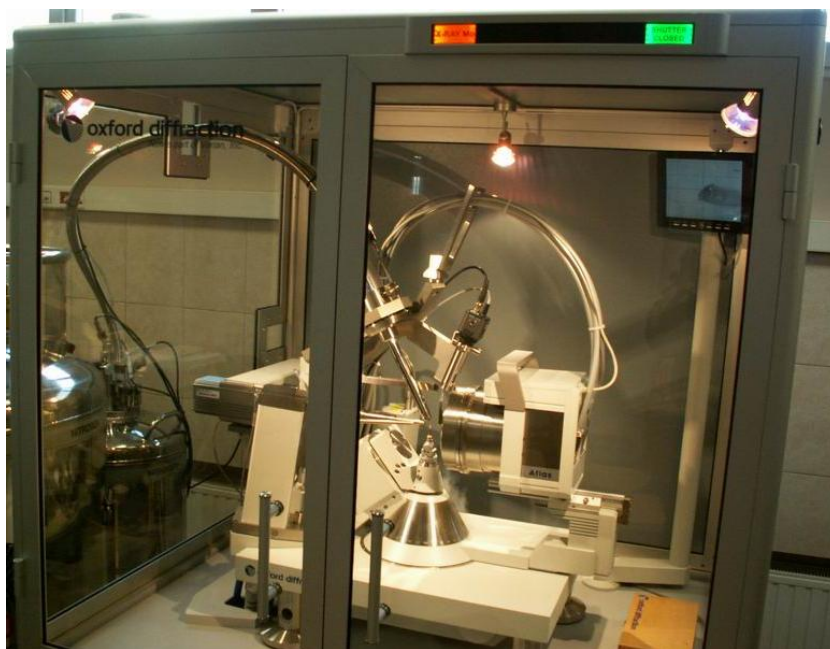


**Figure 4.08: Oxford Diffraction Gemini X-ray diffractometer.**

## Thermogravimetric Analysis

Thermogravimetric analysis monitors the mass of the sample as temperature is increased. This produces a thermal profile of the compound indicating the temperature of desolvation, temperatures of structural changes, and the terminal temperature of the structure.

A Stanton Redcroft STA 780 series thermogravimetric analyser (figure 4.09) was used to carry out the experiments. The balance was tiered in a flow of nitrogen ( $50 \text{ cm}^3 \text{ min}^{-1}$ ) before up to 10 mg of sample was added to the crucible and the initial mass recorded at ambient temperature under the constant flow of nitrogen. The sample was then heated at a rate of  $2 \text{ }^\circ\text{C}$  per minute and the mass change recorded to provide a temperature profile. Most samples were heated to  $400 - 500 \text{ }^\circ\text{C}$  to ensure the full collapse of the framework, before cooling back down to room temperature.



**Figure 4.09: Stanton Redcroft STA 780 series thermogravimetric analyser.**



### **Hot-stage Analysis**

Hot-stage analysis visually monitors crystal stability as temperature is increased or decreased by taking regular photographs of the crystals in correlation to the thermoplot designed. This enables the crystallinity to be monitored as desolvation occurs whilst also confirming if a phase change is observed. Experiments are usually designed to follow the thermal profile obtained from the thermogravimetric analysis so a direct comparison can be made. Reactions using the Linksam hot-stage are controlled by Linksys 32 temperature control, with image control from the Q-capture Pro program that links in with a Q IMAGING QICAM FAST 1394 camera placed above the microscope.

### **X-ray Powder Diffraction**

X-ray powder diffraction is used to determine the purity of the bulk sample of the framework material produced; it also can be used for micro-crystalline material to obtain a unit cell. The powder diffraction experiments in this thesis were carried out by Dr Maggie White of Chemical Engineering and Advanced Materials, Newcastle University.

The instrument used for the powder diffraction experiments was a PANalytical X'Pert Pro Diffractometer fitted with an X'Celerator and secondary monochromator. This instrument is an ultra-fast X-ray detector that uses real-time multiple strip technology. The data recorded for the materials presented in this thesis were acquired over a  $2\theta$  range of 5 to 120 ° in the continuous mode using the X'Celerator detector.

### **Elemental Analysis**

Elemental analysis determines the percentage amount of carbon, nitrogen and hydrogen present in the sample. This is a good indication of the purity of the sample and the solvent content of the framework, allowing confirmation of desolvated structures. The elemental analysis experiments were carried out by Richard Baron of Newcastle University Analytical Services using a Carlo Erba 1108 Elemental Analyser controlled using CE Eager 200 software.

## Gas Adsorption

Gas adsorption was carried out on only one MOF synthesised in this project due to time constraints on the Intelligent Gravimetric Analyser. Adsorption experiments of nitrogen at 77 K and carbon dioxide at 195 K and 273 K were carried out using an Intelligent Gravimetric Analyser (IGA) supplied by Hiden Analytical Ltd. (figure 4.10), designed for both static and flowing, gas and vapour systems. These systems allow the determination of isotherms and corresponding kinetics of adsorption and desorption for set pressure steps.<sup>13</sup>



**Figure 4.10: Intelligent Gravimetric Analyser.**

The microbalance fitted has a long-term stability of  $\pm 1 \mu\text{g}$  with a weighing resolution of  $0.2 \mu\text{g}$ . The sample is degassed at  $< 10^{-6} \text{ Pa}$  at a temperature determined by thermogravimetric analysis to be suitable for desolvation; this is carried out until the sample reaches a constant weight.

To prevent effects from the external environment that would result in vapour condensation both the pressure and balance control system were fully thermostated to 0.1 K. Only ‘dried’ gases were used in the adsorption studies due to the reactivity of the samples to water vapour upon desolvation.

The IGA instruments control the pressure with two pressure transducers with accuracies of 0.02 % over 0 – 0.2 and 0 – 10 KPa; the pressure was maintained at a set point using an active computer control of the inlet and outlet valves for the duration of the experiment. Gas adsorption studies were carried out by Dr Jon Bell and Jayne Knotts of Northern Carbon Laboratories, Chemical Engineering and Advanced Materials, University of Newcastle.

## References:

- 1 G. R. Desiraju, C. V. Krishnamohan, *The Crystal as a Supramolecular Entity*; John Wiley & Sons, **1996**.
- 2 W. Clegg, A. J. Blake, R. O. Gould, P. Main, *Crystal Structure Analysis, Principles and Practice*; IUCr, Oxford University Press, **2001**.
- 3 J. P. Glusker, M. Lewis, M. Rossi, *Crystal Structure Analysis for Chemists and Biologists*; VCH Publishers, UK, **1994**.
- 4 L. Xu, E. Y. Choi, Y. U. Kwon, *Inorg. Chem.*, **2007**, 111, 18794.
- 5 L. Xu, S. Yan, E. Y. Choi, J. Y. Lee, Y. U. Kwon, *Chem. Commun.*, **2009**, 3431.
- 6 K. E. Gutowski, G. A. Broker, H. D. Willaver, J. G. Huddleston, R. P. Swatloski, J. D. Holbrey, R. D. Rogers, *J. Am. Chem. Soc.*, **2003**, 125, 6632.
- 7 E. R. Parnham, R. E. Morris, *Acc. Chem. Res.*, **2007**, 40, 1005.
- 8 E. R. Parnham, R. E. Morris, *Chem. Mater.*, **2006**, 18, 4882.
- 9 H. Arend, J. J. Conelly, *J. Cryst. Growth*, **1982**, 56, 642.
- 10 H. K. Henisch, *Crystals in Gels and Liesegang Rings*; Cambridge University Press, **1988**.
- 11 M. C. Robert, F. Lefaucheux, *J. Cryst. Growth*, **1988**, 90, 258.
- 12 J. Dennis, H. K. Henisch, P. Cherian, *J. Electrochem. Soc.*, **1965**, 112, 1240.
- 13 M. J. Benham, D. K. Ross, *Z. Phys. Neue Folge*, **1989**, 163, 25.

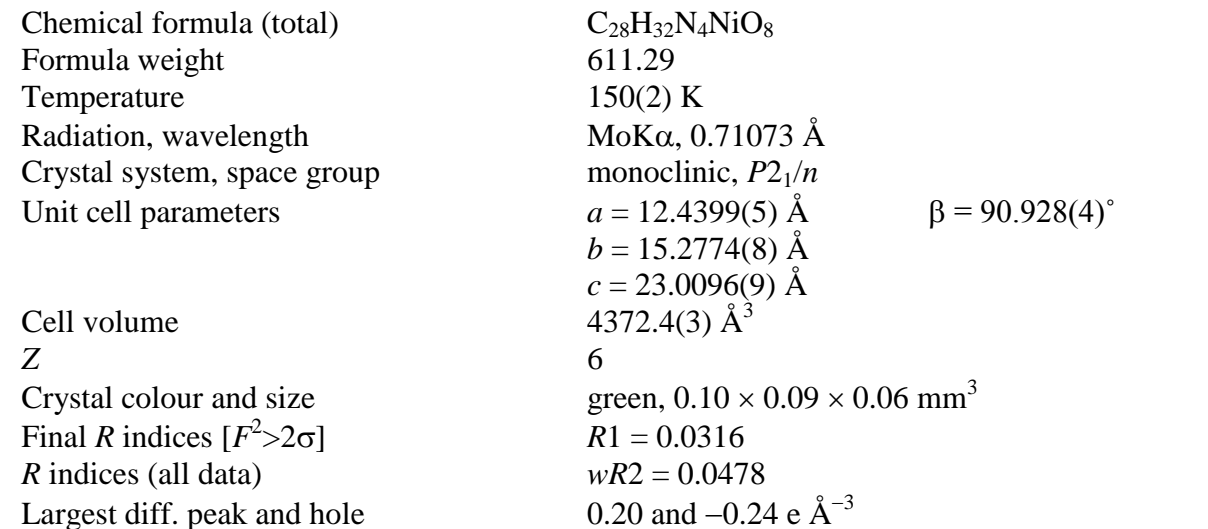
## **Chapter Five – Crystal Structures of Transition Metal and 1,4-benzenedicarboxylic acid Compounds**

### **Introduction**

The following chapter presents compounds produced using the transition metals; cobalt, zinc, nickel, copper and cadmium. These metals were reacted with 1,4-benzenedicarboxylic acid in a range of reaction conditions to investigate the templating effects of different solvents and additional ligands such as 4,4'-bipyridine on topology formation.

The nine compounds presented in this chapter include one dimensional chains (compounds 1 and 2), two dimensional sheets (compounds 3-6) including a porous 4,4' net topology in compound 5, and three dimensional coordinated frameworks (compounds 7-9). Compound 7 presented in this chapter is a dual linker interpenetrated framework that forms 4,4' nets utilizing both the 1,4-benzenedicarboxylate ligand and a 4,4'-bipyridine ligand.

These compounds were analysed further with elemental analysis, powder X-ray diffraction and thermogravimetric analysis, where possible, to determine the purity of the bulk material and the thermostability properties of the compounds.



0.5 mL of a solution of  $\text{Ni}(\text{NO}_3)_2 \cdot 6\text{H}_2\text{O}$  (0.06 g, 0.33 mmol) in dimethylformamide (DMF) (10 mL) and 0.5 mL of a solution of 1,4-benzenedicarboxylic acid (0.028 g, 0.17 mmol) in DMF (10 mL) were placed into a small sample vial. This was covered with Whatman Laboratory Sealing Film and placed inside a larger sample vial. In the larger

sample vial pyridine (0.05 mL, 0.22 mmol) was added before it was covered and left until crystallisation was complete. After two weeks, green block crystals formed.

### Structure Determination

The data were collected at 150 K using molybdenum radiation on an Oxford Diffraction Gemini A Ultra diffractometer. The structure was solved by direct methods. The semi-empirical absorption corrections were applied based on symmetry-equivalent and repeated data. The refinement gave a  $wR2$  of 0.0478 for all 7717 independent reflections and a conventional  $R1$  of 0.0316 for 3352 reflections with  $F^2 > 2\sigma$ . The residual electron density maximum and minimum were 0.20 and  $-0.24 \text{ e\AA}^{-3}$  respectively.

The hydrogen atoms were placed in geometrically calculated positions with  $U$  constrained to  $1.2 U_{eq}(C)$  for aromatic hydrogen atoms and  $U$  constrained to  $1.5 U_{eq}(O)$  for the hydroxyl hydrogen atoms. These were then restrained geometrically using SADI commands. The full data of compound 1 can be found in Appendix 1.

### Structure Analysis

The asymmetric unit of compound 1 (figure 5.01) shows a complete 1,4-benzenedicarboxylate ligand joining two nickel atoms Ni(1) and Ni(2) the latter being on an inversion centre. An additional half 1,4-benzenedicarboxylate ligand is bound to Ni(1) with its symmetry equivalent generated around an inversion centre in the middle of the aromatic ring to complete the ligand. The nickel cations in compound 1 are both six coordinate with octahedral geometries. The Ni(1) atom shows regular octahedral coordination geometry (figure 5.02A) with standard bond angles (table 5.01). Ni(2) also forms a near perfect octahedral geometry (figure 5.02B) through inversion symmetry with angles of O(3)-Ni(2)-N(3)  $90.45(8)^\circ$ , O(3)-Ni(2)-O(11)  $92.04(9)^\circ$  and O(3)-Ni(2)-O(3A)  $180^\circ$ . The two nickel atoms form a secondary building unit (SBU) (figure 5.03) with two 1,4-benzenedicarboxylate ligands coordinated to the nickel atom through one carboxylate oxygen atom in coplanar positions occupying two of the six available coordination sites. The remaining four positions are occupied by trans pyridine ligands and trans water ligands. The asymmetric unit is completed with three additional pyridine

and water molecules that are uncoordinated and involved in the hydrogen bonding network of compound 1. This coordination geometry allows the singly bound carboxylate groups to form one dimensional chains extending down the *a*-axis (figure 5.04). Although the carboxylate group is only singly coordinated it is however fully deprotonated and delocalised with comparable bond lengths of C(7)-O(1) 1.263(4) Å and C(7)-O(2) 1.257(4) Å along with C(8)-O(3) 1.258(4) Å and C(8)-O(4) 1.257(4) Å showing no evidence of a double and single oxygen bond combination in the carboxylate groups. The bond lengths between Ni(1) and the carboxylate oxygens of the ligand (Ni(1)-O(1) 2.056(1) Å, Ni(1)-O(5) 2.051(2) Å and Ni(2)-O(3) 2.065(2) Å) are comparable to similar fully deprotonated structures.<sup>1-4</sup>

The three uncoordinated carboxylate oxygens are also involved as acceptors in hydrogen bonding with uncoordinated water molecules, such as O(12)-H(12A)···O(2) 2.754(3) Å, this water (O(12)) also forms a hydrogen bond to an adjacent chain as a hydrogen bond acceptor via a coordinated water ligand O(11)-H(11A)···O(12) 2.693(3) Å. This coupled with hydrogen bonds from O(4) and O(6) to uncoordinated water molecules (table 5.02) forms hydrogen bonded two dimensional sheets along the *c*-axis and down the *a*-axis. The layers pack together with ring stacking interactions between the overlapping aromatic rings of the pyridine ligands with an interplanar distance of 3.222 Å. Figure 5.05 shows that the sheets are packed in an offset position with the aromatic rings of the 1,4-benzenedicarboxylate almost parallel but tilted slightly out of plane in opposite directions, this is due to the steric bulk of the coordinated pyridine ligands and to the glide plane between each layer producing the offset between the benzene rings and the two-fold screw axis in between each chain tilting the aromatic rings of the 1,4-benzenedicarboxylate in opposite directions.

The pyridine was used in this reaction to deprotonate the 1,4-benzenedicarboxylate ligands and to act as a templating agent using the aromatic-aromatic interactions of the pyridine rings. In both instances the reaction was successful, producing a fully deprotonated structure with pyridine, both coordinated and uncoordinated between the layers, directing the packing of the structure. Due to these factors further investigations were carried out using trimethylamine as an alternative base to probe the effect on topology formation leading to the synthesis of compound 2.



**Table 5.01: Selected Bond Lengths [Å] and Angles [°] for Compound 1**

Ni(1)–O(1)	2.056(2)	Ni(1)–O(5)	2.051(2)
Ni(1)–N(1)	2.101(2)	Ni(1)–N(2)	2.109(2)
Ni(1)–O(9)	2.056(3)	Ni(1)–O(10)	2.059(2)
Ni(2)–O(3)	2.065(2)	Ni(2)–O(3A)	2.065(2)
Ni(2)–N(3)	2.094(2)	Ni(2)–N(3A)	2.094(2)
Ni(2)–O(11)	2.050(2)	Ni(2)–O(11A)	2.050(2)
C(7)–O(1)	1.263(4)	C(7)–O(2)	1.257(4)
C(8)–O(3)	1.258(4)	C(8)–O(4)	1.257(4)
C(15)–O(5)	1.249(4)	C(15)–O(6)	1.259(4)
O(1)–Ni(1)–O(5)	179.62(13)	O(1)–Ni(1)–N(1)	91.07(9 )
O(1)–Ni(1)–N(2)	89.74(9 )	O(1)–Ni(1)–O(9)	90.85(10)
O(1)–Ni(1)–O(10)	87.92(10)	O(5)–Ni(1)–N(1)	89.00(9 )
O(5)–Ni(1)–N(2)	90.18(9 )	O(5)–Ni(1)–O(9)	88.77(10)
O(5)–Ni(1)–O(10)	92.46(10)	N(1)–Ni(1)–N(2)	179.05(13)
N(1)–Ni(1)–O(9)	92.88(10)	N(1)–Ni(1)–O(10)	87.56(11)
N(2)–Ni(1)–O(9)	86.61(10)	N(2)–Ni(1)–O(10)	92.97(11)
O(9)–Ni(1)–O(10)	178.70(10)	O(3)–Ni(2)–N(3)	90.45(8 )
O(3)–Ni(2)–O(11)	92.04(9 )	N(3)–Ni(2)–N(3A)	180.0
N(3)–Ni(2)–O(11)	92.54(10)		

Symmetry operations for equivalent atoms

A  $-x, -y+1, -z+1$ **Table 5.02: Selected Hydrogen bond Lengths [Å] and angles [°] for Compound 1**

D–H...A	d(D–H)	d(H...A)	d(D...A)	(DHA)
O(9)–H(9A)...O(13)	0.813(13)	1.869(16)	2.660(3)	164(3)
O(9)–H(9B)...O(2)	0.817(13)	1.869(15)	2.645(3)	158(3)
O(10)–H(10A)...O(14)	0.810(14)	1.869(14)	2.673(3)	171(3)
O(10)–H(10B)...O(6)	0.818(13)	1.850(15)	2.639(3)	162(3)
O(11)–H(11A)...O(12)	0.820(14)	1.883(15)	2.693(3)	169(3)
O(11)–H(11B)...O(4)	0.810(14)	1.876(16)	2.643(3)	157(3)
O(12)–H(12A)...O(2C)	0.830(14)	1.928(14)	2.754(3)	174(3)
O(12)–H(12B)...N(5)	0.829(14)	2.055(15)	2.882(4)	175(3)
O(13)–H(13A)...O(4D)	0.819(14)	1.930(14)	2.735(4)	167(3)
O(13)–H(13B)...N(4)	0.801(14)	2.002(15)	2.796(4)	172(3)
O(14)–H(14A)...O(6E)	0.826(14)	1.912(14)	2.732(4)	172(3)
O(14)–H(14B)...N(6)	0.812(14)	2.004(15)	2.808(4)	171(3)

Symmetry operations for equivalent atoms

C  $x-1, y, z$  D  $x+1, y, z$  E  $-x+1, -y+1, -z$

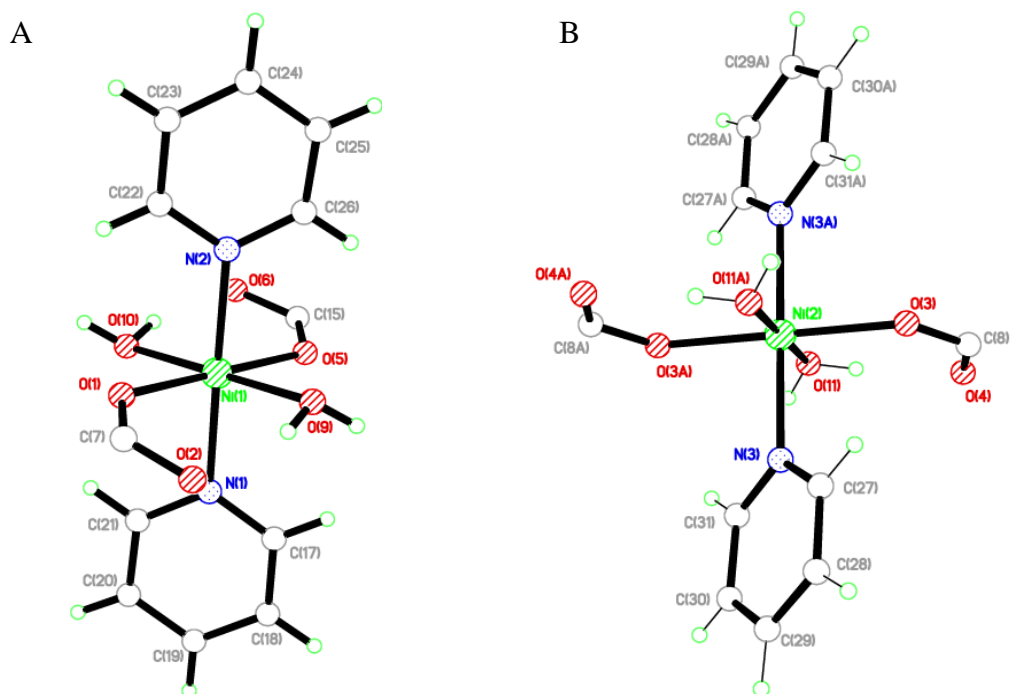


**Figure 5.02: Octahedral coordination environment of A) Ni(1) and B) Ni(2) in compound 1**

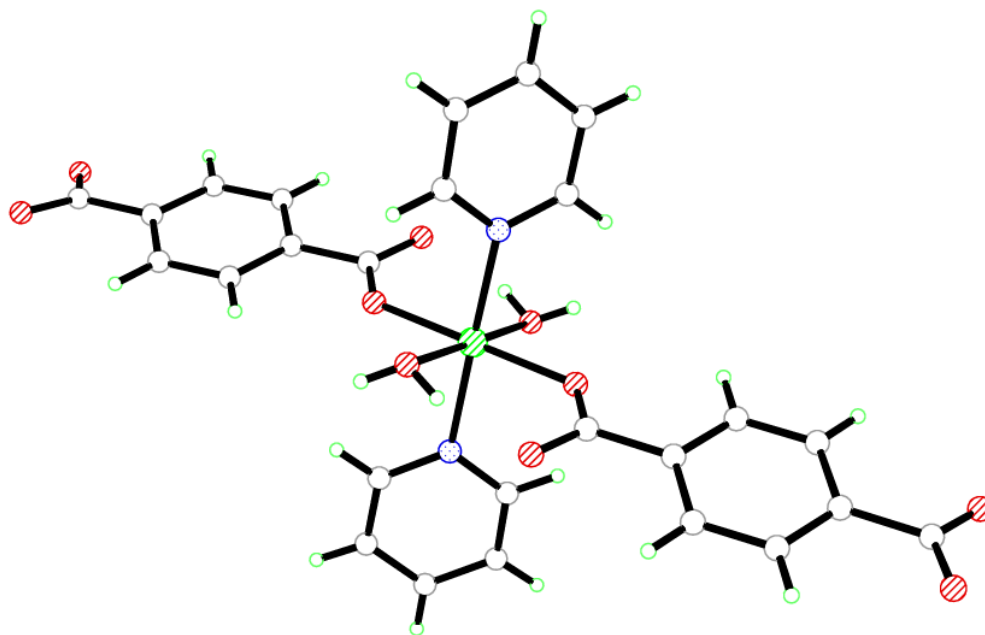


**Figure 5.03: Secondary building unit of Ni(1) in compound 1 (uncoordinated molecules omitted for clarity)**

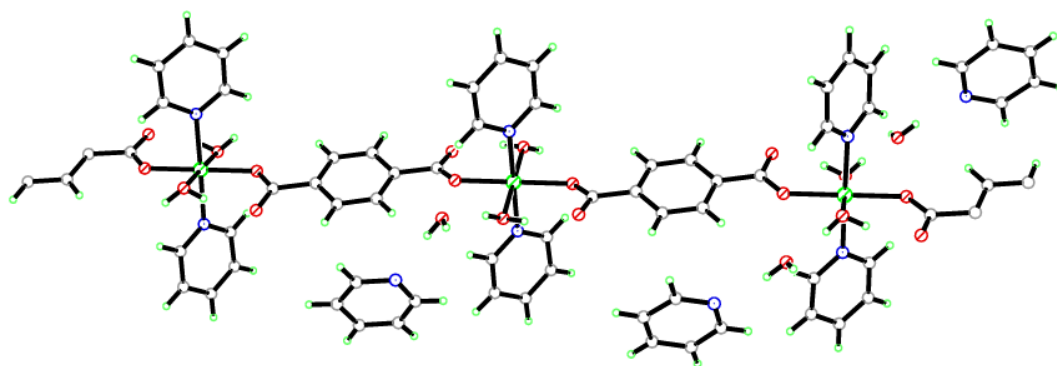


Figure 5.04: One dimensional coordinated chains of compound 1

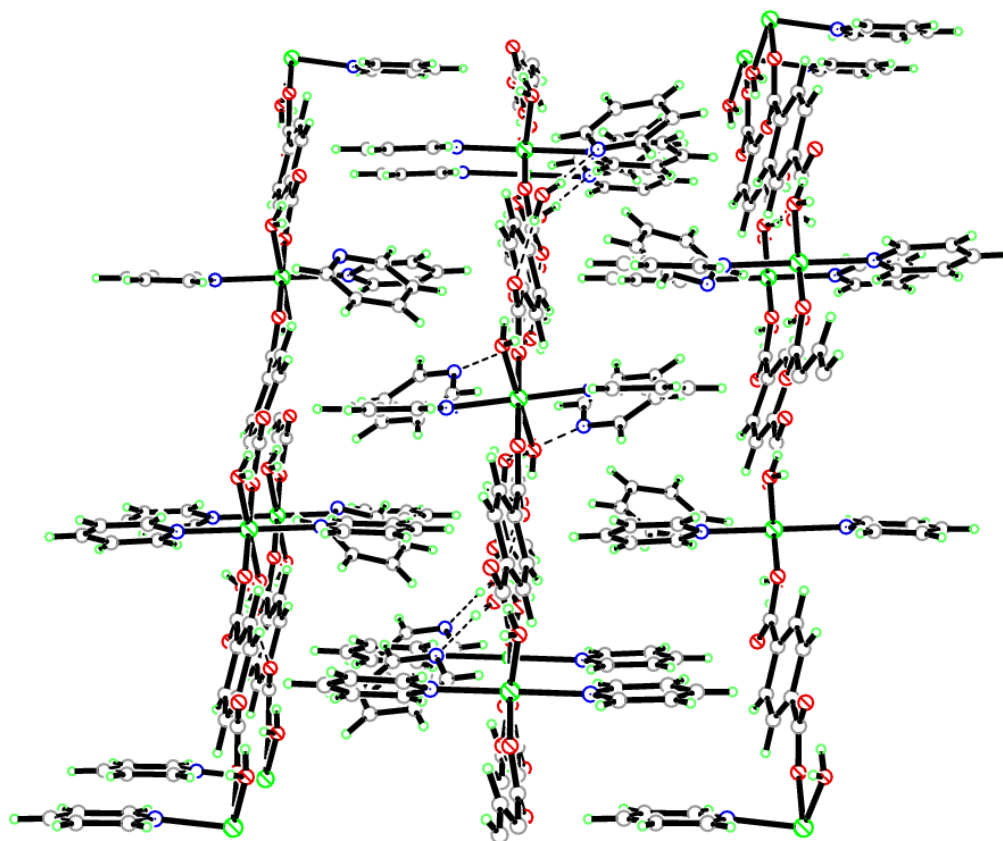
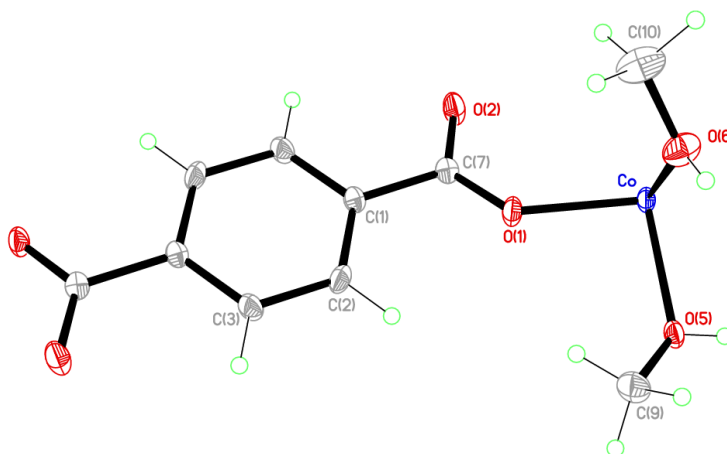


Figure 5.05: Three dimensional packing motif of compound 1 viewed down the *a*-axis

**Compound 2:**  $[\text{Co}(\text{C}_8\text{H}_4\text{O}_4)(\text{CH}_4\text{O})_4]$ 

Chemical formula (total)	$\text{C}_{12}\text{H}_{20}\text{CoO}_8$	
Formula weight	351.21	
Temperature	150(2) K	
Radiation, wavelength	MoK $\alpha$ , 0.71073 Å	
Crystal system, space group	triclinic, $P\bar{1}$	
Unit cell parameters	$a = 6.7623(4)$ Å	$\alpha = 95.953(7)^\circ$
	$b = 6.8567(6)$ Å	$\beta = 95.640(5)^\circ$
	$c = 8.2412(6)$ Å	$\gamma = 95.023(6)^\circ$
Cell volume	$376.37(5)$ Å <sup>3</sup>	
Z	1	
Crystal colour and size	pink, $0.20 \times 0.13 \times 0.10$ mm <sup>3</sup>	
Final $R$ indices [ $F^2 > 2\sigma$ ]	$R1 = 0.0306$	
$R$ indices (all data)	$wR2 = 0.0603$	
Largest diff. peak and hole	0.28 and $-0.28$ e Å <sup>-3</sup>	

**Figure 5.06: Asymmetric Unit of Compound 2 all unique atoms labelled, additional atoms added to complete ligands**

**Synthesis**

0.5 mL of a solution of  $\text{Co}(\text{NO}_3)_2 \cdot 6\text{H}_2\text{O}$  (0.09 g, 0.33 mmol) in methanol (10 mL) and 0.5 mL of a solution of 1,4-benzenedicarboxylic acid (0.028 g, 0.17 mmol) in methanol (10 mL) were placed into a small sample vial. This was covered with Whatman Laboratory Sealing Film and placed inside a larger sample vial. In the larger sample vial trimethylamine (0.05 mL, 0.22 mmol) was added before it was covered and left until crystallisation was complete. After four weeks, pink block crystals formed.

## Structure Determination

The data were collected at 150 K using molybdenum radiation on an Oxford Diffraction Gemini A Ultra diffractometer. The structure was solved by direct methods. The semi-empirical absorption corrections were applied based on symmetry-equivalent and repeated data. The refinement gave a  $wR2$  of 0.0603 for all 1406 independent reflections and a conventional  $R1$  of 0.0306 for 1143 reflections with  $F^2 > 2\sigma$ . The residual electron density maximum and minimum were 0.28 and -0.28 eÅ<sup>-3</sup> respectively.

The hydrogen atoms were placed in geometrically calculated positions with  $U$  constrained to 1.2  $U_{eq}(C)$  for aromatic hydrogen atoms and  $U$  constrained to 1.5  $U_{eq}(C)$  for the methyl hydrogen atoms. The full data of compound 2 can be found in Appendix 1.

## Structure Analysis

The asymmetric unit of compound 2 (figure 5.06) shows half a 1,4-benzenedicarboxylate ligand completed by inversion symmetry through the centre of the aromatic ring, coordinated to a cobalt cation placed on an inversion centre. The cobalt cation in compound 2 is six-coordinate octahedral (figure 5.07) with bond angles of O(1)-Co-O(5) 91.24(6)°, O(1)-Co-O(6) 88.89(6)° and O(5)-Co-O(6) 90.03(6)°. The six coordinate geometry is completed through inversion symmetry forming linear bond angles to the symmetry-equivalent parts, O(1)-Co-O(1A) 180°. Two symmetry-equivalent 1,4-benzenedicarboxylate ligands are coordinated to the cobalt cation through one carboxylate oxygen atom in coplanar positions occupying two of the available coordination sites. The remaining four coordination sites are occupied by two DMF ligands and their trans-symmetry equivalents, O(5)-Co-O(5A) 180° and O(6)-Co-O(6A) 180° that are coordinated in the plane perpendicular to that containing the 1,4-benzenedicarboxylate ligands completing the secondary building unit. (figure 5.08)

The singly coordinated 1,4-benzenedicarboxylate ligands extend the structure down the cell body diagonal to form one dimensional chains. The carboxylate group of the 1,4-benzenedicarboxylate forms a coordination bond with the cobalt cation through the O(1) atom with a bond length of Co-O(1) 2.063(14) Å, the uncoordinated O(2) atom has a comparable bond length of C(7)-O(2) 1.259(3) Å to the C(7)-O(1) 1.258(3) Å

bond, showing no significant difference. This indicates that the carboxylate group is fully deprotonated and delocalised leaving the O(2) atom to be available for hydrogen bonding as a hydrogen acceptor.

Hydrogen bonding between the uncoordinated O(2) atom geometrically constrains the methanol ligands into one orientation, as the intra-molecular hydrogen bond O(5)-H(5)···O(2) 2.609(2) Å forces the methanol to be bound with the O-H pointing towards the carboxylate O(2) atom at a D-H···A angle of 160(3)°. The O(2) atom acts as a bifurcated acceptor forming an additional hydrogen bond with an adjacent chain O(6A)-H(6AA)···O(2) 2.682(2) Å, this not only constrains the geometry of the remaining methanol but also directs the packing motif of the chains into three dimensions (figure 5.09). This results in the staggering of the chains with respect to each other to allow the carboxylate group of chain 1 to be in proximity to the methanol groups of chain 2 which is related by inversion symmetry in between the respective cobalt atoms along the axis.

The trimethylamine was used in this reaction as a deprotonating and templating agent. This structure indicates that, although full deprotonation and delocalisation of the carboxylate group has occurred, the trimethylamine has not coordinated to the cobalt cation or become hydrogen bonded into this structure with compound 2 forming the highly efficient packing motif of the interlocking coordinated methanol ligands. This is most likely due to the inefficient packing through steric bulk and the tendency towards disorder that trimethylamine shows in compounds.<sup>5,6</sup>

**Table 5.03: Selected Bond Lengths [ $\text{\AA}$ ] and Angles [ $^\circ$ ] for Compound 2**

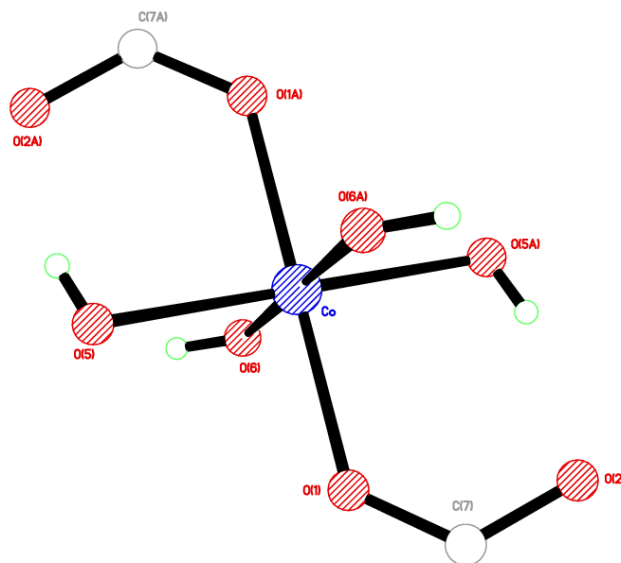
Co–O(1)	2.0630(14)	Co–O(5)	2.1057(17)
Co–O(6)	2.0898(15)	C(7)–O(1)	1.258(3)
C(7)–O(2)	1.259(3)		
O(1)–Co–O(5)	91.24(6)	O(1)–Co–O(5A)	88.76(6)
O(1)–Co–O(6)	88.89(6)	O(1)–Co–O(6A)	91.11(6)
O(5)–Co–O(6)	90.03(6)	O(5)–Co–O(6A)	89.97(6)

Symmetry operations for equivalent atoms

A  $-x+1, -y+1, -z+1$ **Table 5.04: Selected Hydrogen bond Lengths [ $\text{\AA}$ ] and angles [ $^\circ$ ] for Compound 2**

D–H...A	d(D–H)	d(H...A)	d(D...A)	(DHA)
O(5)–H(5)...O(2A)	0.73(3)	1.91(3)	2.609(2)	160(3)
O(6)–H(6)...O(2C)	0.78(3)	1.92(3)	2.682(2)	168(3)

Symmetry operations for equivalent atoms

A  $-x+1, -y+1, -z+1$     C  $x-1, y, z$ **Figure 5.07: Octahedral coordination environment of the Co cation in compound 2**

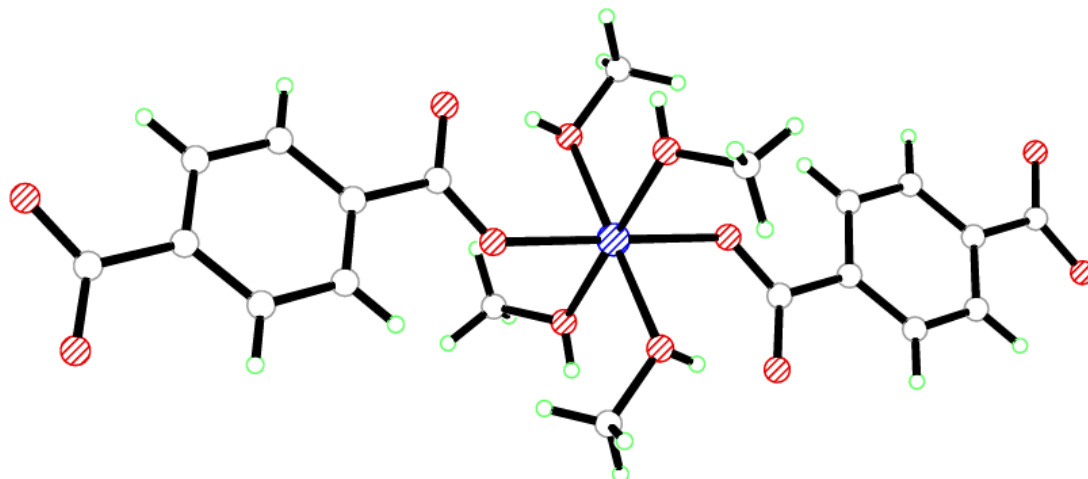


Figure 5.08: Secondary building unit in compound 2

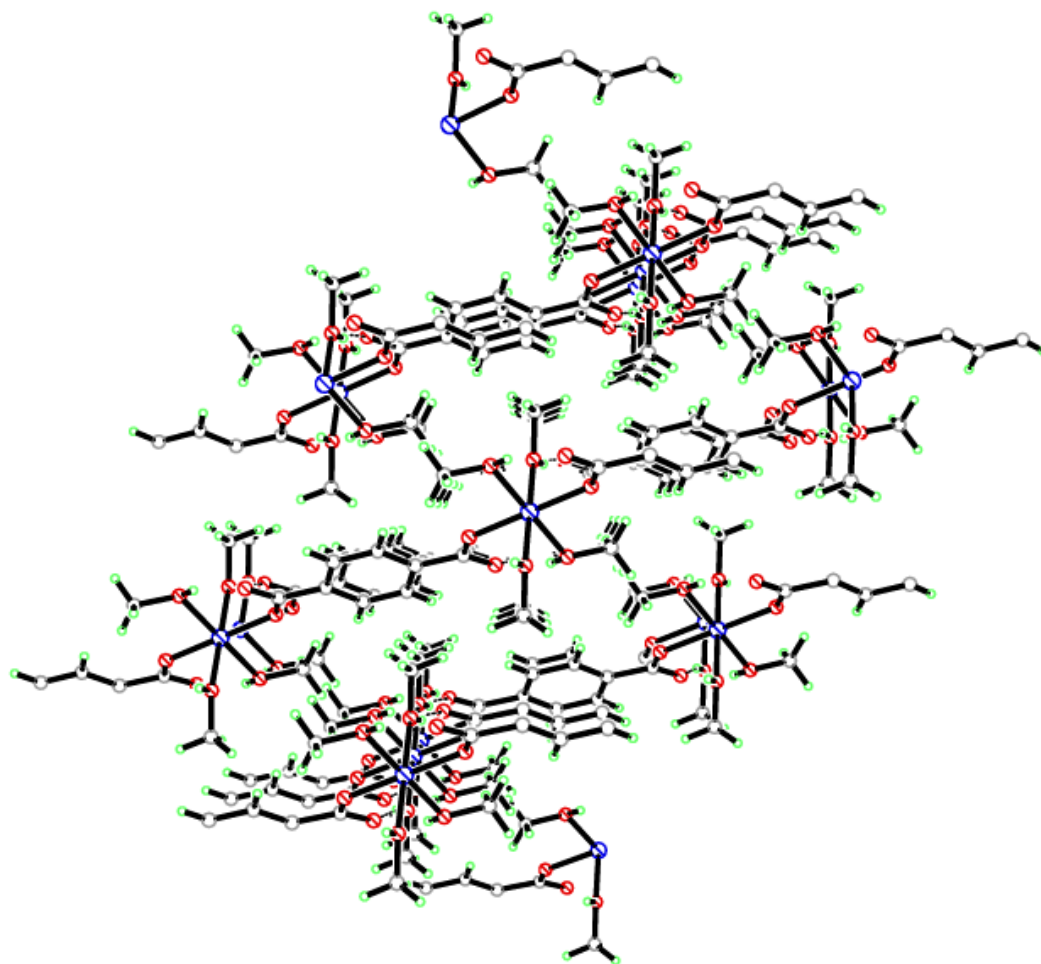
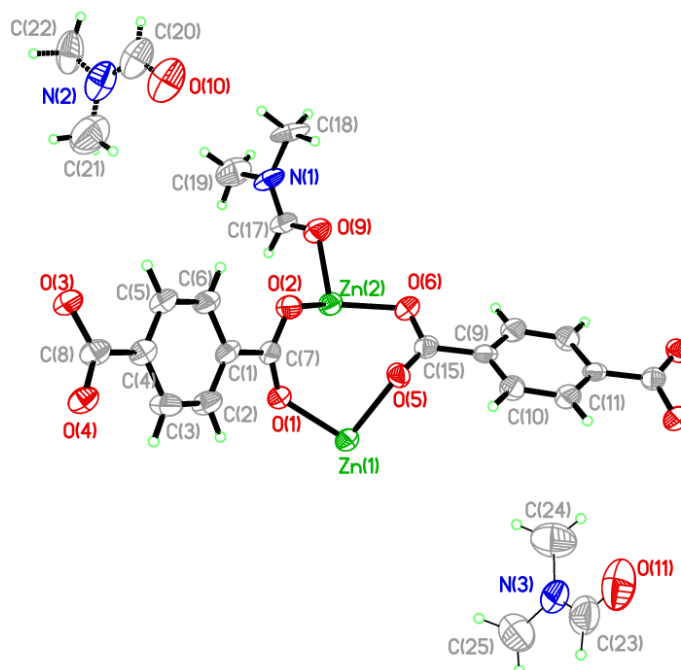


Figure 5.09: Three dimensional packing motif of compound 2 viewed down the *a*-axis



**Compound 3:**  $[\text{Zn}(\text{C}_8\text{H}_4\text{O}_4)(\text{C}_3\text{H}_7\text{NO})] \cdot 2\text{C}_3\text{H}_7\text{NO}$ 

Chemical formula (total)	$\text{C}_{14}\text{H}_{18}\text{N}_2\text{O}_6\text{Zn}$
Formula weight	375.67
Temperature	150(2) K
Radiation, wavelength	CuK $\alpha$ , 1.54178 Å
Crystal system, space group	monoclinic, $P2_1/c$
Unit cell parameters	$a = 15.413(3)$ Å $b = 10.4292(16)$ Å $c = 16.223(3)$ Å $\beta = 103.702(18)^\circ$
Cell volume	$2533.5(7)$ Å <sup>3</sup>
Z	6
Crystal colour and size	colourless, $0.10 \times 0.08 \times 0.06$ mm <sup>3</sup>
Final $R$ indices [ $F^2 > 2\sigma$ ]	$R1 = 0.0745$
$R$ indices (all data)	$wR2 = 0.1431$
Largest diff. peak and hole	0.51 and $-0.37$ e Å <sup>-3</sup>

**Figure 5.10: Asymmetric Unit of Compound 3 all unique atoms labelled, additional atoms added to complete ligands.**

**Synthesis**

1 mL of a solution of  $\text{Zn}(\text{NO}_3)_2 \cdot 6\text{H}_2\text{O}$  (0.1 g, 0.33 mmol) in dimethylformamide (DMF) (10 mL) was layered over 1 mL of a solution of 1,4-benzenedicarboxylic acid (0.028 g, 0.17 mmol) in DMF (10 mL) in small sample vial. The vial was covered and left until crystallisation was complete. After six weeks, colourless block crystals formed.

## Structure Determination

The data were collected at 150 K using copper radiation on an Oxford Diffraction Gemini A Ultra diffractometer. The structure was solved by direct methods. The semi-empirical absorption corrections were applied based on symmetry-equivalent and repeated data. The refinement gave a  $wR2$  of 0.1431 for all 3933 independent reflections and a conventional  $R1$  of 0.0745, for 1736 reflections with  $F^2 > 2\sigma$ . The residual electron density maximum and minimum were 0.51 and  $-0.37 \text{ e}\text{\AA}^{-3}$  respectively.

The hydrogen atoms were placed in geometrically calculated positions with  $U$  constrained to  $1.2 U_{\text{eq}}(\text{C})$  for aromatic hydrogen atoms,  $U$  constrained to  $1.5 U_{\text{eq}}(\text{C})$  for methyl hydrogen atoms and  $U$  constrained to  $1.5 U_{\text{eq}}(\text{O})$  for the hydroxyl hydrogen atoms. The DMF ligands in the structure were heavily disordered and split into two parts for refinement; with SIMU, DELU and FLAT restraints being imposed. The full data of compound 3 can be found in Appendix 1.

## Structure Analysis

The asymmetric unit of compound 3 (figure 5.10) shows a complete 1,4-benzenedicarboxylate ligand and one half 1,4-benzenedicarboxylate ligand completed by inversion symmetry through the centre of the aromatic ring. These ligands join two zinc cations Zn(1) and Zn(2) that are in two different coordination environments in this polymeric compound. The Zn(1) cation is positioned on an inversion centre and forms a six coordinate octahedral geometry through symmetry, the Zn(2) cation is four coordinate distorted tetrahedral.

The six coordinate Zn(1) is coordinated to two unique 1,4-benzenedicarboxylate ligands through one oxygen atom on each carboxylate group in cis positions to one another, O(1)-Zn(1)-O(5)  $91.8(1)^\circ$  and O(4)-Zn(1)-O(5)  $90.8(2)^\circ$ . These coordinate further through their trans symmetry equivalents generated by the inversion symmetry at the centre of the Zn(1) atom, completing the six coordinate geometry (figure 5.11A).

The four coordinate Zn(2) cation forms a distorted tetrahedral geometry coordinating to both carboxylate groups of the complete 1,4-benzenedicarboxylate O(2)-Zn(2)-O(3)  $108.7(2)^\circ$  and the half 1,4-benzenedicarboxylate O(2)-Zn(2)-O(6)  $123.6(2)^\circ$ .

The fourth coordination site is occupied by a disordered DMF, which is coordinated to the zinc cation with a slightly elongated bond of Zn(2)-O(9) 1.986(5) Å compared to the carboxylate bond lengths Zn(2)-O(2) 1.941(5) Å and Zn(2)-O(6) 1.945(5) Å adding emphasis to the distorted geometry of the tetrahedral unit (figure 5.11B).

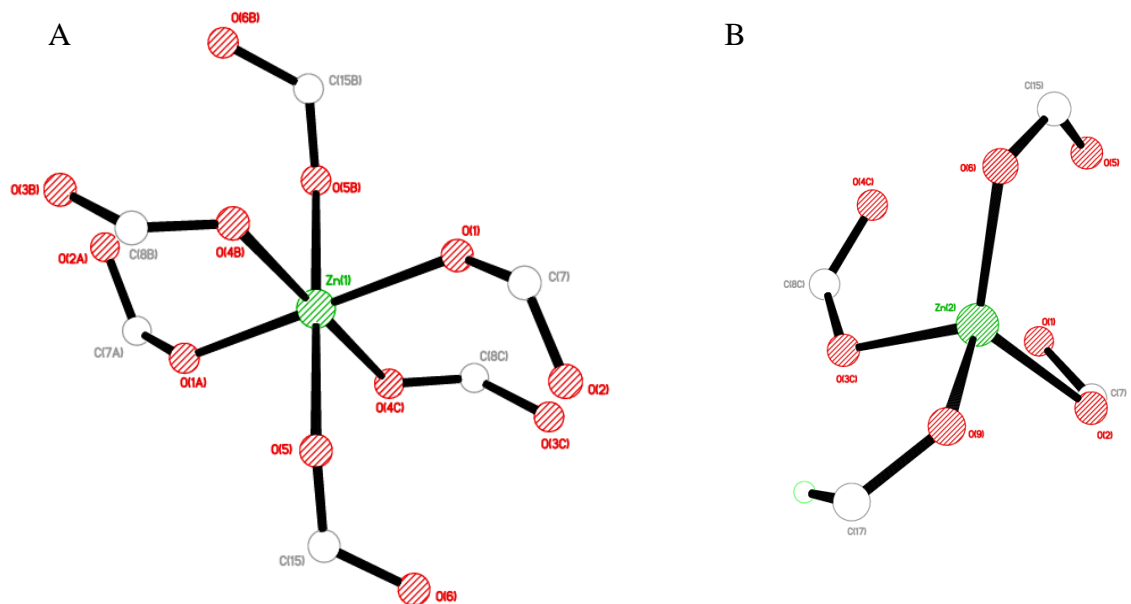
The 1,4-benzenedicarboxylate ligands coordinate through all of their carboxylate oxygen atoms and act as bridging units between the zinc cations to form a zinc trinuclear building unit (figure 5.12). This SBU is capped at both ends by the coordinated DMF molecules preventing the structure expanding in all three dimensions. The SBU is more clearly represented in figure 5.13 where only the coordinated functional groups are shown. The zinc cations are collinear down the *b*-axis; however their bonds to the carboxylate groups are not parallel due to the different coordination geometries they adopt, this is highlighted by the coordination angles C(7)-O(1)-Zn(1) 135.7(5)°, C(7)-O(2)-Zn(2) 118.9(5)°, C(15)-O(5)-Zn(1) 131.2(5)°, C(15)-O(6)-Zn(2) 111.5(5)°, C(8)-O(4)-Zn(1) 128.0(5)° and C(8)-O(3)-Zn(2) 117.3(5)°. This building unit forms a double layer sheet that expands down the *b*-axis and along the *c*-axis (figure 5.14). These sheets stack together to expand the structure into three dimensions by overlapping the terminal DMF ligands to maximise hydrogen bonding between the sheets and additional hydrogen bonding is formed to the uncoordinated DMF molecules; however due to the large disorder of the DMF moieties accurate hydrogen bonds cannot be quantified for analysis. Figure 5.15 shows how this stacking occurs by viewing the crystal structure down the *b*-axis, the dual layer sheets are parallel to one another and packed in a staggered packing motif due to the glide plane between the layers, similar to the packing motif observed in compound 1.

**Table 5.05: Selected Bond Lengths [Å] and Angles [°] for Compound 3**

Zn(1)–O(1)	2.051(5)	Zn(1)–O(4B)	2.081(5)
Zn(1)–O(5)	2.100(5)	Zn(2)–O(2)	1.941(5)
Zn(2)–O(3B)	1.938(5)	Zn(2)–O(6)	1.945(5)
Zn(2)–O(9)	1.986(5)	C(7)–O(1)	1.258(8)
C(7)–O(2)	1.260(8)	C(8)–O(3)	1.278(8)
C(8)–O(4)	1.232(8)		
O(1)–Zn(1)–O(4B)	91.9(2)	O(1)–Zn(1)–O(4C)	88.06(19)
O(1)–Zn(1)–O(5)	91.8(2)	O(1)–Zn(1)–O(5A)	88.2(2)
O(4B)–Zn(1)–O(5)	90.8(2)	O(4B)–Zn(1)–O(5A)	89.2(2)
O(2)–Zn(2)–O(3B)	108.7(2)	O(2)–Zn(2)–O(6)	123.6(2)
O(2)–Zn(2)–O(9)	101.7(2)	O(3B)–Zn(2)–O(6)	116.5(2)
O(3B)–Zn(2)–O(9)	99.7(2)	O(6)–Zn(2)–O(9)	102.0(2)
Zn(1)–O(1)–C(7)	135.7(5)	Zn(2)–O(2)–C(7)	118.9(5)
Zn(1)–O(5)–C(15)	131.2(5)	Zn(2)–O(6)–C(15)	111.5(5)
Zn(1E)–O(4)–C(8)	128.0(5)	Zn(2D)–O(3)–C(8)	117.3(5)
Zn(2)–O(9)–C(17)	119.2(7)		

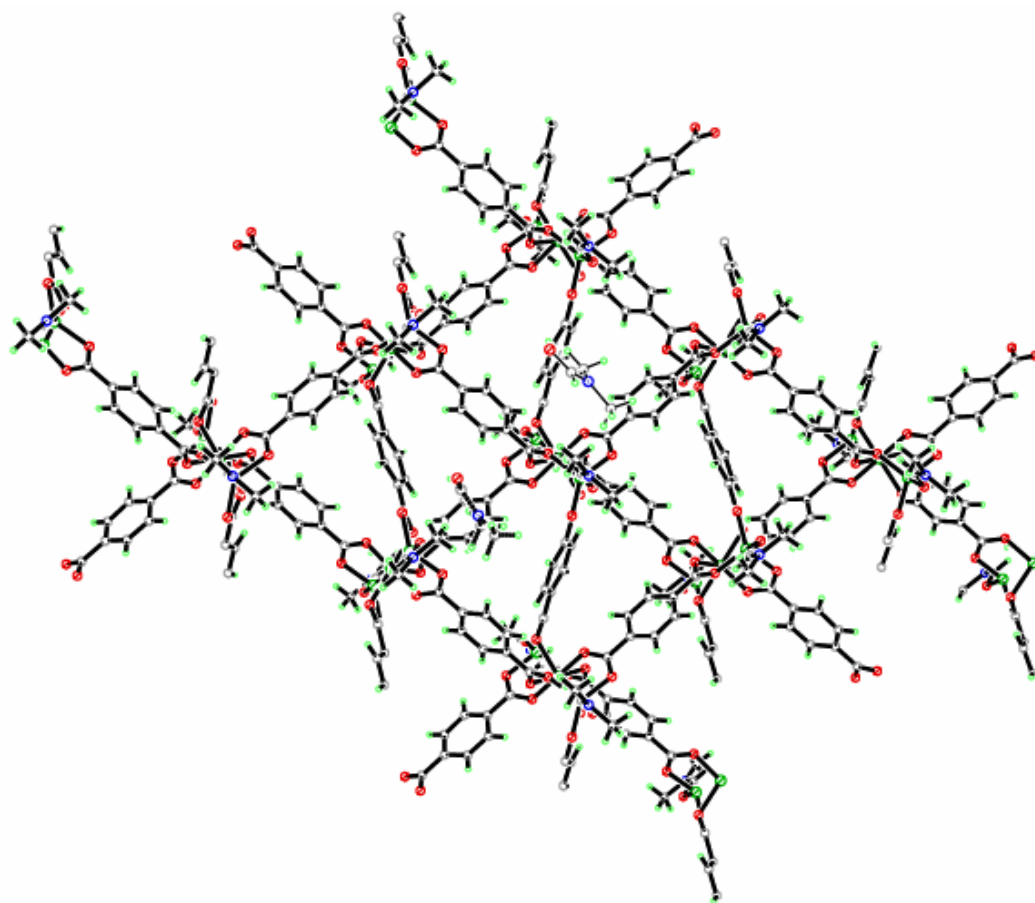
Symmetry operations for equivalent atoms

A  $-x+1, -y+1, -z+1$     B  $x, -y+3/2, z+1/2$     C  $-x+1, y-1/2, -z+1/2$   
D  $x, -y+3/2, z-1/2$     E  $-x+1, y+1/2, -z+1/2$     F  $-x+1, -y, -z+1$

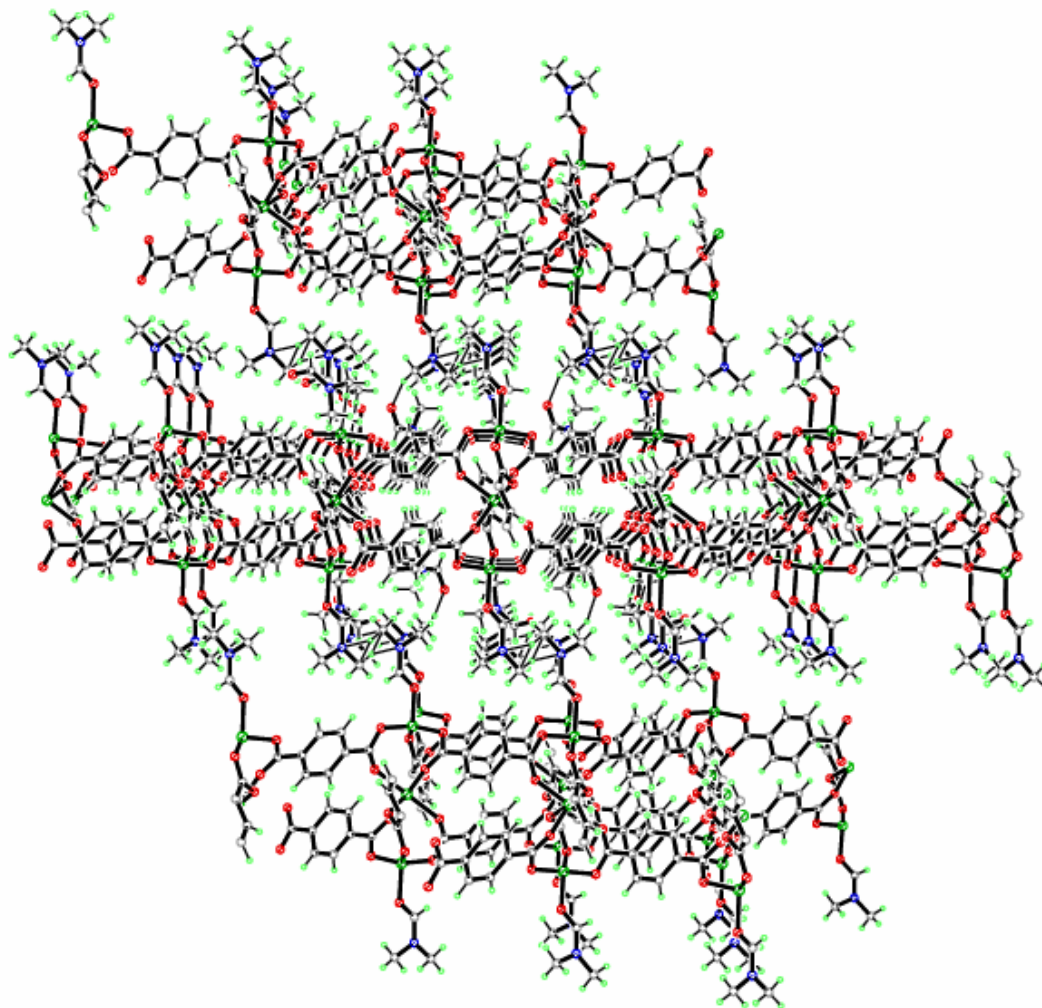


**Figure 5.11: A) Octahedral coordination environment of Zn(1) and B) Tetrahedral coordination environment of Zn(2) in compound 3**

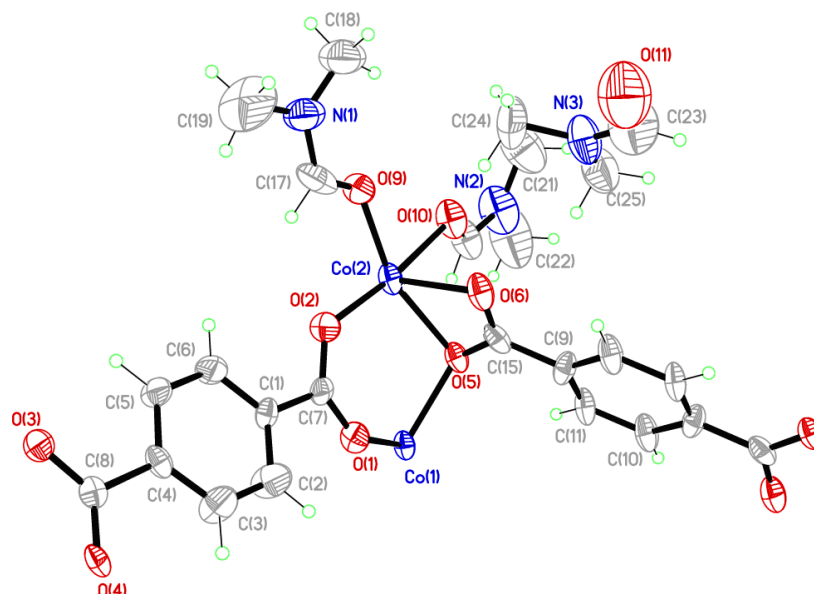




**Figure 5.14:** Two dimensional sheet of compound 3 viewed down the *a*-axis



**Figure 5.15:** Three dimensional packing of double layer sheets in compound 3 viewed down the *b*-axis

**Compound 4:**  $[\text{Co}(\text{C}_8\text{H}_4\text{O}_4)(\text{C}_3\text{H}_7\text{NO})_2]$ 

Chemical formula (total)	$\text{C}_{14}\text{H}_{18}\text{CoN}_2\text{O}_6$
Formula weight	369.23
Temperature	150(2) K
Radiation, wavelength	$\text{CuK}\alpha$ , 1.54178 Å
Crystal system, space group	monoclinic, $P2_1/c$
Unit cell parameters	$a = 14.707(2)$ Å $b = 9.6764(12)$ Å $c = 17.9510(15)$ Å $\beta = 93.958(11)^\circ$
Cell volume	$2548.5(5)$ Å <sup>3</sup>
Z	6
Crystal colour and size	pink, $0.50 \times 0.30 \times 0.04$ mm <sup>3</sup>
Final $R$ indices [ $F^2 > 2\sigma$ ]	$R1 = 0.0640$
$R$ indices (all data)	$wR2 = 0.1590$
Largest diff. peak and hole	0.74 and $-0.58$ e Å <sup>-3</sup>

**Figure 5.16:** Asymmetric Unit of Compound 4 all unique atoms labelled, additional atoms added to complete ligands.

**Synthesis**

1 mL of a solution of  $\text{Co}(\text{NO}_3)_2 \cdot 6\text{H}_2\text{O}$  (0.1 g, 0.33 mmol) in dimethylformamide (DMF) (10 mL) was layered over 1 mL of a solution of 1,4-benzenedicarboxylic acid (0.028 g, 0.17 mmol) in DMF (10 mL) in a small sample vial. The vial was covered and left until crystallisation was complete. After seven weeks, pink plate crystals formed.



## Structure Determination

The data were collected at 150 K using copper radiation on an Oxford Diffraction Gemini A Ultra diffractometer. The structure was solved by direct methods. The semi-empirical absorption corrections were applied based on symmetry-equivalent and repeated data. The refinement gave a  $wR2$  of 0.1590 for all 3121 independent reflections and a conventional  $R1$  of 0.0640, for 1615 reflections with  $F^2 > 2\sigma$ . The residual electron density maximum and minimum were 0.74 and  $-0.58 \text{ e } \text{\AA}^{-3}$  respectively.

The hydrogen atoms were placed in geometrically calculated positions with  $U$  constrained to  $1.2 U_{\text{eq}}(\text{C})$  for aromatic hydrogen atoms,  $U$  constrained to  $1.5 U_{\text{eq}}(\text{C})$  for methyl hydrogen atoms and  $U$  constrained to  $1.5 U_{\text{eq}}(\text{O})$  for the hydroxyl hydrogen atoms. The full data of compound 4 can be found in Appendix 1.

## Structure Analysis

The asymmetric unit of compound 4 (figure 5.16) shows a complete 1,4-benzenedicarboxylate ligand joining two cobalt cations Co(1) and Co(2) the former being on an inversion centre. An additional half 1,4-benzenedicarboxylate ligand is bound to both Co(1) and Co(2) cations with its symmetry equivalent generated around the inversion centre in the middle of the aromatic ring to complete the ligand. The cobalt cations in compound 4 are both six-coordinate with octahedral geometries, the Co(1) cation shows regular octahedral coordination geometry (figure 5.17A) with standard bond angles (table 5.06) as a result of the inversion symmetry at the centre of the atom generating the trans coplanar symmetry equivalents. The Co(2) cation forms a six-coordinate distorted octahedral geometry (figure 5.17B), the distortion originates from a doubly chelating carboxylate group of a 1,4-benzenedicarboxylate ligand. This coordinates to the Co(2) cation with a bite angle of  $\text{O}(5)\text{-Co}(2)\text{-O}(6)$   $61.1(2)^\circ$  much lower than the standard  $90^\circ$  coordination angle. The octahedral geometry is completed by two cis bound 1,4-benzenedicarboxylate ligands  $\text{O}(2)\text{-Co}(2)\text{-O}(3\text{C})$   $97.9(2)^\circ$  that coordinate using one carboxylate oxygen each. The remaining two coordinate sites are occupied by coplanar cis DMF ligands  $\text{O}(9)\text{-Co}(2)\text{-O}(10)$   $83.6(2)^\circ$  that are trans to the carboxylate groups  $\text{O}(5)\text{-Co}(2)\text{-O}(9)$   $158.1(3)^\circ$  and  $\text{O}(2)\text{-Co}(2)\text{-O}(10)$   $172.1(3)^\circ$ .

The single coordinated 1,4-benzenedicarboxylate ligands have fully delocalised carboxylate groups with comparable bond lengths showing no evidence of carbon-oxygen single and double bonds (table 5.06). These carboxylate groups act as bridging groups with the alternate oxygen atom coordinating to Co(1) and then through its inversion symmetry forms a cobalt trinuclear cluster as shown in figure 5.18, this forms a distorted paddle-wheel secondary building unit with distortion emerging from the bifurcated carboxylate coordination. The trinuclear building unit is shown in figure 5.19 with only the functional groups shown to enable the bridging nature of the carboxylate groups to be viewed; these carboxylates hold the cobalt cations coplanar down the *a*-axis. The O(5) carboxylate atom acts as a bridging oxygen coordinating to both Co(1) and Co(2) with the respective Co(1)-O(5) 2.123(5) Å and Co(2)-O(5) 2.167(5) Å bonds that form a bite angle of Co(1)-O(5)-Co(2) 109.8(2)°, with distorted octahedral of the Co(2) cation pulling the bite angle away from the ideal 90°.

The 1,4,-benzenedicarboxylate ligands do not bind the cobalt cations in the standard paddle-wheel motif with bond angles of 120° forming linear bonds placing the cobalt cations at 180°, in contrast they form distorted bond angles of C(7)-O(1)-Co(1) 133.5(5)°, C(7)-O(2)-Co(2) 128.3(5)°, C(8B)-O(4B)-Co(1) 136.9(5)° and C(8B)-O(3B)-Co(2) 123.0(5)°. The cobalt trinuclear cluster is capped at the ends due to the cis bound DMF ligands preventing the formation of a fully coordinated cobalt paddle-wheel building unit that can expand the structure into three dimensions through bridging carboxylates. The 1,4-benzenedicarboxylate ligands expand the building unit into a two dimensional double layer sheet that expands the structure along the *b*-axis and down the *c*-axis (figure 5.20). These sheets stack together to expand the structure into three dimensions by overlapping terminal DMF ligands. Figure 5.21 shows the close packing network of the compound viewed down the crystallographic *b*-axis, the dual layer sheets are parallel to each other packing in a staggered motif due to the DMF molecules and the glide plane.

The compound was synthesised using the same reaction conditions as compound 3 forming a similar framework that is almost isostructural; however the structures differ in the metal coordination geometries due to the metal cations used. Compound 3 has one standard six-coordinate octahedral zinc unit and a distorted four-coordinate tetrahedral

zinc unit, in comparison the metal nodes in compound 4 are both six-coordinate octahedral geometries. The variance in coordination geometry is attributed to the bidentate carboxylate in compound 4, this however does not influence the overall topology of the structure significantly with the formation of the metal trinuclear building unit and the subsequent formation of the dual layer sheets resulting in the similar packing motifs (figure 5.21)(figure 5.15).

Compounds 3 and 4 have similar secondary building units to two compounds reported by Brammer *et al.* (CSD Refcode: IFAXAT02 and LEPKUN).<sup>7</sup> These structures have zinc trinuclear building units with one octahedral and one tetrahedral node bridged by 1,4,benzenedicarboxylate ligands; however these trinuclear clusters are capped with water ligands allowing the sheets to pack in a closer packing motif than compounds 3 and 4, highlighting the templating effect of both water and DMF on the topology formation of the respective compounds.

The reaction conditions used in the formation of compound 3 and 4 were further expanded to adapt the paddle-wheel building motif, resulting in the synthesis of compound 5 with a standardised paddle-wheel building unit.

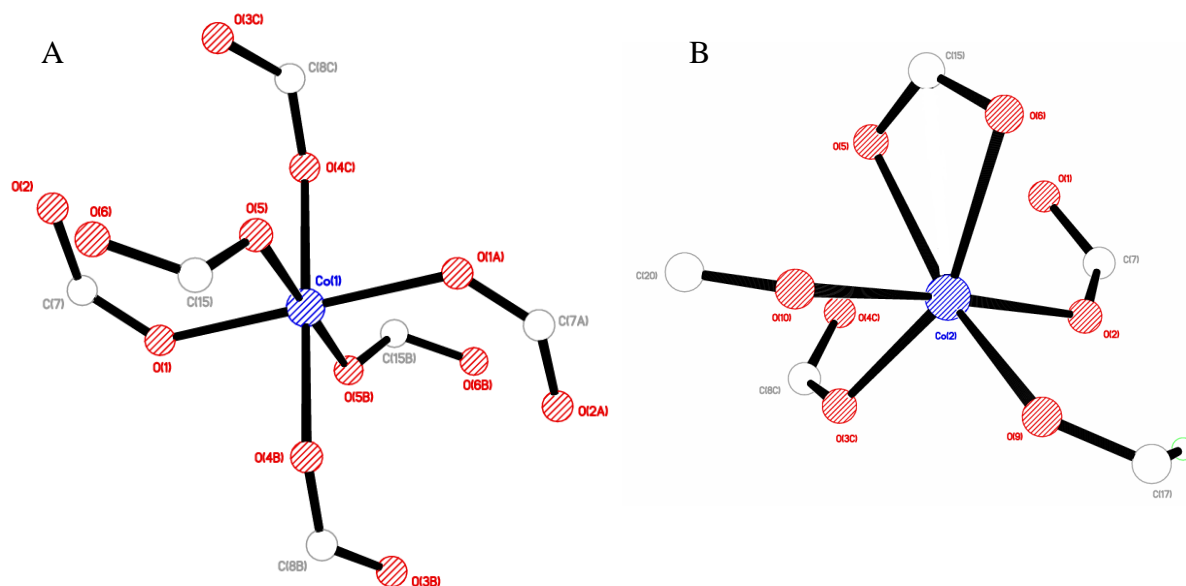
**Table 5.06: Selected Bond Lengths [Å] and Angles [°] for Compound 4**

Co(1)–O(1)	2.047(5)	Co(1)–O(4B)	2.070(5)
Co(1)–O(5)	2.123(5)	Co(2)–O(2)	2.055(5)
Co(2)–O(3B)	2.021(5)	Co(2)–O(5)	2.167(5)
Co(2)–O(6)	2.176(6)	Co(2)–O(9)	2.052(6)
Co(2)–O(10)	2.155(5)	C(7)–O(1)	1.232(9)
C(7)–O(2)	1.272(9)	C(8)–O(3)	1.265(9)
C(8)–O(4)	1.230(9)		
O(1)–Co(1)–O(4B)	94.7(2)	O(1)–Co(1)–O(4C)	85.3(2)
O(1)–Co(1)–O(5)	92.5(2)	O(2)–Co(2)–O(3B)	97.9(2)
O(2)–Co(2)–O(5)	100.6(2)	O(2)–Co(2)–O(6)	96.3(2)
O(2)–Co(2)–O(9)	88.6(2)	O(2)–Co(2)–O(10)	172.1(2)
Co(1)–O(1)–C(7)	133.5(5)	Co(2)–O(2)–C(7)	128.3(5)
Co(1E)–O(4)–C(8)	136.9(5)	Co(2D)–O(3)–C(8)	123.0(5)
Co(1)–O(5)–Co(2)	109.8(2)	Co(1)–O(5)–C(15)	130.2(5)
Co(2)–O(5)–C(15)	89.1(5)	Co(2)–O(6)–C(15)	89.8(5)
Co(2)–O(9)–C(17)	126.5(6)	Co(2)–O(10)–C(20)	119.5(6)
Co(1)–O(5)–Co(2)	109.8(2)		

Symmetry operations for equivalent atoms

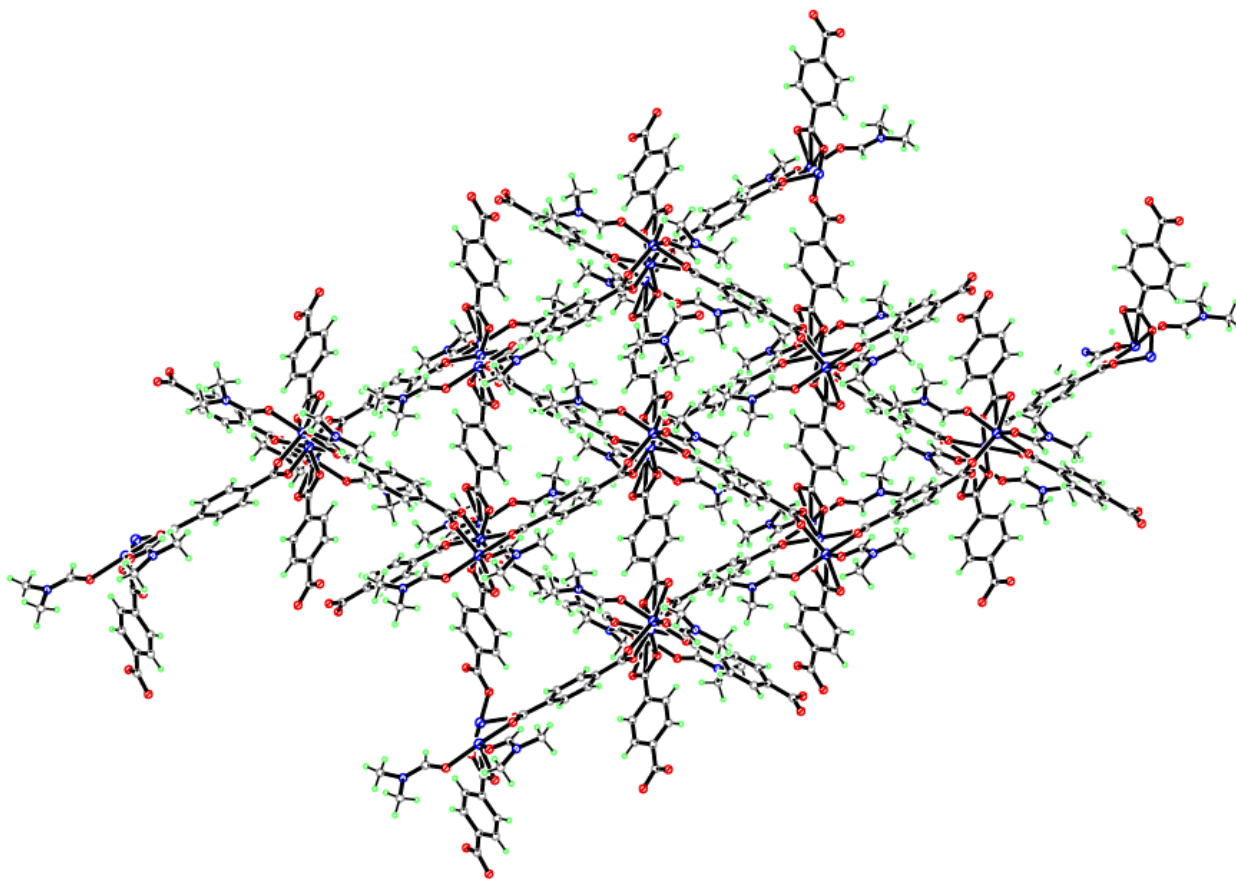
A  $-x+1, -y+1, -z+1$     B  $x, -y+3/2, z-1/2$     C  $-x+1, y-1/2, -z+3/2$

D  $x, -y+3/2, z+1/2$     E  $-x+1, y+1/2, -z+3/2$

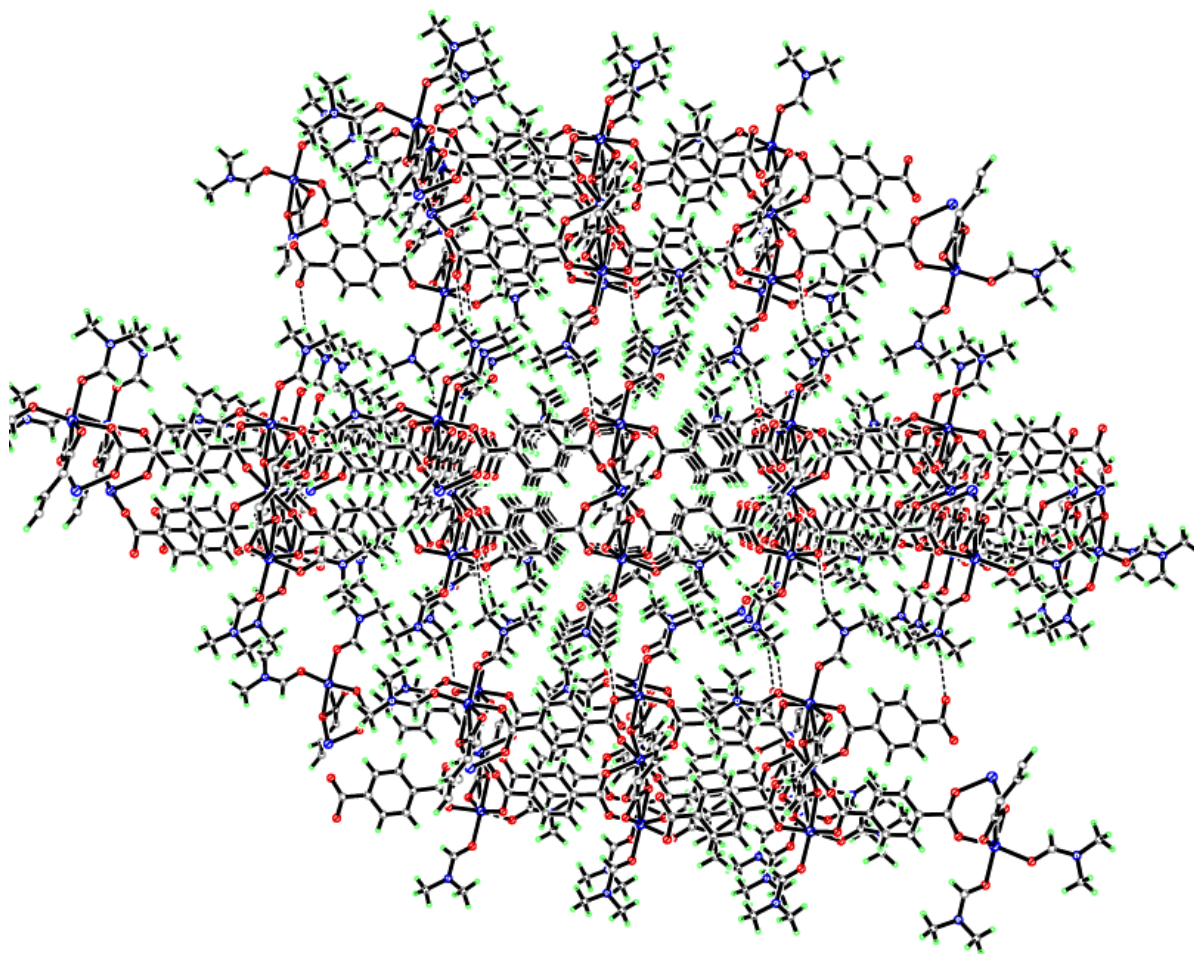


**Figure 5.17: A) Octahedral coordination environment of Co(1) and B) Distorted octahedral coordination environment of Co(2) in compound 4**

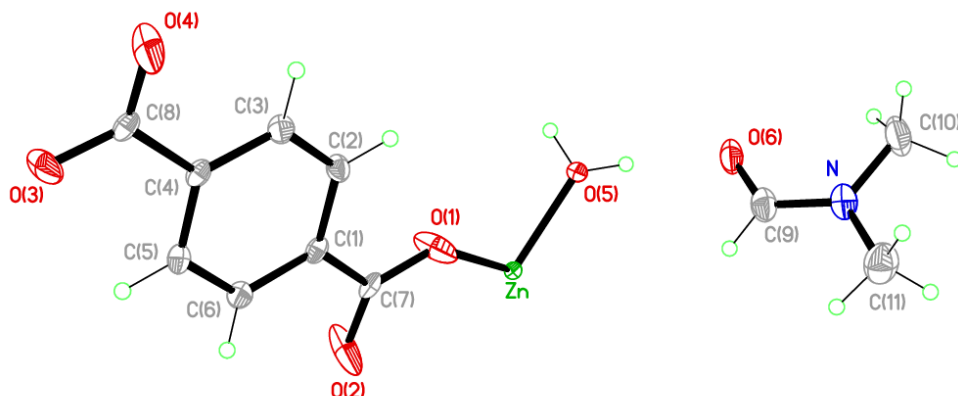




**Figure 5.20:** Two dimensional sheet of compound 4 viewed down the *a*-axis



**Figure 5.21:** Three dimensional packing of double layer sheets in compound 4 viewed down the *b*-axis

**Compound 5:**  $[\text{Zn}(\text{C}_8\text{H}_4\text{O}_4)(\text{H}_2\text{O})] \cdot (\text{C}_3\text{H}_7\text{NO})$ 

Chemical formula (total)	$\text{C}_{11}\text{H}_{13}\text{NO}_6\text{Zn}$
Formula weight	320.59
Temperature	150(2) K
Radiation, wavelength	MoK $\alpha$ , 0.71073 Å
Crystal system, space group	monoclinic, $P2_1/n$
Unit cell parameters	$a = 6.6466(3)$ Å $b = 15.2659(5)$ Å $c = 12.5434(4)$ Å $\beta = 103.794(4)^\circ$
Cell volume	$1236.03(8)$ Å <sup>3</sup>
Z	4
Crystal colour and size	colourless, $0.10 \times 0.02 \times 0.02$ mm <sup>3</sup>
Final $R$ indices [ $F^2 > 2\sigma$ ]	$R1 = 0.0326$
$R$ indices (all data)	$wR2 = 0.0778$
Largest diff. peak and hole	0.60 and $-0.52$ e Å <sup>-3</sup>

**Figure 5.22: Asymmetric Unit of Compound 5 all unique atoms labelled.****Synthesis**

$\text{Zn}(\text{NO}_3)_2 \cdot 6\text{H}_2\text{O}$  (0.09 g, 0.33 mmol) and 1,4-benzenedicarboxylic acid (0.028 g, 0.17 mmol) were added to a reaction mixture of dimethylformamide (DMF) (4 mL), Ethanol (4mL) and water (3mL). This was placed into a 20mL Teflon-lined bomb and heated to 120°C for 24 hours. The vessel was then cooled back down to room temperature at a rate of 0.1°C / min and allowed to stand for 2 hours before colourless needle crystals were retrieved from the vessel.



## Structure Determination

The data were collected at 150 K using molybdenum radiation on an Oxford Diffraction Gemini A Ultra diffractometer. The structure was solved by direct methods. The semi-empirical absorption corrections were applied based on symmetry-equivalent and repeated data. The refinement gave a  $wR2$  of 0.0726 for all 2711 independent reflections and a conventional  $R1$  of 0.0326, for 2354 reflections with  $F^2 > 2\sigma$ . The residual electron density maximum and minimum were 0.60 and  $-0.52 \text{ e } \text{\AA}^{-3}$  respectively.

The hydrogen atoms were placed in geometrically calculated positions with  $U$  constrained to  $1.2 U_{\text{eq}}(\text{C})$  for aromatic hydrogen atoms,  $U$  constrained to  $1.5 U_{\text{eq}}(\text{C})$  for methyl hydrogen atoms and  $U$  constrained to  $1.5 U_{\text{eq}}(\text{O})$  for the hydroxyl hydrogen atoms. The full data of compound 5 can be found in Appendix 1.

## Structure Analysis

The asymmetric unit of compound 5 (figure 5.22) shows a complete 1,4-benzenedicarboxylate ligand coordinated to a zinc cation in a general position. The zinc cation in compound 5 is a five-coordinate distorted square pyramidal (figure 5.23) with bond angles O(1)-Zn-O(2A)  $158.66(9)^\circ$ , O(1)-Zn-O(3B)  $84.89(12)^\circ$ , O(1)-Zn-O(4C)  $88.16(12)^\circ$  and O(1)-Zn-O(5)  $98.47(8)^\circ$ ; these are consistent with known similar distorted square pyramidal geometries.<sup>7,8</sup> The 1,4-benzenedicarboxylate binds to the zinc cation through all four of its carboxylate oxygen atoms through symmetry equivalent ligands. This occupies four of the coplanar coordination sites around the 'base' of the square pyramidal node, the final coordination site perpendicular to the carboxylates is occupied by a water ligand that forms a short strong bond Zn-O(5)  $1.955(18) \text{ \AA}$ . This square pyramidal zinc node expands through an inversion centre to form a more octahedral geometry forming a Zn-Zn interaction, this inversion symmetry is the primary effect that induces the distorted geometry of the square pyramidal with the carboxylates forming bridges between the symmetry equivalent zinc cations. This bridging motif forms a four-blade paddle-wheel secondary building unit with slightly offset bonds diverging away from the ideal  $180^\circ$  trans positions (table 5.07).

The secondary building unit of compound 5 is shown in figure 5.24, this paddle-wheel motif expands the framework in two dimensions to form a 4,4'-sheet (figure 5.25). The sheets of compound 5 pack together along the *c*-axis allowing strong hydrogen bonds to form between the water ligand and adjacent carboxylate groups, O(5)-H(5B)···O(1F) 2.970(3) Å and O(5)-H(5B)···O(3G) 2.991(3) Å expanding the sheet structure into three-dimensions (figure 5.26)(table 5.08).

The 4,4' net motif shown in figure 5.25 creates nanochannels that run down the crystallographic *a*-axis that contain the one unbound DMF molecule shown in the asymmetric unit and its symmetry equivalent, these hydrogen bond to the terminal water ligands of the zinc paddle-wheel structure through the strong hydrogen bond O(5)-H(5A)···O(6) 2.587(3) Å. The presence of the uncoordinated DMF within the structure results in the lack of porosity confirmed by PLATON<sup>9</sup>, however if the DMF molecules were removed from the framework upon using desolvation techniques PLATON calculates the framework of compound 5 will have a pore volume of 524.5 Å<sup>3</sup> per unit cell which is 42.4 %. The potential pores in compound 5 are ideal for gas adsorption studies with dimensions 10.244(6) by 10.244(6) Å producing a porous packing motif shown in figure 5.27. To remove the DMF and activate the structure thermogravimetric analysis showed that structure needed to be heated to 150°C, however upon desolvation the structure continues to collapse fully degrading at 250°C showing low stability upon desolvation.

Further analysis of compound 5 was used to determine the purity of the bulk sample, the elemental analysis gave results of C = 40.67 %, H = 3.49 % and N = 3.54 % that correlate well with the calculated values from the single crystal data; C = 41.16 %, H = 4.05 % and N = 4.36 % with discrepancies in hydrogen and nitrogen as a result of partial desolvation of compound 5. Powder X-ray diffraction of the bulk sample produced a good quality data set shown in figure 5.30 that is consistent with the predicted powder diffraction pattern produced by the single crystal data with all significant peaks at corresponding shifts, indicating the bulk sample was consistent with compound 5 showing overall satisfactory purity.

There are several similar compounds in the CSD to compound 5 with two paddle-wheel structures (CSD Refcode: DAXNOG01 and HIQVUZ01) produced by

Brammer *et al.*<sup>7</sup> and Battern *et al.*<sup>8</sup> respectively. The compound DAXNOG01 comprises of a two dimensional square grid with 4,4' topology shown in figure 5.28, this packing motif is built using a similar paddle-wheel structure to that in compound 5 with Zn-O bond lengths ranging from 1.994(4) – 2.057(4) Å with comparisons to those of compound 5 in table 5.09. The 4,4' net produced has voids with similar dimensions of 10.935 by 10.905 Å, however they are filled with coordinated DMF molecules that protrude from the layers above and below the paddle wheel occupying the equivalent coordination site of the water ligand in compound 5.<sup>7</sup>

The zinc-1,4-benzendicarboxylate MOF of HIQVUZ01<sup>8</sup> is constructed using the zinc paddle-wheel building unit with Zn-O bond lengths ranging from 2.018 – 2.334 Å. The 4,4' net produced again has voids with dimensions 10.896 by 10.901 Å, but adopts a herringbone motif as the angles are skewed by more favourable hydrogen interactions with DMA molecules O-H...O 2.872(3) Å that fill the voids as shown in figure 5.29. These interactions are significant in the length of the Zn-OH<sub>2</sub> bond with elongation to 2.335(2) Å in order to form multiple hydrogen bonds with the DMA molecule, this is significantly longer than the Zn-OH<sub>2</sub> bond in compound 5 at 1.955(18) Å resulting in a wider intermolecular distance between the sheets.<sup>8</sup>(table 5.09)

The potential applications of these structures lead to investigations into solvent systems that would exploit the binding nature and topology directing factors of the solvent and addition ligands. This resulted in the formation of compounds 7 and 8 that are similar in topology to compounds 3,4 and 5.

**Table 5.07: Selected Bond Lengths [Å] and Angles [°] for Compound 5**

Zn–O(1)	2.046(19)	Zn–O(2A)	2.010(2)
Zn–O(3B)	2.052(2)	Zn–O(4C)	2.012(2)
Zn–O(5)	1.9548(18)	C(7)–O(1)	1.243(3)
C(7)–O(2)	1.231(3)	C(8)–O(3)	1.236(3)
C(8)–O(4)	1.240(3)		
O(1)–Zn–O(2A)	158.66(9)	O(1)–Zn–O(3B)	84.89(12)
O(1)–Zn–O(4C)	88.16(12)	O(1)–Zn–O(5)	98.47(8)
Zn–O(1)–C(7)	129.85(18)	ZnA–O(2)–C(7)	127.09(18)
ZnD–O(3)–C(8)	136.08(19)	ZnE–O(4)–C(8)	121.08(18)
Symmetry operations for equivalent atoms			
A	$-x, -y+1, -z+1$	B	$-x+1/2, y-1/2, -z+1/2$
C	$x-1/2, -y+3/2, z+1/2$		
D	$-x+1/2, y+1/2, -z+1/2$	E	$x+1/2, -y+3/2, z-1/2$

**Table 5.08: Selected Hydrogen bond Lengths [Å] and angles [°] for Compound 5**

D–H...A	d(D–H)	d(H...A)	d(D...A)	(DHA)
O(5)–H(5A)...O(6)	0.842(10)	1.750(11)	2.587(3)	173(3)
O(5)–H(5B)...O(1F)	0.828(10)	2.252(19)	2.970(3)	145(3)
O(5)–H(5B)...O(3G)	0.828(10)	2.31(2)	2.991(3)	140(3)
Symmetry operations for equivalent atoms				
F	$-x+1, -y+1, -z+1$	G	$x+1/2, -y+3/2, z+1/2$	

**Table 5.09: Average bond length comparisons between Compound 5, DAXNOG01<sup>7</sup> and HIQVUZ01<sup>8</sup>**

Compound	Bond	Average Bond Length (Å)
Compound 5	Zn–O (carboxylate)	2.031
Compound 5	Zn–O (water)	1.955
DAXNOG01	Zn–O (carboxylate)	2.025
DAXNOG01	Zn–O (DMF)	1.995
HIQVUZ01	Zn–O (carboxylate)	2.031
HIQVUZ01	Zn–O (water)	1.959

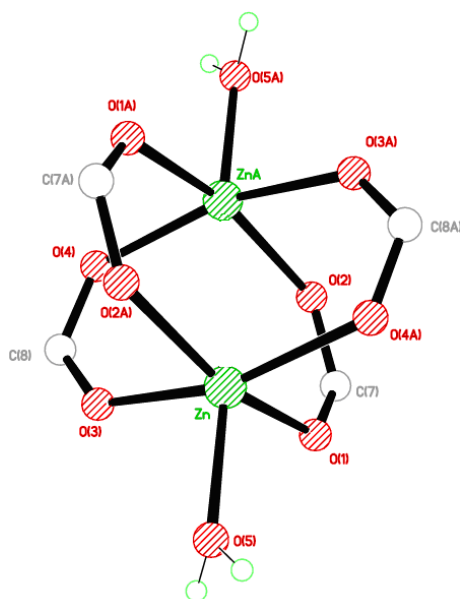


**Figure 5.23:** Square pyramidal geometry of the Zn cation and the symmetry equivalent ZnA cation that forms a distorted octahedral geometry with a Zn-ZnA interaction in compound 5

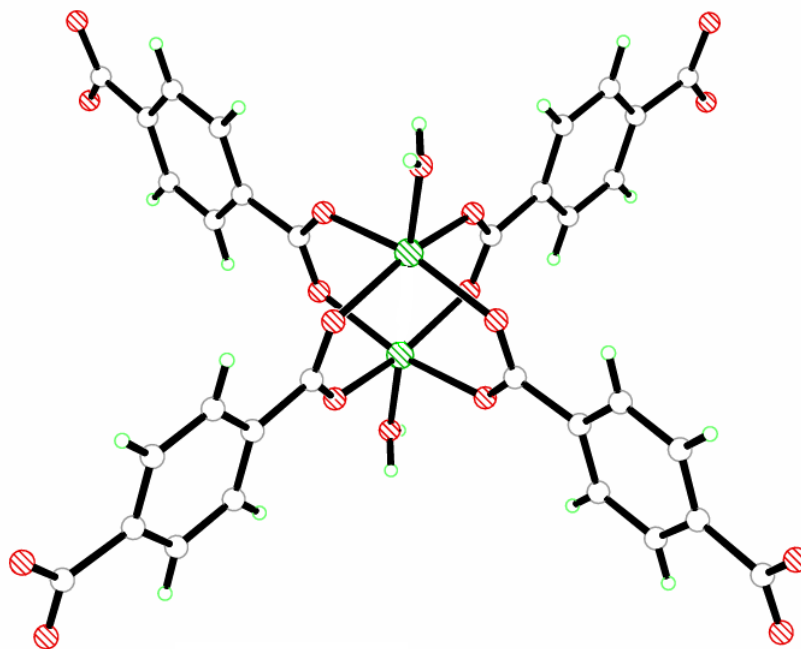


**Figure 5.24:** Secondary building unit of Zn and ZnA paddle-wheel in compound 5 (uncoordinated moieties omitted for clarity)

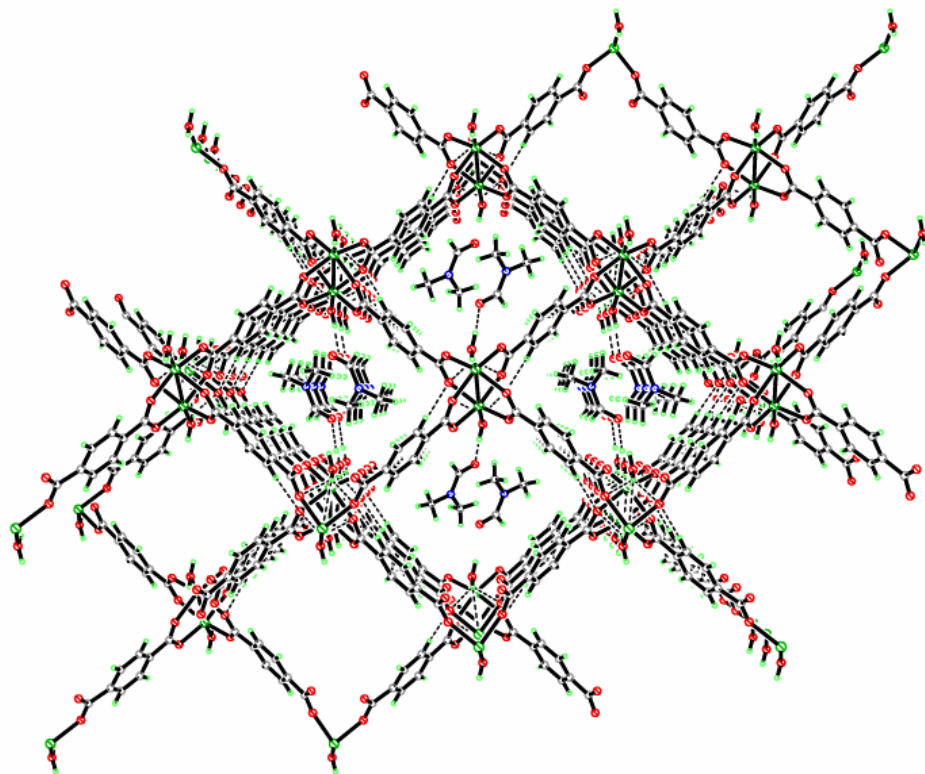


**Figure 5.25:** Two dimensional sheet of compound 5 viewed down the *a*-axis

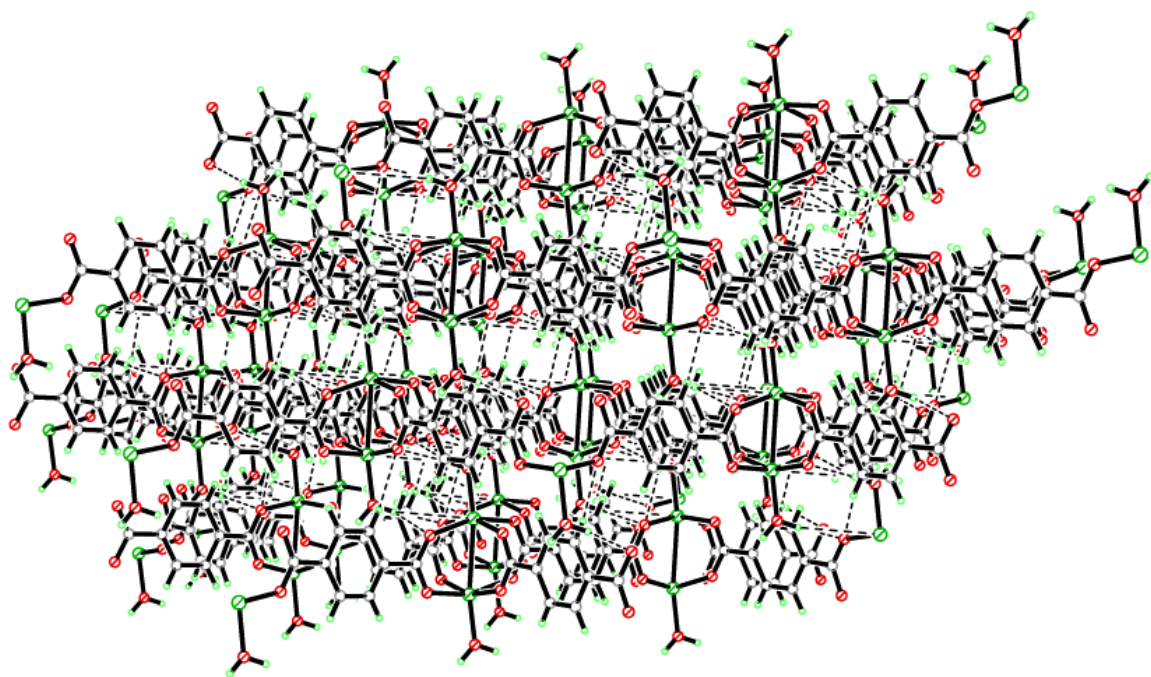


**Figure 5.26:** Three dimensional packing of the sheets in compound 5 viewed down the *c*-axis

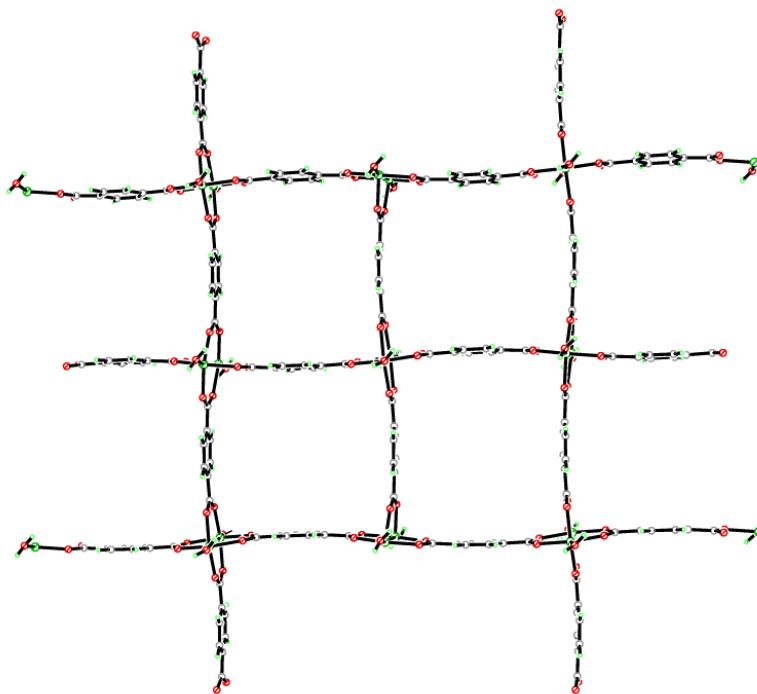


**Figure 5.27:** Two dimensional 4,4' net with voids running down the sheets in compound 5 viewed down the *a*-axis

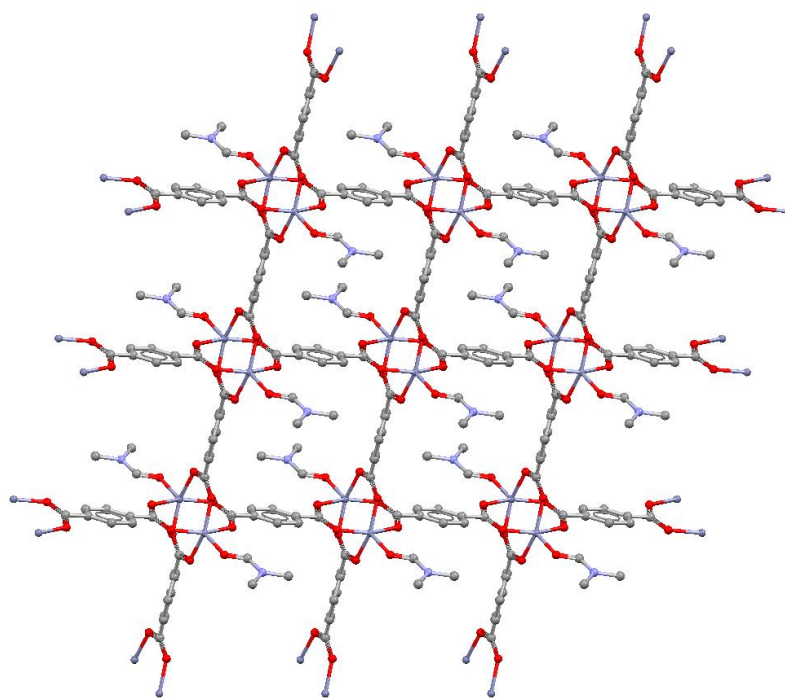


**Figure 5.28:** Two dimensional 4,4' net of DAXNOG01 viewed down the *b*-axis<sup>7</sup>

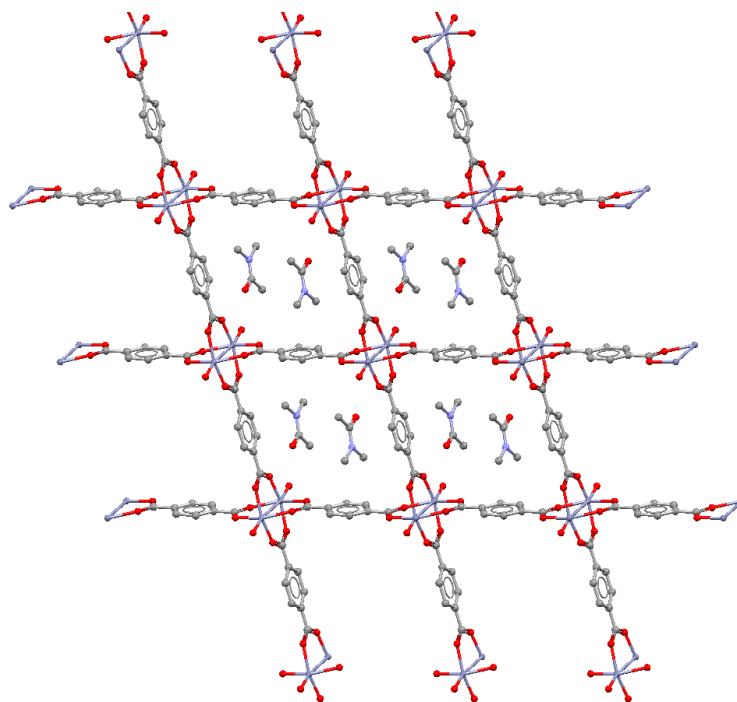


**Figure 5.29: Two dimensional 4,4' of HIQVUZ01 viewed down the *a*-axis<sup>8</sup>**

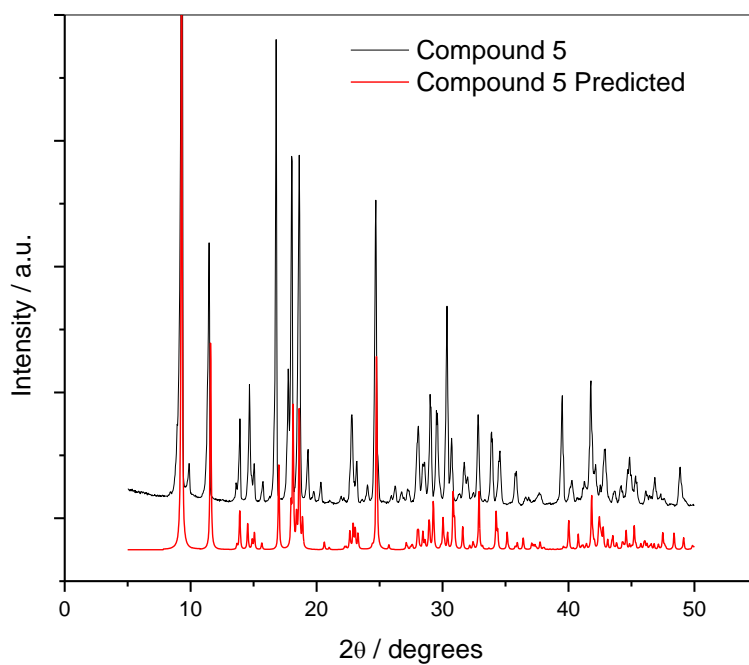
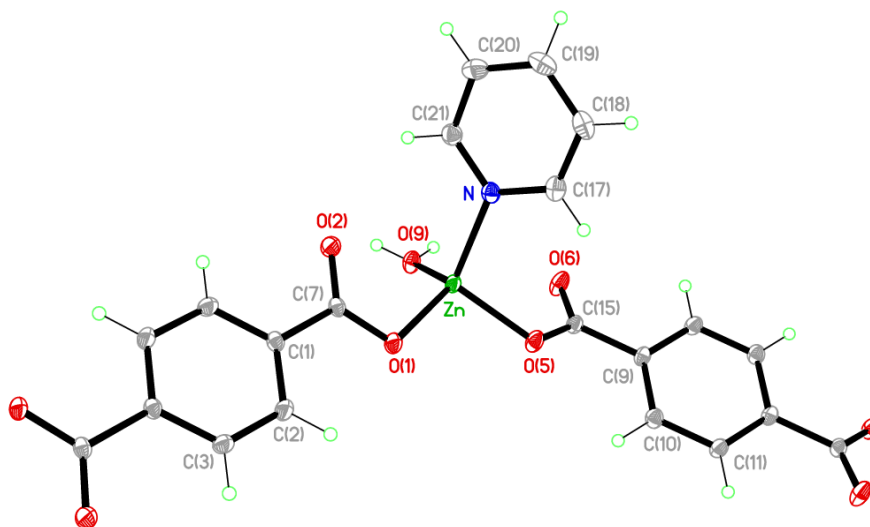


**Figure 5.30: Powder X-ray diffraction pattern of Compound 5**



---



Chemical formula (total)	C <sub>13</sub> H <sub>11</sub> NO <sub>5</sub> Zn	
Formula weight	326.60	
Temperature	120(2) K	
Radiation, wavelength	synchrotron, 0.6889 Å	
Crystal system, space group	monoclinic, <i>P</i> 2 <sub>1</sub> / <i>n</i>	
Unit cell parameters	<i>a</i> = 8.4085(16) Å <i>b</i> = 9.1794(17) Å <i>c</i> = 16.356(3) Å	β = 91.5818(18)°
Cell volume	1262.0(4) Å <sup>3</sup>	
<i>Z</i>	4	
Crystal colour and size	colourless, 0.10 × 0.02 × 0.01 mm <sup>3</sup>	
Final <i>R</i> indices [ <i>F</i> <sup>2</sup> > 2σ]	<i>R</i> 1 = 0.0346	
<i>R</i> indices (all data)	<i>wR</i> 2 = 0.0905	
Largest diff. peak and hole	0.37 and −0.33 e Å <sup>−3</sup>	

**Figure 5.31: Asymmetric Unit of Compound 6 all unique atoms labelled.**

## Synthesis

0.5 mL of a solution of  $\text{Zn}(\text{NO}_3)_2 \cdot 6\text{H}_2\text{O}$  (0.09 g, 0.33 mmol) in water (10 mL) and 0.5 mL of a solution of 1,4-benzenedicarboxylic acid (0.028 g, 0.17 mmol) in water (10 mL) were placed into a small sample vial. This was covered with Whatman Laboratory Sealing Film and placed inside a larger sample vial. In the larger sample vial pyridine (0.05 mL, 0.22 mmol) was added before it was covered and left until crystallisation was complete. After two weeks, colourless needle crystals formed.

## Structure Determination

The data were collected at 120 K using synchrotron radiation on a Crystal Logic diffractometer and Rigaku Saturn 724+ CCD on beamline I19 at the Diamond Light Source facility. The structure was solved by direct methods. The semi-empirical absorption corrections were applied based on symmetry-equivalent and repeated data. The refinement gave a  $wR2$  of 0.0905 for all 5350 independent reflections and a conventional  $R1$  of 0.0346, for 4838 reflections with  $F^2 > 2\sigma$ . The residual electron density maximum and minimum were 0.37 and  $-0.33 \text{ e } \text{\AA}^{-3}$  respectively.

The hydrogen atoms were placed in geometrically calculated positions with  $U$  constrained to  $1.2 U_{\text{eq}}(\text{C})$  for aromatic hydrogen atoms and  $U$  constrained to  $1.5 U_{\text{eq}}(\text{O})$  for the hydroxyl hydrogen atoms. The full data of compound 6 can be found in Appendix 1.

## Structure Analysis

The asymmetric unit of compound 6 (figure 5.31) shows two half 1,4-benzenedicarboxylate ligands completed by inversion symmetry through the centre of the respective aromatic rings, coordinated to a zinc cation placed on a general position. The zinc cation is a four-coordinate tetrahedral shown in figure 5.32 with slight distortions to the bond angles listed in table 5.10. The two half 1,4-benzenedicarboxylates coordinate to the zinc cation forming monodentate bonds occupying two of the coordination sites Zn-O(1) 1.984(18) Å and Zn-O(5) 1.961(19) Å forming a bridging angle of O(1)-Zn-O(5) 99.37(7)°. The remaining two positions are occupied by one pyridine ligand and one water molecule completing the tetrahedral geometry of the zinc cation (figure 5.32).

This building unit allows the 1,4-benzenedicarboxylate to expand the structure into a two dimensional interwoven sheet due to the cis coordination of the ligands. The inversion symmetry at the centre of the aromatic rings then expands the structure in a 'zigzag' motif to form the interwoven sheet. Although the carboxylate groups are individually coordinated they are fully deprotonated and delocalised with comparable bond lengths; C(7)-O(1) 1.279(3) Å, C(7)-O(2) 1.248(2) Å, C(15)-O(5) 1.278(3) Å and

C(15)-O(6) 1.249(3) Å showing no evidence of a carbon-oxygen single and double bond (figure 5.33). These carboxylate oxygens are involved as acceptors in hydrogen bonding with water molecules of adjacent interpenetrating sheets running perpendicular to the plane at 106.07(9)°, forming the hydrogen bonds O(9)-H(9A)⋯O(6C) 2.671(3) Å and O(9)-H(9B)⋯O(2D) 2.698(3) Å (figure 5.34)(table 5.11).

The interpenetrating packing results in the pyridine ligands slotting between the carboxylate ligands of the adjacent sheet, these pyridines form long range  $\sigma$ - $\pi$  interactions from the aromatic hydrogen's of the 1,4-benzenedicarboxylate ligands partially directing the packing motif. The complex interpenetrating nature of this framework results in the compound being unusable for further applications, this coupled with the poor quality and low yield of crystals prevented further analysis of compound 6 by both elemental analysis and powder X-ray diffractometry.

**Table 5.10: Selected Bond Lengths [Å] and Angles [°] for Compound 6**

Zn–O(1)	1.9843(18)	Zn–O(5)	1.9603(19)
Zn–N	2.034(2)	Zn–O(9)	1.9846(19)
C(7)–O(1)	1.279(3)	C(7)–O(1)	1.243(3)
C(7)–O(2)	1.248(3)	C(15)–O(5)	1.278(3)
C(15)–O(6)	1.249(3)		
O(1)–Zn–O(5)	99.37(7)	O(1)–Zn–N	118.40(8)
O(1)–Zn–O(9)	113.79(8)	O(5)–Zn–N	102.93(9)
O(5)–Zn–O(9)	115.82(8)	N–Zn–O(9)	106.32(8)
Zn–O(1)–C(7)	105.33(15)	Zn–O(5)–C(15)	115.10(15)

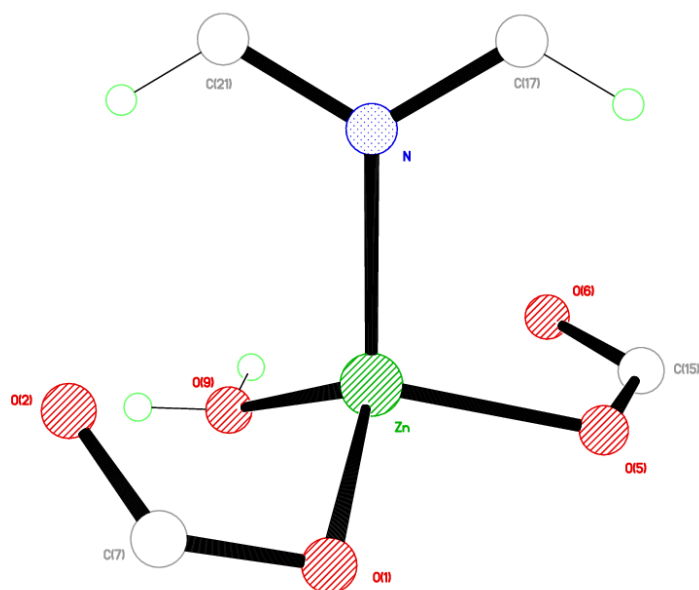
Symmetry operations for equivalent atoms

**Table 5.11: Selected Hydrogen bond Lengths [Å] and angles [°] for Compound 6**

D–H...A	d(D–H)	d(H...A)	d(D...A)	(DHA)
O(9)–H(9A)...O(6C)	0.79(6)	1.88(6)	2.671(3)	171(5)
O(9)–H(9B)...O(2D)	0.78(5)	1.92(5)	2.698(3)	174(5)

Symmetry operations for equivalent atoms

C  $-x+3/2, y+1/2, -z+3/2$  D  $-x+3/2, y-1/2, -z+3/2$

**Figure 5.32: Tetrahedral coordination environment of the Zn cation in compound 6**

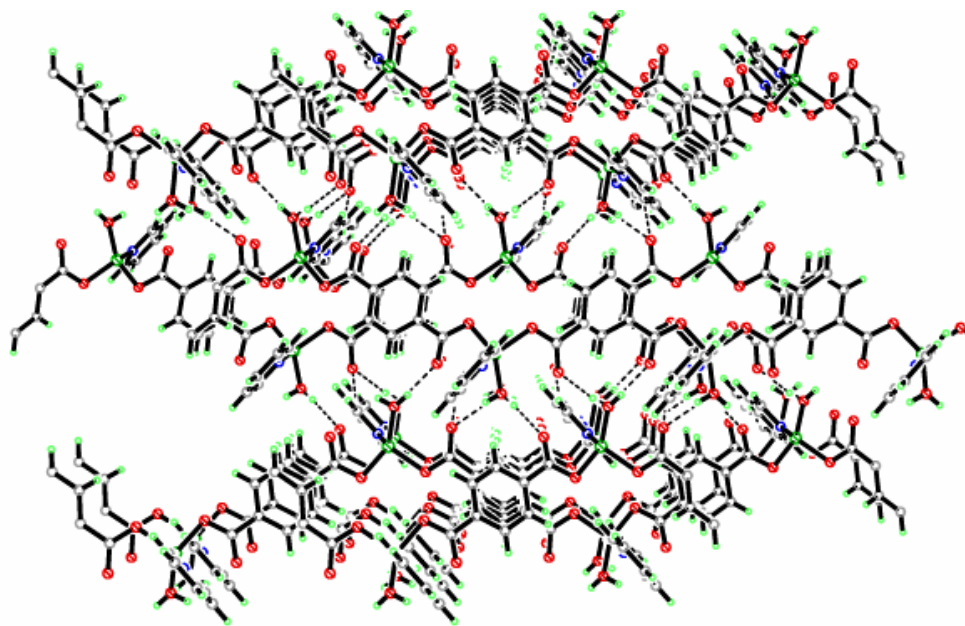


**Figure 5.33:** Two dimensional interpenetrating ‘zigzag’ sheet of compound 6 viewed down the *a*-axis

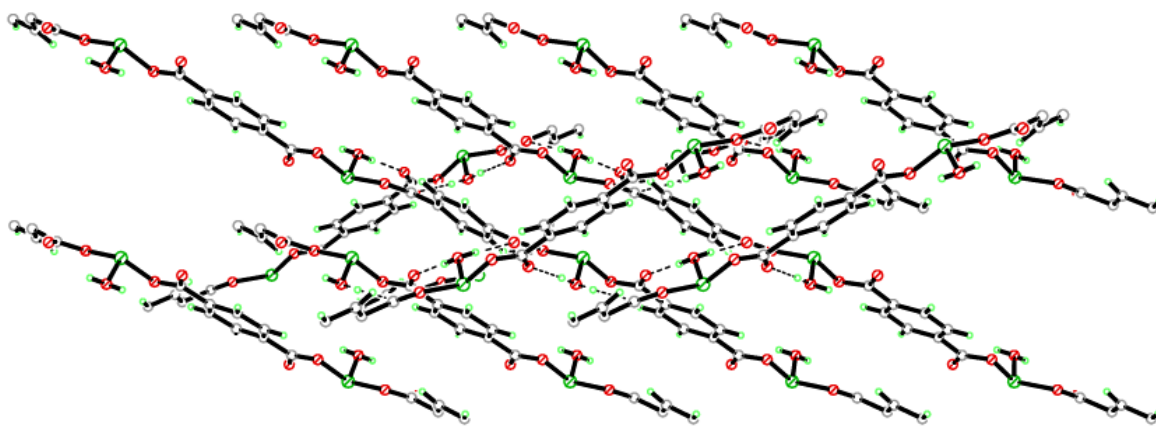


**Figure 5.34:** Three dimensional packing of the interpenetrating sheets in compound 6 viewed down the *b*-axis

**Compound 7:**  $[\text{Cd}(\text{C}_8\text{H}_4\text{O}_4)(\text{C}_{10}\text{H}_8\text{N}_2)]$ 

---

Chemical formula (total)	$\text{C}_{18}\text{H}_{12}\text{CdN}_2\text{O}_4$
Formula weight	432.70
Temperature	120(2) K
Radiation, wavelength	synchrotron, 0.6889 Å
Crystal system, space group	monoclinic, $I2/a$
Unit cell parameters	$a = 16.055(5)$ Å $\beta = 90.160(3)^\circ$ $b = 11.722(3)$ Å $c = 40.187(12)$ Å
Cell volume	$7563(4)$ Å <sup>3</sup>
<i>Z</i>	16
Crystal colour and size	colourless, $0.10 \times 0.04 \times 0.00$ mm <sup>3</sup>
Final <i>R</i> indices [ $F^2 > 2\sigma$ ]	$R1 = 0.1682$
<i>R</i> indices (all data)	$wR2 = 0.4350$
Largest diff. peak and hole	2.01 and $-1.67$ e Å <sup>-3</sup>

---

**Figure 5.35: Asymmetric Unit of Compound 7 all unique atoms labelled****Synthesis**

1 mL of a solution of  $\text{Cd}(\text{NO}_3)_2 \cdot 4\text{H}_2\text{O}$  (0.1 g, 0.33 mmol) in dimethylformamide (DMF) (10 mL) was syringed into one side of the H-Cell vessel, 1 mL of a solution of 1,4-benzenedicarboxylic acid (0.028 g, 0.17 mmol) in DMF (10 mL) and 1 mL of a solution of 4,4'-bipyridine (0.027 g, 0.17 mmol) in DMF (10 mL) were then syringed into the other side of the H-Cell vessel. The independent solutions were bridged by 2 mL water that was carefully layered into the bridging tube. After nine weeks, colourless spindle crystals formed.

## Structure Determination

The data were collected at 120 K using synchrotron radiation on a Crystal Logic diffractometer and Rigaku Saturn 724+ CCD on beamline I19 at the Diamond Light Source facility. The structure was solved by direct methods. The semi-empirical absorption corrections were applied based on symmetry-equivalent and repeated data. The refinement gave a  $wR2$  of 0.4350 for all 6576 independent reflections and a conventional  $R1$  of 0.1682, for 5427 reflections with  $F^2 > 2\sigma$ . The residual electron density maximum and minimum were 2.01 and  $-1.67 \text{ e}\text{\AA}^{-3}$  respectively, the high residual electron density in compound 7 occurs due to unmodelled disorder introduced by twinning.

The hydrogen atoms were placed in geometrically calculated positions with  $U$  constrained to  $1.2 U_{\text{eq}}(\text{C})$  for aromatic hydrogen atoms. The pyridine ligands in the structure were disordered and FLAT restraints were imposed upon them. The full data of compound 7 can be found in Appendix 1.

## Structure Analysis

The asymmetric unit of compound 7 (figure 5.35) shows two complete 1,4-benzenedicarboxylate ligands, coordinating two cadmium cations Cd(1) and Cd(2) to form sheets. The sheets are then coordinated into three dimensions by two 4,4'-bipyridine ligands coordinated cis to the carboxylate ligands on the cadmium cations. The cadmium cations in compound 7 are both six-coordinate distorted octahedral geometries (figure 5.36). The Cd(1) cation is coordinated to two unique 1,4-benzenedicarboxylate ligands, the first ligand is bifurcated coordinating through both carboxylate oxygens to form a bite angle of O(1)-Cd(1)-O(2)  $53.9(7)^\circ$ , much smaller than the normal  $90^\circ$  angle for a octahedral geometry. The second 1,4-benzenedicarboxylate ligand coordinates in a coplanar cis position through the O(5) carboxylate oxygen, O(1)-Cd(1)-O(5)  $89.9(7)^\circ$ , the additional oxygen of this carboxylate (O(6)) coordinates to a symmetry equivalent Cd(1) cation at an angle of O(5)-Cd(1)-O(6A)  $128.4(8)^\circ$  and O(1)-Cd(1)-O(6A)  $141.8(7)^\circ$  completing the carboxylate coordination to Cd(1) occupying four planar coordination sites. The remaining two

coordination sites perpendicular to the carboxylate groups are occupied by a 4,4'-bipyridine ligand and its trans symmetry equivalent O(1)-Cd(1)-N(1) 92.2(7)° and N(1)-Cd(1)-N(2A) 174.9(7)° (figure 5.36A).

The six-coordinate Cd(2) cation also forms a distorted octahedral geometry coordinating to the remaining carboxylate groups of the two unique 1,4-benzenedicarboxylate ligands. In a similar binding motif to the Cd(1) cation it coordinates to both carboxylate oxygens of the bidentate carboxylate group O(7)-C(16)-O(8) with a bite angle of 53.3(8)°. The Cd(2) cation further coordinates to a coplanar cis 1,4-benzenedicarboxylate oxygen O(7)-Cd(2)-O(3) 88.1(9)° and its coplanar symmetry equivalent at angles O(8)-Cd(2)-O(4) 83.7(9)° and O(3)-Cd(2)-O(4D) 131.6(10)° completing the coordination in this plane. Additional coordination sites are occupied by the second 4,4'-bipyridine ligand and its trans symmetry equivalent; N(3)-Cd(2)-N(4) 166.4(11)° to complete the distorted octahedral geometry of the Cd(2) cation (figure 5.36B)(table 5.12).

The Cd(1) and Cd(2) cations form similar secondary building units with their respective symmetry equivalent Cd(1A) and Cd(2A) cations generated through a two-fold screw axis forming a six blade paddle-wheel (figure 5.37). These secondary building units expand the structure into a three dimensions forming 1,4-benzenedicarboxylate sheets down the *a*-axis and along the *c*-axis connecting columns of cadmium cations. These sheets are coordinated together through the 4,4'-bipyridine ligands that form columns down the *b*-axis, this coordination motif forms a 4,4' grid network containing nanochannels with dimensions 10.137(7) by 11.722(7) Å. To minimize natural void space within the crystal, the structure is interpenetrated by an uncoordinated identical anti-parallel framework running through the structure. The interpenetrating system forms strong hydrogen bonds between the aromatic systems of the 4,4'-bipyridine ligands and the aromatic hydrogen's of the 1,4-benzenedicarboxylate ligands in the adjacent framework, forming the  $\sigma$ - $\pi$  hydrogen bonds of an average length of 2.673 Å. The presence of the interpenetrating framework dramatically reduces the pore dimensions to 5.911(2) by 11.036(7) Å and 4.790(2) by 5.911(2) Å (figure 5.38).

PLATON<sup>9</sup> confirms the presence of these pores with a calculated pore volume 1482 Å<sup>3</sup> per unit cell corresponding to 19.6 %. Although the pores have been



dramatically reduced in size by the interpenetration, the ‘free’ accessible voids would aid gas adsorption, along with the dual sized pores compound 7 may be capable of molecular sieving and selective gas adsorption.

Unfortunately further analysis and characterisation of the pores and purity of the sample could not be carried out due to the limitations of the low product yield from the reaction using the H-Cell apparatus. Multiple repeat and scale-up synthesis were carried out but reproducibility and elongated crystallisation times proved a major hindrance in the formation of the pure bulk samples of compound 7.

The structure CUHPUR was reported by Zaworotko *et al.*<sup>10</sup> that shows a packing motif similar to the non interpenetrated topology of compound 7 (figure 5.39). This 4,4’ net is achieved through the inclusion of three DMF and 1 water molecules in the pores to fill the vacant voids. The topology of CUHPUR and compound 7 differ at the metal nodes as CUHPUR has dual bis-bidentate carboxylate moieties per cadmium cation compared to the single bi-bidentate carboxylate and bridging carboxylate present in compound 7. Although this alters the secondary building unit it does not prevent the interpenetration of this compound that forms at higher temperatures.<sup>10</sup> The structure reported by Zaworotko is produced using a rapid solvothermal technique allowing bulk production of both the non-interpenetrated and interpenetrated forms with bulk purity remaining a significant problem preventing further analysis of the compound.<sup>10</sup>

**Table 5.12: Selected Bond Lengths [ $\text{\AA}$ ] and Angles [ $^\circ$ ] for Compound 7**

Cd(1)–O(1)	2.490(2)	Cd(1)–O(2)	2.290(18)
Cd(1)–O(5)	2.226(19)	Cd(1)–O(6A)	2.240(2)
Cd(1)–N(1)	2.340(13)	Cd(1)–N(2B)	2.410(13)
Cd(2A)–O(3)	2.250(2)	Cd(2A)–O(4C)	2.170(3)
Cd(2A)–O(7D)	2.610(3)	Cd(2A)–O(8D)	2.370(2)
Cd(2A)–N(4E)	1.960(4)	Cd(2B)–N(3)	2.070(3)
O(1)–Cd(1)–O(2)	53.9(7)	O(1)–Cd(1)–O(5)	89.8(7)
O(1)–Cd(1)–O(6A)	141.8(7)	O(1)–Cd(1)–N(1)	92.2(7)
O(1)–Cd(1)–N(2B)	92.8(6)	N(1)–Cd(1)–N(2B)	174.9(7)
O(3)–Cd(2A)–O(4C)	131.6(10)	O(3)–Cd(2A)–O(7D)	88.1(9)
O(3)–Cd(2A)–O(8D)	140.5(12)	O(3)–Cd(2A)–N(4E)	91.3(12)
O(3)–Cd(2B)–N(3)	103.3(11)	O(6)–Zn(2)–O(9)	102.0(2)
Cd(1)–O(1)–C(7)	87.2(16)	Cd(1)–O(2)–C(7)	97.0(14)
Cd(2A)–O(3)–C(8)	125.0(2)	Cd(2B)–O(3)–C(8)	127.0(2)
Cd(1)–O(5)–C(15)	118.3(17)	Cd(1A)–O(6)–C(15)	169.0(2)
Cd(2AF)–O(7)–C(16)	89.4(18)	Cd(2AF)–O(8)–C(16)	97.9(16)

Symmetry operations for equivalent atoms

A  $-x+1/2, -y+3/2, -z+3/2$    B  $x, y-1, z$    C  $-x+3/2, y, -z+1$

D  $x, -y+3/2, z-1/2$    E  $x, y+1, z$

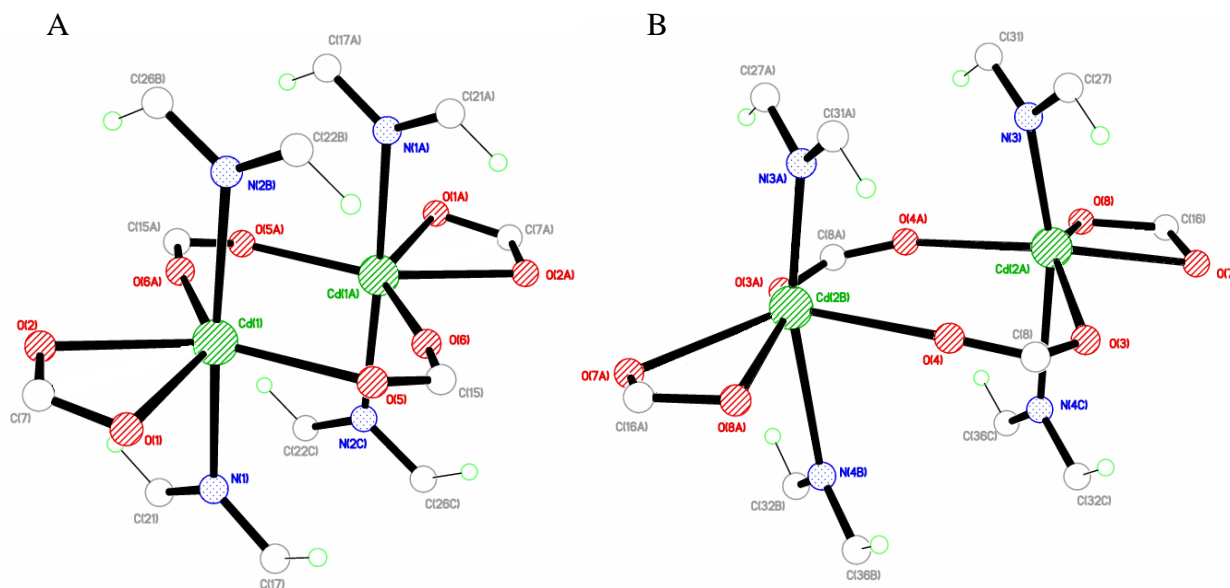


**Figure 5.36:** A) Octahedral coordination environment of Cd(1)-Cd(1A) and B) Octahedral coordination environment of Cd(2)-Cd(2A) in compound 7

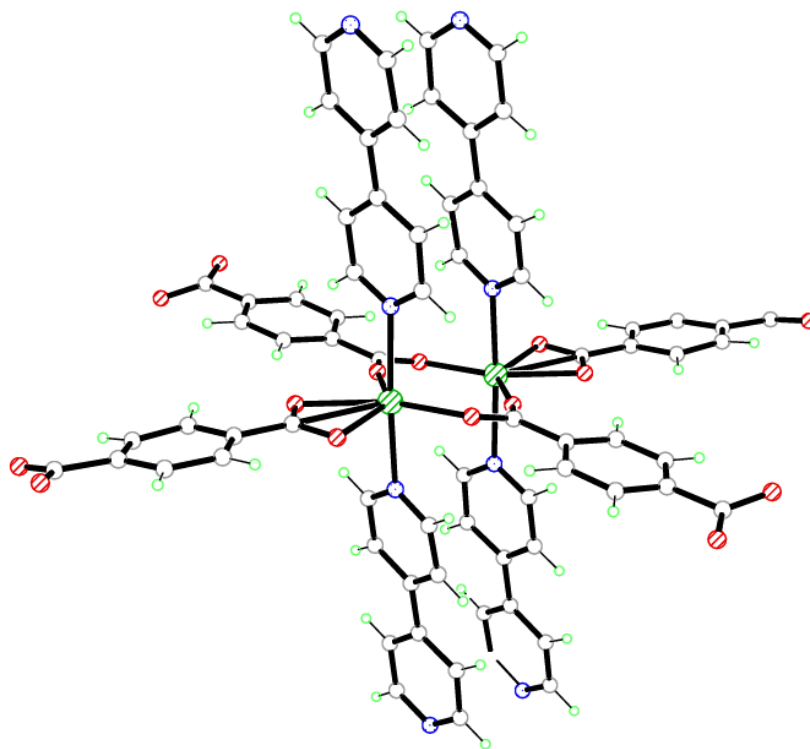


**Figure 5.37:** Secondary building unit of Cd(1)-Cd(1A) and Cd(2)-Cd(2A) six-blade paddle-wheel coordination in compound 7

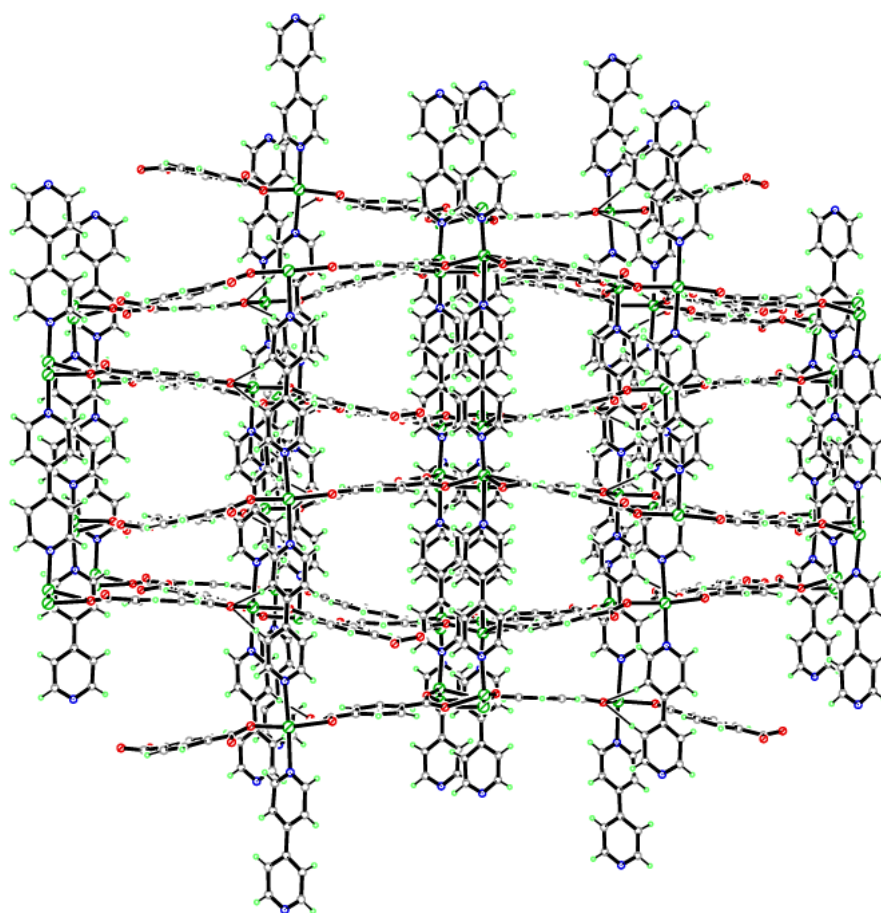


**Figure 5.38:** Three dimensional packing of the interpenetrated compound **7** viewed down the *a*-axis

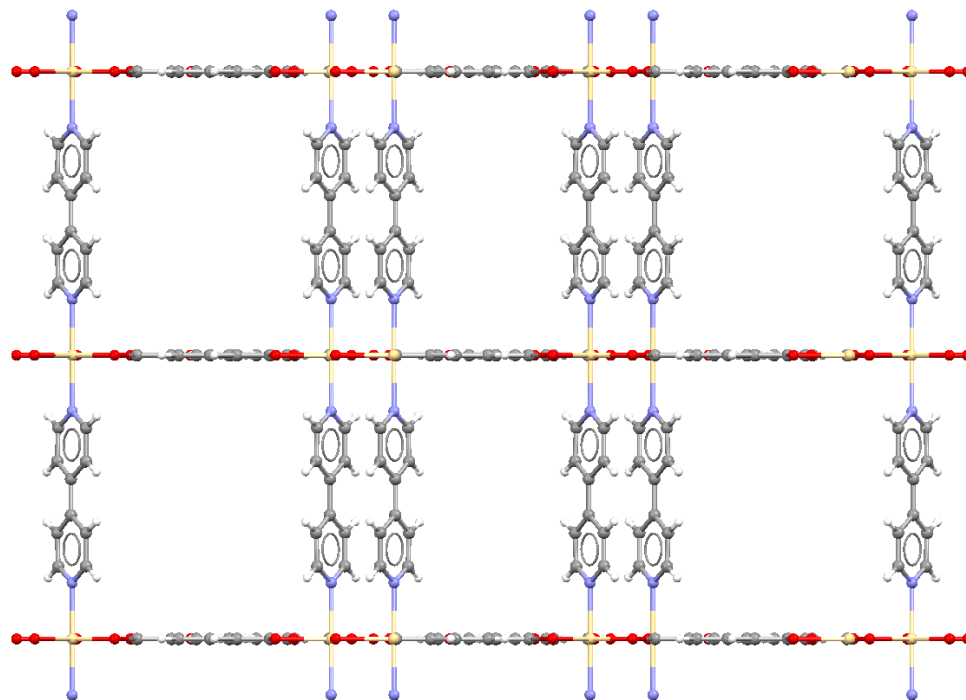
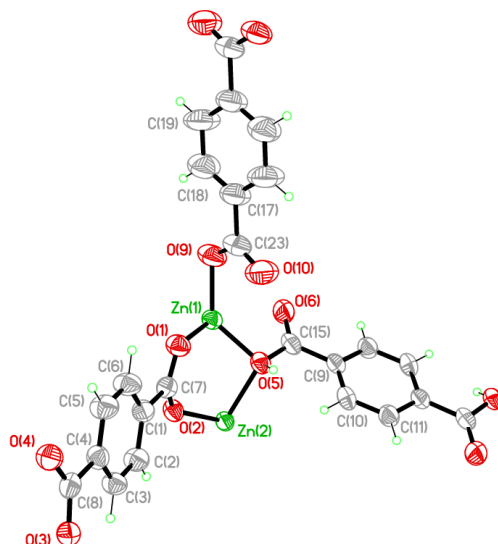


**Figure 5.39:** Three dimensional packing of non-interpenetrated CUHPUR viewed down the *b*-axis<sup>10</sup>

**Compound 8:**  $[\text{Zn}_3(\text{C}_8\text{H}_4\text{O}_4)_3(\text{C}_8\text{H}_6\text{O}_4)]$

---



Chemical formula (total)	$\text{C}_{32}\text{H}_{18}\text{O}_{16}\text{Zn}_3$
Formula weight	854.57
Temperature	120(2) K
Radiation, wavelength	synchrotron, 0.6889 Å
Crystal system, space group	monoclinic, $C2/c$
Unit cell parameters	$a = 32.943(11)$ Å $\beta = 93.922(5)^\circ$ $b = 9.642(3)$ Å $c = 18.253(6)$ Å
Cell volume	$5784(3)$ Å <sup>3</sup>
<i>Z</i>	4
Crystal colour and size	colourless, $0.04 \times 0.02 \times 0.01$ mm <sup>3</sup>
Final <i>R</i> indices [ $F^2 > 2\sigma$ ]	$R1 = 0.0489$
<i>R</i> indices (all data)	$wR2 = 0.1229$
Largest diff. peak and hole	0.57 and $-0.47$ e Å <sup>-3</sup>

**Figure 5.40: Asymmetric Unit of Compound 8 all unique atoms labelled, additional atoms added to complete ligands.**

**Synthesis**

2 mL of a solution of  $\text{Zn}(\text{NO}_3)_2 \cdot 6\text{H}_2\text{O}$  (0.1 g, 0.33 mmol) in water (10 mL) was layered over 2 mL of a solution of 1,4-benzenedicarboxylic acid (0.028 g, 0.17 mmol) in water (10 mL) in small sample vial. The vial was covered and left until crystallisation was complete. After four weeks, colourless plate crystals formed.

## Structure Determination

The data were collected at 120 K using synchrotron radiation on a Crystal Logic diffractometer and Rigaku Saturn 724+ CCD on beamline I19 at the Diamond Light Source facility. The structure was solved by direct methods. The semi-empirical absorption corrections were applied based on symmetry-equivalent and repeated data. The refinement gave a  $wR2$  of 0.1229 for all 5205 independent reflections and a conventional  $R1$  of 0.0489, for 3614 reflections with  $F^2 > 2\sigma$ . The residual electron density maximum and minimum were 0.57 and  $-0.47 \text{ e\AA}^{-3}$  respectively.

The hydrogen atoms were placed in geometrically calculated positions with  $U$  constrained to  $1.2 U_{eq}(C)$  for aromatic hydrogen atoms, no restraints or constraints were imposed on compound 8. The full data of compound 8 can be found in Appendix 1.

## Structure Analysis

The asymmetric unit of compound 8 (figure 5.40) shows a complete 1,4-benzenedicarboxylate ligand and two half 1,4-benzenedicarboxylate ligand completed by inversion symmetry through the centre of the aromatic ring. These ligands join two zinc cations Zn(1) and Zn(2) that are in two different coordination environments in this polymeric compound. The Zn(1) cation is a four-coordinate tetrahedral, whilst the Zn(2) cation is positioned on an inversion centre and forms a six-coordinate octahedral geometry through symmetry (figure 5.41).

The four-coordinate Zn(1) cation is coordinated to all three unique 1,4-benzendicarboxylate ligands through one oxygen atom on each carboxylate group at the angles O(1)-Zn(1)-O(5)  $99.99(11)^\circ$ , O(1)-Zn(1)-O(9)  $104.83(12)^\circ$  and the symmetry equivalent O(1)-Zn(1)-O4A)  $109.35(12)^\circ$  forming the standard tetrahedral geometry shown in figure 5.41A (table 5.13).

The six coordinate Zn(2) cation is connected to the Zn(1) cation by the complete 1,4-benzenedicarboxylate bridging ligand forming the bite angle of Zn(1)-O(1)-C(7)-O(2)-Zn(2)  $118.2(4)^\circ$  with additional coordination by the bridging carboxylate oxygen O(5) with a bite angle of Zn(1)-O(5)-Zn(2)  $101.67(10)^\circ$ . The third coordination position is occupied by the symmetry equivalent of the complete 1,4-benzenedicarboxylate

ligand in the cis position O(2)-Zn(2)-O(3A) 94.41(10)° allowing this ligand to bridge both zinc cations and symmetry equivalents using both carboxylate groups. The remaining coordination sites on the six-coordinate Zn(2) cation are filled by the trans symmetry equivalents of the respective ligands generated through the inversion symmetry at the centre of the Zn(2) cation to form the octahedral geometry shown in figure 5.41B.

The 1,4-benzenedicarboxylates act as bridging ligands between the zinc cations, the inversion symmetry at the centre of the Zn(2) cation expands these bridging units to form a zinc trinuclear building unit (figure 5.42). This secondary building unit is similar to that present in compounds 3 and 4 that both contain a linear trinuclear cluster of cations; however in both these structures the trinuclear clusters are capped at the ends preventing the structure from coordinating in all three dimensions. In contrast the trinuclear cluster in compound 8 has terminal 1,4-benzenedicarboxylate ligands that expand the structure through inversion symmetry at the centre of the ligands aromatic ring. The extensively bridged secondary building unit of compound 8 is clearly shown in figure 5.43 with only the coordinated functional groups visible, this arrangement and the coordination geometries of the zinc nodes can be directly compared to those in the secondary building unit of compound 3 shown previously in figure 5.13. Both compounds have similar bond lengths and angles with a direct comparison shown in table 5.14. Significant differences in the two building units include the differing terminal ligands with compound 8 coordinating to the bridging 1,4-benzenedicarboxylate ligand and the coordination mode of one 1,4-benzenedicarboxylate ligand. In compound 3 both bridging ligands are bidentate coordinating through both carboxylate oxygens, compound 8 has one bidentate carboxylate bridge and a bifurcated bridging oxygen atom O(5) that coordinates both zinc cations and twists the ligand 90° clockwise leaving one carboxylate oxygen uncoordinated. The uncoordinated carboxylate oxygen O(6) has a comparable bond length of C(15)-O(6) 1.241(5) Å to the C(15)-O(5) 1.303(4) Å bond indicating that although it is uncoordinated the carboxylate group is fully delocalised.

The zinc cations in compound 8 form linear columns that run down the *a*-axis and along the *b*-axis. These columns are held together by the bridging 1,4-



benzenedicarboxylate ligands to form double layer sheets that run down the *b*-axis and along the *c*-axis (figure 5.44). This double layer motif is similar to those in both compound 3 (figure 5.15) and compound 4 (figure 5.20), in the previous compounds the sheets then pack together in offset patterns to form strong hydrogen bonding between the layers to hold the structure together. The additional 1,4-benzenedicarboxylate ligand forces the sheets coplanar running parallel with respect to each other, these rigid ligands act as pillars between the sheets running along the *a*-axis preventing the sheets from adopting the off-set packing motif. This highlights the significance of the terminal ligand in the trinuclear building unit on the overall topology and packing motif of the compounds and illustrates the templating effects of alternative solvent molecules.

Compound 8 forms a 4,4' net structure with nanochannels of dimensions 9.125 (4) by 10.488(6) Å running down the *a*-axis (figure 5.44), these nanochannels are then intersected by additional channels running through the structure down the *c*-axis (figure 5.45) creating a highly porous material.

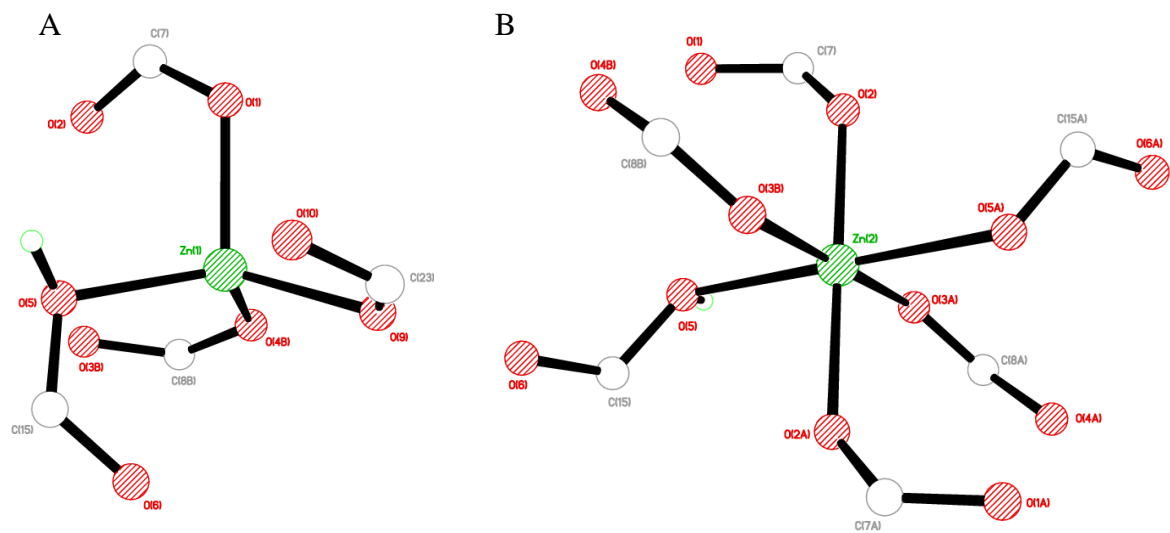
Compound 8 was synthesised using direct addition methods similar to those used to produce compounds 3 and 4 reported in this thesis. These structures clearly show the reproducibility of this method to form a predictable trinuclear secondary building unit using a range of transition metals. They also highlight the importance of the solvent and templating agents on structure topology formation within these structures enabling them to be used as a base for further investigations on structural analogues with different functionalities. The synthesis of compound 8 shows how the 'fine-tuning' of the reaction conditions used to synthesize compounds 3 and 4, can be modified to favour the 1,4-benzenedicarboxylate ligand coordination forming the desired fully coordinated three dimensional porous framework.

**Table 5.13: Selected Bond Lengths [ $\text{\AA}$ ] and Angles [ $^\circ$ ] for Compound 8**

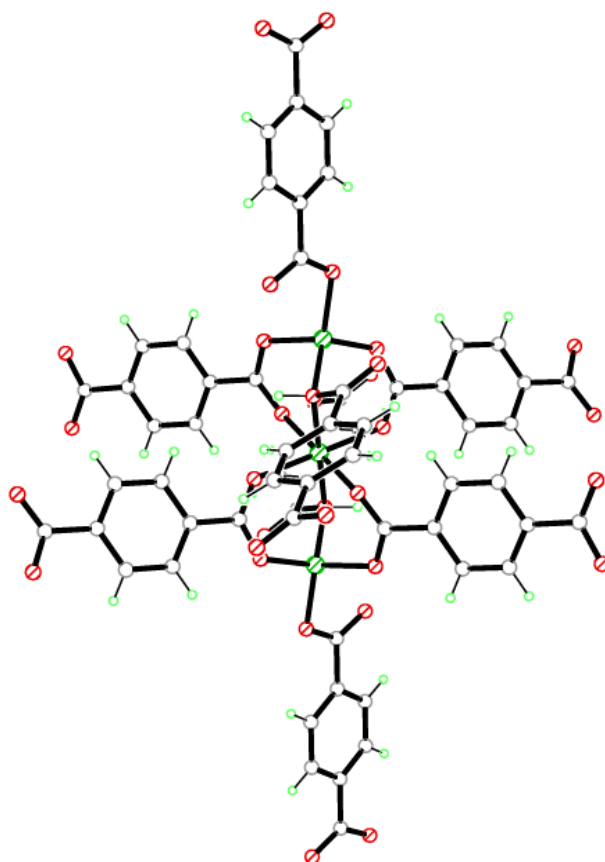
Zn(1)–O(1)	1.970(3)	Zn(1)–O(4A)	1.950(3)
Zn(1)–O(5)	1.965(3)	Zn(1)–O(9)	1.937(3)
Zn(2)–O(2)	2.027(3)	Zn(2)–O(3A)	2.033(3)
Zn(2)–O(5)	2.194(2)	C(7)–O(1)	1.270(5)
C(7)–O(2)	1.243(4)	C(8)–O(3)	1.247(5)
C(8)–O(4)	1.271(4)	C(15)–O(5)	1.303(4)
C(15)–O(6)	1.221(5)	C(23)–O(9)	1.243(6)
C(23)–O(10)	1.237(6)		
O(1)–Zn(1)–O(4A)	109.35(12)	O(1)–Zn(1)–O(5)	99.99(11)
O(1)–Zn(1)–O(9)	104.83(12)	O(2)–Zn(2)–O(2B)	179.997(1)
O(2B)–Zn(2)–O(3A)	85.59(10)	O(2)–Zn(2)–O(3A)	94.41(10)
O(2)–Zn(2)–O(5)	90.82(10)	Zn(1)–O(5)–Zn(2)	101.67(10)
Zn(1)–O(1)–C(7)	115.9(3)	Zn(2)–O(2)–C(7)	135.8(2)
Zn(1E)–O(4)–C(8)	123.5(2)	Zn(2D)–O(3)–C(8)	134.4(3)
Zn(1)–O(5)–C(15)	107.0(2)	Zn(2)–O(5)–C(15)	123.4(2)
Zn(1)–O(9)–C(23)	109.4(3)		
Symmetry operations for equivalent atoms			
A	$x, -y+1, z+1/2$	B	$-x+1/2, -y+3/2, -z+1$
D	$-x+1/2, y-1/2, -z+1/2$		
E	$x, -y+1, z-1/2$		

**Table 5.14: Average bond length comparisons between Compound 8, Compound 3 and Compound 4**

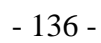
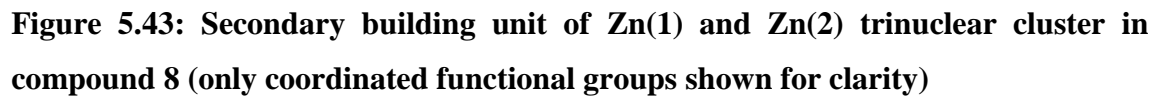
Compound	Bond	Average Bond Length ( $\text{\AA}$ )
Compound 3	Zn–O (carboxylate)	2.004
Compound 3	Zn–O (DMF)	1.986
Compound 4	Zn–O (carboxylate)	2.101
Compound 4	Zn–O (DMF)	2.103
Compound 8	Zn–O (carboxylate)	2.011



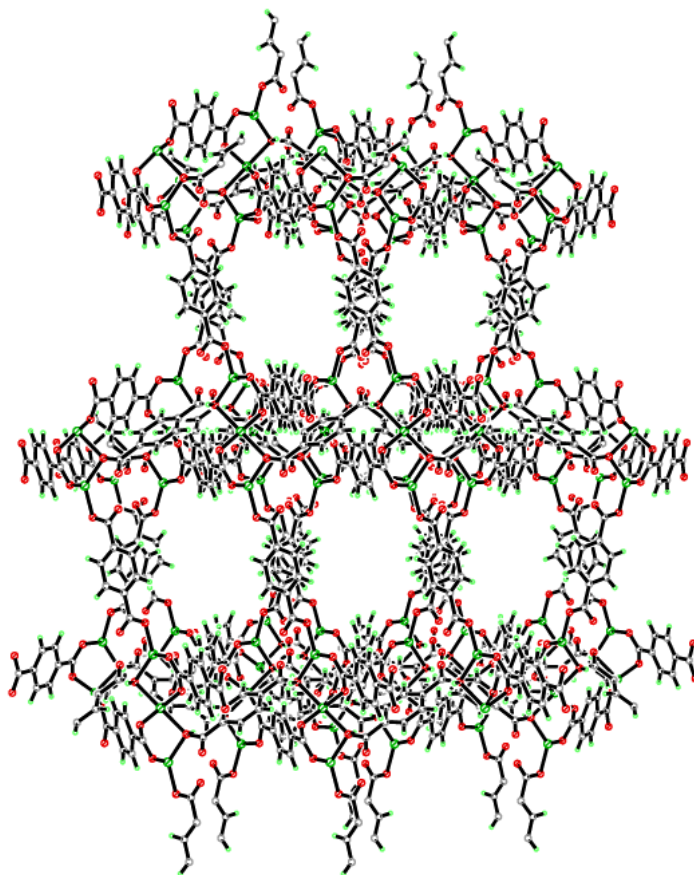
**Figure 5.41: A) Tetrahedral coordination environment of Zn(1) and B) Octahedral coordination environment of Zn(2) in compound 8**



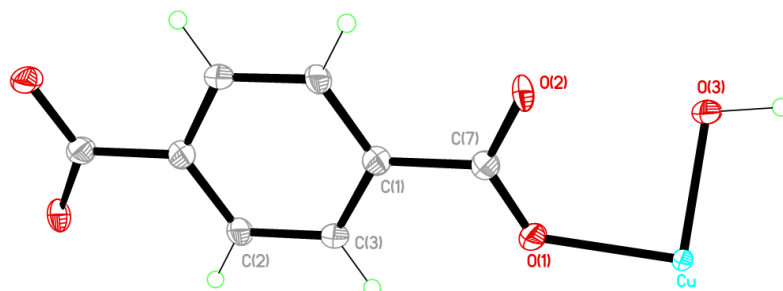
**Figure 5.42: Secondary building unit of Zn(1) and Zn(2) trinuclear cluster in compound 8**



**Figure 5.44: Three dimensional 4,4' net of compound 8 viewed down the *a*-axis**



**Figure 5.45: Three dimensional packing of double layer sheets in compound 8 viewed down the *c*-axis**

**Compound 9:**  $[\text{Cu}_2(\text{C}_8\text{H}_4\text{O}_4)(\text{HO})_2]$ 

Chemical formula (total)	$\text{C}_8\text{H}_6\text{Cu}_2\text{O}_6$
Formula weight	325.21
Temperature	120(2) K
Radiation, wavelength	synchrotron, 0.6889 Å
Crystal system, space group	monoclinic, $P2_1/n$
Unit cell parameters	$a = 3.476(3)$ Å $b = 5.852(5)$ Å $c = 21.630(17)$ Å $\beta = 94.216(8)^\circ$
Cell volume	$438.8(6)$ Å <sup>3</sup>
Z	2
Crystal colour and size	blue, $0.05 \times 0.01 \times 0.01$ mm <sup>3</sup>
Final $R$ indices [ $F^2 > 2\sigma$ ]	$R1 = 0.0668$
$R$ indices (all data)	$wR2 = 0.1981$
Largest diff. peak and hole	1.73 and $-1.17$ e Å <sup>-3</sup>

**Figure 5.46: Asymmetric Unit of Compound 9 all unique atoms labelled, additional atoms added to complete ligands.**

**Synthesis**

2 mL of a solution of  $\text{Cu}(\text{NO}_3)_2 \cdot 6\text{H}_2\text{O}$  (0.09 g, 0.33 mmol) in water (10 mL) was layered over 2 mL of a solution of 1,4-benzenedicarboxylic acid (0.028 g, 0.17 mmol) and sodium hydroxide (0.23g, 6 mmol) in water (10 mL) in small sample vial. The vial was covered and left until crystallisation was complete. After five weeks, blue spindle crystals formed.

**Structure Determination**

The data were collected at 120 K using synchrotron radiation on a Crystal Logic diffractometer and Rigaku Saturn 724+ CCD on beamline I19 at the Diamond Light Source facility. The structure was solved by direct methods. The semi-empirical

absorption corrections were applied based on symmetry-equivalent and repeated data. The refinement gave a  $wR2$  of 0.1981 for all 922 independent reflections and a conventional  $R1$  of 0.0668, for 806 reflections with  $F^2 > 2\sigma$ . The residual electron density maximum and minimum were 1.73 and  $-1.17 \text{ e}\text{\AA}^{-3}$  respectively, the high residual electron density is a result of unmodelled disorder produced from twinning within compound 9

The hydrogen atoms were placed in geometrically calculated positions with  $U$  constrained to  $1.2 U_{\text{eq}}(\text{C})$  for aromatic hydrogen atoms and  $U$  constrained to  $1.5 U_{\text{eq}}(\text{O})$  for the hydroxyl hydrogen atoms., no restraints or constraints were imposed on compound 9. The full data of compound 9 can be found in Appendix 1.

## Structure Analysis

The asymmetric unit of compound 9 (figure 5.46) shows half a 1,4-benzenedicarboxylate ligand completed by inversion symmetry around the centre of its aromatic ring, coordinated to a copper cation placed on a general position. The copper cation in compound 9 is a five-coordinate trigonal bipyramidal (figure 5.47) with distorted bond angles of O(1)-Cu-O(2A)  $167.2(4)^\circ$ , O(1)-Cu-O(3)  $91.5(3)^\circ$  and O(3)-Cu-O(3A)  $133.8(2)^\circ$ . The copper cation coordinates to a symmetry equivalent 1,4-benzenedicarboxylate ligand in the coplanar trans position, acting as a bidentate bridging ligand between symmetry equivalent copper cations by coordinating through both carboxylate oxygen atoms to form strong Cu-O bonds; Cu-O(1)  $2.053(8) \text{ \AA}$  and Cu-O(2)  $2.020(8) \text{ \AA}$ . The remaining three coordination sites are filled by a triply bridging hydroxide group and its cis symmetry equivalents to form the secondary building unit in figure 5.48. The triply bridged hydroxides link the copper cations together to form a sheet running down the  $a$ -axis and along the  $b$ -axis (figure 5.49), with the hydroxide O-H alternating in direction by  $90^\circ$  in the plane of the  $c$ -axis due to two-fold rotation symmetry running down the  $b$ -axis. These sheets are connected by the 1,4-benzenedicarboxylate ligands that run parallel along the  $c$ -axis as shown in figure 5.49, forming coplanar columns that stack down the  $b$ -axis (figure 5.50) with alternating rows that are staggered due to the glide plane running through the  $b$ -axis. This

coordination geometry of the copper cation coupled with the symmetry forms a tightly packed framework with no accessible pore volume.

Further analysis of the bulk material by powder X-ray diffraction and elemental analysis was carried out on the bulk material of compound 9 to determine overall purity. The elemental analysis produced results of C = 34.57 %, H = 2.87% and N = 0.58% which show discrepancies between the calculated values from the single crystal data of C = 29.51 %, H = 1.84 % and N = 0 %. The powder diffraction pattern produced shown in figure 5.51 shows significant discrepancy between the predicted powder diffraction pattern produced by the single crystal data with additional peaks present at 11.2 and 18.1 2-Theta indicating that the bulk of the sample of compound 9 is not pure.

Compound 9 produced an interesting secondary building unit, by the increase in sodium hydroxide concentration creating a system with fully deprotonated 1,4-benzenedicarboxylate ligands along with a triply bridged metal node building unit. This method was successfully employed to produce several 1,2,4,5-benzenetetracarboxylate frameworks discussed later in this thesis.



**Table 5.15: Selected Bond Lengths [Å] and Angles [°] for Compound 9**

Cu—O(1)	2.053(8)	Cu—O(2A)	2.020(8)
Cu—O(3)	2.045(8)	Cu—O(3B)	2.010(8)
Cu—O(3A)	2.099(9)	C(7)—O(1)	1.267(14)
C(7)—O(2)	1.270(14)		
O(1)—Cu—O(2A)	167.2(4)	O(1)—Cu—O(3)	91.5(3)
O(1)—Cu—O(3B)	89.6(3)	Cu—O(1)—C(7)	128.3(8)
CuD—O(2)—C(7)	133.8(8)	Cu—O(3)—CuE	126.7(4)
CuE—O(3)—CuD	115.6(4)	Cu—O(3)—CuD	102.3(4)

Symmetry operations for equivalent atoms

A  $-x+3/2, y+1/2, -z+3/2$       B  $-x+1/2, y+1/2, -z+3/2$

D  $-x+3/2, y-1/2, -z+3/2$       E  $-x+1/2, y-1/2, -z+3/2$

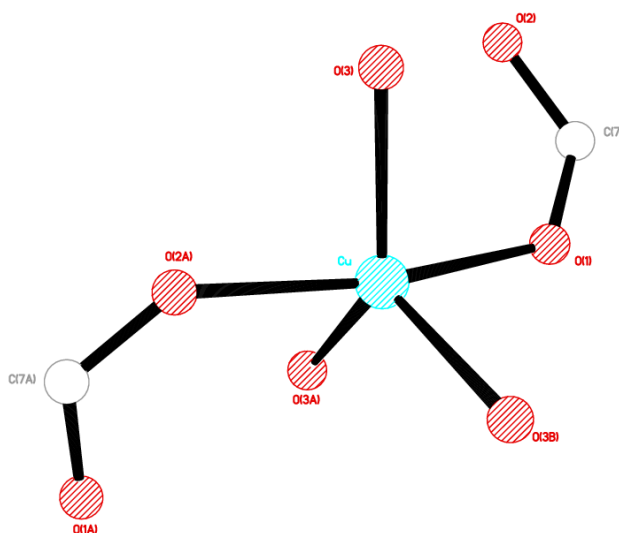


**Figure 5.47: Trigonal bipyramidal coordination environment of the copper cation in compound 9**

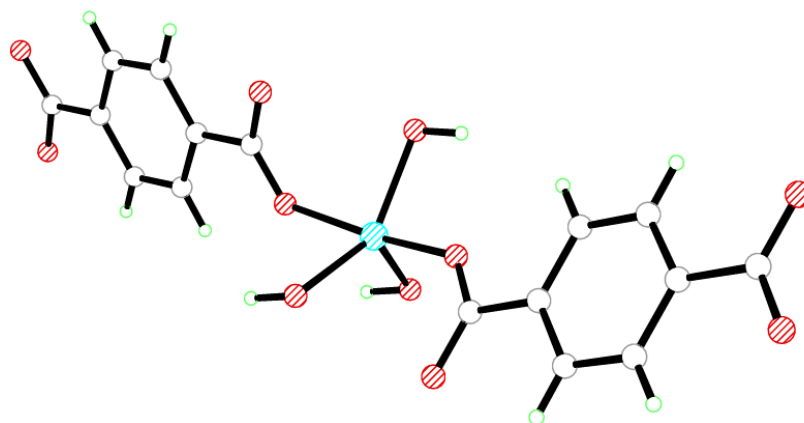


**Figure 5.48:** Secondary building unit of the copper cation in compound 9

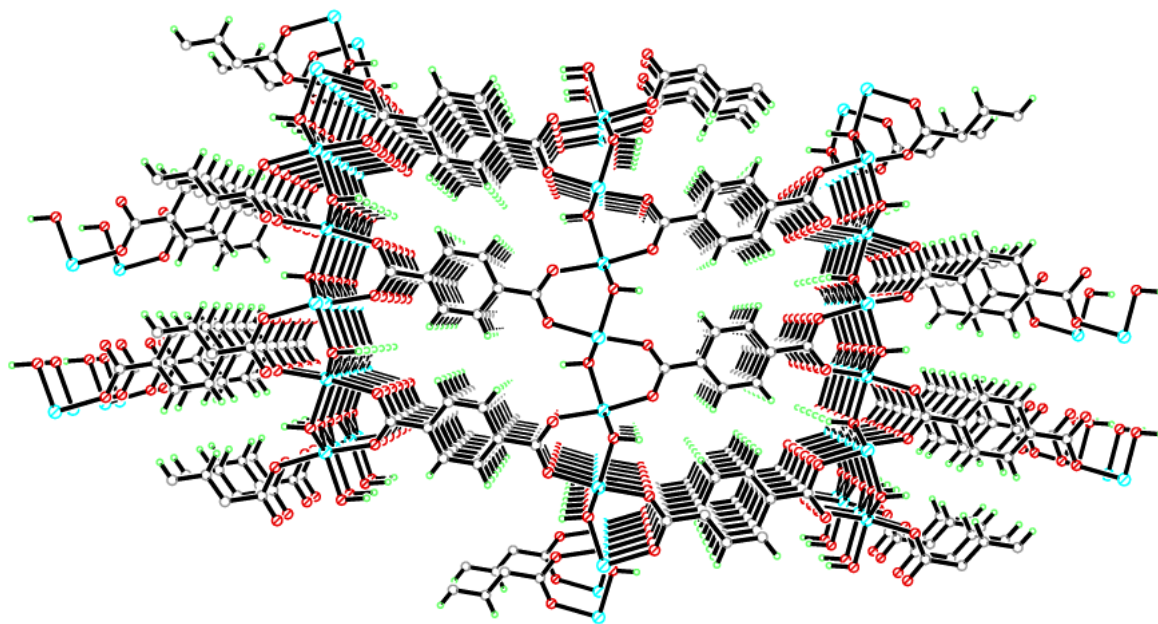


**Figure 5.49:** Three dimensional packing of compound 9 viewed down the *a*-axis

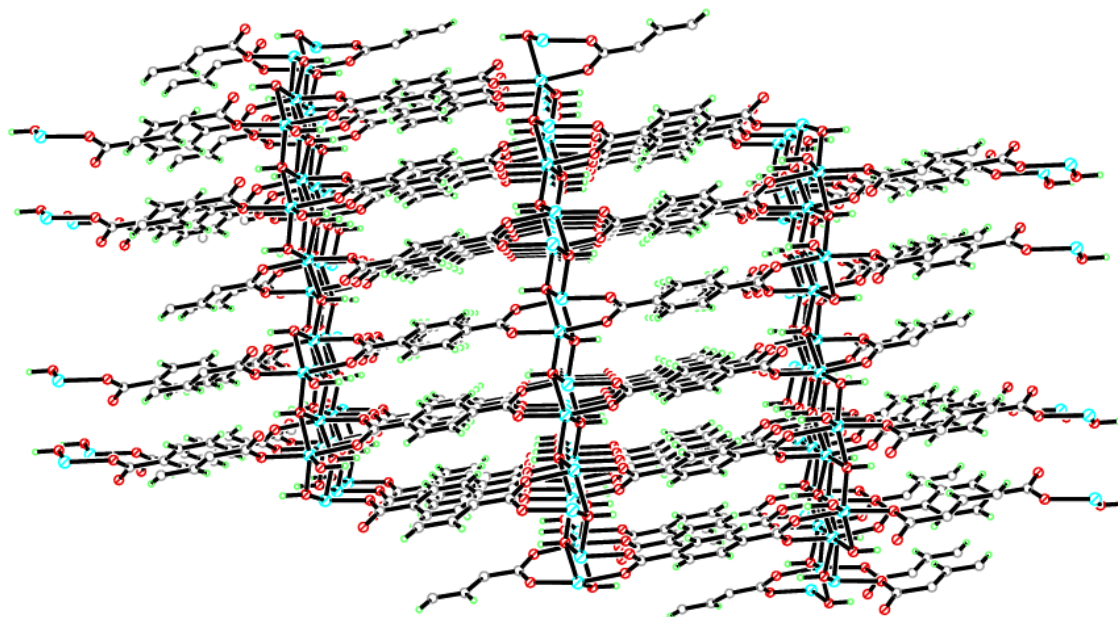


**Figure 5.50:** Three dimensional packing of coplanar columns that coordinate the sheets in compound 9 viewed down the *b*-axis

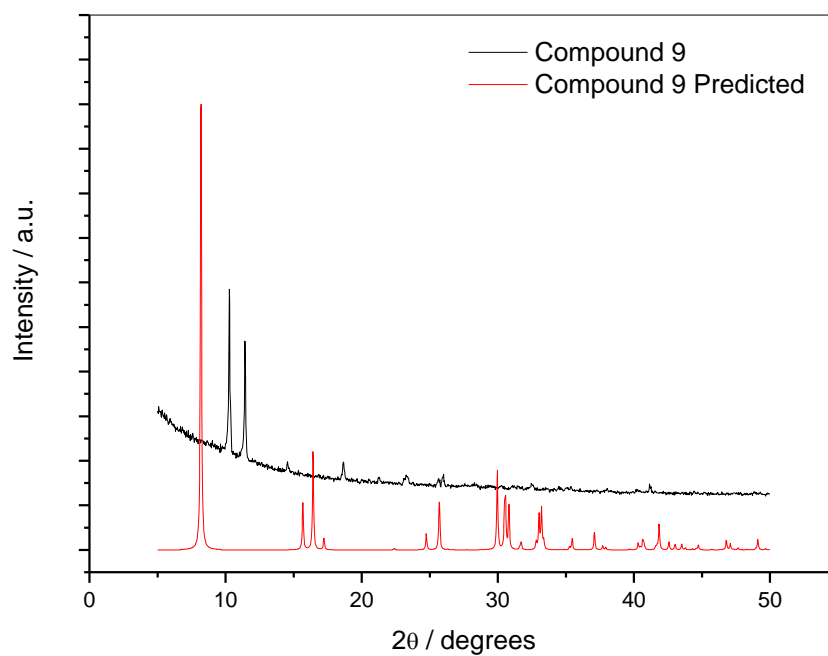


**Figure 5.51:** Powder X-ray diffraction pattern of compound 9

## Conclusion

In this chapter nine compounds with 1,4-benzenedicarboxylic acid were presented; four with zinc, two with cobalt, one with nickel, one with cadmium and one compound with copper. These compounds were formed with a variety of solvents and bases producing frameworks consisting of one dimensional chains to three dimensional coordinated porous grids.

Compound 1 forms one dimensional chains with two octahedral nickel cations linked by 1,4-benzenedicarboxylate ligands. The nickel cations are capped by trans pyridine and trans water molecules that prevent the structure from coordination in three dimensions; instead forming hydrogen bonded sheets via the water molecules that then stack into three dimensions utilizing  $\pi$ - $\pi$  interactions of the coordinated pyridines. Compound 6 was synthesised in similar reaction conditions producing a two dimensional interwoven sheet of tetrahedral zinc cations held together by 1,4-benzenedicarboxylate ligands, with a terminal pyridine coordinated in the axial position templating the topology of the framework through  $\sigma$ - $\pi$  interactions. The pyridine was used in these reactions to deprotonate the 1,4-benzendicarboxylate ligands and to act as a templating agent using the aromatic-aromatic interactions of the pyridine rings. In both instances the reaction was successful; due to significance of the pyridine coordination on the resulting topology further investigations were carried out using trimethylamine as an alternative base to probe the effect on topology formation leading to the synthesis of compound 2.

By changing the base from pyridine to trimethylamine, compound 2 was produced. This compound is a one dimensional chain with octahedral cobalt cations linked by 1,4-benzenedicarboxylate ligands; this structure differs from compound 1 with the coordination of methanol molecules in the absence of pyridine as the trimethylamine does not coordinate into the framework, creating a highly efficient close packing motif in correlation with the space group change and correspond cell volume change of 4372 Å<sup>3</sup> to 376 Å<sup>3</sup>. Direct addition reactions using DMF as a solvent produced compound 3, this compound forms a trinuclear zinc building unit capped by coordinated DMF molecules preventing the structure from expanding into three dimensions resulting in a double-layer sheet. The structure is further directed by DMF molecules with overlapping

of the DMF ligands of adjacent sheets expanding the structure into three dimensions through hydrogen bonding. The prevalence of DMF as a templating agent for topology direction, is exhibited when the zinc cations are substituted for cobalt cations to produce the isostructural compound 4. The structures differ in the metal coordination geometries due to the metal cations used. Compound 3 has one standard six-coordinate octahedral zinc unit and a distorted four-coordinate tetrahedral zinc unit, in comparison the metal nodes in compound 4 are both six-coordinate octahedral geometries; however this does not affect the overall packing topology of the framework with the retention of the trinuclear secondary building units. The SBUs were expanded by altering the reaction conditions in compounds 3 and 4 to reduce the concentration of DMF limiting its coordination and templating effects, resulting in compounds 5 and 8. Compound 5 forms a dinuclear zinc four-blade paddle-wheel SBU capped by one water molecule on the square pyramidal zinc node. This building unit is expanded by 1,4-benzenedicarboxylate ligands to form two dimensional sheets with a 4,4' net topology similar to that present in compounds 3 and 4. Compound 5 was synthesised with a lower concentration of DMF in the reaction medium, resulting in water coordinating with priority; however DMF is still present within the compound situated within the 4,4' nets forming hydrogen bonds to the framework, directing the pore size and shape. The ability of DMF to template the framework in compounds 3-5 resulted in its exclusion from the reaction medium of compound 8 to observe the templating affects of water molecules.

Compound 8 was synthesised using the same reactions conditions as compounds 3 and 4 with DMF substituted for water. This resulted in a trinuclear zinc building unit bridged by 1,4-benzenedicarboxylate ligands in a similar motif to those observed in compounds 3 and 4; however without the presence of DMF the building unit is not capped at each end, instead it expands through an additional 1,4-benzenedicarboxylate ligand to form a three dimensional framework consisting of 4,4' nets with dimensions 9.125 (4) by 10.488(6) Å. The production of compound 8 and compounds 3-5 shows how the solvent medium can be tailored to form structures with consistent paddle-wheel building units that coordinate to either solvent molecules, capping the structure or to linkers allowing coordination into three dimensions, highlighting the templating effects of DMF as a solvent.

## References:

- 1 T. Ohmura, W. Mori, M. Hasegawa, T. Takei, T. Ikeda, E. Hasegawa, *Bull. Chem. Soc. Jpn.*, **2003**, 76, 1387.
- 2 R. H. Groeneman, L. R. MacGillivray, J. L. Atwood, *Inorg. Chem.*, **1999**, 338, 208.
- 3 Z. L. Deng, J. Shi, Z. H. Jiang, D. Z. Liao, S. P. Yan, G. L. Wang, H. G. Wang, R. J. Wang, *Polyhedron*, **1992**, 11, 885.
- 4 C. D. Wu, C. Z. Lu, S. F. Lu, H. H. Zhuang, J. S. Huang, *Inorg. Chem. Commun.*, **2002**, 5, 171.
- 5 K. K. Klausmeyer, F. R. Beckles, *Inorg. Chim. Acta.*, **2005**, 358, 1041.
- 6 J. Sun, Y. Zhou, G. Fang, Z. Chen, L. Wong, G. Zhu, S. Qiu, D. Zhao, *Inorg. Chem.*, **2006**, 45, 8677.
- 7 S. M. Hawxwell, H. Adams, L. Brammer, *Acta. Crystallogr.*, **2006**, B62, 808.
- 8 F. Wang, S. Yang, R. Huang, L. Zheng, S. R. Batten, *Cryst. Eng. Commun.*, **2008**, 10, 1211.
- 9 A. L. Spek, *J. Appl. Crystallogr.*, **2003**, 36, 7.
- 10 J. Zhang, L. Wojtas, R. W. Larsen, M. Eddaoudi, M. J. Zaworotko, *J. Am. Chem. Soc.*, **2009**, 131, 17040.

## **Chapter Six – Crystal Structures of Transition Metal and 1,3,5-benzenetricarboxylic acid Compounds**

### **Introduction**

The following chapter presents compounds produced using the transition metals; cobalt, zinc, nickel, copper, manganese and cadmium. These metals were reacted with 1,3,5-benzenetricarboxylic acid in a range of reaction conditions to investigate the templating effects of different solvents and bases on topology formation.

The twelve compounds presented in this chapter include one dimensional chains (compounds 13-15), two dimensional sheets (compounds 10-12, 16) and three dimensional coordinated frameworks (compounds 17-21). Compound 17 presented in this chapter is a three dimensional framework of significant porosity leading to gas adsorption studies carried out in collaboration with Professor K. M. Thomas of the Northern Carbon Research Laboratories at Newcastle University; with isotherms collected and their respective kinetic data analysed by Dr J. Bell and J. Armstrong. This data was compared to a structural analogue (HKUST-1) that was prepared using the standard synthesis,<sup>9</sup> with carbon dioxide isotherms collected at 192K by Dr J. Bell and Professor K. M. Thomas.

The compounds in this chapter were analysed further with elemental analysis, powder X-ray diffraction and thermogravimetric analysis, where possible, to determine the purity of the bulk material and the thermostability properties of the compounds.





## Structure Determination

The data were collected at 150 K using molybdenum radiation on an Oxford Diffraction Gemini A Ultra diffractometer. The structure was solved by direct methods. The semi-empirical absorption corrections were applied based on symmetry-equivalent and repeated data. The refinement gave a  $wR2$  of 0.0368 for all 3313 independent reflections and a conventional  $R1$  of 0.0337, for 2504 reflections with  $F^2 > 2\sigma$ . The residual electron density maximum and minimum were 0.40 and  $-0.25 \text{ e } \text{\AA}^{-3}$  respectively. Compound 10 crystallised in the chiral space group  $P2_1$  and refined with a Flack parameter of 0.101 indicating the correct handedness has been selected.

The hydrogen atoms were placed in geometrically calculated positions with  $U$  constrained to  $1.2 U_{\text{eq}}(\text{C})$  for aromatic hydrogen atoms and  $U$  constrained to  $1.5 U_{\text{eq}}(\text{C})$  for methyl hydrogen atoms. The ligands in the structure were disordered; with SIMU, DELU and FLAT restraints being imposed for refinement. The full data of compound 10 can be found in Appendix 1.

## Structure Analysis

The asymmetric unit of compound 10 (figure 6.01) shows a five-coordinate square pyramidal copper cation coordinated to one 1,3,5-benzenetricarboxylate ligand and a 4,4'-bipyridine ligand and their trans coplanar symmetry equivalents, with the fifth coordination position occupied by an axial DMF ligand. The square pyramidal geometry is slightly distorted with the bond angles highlighted in table 6.01 (figure 6.02). The copper cation coordinates to two of the three available carboxylate groups of the 1,3,5-benzenetricarboxylate ligand. In each case it forms a monodentate bond coordinating through one carboxylate oxygen atom to form the strong coordination bonds; Cu-O(1) 1.932(5) Å and Cu-O(5A) 1.960(3) Å in its coplanar trans position at a slightly offset angle of O(1)-Cu-O(5A) 170.35(13)°. The coordinating carboxylate groups show that full delocalisation has not occurred with the presence of significantly shorter and longer bond lengths indicating the presence of a carbon-oxygen double and single bond in the carboxylate groups. The comparison of the non-coordinating protonated carboxylate

group O(3)-C(8)-O(4) with single bond C(8)-O(3) 1.309(6) Å and double bond C(8)-O(4) 1.218(6) to the coordinated carboxylate groups shows similar bond lengths; C(7)-O(1) 1.287(5) Å, C(7)-O(2) 1.237(5) Å, C(9)-O(5) 1.289(5) Å and C(9)-O(6) 1.220(5) Å. The protonated carboxylate group is used further in hydrogen bonding within this structure.

Further distorting of the copper geometry is caused by the 4,4'-bipyridine ligand and its trans symmetry equivalent, which binds using both nitrogen atoms available in the trans coplanar positions N(1)-Cu-N(2A) 166.90(16)°. The second ring of the 4,4'-bipyridine ligand is tilted by 33.03(5)° with rotation around the C(12)-C(17) bond causing the rings to flex slightly out of the plane. The 4,4'-bipyridine ligands are in coplanar cis positions to the 1,3,5-benzenetricarboxylate ligands at the angles; O(1)-Cu-N(1) 88.85(14)° and O(1)-Cu-N(2A) 92.74(15)°. The DMF ligand coordinates in the axial position perpendicular to the plane containing the 4,4'-bipyridine and 1,3,5-benzenetricarboxylate ligands, coordinating through its oxygen atom at O(1)-Cu-O(7) 86.73(13)° forming the secondary building unit in figure 6.03.

The secondary building unit expands the structure to form two dimensional sheets that run along the *b*-axis and down the *c*-axis (figure 6.04). The sheets form a net topology with the coordinated DMF molecules pointing inwards to the pore, the remaining available space is occupied by the uncoordinated DMF molecule that is hydrogen bonded to the protonated carboxylate group of the 1,3,5-benzenetricarboxylate ligand via the O(3)-H(3)···O(8) 2.592(5) Å hydrogen bond.

PLATON<sup>1</sup> confirms the presence of pores with a calculated pore volume 537.1 Å<sup>3</sup> per unit cell corresponding to 41.8 %. This porous volume is accessible through the nets with dimensions 9.665(5) by 7.211(5) Å upon desolvation of the DMF.

Thermogravimetric analysis was carried out on compound 10 to determine the thermostability upon desolvation, producing the TGA plot in figure 6.05. The TGA shows a large initial mass loss between 7.685-5.954 mg during stage 1 due to excess surface solvent in the sample. After the excess solvent is removed the sample is stable to 110°C after which desolvation begins. The first solvent to be removed is the uncoordinated DMF molecules at stage 2 contributing to the mass loss of 5.954-5.309 mg between 110-143.3°C. The desolvation is a double step process with further DMF

removal during stage 3 at 145-175°C with the mass loss of 0.928 mg (15.59 %). This mass loss is associated with the uncoordinated DMF that equates for 12.73 % of the theoretical mass, suggesting that the coordinated DMF is irremovable until the critical temperature at 250°C that results in the collapse of the structure at stage 4.

Based on compound 10 only forming the semi-desolvated structure, PLATON<sup>1</sup> calculates the pore volume to be 267.0 Å<sup>3</sup> per unit cell corresponding to 20.8 %. This is based on nanochannels with dimensions 4.921(5) by 9.665(5) Å running down the *a*-axis of compound 10. These nanochannels would be very constrictive only accommodating compounds of sizes up to that of DMF, however they do provide the possibility of hydrogen bonding interactions with the methyl groups of the remaining coordinated DMF molecules. This would show differing adsorption and desorption isotherms with a hysteresis step due to interactions between the adsorbate and the pore walls; these interactions are crucial to several applications including CO<sub>2</sub> and H<sub>2</sub> trapping.

The powder diffraction of this compound showed mostly amorphous background possibly due to the low stability of the structure upon full desolvation. Several attempts were made to gain higher resolution diffraction patterns for data comparison, all proving unsuccessful. Further elemental analysis provided the results C = 55.96 %, H = 5.02% and N = 10.43 % corresponding to the calculated values from the single crystal data of C = 52.26 %, H = 4.53 % and N = 9.76 % with variations a result of excess solvent.

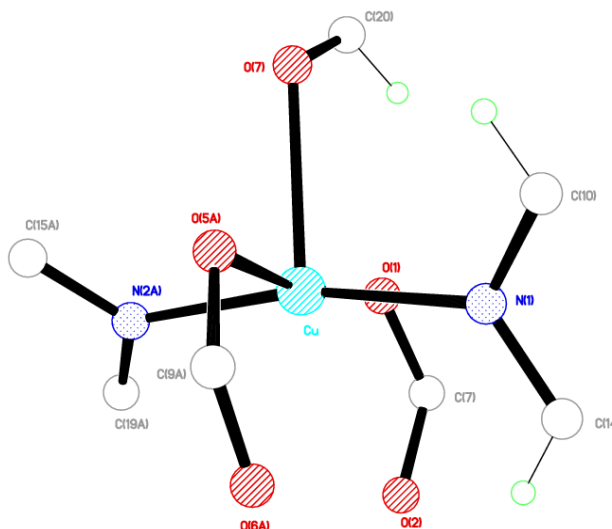
Compound 10 was synthesised using an H-Cell to allow the slow reaction of the 4,4'-bipyridine ligand with the transition metal that would otherwise result in the formation of amorphous product. The difficulty of producing crystals with these reagents is evident from the low number of deposits in the CSD<sup>2</sup>.

**Table 6.01: Selected Bond Lengths [Å] and Angles [°] for Compound 10**

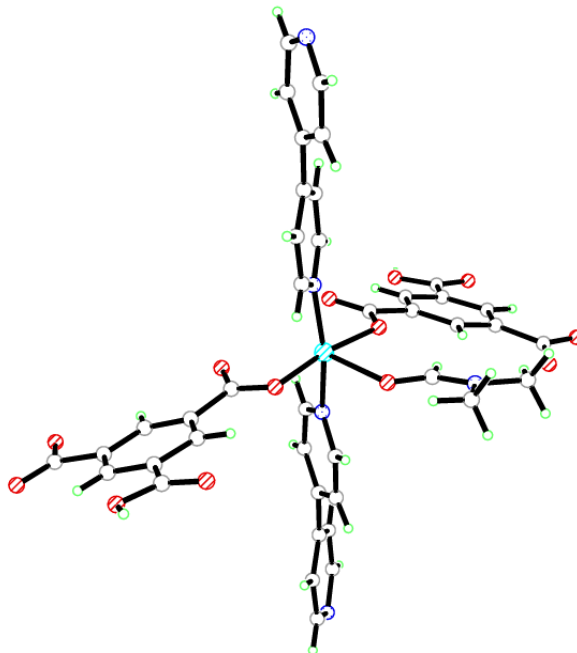
Cu–O(1)	1.932(3)	Cu–O(5A)	1.960(3)
Cu–N(1)	2.027(3)	Cu–N(2B)	2.023(2)
Cu–O(7)	2.380(4)	C(7)–O(1)	1.287(5)
C(7)–O(2)	1.237(5)	C(8)–O(3)	1.309(6)
C(8)–O(4)	1.218(6)	C(9)–O(5)	1.289(5)
C(9)–O(6)	1.220(5)	O(3)–H(3)	0.838(10)
O(1)–Cu–O(5A)	170.35(13)	O(1)–Cu–N(1)	88.85(14)
O(1)–Cu–N(2B)	92.74(15)	O(1)–Cu–O(7)	86.73(13)
Cu–O(1)–C(7)	119.3(3)	Cu–O(5)–C(9)	110.2(3)
Cu–O(7)–C(20)	115.8(3)		
Symmetry operations for equivalent atoms			
A	$-x+1, y-1/2, -z+1$	B	$x-1, y, z-1$
C	$-x+1, y+1/2, -z+1$		

**Table 6.02: Selected Hydrogen bond Lengths [Å] and angles [°] for Compound 10**

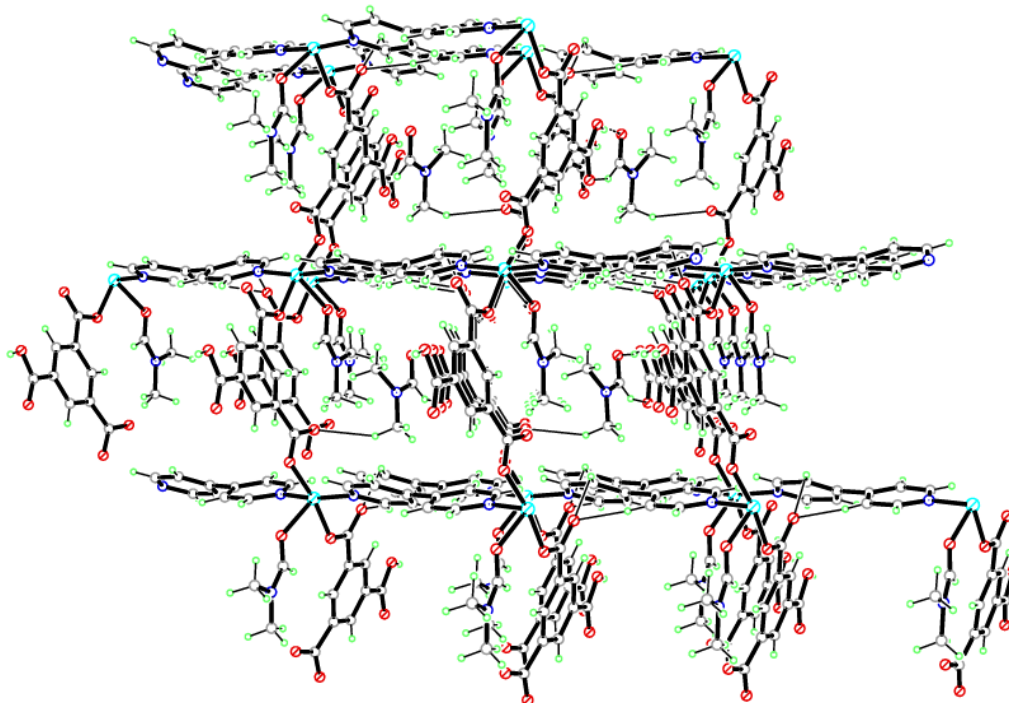
D–H...A	d(D–H)	d(H...A)	d(D...A)	(DHA)
O(3)–H(3)...O(8)	0.838(10)	1.763(14)	2.592(5)	170(5)



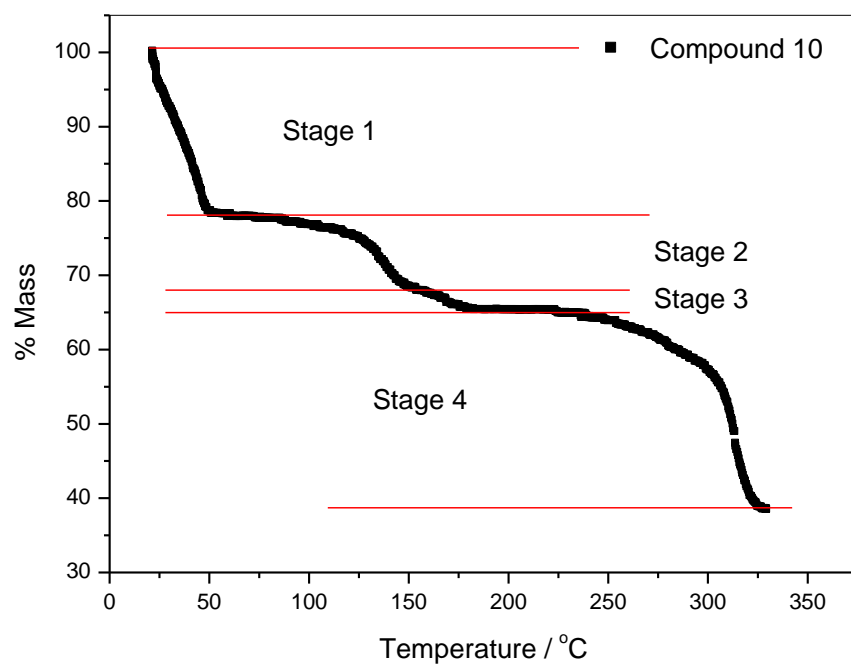
**Figure 6.02: Square pyramidal coordination environment of the copper cation in compound 10**



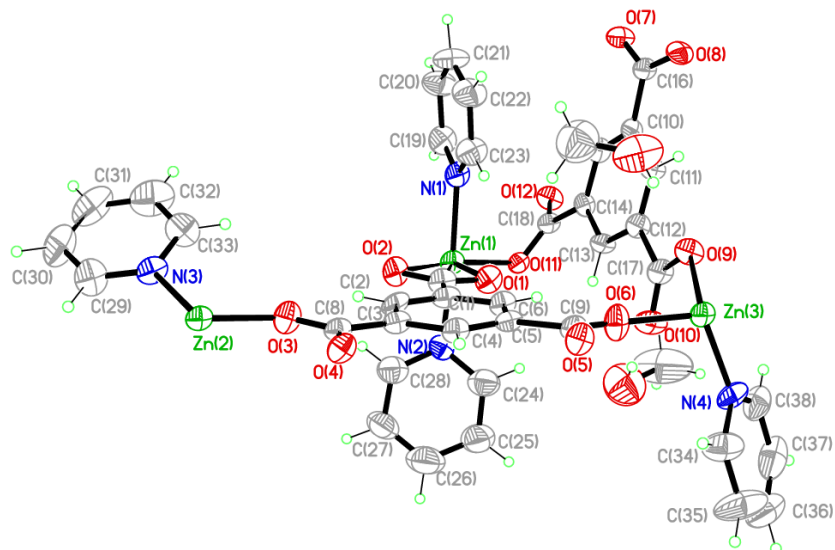
**Figure 6.03: Secondary building unit of the copper cation in compound 10 (uncoordinated moieties omitted for clarity)**



**Figure 6.04: Two dimensional sheet of compound 10 viewed down the  $a$ -axis**



**Figure 6.05: Thermogravimetric analysis plot of compound 10**

**Compound 11:**  $[\text{Zn}_3(\text{C}_9\text{H}_3\text{O}_6)_2(\text{C}_5\text{H}_5\text{N})_4] \cdot 2\text{CH}_4\text{O}$ 

Chemical formula (total)	$\text{C}_{40}\text{H}_{34}\text{N}_4\text{O}_{14}\text{Zn}_3$	
Formula weight	990.82	
Temperature	150(2) K	
Radiation, wavelength	$\text{CuK}\alpha$ , 1.54178 Å	
Crystal system, space group	triclinic, $P\bar{1}$	
Unit cell parameters	$a = 10.1761(6)$ Å	$\alpha = 106.312(7)^\circ$
	$b = 14.3333(13)$ Å	$\beta = 103.661(6)^\circ$
	$c = 15.9560(13)$ Å	$\gamma = 103.012(6)^\circ$
Cell volume	$2061.7(3)$ Å <sup>3</sup>	
$Z$	2	
Crystal colour and size	colourless, $0.50 \times 0.50 \times 0.10$ mm <sup>3</sup>	
Final $R$ indices [ $F^2 > 2\sigma$ ]	$R1 = 0.0731$	
$R$ indices (all data)	$wR2 = 0.2392$	
Largest diff. peak and hole	1.39 and $-1.01$ e Å <sup>-3</sup>	

**Figure 6.06: Asymmetric Unit of Compound 11 all unique atoms labelled.****Synthesis**

2 mL of a solution of  $\text{Zn}(\text{NO}_3)_2 \cdot 6\text{H}_2\text{O}$  (0.1 g, 0.33 mmol) in methanol (10 mL) was layered over 2 mL of a suspension of 1,3,5-benzenetricarboxylic acid (0.028 g, 0.17 mmol) and pyridine (0.05 mL, 0.22 mmol) in water (10 mL) in a small sample vial. The vial was covered and left until crystallisation was complete. After two weeks, colourless block crystals formed.

## Structure Determination

The data were collected at 150 K using copper radiation on an Oxford Diffraction Gemini A Ultra diffractometer. The structure was solved by direct methods. The semi-empirical absorption corrections were applied based on symmetry-equivalent and repeated data. The refinement gave a  $wR2$  of 0.2392 for all 7139 independent reflections and a conventional  $R1$  of 0.0731, for 4388 reflections with  $F^2 > 2\sigma$ . The residual electron density maximum and minimum were 1.39 and  $-1.01 \text{ e } \text{\AA}^{-3}$  respectively, the slightly high residual electron density is a result of disorder within the uncoordinated DMF molecules.

The hydrogen atoms were placed in geometrically calculated positions with  $U$  constrained to  $1.2 U_{\text{eq}}(\text{C})$  for aromatic hydrogen atoms,  $U$  constrained to  $1.5 U_{\text{eq}}(\text{C})$  for methyl hydrogen atoms and  $U$  constrained to  $1.5 U_{\text{eq}}(\text{O})$  for the hydroxyl hydrogen atoms. The full data of compound 11 can be found in Appendix 1.

## Structure Analysis

The asymmetric unit of compound 11 (figure 6.06) shows two complete 1,3,5-benzenetricarboxylate ligands coordinating to three zinc cations, Zn(1), Zn(2) and Zn(3) that are in two different coordination environments in this polymeric compound. The zinc cations are all in general positions with Zn(1) forming a six-coordinate distorted octahedral geometry, Zn(2) and Zn(3) are four-coordinate and adopt the tetrahedral geometry (figure 6.07).

The six-coordinate Zn(1) (figure 6.07A) is coordinated to two unique 1,3,5-benzenetricarboxylate ligands using three unique carboxylate groups. The carboxylate group O(1)-C(7)-O(2) forms a bidentate coordination to the Zn(1) cation with a bite angle of  $58.8(2)^\circ$ , this angle is less than the ideal  $90^\circ$  angle for a cis position coordination in the octahedral geometry inducing the disorder observed at the Zn(1) node. A second carboxylate group of a symmetry equivalent of the same 1,3,5-benzenetricarboxylate ligand is coordinated in the coplanar cis position at an angle O(2)-Zn(1)-O(5A)  $97.1(2)^\circ$ . This carboxylate group coordinates to the Zn(1) cation using one carboxylate oxygen atom O(5), whilst the second forms a monodentate bond to the



Zn(3) cation forming a bridge between the two cations. The final carboxylate groups coordinated to the Zn(1) cation coordinates in the coplanar cis position to the O(1) oxygen, O(1)-Zn(1)-O(11) 101.7(2)°. This carboxylate group coordinates forming the monodentate bond Zn(1)-O(11), the O(12) oxygen then forms a monodentate bond to a symmetry equivalent Zn(3) cation forming a second bridge between the Zn(1) and Zn(3) cations. This bridge is formed as the 1,3,5-benzenetricarboxylate ligand twists out of the plane of the carboxylate oxygens by 36.67(6)°, with the aromatic ring perpendicular to that of the other 1,3,5-benzenetricarboxylate ligand. This results in the second carboxylate oxygen O(12) being positioned out of the plane of the Zn(1)-O(11) pointing in the direction of the Zn(3) symmetry equivalent. The carboxylate oxygens occupy four of the six available coordination sites on Zn(1), the remaining two positions cis and perpendicular to the oxygen atoms are occupied by two mutually trans pyridine ligands; N(1)-Zn(1)-N(2) 174.9(3)° (figure 6.07A).

The four coordinate Zn(2) cation (figure 6.07B) is coordinated to the two unique 1,3,5-benzenetricarboxylate ligands through one carboxylate group on each ligand. The carboxylate groups initially coordinate with monodentate bonds in the coplanar cis positions, O(3)-Zn(2)-O(7) 89.3(3)°. The remaining carboxylate oxygens then coordinate to a symmetry equivalent Zn(2) cation in the coplanar cis position O(4)-Zn(2A)-O(8) 88.3(3)° with respect to each other. As a result of inversion symmetry between the two Zn(2) cations a paddle-wheel secondary building unit is formed with the carboxylate groups trans to their symmetry equivalents O(3)-Zn(2)-O(4A) 159.9(2)° and O(7)-Zn(2)-O(8A) 158.9(2)°. This paddle-wheel secondary building unit is capped in the axial positions by a pyridine ligand O(3)-Zn(2)-N(3) 96.2(3)° completing the Zn(2) coordination sphere (figure 6.07B) (table 6.03).

The Zn(3) cation forms a four-coordinate tetrahedral geometry (figure 6.07C) coordinating to two unique 1,3,5-benzenetricarboxylate ligands through monodentate bonds on three coplanar carboxylates that coordinate cis to one another; O(6)-Zn(3)-O(9) 98.3(3)° and O(6)-Zn(3)-O(12A) 119.5(3)°. The third carboxylate group O(11)-C(18)-O(12) is from a symmetry equivalent 1,3,5-benzenetricarboxylate ligand that acts as a bridging group between the Zn(3) and Zn(1) cations allowing the structure to expand in two dimensions. The final coordination site is filled by an axial pyridine

ligand cis to the carboxylate groups O(6)-Zn(3)-N(4)  $109.1(3)^\circ$  that forms a slightly stronger bond of  $2.001(3) \text{ \AA}$ .

The secondary building units of the zinc cations and the orientation of the 1,3,5-benzenetricarboxylate ligands form columns that run down the *a*-axis and along the *b*-axis (figure 6.08). These columns contain grids of dimensions  $11.213(3)$  by  $7.633(3) \text{ \AA}$  that are connected by the Zn(2) paddle-wheel building unit. The grids contain one coordinated pyridine ligand and one uncoordinated methanol molecule and their symmetry equivalents generated by inversion symmetry at the centre of the grid, resulting in two pyridines and two uncoordinated methanols in each potential pore. It is unlikely that the pyridine molecules can be removed from the framework without the structure collapsing; however, if the uncoordinated methanol molecules were removed, PLATON<sup>1</sup> confirms the presence of pores with a calculated pore volume  $376.8 \text{ \AA}^3$  per unit cell corresponding to 18.3 %. This porous volume would be accessible in the form of a channel running down the *a*-axis.

Thermogravimetric analysis was carried out on compound 11 to determine the thermostability upon desolvation producing the TGA plot shown in figure 6.09. The TGA shows a gradual mass loss between 50-350°C, stage 1 shows a significant mass loss of 0.5 mg between 50-100°C with an unstable plateau following and stage 2 shows further mass loss of 0.75 mg between 125-200°C. The desolvation is a double step process with a total mass loss of 1.25 mg (19.23 %). The first mass loss of 7.69 % can be associated with methanol that equates for 6.46 % of the calculated mass. The additional mass loss is associated with pyridine removal and the subsequent collapse of the structure at 200°C due to destabilisation upon the pyridine removal. The relatively low thermostability of the compound is primarily due to the two dimensional nature of the coordination in compound 11. The columns that are coordinated together to form a sheet running down the *a*-axis and *b*-axis then pack together in offset positions to maximise  $\pi$ - $\pi$  interactions at  $3.752(3) \text{ \AA}$  with adjacent pyridine ligands of the parallel sheet. Additional weak hydrogen bonds with uncoordinated methanol molecules add further to the long range stability by forming weak  $\sigma$ - $\pi$  interactions at  $4.098(5) \text{ \AA}$  between O-H(40A)···C(34)-N(4) aromatic ring. These  $\pi$ - $\pi$  and  $\sigma$ - $\pi$  interactions allow the structure to expand into three dimensions as shown in figure 6.08.

The powder diffraction of the bulk sample of compound 11 showed a good quality data set (figure 6.10) that correlates well with the predicted powder diffraction pattern produced from the single crystal data, with all significant peaks present at corresponding angles. Additional analysis of the purity of the bulk sample was conducted using elemental analysis that produced the results C = 43.92 %, H = 2.82 % and N = 4.61 %. These correlate with the calculated values from the single crystal data of C = 48.48 %, H = 3.43 % and N = 5.65 % with discrepancies in hydrogen and nitrogen due to a partially wet sample with excess solvent.

Although the bulk sample was pure with high repeatability the thermostability of the compound was not sufficient to enable further investigation for potential porosity and subsequent applications. However due to the potential replication of the grid network further reactions were carried out to synthesize analogues resulting in compound 12.

**Table 6.03: Selected Bond Lengths [ $\text{\AA}$ ] and Angles [ $^\circ$ ] for Compound 11**

Zn(1)–O(1)	2.072(6)	Zn(1)–O(2)	2.390(6)
Zn(1)–O(5A)	2.038(5)	Zn(1)–O(11)	2.088(6)
Zn(1)–N(1)	2.164(7)	Zn(1)–N(2)	2.131(7)
Zn(2)–O(3)	2.011(6)	Zn(2)–O(4B)	2.052(6)
Zn(2)–O(7C)	2.031(6)	Zn(2)–O(8D)	2.064(6)
Zn(2)–N(3)	2.018(6)	Zn(3)–O(6)	1.955(7)
Zn(3)–O(9)	1.974(6)	Zn(3)–O(12E)	1.994(6)
Zn(3)–N(4)	2.001(7)	C(7)–O(1)	1.270(11)
C(7)–O(2)	1.247(10)	C(8)–O(3)	1.272(10)
C(8)–O(4)	1.266(10)	C(9)–O(5)	1.269(10)
C(9)–O(6)	1.255(11)		
O(1)–Zn(1)–O(2)	58.8(2)	O(1)–Zn(1)–O(5A)	155.7(3)
O(1)–Zn(1)–O(11)	101.7(2)	O(1)–Zn(1)–N(1)	91.6(3)
O(1)–Zn(1)–N(2)	87.4(3)	O(3)–Zn(2)–O(4B)	159.2(2)
O(3)–Zn(2)–O(7C)	89.9(3)	O(3)–Zn(2)–O(8D)	86.7(3)
O(3)–Zn(2)–N(3)	102.5(3)	O(6)–Zn(3)–O(9)	98.3(3)
O(6)–Zn(3)–O(12E)	119.5(3)	O(6)–Zn(3)–N(4)	109.1(3)
Zn(1)–O(1)–C(7)	96.3(5)	Zn(1)–O(2)–C(7)	82.4(5)
Zn(2)–O(3)–C(8)	125.0(6)	Zn(2B)–O(4)–C(8)	131.1(6)
Zn(1E)–O(5)–C(9)	133.9(6)	Zn(3)–O(6)–C(9)	154.1(6)
Zn(2F)–O(7)–C(16)	117.2(5)	Zn(2D)–O(8)–C(16)	138.8(6)
Zn(3A)–O(12)–C(18)	106.2(5)	Zn(1)–O(11)–C(18)	122.2(5)

Symmetry operations for equivalent atoms

A  $x+1,y,z$     B  $-x+1,-y+2,-z+2$     C  $x,y+1,z$ D  $-x+1,-y+1,-z+2$     E  $x-1,y,z$     F  $x,y-1,z$ **Table 6.04: Selected Hydrogen bond Lengths [ $\text{\AA}$ ] and angles [ $^\circ$ ] for Compound 11**

D–H...A	d(D–H)	d(H...A)	d(D...A)	(DHA)
O(13)–H(13O)...O(9)	0.84	2.08	2.924(11)	180
O(14)–H(14O)...O(10)	0.84	2.01	2.849(13)	180

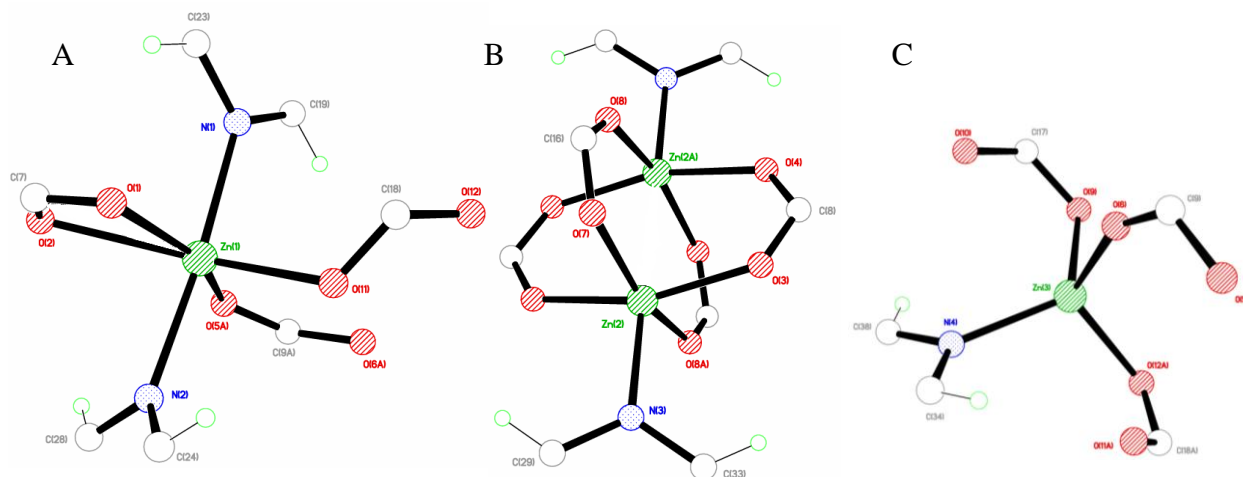


**Figure 6.07:** A) Octahedral coordination environment of Zn(1), B) Square pyramidal geometry of the Zn(2) cation and the symmetry equivalent Zn(2A) cation that forms a distorted octahedral geometry and C) Tetrahedral coordination environment of Zn(3) in compound 11

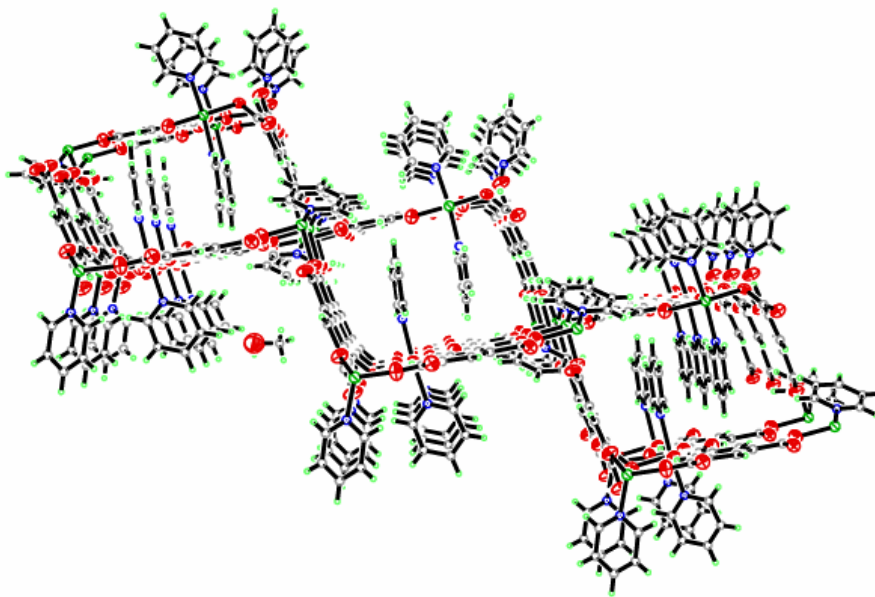


**Figure 6.08:** Two dimensional columns in compound 11 viewed down the *a*-axis

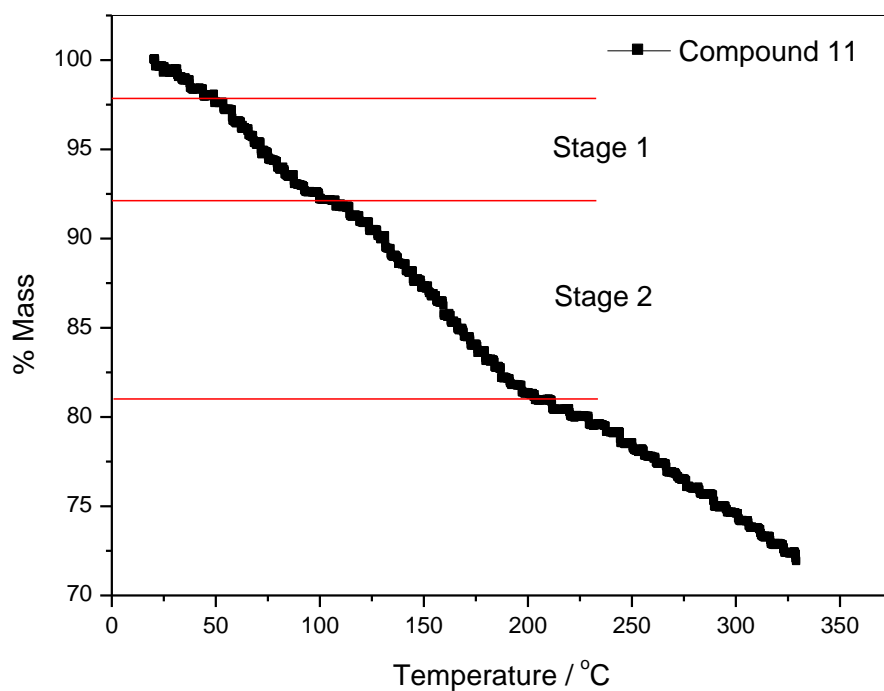


**Figure 6.09: Thermogravimetric analysis plot of compound 11**

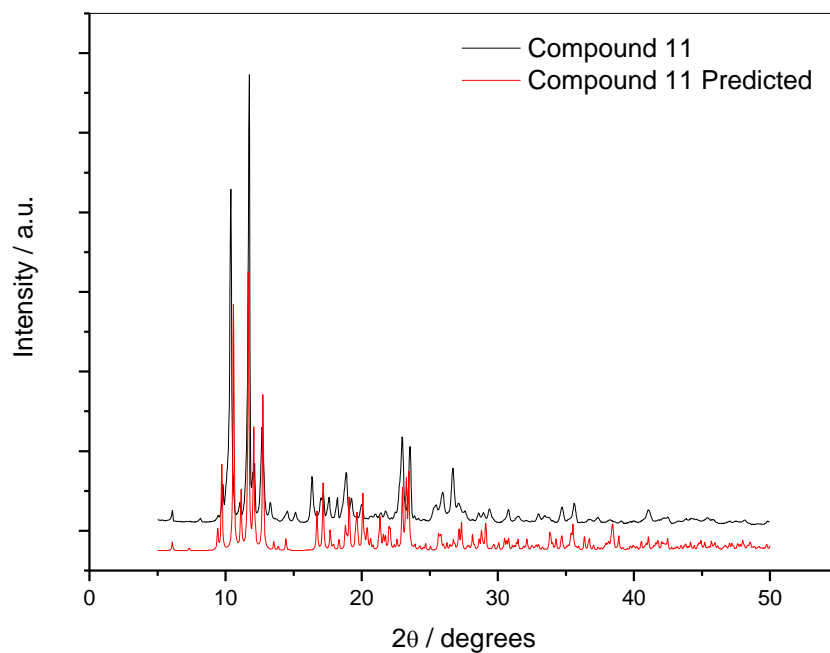
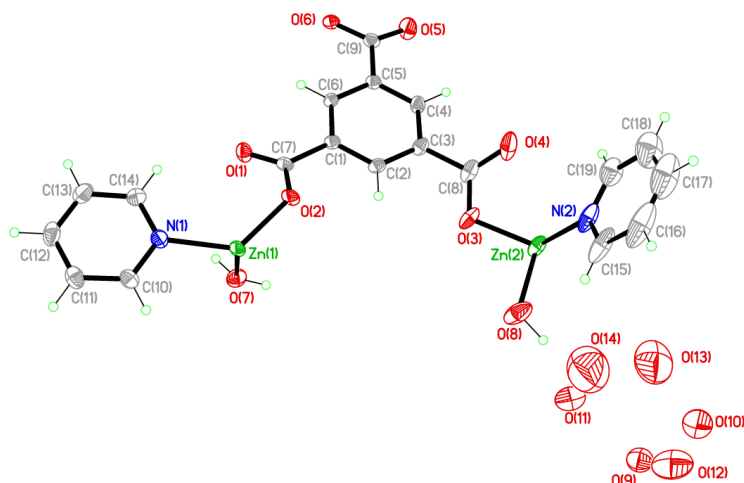


**Figure 6.10: Powder X-ray diffraction pattern of Compound 11**

**Compound 12:**  $[\text{Zn}_3(\text{C}_9\text{H}_3\text{O}_6)_2(\text{C}_5\text{H}_5\text{N})_3(\text{H}_2\text{O})_3] \cdot 6\text{H}_2\text{O}$



Chemical formula (total)	$\text{C}_{33}\text{H}_{39}\text{N}_3\text{O}_{21}\text{Zn}_3$
Formula weight	1009.78
Temperature	150(2) K
Radiation, wavelength	$\text{CuK}\alpha$ , 1.54178 Å
Crystal system, space group	monoclinic, $P2_1/m$
Unit cell parameters	$a = 8.1241(2)$ Å $b = 28.8013(6)$ Å $c = 9.4023(3)$ Å $\beta = 114.008(3)^\circ$
Cell volume	$2009.67(9)$ Å <sup>3</sup>
<i>Z</i>	2
Crystal colour and size	colourless, $0.70 \times 0.10 \times 0.05$ mm <sup>3</sup>
Final <i>R</i> indices [ $F^2 > 2\sigma$ ]	$R1 = 0.0394$
<i>R</i> indices (all data)	$wR2 = 0.1118$
Largest diff. peak and hole	0.93 and $-0.48$ e Å <sup>-3</sup>

**Figure 6.11: Asymmetric Unit of Compound 12 all unique atoms labelled, additional atoms added to complete ligands (hydrogens on uncoordinated waters omitted).**

### Synthesis

0.5 mL of a solution of  $\text{Zn}(\text{NO}_3)_2 \cdot 6\text{H}_2\text{O}$  (0.09 g, 0.33 mmol) in water (10 mL) and 0.5 mL of a solution of 1,3,5-benzenetricarboxylic acid (0.035 g, 0.17 mmol) in water (10 mL) were placed into a small sample vial. This was covered with Whatman Laboratory Sealing Film and placed inside a larger sample vial. In the larger sample vial pyridine (0.05 mL, 0.22 mmol) was added before it was covered and left until crystallisation was complete. After two weeks, colourless crystals formed.

## Structure Determination

The data were collected at 150 K using copper radiation on an Oxford Diffraction Gemini A Ultra diffractometer. The structure was solved by direct methods. The semi-empirical absorption corrections were applied based on symmetry-equivalent and repeated data. The refinement gave a  $wR2$  of 0.1118 for all 3627 independent reflections and a conventional  $R1$  of 0.0394, for 3383 reflections with  $F^2 > 2\sigma$ . The residual electron density maximum and minimum were 0.93 and  $-0.48 \text{ e } \text{\AA}^{-3}$  respectively.

The hydrogen atoms were placed in geometrically calculated positions with  $U$  constrained to  $1.2 U_{\text{eq}}(\text{C})$  for aromatic hydrogen atoms and  $U$  constrained to  $1.5 U_{\text{eq}}(\text{O})$  for the hydroxyl hydrogen atoms. The coordinated water ligands in the structure were disordered; with SIMU and DELU restraints being imposed during refinement. The full data of compound 12 can be found in Appendix 1.

## Structure Analysis

The asymmetric unit of compound 12 (figure 6.11) shows a complete 1,3,5-benzenetricarboxylate ligand coordinating two zinc cations, Zn(1) and Zn(2) the latter placed on a mirror plane. The zinc cations in compound 12 are both four-coordinate with tetrahedral geometries (figure 6.12).

The Zn(1) cation is in a general position and forms the slightly distorted tetrahedral coordination geometry shown in figure 6.12A with bond angles between the carboxylate groups and pyridine ligands deviating from the expected values; O(2)-Zn(1)-O(6A)  $121.65(8)^\circ$  and O(2)-Zn(1)-N(1)  $128.72(9)^\circ$ . (table 6.05) The Zn(1) cation is coordinated to the 1,3,5-benzenetricarboxylate ligand using two unique carboxylate groups. The zinc cation coordinates to the carboxylate groups using one oxygen on each carboxylate group forming the monodentate bonds; Zn(1)-O(2)  $1.926(19) \text{ \AA}$  and the symmetry equivalent ligand Zn(1)-O(6A)  $1.941(19) \text{ \AA}$ . These carboxylates coordinate coplanar with a bite angle of O(2)-Zn(1)-O(6A)  $120.65(8)^\circ$  creating a planar stepped chain that runs down the cell body diagonal. The remaining two coordination sites on the Zn(1) cation are occupied by a pyridine ligand Zn(1)-N(1)  $2.023(2) \text{ \AA}$  and a water molecule Zn(1)-O(7)  $2.076(2) \text{ \AA}$ , these are coordinated at almost



cis positions with respect to one another with an angle of N(1)-Zn(1)-O(7)  $93.44(9)^\circ$  and caps the Zn(1) building unit in the *b*-axis (figure 6.12A) (table 6.05).

The four-coordinate Zn(2) cation (figure 6.12B) coordinates to the 1,3,5-benzenetricarboxylate ligand through the remaining uncoordinated carboxylate group forming the monodentate bond Zn(2)-O(3) 1.960(2) Å. The Zn(2) cation is situated on a mirror plane and is coordinated to a pyridine ligand that is also in the mirror plane with a angle O(3)-Zn(2)-N(2)  $118.66(7)^\circ$  to the carboxylate group. An additional water molecule occupies the third coordination site and is also situated in the mirror plane; however its hydrogen atom H(8) is at an angle to the mirror plane allowing the second hydrogen to be generated through mirror symmetry. The final coordination site is occupied by the mirror symmetry generated O(3) carboxylate group that forms a bridging angle of O(3)-Zn(2)-O(3B)  $116.71(13)^\circ$  between two symmetry related parallel 1,3,5-benzenetricarboxylate-zinc chains to form a sheet.

These sheets pack together one on top of the other up the *a*-axis, with each stacked sheet staggered by 4.325 Å with respect to the Zn(2) cations to reduce the steric hindrance of the axial pyridine ligands, this allows the sheets to pack more efficiently as shown in figure 6.13. The sheet then alternates with a flip of  $180^\circ$  in the *a*-axis as the structure expands down the *b*-axis, this is due to an inversion symmetry point resulting in the formation of a 'zip-lock' packing motif. The sheets are held together by an extensive hydrogen bonding network between the coordinated water molecules and adjacent uncoordinated carboxylate oxygens that act as hydrogen bond acceptors; O(7)-H(7A)⋯O(1D) 2.689(3) Å (table 6.06) along with multiple hydrogen bonds to uncoordinated water molecules that act as both hydrogen bond acceptors and bifurcated hydrogen bond donors (figure 6.14).

Elemental analysis of the bulk sample of compound 12 shows impurities with the results C = 42.96 %, H = 4.32 % and N = 5.01 % significantly different to the calculated values from the single crystal data of C = 39.22 %, H = 3.86 % and N = 4.16 %. This variation is a result of the presence of excess pyridine in the compound from the original reaction solution. Further analysis of the purity of compound 12 could not be carried out via powder X-ray diffraction analysis due to the low stability of the compound once removed from the reaction solution.

The pyridine was used in this reaction to deprotonate the 1,3,5-benzenetricarboxylate ligands, with the use of the vapour diffusion technique to slow the reaction and reduce the concentration of pyridine in the product. This reaction was designed to reproduce a 'pyridine-free' compound 11 that shows significant templating by the pyridine ligands. Unfortunately a large concentration of pyridine is still coordinated to the zinc cations in compound 12 and although both compounds 11 and 12 have similar cation environments the structures form different packing motifs with different intermolecular interactions.

**Table 6.05: Selected Bond Lengths [Å] and Angles [°] for Compound 12**

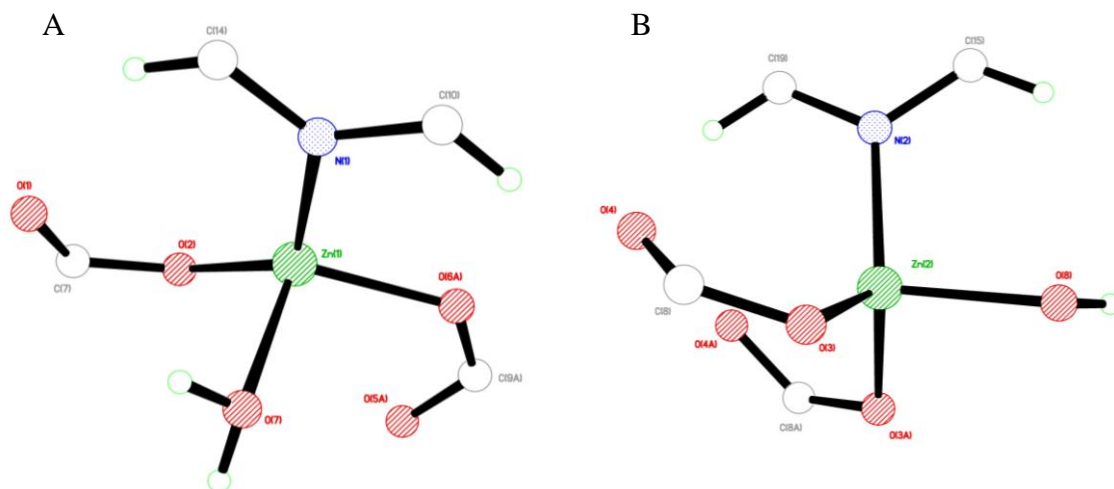
Zn(1)–O(2)	1.9264(19)	Zn(1)–O(6A)	1.9410(19)
Zn(1)–N(1)	2.023(2)	Zn(1)–O(7)	2.076(2)
Zn(2)–O(3)	1.960(2)	Zn(2)–O(8)	2.013(4)
Zn(2)–N(2)	2.026(4)	C(7)–O(2)	1.284(3)
C(7)–O(1)	1.234(4)	C(8)–O(4)	1.245(4)
C(8)–O(3)	1.281(4)	C(9)–O(6)	1.272(4)
C(9)–O(5)	1.242(4)		
O(2)–Zn(1)–O(6A)	121.65(8)	O(2)–Zn(1)–N(1)	128.72(9)
O(2)–Zn(1)–O(7)	102.62(9)	O(3)–Zn(2)–O(3B)	116.71(13)
O(3)–Zn(2)–N(2)	118.66(7)	O(3)–Zn(2)–O(8)	96.66(10)
Zn(1)–O(2)–C(7)	117.77(17)	Zn(2)–O(3)–C(8)	112.3(2)

Symmetry operations for equivalent atoms

A  $x-1, y, z-1$     B  $x, -y+3/2, z$ **Table 6.06: Selected Hydrogen bond Lengths [Å] and angles [°] for Compound 12**

D–H...A	d(D–H)	d(H...A)	d(D...A)	(DHA)
O(7)–H(7A)...O(1D)	0.93(3)	1.78(3)	2.689(3)	167(4)
O(7)–H(7B)...O(12E)	0.93(3)	1.84(3)	2.701(14)	154(4)
O(7)–H(7B)...O(9E)	0.93(3)	1.94(3)	2.844(4)	165(4)
O(8)–H(8A)...O(11)	0.96(3)	1.73(3)	2.639(4)	158(5)

Symmetry operations for equivalent atoms

D  $-x+2, -y+2, -z+1$     E  $x+1, -y+3/2, z$ **Figure 6.12: A) Tetrahedral coordination environment of Zn(1) and B) Tetrahedral coordination environment of Zn(2) in compound 12**

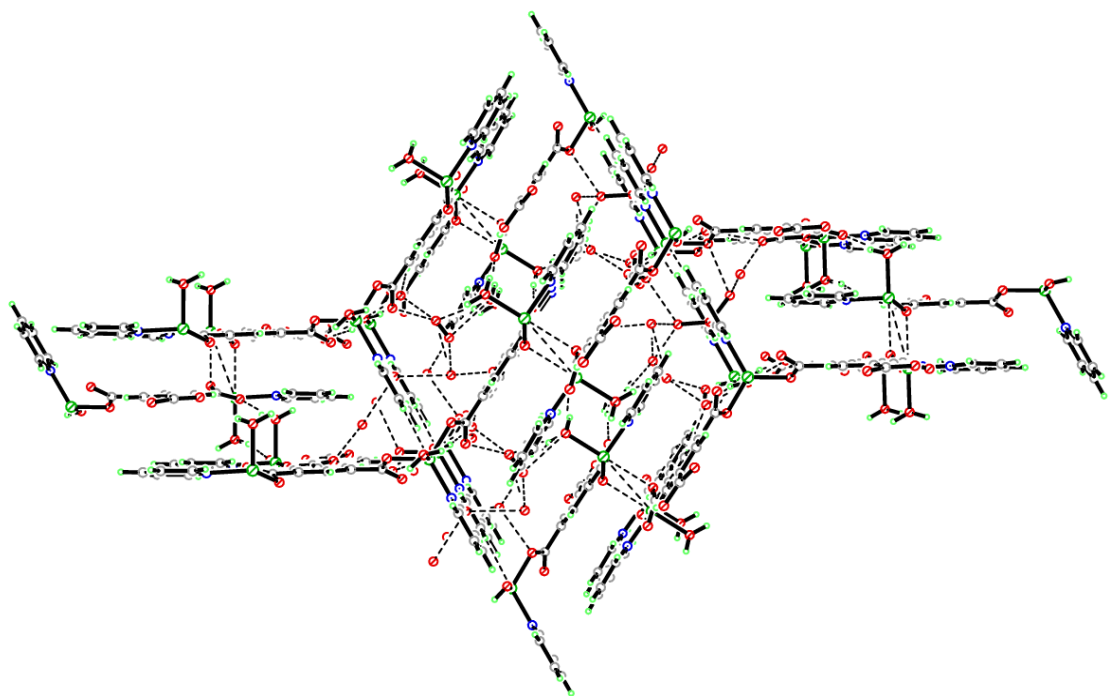


**Figure 6.13:** Packing motif of the two dimensional sheets of compound 12 viewed down the *c*-axis (dashed lines indicate hydrogen bonding).

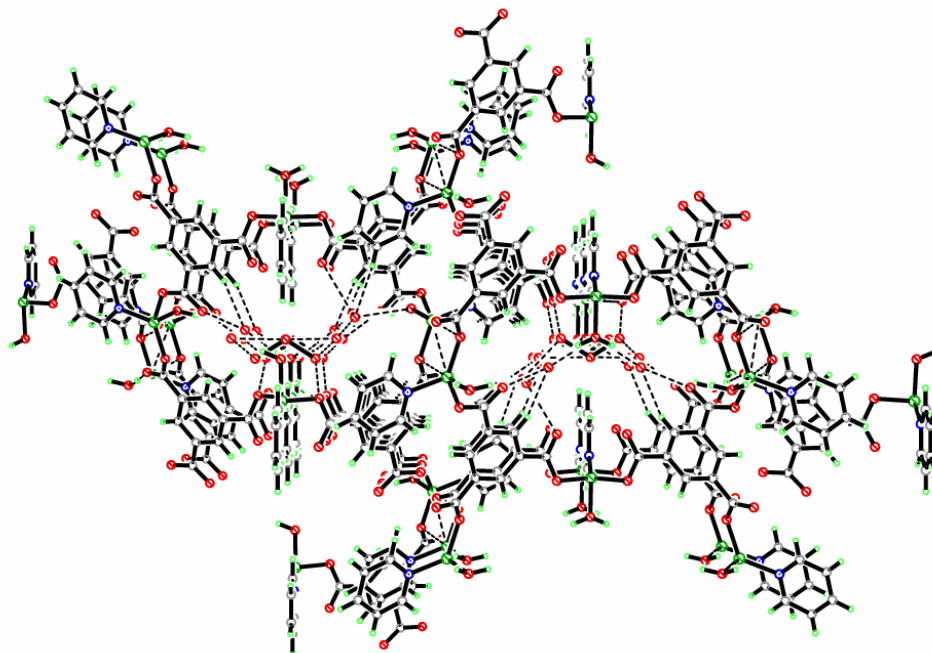
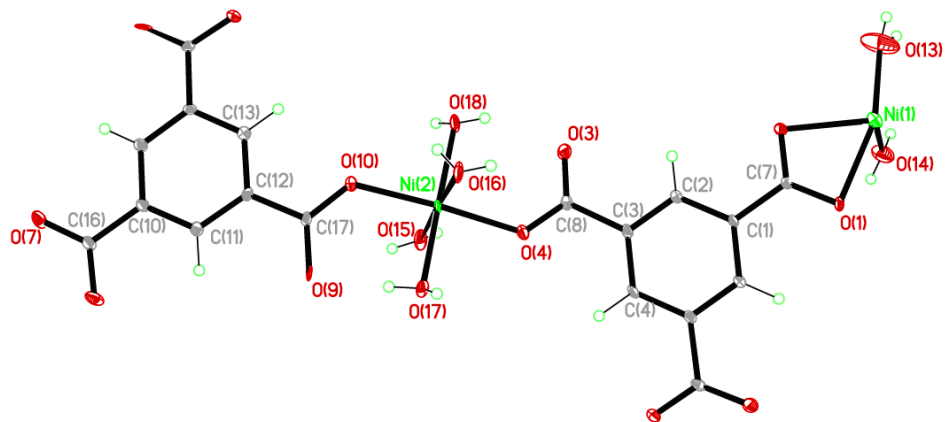


**Figure 6.14:** Three dimensional packing of the sheets in compound 12 viewed down the *b*-axis (dashed lines indicate hydrogen bonding)

**Compound 13:**  $[\text{Ni}_3(\text{C}_9\text{H}_3\text{O}_6)_2(\text{H}_2\text{O})_{12}]$



Chemical formula (total)	$\text{C}_{18}\text{H}_{30}\text{Ni}_3\text{O}_{24}$
Formula weight	806.55
Temperature	150(2) K
Radiation, wavelength	MoK $\alpha$ , 0.71073 Å
Crystal system, space group	monoclinic, $C2$
Unit cell parameters	$a = 17.2444(13)$ Å $\beta = 111.369(8)^\circ$ $b = 12.8990(7)$ Å $c = 6.4781(4)$ Å
Cell volume	$1341.90(15)$ Å <sup>3</sup>
$Z$	2
Crystal colour and size	green, $0.70 \times 0.10 \times 0.10$ mm <sup>3</sup>
Final $R$ indices [ $F^2 > 2\sigma$ ]	$R1 = 0.0422$
$R$ indices (all data)	$wR2 = 0.1089$
Largest diff. peak and hole	2.66 and $-0.57$ e Å <sup>-3</sup>
Absolute structure parameter	0.48(3)

**Figure 6.15:** Asymmetric Unit of Compound 13 all unique atoms labelled, additional atoms added to complete ligands.

**Synthesis**

$\text{Ni}(\text{NO}_3)_2 \cdot 6\text{H}_2\text{O}$  (0.09 g, 0.33 mmol) and 1,3,5-benzenetricarboxylic acid (0.035 g, 0.17 mmol) were added to a reaction mixture of ethanol (4mL) and water (3mL). This was placed into a 20mL Teflon-lined bomb and heated to 120°C for 24 hours. The vessel was then cooled back down to room temperature at a rate of 0.1°C / min and allowed to stand for 2 hours before green block crystals were retrieved from the vessel.

## Structure Determination

The data were collected at 150 K using molybdenum radiation on an Oxford Diffraction Gemini A Ultra diffractometer. The structure was solved by direct methods. The semi-empirical absorption corrections were applied based on symmetry-equivalent and repeated data. The refinement gave a  $wR2$  of 0.1089 for all 1506 independent reflections and a conventional  $R1$  of 0.0422, for 1415 reflections with  $F^2 > 2\sigma$ . The residual electron density maximum and minimum were 2.66 and  $-0.57 \text{ e } \text{\AA}^{-3}$  respectively. Compound 13 crystallised in the chiral space group  $C2$  and refined with a Flack parameter of 0.48 indicating the structure may be twinned with inversion, it was not possible to define the twinning within the refinement which resulted in the high Flack parameter and the high residual electron density.

The hydrogen atoms were placed in geometrically calculated positions with  $U$  constrained to  $1.2 U_{\text{eq}}(\text{C})$  for aromatic hydrogen atoms and  $U$  constrained to  $1.5 U_{\text{eq}}(\text{O})$  for the hydroxyl hydrogen atoms. The ligands in the structure were slightly disordered and refined with SIMU and DELU restraints. The full data of compound 13 can be found in Appendix 1.

## Structure Analysis

The asymmetric unit of compound 13 (figure 6.15) shows two 1,3,5-benzenetricarboxylate ligands completed by two-fold rotation axis that run through the centre of the respective aromatic rings, coordinated to two nickel cations Ni(1) and Ni(2). The nickel cations in compound 13 are both six-coordinate octahedral geometries with Ni(1) located on a two-fold rotation axis completing its coordination geometry through symmetry.

The Ni(1) cation forms a distorted octahedral geometry (figure 6.16A) coordinating to a bidentate carboxylate group of the 1,3,5-benzenetricarboxylate ligand with a bite angle of  $\text{O}(1)\text{-Ni}(1)\text{-O}(1\text{A})$   $62.5(3)^\circ$ . The Ni(1) cation also coordinates to two cis water molecules  $\text{O}(13)\text{-Ni}(1)\text{-O}(14)$   $85.1(3)^\circ$  with the remaining two coordination sites occupied by their symmetry equivalents generated by the two-fold rotation symmetry;  $\text{O}(13)\text{-Ni}(1)\text{-O}(13\text{A})$   $99.6(5)^\circ$  and  $\text{O}(14)\text{-Ni}(1)\text{-O}(14\text{A})$   $175.9(4)^\circ$ . These

ligands effectively cap the Ni(1) cation making it a terminal node. Compound 13 expands through the 1,3,5-benzenetricarboxylate ligand that bridges the Ni(1) and Ni(2) cations. The Ni(2) cation is coordinated by two trans monodentate coplanar carboxylate groups of unique 1,3,5-benzenetricarboxylate ligands O(4)-Ni(2)-O(10) 175.8(2)°. The four remaining coordination sites cis to the carboxylate groups are occupied by water molecules that form the equatorial belt of the octahedral Ni(2) cation completing its coordination sphere (figure 6.16B).

The terminal Ni(1) and the bridging Ni(2) cations form a secondary building unit shown in figure 6.17, this building unit expands the structure down the *b*-axis and along the *c*-axis to form one dimensional chains (figure 6.18). These chains ‘zigzag’ and are linked together via hydrogen bonds and  $\pi$ - $\pi$  interactions. The four monodentate carboxylate groups of the 1,3,5-benzenetricarboxylate ligands show full deprotonation and delocalisation with comparable carbon-oxygen bonds listed in table 6.07. These carboxylate groups act as hydrogen bond acceptors forming hydrogen bonds to the coordinated water molecules of adjacent chains; O(13)-H(13B)⋯O(7D) 2.853(8) Å, O(15)-H(15A)⋯O(36) 2.775(8) Å, O(18)-H(18B)⋯O(3) 2.620(7) Å, O(18)-H(18A)⋯O(12) 2.883(6) Å (table 6.08). They form further hydrogen bonds acting as both hydrogen bond acceptors and donors to form a hydrogen bonding network throughout the structure (figure 6.19). The chains layer in an anti-parallel motif to maximise the  $\pi$ - $\pi$  stacking interactions between rings C(1)-C(8) and the adjacent rings of C(10)-C(17) at a distance of 3.581(2) Å with an interplanar staggering of 3.273(4) Å, expanding the structure down the *c*-axis and into three dimensions (figure 6.20).

During the course of this research compound 13 was synthesised and published by Hsu *et al.* (CSD Ref code: XUBLUC),<sup>3</sup> the structure was crystallised in the same space group with similar bond lengths and angles with selected comparisons in table 6.09.

Compound 13 was synthesised using solvothermal synthesis; this rapid synthesis technique enabled the rapid systematic variation of the reaction conditions to attempt to yield structural analogues or expanded structures with full deprotonation and coordination of all carboxylate groups. This resulted in the synthesis of compounds 14 and 15.

**Table 6.07: Selected Bond Lengths [Å] and Angles [°] for Compound 13**

Ni(1)–O(1)	2.109(5)	Ni(1)–O(13)	1.988(6)
Ni(1)–O(14)	2.079(5)	Ni(2)–O(4)	2.021(5)
Ni(2)–O(10)	2.022(5)	Ni(2)–O(15)	2.086(5)
Ni(2)–O(16)	2.069(5)	Ni(2)–O(17)	2.057(5)
Ni(2)–O(18)	2.065(5)	C(7)–O(1)	1.267(7)
C(8)–O(3)	1.256(8)	C(8)–O(4)	1.258(9)
C(16)–O(7)	1.259(7)	C(17)–O(9)	1.260(8)
C(17)–O(10)	1.273(9)		
O(1)–Ni(1)–O(1A)	62.5(3)	O(1)–Ni(1)–O(13)	159.6(3)
O(1)–Ni(1)–O(14)	87.3(2)	O(4)–Ni(2)–O(10)	175.8(2)
O(4)–Ni(2)–O(15)	89.2(2)	O(4)–Ni(2)–O(16)	89.81(19)
O(4)–Ni(2)–O(17)	86.4(2)	O(4)–Ni(2)–O(18)	93.6(2)
Ni(1)–O(1)–C(7)	89.1(4)	Ni(2)–O(4)–C(8)	128.7(4)
Ni(2)–O(10)–C(17)	127.6(4)	Ni(1)–O(13)–H(13A)	114(8)

Symmetry operations for equivalent atoms

A  $-x+1, y, -z+1$ **Table 6.08: Selected Hydrogen bond Lengths [Å] and angles [°] for Compound 13**

D–H...A	d(D–H)	d(H...A)	d(D...A)	(DHA)
O(13)–H(13A)...O(17C)	0.76(3)	1.85(3)	2.608(7)	178(12)
O(13)–H(13B)...O(7D)	0.75(3)	2.15(5)	2.853(8)	156(10)
O(14)–H(14A)...O(18E)	0.76(3)	2.13(4)	2.866(8)	164(9)
O(14)–H(14B)...O(7F)	0.76(3)	2.23(6)	2.880(8)	144(9)
O(15)–H(15A)...O(3G)	0.77(3)	2.00(3)	2.755(7)	171(7)
O(15)–H(15B)...O(16H)	0.76(3)	2.54(4)	3.244(7)	155(8)
O(16)–H(16A)...O(1I)	0.76(3)	2.18(3)	2.926(7)	168(9)
O(16)–H(16B)...O(9J)	0.76(3)	1.96(4)	2.680(7)	159(8)
O(17)–H(17A)...O(7K)	0.75(3)	2.12(5)	2.800(6)	152(8)
O(17)–H(17B)...O(9)	0.75(3)	1.83(3)	2.541(7)	158(7)
O(18)–H(18A)...O(1L)	0.76(3)	2.17(4)	2.883(7)	155(7)
O(18)–H(18B)...O(3)	0.75(3)	2.00(5)	2.620(7)	140(8)

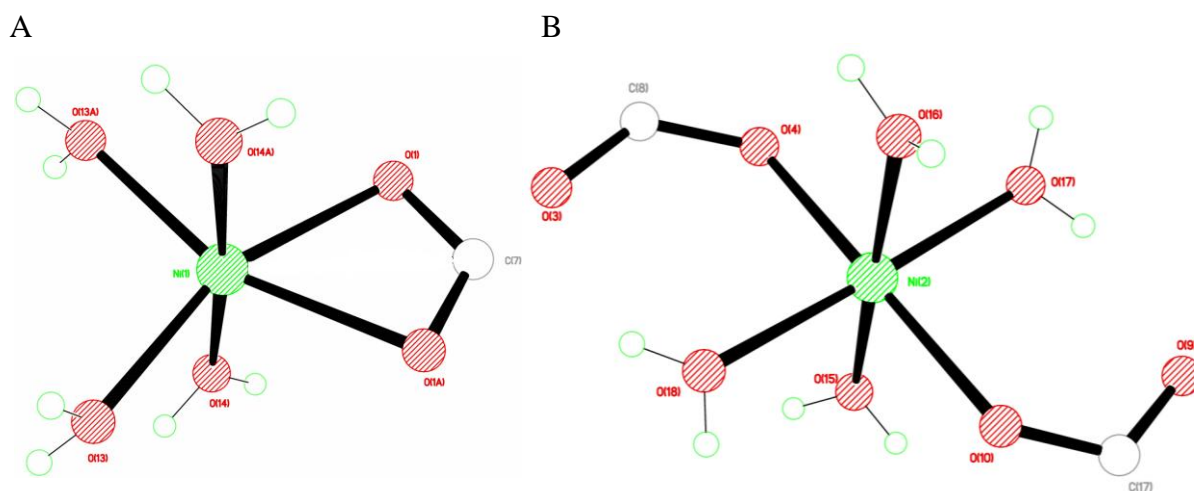
Symmetry operations for equivalent atoms

C  $x, y+1, z$  D  $x+1/2, y+3/2, z$  E  $x+1/2, y+1/2, z$ F  $-x+1/2, y+3/2, -z$  G  $-x+1/2, y-1/2, -z$  H  $x, y, z-1$ I  $x-1/2, y-1/2, z$  J  $-x+1/2, y+1/2, -z+1$  K  $x+1/2, y+1/2, z+1$ L  $x-1/2, y-1/2, z-1$

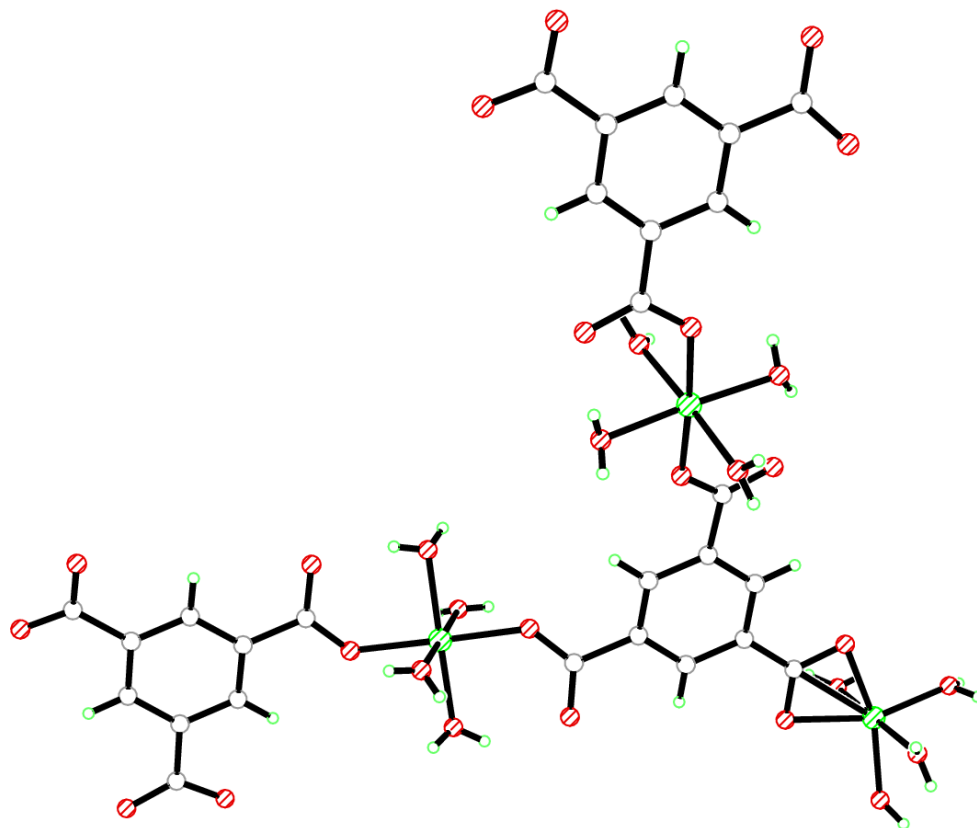


**Table 6.09: Average bond length comparisons between Compound 13 and XUBLUC<sup>3</sup>**

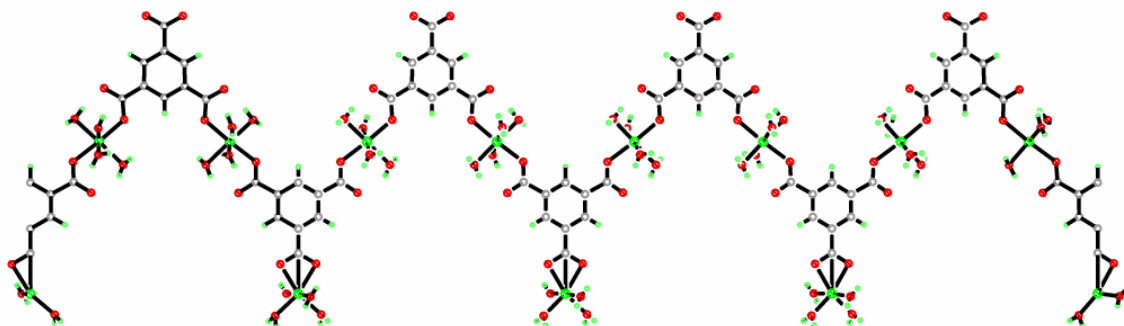
Compound	Bond	Average Bond Length (Å)
Compound 13	Ni-O (carboxylate)	2.031
Compound 13	Ni-O (water)	2.033
XUBLUC	Ni-O (carboxylate)	2.038
XUBLUC	Ni-O (water)	2.039



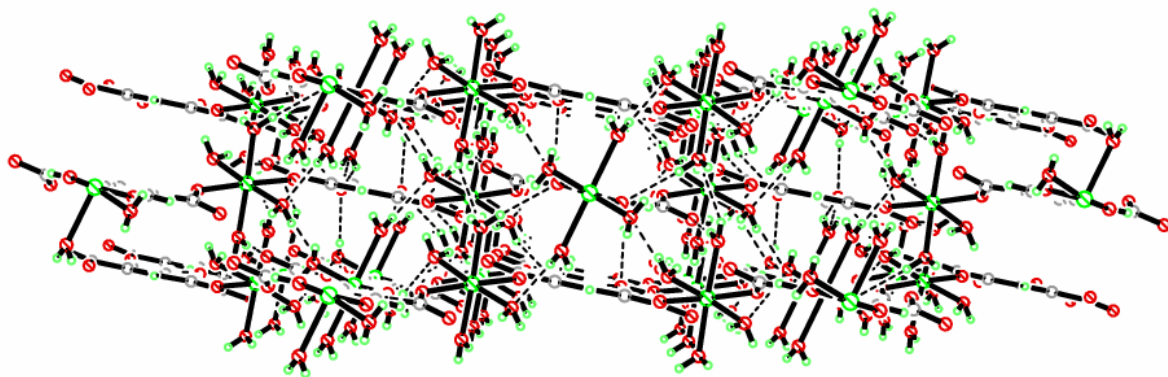
**Figure 6.16: A) Octahedral coordination environment of Ni(1) and B) Octahedral coordination environment of Ni(2) in compound 13**



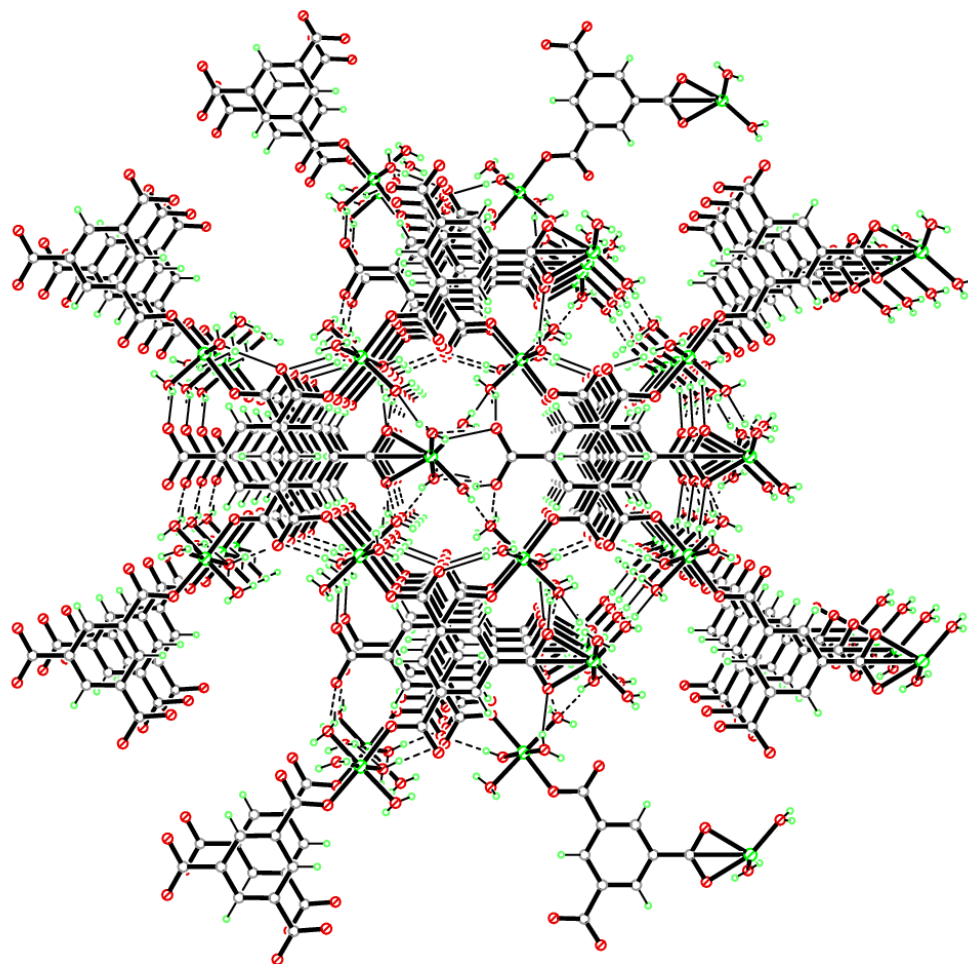
**Figure 6.17: Secondary building unit of Ni(1) and Ni(2) in compound 13**



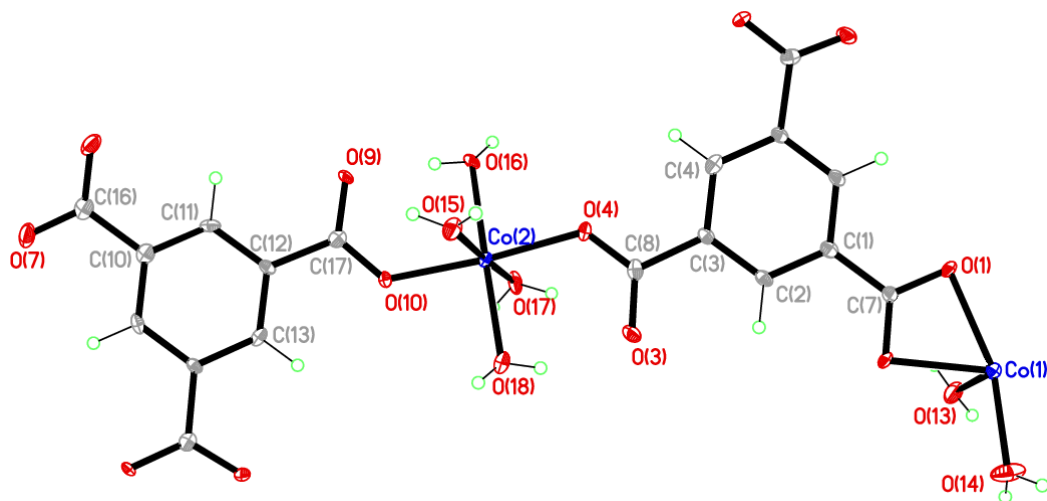
**Figure 6.18: One dimensional chains in compound 13 viewed down the *a*-axis**



**Figure 6.19:** Two dimensional packing and hydrogen bonding of the chains of compound 13 viewed down the *b*-axis



**Figure 6.20:** Three dimensional packing of layers of chains in compound 13 viewed down the *c*-axis

**Compound 14:**  $[\text{Co}_3(\text{C}_9\text{H}_3\text{O}_6)_2(\text{H}_2\text{O})_{12}]$ 

Chemical formula (total)	$\text{C}_{18}\text{H}_{30}\text{Co}_3\text{O}_{24}$
Formula weight	807.21
Temperature	150(2) K
Radiation, wavelength	MoK $\alpha$ , 0.71073 Å
Crystal system, space group	monoclinic, <i>I</i> 2
Unit cell parameters	$a = 6.5000(3)$ Å $\beta = 90.102(7)^\circ$ $b = 12.9415(5)$ Å $c = 16.1703(12)$ Å
Cell volume	$1360.24(13)$ Å <sup>3</sup>
<i>Z</i>	2
Crystal colour and size	purple, $0.80 \times 0.30 \times 0.10$ mm <sup>3</sup>
Final <i>R</i> indices [ <i>F</i> <sup>2</sup> > 2σ]	<i>R</i> 1 = 0.0237
<i>R</i> indices (all data)	<i>wR</i> 2 = 0.0611
Largest diff. peak and hole	0.90 and −0.29 e Å <sup>−3</sup>
Absolute structure parameter	0.703(18)

**Figure 6.21: Asymmetric Unit of Compound 14 all unique atoms labelled, additional atoms added to complete ligands.**

**Synthesis**

$\text{Co}(\text{NO}_3)_2 \cdot 6\text{H}_2\text{O}$  (0.09 g, 0.33 mmol) and 1,3,5-benzenetricarboxylic acid (0.035 g, 0.17 mmol) were added to a reaction mixture of ethanol (4mL) and water (3mL). This was placed into a 20mL Teflon-lined bomb and heated to 120°C for 24 hours. The vessel was then cooled back down to room temperature at a rate of 0.1°C / min and allowed to stand for 2 hours before purple block crystals were retrieved from the vessel.

## Structure Determination

The data were collected at 150 K using molybdenum radiation on an Oxford Diffraction Gemini A Ultra diffractometer. The structure was solved by direct methods. The semi-empirical absorption corrections were applied based on symmetry-equivalent and repeated data. The refinement gave a  $wR2$  of 0.0611 for all 1389 independent reflections and a conventional  $R1$  of 0.0237, for 1349 reflections with  $F^2 > 2\sigma$ . The residual electron density maximum and minimum were 0.90 and  $-0.29 \text{ e } \text{\AA}^{-3}$  respectively. Compound 14 crystallised in the chiral space group  $I2$  and refined with a Flack parameter of 0.703 indicating the structure may be twinned with inversion, it was not possible to define the twinning within the refinement which resulted in the high Flack parameter and the high residual electron density.

The hydrogen atoms were placed in geometrically calculated positions with  $U$  constrained to  $1.2 U_{\text{eq}}(\text{C})$  for aromatic hydrogen atoms and  $U$  constrained to  $1.5 U_{\text{eq}}(\text{O})$  for the hydroxyl hydrogen atoms. The ligands in the structure were slightly disordered and refined with SIMU and DELU restraints. The full data of compound 14 can be found in Appendix 1.

## Structure Analysis

Compound 14 is a structural analogue to compound 13 and XUBLUC,<sup>3</sup> however compound 14 is crystallised in the monoclinic space group  $I2$ . The asymmetric unit of compound 14 (figure 6.21) shows two 1,3,5-benzenetricarboxylate ligands completed by two-fold rotation axis that run through the centre of the respective aromatic rings, coordinated to two cobalt cations Co(1) and Co(2). The Co(1) cation is positioned on a two-fold rotation axis and forms a distorted six-coordinate octahedral geometry as shown in figure 6.22A. The Co(1) cation coordinates to a bidentate carboxylate group of the 1,3,5-benzenetricarboxylate ligand with a bite angle of O(1)-Co(1)-O(1A)  $61.22(16)^\circ$ . This bite angle is similar to that observed in the nickel analogue compound 13; O(1)-Ni(1)-O(1A)  $62.5(3)^\circ$  with a similar bond length of Co(1)-O(1)  $2.150(3) \text{ \AA}$  (table 6.10). The Co(1) cation coordinates further to two cis water molecules O(13)-Co(1)-O(14)  $85.11(13)^\circ$ , the remaining coordination sites are occupied by the symmetry

equivalent water ligands generated by the two fold rotation symmetry with O(13)-Co(1)-O(13A) 176.1(17)° in the trans position and O(14)-Co(1)-O(14A) 103.7(2)° at the distorted cis position. The coordination of these water ligands caps the Co(1) node preventing it expanding further down the *b*-axis and *a*-axis, further expansion is through the coordinated bridging 1,3,5-benzenetricarboxylate ligand that also coordinates to the coplanar Co(2) cation (figure 6.22A).

The Co(2) cation coordinates to two monodentate coplanar carboxylate groups of unique 1,3,5-benzenetricarboxylate ligands with a bridging angle of O(4)-Co(2)-O(10) 174.79(11)°. The four remaining equatorial coordination sites are occupied by water ligands that coordinate cis to the carboxylate groups; O(4)-Co(2)-O(15) 89.92(11)°, O(4)-Co(2)-O(16) 86.91(12)°, O(4)-Co(2)-O(17) 89.76(11)° and O(4)-Co(2)-O(18) 92.90(12)° (figure 6.22B).

The coordinated 1,3,5-benzenetricarboxylate ligands are completed by the two-fold rotation symmetry forming the secondary building unit shown in figure 6.23. The second 1,3,5-benzenetricarboxylate ligand that bridges the two Co(2) cations via symmetry is fully deprotonated; however the O(7)-C(16)-O(7A) carboxylate group does not coordinate to a cobalt cation, both the group and the monodentate carboxylate groups are fully delocalised with no evidence of carbon-oxygen double or single bonds (table 6.10). The uncoordinated carboxylate group coupled with the terminal Co(1) node results in the compound forming ‘zigzag’ one dimensional chains that expand down the *b*-axis (figure 6.24). The chains are linked together by an extensive hydrogen bonding network and  $\pi$ - $\pi$  stacking interactions. The monodentate and uncoordinated carboxylate groups act as hydrogen bond acceptors forming strong hydrogen bonds to coordinated water molecules of adjacent chains; O(18)-H(18B)⋯O(3) 2.613(4) Å, O(15)-H(15B)⋯O(3H) 2.25(4) Å, O(13)-H(13A)⋯O(7C) 2.833(4) Å, with a full list of hydrogen bonds in table 6.11. These hydrogen bonds form an extensive network allowing the chains to form a close packing motif shown in figure 6.25. The chains layer in an anti-parallel motif to maximise the  $\pi$ - $\pi$  stacking between the adjacent aromatic rings with a interplanar distance of 3.55(3) Å with a interplanar staggering of 3.22(5) Å expanding the structure into three dimensions.

Further analysis of the bulk material of compound 14 was carried out using elemental analysis to determine its purity with results of C = 26.97 %, H = 3.67 % and N = 0.06 % correlating with the calculated values from the single crystal data of C = 26.7 %, H = 3.71 % and N = 0 %, showing a high purity of the bulk material.

Compound 14 is the structural analogue of compound 13/XUBLUC<sup>3</sup> and is isostructural with comparable bond lengths and angles, compound 14 is also similar to a compound synthesised by Stride *et al.* (CSD Refcode: EKEXEY)<sup>4</sup> that is formed using the same ligands; the bond lengths of these compounds are compared in table 6.12. Compounds 14 and 13 were prepared using the solvothermal synthesis technique; this method has high reproducibility providing a highly pure compound making it an ideal platform to design new compounds from. The slight alterations in the synthesis protocol in preparing both the nickel and cobalt analogues also yielded the new cadmium analogue, compound 15.

**Table 6.10: Selected Bond Lengths [Å] and Angles [°] for Compound 14**

Co(1)–O(1)	2.150(3)	Co(1)–O(13)	2.118(3)
Co(1)–O(14)	2.004(3)	Co(2)–O(4)	2.061(3)
Co(2)–O(10)	2.060(3)	Co(2)–O(15)	2.123(3)
Co(2)–O(16)	2.083(3)	Co(2)–O(17)	2.136(3)
Co(2)–O(18)	2.098(4)	C(7)–O(1)	1.275(4)
C(8)–O(3)	1.264(5)	C(8)–O(4)	1.259(5)
C(16)–O(7)	1.269(4)	C(17)–O(9)	1.262(5)
C(17)–O(10)	1.259(5)		
O(1)–Co(1)–O(1A)	61.22(16)	O(1)–Co(1)–O(13)	97.44(11)
O(1)–Co(1)–O(14)	156.41(14)	O(4)–Co(2)–O(10)	174.79(11)
O(4)–Co(2)–O(15)	89.92(11)	O(4)–Co(2)–O(16)	86.91(12)
O(4)–Co(2)–O(17)	89.76(11)	O(4)–Co(2)–O(18)	92.90(12)
Co(1)–O(1)–C(7)	90.2(3)	Co(2)–O(4)–C(8)	128.4(3)
Co(2)–O(10)–C(17)	128.9(3)		

Symmetry operations for equivalent atoms

A  $-x+1, y, -z+1$ **Table 6.11: Selected Hydrogen bond Lengths [Å] and angles [°] for Compound 14**

D–H...A	d(D–H)	d(H...A)	d(D...A)	(DHA)
O(13)–H(13A)...O(7C)	0.792(18)	2.05(2)	2.833(4)	168(5)
O(13)–H(13B)...O(18D)	0.788(18)	2.46(5)	2.906(4)	117(5)
O(14)–H(14A)...O(7E)	0.787(18)	2.11(3)	2.837(5)	154(6)
O(14)–H(14B)...O(16F)	0.789(18)	1.866(19)	2.650(3)	172(5)
O(15)–H(15A)...O(7G)	0.793(18)	2.41(3)	3.130(4)	151(4)
O(15)–H(15B)...O(3H)	0.795(18)	1.94(2)	2.725(4)	172(5)
O(16)–H(16A)...O(7I)	0.783(18)	2.006(19)	2.788(5)	177(5)
O(16)–H(16B)...O(9)	0.786(18)	1.80(2)	2.537(4)	155(4)
O(17)–H(17A)...O(9D)	0.792(18)	1.883(19)	2.667(4)	170(4)
O(17)–H(17B)...O(1J)	0.791(18)	2.12(2)	2.897(4)	168(4)
O(18)–H(18A)...O(1K)	0.803(19)	2.08(2)	2.877(5)	175(4)
O(18)–H(18B)...O(3)	0.790(18)	1.89(3)	2.613(4)	151(5)

Symmetry operations for equivalent atoms

C  $x-1/2, y-3/2, z-1/2$  D  $-x+1/2, y-1/2, -z+3/2$ E  $x+1/2, y-3/2, z-1/2$  F  $x, y-1, z$  G  $x+1/2, y-1/2, z-1/2$ H  $-x+3/2, y+1/2, -z+3/2$  I  $x-1/2, y-1/2, z-1/2$ J  $x-1/2, y+1/2, z+1/2$  K  $x+1/2, y+1/2, z+1/2$



**Table 6.12: Average bond length comparisons between Compound 14, Compound 13, XUBLUC<sup>3</sup> and EKEXEY<sup>4</sup>**

Compound	Bond	Average Bond Length (Å)
Compound 13	Ni-O (carboxylate)	2.031
Compound 14	Co-O (carboxylate)	2.047
XUBLUC	Ni-O (carboxylate)	2.088
EKEXEY	Co-O (carboxylate)	2.102

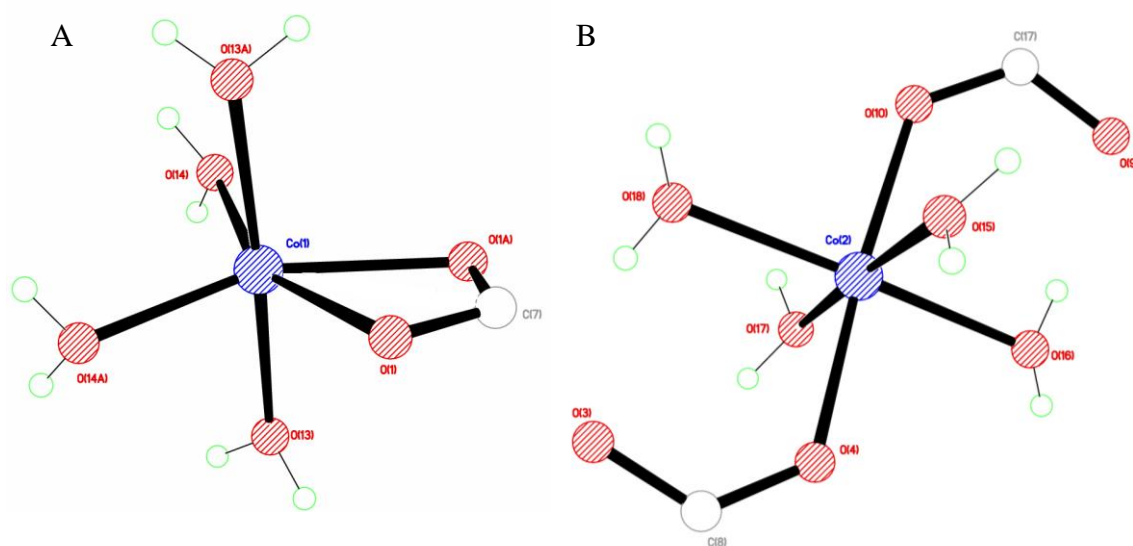


**Figure 6.22: A) Octahedral coordination environment of Co(1) and B) Octahedral coordination environment of Co(2) in compound 14**

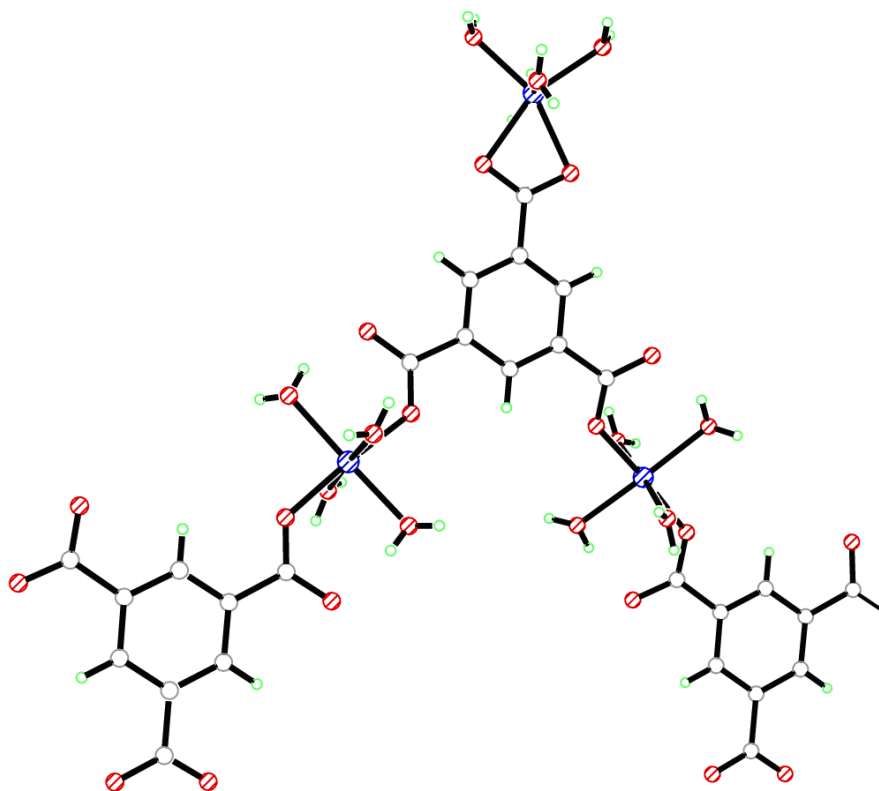


**Figure 6.23:** Secondary building unit of Co(1) and Co(2) in compound 14

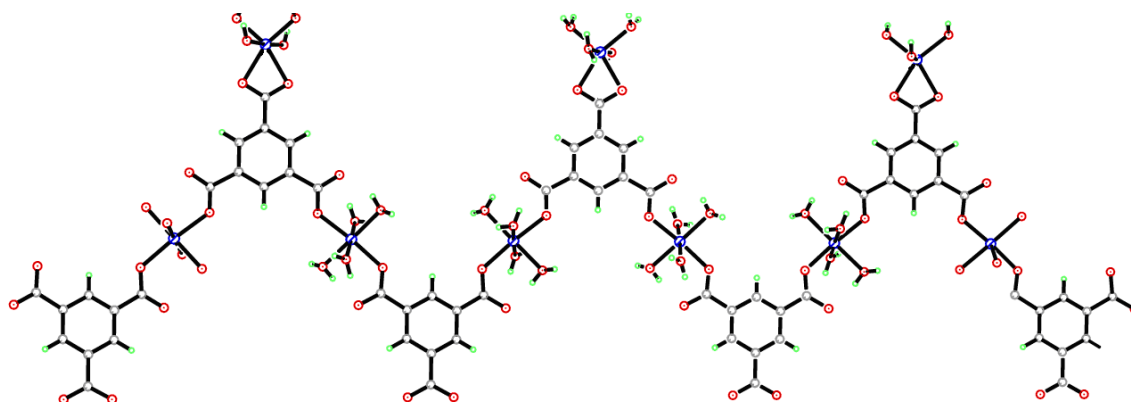


**Figure 6.24:** One dimensional chains in compound 14 viewed down the *a*-axis

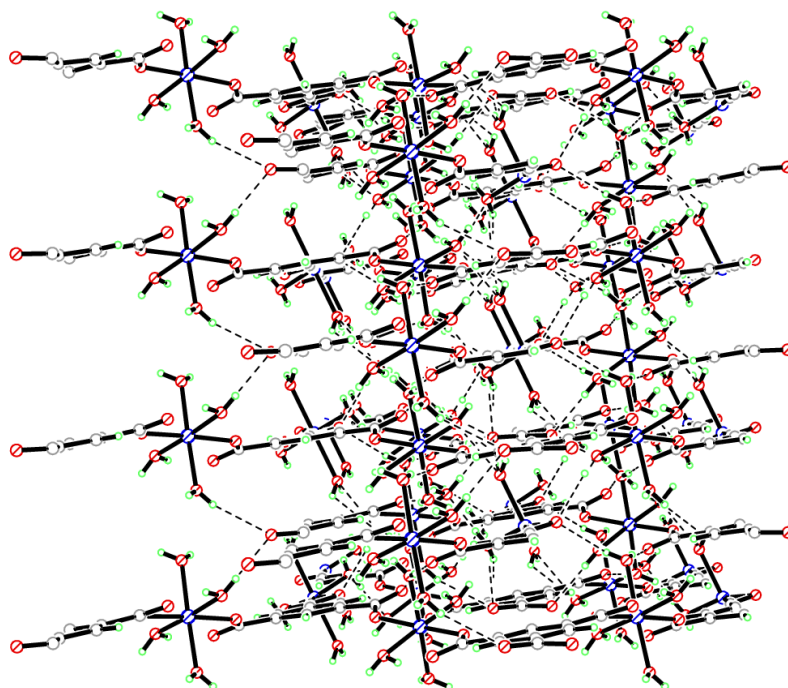
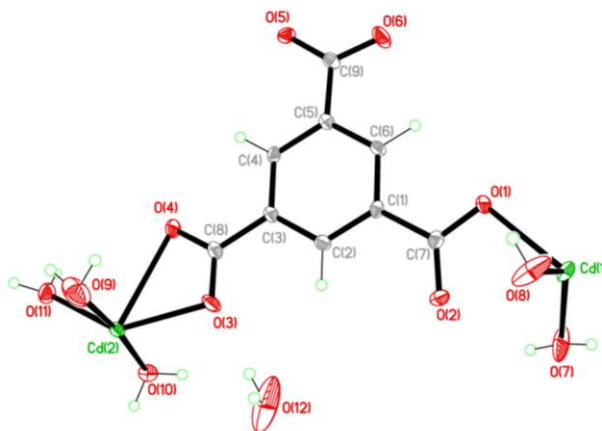


**Figure 6.25:** Two dimensional packing and hydrogen bonding of the chains of compound 14 viewed down the *b*-axis

**Compound 15:**  $[\text{Cd}_3(\text{C}_9\text{H}_3\text{O}_6)_2(\text{H}_2\text{O})_9] \cdot 2(\text{H}_2\text{O})$



Chemical formula (total)	$\text{C}_{18}\text{H}_{28}\text{Cd}_3\text{O}_{23}$
Formula weight	949.60
Temperature	150(2) K
Radiation, wavelength	MoK $\alpha$ , 0.71073 Å
Crystal system, space group	monoclinic, $C2/c$
Unit cell parameters	$a = 18.9932(5)$ Å $b = 7.34117(19)$ Å $c = 20.3954(5)$ Å $\beta = 97.205(2)^\circ$
Cell volume	$2821.32(13)$ Å <sup>3</sup>
Z	4
Crystal colour and size	colourless, $0.30 \times 0.20 \times 0.05$ mm <sup>3</sup>
Final $R$ indices [ $F^2 > 2\sigma$ ]	$R1 = 0.0254$
$R$ indices (all data)	$wR2 = 0.0605$
Largest diff. peak and hole	1.29 and $-1.09$ e Å <sup>-3</sup>

**Figure 6.26:** Asymmetric Unit of Compound 15 all unique atoms labelled, additional atoms added to complete ligands.

**Synthesis**

$\text{Cd}(\text{NO}_3)_2 \cdot 4\text{H}_2\text{O}$  (0.101 g, 0.33 mmol) and 1,3,5-benzenetricarboxylic acid (0.035 g, 0.17 mmol) were added to a reaction mixture of ethanol (4mL) and water (3mL). This was placed into a 20mL Teflon-lined bomb and heated to 120°C for 24 hours. The vessel was then cooled back down to room temperature at a rate of 0.1°C / min and allowed to stand for 2 hours before colourless block crystals were retrieved from the vessel.

## Structure Determination

The data were collected at 150 K using molybdenum radiation on an Oxford Diffraction Gemini A Ultra diffractometer. The structure was solved by direct methods. The semi-empirical absorption corrections were applied based on symmetry-equivalent and repeated data. The refinement gave a  $wR2$  of 0.0605 for all 3377 independent reflections and a conventional  $R1$  of 0.0254, for 2883 reflections with  $F^2 > 2\sigma$ . The residual electron density maximum and minimum were 1.29 and  $-1.09 \text{ e } \text{\AA}^{-3}$  respectively, the high residual electron density in compound 15 is primarily caused by unmodelled disorder in coordinated and uncoordinated water molecules.

The hydrogen atoms were placed in geometrically calculated positions with  $U$  constrained to  $1.2 U_{\text{eq}}(\text{C})$  for aromatic hydrogen atoms and  $U$  constrained to  $1.5 U_{\text{eq}}(\text{O})$  for the hydroxyl hydrogen atoms. The water molecules in the structure were slightly disordered and refined with SADI restraints. The full data of compound 15 can be found in Appendix 1.

## Structure Analysis

The asymmetric unit of compound 15 (figure 6.26) shows a complete 1,3,5-benzenetricarboxylate ligand bridging two unique cadmium cations Cd(1) and Cd(2) and one symmetry related cadmium cation Cd(2A). The cadmium cations are in two different coordination environments in this polymeric compound, with Cd(1) positioned on a two-fold rotation axis and Cd(2) in a general position.

The Cd(1) cation forms a five-coordinate distorted trigonal bipyramidal node (figure 6.27A), coordinating to two monodentate symmetry related 1,3,5-benzenetricarboxylate ligands through the O(1) carboxylate oxygen forming the Cd(1)-O(1) 2.248(19) Å bond. The second symmetry equivalent bond coordinates in the trans coplanar position O(1)-Cd(1)-O(1A)  $171.59(11)^\circ$ , generated by the two-fold rotation symmetry around the centre of the Cd(1) cation. The remaining O(2) carboxylate does not form a direct covalent bond; however it forms a long range interaction at 2.737(2) Å almost allowing the carboxylate group to form a bidentate bond with a bite angle of  $80.95(3)^\circ$ , this interaction is partially responsible for the distortion within the Cd(1)

geometry bringing the O(1)-Cd(1)-O(1A) angle away from the ideal 180°. The remaining coordination sites are occupied by two unique water molecules O(7) and O(8), the O(8) water is situated on a two-fold rotation axis with its second hydrogen generated by rotation symmetry. The O(7) water molecule coordinates at O(7)-Cd(1)-O(8) 132.52(8)°, its symmetry equivalent is generated by the two-fold axis and fills the final coordination site at O(7)-Cd(1)-O(7A) 94.96(16)° (figure 6.27A) (table 6.13).

The remaining carboxylate groups on the 1,3,5-benzenetricarboxylate ligand form bidentate coordination bonds to the Cd(2) cations. The Cd(2) cation coordinates to the O(3)-C(8)-O(4) carboxylate group with a bite angle of 52.73(3)°. This bidentate coordination mode shows an unusual bond length arrangement with the Cd(2)-O(3) forming the strong bond at 2.258(19) Å, whilst the Cd(2)-O(4) forms a much weaker bond of length 2.623(2) Å. This is also present in the carboxylate group of the symmetry equivalent ligand O(5B)-C(9B)-O(6B) that coordinates with a bite angle of 53.81(7)° and bond lengths; Cd(2)-O(5B) 2.528(19) Å and Cd(2)-O(6B) 2.313(2) Å. The carboxylate groups coordinate to the Cd(2) cation in a distorted cis position O(3)-Cd(2)-O(6B) 83.72(7)°, with the remaining coordination sites filled with water molecules O(9)-O(11) perpendicular to the carboxylate groups; O(3)-Cd(2)-O(9) 88.18(9)°. This completes the coordination sphere of the seven-coordinate distorted pentagonal bipyramidal Cd(2) cation shown in figure 6.27B. The combination of the coordination motifs of the Cd(1) and Cd(2) cations forms the secondary building unit in figure 6.28.

The 1,3,5-benzenetricarboxylates twist out of the cadmium cation plane with an angle of 60.70(2)° to one another forming a non-planar 'zigzag' chain similar to that in compounds 13 and 14. These chains expand into two dimensional columns that stack on top of one another down the *c*-axis (figure 6.29). These columns are then interpenetrated by an inverse column generated by an inversion centre in-between the two columns. These run in opposite directions and form close  $\pi$ - $\pi$  stacking interactions of 3.797(13) Å with an offset of 3.424(8) Å between adjacent rings (figure 6.30).

The structure is further stabilised by hydrogen bonding between coordinated water molecules and the hydrogen bond accepting carboxylate groups that form strong almost linear hydrogen bonds; O(7)-H(7A)⋯O(5D) 2.683(3) Å with an angle of 173(4)° and O(10)-H(10A)⋯O(2I) 2.648(3) Å with a linear angle of 175(3)°. The packing of

compound 15 yields small closed pores between the interpenetrating columns that contain one uncoordinated water molecule, this forms two strong hydrogen bonds between O(3) and an adjacent O(6F) of 2.854(4) Å and 3.189(4) Å respectively with a bite angle of 104(2)° (table 6.14).

The presence of a closed micropore resulted in compound 15 undergoing further analysis with the intention of opening the pores by overcoming the  $\pi$ - $\pi$  stacking and hydrogen bonds, then dehydrating the structure to allow gas or liquid adsorption. The removal would require a structural change that the thermogravimetric analysis confirms to be too dramatic as the TGA plot shown in figure 6.31 indicates complete dissociation of the compound after 55°C during stage 1, suggesting the structure would not be suitable for further application investigations.

Additional analysis of the bulk sample was carried out to confirm the purity of the compound and to give validity to the synthesis protocol for further adaptations. The powder X-ray diffraction data produced from compound 15 was of a sufficient quality for comparison with the predicted powder diffraction pattern obtained from the single crystal data (figure 6.32). Both the powder patterns correlate well with the only significant difference in the background signals at 45 2-Theta, with all significant peaks at 8.6, 15.2, 15.9, 18.7 and 26 2-Theta present with appropriate intensities.

Elemental analysis of compound 15 gave the results C = 24.88 %, H = 2.75 % and N = 0 %, these correspond to the calculated values from the single crystal data of C = 22.75 %, H = 2.95 % and N = 0 %. The further analysis of the compound confirms the validity of the synthesis protocol with the synthesis of a pure bulk product.

Compound 15 was synthesised using solvothermal synthesis with replicated conditions of compounds 13 and 14 to continue the structural series. Compound 15 crystallises in the higher symmetry space group of monoclinic  $C2/c$  and contains significant differences that result in the ‘zigzag’ chain formation that further expands into an interpenetrated column. The primary difference in compound 15 when compared to compounds 13 and 14 is the coordination geometry of the Cd(1) and Cd(2) cations. In the previous compounds the similar atomic radii of nickel and cobalt cations formed slightly distorted octahedral geometries that are common in compounds of this nature.<sup>3-6</sup> This is in stark contrast to the disordered trigonal bipyramidal and pentagonal

bipyramidal geometries of the Cd(1) and Cd(2) cations respectively. The cadmiums can adopt these geometries due to their larger coordination sphere; this allows the cation to form multiple bidentate coordinations to the carboxylate groups of the 1,3,5-benzenetricarboxylate ligands. The presence of the trigonal bipyramidal and pentagonal bipyramidal geometries also prevents the formation of terminal nodes observed in compounds 13 and 14, with the presence of a fully deprotonated and delocalised 1,3,5-benzenetricarboxylate bridging linker the structure forms the two dimensional columns. A comparison of the significant bond lengths is presented in table 6.15 and highlights the weaker 'second' bond in the bidentate carboxylates of compound 15.

Along with compound 13 and 14 presented in this thesis additional compounds such as XUBLUC,<sup>3</sup> EKEXEY,<sup>4</sup> EXOKOR<sup>5</sup> and DERYAB<sup>6</sup> published in the literature show the potentials for expanding this synthesis protocol and structure motif. The copper analogue EXOKOR published by Murugavel *et al.*<sup>5</sup> shows that for the late first-row transition metals the structural motif exhibited in compounds 13 and 14 can be further extended. The bimellitic compound of DERYAB<sup>6</sup> indicates how a substitution of one metal site can occur in this structure without affecting the overall structural motif. The dual zinc, nickel structure affords octahedral nodes that form the 'zigzag' chains with the zinc cation acting as the terminal node. The synthesis procedure of DERYAB is similar to that of the previous compounds with the nickel concentration halved with the addition of the zinc metal. The prospect of producing dual-metal frameworks led to new synthesis protocols being devised. As part of these new reactions the addition of DMF was selected due to its properties under solvothermal conditions to act as a deprotonating and templating agent. These reactions resulted in compounds 16, 17 and 19-21.



**Table 6.13: Selected Bond Lengths [Å] and Angles [°] for Compound 15**

Cd(1)–O(1)	2.2481(19)	Cd(1)–O(7)	2.265(2)
Cd(1)–O(8)	2.244(3)	Cd(2)–O(3)	2.2581(19)
Cd(2)–O(4)	2.623(2)	Cd(2)–O(5B)	2.5281(19)
Cd(2)–O(6B)	2.313(2)	Cd(2)–O(9)	2.277(3)
Cd(2)–O(10)	2.293(2)	Cd(2)–O(11)	2.269(2)
C(7)–O(1)	1.271(3)	C(7)–O(2)	1.243(3)
C(8)–O(3)	1.257(3)	C(8)–O(4)	1.261(3)
C(9)–O(5)	1.270(3)	C(9)–O(6)	1.256(3)
O(1)–Cd(1)–O(1A)	171.59(11)	O(1)–Cd(1)–O(7)	106.56(8)
O(1)–Cd(1)–O(8)	85.80(6)	O(3)–Cd(2)–O(4)	52.73(7)
O(3)–Cd(2)–O(5B)	136.61(7)	O(3)–Cd(2)–O(6B)	83.72(7)
O(3)–Cd(2)–O(9)	88.18(9)	O(3)–Cd(2)–O(10)	95.91(8)
O(3)–Cd(2)–O(11)	138.56(8)	Cd(1)–O(1)–C(7)	105.22(17)
Cd(2)–O(3)–C(8)	101.71(17)	Cd(2)–O(4)–C(8)	84.43(16)

Symmetry operations for equivalent atoms

A  $-x+1, y, -z+3/2$  B  $x+1/2, y-1/2, z$  C  $x-1/2, y+1/2, z$ **Table 6.14: Selected Hydrogen bond Lengths [Å] and angles [°] for Compound 15**

D–H...A	d(D–H)	d(H...A)	d(D...A)	(DHA)
O(7)–H(7A)...O(5D)	0.813(15)	1.874(16)	2.683(3)	173(4)
O(7)–H(7B)...O(4E)	0.815(15)	1.97(2)	2.755(3)	161(4)
O(8)–H(8A)...O(4F)	0.820(14)	1.943(12)	2.753(3)	169(2)
O(9)–H(9A)...O(1F)	0.861(15)	1.804(18)	2.651(3)	167(3)
O(9)–H(9B)...O(11G)	0.858(15)	2.72(4)	2.982(3)	99(3)
O(9)–H(9B)...O(7H)	0.858(15)	2.65(4)	3.041(4)	110(3)
O(10)–H(10A)...O(2I)	0.829(14)	1.821(14)	2.648(3)	175(3)
O(10)–H(10B)...O(12I)	0.804(14)	1.788(16)	2.582(4)	169(4)
O(11)–H(11A)...O(10G)	0.822(14)	1.886(16)	2.704(3)	173(3)
O(11)–H(11B)...O(5J)	0.817(14)	1.990(16)	2.802(3)	172(3)
O(12)–H(12A)...O(3)	0.84	2.01	2.854(4)	179
O(12)–H(12B)...O(6F)	0.84	2.35	3.189(4)	179

Symmetry operations for equivalent atoms

D  $-x+1, -y+1, -z+1$  E  $x, -y+1, z+1/2$  F  $-x+1, -y, -z+1$ G  $-x+3/2, y-1/2, -z+1/2$  H  $x, -y, z-1/2$  I  $-x+3/2, -y+1/2, -z+1$ J  $-x+1, y, -z+1/2$

**Table 6.15: Bond length comparisons between Compound 15, Compound 13, and Compound 14**

Compound	Bond	Average Bond Length (Å)
Compound 13	Ni(1)-O(1) (carboxylate)	2.031
Compound 14	Co(1)-O(1) (carboxylate)	2.047
Compound 15	Cd(2)-O(3) (carboxylate)	2.258
Compound 15	Cd(2)-O(4) (carboxylate)	2.623
Compound 15	Cd(2)-O(5) (carboxylate)	2.528
Compound 15	Cd(2)-O(6) (carboxylate)	2.313

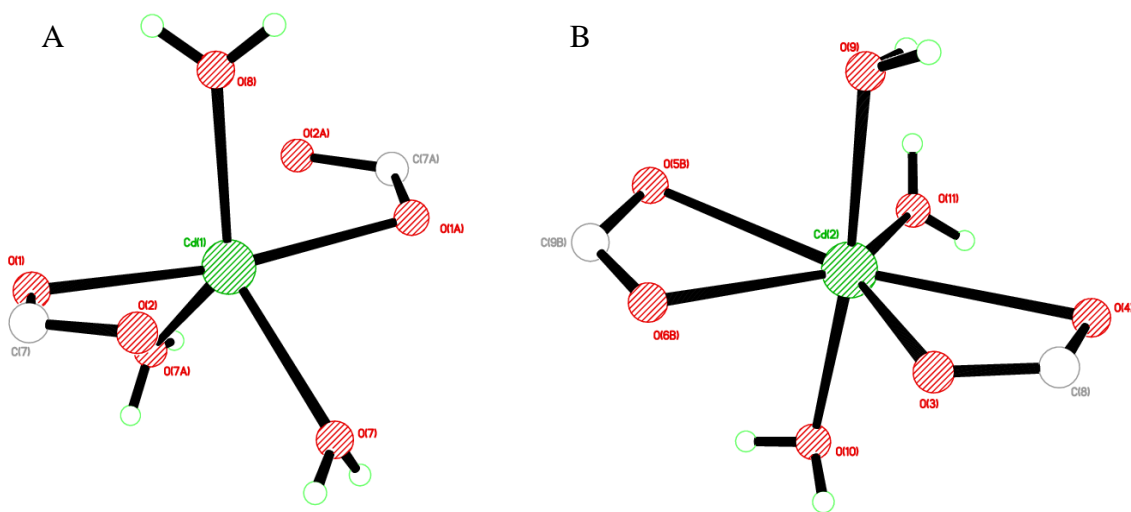


**Figure 6.27: A) Trigonal bipyramidal coordination environment of Cd(1) and B) Pentagonal bipyramidal coordination environment of Cd(2) in compound 15**

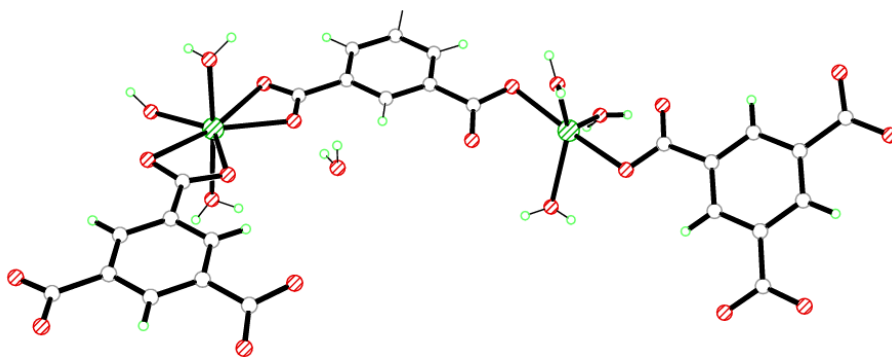


**Figure 6.28:** Secondary building unit of Cd(1) and Cd(2) in compound 15

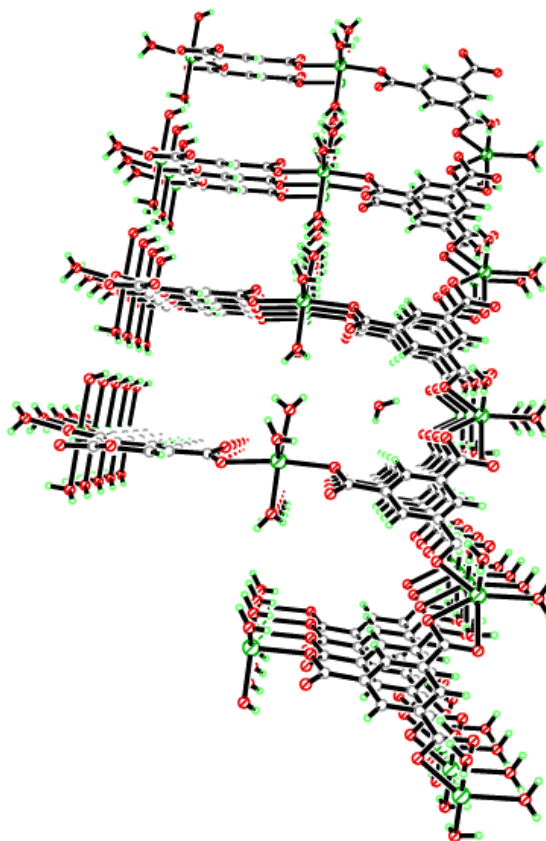


**Figure 6.29:** Two dimensional columns in compound 15 viewed down the *c*-axis

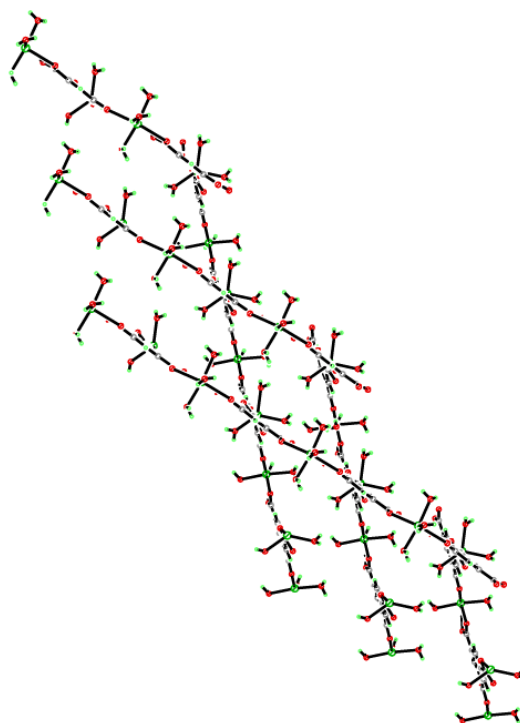


**Figure 6.30:** Two dimensional packing and interpenetration of the columns of compound 15 viewed down the *b*-axis

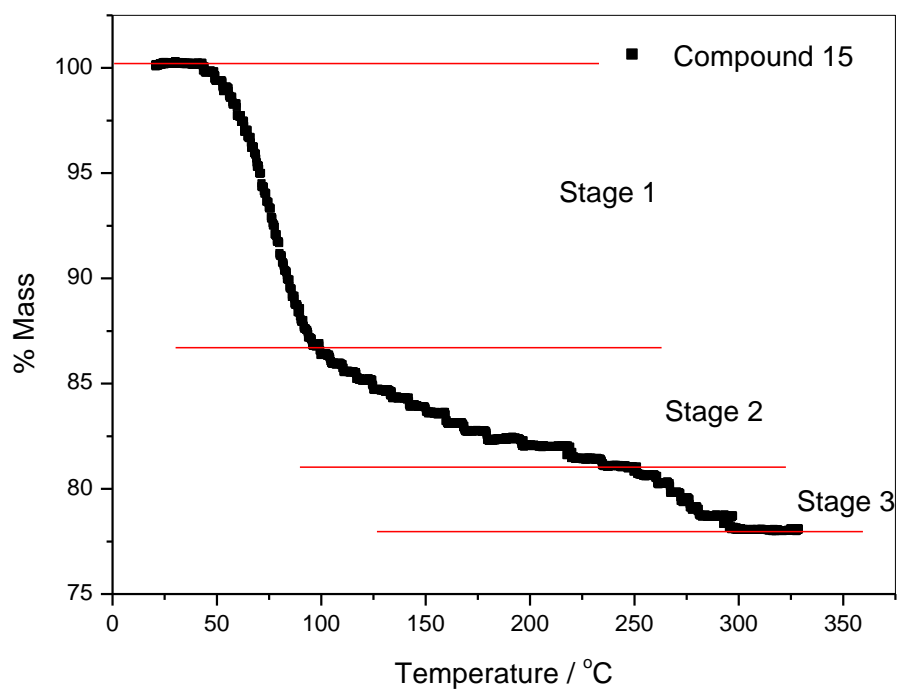


**Figure 6.31:** Thermogravimetric analysis plot of compound 15

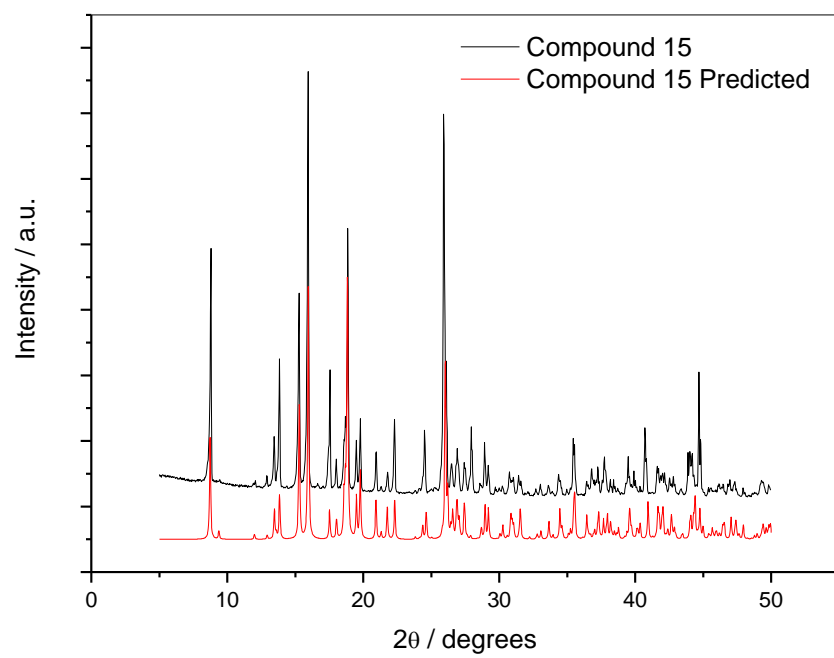
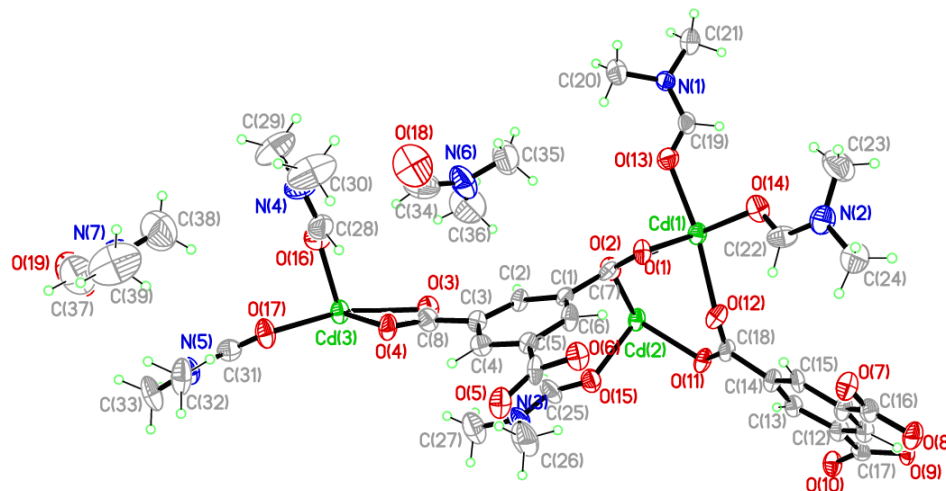


**Figure 6.32: Powder X-ray diffraction pattern of Compound 15**

**Compound 16:**  $[\text{Cd}_3(\text{C}_9\text{H}_3\text{O}_6)_2(\text{C}_3\text{H}_7\text{NO})_5] \cdot 2(\text{C}_3\text{H}_7\text{NO})$



Chemical formula (total)	$\text{C}_{39}\text{H}_{55}\text{Cd}_3\text{N}_7\text{O}_{19}$	
Formula weight	1263.10	
Temperature	150(2) K	
Radiation, wavelength	$\text{CuK}\alpha$ , 1.54184 Å	
Crystal system, space group	triclinic, $P\bar{1}$	
Unit cell parameters	$a = 10.1839(6)$ Å	$\alpha = 96.126(6)^\circ$
	$b = 11.1884(9)$ Å	$\beta = 100.103(5)^\circ$
	$c = 21.8343(14)$ Å	$\gamma = 93.186(6)^\circ$
Cell volume	2428.2(3) Å <sup>3</sup>	
Z	2	
Crystal colour and size	colourless, 0.50 × 0.07 × 0.05 mm <sup>3</sup>	
Final $R$ indices [ $F^2 > 2\sigma$ ]	$R1 = 0.0642$	
$R$ indices (all data)	$wR2 = 0.1528$	
Largest diff. peak and hole	1.60 and $-1.03$ e Å <sup>-3</sup>	

**Figure 6.33:** Asymmetric Unit of Compound 16 all unique atoms labelled, additional atoms added to complete ligands.

### Synthesis

$\text{Cd}(\text{NO}_3)_2 \cdot 4\text{H}_2\text{O}$  (0.101 g, 0.33 mmol) and 1,3,5-benzenetricarboxylic acid (0.035 g, 0.17 mmol) were added to a reaction mixture of dimethylformamide (DMF) (4 mL), ethanol (4mL) and water (3mL). This was placed into a 20mL Teflon-lined bomb and heated to 120°C for 24 hours. The vessel was then cooled back down to room temperature at a rate of 0.1°C / min and allowed to stand for 2 hours before colourless block crystals were retrieved from the vessel.

## Structure Determination

The data were collected at 150 K using copper radiation on an Oxford Diffraction Gemini A Ultra diffractometer. The structure was solved by direct methods. The semi-empirical absorption corrections were applied based on symmetry-equivalent and repeated data. The refinement gave a  $wR2$  of 0.1528 for all 7504 independent reflections and a conventional  $R1$  of 0.0642, for 4518 reflections with  $F^2 > 2\sigma$ . The residual electron density maximum and minimum were 1.60 and  $-1.03 \text{ e } \text{\AA}^{-3}$  respectively, the high residual electron density is a result of unmodelled disorder in coordinated DMF.

The hydrogen atoms were placed in geometrically calculated positions with  $U$  constrained to  $1.2 U_{eq}(\text{C})$  for aromatic hydrogen atoms and  $U$  constrained to  $1.5 U_{eq}(\text{O})$  for the hydroxyl hydrogen atoms. The DMF molecules in the structure were slightly disordered and refined with SIMU and DELU restraints. The full data of compound 16 can be found in Appendix 1.

## Structure Analysis

The asymmetric unit of compound 16 (figure 6.33) shows two complete 1,3,5-benzenetricarboxylate ligands coordinating three cadmium cations Cd(1), Cd(2) and Cd(3). The cadmium cations are in general positions and adopt two different coordination geometries in this polymeric compound; Cd(1) forms a seven-coordinate pentagonal bipyramidal geometry whilst both Cd(2) and Cd(3) form distorted six-coordinate octahedral geometries (figure 6.34) (table 6.16).

The seven-coordinate Cd(1) (figure 6.34A) is coordinated by two bidentate carboxylate groups of unique 1,3,5-benzenetricarboxylate ligands, and monodentate coordination to a bifurcated carboxylate group that bridges both Cd(1) and Cd(2) through individual bonds of a symmetry equivalent 1,3,5-benzenetricarboxylate ligand. The cadmium cation forms a bidentate bond to the carboxylate group O(1)-C(7)-O(2) with a bite angle of  $54.2(2)^\circ$ , a second carboxylate group O(9)-C(17)-O(10) coordinates with the O(10) trans to the O(1) atom; O(1)-Cd(1)-O(10)  $162.2(3)^\circ$  and the O(9) cis to the O(2) atom O(2)-Cd(1)-O(9)  $72.1(2)^\circ$ . This carboxylate group coordinates with a bite angle of  $54.5(2)^\circ$  comparable to that of the O(1)-C(7)-O(2) bidentate carboxylate group,

these carboxylates coordinate coplanar with alternating bond lengths; Cd(1)-O(1) 2.272(7) Å, Cd(1)-O(2) 2.573(7) Å, Cd(1)-O(9) 2.541(7) Å and Cd(1)-O(10) 2.298(7) Å. These alternating bond lengths are also observed in the seven-coordinate pentagonal bipyramidal Cd(2) cation of compound 15. Although the oxygens are coplanar the 1,3,5-benzenetricarboxylates twist out of plane at the carboxylate carbons C(7) and C(17) at an angle of 122.31(7)°. An additional carboxylate coordinates cis with respect to the other carboxylate groups; O(9)-Cd(1)-O(12) 86.6(2)° and O(1)-Cd(1)-O(12) 80.2(3)° forming a standard monodentate bond Cd(1)-O(12) 2.3226(7) Å. This additional carboxylate is part of a symmetry equivalent 1,3,5-benzenetricarboxylate ligand of the ligand containing the O(9)-C(17)-O(10) carboxylate, and acts as a bridge between Cd(1) and Cd(2) allowing the structure to expand in both the *b*-axis and *c*-axis. The remaining two coordination sites on the Cd(1) cation are capped by coordinated DMF molecules cis to one another at an angle of 94.1(13)°, this completes the coordination sphere of the Cd(1) cation (figure 6.34A).

The Cd(2) cation is located 3.524(3) Å below the Cd(1) cation in the *b*-axis linked by three bridging carboxylate groups; O(1)-C(7)-O(2), O(10)-C(17)-O(9) and O(12)-C(18)-O(11) shown in figure 6.34B. As previously mentioned the monodentate coordination from the O(12)-C(18)-O(11) carboxylate forms a standard coordination bridge between Cd(1) and Cd(2) with a conventional bite angle of 67.46(2)° and strong monodentate bonds to each respective cadmium cations Cd(1)-O(12) 2.326(7) Å and Cd(2)-O(11) 2.206(6) Å. The remaining two bridging carboxylates coordinate originally to the Cd(1) cation as bidentate ligands with bonds formed with both carboxylate oxygens. One oxygen from each of these groups (O(2) and O(9)) then coordinate to the Cd(2) cation with bite angles of Cd(1)-O(2)-Cd(2) 92.7(2)° and Cd(1)-O(9)-Cd(2) 91.9(2)° placing the bond perpendicular to the bidentate carboxylate group. Although this bridge is unconventional, the bond lengths of Cd(2)-O(2) 2.290(7) Å and Cd(2)-O(9) 2.360(7) Å suggest that these are the primary bonds to the carboxylate oxygens compared to the much longer weaker bonds to the Cd(1) cation partially explaining the short-long bidentate bonds observed at the Cd(1) cation. The final two equatorial coordination sites are occupied by the bidentate O(7B)-C(16B)-O(8B) carboxylate group of the cis coplanar symmetry equivalent 1,3,5-benzenetricarboxylate of the C(11)-



C(18) ligand coordinated through the O(11)-C(18)-O(12) carboxylate group at an angle of O(7B)-Cd(2)-O(11)  $87.4(2)^\circ$ . This carboxylate group coordinates through both oxygens to form the bonds Cd(2)-O(7B) 2.273(6) Å and Cd(2)-O(8B) 2.391(7) Å. The Cd(2) octahedral geometry is completed with coordination to an axial DMF ligand trans to the O(A)-C(17A)-O(10A) carboxylate bridge at an angle of  $169.2(3)^\circ$  and perpendicular to the carboxylate equatorial belt; O(2)-Cd(2)-O(15)  $91.0(3)^\circ$  (figure 6.34B).

The array of bridging carboxylate groups holds the Cd(1) and Cd(2) cations in close proximity forming columns of the cations down the *a*-axis linked by two 1,3,5-benzenetricarboxylate ligands related by inversion symmetry to form a double layer of ligands as shown in figure 6.36. These columns are further expanded with coordination to a third cadmium cation Cd(3) through the primary 1,3,5-benzenetricarboxylate ligand C(1)-O(6) that acts as a linker between the Cd(1) and Cd(3) cations. The ligand is positioned perpendicular to the other 1,3,5-benzenetricarboxylate ligand at an angle of  $116.44(2)^\circ$  and coordinates using all of its carboxylate oxygen atoms. The O(1)-C(7)-O(2) carboxylate group is a bridge between both Cd(1) and Cd(2), the remaining two carboxylate groups O(3)-C(8)-O(4) and O(5)-C(9)-O(6) are coordinated to symmetry equivalent Cd(3) cations.

The Cd(3) cation forms a six-coordinate distorted octahedron (figure 6.34C) coordinating to three carboxylate groups of symmetry equivalent 1,3,5-benzenetricarboxylate ligands and two cis DMF molecules that cap the node in the *b*-axis and *c*-axis at an angle of O(16)-Cd(3)-O(17)  $80.9(3)^\circ$ . The Cd(3) cation forms a bidentate bond to the O(3)-C(8)-O(4) carboxylate group with a bite angle of O(3)-Cd(3)-O(4)  $55.4(2)^\circ$  similar to the bite angles formed by other carboxylates in this compound. The completion of the Cd(3) coordination geometry occurs with the formation of monodentate bonds to each of the oxygens O(5) and O(6) of the symmetry equivalent 1,3,5-benzenetricarboxylate ligands. The O(5A) oxygen atom coordinates perpendicular in the cis position to the bidentate O(3)-C(8)-O(4) carboxylate group whilst its symmetry equivalent O(6B) coordinates in the cis coplanar position at O(3)-Cd(3)-O(6B)  $85.1(2)^\circ$ . This cis coordination motif shown in figure 6.34C allows the Cd(3) cation to act as a central node expanding the structure down the *a*-axis and *c*-axis to

form a 'zigzag' sheet via the secondary building unit shown in figure 6.35. These sheets expand down the *a*-axis and *c*-axis but are capped in the *b*-axis by the coordinated DMF molecules on both the Cd(3) and Cd(1) cations. The DMF ligands alternate in direction at each symmetry equivalent cadmium cation due to an inversion centre between each pair of adjacent Cd(3) cations, and an inversion centre between the linking 1,3,5-benzenetricarboxylate ligands that bridge the columns of Cd(1) and Cd(2) cations. The DMF ligands coordinated to the Cd(1) and Cd(3) cations are in the *cis* positions with respect to each other forming 'L'-shaped connectivity, with one DMF pointing along the *b*-axis and the other along the *c*-axis. These ligands flip by 180° at each alternating cadmium due to the inversion symmetry, this rotation enables strong intramolecular overlapping between the DMF molecules of the Cd(1) and those of an adjacent Cd(3) cation. Further intermolecular interactions between adjacent sheets are formed by the DMF molecules pointing 'up and down' in the *b*-axis to form the close packing observed down the *a*-axis in figure 6.36, that optimises the packing based on the steric bulk of the DMF molecules as they template the packing motif in compound 16.

The sheets pack parallel along the *b*-axis and *c*-axis with slight staggering along the *a*-axis due to the symmetry operators. This staggering creates a 'zip-lock' packing motif of the DMF molecules with a distance of 5.585(4) Å from respective adjacent nitrogens of the DMF molecules. This packing coupled with the 'zigzag' nature of the sheets creates micropores observed in figure 6.36. These potential pores have dimensions 6.505(2) by 5.774(4) Å and contain one uncoordinated DMF molecule that forms hydrogen bonds with the coordinated DMF molecules of the Cd(2) cation and appears to be trapped within the pore by the steric bulk of the alternating DMF molecules.

Additional analysis of the bulk sample was carried out to investigate the purity of compound 16, and gauge if the addition of DMF into the reaction media has any adverse effects. The powder X-ray diffraction data produced the diffraction pattern shown in figure 6.37; this is consistent with the calculated powder diffraction pattern from the single crystal data with correlating intense peaks.

Elemental analysis was used to analyse if residual DMF was present in the dry compound, results show the C = 29.22 %, H = 3.27 % and N = 2.91 %; these do not

correlate with the calculated values from the single crystal data of C = 37.05 %, H = 4.35 % and N = 7.76 %. The difference in values is most likely a result of the desolvation of the framework upon drying and the subsequent collapse of the compound resulting in the loss of approximately three DMF molecules.

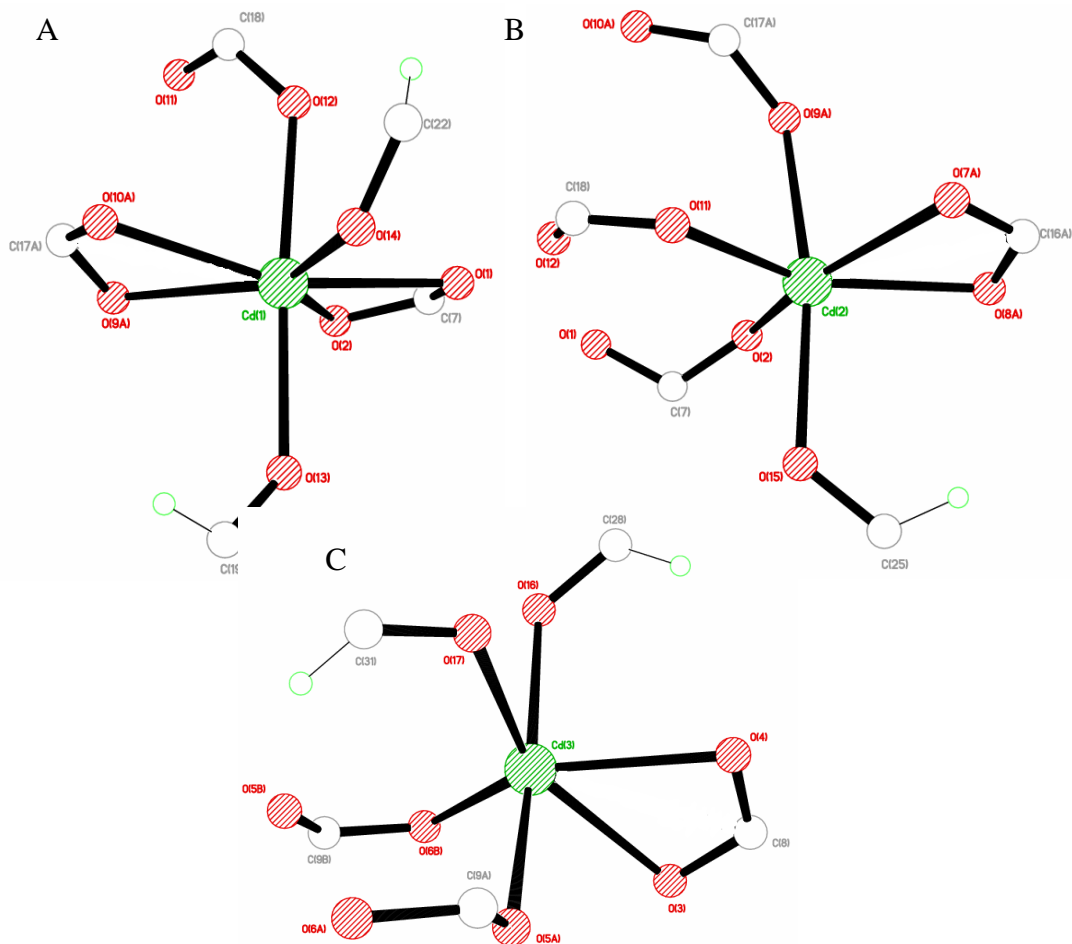
The lack of stability in compound 16 suggests it will not be ideal for further studies; however the synthesis was designed to investigate the potential of DMF for fully deprotonating the 1,3,5-benzenetricarboxylate ligands under solvothermal conditions, with potential products giving results to investigate the influence of DMF on the structural packing motifs. Compound 16 shows that DMF both fully deprotonates the ligands and also coordinates to the metal centres to produce metal-ligand coordination geometries that may be useful in creating microporous structures with DMF present in the pores.

**Table 6.16: Selected Bond Lengths [ $\text{\AA}$ ] and Angles [ $^\circ$ ] for Compound 16**

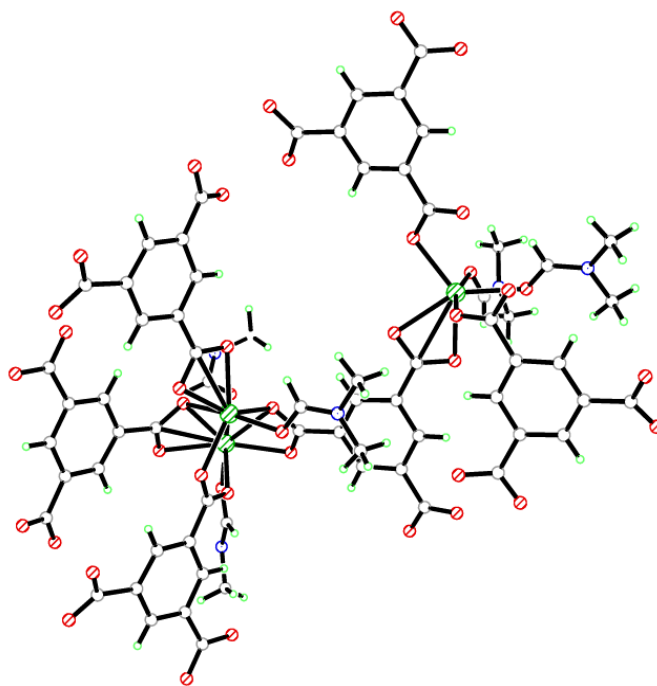
Cd(1)–O(1)	2.272(7)	Cd(1)–O(2)	2.573(7)
Cd(1)–O(9A)	2.541(7)	Cd(1)–O(10A)	2.298(7)
Cd(1)–O(12)	2.326(7)	Cd(1)–O(13)	2.225(8)
Cd(1)–O(14)	2.302(8)	Cd(2)–O(2)	2.290(7)
Cd(2)–O(7B)	2.273(6)	Cd(2)–O(8B)	2.391(7)
Cd(2)–O(9A)	2.360(7)	Cd(2)–O(11)	2.206(6)
Cd(2)–O(15)	2.281(7)	Cd(3)–O(3)	2.420(7)
Cd(3)–O(4)	2.337(6)	Cd(3)–O(5C)	2.315(8)
Cd(3)–O(6B)	2.238(7)	Cd(3)–O(16)	2.287(9)
Cd(3)–O(17)	2.280(7)	C(7)–O(1)	1.267(12)
C(7)–O(2)	1.286(13)	C(8)–O(3)	1.276(12)
C(8)–O(4)	1.256(12)	C(9)–O(5)	1.241(12)
C(9)–O(6)	1.284(11)	C(16)–O(7)	1.273(12)
C(16)–O(8)	1.260(11)	C(17)–O(9)	1.280(11)
C(17)–O(10)	1.257(12)	C(18)–O(11)	1.252(12)
C(18)–O(12)	1.267(12)		
O(1)–Cd(1)–O(2)	54.2(2)	O(1)–Cd(1)–O(9A)	125.9(2)
O(1)–Cd(1)–O(10A)	162.0(3)	O(1)–Cd(1)–O(12)	80.2(3)
O(1)–Cd(1)–O(13)	93.9(3)	O(1)–Cd(1)–O(14)	90.4(3)
O(2)–Cd(2)–O(7B)	100.5(2)	O(2)–Cd(2)–O(8B)	155.3(2)
O(2)–Cd(2)–O(9A)	80.6(2)	O(2)–Cd(2)–O(11)	115.2(3)
O(2)–Cd(2)–O(15)	91.0(3)	O(3)–Cd(3)–O(4)	55.4(2)
O(3)–Cd(3)–O(5C)	87.7(3)	O(3)–Cd(3)–O(6B)	85.1(2)
O(3)–Cd(3)–O(16)	102.8(3)	O(3)–Cd(3)–O(17)	150.0(2)
Cd(1)–O(2)–Cd(2)	92.7(2)		

Symmetry operations for equivalent atoms

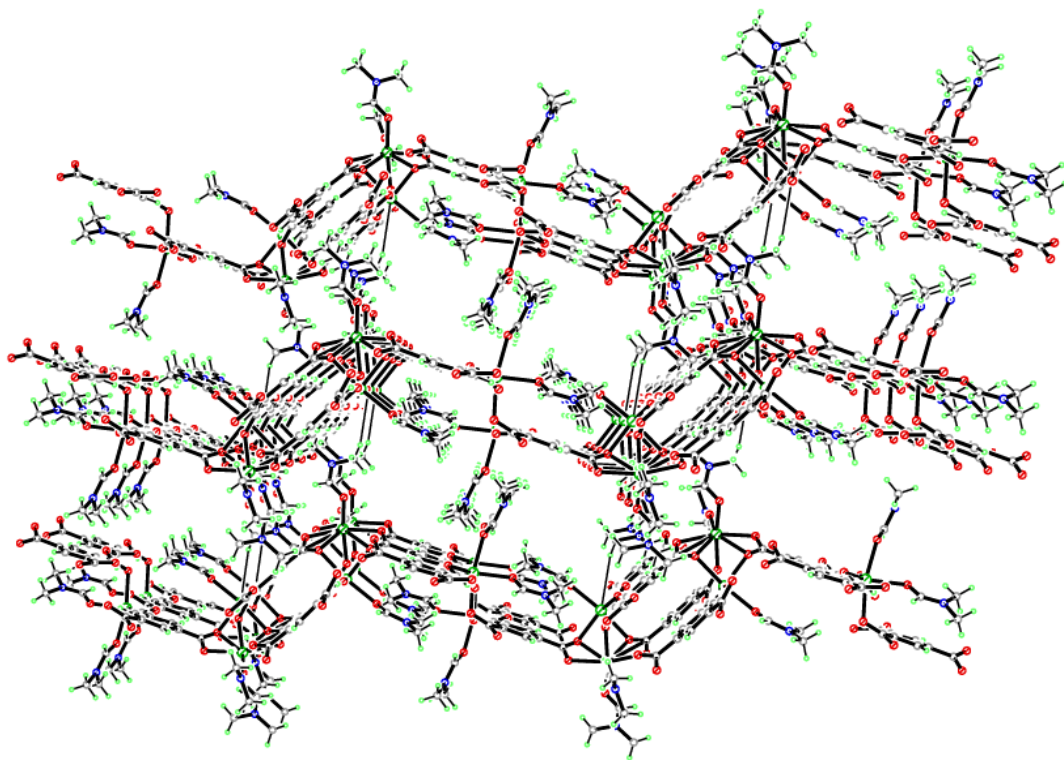
A  $-x, -y+1, -z$  B  $x+1, y, z$  C  $-x+1, -y+1, -z+1$



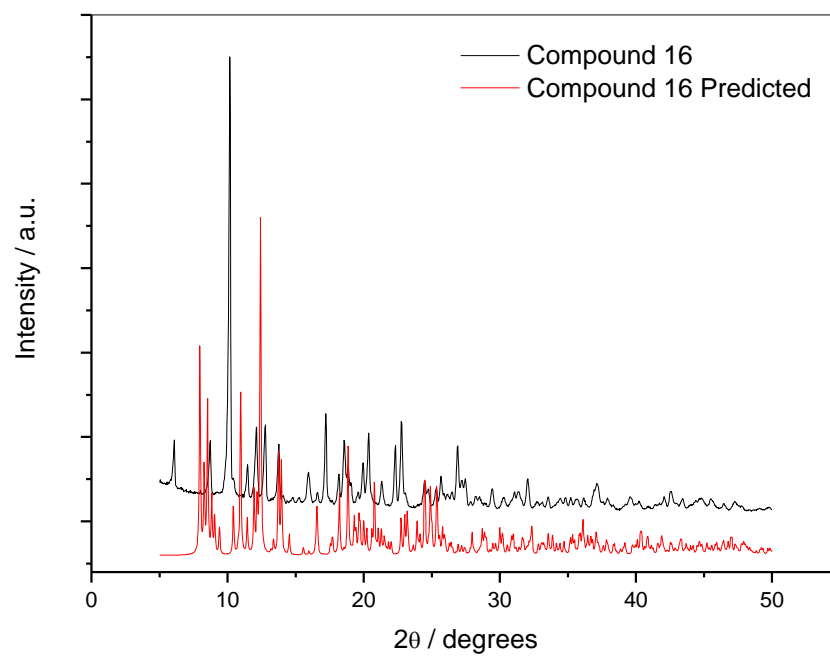
**Figure 6.34: A) Pentagonal bipyramidal coordination environment of Cd(1), B) Octahedral coordination environment of Cd(2) and C) Octahedral coordination environment of Cd(3) in compound 16**



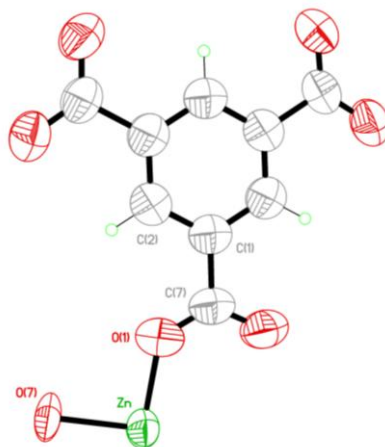
**Figure 6.35:** Secondary building unit of Cd(1), Cd(2) and Cd(3) in compound 16



**Figure 6.36:** Two dimensional layers in compound 16 viewed down the *a*-axis



**Figure 6.37: Powder X-ray diffraction pattern of Compound 16**

**Compound 17:**  $[\text{Zn}_3(\text{C}_9\text{H}_3\text{O}_6)_2(\text{H}_2\text{O})_3 \cdot 3(\text{C}_3\text{H}_7\text{NO})]$ 

Chemical formula (total)	$\text{C}_{18}\text{H}_{12}\text{O}_{15}\text{Zn}_3$
Formula weight	664.39
Temperature	150(2) K
Radiation, wavelength	MoK $\alpha$ , 0.71073 Å
Crystal system, space group	cubic, $Fm\bar{3}m$
Unit cell parameters	$a = 26.5165(2)$ Å
Cell volume	$18644.4(2)$ Å <sup>3</sup>
Z	16
Crystal colour and size	colourless, $0.20 \times 0.16 \times 0.10$ mm <sup>3</sup>
Final $R$ indices [ $F^2 > 2\sigma$ ]	$R1 = 0.0906$
$R$ indices (all data)	$wR2 = 0.2633$
Largest diff. peak and hole	0.93 and $-0.38$ e Å <sup>-3</sup>

**Figure 6.38:** Asymmetric Unit of Compound 17 all unique atoms labelled, additional atoms added to complete ligands

**Synthesis**

$\text{Zn}(\text{NO}_3)_2 \cdot 6\text{H}_2\text{O}$  (0.09 g, 0.33 mmol) and 1,3,5-benzenetricarboxylic acid (0.028 g, 0.17 mmol) were added to a reaction mixture of dimethylformamide (DMF) (4 mL), ethanol (4mL) and water (3mL). This was placed into a 20mL Teflon-lined bomb and heated to 160°C for 24 hours. The vessel was then cooled back down to room temperature at a rate of 0.1°C / min and allowed to stand for 2 hours before colourless block crystals were retrieved from the vessel.



## Structure Determination

The data were collected at 150 K using molybdenum radiation on an Oxford Diffraction Gemini A Ultra diffractometer. The structure was solved by direct methods. The semi-empirical absorption corrections were applied based on symmetry-equivalent and repeated data. The refinement gave a  $wR2$  of 0.2633 for all 887 independent reflections and a conventional  $R1$  of 0.0906 for 719 reflections with  $F^2 > 2\sigma$ . The residual electron density maximum and minimum were 0.93 and  $-0.38 \text{ e } \text{\AA}^{-3}$  respectively, the high residual electron density in compound 17 is a result of the unmodelled disordered solvent molecules present in the pores of the framework.

The hydrogen atoms were placed in geometrically calculated positions with  $U$  constrained to  $1.2 U_{eq}(\text{C})$  for aromatic hydrogen atoms. The full data of compound 17 can be found in Appendix 1.

## Structure Analysis

The asymmetric unit of compound 17 (figure 6.38) shows one third of a 1,3,5-benzenetricarboxylate ligand completed by three-fold rotation symmetry around the centre of the aromatic ring, connecting a zinc cation positioned on a two-fold rotation axis. The zinc cation in compound 17 is a five coordinate square pyramidal (figure 6.39) with slight distortions in the bond angles shown in table 6.17.

The one third 1,3,5-benzenetricarboxylate ligand coordinates to the zinc cation with a monodentate bond through O(1), Zn(1)-O(1) 2.021(4) Å, additional symmetry equivalents of this carboxylate group coordinate in the coplanar cis-position forming the base of the square pyramidal unit. The zinc cation is capped by an axial water molecule positioned in the two-fold rotation axis at O(1)-Zn(1)-O(7) 91.4(3)° perpendicular to the equatorial bond of the carboxylates completing the five-coordinate geometry of the zinc cation.

The completion of the fully deprotonated and coordinated 1,3,5-benzenetricarboxylate ligand via the three-fold symmetry creates dimeric zinc tetracarboxylate units (figure 6.40), with a short Zn-Zn internuclear separation of 2.968(2) Å trans to the axial coordinated water molecule. This paddle wheel secondary building unit has four-fold symmetry around its centre and coupled with the three-fold

symmetry of the 1,3,5-benzenetricarboxylate ligand forms a fully coordinated porous three dimensional MOF. It achieves this by utilizing larger building units of zinc dimers at the six vertices of four 1,3,5-benzenetricarboxylate ligands connecting these by sharing the octahedra around the two-fold zinc dimers that act as bridging units. This building motif creates octahedral channels with four-fold symmetry running down the [100] axis of the cubic cell (figure 6.41). These pores are 7.190(2) Å by 7.190(2) Å and run through the cell body axis intersecting with one another. The octahedral nanochannels are also intersected by triangular pores along the [111] cell body diagonal (figure 6.42) to provide a three dimensional network of pores throughout the structure.

In compound 17, the terminal axial water ligands are directed into the interior of the nanochannels, additional disordered electron density is also present inside the pores and the contents could not be directly located in the crystal structure analysis. The disordered electron density is accounted for by thermogravimetric analysis that produced the TGA plot in figure 6.43. Further analysis of the bulk sample of compound 17 was carried out using thermogravimetric analysis, powder X-ray diffraction and elemental analysis to determine the bulk purity of the compound. The samples were prepared for each further analysis by removing compound 17 from the reaction solution by filtration under vacuum before being left to dry for 30 minutes.

The TGA plot (figure 6.43) shows a four stage temperature profile; stage 1 is associated with excess surface solvent being removed from the partially wet sample, stage 2 shows a mass loss of 3.54 mg (17.9 %) between 150-220°C, this correlates with three disordered DMF molecules per unit cell. The TGA shows that desolvation fully occurs at 220°C; however stage 3 indicates compound 17 does not form a stable plateau and continues to lose mass as the coordinated water molecules are slowly removed before the structure finally loses stability and degrades at 275°C during stage 4. If the compound was desolvated at 220°C and held at this temperature PLATON<sup>1</sup> confirms the presence of an extensive pore network with a total potential solvent-accessible volume of 12578.3 Å<sup>3</sup> per unit cell volume of 18634.5 Å<sup>3</sup> (67.5 %). The high potential pore volume available makes compound 17 ideal for further gas adsorption studies. This coupled with its high yielding synthesis (89.7%) with high purity in the form of only

single crystals produced led to the further analysis of compound 17 using CO<sub>2</sub> gas adsorption on an Intelligent Gravimetric Analyser (IGA).

Elemental analysis produced the results C = 34.21 %, H = 2.13 % and N = 0.07 % that correlate with the calculated values from the single crystal data; C = 32.51%, H = 1.81 % and N = 0 %. The sample was analysed using powder X-ray diffraction after the initial drying process was complete on compound 17 producing the powder diffraction pattern shown in figure 6.44, the data points of this plot are not consistent with those of the predicted powder diffraction pattern generated from the single crystal data. The diffraction pattern shows a lack of intensity at 6.715 and 9.439 2-Theta that correspond to two of the highest intensity peaks in the predicted diffraction pattern, the highest intensity peak at 11.457 2-Theta is present in both diffraction patterns with the obtained pattern showing additional peaks at 9.251, 9.853, 18.428, 19.306 and 23.766 2-Theta. A second sample of compound 17 was heated to the desolvation temperature of 220°C for 2 hours before cooling to room temperature, a powder diffraction pattern of this sample was obtained and compared to the initial drying and predicted powder diffraction patterns in figure 6.44 to highlight any further structural change upon full desolvation. The third powder diffraction pattern shown in figure 6.44 was measured after the sample of compound 17 had undergone gas adsorption measurements of CO<sub>2</sub> at 303 K and shows the compound remains in the desolvated conformation. The consistency of the elemental analysis and the diverging powder diffraction patterns suggests that the structure of compound 17 undergoes a conformation change upon desolvation altering the packing structure of the powder sample.

There are several similar compounds in the crystallographic database to compound 17 with the dimeric metal tetracarboxylate units appearing in several compounds such as MOF 4 produced by Yaghi *et al.*<sup>7</sup> and USF-3<sup>8</sup>. Compound 17 is also a structural analogue of FIQCEN (HKUST-1)<sup>9</sup> and the iron centred analogue NINVAI.<sup>10</sup> Compound 17 is synthesised in similar conditions to those used to prepare HKUST-1, both structures show identical asymmetric units with slight variations in M-O bond lengths and angles which is to be expected by switching from the copper nodes in HKUST-1 to the zinc nodes in compound 17, these discrepancies are compared in table 6.18. The overall structural topology remains the same with the structures

superimposable, the major variation is in the contents of the nanochannels of the structures. Compound 17 is reported to contain three DMF molecules per  $[\text{Zn}_3(\text{C}_9\text{H}_3\text{O}_6)_2(\text{H}_2\text{O})_3]$  unit, in contrast HKUST-1 reveals that its nanochannels are filled with ten water molecules per  $[\text{Cu}_3(\text{C}_9\text{H}_3\text{O}_6)_2(\text{H}_2\text{O})_3]$  moiety. This has drastic consequences on the accessibility of the channels within each structure as HKUST-1 is desolvated at 100°C and remains stable until 250°C,<sup>9</sup> a large difference to the desolvation temperature in compound 17 of 220°C needed to remove the DMF molecules used to template the structure. A further comparison of HKUST-1 to compound 17 was carried out with analysis of the CO<sub>2</sub> adsorption onto both compounds to investigate relative pore characteristics.

### **Gas adsorption of compound 17**

The metal-organic framework of compound 17 is a structural analogue of HKUST-1, a compound that has been shown to have useful applications in gas/vapour adsorption and storage with HKUST-1 showing high affinity for CO, CO<sub>2</sub>, N<sub>2</sub>, NO and H<sub>2</sub>.<sup>9,11-13</sup> The high adsorption capacity of HKUST-1 for both nitric oxide and hydrogen confirms its applicability as a gas storage material and for pharmaceutical and biological applications as a NO adsorbant,<sup>11,12</sup> making compound 17 an ideal target molecule for these applications.

### **Porous structure characterisation**

The usual method for characterisation of a porous structure involves a series of adsorption isotherms of nitrogen at 77 K and carbon dioxide at 273 and 303 K. The adsorption of nitrogen at 77 K showed low uptake and could not be used for quantitative analysis and the carbon dioxide adsorption at 273 K was too slow, failing to reach equilibrium. Therefore carbon dioxide at 303 K was used to characterise the structure.

A sample of compound 17 (26.45 mg) was prepared by desolvating in the IGA through exposing the sample to vacuum at 10<sup>-6</sup> mbar and heating to 150°C for five hours, until a stable mass profile was reached. Typical mass loss due to removal of volatile species within the pores was 17.9%.

The adsorption isotherm of carbon dioxide on 26.45 mg of compound 17 at 303 K is plotted in figure 6.45. The isotherm is type 1 according to the IUPAC classification system,<sup>[14]</sup> suggesting it can be analysed using virial analysis to obtain the interaction between the gas and the sample: this is in conjunction with analysis using the D-R equation to gain information on the micropore volume. The carbon dioxide adsorption isotherm at 303 K shows a fast uptake of carbon dioxide into compound 17; however the total carbon dioxide uptake of 0.375 mmol g<sup>-1</sup> is not consistent with a compound containing 67.5 % porosity and is significantly less than that of HKUST-1 which adsorbs 16.52 mmol g<sup>-1</sup>.<sup>12</sup>

The virial analysis of the carbon dioxide isotherm at 303 K was used to determine the interactive force between the gas and the sample.

$$\ln \frac{n}{p} = A_0 + A_1 n + A_2 n^2 \dots$$

n = amount adsorbed

p = pressure

A = virial parameter related to Henry's constant

Figure 6.46 shows the virial plot for carbon dioxide at 303 K, the graph is linear and the gradient gives an  $A_1$  value of  $-2056.1833 \pm (49.66)$  g mol<sup>-1</sup>. The significant size of the  $A_1$  value demonstrates the CO<sub>2</sub>-sample interaction strength suggesting extensive constriction of the nanochannels in compound 17. The extent of this contraction is exemplified by comparison of the virial analysis  $A_1$  value of carbon dioxide at 303 K for compound 17 to that of carbon molecular sieves with  $A_1$  values of -600 mmol g<sup>-1</sup> to -1450 mmol g<sup>-1</sup> with pore sizes ranging from 4.0 to 4.5 Å.<sup>15,16</sup> This would suggest that compound 17 has smaller pores than those present in carbon molecular sieves.

Further analysis using the D-R equation on the carbon dioxide adsorption isotherm at 303 K produced the D-R plot shown in figure 6.46. The D-R equation can be rearranged to give:

$$\log n = \log n_m - D \log^2 \frac{P}{P_0}$$

Where:

$$D = B \left( \frac{T}{\beta} \right)^2$$

Therefore the plot of  $\log_{10} n$  against  $\log^2(P/P_0)$  should be linear with an intercept equal to  $\log_{10} n_m$ , where  $n_m$  is the micropore volume. The D-R plot in figure 6.47 is almost linear across the pressure range 500-900 mbar with an intercept value of  $3.76204 \times 10^{-4} \pm 0.00703 \text{ mmol g}^{-1}$  that equates to a micropore volume of  $2.173 \times 10^{-5} \pm 1.360 \times 10^{-4} \text{ cm}^3 \text{ g}^{-1}$ . This is significantly lower than the predicted pore volume of  $1.82 \text{ cm}^3 \text{ g}^{-1}$  calculated from the crystallographic data by PLATON.<sup>1</sup> This suggests that compound 17 forms a microporous compound upon desolvation with a low total pore volume.

### **Kinetics for adsorption of carbon dioxide at 303 K on compound 17**

The isotherm for the adsorption of carbon dioxide on compound 17 at 303 K is shown in figure 6.45. The kinetic profiles for each pressure increment were analysed using the stretched exponential model<sup>17</sup> to gain the rate constants for the equilibrium of mass uptake. The stretched exponential kinetic model (SE) has been used to study the adsorption and desorption of a wide range of gases and vapours on metal-organic framework materials.<sup>18,19</sup> Klafter and Shlesinger<sup>17</sup> showed that the SE model is the mathematical structure relating the relaxation via parallel channels and the serial hierarchically constrained dynamics<sup>20</sup> and deflect diffusion model.<sup>21</sup> The SE model is described by the following equation:

$$\frac{M_t}{M_e} = 1 - e^{-(kt)^\beta}$$

Where:  $M_t$  is mass at time

$M_e$  is mass at equilibrium

$K$  is the mass transfer rate constant ( $\text{s}^{-1}$ )

t is time (s)

$\beta$  is the material dependent parameter

The kinetic profiles for 50-1000 mbar are shown in figures 6.47-6.56 for the adsorption isotherm of carbon dioxide on compound 17 at 303 K.

Figure 6.48 and 6.49 are for pressure steps within the early region of the isotherm. For these two steps the kinetics are fast with values of  $0.00186 \pm 3 \times 10^{-5} \text{ s}^{-1}$  and  $0.00205 \pm 4 \times 10^{-5} \text{ s}^{-1}$ , the values for  $\beta$  are  $0.69211 \pm 5.99 \times 10^{-3}$  and  $0.71409 \pm 8.18 \times 10^{-3}$ . The kinetic profiles for these two pressure steps fit the SE model very well as the residuals for the fit are well within the ideal range.

Figure 6.51, 6.52 and 6.53 show the transition into the second part of the type I isotherm with rate constants steadily increasing with pressure;  $0.00228 \pm 4 \times 10^{-5} \text{ s}^{-1}$ ,  $0.00241 \pm 4 \times 10^{-5} \text{ s}^{-1}$  and  $0.00242 \pm 4 \times 10^{-5} \text{ s}^{-1}$  with the  $\beta$  values compared in table 6.19.

Figure 6.55 and 6.57 in the latter region of the isotherm show the rate constant has continued to increase with pressure with values;  $0.00291 \pm 5 \times 10^{-5} \text{ s}^{-1}$  and  $0.003 \pm 6 \times 10^{-5} \text{ s}^{-1}$  with the  $\beta$  values  $0.76514 \pm 9.29 \times 10^{-3}$  and  $0.8339 \pm 1.29 \times 10^{-2}$  (table 6.19).

All the kinetic profiles show equilibrium of mass uptake within 4000 seconds and all fit the SE model within 4 %. The rate constant calculated show the rate of adsorption increases as the isotherm increases in pressure with increasing uptake as shown in figures 6.58 and 6.59. For the SE model the  $\beta$  values represent a variable that can be used to determine if a process is one dimensional or three dimensional, if the  $\beta$  value  $\approx 1$  then the process is one dimensional and if the  $\beta$  value  $\approx 0.5$  the process is three dimensional. The  $\beta$  values plotted in figure 6.58 show that compound 17 approaches  $\beta \approx 1$ .

Comparison of the adsorption properties of compound 17 and HKUST-1 shows significant differences in pore volume, uptake and kinetic rates. Compound 17 has a maximum uptake of  $0.375 \pm 4.96 \times 10^{-2} \text{ mmol g}^{-1}$  with a pore volume of  $2.173 \times 10^{-5} \pm 1.360 \times 10^{-4} \text{ cm}^3 \text{ g}^{-1}$ , compared to HKUST-1 that has an uptake of  $16.52 \pm 4.62 \times 10^{-2} \text{ mmol g}^{-1}$  (figure 6.60 and 6.64) with a pore volume of  $0.709 \pm 2.07 \times 10^{-3} \text{ cm}^3 \text{ g}^{-1}$  for carbon dioxide adsorption at 195 K (figure 6.61). The kinetic rates of adsorption in compound 17 and HKUST-1 are compared in table 6.20 with HKUST-1 showing faster

adsorption throughout the adsorption pressure steps, on average adsorption is twice as fast. The adsorption properties of compound 17 further confirm the structural rearrangement of the zinc-HKUST-1 analogue upon desolvation, yielding a microporous material with pores similar in size and volume to those observed in carbon molecular sieves. This unique rearrangement and formation of a microporous compound based around the HKUST-1 structure provides a compound with potential applications in kinetic molecular sieving of gases, a stark contrast to the conventional applications of HKUST-1.

**Table 6.17: Selected Bond Lengths [Å] and Angles [°] for Compound 17**

Zn–O(1)	2.021(4)	Zn–O(7)	1.978(7)
C(7)–O(1)	1.249(5)		
O(1)–Zn–O(1A)	87.7(3)	O(1)–Zn–O(1B)	88.4(2)
O(1)–Zn–O(1C)	158.7(3)	O(1)–Zn–O(7)	91.4(3)
Zn–O(1)–C(7)	127.7(5)	C(1)–C(7)–O(1)	117.2(4)
Symmetry operations for equivalent atoms			
A y,x,z    B x,y,–z    C y,x,–z			

**Table 6.18: Bond length comparisons between Compound 17 and HKUST-1<sup>9</sup>**

Compound	Bond	Bond Length (Å)
Compound 17	Zn–O (carboxylate)	2.021(4)
Compound 17	Zn–O (water)	1.978(7)
HKUST-1	Cu–O (carboxylate)	1.952(4)
HKUST-1	Cu–O (water)	2.165(4)

**Table 6.19: Rate constants and exponent values for 50-1000 mbar pressure steps for carbon dioxide adsorption on compound 17 at 303 K**

Pressure step (mbar)	Rate constant (s <sup>-1</sup> )	Exponent value (β)
50-100	0.00186 ±3 x 10 <sup>-5</sup>	0.69211 ±5.99 x 10 <sup>-3</sup>
100-150	0.00205 ±4 x 10 <sup>-5</sup>	0.71409 ±8.18 x 10 <sup>-3</sup>
150-200	0.00211 ±4 x 10 <sup>-5</sup>	0.67203 ±6.71 x 10 <sup>-3</sup>
200-300	0.00228 ±4 x 10 <sup>-5</sup>	0.65439 ±5.97 x 10 <sup>-3</sup>
300-400	0.00241 ±4 x 10 <sup>-5</sup>	0.68697 ±6.51 x 10 <sup>-3</sup>
400-500	0.00242 ±4 x 10 <sup>-5</sup>	0.74526 ±6.88 x 10 <sup>-3</sup>
500-600	0.00256 ±5 x 10 <sup>-5</sup>	0.71650 ±9.50 x 10 <sup>-3</sup>



600-700	$0.00291 \pm 5 \times 10^{-5}$	$0.76514 \pm 9.29 \times 10^{-3}$
700-800	$0.00293 \pm 5 \times 10^{-5}$	$0.74458 \pm 8.65 \times 10^{-3}$
800-900	$0.00300 \pm 6 \times 10^{-5}$	$0.83390 \pm 1.29 \times 10^{-2}$

**Table 6.20: Rate constants comparison for 50-1000 mbar pressure steps for carbon dioxide adsorption on compound 17 at 303 K and HKUST-1 at 192 K**

Pressure step (mbar)	Compound 17 – 303 K Rate constant ( $s^{-1}$ )	HKUST-1 – 192 K Rate constant ( $s^{-1}$ )
50-100	$0.00186 \pm 3 \times 10^{-5}$	$0.00322 \pm 3 \times 10^{-5}$
100-150	$0.00205 \pm 4 \times 10^{-5}$	$0.00365 \pm 7 \times 10^{-6}$
150-200	$0.00211 \pm 4 \times 10^{-5}$	$0.00455 \pm 4 \times 10^{-5}$
200-300	$0.00228 \pm 4 \times 10^{-5}$	$0.00549 \pm 5 \times 10^{-5}$
300-400	$0.00241 \pm 4 \times 10^{-5}$	$0.00485 \pm 3 \times 10^{-5}$
400-500	$0.00242 \pm 4 \times 10^{-5}$	$0.00706 \pm 1 \times 10^{-4}$
500-600	$0.00256 \pm 5 \times 10^{-5}$	$0.00731 \pm 1 \times 10^{-4}$
600-700	$0.00291 \pm 5 \times 10^{-5}$	$0.00569 \pm 2 \times 10^{-5}$
700-800	$0.00293 \pm 5 \times 10^{-5}$	$0.00577 \pm 3 \times 10^{-5}$
800-900	$0.00300 \pm 6 \times 10^{-5}$	$0.00582 \pm 3 \times 10^{-5}$

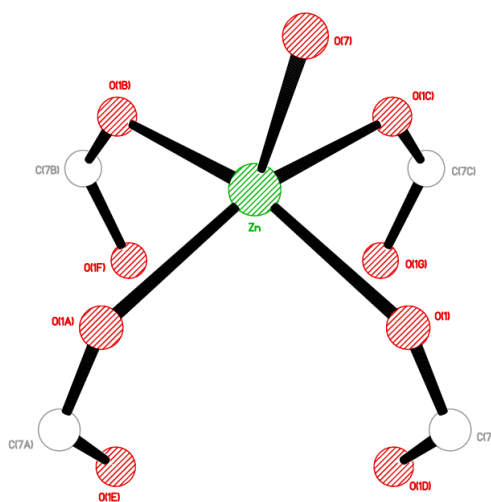


**Figure 6.39: Square pyramidal coordination environment of the Zn cation in compound 17**

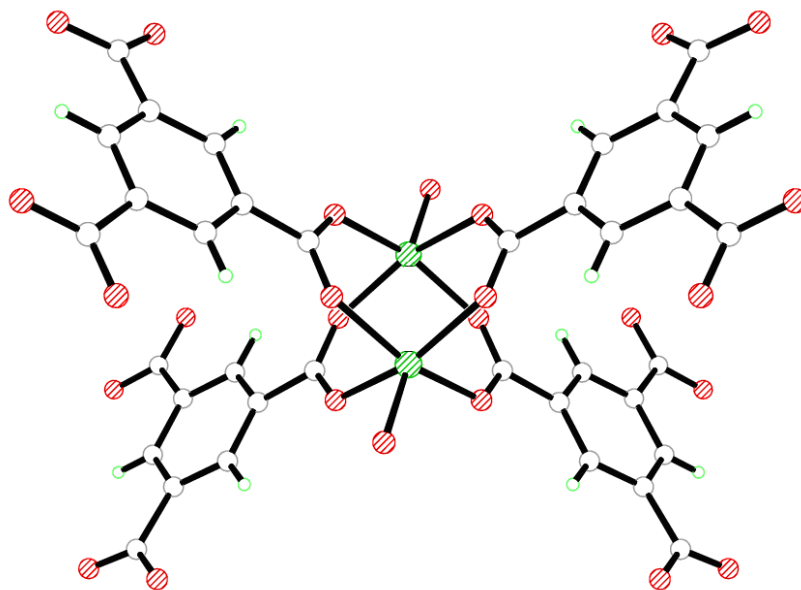


**Figure 6.40: Paddle-wheel secondary building unit in compound 17**

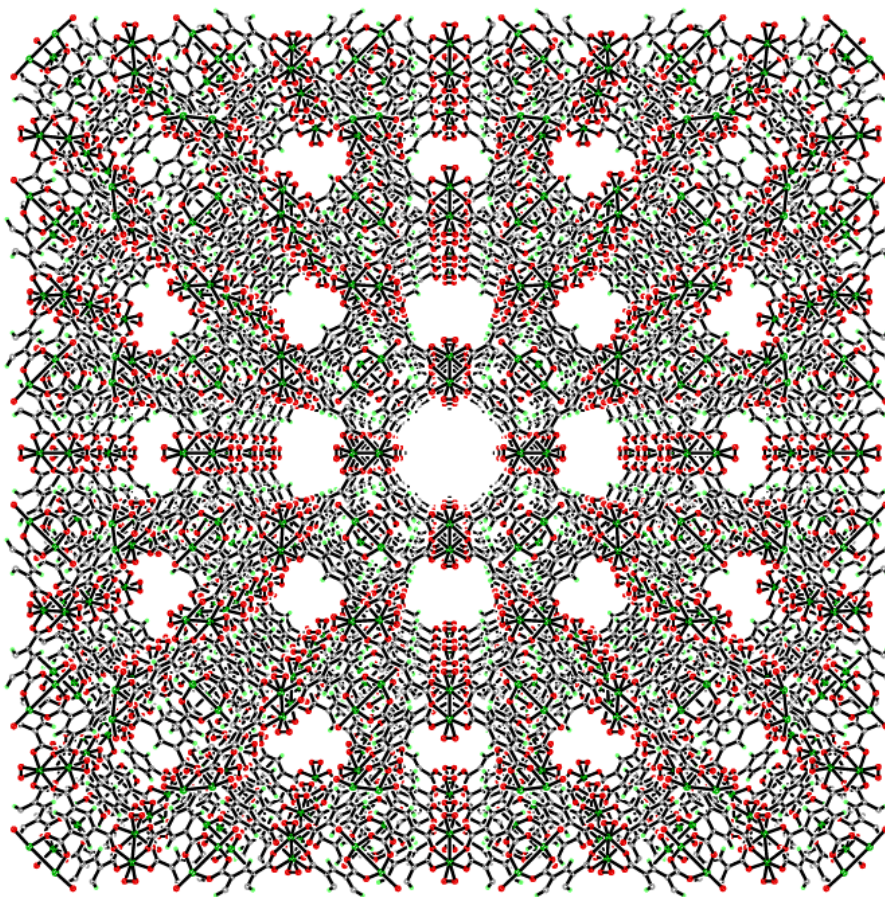


**Figure 6.41: Three dimensional packing of compound 17 viewed down the *a*-axis**

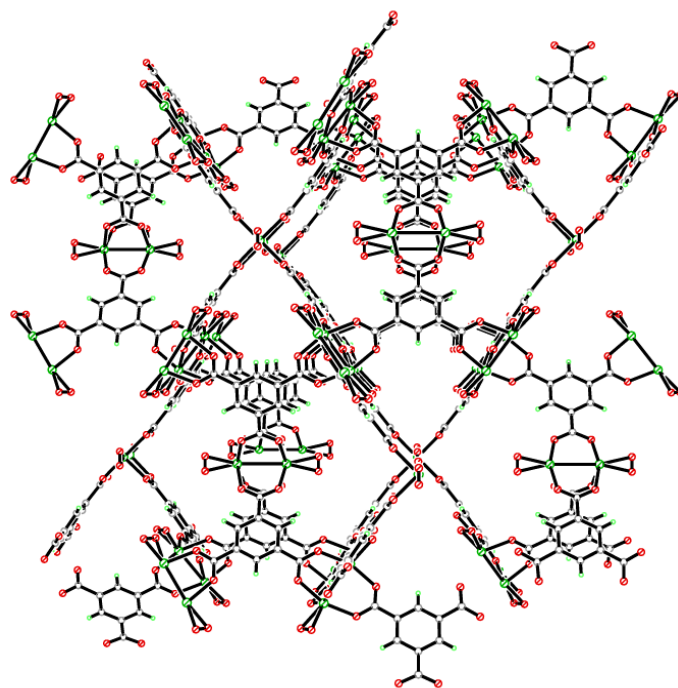


**Figure 6.42:** Three dimensional packing motif of compound 17 viewed down the [111]-axis cell body diagonal.

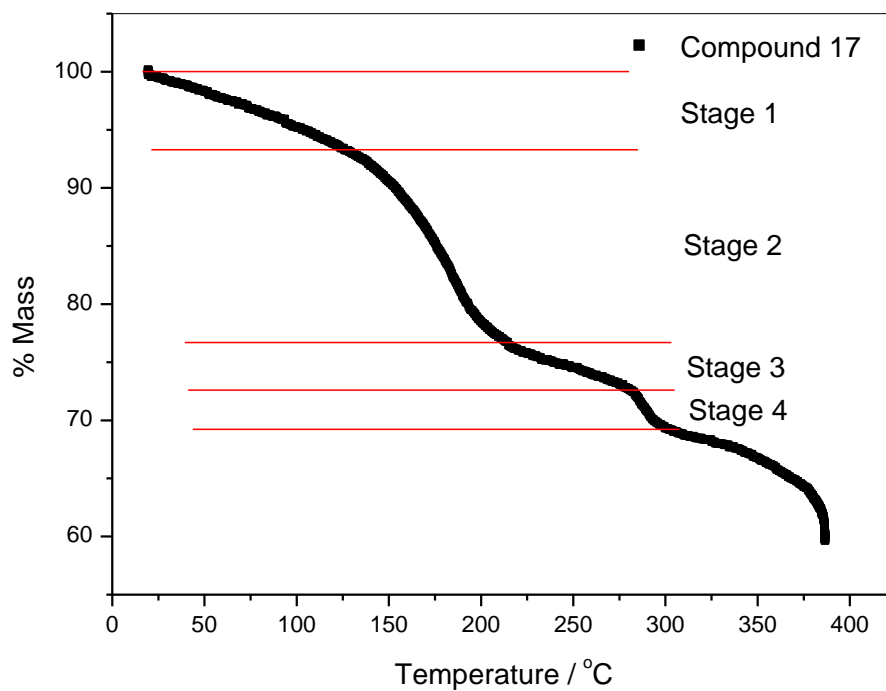


**Figure 6.43:** Thermogravimetric analysis plot of compound 17

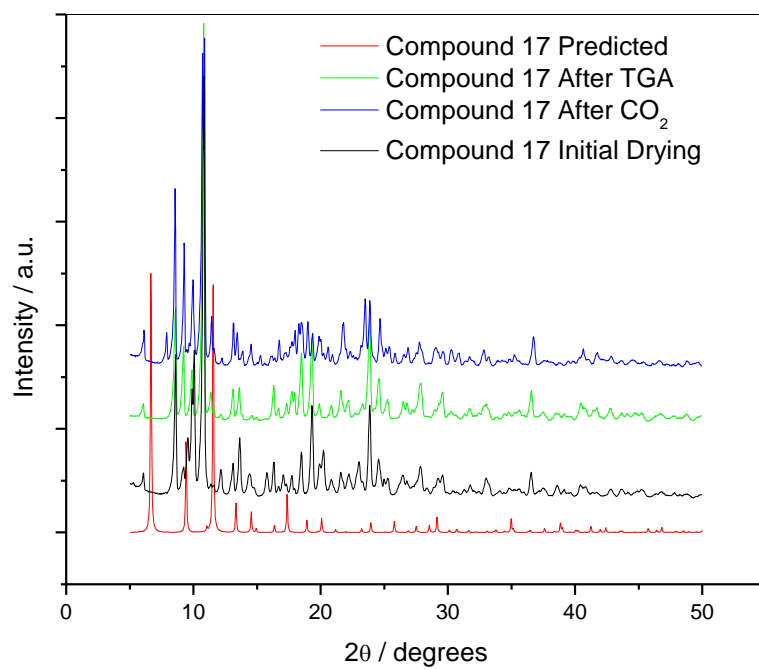


**Figure 6.44: Powder X-ray diffraction pattern of Compound 17**

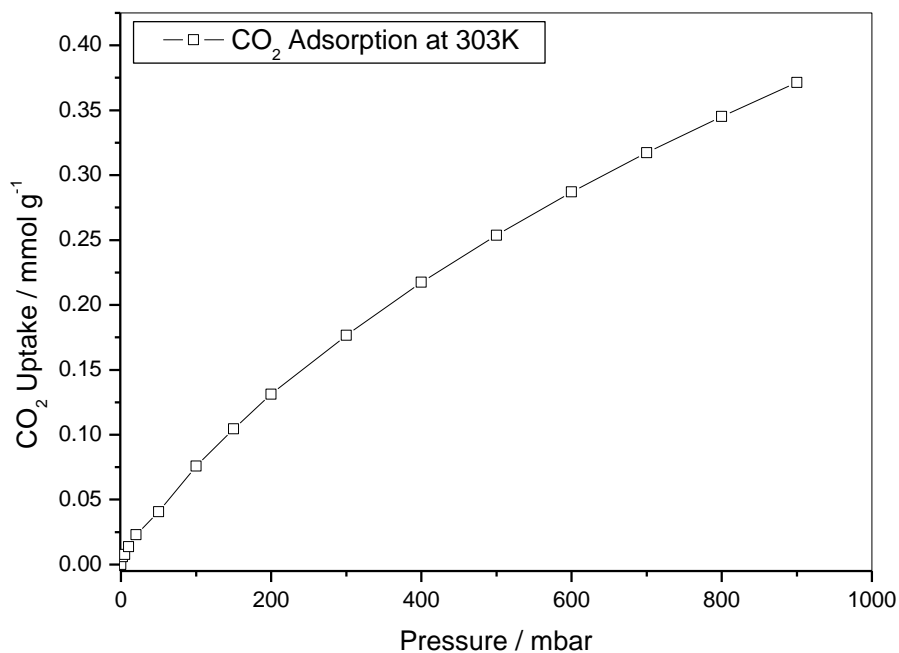


**Figure 6.45: Purified carbon dioxide adsorption on Compound 17 at 303 K**

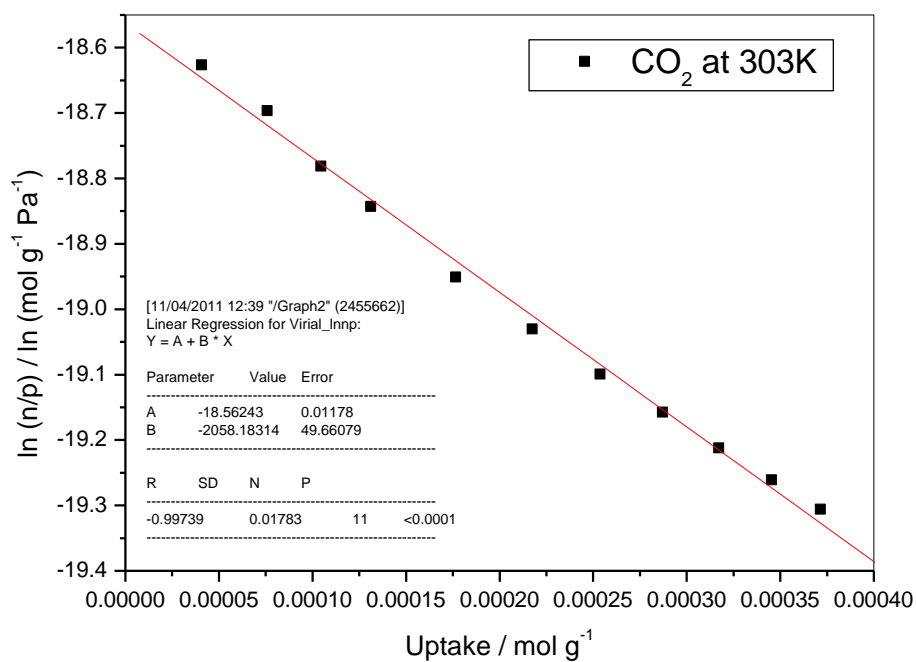


**Figure 6.46: Virial plot for carbon dioxide adsorption on Compound 17 at 303 K**

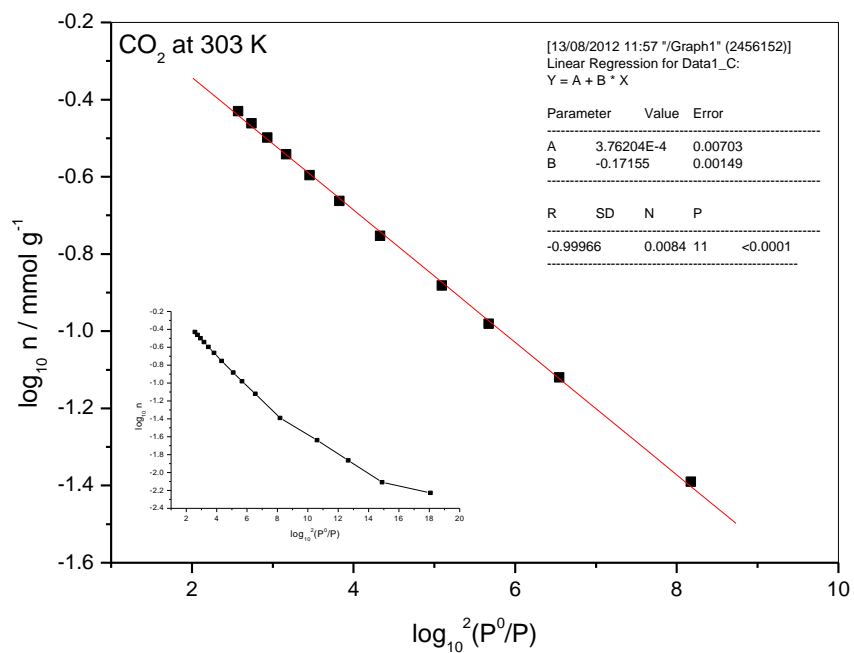


**Figure 6.47: D-R analysis for carbon dioxide adsorption on Compound 17 at 303 K**

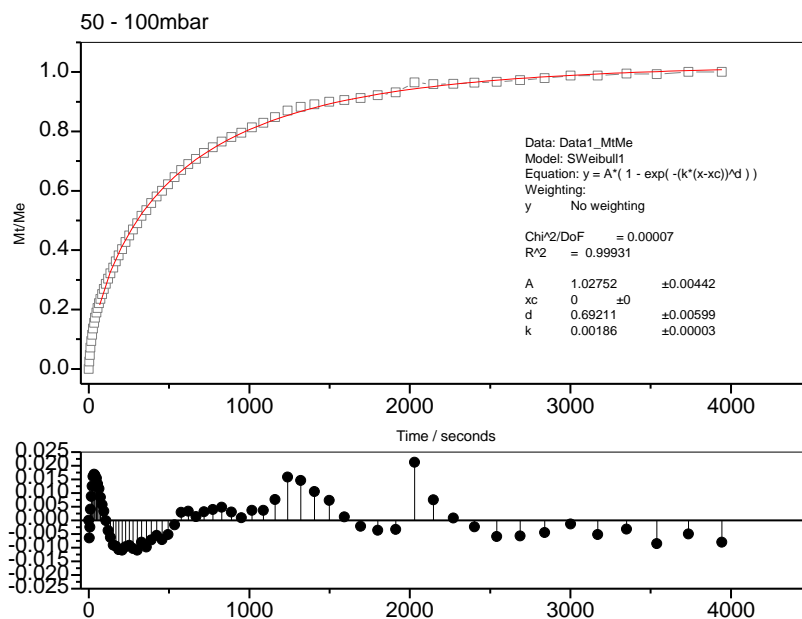


**Figure 6.48: Normalization adsorption profile for carbon dioxide adsorption on Compound 17 at 303 K - pressure step 50-100 mbar**

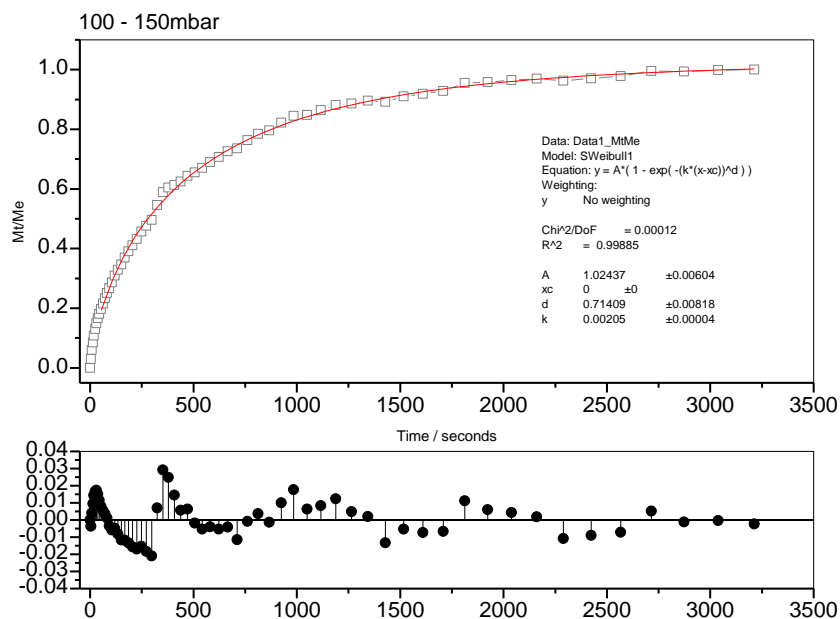


**Figure 6.49: Normalization adsorption profile for carbon dioxide adsorption on Compound 17 at 303 K - pressure step 100-150 mbar**

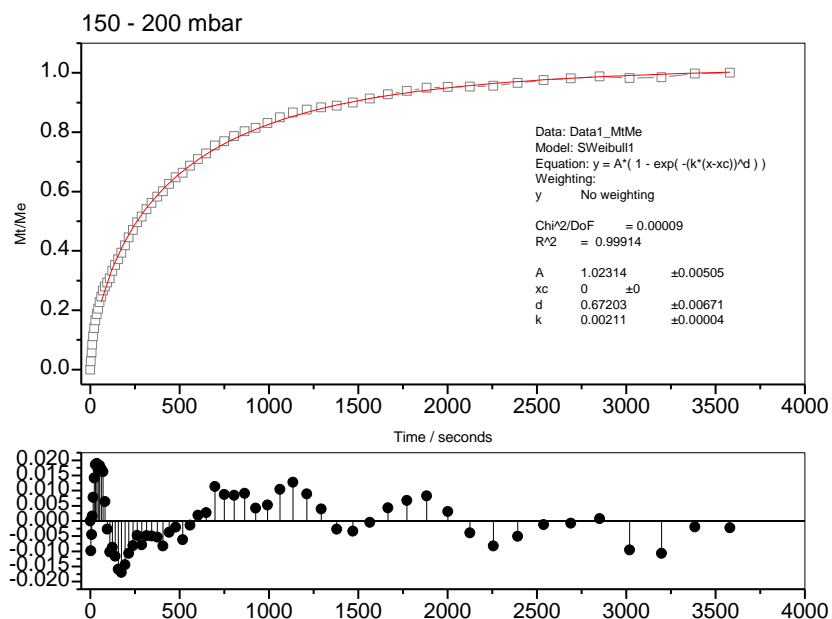


**Figure 6.50: Normalization adsorption profile for carbon dioxide adsorption on Compound 17 at 303 K - pressure step 150-200 mbar**

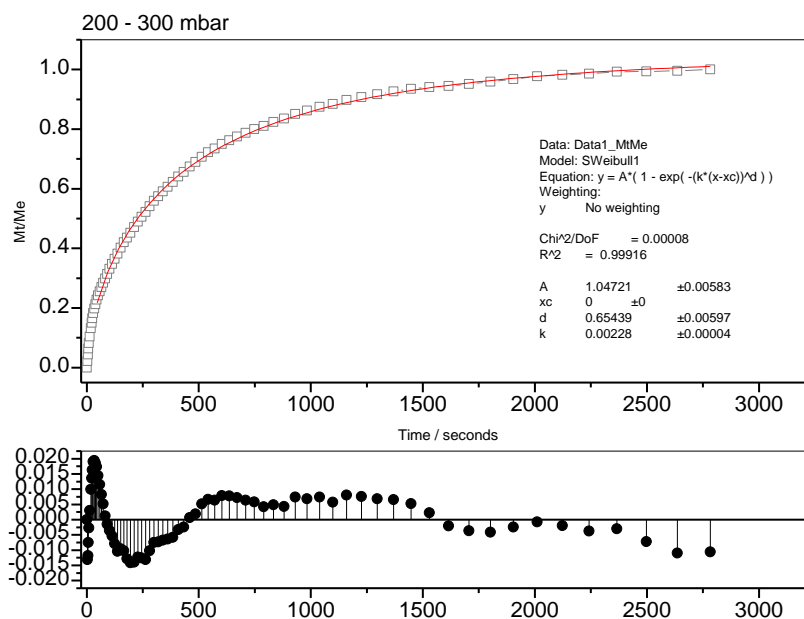


**Figure 6.51: Normalization adsorption profile for carbon dioxide adsorption on Compound 17 at 303 K - pressure step 200-300 mbar**

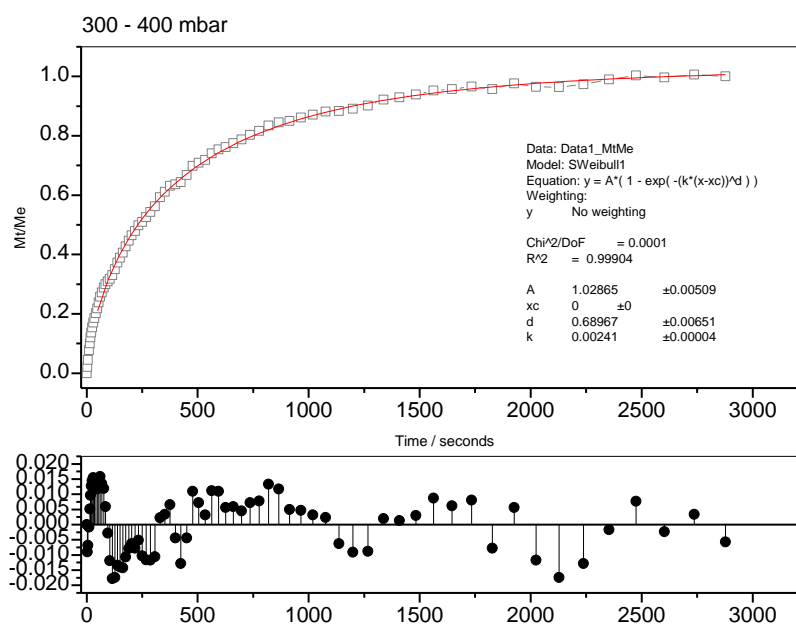


**Figure 6.52: Normalization adsorption profile for carbon dioxide adsorption on Compound 17 at 303 K - pressure step 300-400 mbar**

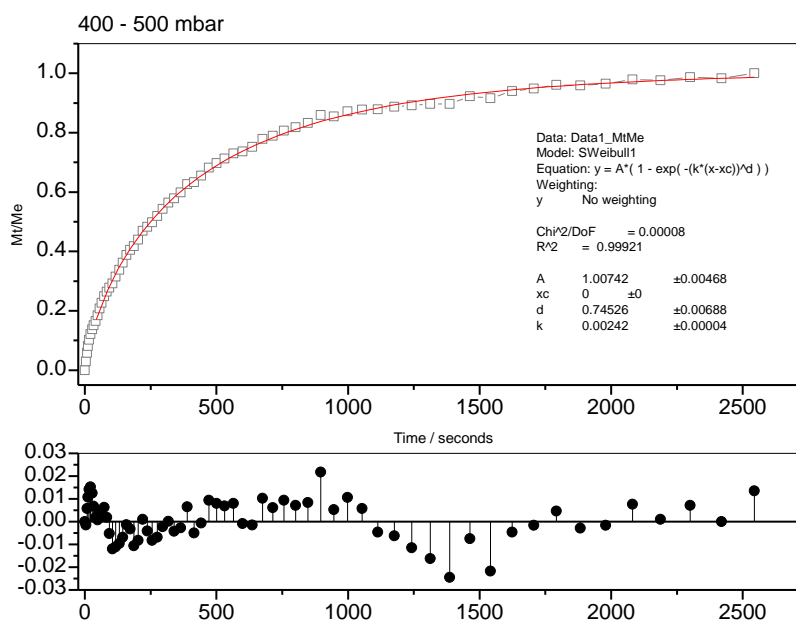


**Figure 6.53: Normalization adsorption profile for carbon dioxide adsorption on Compound 17 at 303 K - pressure step 400-500 mbar**



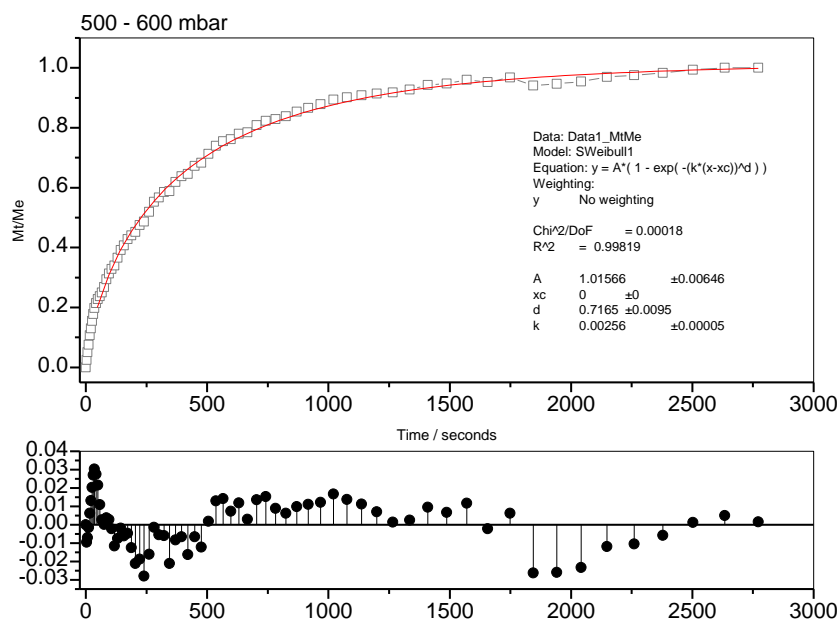


**Figure 6.54: Normalization adsorption profile for carbon dioxide adsorption on Compound 17 at 303 K - pressure step 500-600 mbar**

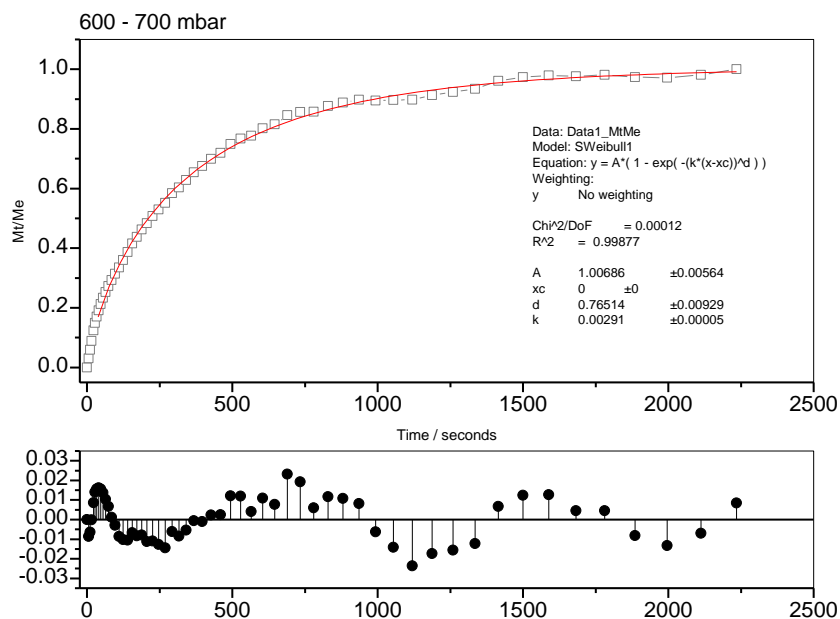


**Figure 6.55: Normalization adsorption profile for carbon dioxide adsorption on Compound 17 at 303 K - pressure step 600-700 mbar**

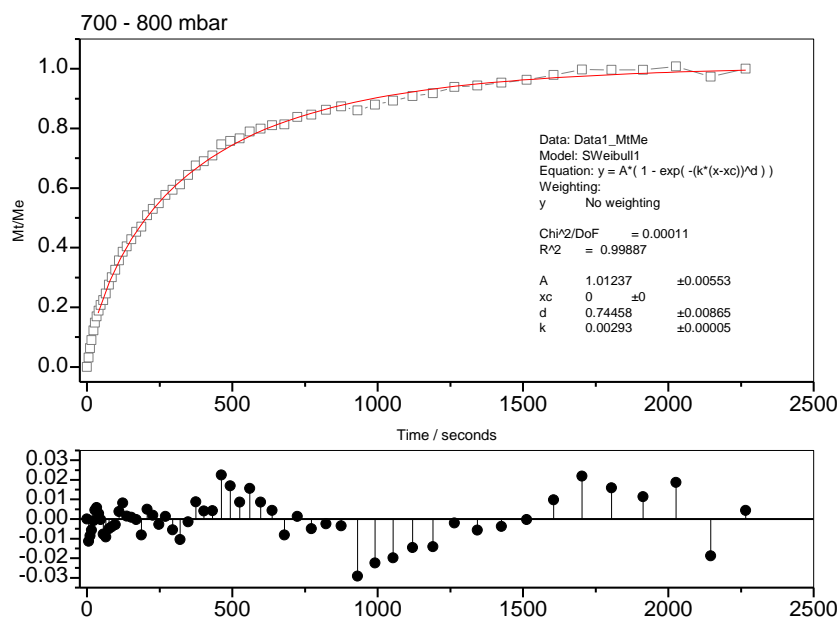


**Figure 6.56: Normalization adsorption profile for carbon dioxide adsorption on Compound 17 at 303 K - pressure step 700-800 mbar**

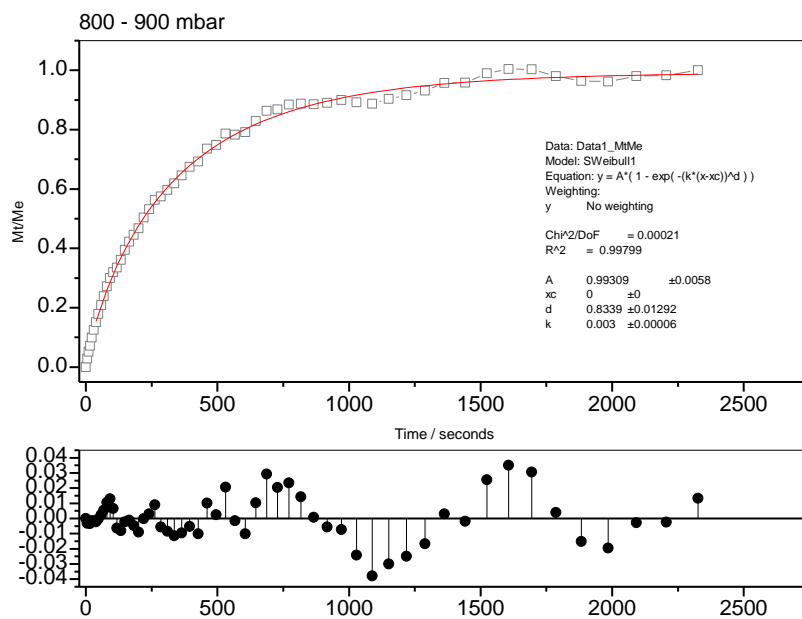


**Figure 6.57: Normalization adsorption profile for carbon dioxide adsorption on Compound 17 at 303 K - pressure step 800-900 mbar**

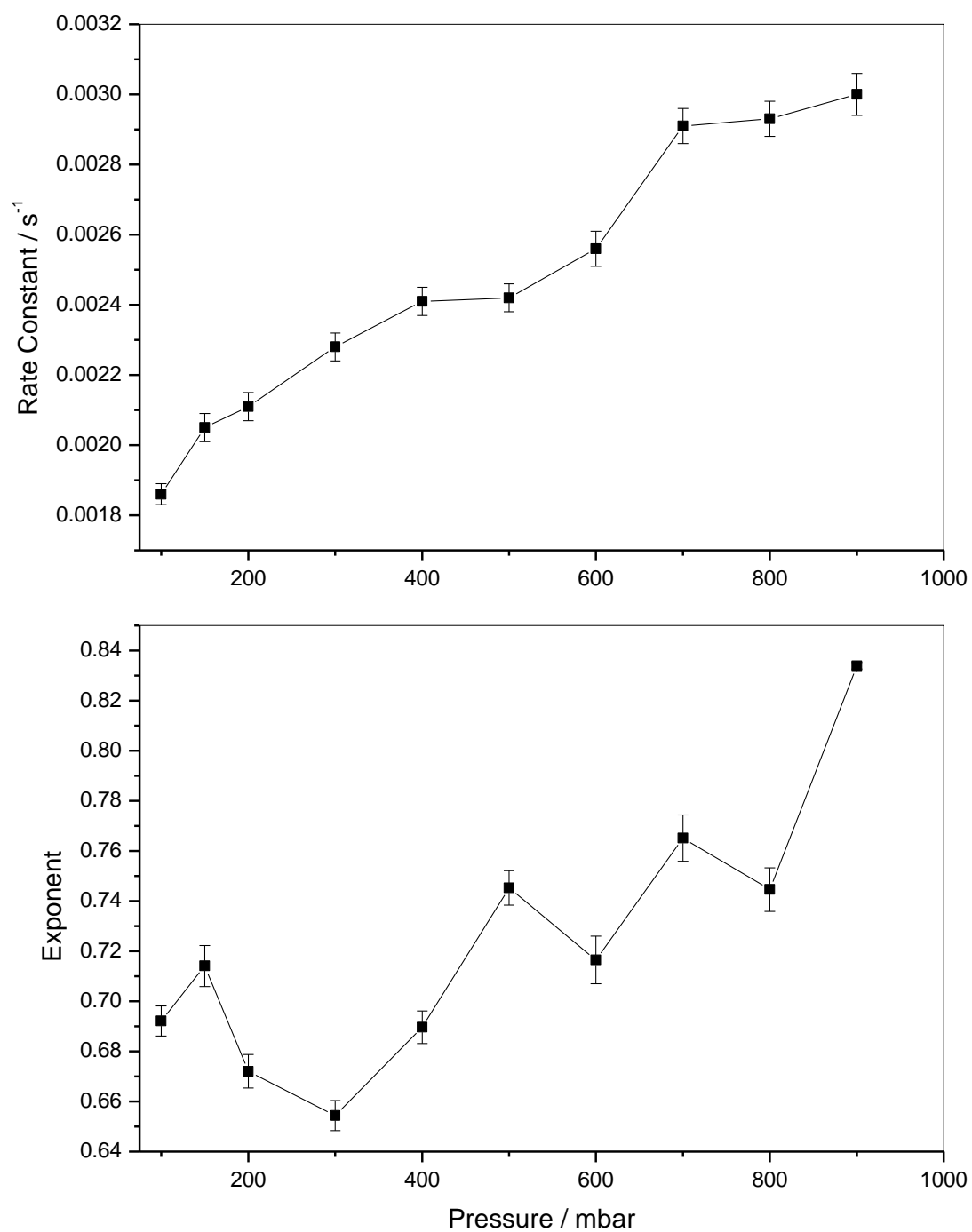


**Figure 6.58: Rate constant and Exponent plots for carbon dioxide adsorption on Compound 17 at 303 K**

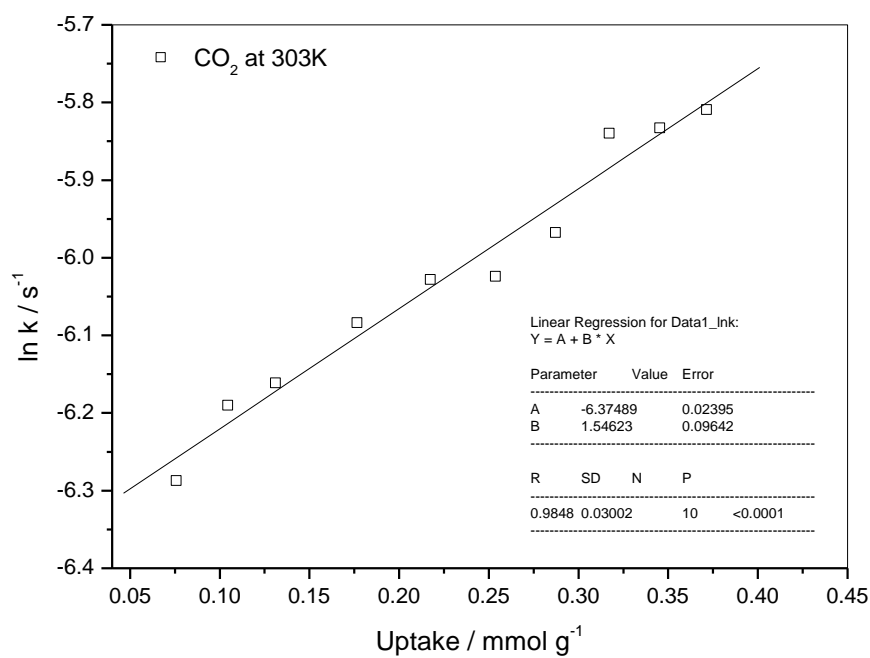


**Figure 6.59: ln k plot against carbon dioxide uptake on Compound 17 at 303 K**

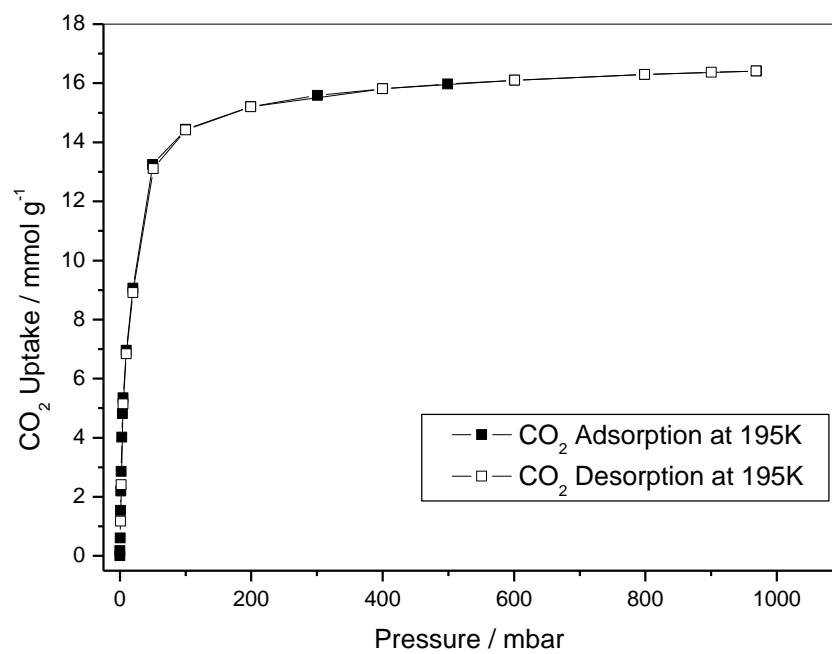


**Figure 6.60: Purified carbon dioxide adsorption on HKUST-1 at 192 K**

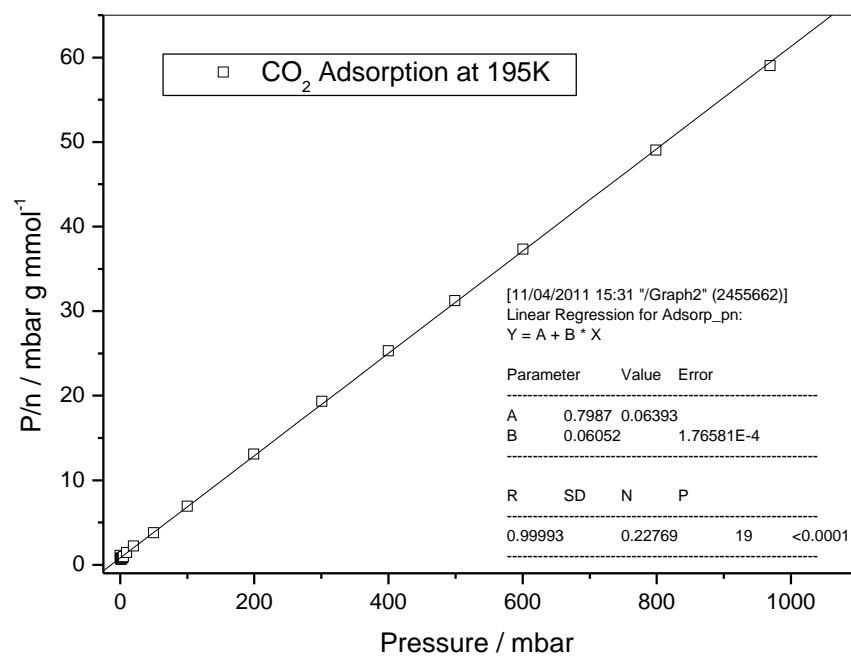


**Figure 6.61: Langmuir analysis plot for purified carbon dioxide adsorption on HKUST-1 at 192 K**

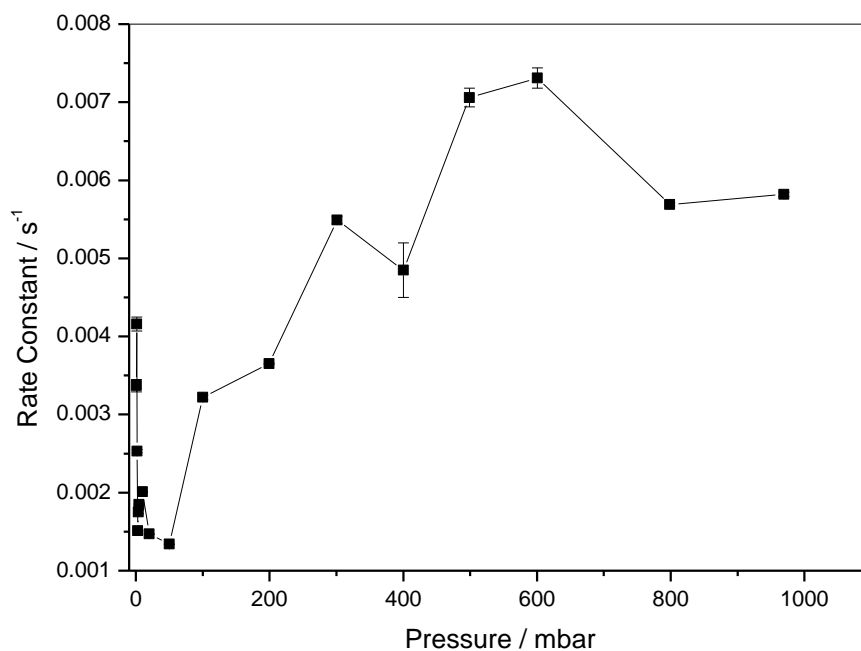


**Figure 6.62: Rate constant plot for carbon dioxide adsorption on HKUST-1 - 192 K**

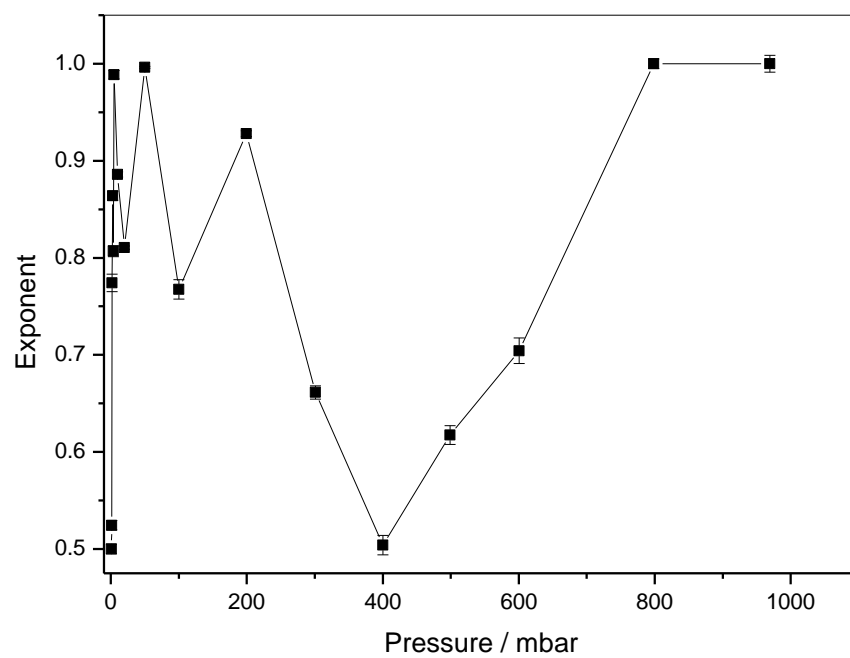


**Figure 6.63: Exponent plot for carbon dioxide adsorption on HKUST-1 at 192 K**

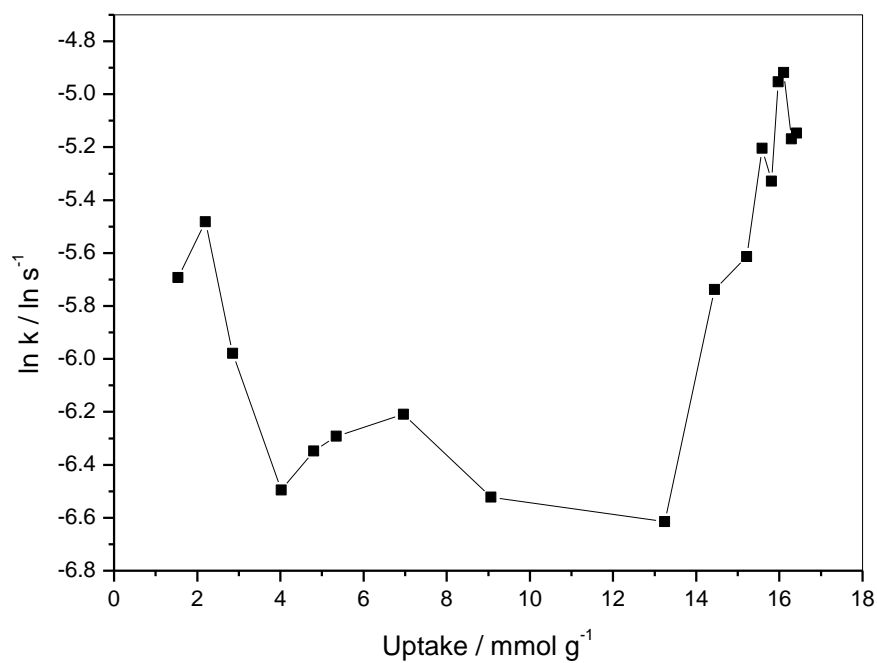
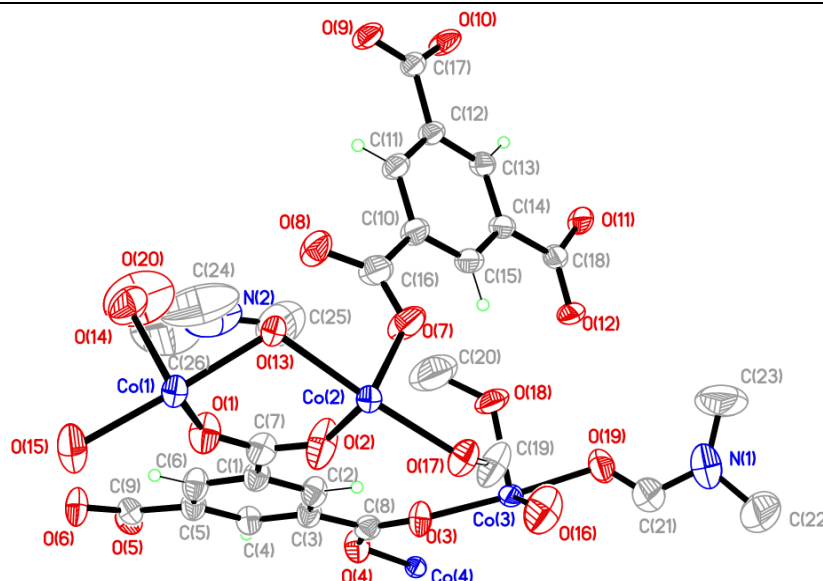


**Figure 6.64: ln k plot against carbon dioxide uptake on HKUST-1 at 192 K**

**Compound 18:**  $[\text{Co}_3(\text{C}_9\text{H}_3\text{O}_6)_2(\text{H}_2\text{O})_{3.25}(\text{CH}_4\text{O})_{1.25}(\text{C}_3\text{H}_7\text{NO})] \cdot (\text{C}_3\text{H}_7\text{NO})$



Chemical formula (total)	$\text{C}_{25.25}\text{H}_{31.5}\text{Co}_3\text{N}_2\text{O}_{18.5}$
Formula weight	835.81
Temperature	150(2) K
Radiation, wavelength	MoK $\alpha$ , 0.71073 Å
Crystal system, space group	orthorhombic, <i>Pnma</i>
Unit cell parameters	$a = 24.6079(6)$ Å $b = 27.9687(8)$ Å $c = 14.6579(4)$ Å
Cell volume	10088.3(5) Å <sup>3</sup>
Z	8
Crystal colour and size	purple, 0.20 × 0.10 × 0.05 mm <sup>3</sup>
Final <i>R</i> indices [ $F^2 > 2\sigma$ ]	$R1 = 0.0595$
<i>R</i> indices (all data)	$wR2 = 0.1754$
Largest diff. peak and hole	1.66 and −0.59 e Å <sup>−3</sup>

**Figure 6.65:** Asymmetric Unit of Compound 18 all unique atoms labelled,

### Synthesis

1 mL of a solution of  $\text{Co}(\text{NO}_3)_2 \cdot 6\text{H}_2\text{O}$  (0.09 g, 0.33 mmol) in dimethylformamide (DMF) (10 mL) was syringed into one side of the H-Cell vessel, 1 mL of a solution of 1,3,5-benzenetricarboxylic acid (0.035 g, 0.17 mmol) in DMF (10 mL) was then syringed into the other side of the H-Cell vessel. The independent solutions were bridged by 2 mL water that was carefully layered into the bridging tube. After four weeks, purple needle crystals formed.

## Structure Determination

The data were collected at 150 K using molybdenum radiation on an Oxford Diffraction Gemini A Ultra diffractometer. The structure was solved by direct methods. The semi-empirical absorption corrections were applied based on symmetry-equivalent and repeated data. The refinement gave a  $wR2$  of 0.1754 for all 11348 independent reflections and a conventional  $R1$  of 0.0595, for 6929 reflections with  $F^2 > 2\sigma$ . The residual electron density maximum and minimum were 1.66 and  $-0.59 \text{ e } \text{\AA}^{-3}$  respectively, the high residual electron density in compound 18 results from heavily disordered DMF molecules where it was not possible to model all the disorder.

The hydrogen atoms were placed in geometrically calculated positions with  $U$  constrained to  $1.2 U_{eq}(\text{C})$  for aromatic hydrogen atoms. The DMF molecules in the structure coordinated to the Co(3) cation were heavily disordered and split into two parts for refinement; with SIMU, DELU and FLAT restraints imposed. The full data of compound 18 can be found in Appendix 1.

## Structure Analysis

The asymmetric unit of compound 18 (figure 6.65) shows two complete 1,3,5-benzenetricarboxylate ligands coordinating to four cobalt cations, Co(1), Co(2), Co(3) and Co(4) that are in two different coordination environments in this polymeric compound. The Co(1) and Co(2) cations form standard octahedral geometries as they are situated coplanar in a mirror plane joined by two symmetry equivalent 1,3,5-benzenetricarboxylate ligands and a bridging water molecule O(13). (figure 6.66) The Co(3) and Co(4) cations also form a connected building unit shown in figure 6.67; however the Co(3) cation adopts the standard octahedral geometry with bond angles in table 6.21, whilst the Co(4) forms a distorted square pyramidal geometry. This is a direct result of the trifurcating O(5)-C(9)-O(6) carboxylate that coordinates to Co(4) with a bidentate coordination forming the bite angle O(5)-Co(4)-O(6)  $58.68(11)^\circ$  with an additional bond from the O(5) to Co(3) forming a bridge with an angle of Co(3)-O(5)-Co(4)  $106.67(12)^\circ$ . The bond lengths to Co(4) from the O(5)-C(9)-O(6) carboxylate vary drastically with the Co(4)-O(6) at  $2.001(3) \text{ \AA}$  one of the strongest



cobalt-oxygen bonds in the compound, whilst the Co(4)-O(5) bond is 2.385(3) Å which is the weakest cobalt-oxygen bond in the compound. The Co(3)-O(5) bond length is 2.099(3) Å comparable to the primary Co(4)-O(6) bond, suggesting that the Co(4)-O(5) bond is a weaker ‘secondary’ interaction. This is further exemplified by the other bond angles in the distorted square pyramidal geometry of Co(4) with O(4)-Co(4)-O(6) 132.11(14)° and O(4)-Co(4)-O(11) 105.41(13)°, indicating that if the O(5) bond is not fully coordinated the Co(4) would adopt a more tetrahedral geometry.

These cobalt cations are linked together by the two 1,3,5-benzenetricarboxylate ligands C(1)-O(6) and C(10)-O(12). The C(1)-O(6) 1,3,5-benzenetricarboxylate has fully delocalised carboxylate groups coordinating through all its carboxylate oxygens. The O(1)-C(7)-O(2) carboxylate group bridges the Co(1) and Co(2) cations with monodentate bonds Co(1)-O(1) and Co(2)-O(2), its symmetry equivalent carboxylate group generated by the mirror plane also coordinates perpendicular in the cis position O(1)-Co(1)-O(1A) 98.54(19)° completing the bridging group with a bifurcated water molecule O(13) (figure 6.66). The remaining two carboxylate groups are used to bridge the Co(3) and Co(4) cations with the O(3)-C(8)-O(4) carboxylate group forming monodentate bonds to respective cobalt cations generating a bridge similar to that present between the Co(3) and Co(4) bridging unit. The last carboxylate of the C(1)-O(6) ligand coordinates in a trifurcated bridge between symmetry equivalent Co(4) (bidentate) and Co(3) (monodentate) generating the distorted geometry in the Co(4) cation. This bridging carboxylate is present in a similar position within the bridging cluster to the bidentate water molecule O(13), and is able to coordinate in this position and motif due to the lack of a mirror plane through the Co(3)-Co(4) bridging cluster (figure 6.67).

The second 1,3,5-benzenetricarboxylate ligand C(10)-O(12) has fully delocalised carboxylate groups coordinating through all but two O(8) and O(12) carboxylate oxygens. These uncoordinated carboxylates show fully delocalisation and deprotonation with no indication of carbon-oxygen single and double bonds present within the structure (table 6.21). The ligand acts as a bridge between the Co(1)-Co(2) building unit and the Co(3)-Co(4) building unit shown in figure 6.66 and 6.67 respectively. This occurs with the coordination to Co(2) through the monodentate bond trans to the

bridging cluster via the O(7) carboxylate oxygen, its remaining two carboxylate groups coordinate solely to symmetry equivalent Co(3) and Co(4) cations. The O(9)-C(17)-O(1) carboxylate group forms the second primary bridging carboxylate in the Co(3)-Co(4) building unit coordinating with the monodentate bonds Co(3)-O(9) and Co(4)-O(10). This carboxylate group coordinates perpendicular to the O(3)-C(8)-O(4) bridging carboxylate at  $97.64(13)^\circ$  completing the carboxylate bridging between the Co(3)-Co(4) cations. The remaining carboxylate group of the C(10)-O(12) ligand coordinates with a monodentate bond to the Co(4) cation; Co(4)-O(11) in a symmetry equivalent Co(3)-Co(4) building unit in the trans position to the Co(3)-Co(4) carboxylate bridges. The Co(3)-Co(4) building unit is similar to that observed between the Co(1)-Co(2) with both units placing the respective cobalts  $3.601(12) \text{ \AA}$  and  $3.547(10) \text{ \AA}$  apart. The building units contain two bidentate bridging carboxylates and bifurcated bridging oxygen all in the cis positions with respect to each other.

The Co(1) and Co(3) cations act as semi-capped nodes with Co(1) coordinating to a bridging water molecule O(13) and two terminal water molecules cis to one another O(14)-Co(1)-O(15)  $89.92(12)^\circ$ , with the final coordination site occupied by the symmetry equivalent O(14) water molecule generated by the mirror symmetry. The Co(3) cation is also capped trans to the bridging carboxylate groups with coordination to a terminal water ligand O(16), a terminal methanol O(18) coordinated cis to O(16); and a DMF molecule completes the octahedral geometry cis to the other terminal ligands. The Co(2) and Co(4) cations act as fully bridging nodes coordinating to the C(10)-O(12) 1,3,5-benzenetricarboxylate ligand expanding the structure down the cell body diagonals. The linking of the two building units of Co(1)-Co(2) and Co(3)-Co(4) creates the molecular unit shown in figure 6.68. This molecular building unit expands the structure into a fully coordinated three dimensional porous network. The Co(1)-Co(2) bridging unit forms columns down the *a*-axis that are stacked up the *c*-axis (figure 6.69) forming a central building point in the (101) mirror plane. These columns are linked by the bridging 1,3,5-benzenetricarboxylate ligands diverging at  $90.51(3)^\circ$  to one another, these form double layer sheets connected by the Co(3)-Co(4) bridging units and expand along the *a*-axis and down the *c*-axis (figure 6.70). This packing motif creates almost circular pores that run down the *c*-axis shown in figure 6.70, these pores have the

dimensions 9.041(3) by 6.223(6) Å and are created due to the capped ligands on Co(1), Co(2) and Co(3) that form the walls of the pore. Each pore has one disordered methanol, two disordered DMF and four water molecules pointing in towards the pore creating multiple interaction sites for potential adsorbates. These pores are free of solvent and are connected by smaller triangular pores down the cell body diagonal with dimensions 6.223(8) by 8.019(2) Å which contain one uncoordinated DMF molecule.

PLATON<sup>1</sup> confirms the presence of pores upon desolvation of the compound, with a calculated pore volume 6287.2 Å<sup>3</sup> per unit cell corresponding to 62.3 %.

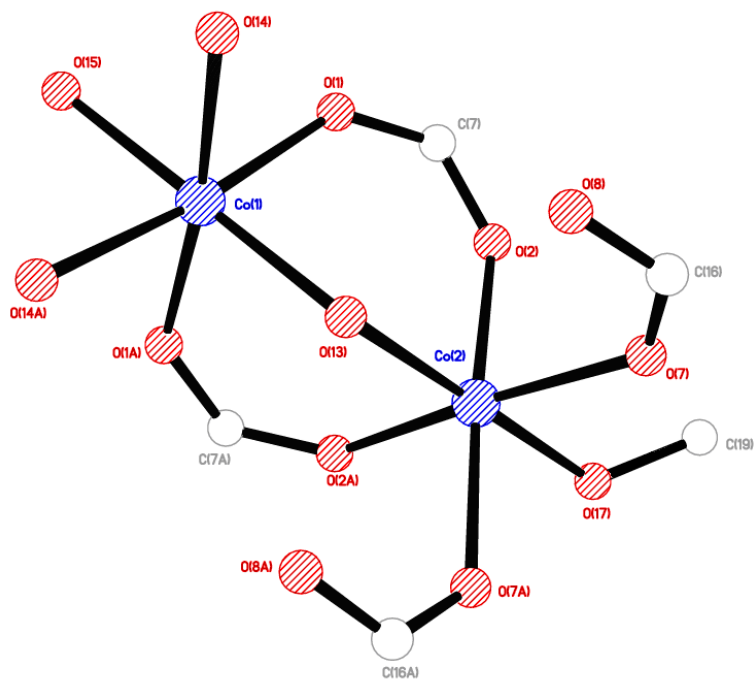
The high porosity of compound 18 and the similar pore motifs to compound 17 and HKUST-1<sup>9</sup> suggest the potential applications for gas and vapour separation based on molecular interactions with the pore walls, making compound 18 a very desirable compound. The synthesis protocol used to form compound 18 differs drastically from those used to bulk prepare compound 17 and HKUST-1.<sup>9</sup> The H-Cell synthesis technique yielded only two small crystals of compound 18 in 4 weeks making this method invalid for bulk scale up reactions required for gas adsorption studies. Further attempts to synthesize this product using solvothermal synthesis failed with powder products failing to correlate with the predicted powder diffraction pattern calculated from the single crystal data of compound 18. The synthesis of this compound however does show that the solvent system used for compound 17 is adaptable to crystallise previously unobtainable frameworks across a range of synthesis vessels. In addition to compound 18 a second compound was formed using the H-Cell apparatus; compound 19.

**Table 6.21: Selected Bond Lengths [Å] and Angles [°] for Compound 18**

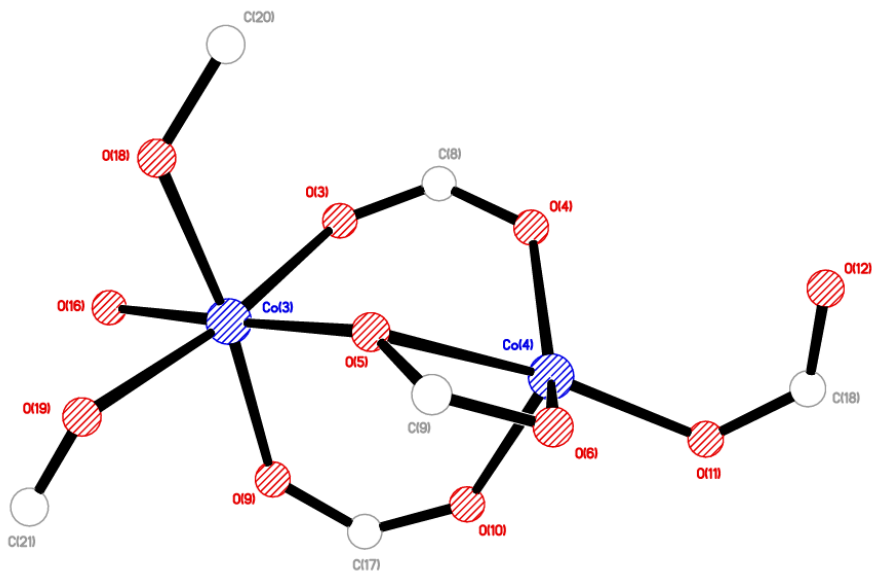
Co(1)–O(1)	2.050(3)	Co(1)–O(13)	2.093(4)
Co(1)–O(14)	2.124(3)	Co(1)–O(15)	2.111(5)
Co(2)–O(2)	2.017(3)	Co(2)–O(7)	2.035(3)
Co(2)–O(13)	2.190(4)	Co(2)–O(17)	2.124(4)
Co(3)–O(3)	2.071(3)	Co(3)–O(5B)	2.099(3)
Co(3)–O(9C)	2.033(3)	Co(3)–O(16)	2.092(4)
Co(3)–O(18)	2.085(3)	Co(3)–O(19)	2.081(4)
Co(4)–O(4)	1.941(3)	Co(4)–O(5B)	2.385(3)
Co(4)–O(6B)	2.001(3)	Co(4)–O(10C)	1.971(3)
Co(4)–O(11D)	1.973(3)	C(7)–O(1)	1.260(5)
C(7)–O(2)	1.242(5)	C(8)–O(3)	1.240(5)
C(8)–O(4)	1.263(5)	C(9)–O(5)	1.240(5)
C(9)–O(6)	1.277(5)	C(16)–O(7)	1.268(5)
C(16)–O(8)	1.252(5)	C(17)–O(9)	1.248(5)
C(17)–O(10)	1.254(5)	C(18)–O(11)	1.269(5)
C(18)–O(12)	1.245(5)		
O(1)–Co(1)–O(1A)	98.54(19)	O(1)–Co(1)–O(13)	92.95(11)
O(1)–Co(1)–O(14)	87.76(13)	O(1)–Co(1)–O(15)	88.55(14)
O(2)–Co(2)–O(2A)	91.5(2)	O(2)–Co(2)–O(7)	88.76(18)
O(2)–Co(2)–O(13)	94.27(12)	O(2)–Co(2)–O(17)	88.08(13)
O(3)–Co(3)–O(5B)	89.06(11)	O(3)–Co(3)–O(9C)	97.64(13)
O(3)–Co(3)–O(16)	88.18(14)	O(3)–Co(3)–O(18)	89.86(14)
O(3)–Co(3)–O(19)	171.32(15)	O(4)–Co(4)–O(5B)	90.99(11)
O(4)–Co(4)–O(6B)	132.11(14)	O(4)–Co(4)–O(10C)	112.19(14)
O(4)–Co(4)–O(11D)	105.41(13)	Co(1)–O(1)–C(7)	135.1(3)
Co(2)–O(2)–C(7)	135.7(3)	Co(3)–O(3)–C(8)	140.7(3)
Co(4)–O(4)–C(8)	127.6(3)	Co(3D)–O(5)–C(9)	150.2(3)
Co(4D)–O(5)–C(9)	82.1(2)	Co(4D)–O(6)–C(9)	98.8(3)
Co(2)–O(7)–C(16)	128.9(3)	Co(3E)–O(9)–C(17)	135.3(3)
Co(4B)–O(11)–C(18)	123.7(3)	Co(4E)–O(10)–C(17)	137.1(3)
Co(1)–O(13)–Co(2)	111.82(17)	Co(3D)–O(5)–Co(4D)	106.67(12)

Symmetry operations for equivalent atoms

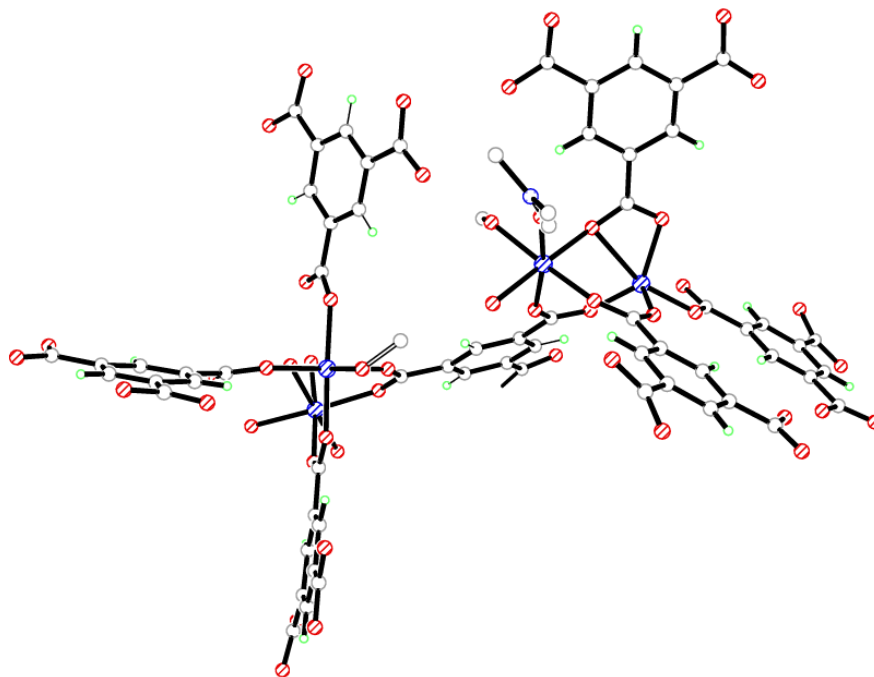
A  $x, -y+3/2, z$     B  $-x+3/2, -y+1, z-1/2$     C  $x+1/2, y, -z+1/2$ D  $-x+3/2, -y+1, z+1/2$     E  $x-1/2, y, -z+1/2$



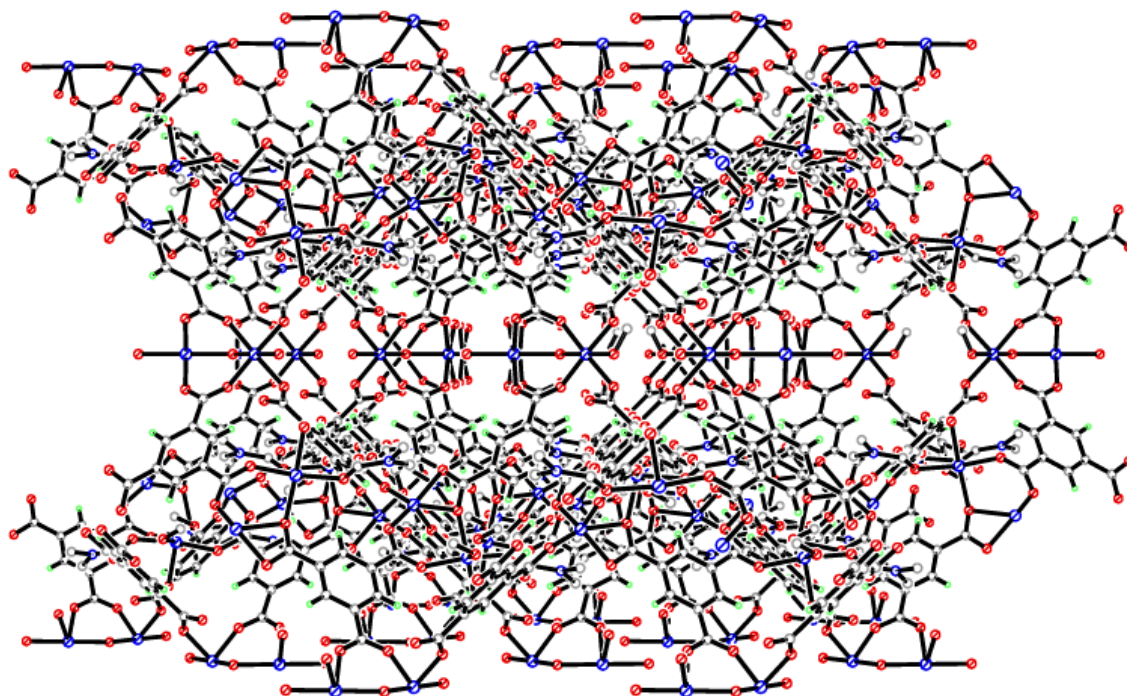
**Figure 6.66:** Octahedral coordination environment of Co(1) and Co(2) forming the Co(1)-Co(2) bridging unit in compound 18



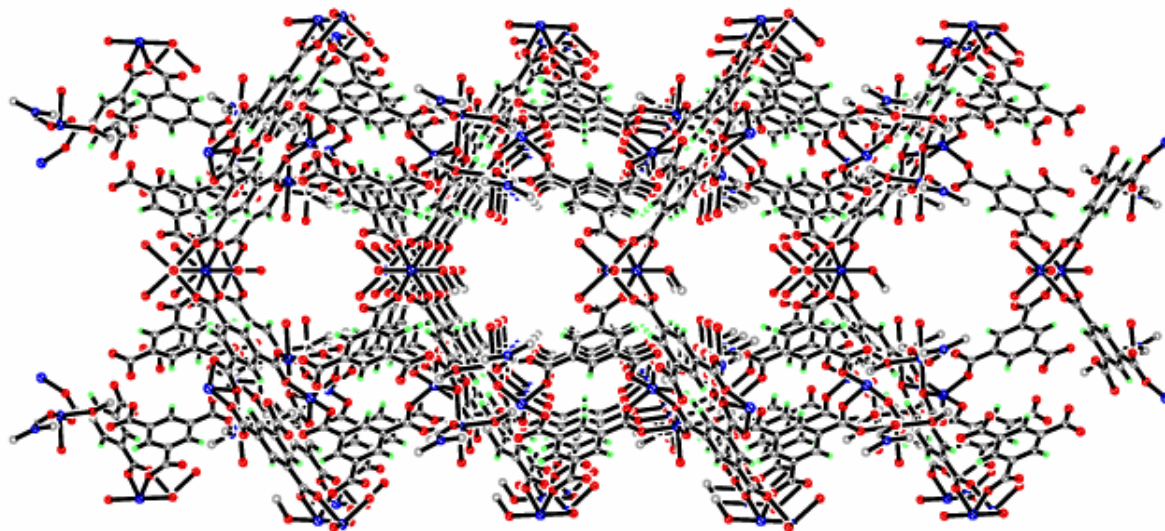
**Figure 6.67:** Octahedral coordination environment of Co(3) and tetrahedral coordination of Co(4) forming the Co(3)-Co(4) bridging unit in compound 18



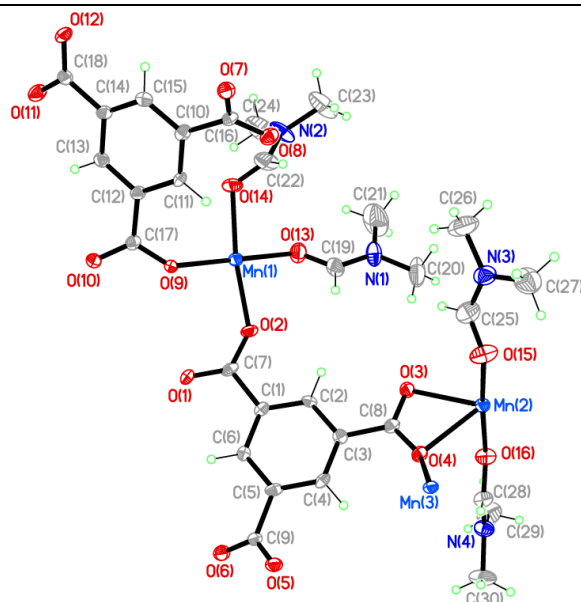
**Figure 6.68:** Secondary building unit of Co(1)-Co(2) and Co(3)-Co(4) bridging units in compound 18



**Figure 6.69:** Three dimensional packing in compound 18 viewed down the *a*-axis



**Figure 6.70:** Three dimensional packing of compound 18 viewed down the *c*-axis showing the nanochannels that run through the compound

**Compound 19:**  $[\text{Mn}_3(\text{C}_9\text{H}_3\text{O}_6)_2(\text{C}_3\text{H}_7\text{NO})_4]$ 

Chemical formula (total)	$\text{C}_{30}\text{H}_{34}\text{Mn}_3\text{N}_4\text{O}_{16}$
Formula weight	871.43
Temperature	150(2) K
Radiation, wavelength	MoK $\alpha$ , 0.71073 Å
Crystal system, space group	monoclinic, $P2_1/c$
Unit cell parameters	$a = 17.979(4)$ Å $b = 11.8057(16)$ Å $c = 18.827(9)$ Å $\beta = 116.48(4)^\circ$
Cell volume	$3577(2)$ Å <sup>3</sup>
<i>Z</i>	4
Crystal colour and size	colourless, $0.40 \times 0.30 \times 0.02$ mm <sup>3</sup>
Final <i>R</i> indices [ $F^2 > 2\sigma$ ]	$R1 = 0.0628$
<i>R</i> indices (all data)	$wR2 = 0.1834$
Largest diff. peak and hole	1.03 and $-0.87$ e Å <sup>-3</sup>

**Figure 6.71: Asymmetric Unit of Compound 19 all unique atoms labelled****Synthesis**

1 mL of a solution of  $\text{Mn}(\text{NO}_3)_2$  (0.059 g, 0.33 mmol) in dimethylformamide (DMF) (10 mL) was syringed into one side of the H-Cell vessel, 1 mL of a solution of 1,3,5-benzenetricarboxylic acid (0.035 g, 0.17 mmol) in DMF (10 mL) was then syringed into the other side of the H-Cell vessel. The independent solutions were bridged by 2 mL water that was carefully layered into the bridging tube. After three weeks, colourless plate crystals formed.



## Structure Determination

The data were collected at 150 K using molybdenum radiation on an Oxford Diffraction Gemini A Ultra diffractometer. The structure was solved by direct methods. The semi-empirical absorption corrections were applied based on symmetry-equivalent and repeated data. The refinement gave a  $wR2$  of 0.1834 for all 6306 independent reflections and a conventional  $R1$  of 0.0628, for 4812 reflections with  $F^2 > 2\sigma$ . The residual electron density maximum and minimum were 1.03 and  $-0.87 \text{ e } \text{\AA}^{-3}$  respectively.

The hydrogen atoms were placed in geometrically calculated positions with  $U$  constrained to  $1.2 U_{\text{eq}}(\text{C})$  for aromatic hydrogen atoms and  $1.5 U_{\text{eq}}(\text{C})$  for methyl hydrogens. The full data of compound 19 can be found in Appendix 1.

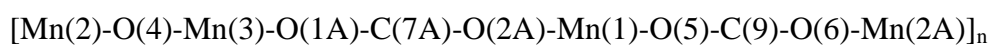
## Structure Analysis

The asymmetric unit of compound 19 (figure 6.71) shows two complete 1,3,5-benzenetricarboxylate ligands coordinating to three manganese cations, Mn(1), Mn(2) and Mn(3) that all form distorted octahedral geometries (figure 6.72) (table 6.22).

The distorted octahedral geometries in Mn(2) and Mn(3) are generated by bidentate carboxylate groups that reduce the bond angles significantly with the O(3)-Mn(2)-O(4) bite angle of  $57.45(11)^\circ$  and the O(9A)-Mn(3)-O(10A) bite angle  $57.00(11)^\circ$  lower than the ideal cis  $90^\circ$  octahedral bond angle.

The manganese cations are linked together by the two 1,3,5-benzenetricarboxylate ligands C(1)-O(6) and C(10)-O(12), both these ligands have fully deprotonated and delocalised carboxylate groups, that are bifurcated forming monodentate bonds through each carboxylate oxygen to manganese cations creating a carboxylate bridge. The individual carboxylate bonds to the respective manganese cations are shown in figure 6.72. When these carboxylate groups are bridged they form a complex chain of manganese cations running down the [011] diagonal in the order;  $[\text{Mn}(2)\text{-Mn}(1)\text{-Mn}(3)\text{-Mn}(2)\cdots]_n$ . These are connected primarily by the C(1)-O(6) 1,3,5-benzenetricarboxylate ligand that coordinates to Mn(2) with the bidentate carboxylate group O(3)-C(8)-O(4) with a bite angle of  $57.45(11)^\circ$ , this carboxylate group also coordinates to the Mn(3) cation. This creates a bridging angle of Mn(2)-O(4)-Mn(3)

114.42(13)° with the Mn(3) positioned 2.343(6) Å out of the Mn(2)-carboxylate plane. The O(5)-C(9)-O(6) carboxylate group then coordinates to the Mn(1) cation and a symmetry equivalent Mn(2) cation with the monodentate bonds Mn(1)-O(5) 2.224(3) Å and Mn(2)-O(6) 2.123(3) Å. It coordinates to the Mn(1) cation with a C(9)-O(5)-Mn(1) bond angle of 145.4(3)° placing the Mn(1) at 106.85(4)° to the Mn(2A) cation with a distance of 5.441(5) Å, this places the Mn(1) cation coplanar to the Mn(3) cation at a distance of 3.632(2) Å. The Mn(1) and Mn(3) cations are also bridged by the symmetry equivalent of the C(1)-O(6) ligand that is generated by an inversion symmetry point at 1.808(2) Å directly below the C(1) carbon of the ligand. This symmetry equivalent ligand runs parallel at a  $\pi$ - $\pi$  distance of 3.618(4) Å and coordinates to the Mn(1) and Mn(3) cations via the monodentate bonds Mn(1)-O(2) 2.124(3) Å cis to the symmetry equivalent O(5)-C(9)-O(6) carboxylate at 89.72(12)°; and the Mn(3)-O(1) 2.133(3) Å bond in the cis position with respect to its symmetry equivalent O(3)-C(8)-O(4) carboxylate group at 82.89(12)°. This bridges the manganese cations in the following system;



This chain is further bridged by the second 1,3,5-benzenetricarboxylate ligand C(10)-O(12) that is perpendicular at an offset angle of 107.46(12)° to the plane of the C(1)-O(6) aromatic ring. This ligand alternates between each manganese chain due to the inversion symmetry at the centre of two respective cation chains, flipping the ligand by 180° creating a 'zigzag' sheet. The C(10)-O(12) ligand coordinates to the manganese chain by the bidentate carboxylate O(9)-C(17)-O(10) to the Mn(3) cation with a bite angle of 57.00(11)°, this carboxylate coordinates further to the coplanar Mn(1) cation creating a bridging angle of Mn(1)-O(9)-Mn(3) of 112.41(3)°. The O(11)-C(18)-O(12) carboxylate further bridges a symmetry equivalent Mn(1) and Mn(3) cluster coordinating with monodentate bonds Mn(1)-O(11) 2.110(3) Å and Mn(3)-O(12) 2.162(3) Å coplanar to the manganese cations and perpendicular to the O(9)-C(17)-O(10) carboxylate bridge at 90.53(13)°. The remaining carboxylate group O(7)-C(16)-O(8) of the C(10)-O(12) ligand coordinates to the Mn(2A) cation with a monodentate bond Mn(2)-O(8) creating a bite angle of 112.84(13)° between the O(6) of the C(1)-O(6) 1,3,5-benzenetricarboxylate ligand. The remaining oxygen O(7) coordinates to a

symmetry equivalent Mn(3) cation cis to the carboxylate oxygens O(4) and O(10) filling the last coordination site of the six-coordinate octahedral Mn(3) cation, this also forms the last carboxylate bridge of the manganese cluster (figure 6.72C).

The remaining two coordination sites of both Mn(1) and Mn(2) are filled with DMF ligands that coordinate cis to one another on the Mn(1) cation with an angle of O(14)-Mn(1)-O(13)  $83.82(14)^\circ$  pointing them out away from the manganese chain. The Mn(2) coordinates to two trans DMF molecules that take up the axial positions cis to the carboxylate equatorial belt; O(15)-Mn(2)-O(16)  $174.45(13)^\circ$  placing them above and below the manganese chains (figure 6.72B).

The bridging coordination mode of all the carboxylates of multiple symmetry equivalent 1,3,5-benzenetricarboxylates forms the molecular building unit shown in figure 6.73 with the two symmetry related C(1)-O(6) ligands overlapped with the inversion point positioned between them. The building unit expands the structure into a three dimensional coordinated framework with the 'zigzag' sheets of 1,3,5-benzenetricarboxylate criss-crossing, connecting the non-planar chains manganese cations as shown in figure 6.74. This figure shows compound 19 down the *c*-axis with the coordinated DMF ligands removed for clarity revealing potential micropores. This porous network is further expanded when the structure is viewed down the *a*-axis (figure 6.75), which shows the DMF molecules pointing inwards towards each other. If these DMF molecules were removed it reveals a porous network following the classical herringbone motif shown in figure 6.76 with potential pores of dimensions 8.365(8) by 10.237(13) Å.

Further analysis of the bulk material was carried out to determine purity using powder X-ray diffraction and elemental analysis. The elemental analysis of compound 19 provided the results C = 40.54 %, H = 3.70 % and N = 6.13 %. These are consistent with the calculated values from the single crystal data of C = 41.31 %, H = 3.90 % and N = 6.43 %. The powder diffraction data of compound 19 produced the diffraction pattern in figure 6.77. This is almost identical to the predicted powder diffraction pattern from the single crystal data with the significant peaks at 9.137, 9.339, 10.953, 11.760 and 16.906 2-Theta present in both sets of data with similar intensities.

The high purity and reproducibility of this compound made it an ideal target for further studies in both gas adsorption and magnetic properties, to investigate potential magnetism through the Mn-O-Mn bonds. The synthesis protocol of compound 19 uses the H-Cell apparatus to crystallise the material, this proved to be a major setback in further analysis of this compound with small quantities of compound 19 produced once every three weeks, and this coupled with the high affinity of DMF limited its potential for the further investigations. Compound 19 resulted in additional reaction methods employed to develop structures templated with the same ligands but without the DMF coordinated in the structure, leading to the production of compounds 20 and 21.

**Table 6.22: Selected Bond Lengths [Å] and Angles [°] for Compound 19**

Mn(1)–O(2)	2.124(3)	Mn(1)–O(5A)	2.224(3)
Mn(1)–O(9)	2.145(3)	Mn(1)–O(11B)	2.110(3)
Mn(1)–O(13)	2.185(3)	Mn(1)–O(14)	2.176(3)
Mn(2)–O(3)	2.221(3)	Mn(2)–O(4)	2.371(3)
Mn(2)–O(6C)	2.123(3)	Mn(2)–O(8D)	2.098(3)
Mn(2)–O(15)	2.221(4)	Mn(2)–O(16)	2.185(3)
Mn(3)–O(1A)	2.133(3)	Mn(3)–O(4)	2.293(3)
Mn(3)–O(7D)	2.084(3)	Mn(3)–O(9A)	2.226(3)
Mn(3)–O(10A)	2.368(3)	Mn(3)–O(12E)	2.162(3)
C(7)–O(1)	1.263(5)	C(7)–O(2)	1.258(5)
C(8)–O(3)	1.263(5)	C(8)–O(4)	1.277(5)
C(9)–O(5)	1.258(5)	C(9)–O(6)	1.271(5)
C(16)–O(7)	1.253(5)	C(16)–O(8)	1.269(5)
C(17)–O(9)	1.285(5)	C(17)–O(10)	1.238(5)
C(18)–O(11)	1.260(5)	C(18)–O(12)	1.256(5)
O(2)–Mn(1)–O(5A)	89.72(12)	O(2)–Mn(1)–O(9)	92.54(12)
O(2)–Mn(1)–O(11B)	92.67(13)	O(2)–Mn(1)–O(13)	87.63(13)
O(2)–Mn(1)–O(14)	171.30(13)	O(3)–Mn(2)–O(4)	57.45(11)
O(3)–Mn(2)–O(6C)	99.34(12)	O(3)–Mn(2)–O(8D)	146.59(12)
O(3)–Mn(2)–O(15)	91.39(14)	O(3)–Mn(2)–O(16)	93.24(13)
O(1A)–Mn(3)–O(4)	82.89(12)	O(1A)–Mn(3)–O(7D)	112.53(12)
O(1A)–Mn(3)–O(9A)	100.12(12)	O(1A)–Mn(3)–O(10A)	154.47(12)
O(1A)–Mn(3)–O(12E)	101.23(13)	Mn(3A)–O(1)–C(7)	127.4(3)
Mn(1)–O(2)–C(7)	141.7(3)	Mn(2)–O(3)–C(8)	94.2(3)
Mn(2)–O(4)–Mn(3)	114.42(13)	Mn(2)–O(4)–C(8)	87.1(3)
Mn(3)–O(4)–C(8)	139.0(3)	Mn(1A)–O(5)–C(9)	145.4(3)
Mn(2F)–O(6)–C(9)	120.6(3)	Mn(3G)–O(7)–C(16)	133.6(3)
Mn(2G)–O(8)–C(16)	128.1(3)	Mn(1)–O(9)–Mn(3A)	112.41(13)
Mn(1)–O(9)–C(17)	141.2(3)	Mn(3A)–O(9)–C(17)	93.6(3)
Mn(3A)–O(10)–C(17)	88.3(3)	Mn(1H)–O(11)–C(18)	138.4(3)
Mn(3I)–O(12)–C(18)	127.8(3)		
Symmetry operations for equivalent atoms			
A	$-x+1, -y+1, -z+1$	B	$-x, y-1/2, -z+1/2$
C	$x, -y+1/2, z-1/2$		
D	$-x+1, y-1/2, -z+1/2$	E	$x+1, -y+3/2, z+1/2$
F	$x, -y+1/2, z+1/2$		
G	$-x+1, y+1/2, -z+1/2$	H	$-x, y+1/2, -z+1/2$
I	$x-1, -y+3/2, z-1/2$		



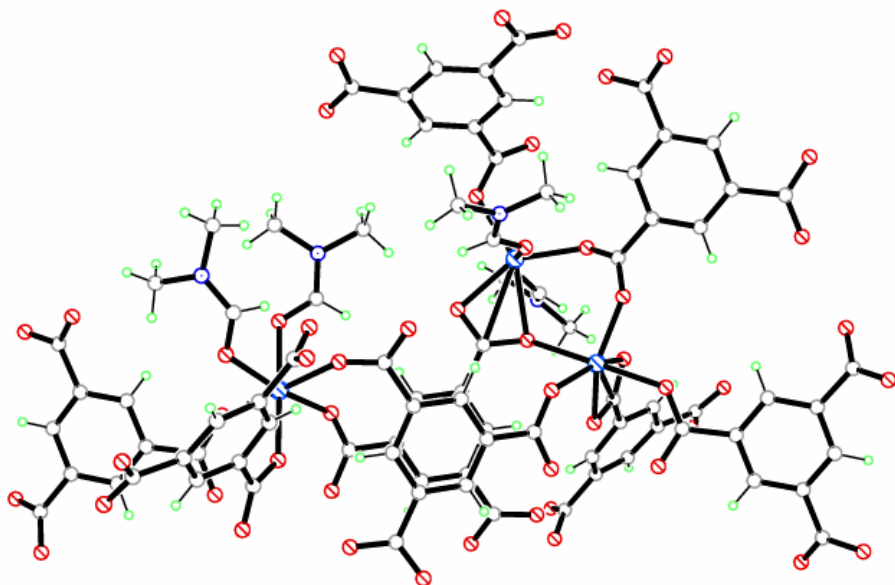


**Figure 6.73:** Secondary building unit of the bridged Mn(1), Mn(2) and Mn(3) cations in compound 19

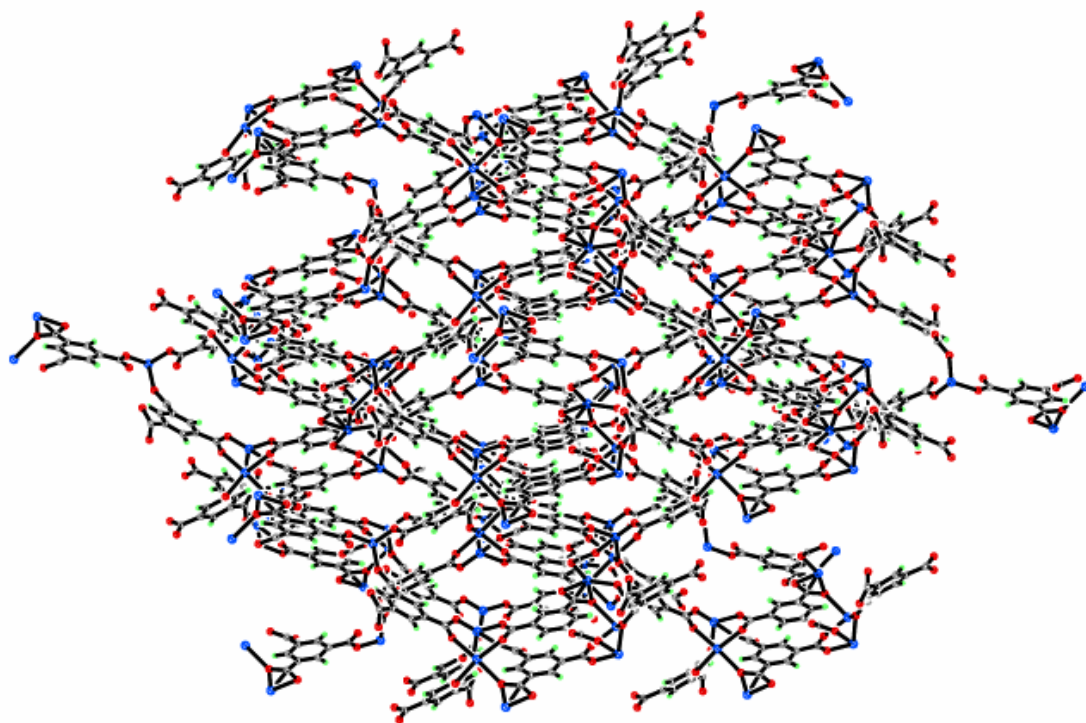


**Figure 6.74:** Three dimensional packing in compound 19 viewed down the *c*-axis

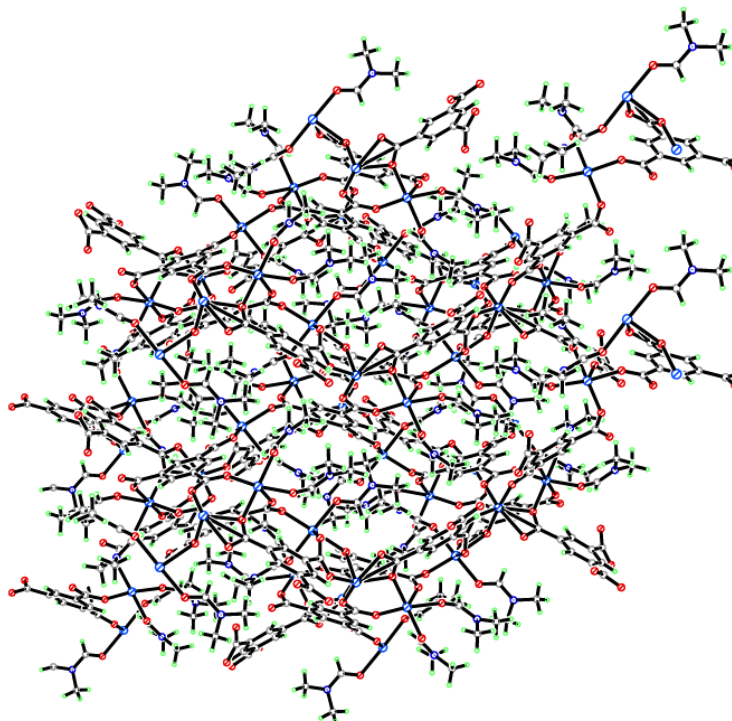


**Figure 6.75:** Three dimensional packing of compound 19 viewed down the *a*-axis showing the nanochannels that run through the compound filled with DMF

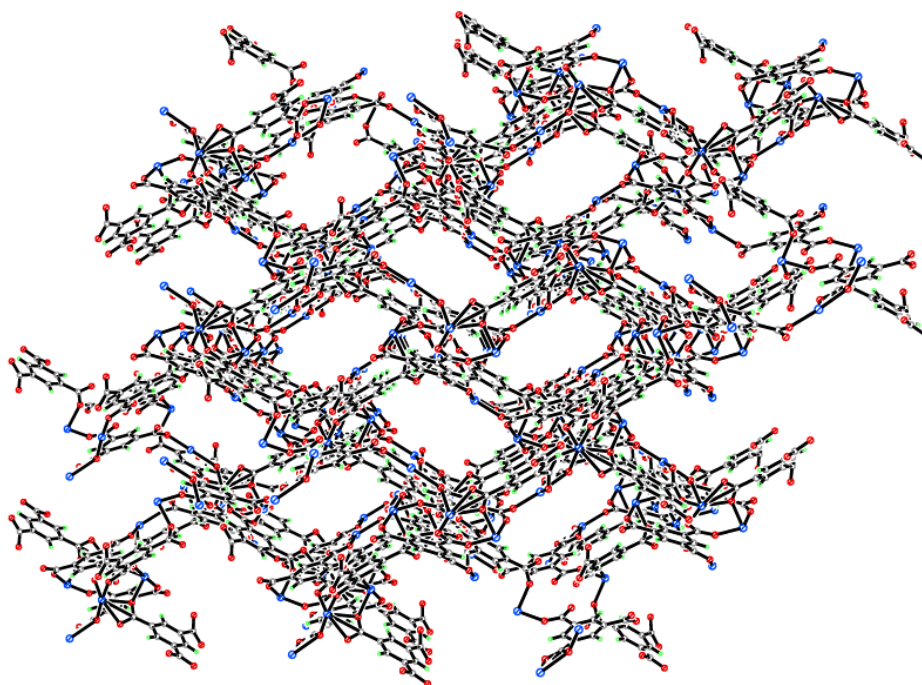


**Figure 6.76:** Three dimensional herringbone packing of compound 19 viewed down the *a*-axis showing (DMF removed for clarity)



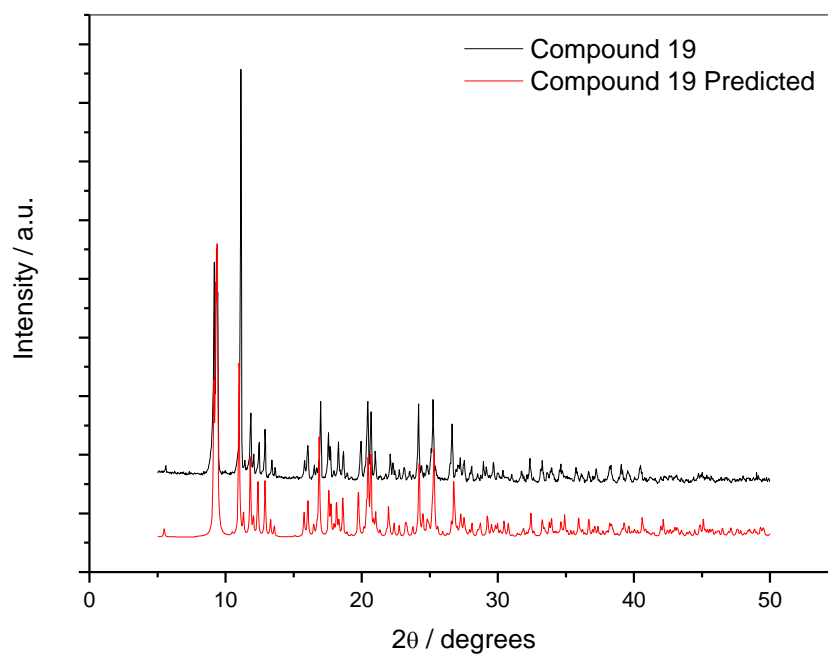
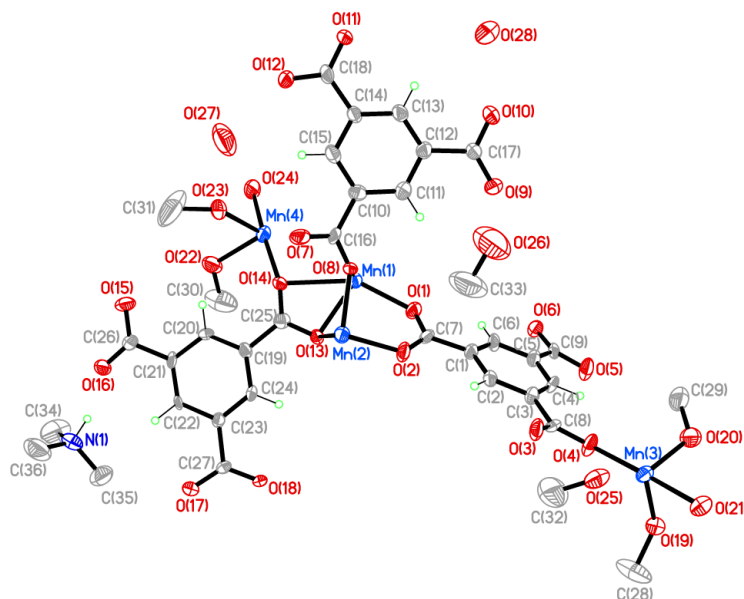


**Figure 6.77: Powder X-ray diffraction pattern of Compound 19**

**Compound 20:**  $[\text{Mn}_4(\text{C}_9\text{H}_3\text{O}_6)_3(\text{CH}_4\text{O})_5(\text{H}_2\text{O})_2]^- \cdot (\text{C}_3\text{H}_9\text{N})^+ \cdot (\text{CH}_4\text{O}) \cdot 2(\text{H}_2\text{O})$



Chemical formula (total)	$\text{C}_{36}\text{H}_{51}\text{Mn}_4\text{NO}_{28}$
Formula weight	1165.54
Temperature	150(2) K
Radiation, wavelength	MoK $\alpha$ , 0.71073 Å
Crystal system, space group	monoclinic, $P2_1/c$
Unit cell parameters	$a = 13.7180(16)$ Å $\beta = 109.272(13)^\circ$ $b = 20.3721(14)$ Å $c = 18.927(2)$ Å
Cell volume	$4993.0(9)$ Å <sup>3</sup>
<i>Z</i>	4
Crystal colour and size	colourless, $0.05 \times 0.05 \times 0.01$ mm <sup>3</sup>
Final <i>R</i> indices [ $F^2 > 2\sigma$ ]	$R1 = 0.0814$
<i>R</i> indices (all data)	$wR2 = 0.2269$
Largest diff. peak and hole	0.91 and $-0.60$ e Å <sup>-3</sup>

**Figure 6.78: Asymmetric Unit of Compound 20 all unique atoms labelled.**

### Synthesis

0.5 mL of a solution of  $\text{Mn}(\text{NO}_3)_2$  (0.059 g, 0.33 mmol) in methanol (10 mL) and 0.5 mL of a solution of 1,3,5-benzenetricarboxylic acid (0.032 g, 0.17 mmol) in methanol (10 mL) were placed into a small sample vial. This was covered with Whatman Laboratory Sealing Film and placed inside a larger sample vial. In the larger sample vial trimethylamine (0.05 mL, 0.22 mmol) was added before it was covered and left until crystallisation was complete. After one week, colourless spindle crystals formed.

## Structure Determination

The data were collected at 150 K using molybdenum radiation on an Oxford Diffraction Gemini A Ultra diffractometer. The structure was solved by direct methods. The semi-empirical absorption corrections were applied based on symmetry-equivalent and repeated data. The refinement gave a  $wR2$  of 0.2269 for all 6512 independent reflections and a conventional  $R1$  of 0.0814, for 2775 reflections with  $F^2 > 2\sigma$ . The residual electron density maximum and minimum were 0.91 and  $-0.60 \text{ e } \text{\AA}^{-3}$  respectively.

The hydrogen atoms were placed in geometrically calculated positions with  $U$  constrained to  $1.2 U_{\text{eq}}(\text{C})$  for aromatic hydrogen atoms and  $U$  constrained to  $1.2 U_{\text{eq}}(\text{N})$  for the protonated nitrogen hydrogen atoms. The methanol ligands in the structure were disordered; with SIMU and DELU restraints being imposed during refinement. The full data of compound 20 can be found in Appendix 1.

## Structure Analysis

The asymmetric unit of compound 20 (figure 6.78) shows three complete 1,3,5-benzenetricarboxylate ligands coordinating to four manganese cations; Mn(1), Mn(2), Mn(3) and Mn(4) that form slightly distorted octahedral geometries shown in figures 6.79 and 6.80. This forms an anionic framework which is balanced in charge by an uncoordinated trimethylammonium cation in the pores of the structure. The manganese cations are linked together to form a 'C'-shaped unit with the manganese cations linked by bridging carboxylate groups of the three 1,3,5-benzenetricarboxylate ligands; C(1)-O(6), C(10)-O(12) and C(19)-O(18). The C(10)-O(12) and C(19)-O(18) ligands are not fully coordinated with the respective O(9)-C(17)-O(10) and O(15)-C(26)-O(16) carboxylate groups remaining uncoordinated. The ligands do however show full delocalisation of the carboxylate groups with no evidence of carbon-oxygen double bonds or single bonds present within the aforementioned groups; C(17)-O(9) 1.242(14) Å and C(17)-O(10) 1.241(14) Å. (table 6.23) These groups do not form dative covalent bonds and are instead involved as hydrogen bond acceptors to adjacent manganese 'C'-shaped clusters. The O(9) and O(10) carboxylate oxygens form hydrogen bonds with terminal cis methanols O(19) and O(20) respectively on the Mn(3) node, the O(15) and

O(16) carboxylate oxygens form hydrogen bonds to the methanol O(22) and water ligand O(24) coordinated to the Mn(4) node.

The primary ligand in compound 20 is the 1,3,5-benzenetricarboxylate C(1)-O(6), this ligand shows full deprotonation and delocalisation of its carboxylate groups that then coordinate through monodentate bonds from each carboxylate oxygen to the manganese cations. These carboxylate groups form bridges connecting the octahedral manganese to form the 'C'-shaped building unit in figure 6.81, which runs in the order [Mn(4)-Mn(1)-Mn(2)-Mn(3)]. The Mn(3) is out of plane at 2.214(8) Å above in the *c*-axis of the coplanar Mn(1), Mn(2) and Mn(4) that coordinate in the plane of the C(1)-O(6) 1,3,5-benzenetricarboxylate ligand. The O(1)-C(7)-O(2) carboxylate coordinates to the coplanar Mn(1) and Mn(2) with monodentate bonds Mn(1)-O(1) 2.115(8) Å and Mn(2)-O(2) 2.061(7) Å forming the first bridge of the cluster holding the Mn(1) and Mn(2) cations coplanar with the metal-metal distance of 3.258(4) Å. The remaining two carboxylate groups O(3)-C(8)-O(11) and O(5)-C(9)-O(6) form similar bridging carboxylate units to Mn(2)-Mn(3) and Mn(1)-Mn(4) of two symmetry equivalent 'C'-shaped manganese clusters. The symmetry equivalent C(1)-O(6) ligands that coordinate to the manganese 'C'-shaped cluster shown in figure 6.81 are the product of a coplanar inversion centre that is positioned 3.525(4) Å either side of the C(1) atom in the *a*-axis that generates the two symmetry equivalent coplanar ligands. The symmetry equivalent O(3)-C(8)-O(4) carboxylate group coordinates to the Mn(2) and Mn(3) cations via monodentate bonds Mn(2)-O(3) and Mn(2)-O(4) (table 6.23). This group coordinates in the *cis* position to the O(1)-C(7)-O(2) carboxylate of the C(1)-O(6) ligand at an angle of O(2)-Mn(2)-O(3C) 96.9(3)° with the carboxylate group twisting out of plane towards the Mn(3) cation.

The last bridging unit of the C(1)-O(6) ligand forms between the Mn(1) and Mn(4) cations with the monodentate bonds Mn(1)-O(6) and Mn(4)-O(5) from the O(5)-C(9)-O(6) symmetry equivalent carboxylate group that coordinates *cis* with respect to the O(1)-C(7)-O(2) carboxylate; O(1)-Mn(1)-O(6A) 93.5(3)°. This creates a column of 'C'-shaped clusters running down the *a*-axis on either side of a chain of 1,3,5-benzenetricarboxylate ligands that connect them in the *b*-axis. These columns do not form sheets as they are capped in the *b*-axis at the Mn(3) and Mn(4) nodes. The Mn(3)

cation is capped by coordination to a water molecule O(21) trans to the O(3)-C(8)-O(4) bridge and coordination to two coplanar cis methanols O(19) and O(20) that are within hydrogen bonding distance of the C(9)-C(17)-O(10) carboxylate (figure 6.80A). The Mn(4) cation is also capped by one water ligand cis to the O(5)-C(9)-O(6) carboxylate bridge with one trans and one cis methanol, O(23) and O(22) respectively to the O(5) bridge.(figure 6.80B) These capped columns are connected by the remaining two 1,3,5-benzenetricarboxylate ligands C(10)-O(12) and C(19)-O(18) that coordinate to the 'C'-shaped manganese clusters at 106.69(13)° almost perpendicular to the plane of the C(1)-O(6) ligand. They run parallel to one another down the *c*-axis separated by 3.308(4) Å with respect to the planes of their aromatic rings, with an offset down the *c*-axis and *b*-axis of 0.798(5) Å, indicating both aromatic rings are involved in  $\pi$ - $\pi$  stacking interactions.

The C(10)-O(12) ligand coordinates to the manganese cluster using the trifurcated O(7)-C(16)-O(8) carboxylate that forms a bridge between Mn(1), Mn(2) and Mn(3). The O(8) carboxylate oxygen forms a bidentate coordination to the Mn(1) and Mn(2) in conjunction to the monodentate coordination of the O(7) carboxylate oxygen to the Mn(3) node. The O(8) carboxylate forms strong bonds to Mn(1) 2.183(9) Å and Mn(2) 2.124(7) Å coordination cis to the O(13) carboxylate bridge; O(8)-Mn(1)-O(13) 78.7(3)°, with a bridging bite angle of Mn(1)-O(8)-Mn(2) 98.3(3)°. The O(7) coordinates cis to the O(4) carboxylate and trans to the capping O(20) methanol. The last coordinating carboxylate of the C(10)-O(12) ligands, O(11)-C(18)-O(12) coordinates trans to the symmetry equivalent O(7)-C(16)-O(8) bridging carboxylate forming a bridge between Mn(2) and Mn(3). The trifurcated carboxylate forms a bidentate coordination to the Mn(2) cation completing its coordination sphere whilst bridging to the Mn(3) via the O(1) carboxylate oxygen that forms a bridge with a bite angle of 105.3(3)° completing the coordination sphere of the Mn(3) cation.(figure 6.81)

The final 1,3,5-benzenetricarboxylate ligand C(19)-O(18) coordinates in a similar motif to the C(10)-O(12) ligand, coordinating with a trifurcated carboxylate O(13)-C(25)-O(14) that bridges Mn(1), Mn(2) and Mn(4) along with a standard bridging carboxylate O(17)-C(27)-O(18) that forms monodentate bonds to Mn(1) and Mn(4). The

O(13)-C(25)-O(14) carboxylate coordinates at an offset angle to the trans position of the symmetry equivalent O(17)-C(27)-O(18) at 159.8(3)°.

The coordination of these 1,3,5-benzenetricarboxylate ligands creates the molecular building unit shown in figure 6.82, showing the planar chains of the 1,3,5-benzenetricarboxylate ligand coordinating to the dual layer columns. This molecular building unit expands the structure in three dimensions to create a microporous three dimensional coordinated framework. The structure packs with the manganese cluster-1,3,5-benzenetricarboxylate-manganese cluster unit staggered in the *c*-axis as the structure expands down the *b*-axis, this is clearly shown in figure 6.83 when the structure is viewed down the *a*-axis. The staggering is a result of the glide plane down the [101] axis and creates the micropores between the capped ends of one manganese cluster and the aromatic ring of the bridging 1,3,5-benzenetricarboxylate C(1)-O(6) of the adjacent column. The micropores have dimensions 8.18(2) by 6.21(7) Å and contain one trimethylammonium cation that hydrogen bonds to the uncoordinated O(16) carboxylate oxygen with a strong hydrogen bond of 2.702(4) Å, the pores also contain one disordered methanol and two uncoordinated water molecules. Figure 6.84 shows the micropores running between the 1,3,5-benzenetricarboxylate ligands that form the columns down the *c*-axis and highlights the possible hydrogen bonding between the predicted hydrogens on the disordered methanol. The micropores are also visible down the *b*-axis that shows the packing motif of the axial columns and manganese clusters (figure 6.85).

The anionic nature of this framework balanced by the cationic trimethylammonium that templates the pores around itself, results in compound 20 being highly unstable to desolvation or solvent exchange with the compound decomposing if removed from its original reaction medium for elongated periods of time. This prevented the acquisition of a clean powder diffraction pattern and reliable elemental analysis.

The structure did provide interesting structural comparisons with compounds 19 and 21, showing the templating effects and results in minor changes in the reaction medium on the overall packing and coordination motifs of the compounds. This is discussed after the presentation of compound 21.

**Table 6.23: Selected Bond Lengths [Å] and Angles [°] for Compound 20**

Mn(1)–O(1)	2.115(8)	Mn(1)–O(6A)	2.111(8)
Mn(1)–O(8)	2.183(9)	Mn(1)–O(13)	2.262(7)
Mn(1)–O(14)	2.431(7)	Mn(1)–O(17B)	2.073(8)
Mn(2)–O(2)	2.061(7)	Mn(2)–O(3C)	2.055(9)
Mn(2)–O(8)	2.124(7)	Mn(2)–O(11D)	2.375(7)
Mn(2)–O(12D)	2.168(8)	Mn(2)–O(13)	2.270(8)
Mn(3)–O(4)	2.166(8)	Mn(3)–O(7C)	2.143(8)
Mn(3)–O(11E)	2.214(8)	Mn(3)–O(19)	2.189(9)
Mn(3)–O(20)	2.152(8)	Mn(3)–O(21)	2.197(9)
Mn(4)–O(5A)	2.134(8)	Mn(4)–O(14)	2.210(8)
Mn(4)–O(18B)	2.175(8)	Mn(4)–O(22)	2.245(8)
Mn(4)–O(23)	2.182(9)	Mn(4)–O(24)	2.188(9)
C(7)–O(1)	1.272(12)	C(7)–O(2)	1.264(13)
C(8)–O(3)	1.227(13)	C(8)–O(4)	1.309(13)
C(9)–O(5)	1.238(13)	C(9)–O(6)	1.269(13)
C(16)–O(7)	1.249(13)	C(16)–O(8)	1.284(13)
C(17)–O(9)	1.242(14)	C(17)–O(10)	1.241(14)
C(18)–O(11)	1.260(13)	C(18)–O(12)	1.265(13)
C(25)–O(13)	1.301(12)	C(25)–O(14)	1.243(13)
C(26)–O(15)	1.254(14)	C(26)–O(16)	1.260(13)
C(27)–O(17)	1.256(13)	C(27)–O(18)	1.237(12)
O(1)–Mn(1)–O(6A)	93.5(3)	O(1)–Mn(1)–O(8)	88.6(3)
O(1)–Mn(1)–O(13)	93.8(3)	O(1)–Mn(1)–O(14)	149.7(3)
O(1)–Mn(1)–O(17B)	105.7(3)	O(2)–Mn(2)–O(3C)	96.9(3)
O(2)–Mn(2)–O(8)	93.4(3)	O(2)–Mn(2)–O(11D)	162.1(3)
O(2)–Mn(2)–O(12D)	105.3(3)	O(2)–Mn(2)–O(13)	91.8(3)
O(4)–Mn(3)–O(7C)	94.9(3)	O(4)–Mn(3)–O(11E)	89.7(3)
O(4)–Mn(3)–O(19)	91.8(3)	O(4)–Mn(3)–O(20)	88.7(3)
O(4)–Mn(3)–O(21)	176.5(3)	Mn(1)–O(1)–C(7)	131.7(8)
Mn(2)–O(2)–C(7)	131.7(7)	Mn(2C)–O(3)–C(8)	134.3(8)
Mn(3)–O(4)–C(8)	127.1(8)	Mn(4A)–O(5)–C(9)	141.6(9)
Mn(1A)–O(6)–C(9)	123.4(8)	Mn(1)–O(8)–Mn(2)	98.3(3)
Mn(3C)–O(7)–C(16)	147.8(8)	Mn(2)–O(8)–C(16)	123.0(8)
Mn(1)–O(8)–C(16)	130.9(7)	Mn(2B)–O(11)–C(18)	85.4(7)
Mn(2B)–O(11)–Mn(3F)	105.3(3)	Mn(2B)–O(12)–C(18)	94.7(7)
Mn(3F)–O(11)–C(18)	144.0(9)	Mn(1)–O(13)–Mn(2)	91.9(3)
Mn(1)–O(13)–C(25)	94.1(7)	Mn(2)–O(13)–C(25)	125.6(7)
Mn(1)–O(14)–Mn(4)	105.1(3)	Mn(1)–O(14)–C(25)	87.9(7)
Mn(4)–O(14)–C(25)	152.3(8)	Mn(1D)–O(17)–C(27)	128.2(7)
Mn(4D)–O(18)–C(27)	133.1(8)	Mn(3)–O(19)–C(28)	126.0(8)
Mn(3)–O(20)–C(29)	127.2(7)	Mn(4)–O(22)–C(30)	118.9(9)

Symmetry operations for equivalent atoms

A  $-x+1, -y+1, -z+1$     B  $x, -y+1/2, z-1/2$     C  $-x, -y+1, -z+1$   
D  $x, -y+1/2, z+1/2$     E  $-x, y+1/2, -z+1/2$     F  $-x, y-1/2, -z+1/2$

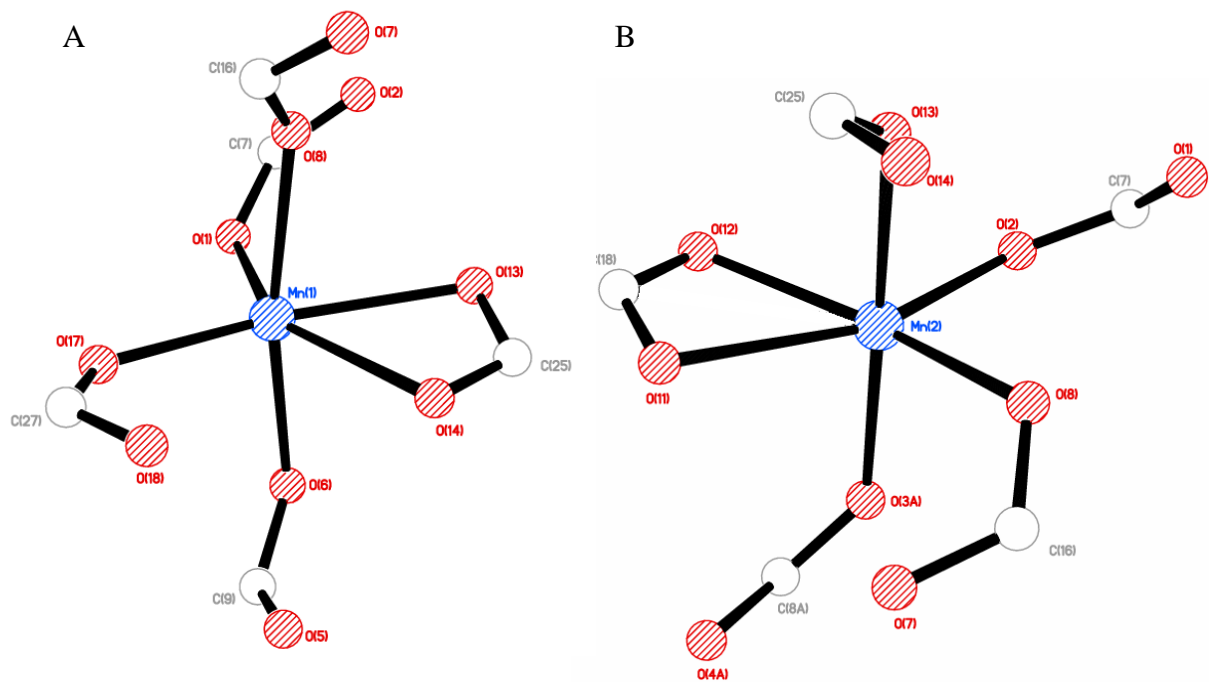


**Figure 6.79: A) Octahedral coordination environment of Mn(1) and B) Octahedral coordination environment of Mn(2) in compound 20**

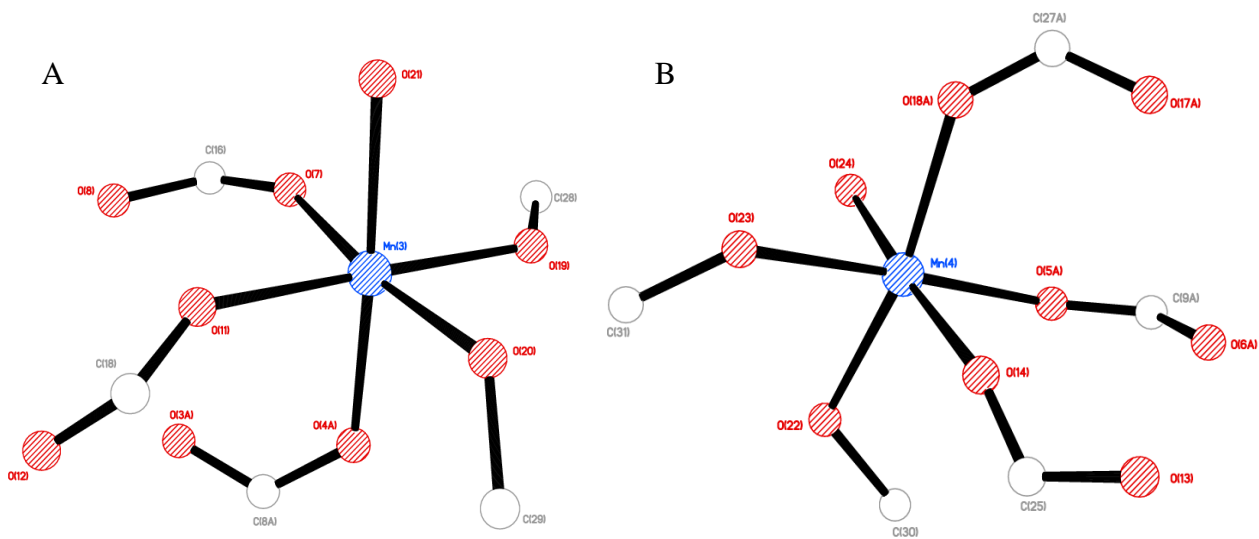


**Figure 6.80: A) Octahedral coordination environment of Mn(3) and B) Octahedral coordination environment of Mn(4) in compound 20**



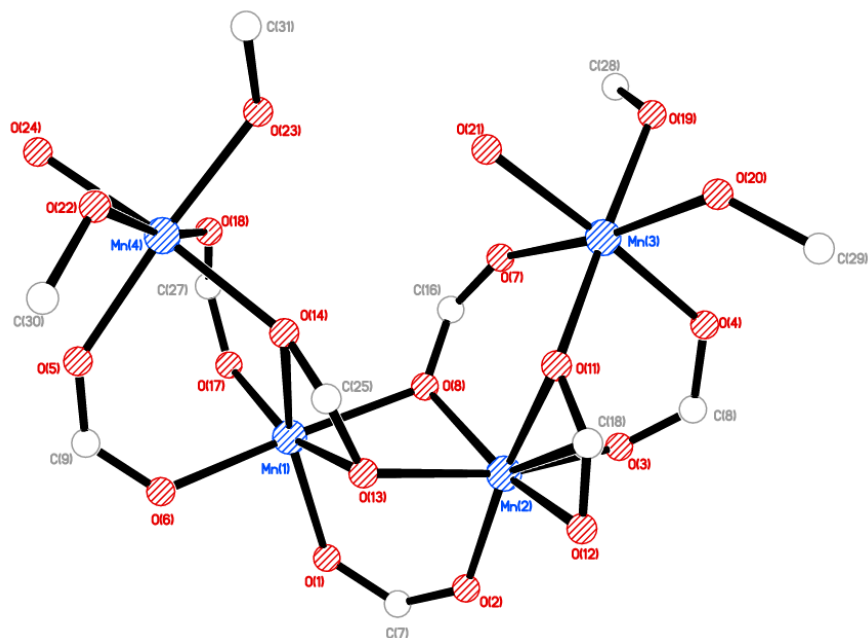


**Figure 6.81: ‘C’-shaped building unit of manganese cations in compound 20**

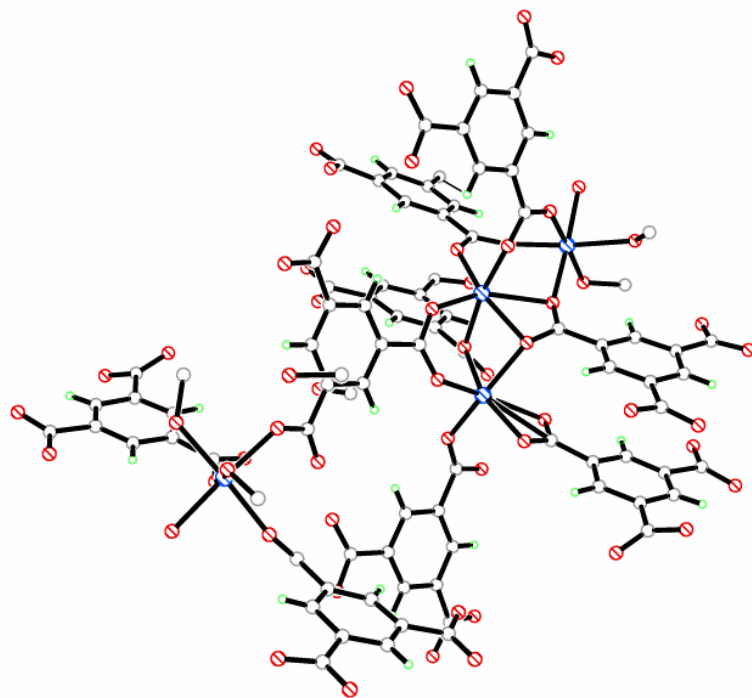


**Figure 6.82: Molecular building unit in compound 20 (uncoordinated ligands omitted for clarity)**

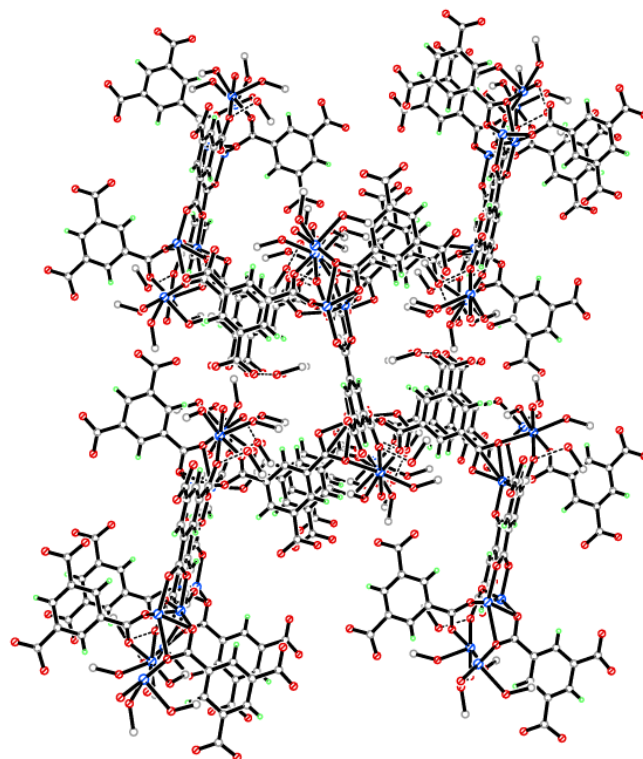


**Figure 6.83:** Three dimensional packing in compound 20 viewed down the *a*-axis

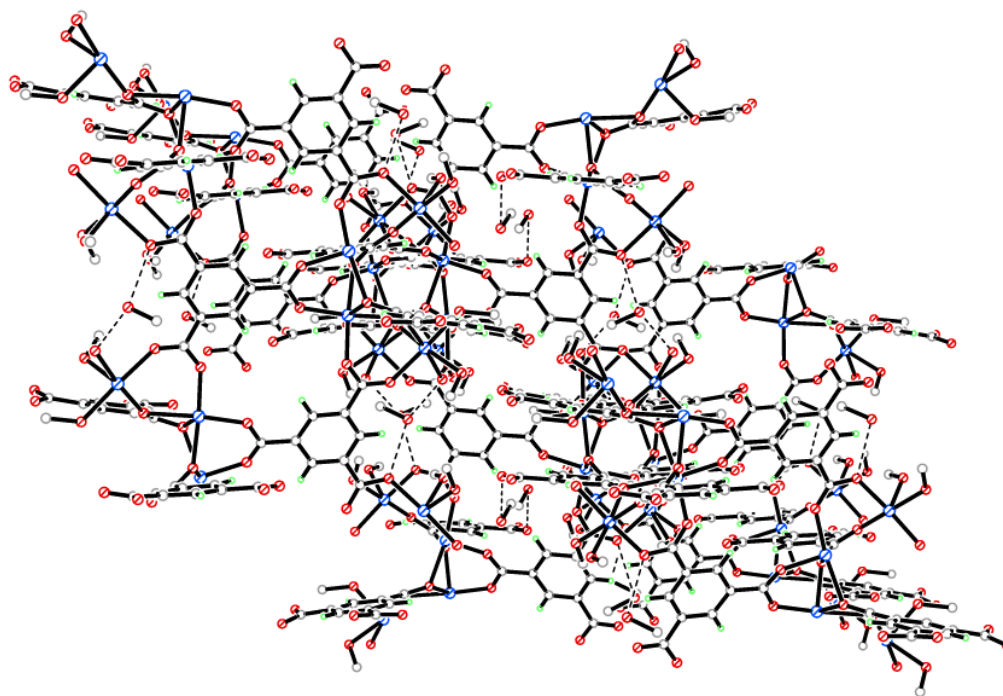


**Figure 6.84:** Three dimensional packing in compound 20 viewed down the *c*-axis

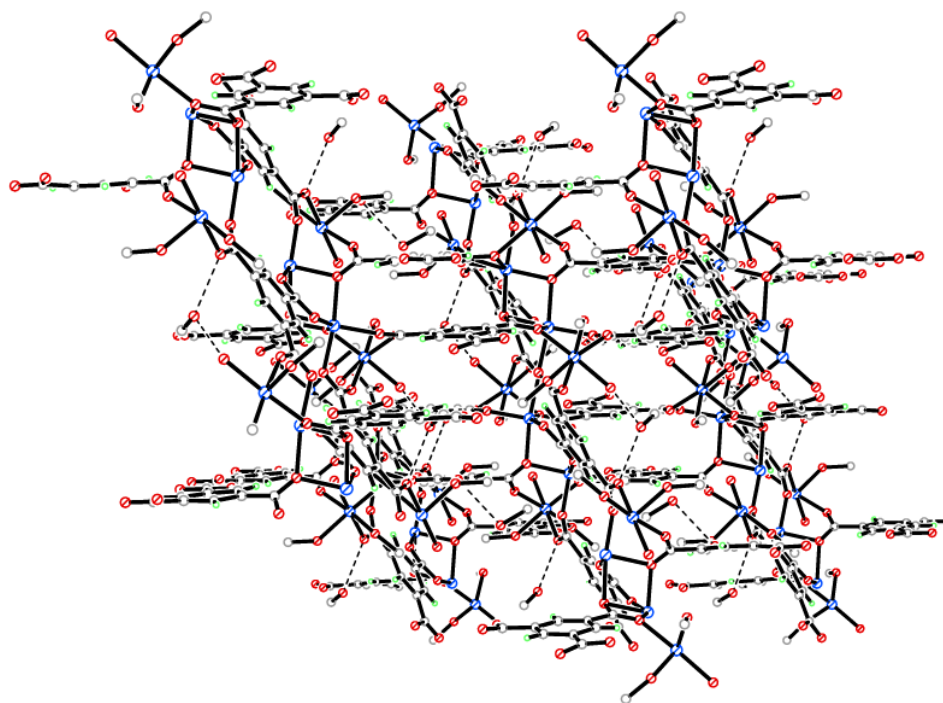
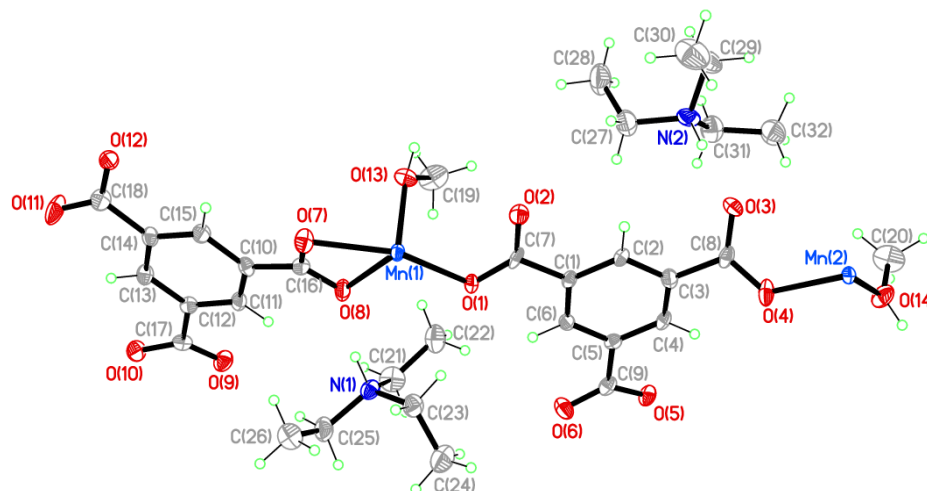


**Figure 6.85:** Three dimensional packing in compound 20 viewed down the *b*-axis

**Compound 21:**  $[\text{Mn}_2(\text{C}_9\text{H}_3\text{O}_6)_2(\text{CH}_4\text{O})_2]^{-2} \cdot 2(\text{C}_6\text{H}_{16}\text{N})^+$



Chemical formula (total)	$\text{C}_{16}\text{H}_{23}\text{MnNO}_7$
Formula weight	396.29
Temperature	150(2) K
Radiation, wavelength	CuK $\alpha$ , 1.54178 Å
Crystal system, space group	monoclinic, $P2_1/c$
Unit cell parameters	$a = 20.5137(7)$ Å $b = 10.2049(3)$ Å $c = 18.5187(7)$ Å $\beta = 111.174(4)^\circ$
Cell volume	$3615.0(2)$ Å <sup>3</sup>
Z	8
Crystal colour and size	colourless, $0.50 \times 0.24 \times 0.05$ mm <sup>3</sup>
Final $R$ indices [ $F^2 > 2\sigma$ ]	$R1 = 0.0568$
$R$ indices (all data)	$wR2 = 0.1417$
Largest diff. peak and hole	0.58 and $-0.44$ e Å <sup>-3</sup>

**Figure 6.86:** Asymmetric Unit of Compound 21 all unique atoms labelled.

### Synthesis

0.5 mL of a solution of  $\text{Mn}(\text{NO}_3)_2$  (0.059 g, 0.33 mmol) in methanol (10 mL) and 0.5 mL of a solution of 1,3,5-benzenetricarboxylic acid (0.032 g, 0.17 mmol) in methanol (10 mL) were placed into a small sample vial. This was covered with Whatman Laboratory Sealing Film and placed inside a larger sample vial. In the larger sample vial triethylamine (0.05 mL, 0.22 mmol) was added before it was covered and left until crystallisation was complete. After two weeks, colourless spindle crystals formed.

## Structure Determination

The data were collected at 150 K using copper radiation on an Oxford Diffraction Gemini A Ultra diffractometer. The structure was solved by direct methods. The semi-empirical absorption corrections were applied based on symmetry-equivalent and repeated data. The refinement gave a  $wR2$  of 0.1417 for all 5622 independent reflections and a conventional  $R1$  of 0.0568, for 3393 reflections with  $F^2 > 2\sigma$ . The residual electron density maximum and minimum were 0.58 and  $-0.44 \text{ e } \text{\AA}^{-3}$  respectively.

The hydrogen atoms were placed in geometrically calculated positions with  $U$  constrained to  $1.2 U_{\text{eq}}(\text{C})$  for aromatic hydrogen atoms,  $1.5 U_{\text{eq}}(\text{C})$  for methyl and  $U$  constrained to  $1.2 U_{\text{eq}}(\text{N})$  hydrogen atoms for the protonated nitrogen hydrogen atoms. The triethylammonium cations in the structure were disordered; with SIMU and DELU restraints being imposed during refinement. The full data of compound 21 can be found in Appendix 1.

## Structure Analysis

The asymmetric unit of compound 21 (figure 6.86) shows two complete 1,3,5-benzenetricarboxylate ligands coordinating to two manganese cations Mn(1) and Mn(2). The manganese cations form trigonal bipyramidal geometries coordinating to four carboxylates and a terminal methanol ligand each to complete the five-coordinate geometry as shown in figure 6.87. This forms an anionic framework which is charge balanced by the presence of two ammonium cations.

The Mn(1) cation forms a distorted trigonal bipyramidal geometry shown in figure 6.87A, the distortion in the bond angles emerges from the bidentate carboxylate group that coordinates with a O(7)-Mn(1)-O(8) bite angle of  $56.02(12)^\circ$ , this alters the positioning of the equatorial ligands with O(7)-Mn(1)-O(1)  $144.36(14)^\circ$  distorted away from the ideal  $120^\circ$  bond angle. The Mn(1) cation coordinates to the 1,3,5-benzenetricarboxylate ligand C(1)-O(6) through a monodentate bond with O(1), it then further coordinates with a symmetry equivalent of this carboxylate group at O(1)-Mn(1)-O(2A)  $126.44(13)^\circ$  which is generated through an inversion symmetry centre  $1.971(4) \text{ \AA}$  away from the Mn(1) in the  $a$ -axis. This creates a dinuclear manganese

building unit with the O(1)-C(7)-O(2) carboxylate bridging two symmetry equivalent manganese cations. The Mn(1) coordinates to a separate symmetry equivalent C(1)-O(6) ligand through the O(5)-C(9)-O(6) carboxylate that forms a monodentate bond to one of the axial sites on the Mn(1) cation; O(1)-Mn(1)-O(5B)  $89.95(13)^\circ$  cis to the O(1)-C(7)-O(2) carboxylate. This carboxylate does not bridge to the Mn(1) via the O(6) carboxylate oxygen that remains uncoordinated as a trans axial methanol O(5)-Mn(1)-O(13)  $175.49(14)^\circ$  occupies the remaining coordination site. The O(5)-C(9)-O(6) carboxylate rotates  $37.48(12)^\circ$  to create space for the symmetry equivalent methanol that is generated in the inverted  $180^\circ$  position on Mn(1A). The remaining carboxylate group on the C(1)-O(6) 1,3,5-benzenetricarboxylate ligand coordinates to the second manganese cation Mn(2) with a monodentate bond from the O(4) carboxylate oxygen.

The Mn(2) cation also forms a dinuclear manganese building unit by further coordinating to the second 1,3,5-benzenetricarboxylate ligand C(10)-O(12) in a similar motif to that observed by the O(1)-C(7)-O(12) carboxylate and the Mn(1) cation. The C(10)-C(17)-O(9) carboxylate group coordinates in the second equatorial coordination site at an angle of O(9)-Mn(2)-O(4)  $98.55(14)^\circ$ . Its symmetry equivalent coordinates at an angle of O(9)-Mn(2)-O(10A)  $134.75(14)^\circ$  through the carboxylate oxygen O(10) creating a dimeric manganese building unit through a inversion centre located 1.902(4) away from the Mn(2) cation in the *a*-axis. The remaining uncoordinated carboxylate group of the C(10)-O(12) ligand coordinates to a symmetry equivalent Mn(2) cation in the axial coordination site cis to the equatorial bridging carboxylates O(9)-Mn(2)-O(12B)  $92.35(14)^\circ$ , with a trans methanol completing the coordination geometry of the Mn(2) cation (figure 6.87B).

The 1,3,5-benzenecarboxylate ligands link the Mn(1) and Mn(2) cations together to create the molecular building unit in figure 6.88. This building unit doubles through the inversion symmetry to create dinuclear manganese tetracarboxylate building units at each manganese cation. This expands the structure into three-dimensions creating sheets of 1,3,5-benzenetricarboxylate and dinuclear manganese units that expand along the *a*-axis and *c*-axis, connected by axial ligands that run down the cell body diagonal.(figure 6.89) This creates a porous three dimensional compound that packs together in the herringbone motif when viewed down the cell body diagonal [111], figure 6.90 shows

this packing motif with the triethylammonium cations removed for clarity. The framework produces nets of dimensions 10.216(5) by 8.531(8) Å that are restricted in the centre by coordinated methanols that create segmented channels down the [111] axis with dimensions 10.216(5) by 8.531(8) by 10.680(13) Å. These nanochannels are intersected by irregular pores that are templated around the triethylammonium cations and run down the *a*-axis with the widest point at 14.536(13) Å and the narrowest at 5.949(10) Å with a slightly alternating height of 8.289(12) Å.

The triethylammonium cations are positioned within the nanochannels with the N(1)H(1) cation forming strong hydrogen bonds to the carboxylate oxygen O(8) of N(1)-H(1)⋯O(8) 2.715(5) Å with a near linear bond angle of 165°. The second triethylammonium cation is disordered over two positions and solved in two parts; however both protonated nitrogens form similar hydrogen bonds to the uncoordinated carboxylate oxygen O(3); N(2)-H(2)⋯O(3) 2.618(14) Å with a similar angle of 165°. The structure is further stabilised by intramolecular hydrogen bonds between the coordinated methanol ligands O(13)-H(13) and the uncoordinated carboxylate oxygen O(6) along with the O(14)-H(14) to the O(11) carboxylate oxygen (table 6.25).

Although the triethylammonium cations form strong hydrogen bonds to the anionic (-2) framework and counter-balances the charge, thermogravimetric analysis of compound 21 suggests that the templating agent can be removed without destabilising the framework material. The TGA plot shown in figure 6.92 shows stage 1 contains a dramatic weight loss at 80-110°C from 4.316 mg to 4.04 mg, the mass loss of 0.276 mg equates to 25 % of the mass lost in the temperature profile. This mass loss correlates with the calculated mass of triethylamine in compound 21 from the single crystal data at 25.74 % of the molecular weight. After compound 21 is desolvated at 110°C it remains stable forming a plateau up to 180°C after which it begins to slowly degrade with the rapid collapse occurring at 210°C during stage 2. This thermal stability gives an extended temperature window in which the sample can be heated, desolvated and have adsorption tested.

Analysis of the purity of the bulk sample and potential excess triethylamine in the dried compound was carried out using elemental analysis, this produced the results of C = 42.65 %, H = 5.80 % and N = 4.21 %. When these are compared to the solvated

crystal structure values of C = 48.44 %, H = 5.80 % and N = 3.53 % they correlate well, suggesting the structure remains solvated upon removal from the reaction medium and is more stable than compound 20 the trimethylammonium analogue.

Compounds 19, 20 and 21 were synthesised using the same reagents with variations in templating agents to determine the effect on structural motif formation. Compound 19 was synthesised using the slow diffusion technique forming a potentially porous material templated around DMF, with the walls of the pores formed by capped nodes with DMF pointing into the nanochannels of the herringbone motif. Due to the slow reaction and crystallisation times of compound 19 the rapid vapour diffusion technique was employed with deprotonation occurring from volatile bases. Compound 20 shows the dramatic effect of templating around the trimethylamine as it forms an anionic framework with a (-1) charge counter-balanced by a trimethylammonium cation making the structure harder to desolvate without collapse of the framework. Both compounds 20 and 19 show similarities in the molecular building units with compound 19 forming chains of manganese cations joined by 1,3,5-benzenetricarboxylate ligands that use a series of bridging carboxylate groups to coordinate the chains together. Compound 20 also forms a similar structure; however the manganese cations do not form chains that run through the structure. In contrast it forms shortened chains in a 'C'-shape building unit capped by methanol ligands that now coordinate with no competition from the DMF ligands used in the reaction medium of compound 19. The 'C'-shaped clusters prevent the formation of regular arrays of pores observed by the herringbone motif of compound 19, instead forming the micropore system templated around the small trimethylammonium cations that form strong hydrogen bonds to the pore walls.

Further experiments were carried out investigating the packing effect of the larger and high steric bulk templater triethylamine with the aim of creating a compound with larger pores containing a disordered, labile templating agent for easier removal upon heating. This resulted in the formation of the anionic (-2) framework compound 21, unlike both compounds 19 and 20 it does not form chains of manganese cations; but relies on a partial paddle-wheel building unit that results in the herringbone packing motif similar to that of compound 19. This occurs as the paddle-wheel building unit



forms a extended building unit with the regular arrays of coordination ‘pillars’ that are expanded by inversion symmetry. The nanochannels in both compound 19 and 21 are of similar size (table 6.26); however compound 21 forms irregular interconnecting nanochannels similar to those in compound 20 that vary in size along the channel growing and shrinking with respect to the bulk templating agent.

The structural progression and packing alterations of compound 19, 20 and 21 show the importance and potential of deprotonating agents that act as templating agents, with the ‘pros’ of large potential pore volume and ‘cons’ of anionic unstable frameworks, in using larger deprotonating agents. A comparison of the structures is presented in table 6.26 highlighting the consistency throughout the structures.

**Table 6.24: Selected Bond Lengths [Å] and Angles [°] for Compound 21**

Mn(1)–O(1)	2.142(3)	Mn(1)–O(2A)	2.103(3)
Mn(1)–O(5B)	2.151(4)	Mn(1)–O(7)	2.200(3)
Mn(1)–O(8)	2.469(4)	Mn(1)–O(13)	2.221(4)
Mn(2)–O(4)	2.102(3)	Mn(2)–O(9B)	2.087(4)
Mn(2)–O(10C)	2.089(3)	Mn(2)–O(12A)	2.100(4)
Mn(2)–O(14)	2.192(4)	C(7)–O(1)	1.253(6)
C(7)–O(2)	1.258(6)	C(8)–O(3)	1.243(6)
C(8)–O(4)	1.271(6)	C(9)–O(5)	1.273(6)
C(9)–O(6)	1.247(6)	C(16)–O(7)	1.261(6)
C(16)–O(8)	1.269(6)	C(17)–O(9)	1.253(6)
C(17)–O(10)	1.250(6)	C(18)–O(11)	1.244(6)
C(18)–O(12)	1.274(6)		
O(1)–Mn(1)–O(2A)	126.44(13)	O(1)–Mn(1)–O(5B)	89.95(13)
O(1)–Mn(1)–O(7)	144.36(14)	O(1)–Mn(1)–O(8)	88.50(12)
O(1)–Mn(1)–O(13)	86.66(13)	O(4)–Mn(2)–O(9B)	98.55(14)
O(4)–Mn(2)–O(10C)	125.75(16)	O(4)–Mn(2)–O(12A)	98.43(14)
O(4)–Mn(2)–O(14)	89.15(15)	Mn(1)–O(1)–C(7)	113.7(3)
Mn(1A)–O(2)–C(7)	165.9(4)	Mn(2)–O(4)–C(8)	120.1(3)
Mn(1D)–O(5)–C(9)	123.0(3)	Mn(1)–O(7)–C(16)	97.5(3)
Mn(2D)–O(9)–C(17)	142.8(3)	Mn(1)–O(8)–C(16)	84.9(3)
Mn(2)–O(14)–C(20)	125.0(3)	Mn(2A)–O(12)–C(18)	129.7(3)
Mn(1)–O(13)–C(19)	125.9(3)		
Symmetry operations for equivalent atoms			
A $-x+1, -y+2, -z+1$ B $-x+1, y+1/2, -z+3/2$ C $x+1, -y+3/2, z+1/2$			
D $-x+1, y-1/2, -z+3/2$			

**Table 6.25: Selected Hydrogen bond Lengths [Å] and angles [°] for Compound 21**

D–H...A	d(D–H)	d(H...A)	d(D...A)	(DHA)
O(13)–H(13)...O(6F)	0.837(10)	1.786(14)	2.616(5)	171(6)
O(14)–H(14)...O(11G)	0.844(10)	1.745(19)	2.565(5)	163(6)
N(1)–H(1)...O(8)	0.93	1.81	2.715(5)	165
N(2)–H(2A)...O(3)	0.93	1.77	2.681(14)	165
N(2A)–H(2A1)...O(3)	0.93	1.86	2.770(16)	166
Symmetry operations for equivalent atoms				
F $x, -y+3/2, z-1/2$ G $x+1, y, z+1$				

**Table 6.26: Comparisons between Compound 21, Compound 20 and Compound 19**

	Compound 19	Compound 20	Compound 21
Node geometries	Octahedral	Octahedral	Octahedral
M-O average bond length (Å)	2.133	2.124	2.157
Type of building unit	Bridged Chains	Capped Chain	Paddle-wheel
Pore dimensions (Å)	8.365 x 10.237	8.180 x 6.210	8.531 x 10.216

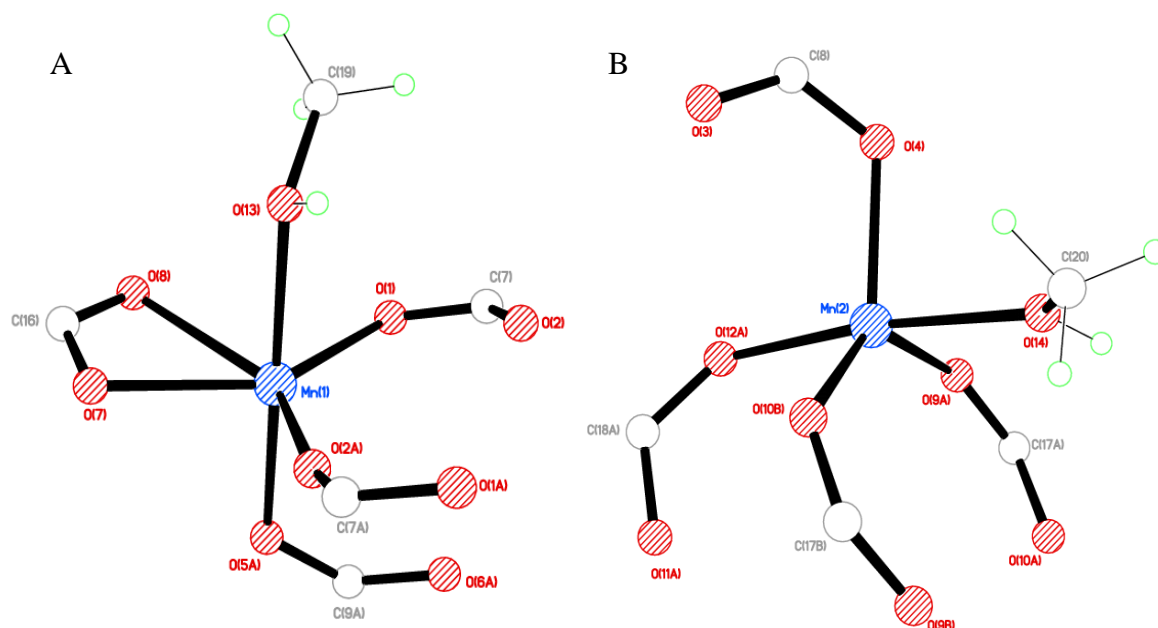


**Figure 6.87: A) Octahedral coordination environment of Mn(1) and B) Octahedral coordination environment of Mn(2) in compound 21**

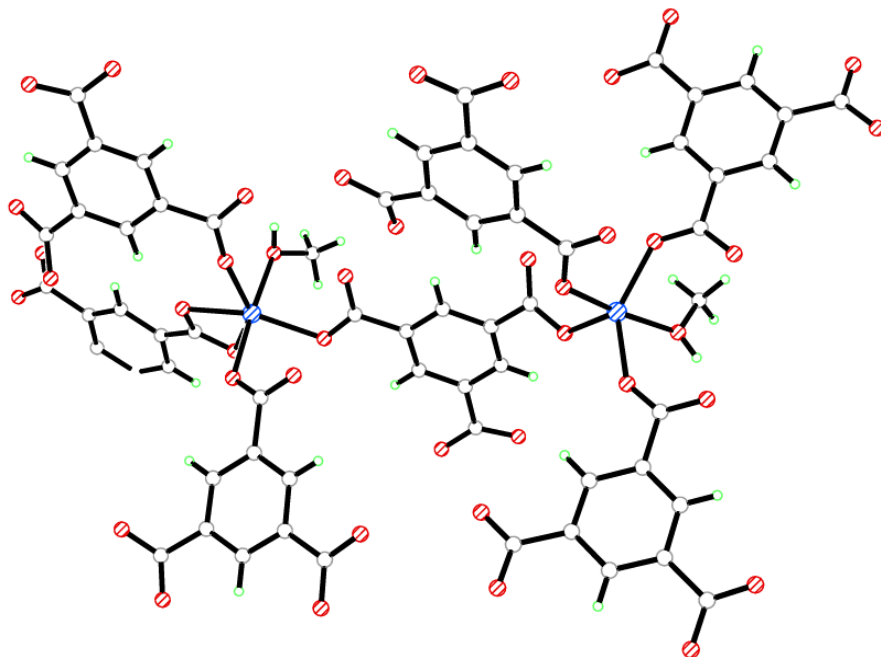


**Figure 6.88:** Molecular building unit in compound 21 (uncoordinated ligands omitted for clarity)

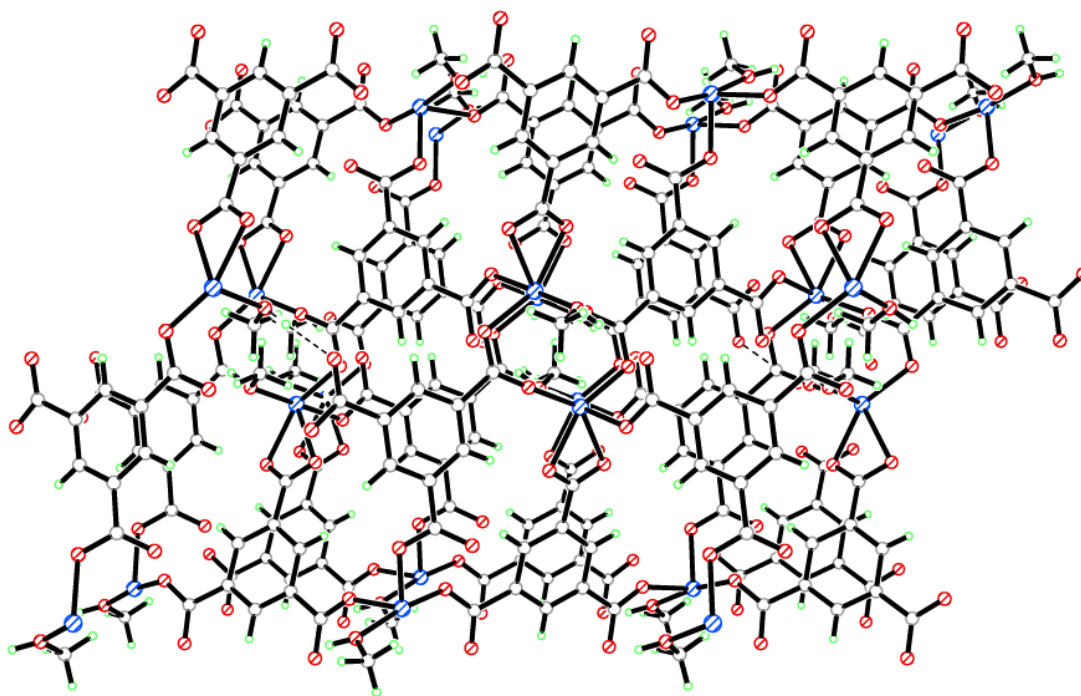


**Figure 6.89:** Three dimensional packing in compound 21 viewed down the *b*-axis

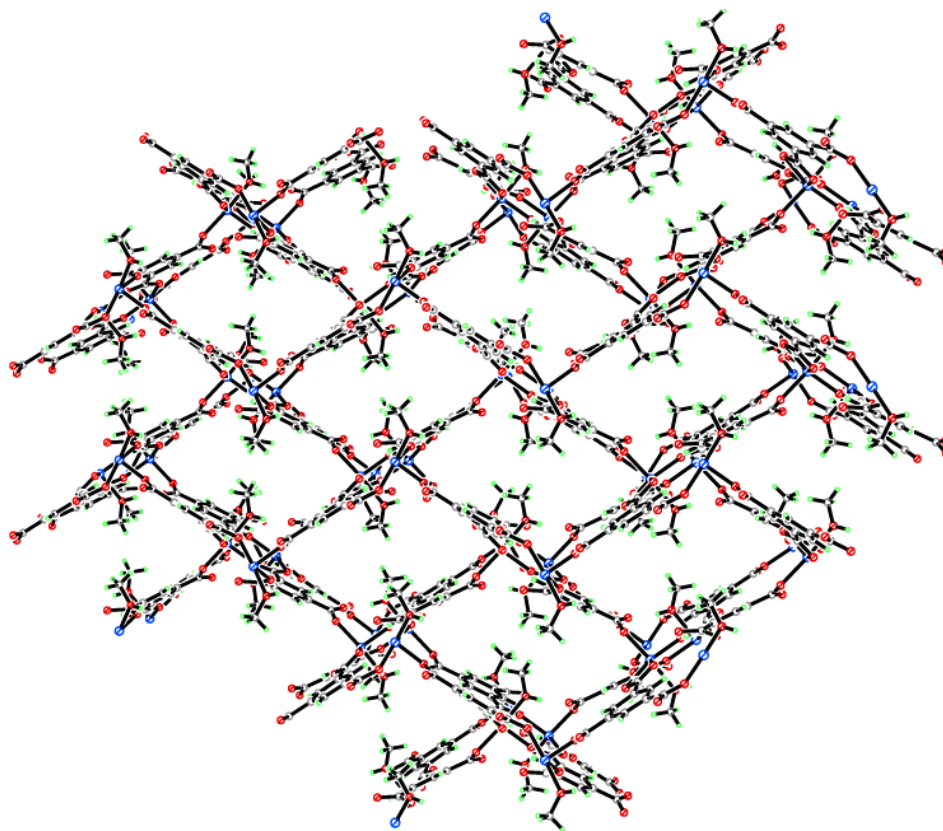


**Figure 6.90:** Three dimensional herringbone packing motif in compound 21 viewed down the [111] cell body diagonal.

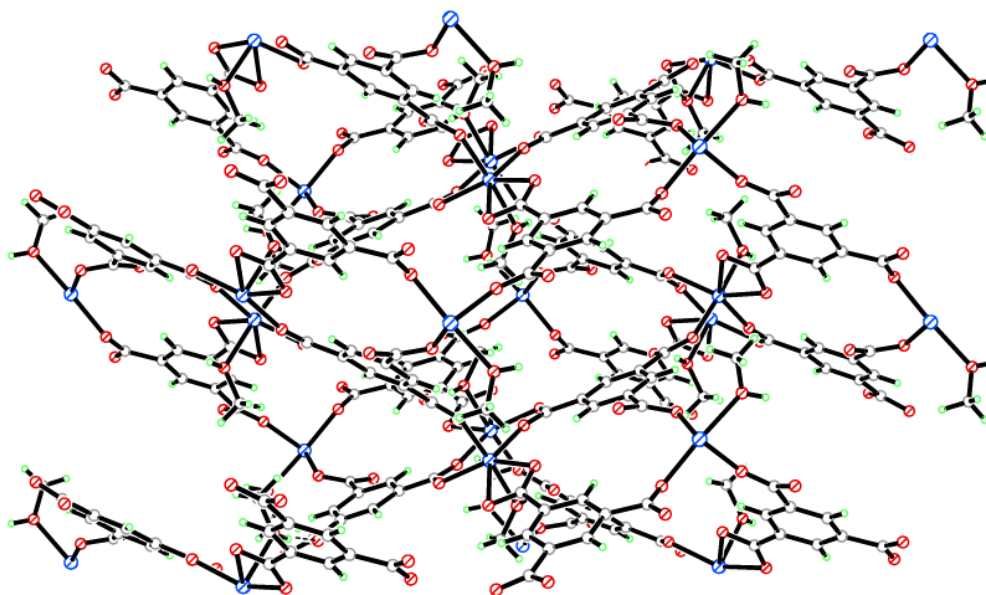


**Figure 6.91:** Three dimensional packing in compound 21 viewed down the *a*-axis

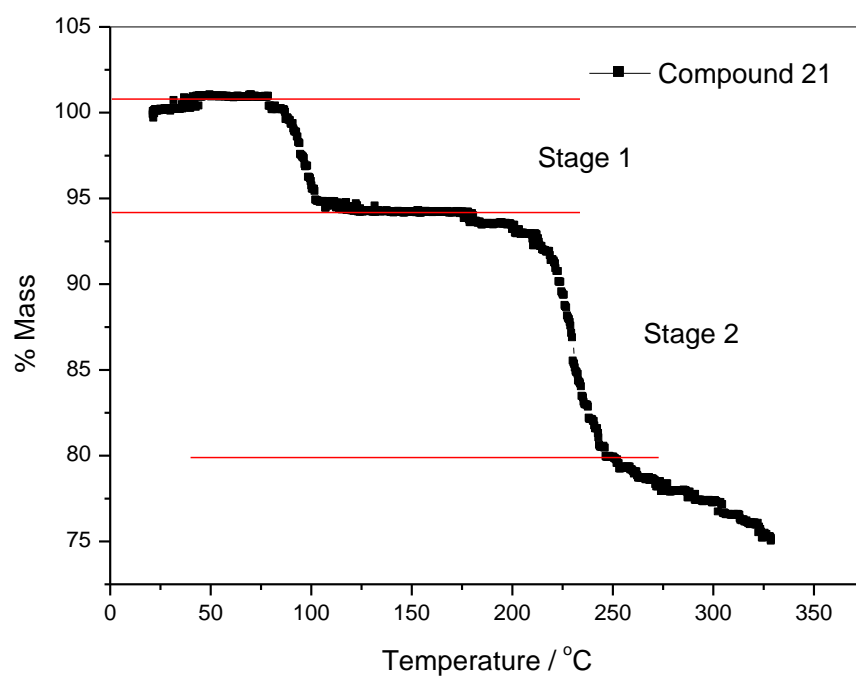


**Figure 6.92: Thermogravimetric analysis plot of compound 21**

## Conclusion

In this chapter twelve compounds with 1,3,5-benzenetricarboxylic acid were presented; three with zinc, two with cobalt, one with nickel, two with cadmium, three with manganese and one compound with copper. These compounds were formed with a variety of solvents and bases producing frameworks consisting of one dimensional chains to three dimensional coordinated porous grids.

Compound 10 forms two dimensional sheets of 1,3,5-benzenetricarboxylic acid and 4,4'-bipyridine with a net topology; the coordinated DMF molecules point inwards to the pore, the remaining available space is occupied by the uncoordinated DMF molecule that is hydrogen bonded to the framework. The pores have dimensions 9.665(5) by 7.211(5) Å upon desolvation of the DMF molecules with a pore volume of 41.8 %; however the TGA shows only partial desolvation at 110°C giving a pore volume of 20.8 %. Compound 10 was synthesised using an H-Cell to allow the slow reaction of the 4,4'-bipyridine ligand with the transition metal that would otherwise result in the formation of amorphous product. Unfortunately this yielded small amounts of product preventing its further analysis, future work on this compound will orientate scale up of reactions to produce samples from direct addition reactions that match the predicted powder diffraction pattern.

Investigations into pyridine templating within 1,3,5-benzenetricarboxylic acid frameworks was carried out due to its success in the 1,4-benzenedicarboxylic acid frameworks. This produced the compounds 11 and 12. Compound 11 was synthesised with directed addition of pyridine producing a two dimensional framework consisting of columns of 1,3,5-benzenetricarboxylic acid and zinc cations, that are connected through a zinc paddle-wheel building wheel unit. The compound packs together to form a grid network that contains two pyridines and two uncoordinated methanols per pore, these can be removed upon heating to 50°C for methanol removal and 125°C for the pyridine to be removed from the framework. This compound is unstable upon desolvation and proceeds to decompose after the pyridine is removed. Compound 11 is strongly templated by the pyridine molecules with two coordinating to each zinc cation that allow the columns to expand in three dimensions through  $\pi$ - $\pi$  interactions. It was theorised that reducing the pyridine concentration in the reaction mixture by slow

diffusion techniques would yield a fully coordinated structure with the carboxylate groups coordinated in preference over the pyridine molecules. This produced compound 12, that consists of two tetrahedral zinc cations coordinated by one 1,3,5-benzenetricarboxylate linker with each cation capped by one pyridine. Compound 12 forms two dimensional sheets that pack in a staggered conformation to reduce the steric effects from the coordinated pyridine ligands. Although the amount of pyridine has been reduced the conformational change at the zinc nodes, results in the pyridine ligand directing the packing motif of the compound, forming an unusual 'zip-lock' packing motif different to that observed in compound 13. To prevent pyridine from templating the structures of the frameworks, further work will need to be invested in vapour diffusion reactions using lower concentrations of pyridine; to yield structures that give an insight into the directing effects upon node geometry and topology formation.

Investigations into solvent templating effects were carried out using solvothermal synthesis techniques that enabled rapid alterations and fine-tuning of reaction conditions, producing compounds 13-17. Compound 13 forms a one dimensional zigzag chains of octahedral nickel cations linked by 1,3,5-benzenetricarboxylates in hydrogen bonded layers that stack anti-parallel to maximise  $\pi$ - $\pi$  interactions. The synthesis method utilised ethanol and water as solvents resulting in water templating the structure. This was also observed in the structural analogue compound 14 that was produced using the same reaction conditions with cobalt nitrate. This solvent system has consistent templating effects with the production of a third compound, compound 15 the cadmium analogue. Compound 15 consists of trigonal bipyramidal and pentagonal bipyramidal nodes that alter the packing motif slightly forming one dimensional zigzag chains that pack together to form columns that interpenetrate each other; a stark contrast to the two dimensional sheet packing of compounds 13 and 14. These compounds and additional compounds such as XUBLUC,<sup>3</sup> EKEXEY,<sup>4</sup> EXOKOR<sup>5</sup> and DERYAB<sup>6</sup> published in the literature show the potentials for expanding this synthesis protocol and structure motif in future work. The research carried out here expanded this area with new reactions; the addition of DMF was selected due to its properties under solvothermal conditions to act as a deprotonating and templating agent. These reactions resulted in compounds 16, 17 and 19-21.



Compound 16 was formed under solvothermal conditions with a solvent mixture of water, ethanol and DMF. This produced an array of bridging carboxylate groups holds the Cd(1) and Cd(2) cations in close proximity forming columns of the cations, linked by two 1,3,5-benzenetricarboxylate ligands related by inversion symmetry to form a double layer of ligands. The DMF ligands coordinated to the Cd(1) and Cd(3) cations form 'L'-shaped connectivity, with one DMF pointing along the *b*-axis and the other along the *c*-axis. These ligands flip by 180° at each alternating cadmium due to the inversion symmetry, this rotation enables strong intramolecular overlapping between the DMF molecules. The sheets pack in a staggered conformation creating a 'zip-lock' packing motif of the DMF; this packing coupled with the 'zigzag' nature of the sheets creates micropores with dimensions 6.505(2) by 5.774(4) Å that contain one uncoordinated DMF molecule that forms hydrogen bonds with the coordinated DMF molecules. Compound 16 shows that DMF both fully deprotonates the ligands and also coordinates to the metal centres to produce metal-ligand coordination geometries that may be useful in creating microporous structures with DMF present in the pores. Further reactions produced the microporous compound 17, which is an analogue to the highly porous HKUST-1<sup>9</sup>. The compound is composed of a dimeric zinc paddle-wheel unit that expands the structure into a fully coordinated three dimensional framework, with pores of 7.190(2) Å by 7.190(2) Å, giving a total pore volume of 67.5 %. The structure is desolvated between 150-220°C; however the structure does not stabilise and continues to lose mass associated with the labile coordinated water molecules, producing highly reactive open metal centres at the zinc nodes. This induces a conformational change of compound 17, confirmed by powder diffraction and elemental analysis. The new structure formed by post synthetic rearrangement upon desolvation exhibits uncharacteristic adsorption properties when compared to carbon dioxide adsorption at 195 K of HKUST-1. Compound 17 upon rearrangement forms a nanoporous framework with a maximum uptake of  $0.375 \pm 4.96 \times 10^{-2} \text{ mmol g}^{-1}$  with a pore volume of  $2.173 \times 10^{-5} \pm 1.360 \times 10^{-4} \text{ cm}^3 \text{ g}^{-1}$ ; compared to HKUST-1 that has an uptake of  $16.52 \pm 4.62 \times 10^{-2} \text{ mmol g}^{-1}$  with a pore volume of  $0.709 \pm 2.07 \times 10^{-3} \text{ cm}^3 \text{ g}^{-1}$  for carbon dioxide adsorption at 195 K. This shows that compound 17 has rearranged from the highly porous framework of HKUST-1 to a framework with similar size pores to carbon

molecular sieves, this has dramatic consequences on the range of applications for compound 17; instead of high storage fuel cells and biomedical delivery applications, the compound could be used in the application of kinetic molecular sieving of gases, a rare application for MOF compounds. Further work on this material is required with investigations into mounts and active solutions that may help stabilize the framework for catalytic applications.

As a result of the improved reaction conditions containing DMF for the production of porous frameworks including compound 18, reactions involving manganese were carried out producing compounds 19-21. Compound 19 was synthesised using DMF within a H-Cell, forming a three dimensional framework of chains of manganese cations:  $[\text{Mn}(2)\text{-O}(4)\text{-Mn}(3)\text{-O}(1\text{A})\text{-C}(7\text{A})\text{-O}(2\text{A})\text{-Mn}(1)\text{-O}(5)\text{-C}(9)\text{-O}(6)\text{-Mn}(2\text{A})]_n$  bridged by 1,3,5-benzenetricarboxylate ligands. This forms zigzag sheets of 1,3,5-benzenetricarboxylate criss-crossing, connecting the non-planar chains manganese cations into a herringbone packing motif with pores of dimensions 8.365(8) by 10.237(13) Å. The high affinity of DMF limited its potential for the further investigations. Previous success was obtained in producing compounds without DMF and pyridine coordinated in the framework by altering the bases to trimethylamine and triethylamine; leading to the production of compounds 20 and 21. The templating effects of trimethylamine in compound 20 produces manganese cations linked together to form a 'C'-shaped unit linked by bridging carboxylate groups of the three 1,3,5-benzenetricarboxylate ligands. This expands into three dimensions to create a microporous three dimensional coordinated framework, with pores of dimensions 8.18(2) by 6.21(7) Å containing one trimethylammonium that templates the anionic framework of compound 20. A similar structure is observed in compound 21 that consists of dinuclear clusters that form a three dimensional anionic framework templated around the triethylammonium cations in the 10.216(5) by 8.531(8) Å pores. The structural progression and packing alterations of compound 19, 20 and 21 show the importance and potential of deprotonating agents that act as templating agents, with the 'pros' of large potential pore volume and 'cons' of anionic unstable frameworks, in using larger deprotonating agents.

## References:

- 1 A. L. Spek, *J. Appl. Crystallogr.*, **2003**, 36, 7.
- 2 F. H. Allen, *Acta. Crystallogr.*, **2002**, B58, 380.
- 3 S. C. Hsu, P. H. Chiang, C. H. Chang, C. H. Lin, *Acta. Crystallogr.*, **2009**, E65, 625.
- 4 M. A. Nadeem, M. Bhadbhade, J. A. Stride, *Dalton Trans.*, **2010**, 39, 9860.
- 5 D. Krishnamurthy, R. Murugavel, *Indian J. Chem.Sect. A: Inorg. Bio-inorg., Phys., Theor. Anal. Chem.*, **2003**, 42, 2267.
- 6 S. Liang, H. Wang, Z. Wang, J. Y. Han, *Acta. Crystallogr. Sect. E: Strcut. Rep. Online*, **2006**, 62, 3014.
- 7 M. Eddaoudi, H. Li, O. M. Yaghi, *J. Am. Chem. Soc.*, **2000**, 122, 1391.
- 8 Z. Wang, V. Kravtsov, M. J. Zaworotko, *Angew. Chem.*, **2005**, 117, 2937.
- 9 S. Y. Chui, S. M. Lo, J. P. H. Charmant, A. G. Orphan, I. D. Williams, *Science*, **1999**, 283, 1148.
- 10 L. Xie, S. Liu, C. Gao, R. Cao, J. Cao, C. Sun, Z. Su, *Inorg. Chem.*, **2007**, 46, 7782.
- 11 S. Bordiga, L. Regli, F. Bonino, E. Groppo, C. Lamberti, B. Xiao, P. S. Wheatley, R. E. Morris, A. Zecchina, *Phys. Chem. Chem. Phys.*, **2007**, 9, 2676.
- 12 B. Xiao, P. S. Wheatley, X. Zhao, A. J. Fletcher, S. Fox, A. G. Rossi, I. L. Megson, S. Bordiga, L. Regli, K. M. Thomas, R. E. Morris, *J. Am. Chem. Soc.*, **2007**, 129, 1203.
- 13 J. Y. Lee, J. Li, J. Jagiello, *J. Solid State Chem.*, **2005**, 178, 2527.
- 14 K. S. W. Sing, D. H. Everett, R. A. W. Haul, L. Moscou, R. A. Pierotti, J. Rouquerol, T. Siemieniewska, *Pure Appl. Chem.*, **1985**, 57, 603.
- 15 C. R. Reid, K. M. Thomas, *Langmuir*, **1999**, 15, 3206.
- 16 C. R. Reid, I. P. O'Koge, K. M. Thomas, *Langmuir*, **1998**, 14, 2415.
- 17 K. J. Klafter, M. F. Shlesinger, *Proc. Natl. Acad. Sci. USA*, **1986**, 83, 848.
- 18 A. J. Fletcher, E. J. Cussen, D. Bradshaw, M. J. Rosseinsky, K. M. Thomas, *J. Am. Chem. Soc.*, **2004**, 126, 1750.
- 19 B. Chen, X. Zhao, A. Putkham, K. Hong, E. B. Lobkovsky, E. J. Hurtado, A. J. Fletcher, K. M. Thomas, *J. Am. Chem. Soc.*, **2008**, 130, 20, 6411.

- 20 R. G. Palmer, D. L. Stein, E. Abraham, P. W. Anderson, *Phys. Rev. Let.*, **1984**, 53, 10, 958.
- 21 S. H. Glarum, *J. Chem. Phys.*, **1960**, 33, 1371.

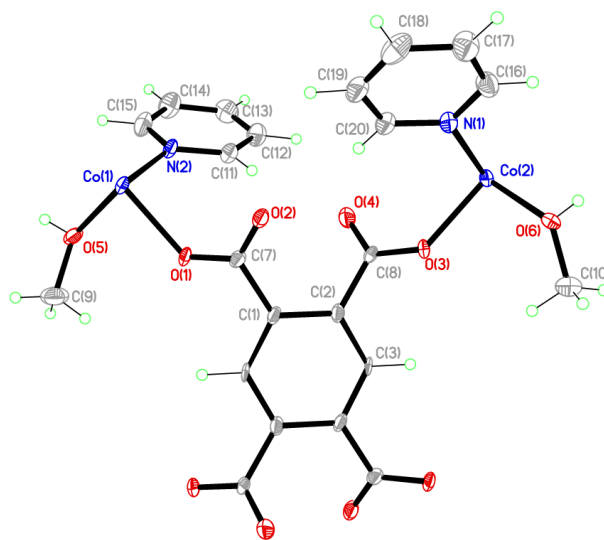
## **Chapter Seven – Crystal Structures of Transition Metal and 1,2,4,5-benzenetetracarboxylic acid Compounds**

### **Introduction**

The following chapter presents compounds produced using the transition metals; cobalt, zinc, nickel, copper and cadmium. These metals were reacted with 1,2,4,5-benzenetetracarboxylic acid in a range of reaction conditions to investigate the templating effects of different solvents, bases, alkali earth metals and additional ligands such 4,4'-bipyridine on topology formation.

The fifteen compounds presented in this chapter include two dimensional sheets (compounds 22-27) and three dimensional coordinated frameworks (compounds 28-36). Compounds 27-31 presented in this chapter show the templating effects of the alkali metals sodium and potassium. Compounds 32-35 highlight the importance of solvent control in framework synthesis with the templating effects of DMF upon porous three dimensional frameworks.

The compounds present in this chapter were analysed further with elemental analysis, powder X-ray diffraction, Hot-stage microscopy and thermogravimetric analysis, where possible, to determine the purity of the bulk material and the thermostability properties of the compounds.

**Compound 22:**  $[\text{Co}_2(\text{C}_{10}\text{H}_2\text{O}_8)(\text{CH}_4\text{O})_4(\text{C}_5\text{H}_5\text{N})_4]$ 

Chemical formula (total)	$\text{C}_{34}\text{H}_{38}\text{Co}_2\text{N}_4\text{O}_{12}$	
Formula weight	812.54	
Temperature	150(2) K	
Radiation, wavelength	MoK $\alpha$ , 0.71073 Å	
Crystal system, space group	triclinic, $P\bar{1}$	
Unit cell parameters	$a = 8.1575(5)$ Å	$\alpha = 77.630(6)^\circ$
	$b = 11.2091(7)$ Å	$\beta = 75.663(6)^\circ$
	$c = 11.4524(10)$ Å	$\gamma = 70.354(6)^\circ$
Cell volume	$945.62(12)$ Å <sup>3</sup>	
Z	1	
Crystal colour and size	pink, $0.30 \times 0.25 \times 0.20$ mm <sup>3</sup>	
Final $R$ indices [ $F^2 > 2\sigma$ ]	$R1 = 0.0497$	
$R$ indices (all data)	$wR2 = 0.1112$	
Largest diff. peak and hole	1.16 and $-0.34$ e Å <sup>-3</sup>	

**Figure 7.01: Asymmetric Unit of Compound 22 all unique atoms labelled, additional atoms added to complete ligands**

**Synthesis**

0.5 mL of a solution of  $\text{Co}(\text{NO}_3)_2 \cdot 6\text{H}_2\text{O}$  (0.09 g, 0.33 mmol) in methanol (10 mL) and 0.5 mL of a solution of 1,2,4,5-benzenetetracarboxylic acid (0.043 g, 0.17 mmol) in methanol (10 mL) were placed into a small sample vial. This was covered with Whatman Laboratory Sealing Film and placed inside a larger sample vial. In the larger sample vial pyridine (0.05 mL, 0.22 mmol) was added before it was covered and left until crystallisation was complete. After one week, pink block crystals formed.

## Structure Determination

The data were collected at 150 K using molybdenum radiation on an Oxford Diffraction Gemini A Ultra diffractometer. The structure was solved by direct methods. The semi-empirical absorption corrections were applied based on symmetry-equivalent and repeated data. The refinement gave a  $wR2$  of 0.1112 for all 3332 independent reflections and a conventional  $R1$  of 0.0497, for 1863 reflections with  $F^2 > 2\sigma$ . The residual electron density maximum and minimum were 1.16 and  $-0.34 \text{ e } \text{\AA}^{-3}$  respectively.

The hydrogen atoms were placed in geometrically calculated positions with  $U$  constrained to  $1.2 U_{\text{eq}}(\text{C})$  for aromatic hydrogen atoms and  $U$  constrained to  $1.5 U_{\text{eq}}(\text{C})$  for methyl hydrogen atoms. The full data of compound 22 can be found in Appendix 1.

## Structure Analysis

The asymmetric unit of compound 22 (figure 7.01) shows half a 1,2,4,5-benzenetetracarboxylate ligand completed by inversion symmetry through the centre of its aromatic ring, coordinated to two cobalt cations Co(1) and Co(2) placed on inversion centres. The cobalt cations in compound 22 both form standard octahedral geometries shown in figure 7.02 with the bond angles listed in table 7.01.

The Co(1) cation forms the six-coordinate octahedral by coordinating to the O(1)-C(7)-O(2) carboxylate group through the monodentate Co(1)-O(1)  $2.076(3) \text{ \AA}$  bond and its coplanar trans symmetry equivalent O(1A) at  $180^\circ$  generated by inversion symmetry. The Co(1) cation coordinates to two terminal ligands cis to the carboxylate group in the form of a pyridine ligand; O(1)-Co(1)-N(2)  $91.56(12)^\circ$  and a methanol ligand O(1)-Co(1)-O(5)  $89.73(13)^\circ$ . The six-coordinate geometry is completed by the inversion symmetry that generates the respective trans-coplanar symmetry equivalents as shown in figure 7.02A.

The Co(2) cation coordinates to the remaining carboxylate group O(3)-C(8)-O(4) of the 1,2,4,5-benzenetetracarboxylate ligand forming the monodentate Co(2)-O(3)  $2.076(3) \text{ \AA}$  monodentate bond, identical to the Co(1)-O(1) bond. Co(2) also coordinates to two cis terminal ligands creating a similar node to Co(1) with coordination to one pyridine and one methanol ligand shown in figure 7.02B. Co(2) is placed on a inversion

centre and completes its six-coordinate geometry through the trans-coplanar symmetry equivalents generated through this symmetry point. The uncoordinated carboxylate oxygens O(2) and O(4) are fully delocalised as the C(7)-O(2) and C(8)-O(4) bond lengths of 1.254(5) Å and 1.255(5) Å respectively are comparable to their coordinated counterparts (table 7.01). This delocalisation allows these uncoordinated carboxylate oxygens to be involved as hydrogen bond acceptors through intramolecular hydrogen bonds with the hydrogens of adjacent coordinated cis methanol ligands. These hydrogen bonds force the carboxylate groups to rotate so that the O(2) oxygen is coplanar and opposite the O(5) methanol; creating the hydrogen bond O(5)-H(5)⋯O(2) 2.585(4) Å (figure 7.02A). This also occurs on the Co(2) cation forming the hydrogen bond O(6)-H(6)⋯O(4) 2.567(5) Å shown in figure 7.02B (table 7.02). This results in the carboxylates twisting out of the plane of the 1,2,4,5-benzenetetracarboxylate aromatic ring by 116.1(4)° to coordinate with the coplanar cobalt cations with the optimised hydrogen bonding to the cis methanol ligands.

The 1,2,4,5-benzenetetracarboxylate linker is completed by inversion symmetry around the centre of its aromatic ring, this creates the molecular building unit in figure 7.03. This allows compound 22 to expand in two dimensions to form sheets running along the *b*-axis and down the *c*-axis, when these sheets are viewed down the *a*-axis (figure 7.04) the methanol ligands are pointing inwards towards each other with one pointing above the plane of the sheet and its opposite counterpart related by inversion symmetry pointing below the plane of the sheet. The four methanols fill the gaps between the four coplanar linkers with the pyridine ligands pointing axial to the sheets. The pyridine stack the sheets parallel with no offset between the respective sheets, this occurs as the pyridines are not directly perpendicular to the plane of the sheet but point out at angles of 45.71(5)° for the C(11)-N(2) pyridine and 21.55(3)° for the C(16)-N(1) pyridine. This allows the pyridines to overlap with their counterparts on adjacent sheets creating strong  $\pi$ - $\pi$  stacking interactions with the C(16)-N(1) stacking at a distance of 3.759(5) Å to the opposite C(16)-N(1) and C(11)-N(2) stacking with a  $\pi$ - $\pi$  distance of 3.710(2) Å to its counterpart (figure 7.05 and figure 7.06).

The extensive  $\pi$ - $\pi$  stacking interactions that hold this structure together in three dimensions via templating around the coordinated pyridine ligands proved to be



insufficient to allow desolvation of the coordinated methanol molecules in an attempt to create 11.433(2) by 11.433(2) Å pores between the linkers. The thermostability of compound 22 is extremely low with stage 1 of the TGA plot (figure 7.07) indicating the compound begins to degrade immediately upon heating; with stage 2 showing only a minor stability at 62-82°C, which still undergoes mass loss failing to provide a substantial plateau before the compound fully degrades at 200°C during stage 3.

The low stability of compound 22 prevented the acquisition of a powder X-ray diffraction pattern as the sample degraded upon drying forming an amorphous powder. The desolvation of compound 22 upon drying was observed by elemental analysis that gave results of C = 46.7 %, H = 3.56 % and N = 6.84 %; compared to the calculated values from the single crystal data of C = 50.21 %, H = 4.68 % and N = 6.89 %. The nitrogen content is consistent with both the carbon and hydrogen contents lower, the difference of 3.51 % in carbon can be attributed to the loss of methanol within the compounds that accounts for C = 3.9 % of compound 22.

Compound 22 was synthesised as an expansion of the extensive vapour diffusion reactions investigating the templating effects of volatile bases on topology formation. This structure is comparable to compounds 23 and 24 with both compounds synthesised using similar reaction conditions. Compound 23 shows the effect of switching the cobalt cation for a copper cation and how the resulting coordination geometry change alters the packing motif of the pyridines.

**Table 7.01: Selected Bond Lengths [Å] and Angles [°] for Compound 22**

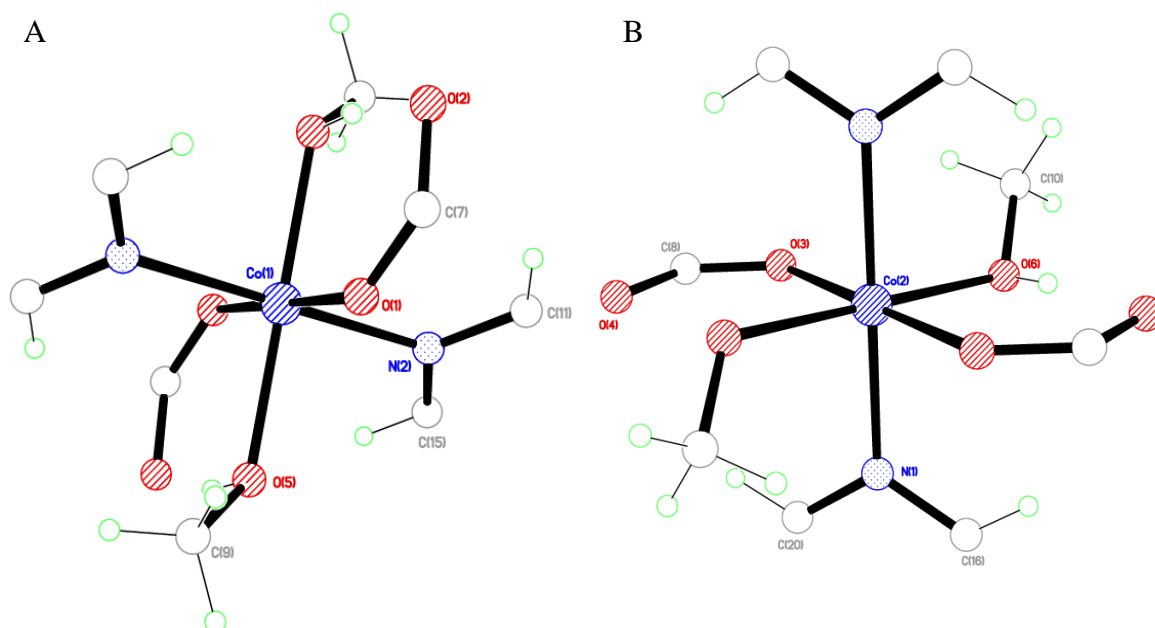
Co(1)–O(1)	2.076(3)	Co(1)–O(5)	2.118(3)
Co(1)–N(2)	2.164(4)	Co(2)–O(3)	2.076(3)
Co(2)–O(6)	2.126(3)	Co(2)–N(1)	2.152(4)
C(7)–O(1)	1.264(5)	C(7)–O(2)	1.254(5)
C(8)–O(3)	1.268(5)	C(8)–O(4)	1.255(5)
O(1)–Co(1)–O(1A)	180.0	O(1)–Co(1)–O(5)	89.73(13)
O(1)–Co(1)–N(2)	91.56(13)	O(3)–Co(2)–O(3B)	180.0
O(3)–Co(2)–O(6)	88.90(13)	O(3)–Co(2)–N(1)	91.35(13)
Co(1)–O(1)–C(7)	129.7(3)	Co(2)–O(3)–C(8)	128.6(3)

Symmetry operations for equivalent atoms

A  $-x, -y+2, -z$     B  $-x+1, -y+1, -z+1$ **Table 7.02: Selected Hydrogen bond Lengths [Å] and angles [°] for Compound 22**

D–H...A	d(D–H)	d(H...A)	d(D...A)	(DHA)
O(5)–H(5)...O(2A)	0.74(6)	1.88(7)	2.585(4)	159(7)
O(6)–H(6)...O(4B)	0.71(6)	1.88(7)	2.567(5)	165(8)

Symmetry operations for equivalent atoms

A  $-x, -y+2, -z$     B  $-x+1, -y+1, -z+1$ **Figure 7.02: A) Octahedral coordination environment of Co(1) and B) Octahedral coordination environment of Co(2) in compound 22 (all unique atoms labeled)**

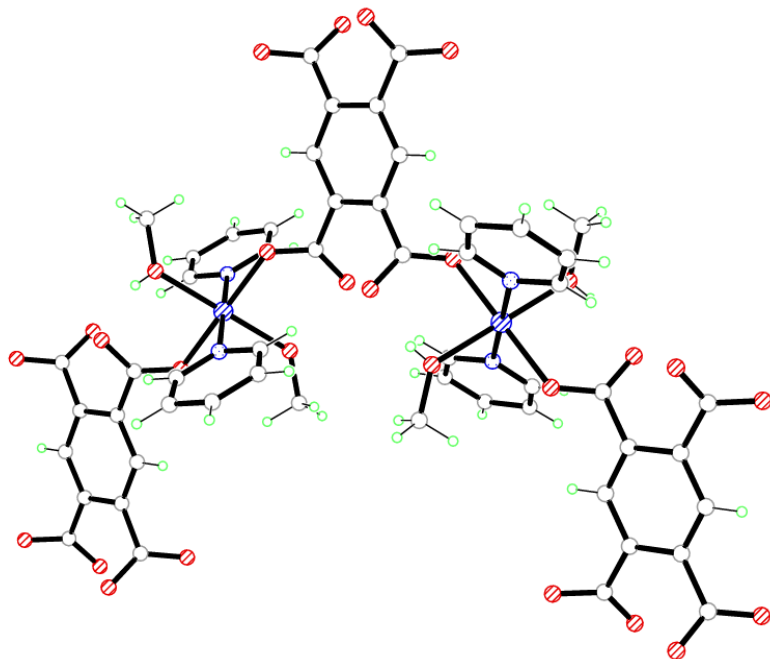


**Figure 7.03: Molecular building unit of Co(1) and CO(2) in compound 22**

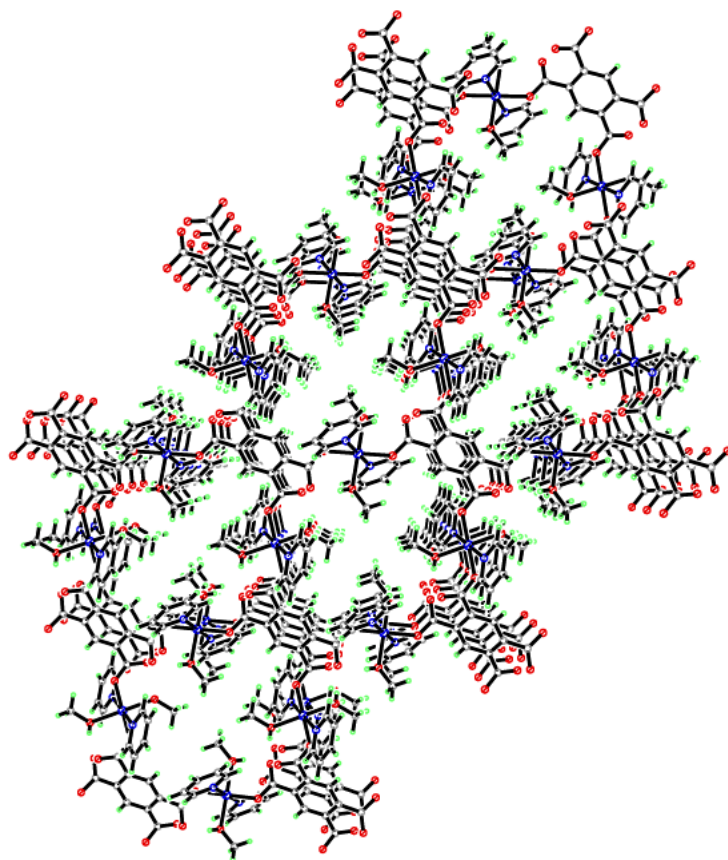


**Figure 7.04: Two dimensional sheet of compound 22 viewed down the *a*-axis**

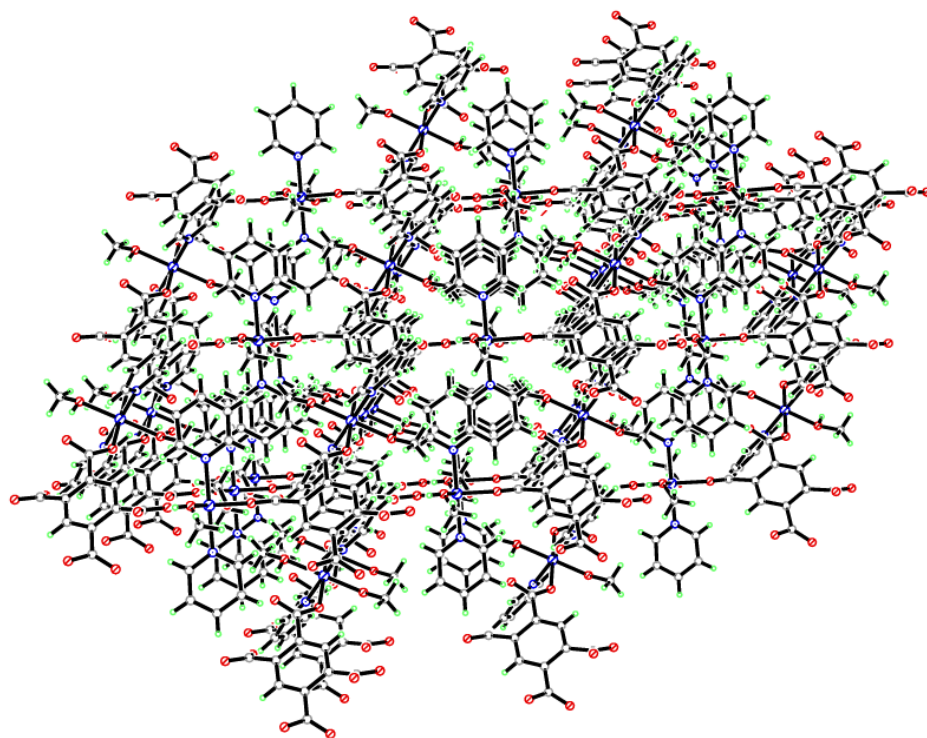


**Figure 7.05:** Three dimensional overlapping packing of the sheets in compound 22 viewed down the *b*-axis

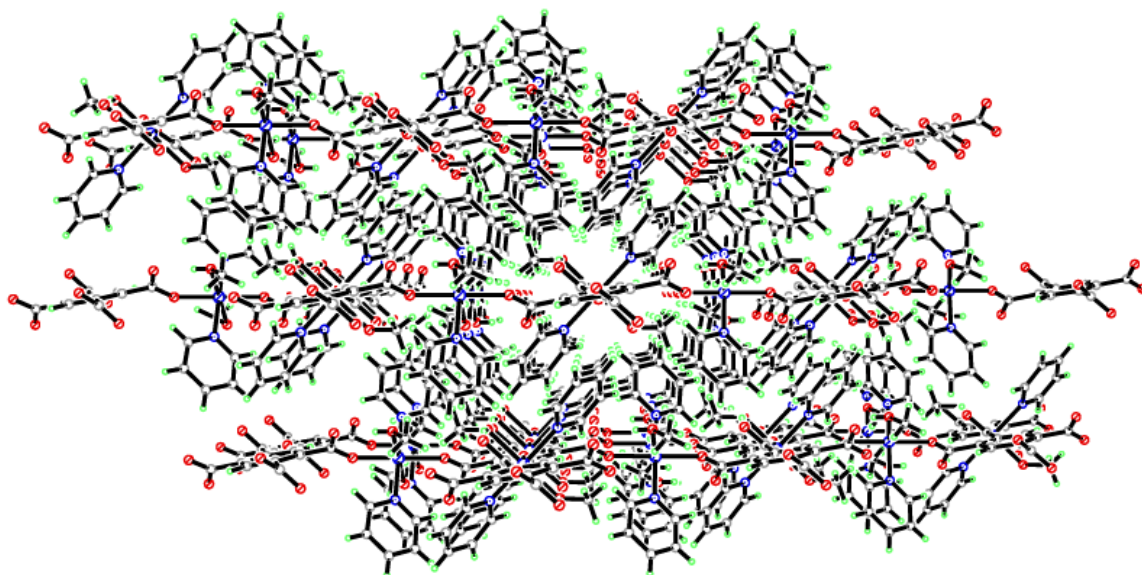


**Figure 7.06:** Three dimensional overlapping packing of the sheets in compound 22 viewed down the *c*-axis

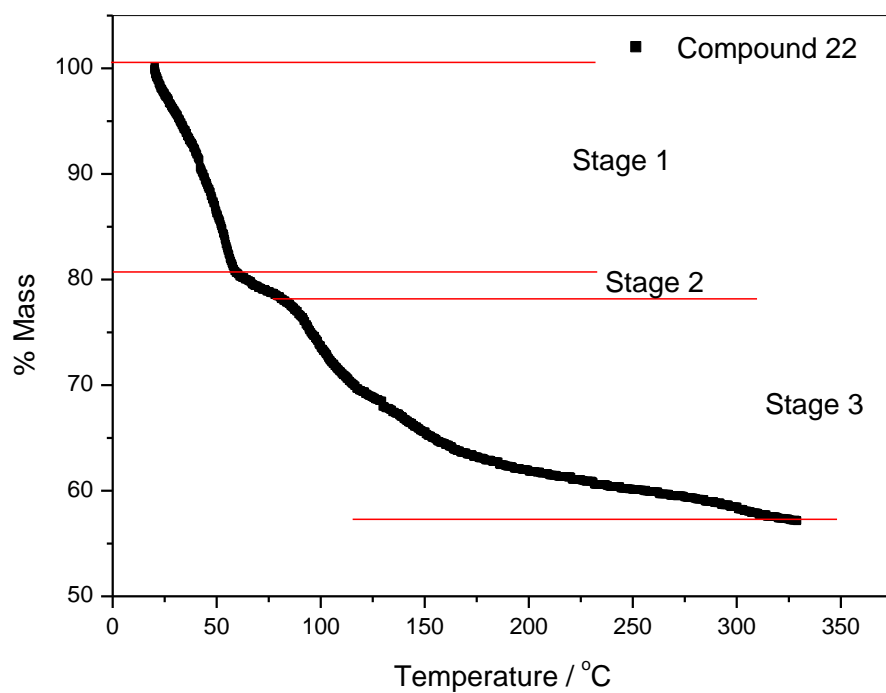
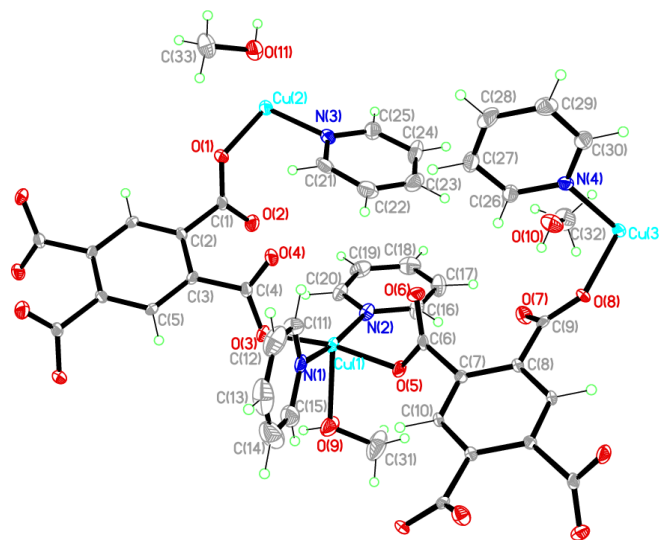


**Figure 7.07: Thermogravimetric analysis plot of compound 22**

**Compound 23:**  $[\text{Cu}_2(\text{C}_{10}\text{H}_2\text{O}_8)(\text{CH}_4\text{O})(\text{C}_5\text{H}_5\text{N})_4] \cdot 2(\text{CH}_4\text{O})$



Chemical formula (total)	$\text{C}_{33}\text{H}_{34}\text{Cu}_2\text{N}_4\text{O}_{11}$	
Formula weight	789.72	
Temperature	150(2) K	
Radiation, wavelength	MoK $\alpha$ , 0.71073 Å	
Crystal system, space group	triclinic, $P\bar{1}$	
Unit cell parameters	$a = 8.7980(3)$ Å	$\alpha = 94.840(3)^\circ$
	$b = 10.6480(4)$ Å	$\beta = 90.453(3)^\circ$
	$c = 19.1470(8)$ Å	$\gamma = 110.355(4)^\circ$
Cell volume	$1674.37(11)$ Å <sup>3</sup>	
Z	2	
Crystal colour and size	blue, $0.25 \times 0.2 \times 0.20$ mm <sup>3</sup>	
Final $R$ indices [ $F^2 > 2\sigma$ ]	$R1 = 0.0451$	
$R$ indices (all data)	$wR2 = 0.1041$	
Largest diff. peak and hole	0.56 and $-0.84$ e Å <sup>-3</sup>	

**Figure 7.08: Asymmetric Unit of Compound 23 all unique atoms labelled, additional atoms added to complete ligands**

### Synthesis

0.5 mL of a solution of  $\text{Cu}(\text{NO}_3)_2 \cdot 4\text{H}_2\text{O}$  (0.079 g, 0.33 mmol) in methanol (10 mL) and 0.5 mL of a solution of 1,2,4,5-benzenetetracarboxylic acid (0.043 g, 0.17 mmol) in methanol (10 mL) were placed into a small sample vial. This was covered with Whatman Laboratory Sealing Film and placed inside a larger sample vial. In the larger sample vial pyridine (0.05 mL, 0.22 mmol) was added before it was covered and left until crystallisation was complete. After four days, blue block crystals formed.

## Structure Determination

The data were collected at 150 K using molybdenum radiation on an Oxford Diffraction Gemini A Ultra diffractometer. The structure was solved by direct methods. The semi-empirical absorption corrections were applied based on symmetry-equivalent and repeated data. The refinement gave a  $wR2$  of 0.1041 for all 6640 independent reflections and a conventional  $R1$  of 0.0451, for 4652 reflections with  $F^2 > 2\sigma$ . The residual electron density maximum and minimum were 0.56 and  $-0.84 \text{ e } \text{\AA}^{-3}$  respectively.

The hydrogen atoms were placed in geometrically calculated positions with  $U$  constrained to  $1.2 U_{\text{eq}}(\text{C})$  for aromatic hydrogen atoms and  $U$  constrained to  $1.5 U_{\text{eq}}(\text{C})$  for methyl hydrogen atoms. The full data of compound 23 can be found in Appendix 1.

## Structure Analysis

The asymmetric unit of compound 23 (figure 7.08) shows two half 1,2,4,5-benzenetetracarboxylate ligand completed by inversion symmetry through the centre of the respective aromatic rings, coordinated to three copper cations Cu(1), Cu(2) and Cu(3). The copper cations are in two different coordination environments in this polymeric compound with Cu(1) placed on a general position forming a five-coordinate square based pyramidal (figure 7.09A); whilst Cu(2) and Cu(3) are positioned on inversion symmetry centres and form standard octahedral geometries (figure 7.09B and 7.09C).

The Cu(1) cation forms a five-coordinate square based pyramid coordinating to two trans carboxylates from the individual 1,2,4,5-benzenetetracarboxylate ligands via the monodentate bonds to O(3) and O(5) that coordinate at an angle of O(3)-Cu(1)-O(5)  $169.89(10)^\circ$ . The remaining two equatorial coordination sites are occupied by individual trans pyridine ligands N(1)-Cu(1)-N(2)  $166.00(12)^\circ$  which are rotated  $90^\circ$  around the Cu-N bond with respect to each other. The fifth coordination site is occupied by an axial methanol ligand that coordinates cis with respect to the other ligands coordinated to the Cu(1) cation (table 7.03), forming a elongated Cu(1)-O(9) bond of  $2.359(3) \text{ \AA}$ . The Cu(1) cation acts as a central connecting node with the two 1,2,4,5-benzenetetracarboxylate ligands linking all the copper cations with each carboxylate

coordinating to a copper cation. These linkers are not coplanar and diverge away from the Cu(1) cation with different angles with respect to their aromatic rings, this occurs as the carboxylate groups rotate around the carbon-carbon bonds out of the aromatic plane. The aromatic ring of the C(1)-O(4) ligand is angled at  $56.96(2)^\circ$  to the plane of the copper-carboxylates whilst the aromatic ring of the C(6)-O(8) ligand is angled at  $62.33(2)^\circ$  with respect to the plane, this creates a non-planar sheet upon further coordination to Cu(2) and Cu(3) cations adopting a 'zigzag' sheet motif which differs from the planar sheet observed in compound 22.

The Cu(2) cation is linked to the Cu(1) cation via the C(1)-O(4) ligand by coordinating to its remaining carboxylate group to form the monodentate bond Cu(2)-O(1) 1.961(2) Å and its trans symmetry equivalent O(1)-Cu(2)-O(1A)  $180^\circ$  generated by the inversion symmetry. The Cu(2) cation adopts a similar coordination motif of the Co(1) and Co(2) cations in compound 22 coordinating to one axial methanol perpendicular to the plane of the aromatic ring of the C(1)-O(4) ligand; and one cis pyridine ligand that runs parallel to the 1,2,4,5-benzenetetracarboxylate ligand stacking below the C(16)-N(2) pyridine coordinated to the Cu(1) cation to form an intramolecular  $\pi$ - $\pi$  stacking interaction of 3.945(2) Å. The coordination geometry of the Cu(2) cation is completed by the generation of the respective trans symmetry equivalent ligands through the inversion centre (figure 7.09B).

The remaining Cu(3) cation is linked to the Cu(1) cation by the C(6)-O(8) ligand that coordinates via the O(8) carboxylate oxygen forming a monodentate bond. Cu(3) also coordinates to a methanol in the coplanar cis position to the carboxylate group allowing the intramolecular hydrogen bonding between the uncoordinated O(7) carboxylate oxygen and the O-H of the methanol (table 7.04). The remaining coordination site is occupied by an axial pyridine ligand that coordinates perpendicular to the carboxylate group; O(8)-Cu(3)-N(4)  $91.56(10)^\circ$  with the completion of the octahedral geometry via the generation of the coplanar trans symmetry equivalent ligands through the inversion centre at the Cu(3) cation (figure 7.09C). The Cu(3) cation is rotated with respect to the plane of the 1,2,4,5-benzenetetracarboxylates aromatic ring pointing the axial pyridines off-centre from the perpendicular  $90^\circ$  at an angle of  $108.27(5)^\circ$ . This allows the pyridine ligand C(26)-N(4) to point perpendicular to the



C(11)-N(1) pyridine coordinated to the Cu(1) forming a  $\sigma$ - $\pi$  (C-H- $\pi$ ) interaction from the C(13)-H(13)···C(26)-C(30) aromatic ring at 3.394(2)°.

The linking 1,2,4,5-benzenetetracarboxylate ligands are expanded through the inversion symmetry at the centre of the aromatic rings to form the building unit shown in figure 7.10. This molecular building unit expands compound 23 into a coordinated two dimensional sheet with a similar packing motif to that of compound 22 (figure 7.11). In contrast to the three methanol ligands pointing inwards to the potential pore as observed in compound 22, compound 23 has two pyridines and two methanols pointing inwards as a result of the square pyramidal geometry of the Cu(1) cation. These sheets expand down the *c*-axis and along the *b*-axis with a 'zigzag' motif producing a wave-like sheet that is visible when compound 23 is viewed down the *b*-axis (figure 7.12).

These sheets are stacked together utilizing the C(26)-N(4) pyridine ligand and its symmetry equivalent of an adjacent sheet generated through an inversion centre 1.852(4) Å away from its aromatic ring in the *c*-axis. This creates a  $\pi$ - $\pi$  stacking of 3.721(4) Å in the *c*-axis, stacking two adjacent sheets in the *a*-axis. The structure is further stabilised by hydrogen bonds from the coordinated methanol ligands to uncoordinated water molecules; O(10)-H(10)···O(7) 2.656(4) Å and O(9)-H(9)···O(11E) 2.763(4) Å (table 7.04).

Compound 23 was synthesised as an analogue of compound 22; however upon substituting cobalt by copper, variations in the structure and packing motifs were able to form. The majority of differences arise from the addition of an extra square pyramidal Cu(1) cation in compound 23 that alters the coordination motif of the 1,2,4,5-benzenetetracarboxylate ligands. The structures do have significant similarities with both Co(1) and Co(2) in compound 22 (figure 7.02) forming the same coordination geometries as Cu(2) and Cu(3) in compound 23 (figure 7.09) with all four cations positioned on inversion centres. These cations also show the preferential orientation of the carboxylate with respect to the pyridine and methanol ligands, indicating the coordinated monodentate carboxylate groups avoids the steric bulk of the pyridine and moves coplanar to the methanol ligand to form a strong intramolecular hydrogen bond. The compounds also form 4,4' netted sheets where four linkers join four nodes to form a square that expands into a sheet. Compound 22 has four methanol ligands pointing in

towards the 4,4' net blocking the potential pore, in contrast compound 23 has similar sized nets that accommodate two pyridine and two methanol ligands. The packing motifs of the two compounds differ with compound 22 forming planar sheets packed together utilizing an extensive network of  $\pi$ - $\pi$  stacking with its regular arrays of axial pyridine ligands, whilst compound 23 forms a 'zigzag' sheet that forms several intramolecular  $\pi$ - $\pi$  stacking and  $\sigma$ - $\pi$  interactions with only one intermolecular  $\pi$ - $\pi$  stacking between symmetry equivalent C(26)-N(4) pyridines around an inversion centre.

The differing reliance on pyridine stacking between the two compounds resulted in the investigations involving lower concentrations of pyridine in the reaction media. This was designed to develop products with similar motifs that do not pack around the pyridine ligands leading to the formation of compound 24. Additional reactions based on these packing motifs were developed to include elongated 4,4'-bipyridine ligands to fully coordinate the layers of 1,2,4,5-benzenetetracarboxylate linkers with regular arrays of 4,4'-bipyridine forming columns throughout the structure. These reactions led to the formation of compounds 25 and 26.

**Table 7.03: Selected Bond Lengths [ $\text{\AA}$ ] and Angles [ $^\circ$ ] for Compound 23**

Cu(1)–O(3)	1.971(2)	Cu(1)–O(5)	1.946(2)
Cu(1)–O(9)	2.359(3)	Cu(1)–N(1)	2.029(3)
Cu(1)–N(2)	2.026(3)	Cu(2)–O(1)	1.961(2)
Cu(2)–N(3)	2.047(3)	Cu(3)–O(8)	1.973(2)
Cu(3)–N(4)	2.023(3)	O(1)–C(1)	1.284(4)
O(2)–C(1)	1.241(4)	O(3)–C(4)	1.279(4)
O(4)–C(4)	1.235(4)	O(5)–C(6)	1.289(4)
O(6)–C(6)	1.229(4)	O(7)–C(9)	1.242(4)
O(8)–C(9)	1.277(4)		
O(3)–Cu(1)–O(5)	169.89(10)	O(3)–Cu(1)–O(9)	88.27(9)
O(3)–Cu(1)–N(1)	88.61(10)	O(3)–Cu(1)–N(2)	95.07(10)
O(1)–Cu(2)–O(1A)	180.0	O(1)–Cu(2)–N(3)	92.69(10)
O(8)–Cu(3)–O(8B)	180.0	O(8)–Cu(3)–N(4)	88.44(10)
Cu(2)–O(1)–C(1)	125.3(2)	Cu(1)–O(3)–C(4)	109.7(2)
Cu(1)–O(5)–C(6)	119.4(2)	Cu(3)–O(8)–C(9)	128.6(2)

Symmetry operations for equivalent atoms

A  $-x+1, -y+2, -z$     B  $-x+2, -y+2, -z+1$ **Table 7.04: Selected Hydrogen bond Lengths [ $\text{\AA}$ ] and angles [ $^\circ$ ] for Compound 23**

D–H...A	d(D–H)	d(H...A)	d(D...A)	(DHA)
O(9)–H(9)...O(11E)	0.96(6)	1.81(6)	2.763(4)	175(5)
O(10)–H(10)...O(7)	0.72(4)	1.94(4)	2.656(4)	170(4)
O(11)–H(11)...O(2A)	0.94(7)	1.73(7)	2.636(4)	160(6)

Symmetry operations for equivalent atoms

A  $-x+1, -y+2, -z$     E  $x, y-1, z$



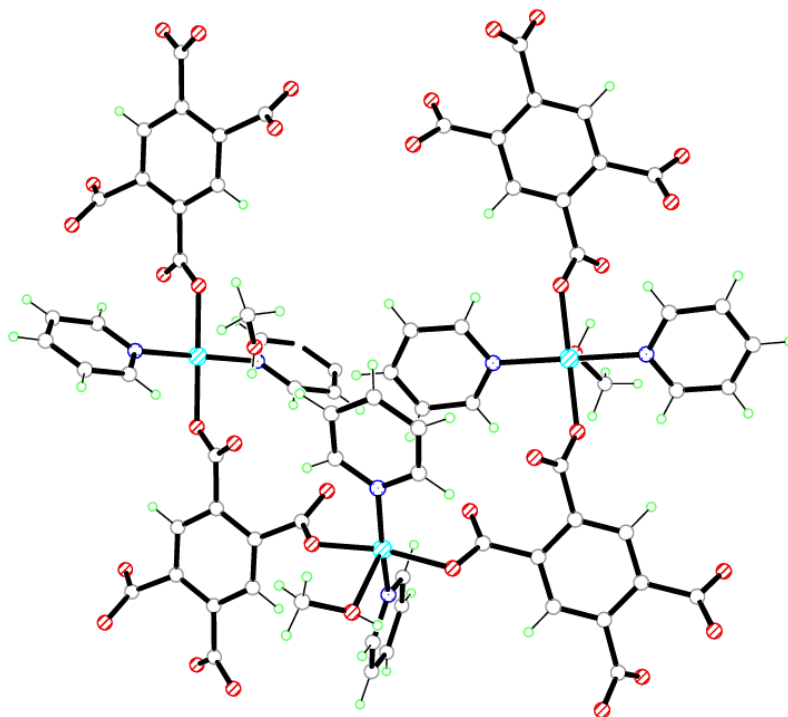


**Figure 7.10:** Molecular building unit of Cu(1), Cu(2) and Cu(3) in compound 23

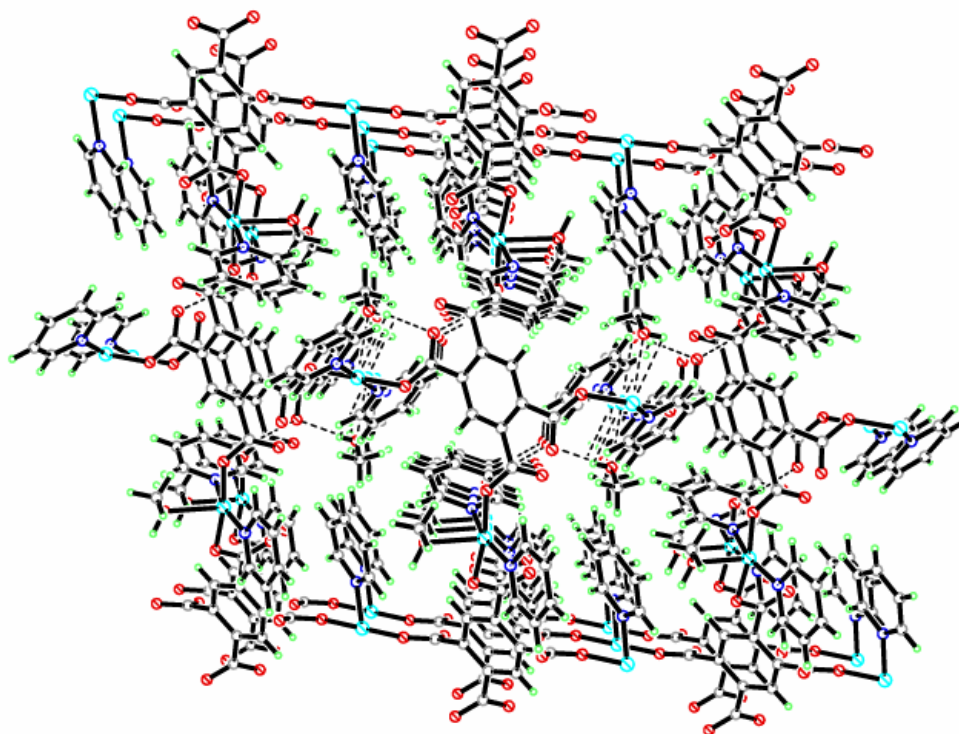


**Figure 7.11:** Two dimensional sheet of compound 23 viewed down the *a*-axis

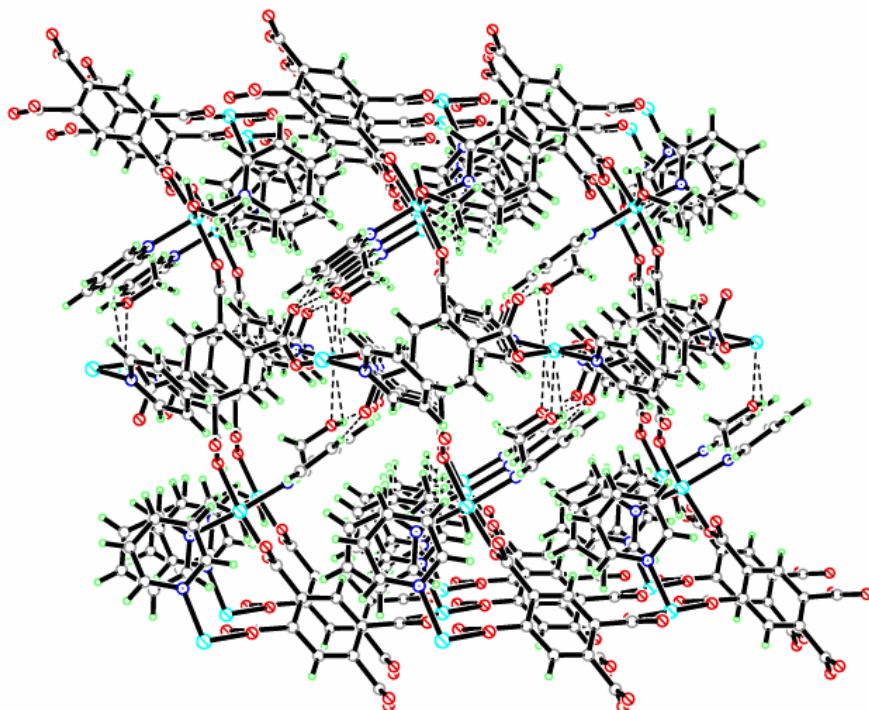
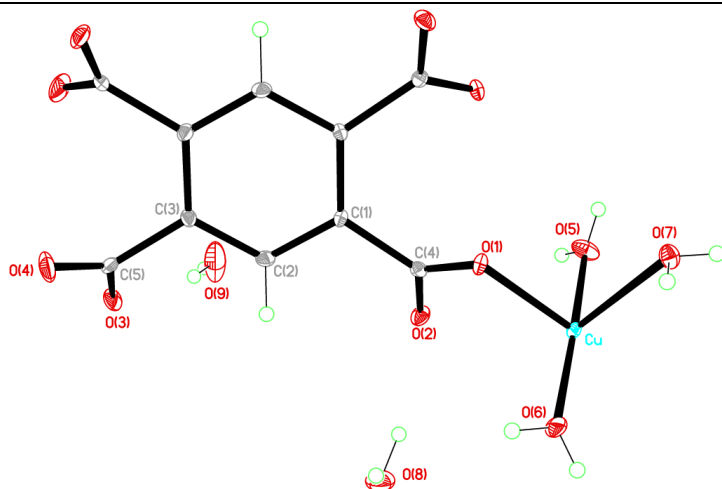


**Figure 7.12:** Three dimensional packing of the zigzag sheets in compound 23 viewed down the *b*-axis

**Compound 24:**  $[\text{Cu}_2(\text{C}_{10}\text{H}_2\text{O}_8)(\text{H}_2\text{O})_6] \cdot 4(\text{H}_2\text{O})$



Chemical formula (total)	$\text{C}_{10}\text{H}_{22}\text{Cu}_2\text{O}_{18}$
Formula weight	557.36
Temperature	150(2) K
Radiation, wavelength	MoK $\alpha$ , 0.71073 Å
Crystal system, space group	monoclinic, $C2/c$
Unit cell parameters	$a = 12.1433(3)$ Å $b = 18.1282(4)$ Å $c = 9.5587(3)$ Å $\beta = 113.464(3)^\circ$
Cell volume	$1930.22(9)$ Å <sup>3</sup>
Z	4
Crystal colour and size	blue, $0.10 \times 0.09 \times 0.08$ mm <sup>3</sup>
Final $R$ indices [ $F^2 > 2\sigma$ ]	$R1 = 0.0230$
$R$ indices (all data)	$wR2 = 0.0548$
Largest diff. peak and hole	0.50 and $-0.36$ e Å <sup>-3</sup>

**Figure 7.13: Asymmetric Unit of Compound 24 all unique atoms labelled, additional atoms added to complete ligands**

### Synthesis

0.5 mL of a solution of  $\text{Cu}(\text{NO}_3)_2 \cdot 4\text{H}_2\text{O}$  (0.079 g, 0.33 mmol) in methanol (10 mL) and 0.5 mL of a solution of 1,2,4,5-benzenetetracarboxylic acid (0.043 g, 0.17 mmol) in water (10 mL) were placed into a small sample vial. This was covered with Whatman Laboratory Sealing Film and placed inside a larger sample vial. In the larger sample vial pyridine (0.02 mL, 0.11 mmol) was added before it was covered and left until crystallisation was complete. After three days, blue block crystals formed.

## Structure Determination

The data were collected at 150 K using molybdenum radiation on an Oxford Diffraction Gemini A Ultra diffractometer. The structure was solved by direct methods. The semi-empirical absorption corrections were applied based on symmetry-equivalent and repeated data. The refinement gave a  $wR2$  of 0.0548 for all 2301 independent reflections and a conventional  $R1$  of 0.0230, for 1853 reflections with  $F^2 > 2\sigma$ . The residual electron density maximum and minimum were 0.50 and  $-0.36 \text{ e } \text{\AA}^{-3}$  respectively.

The hydrogen atoms were placed in geometrically calculated positions with  $U$  constrained to  $1.2 U_{\text{eq}}(\text{C})$  for aromatic hydrogen atoms and  $U$  constrained to  $1.5 U_{\text{eq}}(\text{O})$  for hydroxyl hydrogen atoms. SADI restraints were imposed on the coordinated and uncoordinated water molecules within compound 24 during refinement. The full data of compound 24 can be found in Appendix 1.

## Structure Analysis

The asymmetric unit of compound 24 (figure 7.13) shows one half 1,2,4,5-benzenetetracarboxylate ligand completed by two-fold rotation symmetry in the plane of the aromatic ring, coordinating to one copper cation placed in a general position. The copper cation (Cu) forms a five-coordinate square pyramidal geometry similar to that observed in compound 23 at the Cu(1) node (figure 7.09A) coordinating to two trans coplanar carboxylate groups of symmetry equivalent 1,2,4,5-benzenetetracarboxylate ligands with the monodentate bonds Cu-O(1) 2.009(12) Å and Cu-O(3) 1.954(13) Å at an angle of  $175.13(5)^\circ$ . Three water ligands O(5), O(6) and O(7) coordinate cis to the carboxylate groups with the bond lengths listed in table 7.05, the water ligands complete the Cu cation geometry to form the five-coordinate node shown in figure 7.14. The copper cation connects two symmetry equivalent 1,2,4,5-benzenetetracarboxylate ligands that are completed by the two-fold rotation symmetry in the plane of the aromatic ring, forming the molecular building unit in figure 7.15. The molecular building unit expands the structure into a two dimensional sheet that runs along the  $a$ -axis and down the  $b$ -axis, figure 7.16 shows the layers of these sheets when compound 24 is viewed down the  $c$ -axis. The sheets consist of 4,4' nets similar to those seen in



compounds 22 and 23, in the case of this compound the net is once again formed around four nodes and four linkers; each linker bridging between two nodes in the net. The nets have dimensions 6.934(5) by 8.608(4) Å and have four coordinated molecules pointing inwards towards the net. These form hydrogen bonds with the uncoordinated water molecules that act as both acceptor and donor groups forming further hydrogen bonds to the uncoordinated carboxylate oxygen atoms O(2) and O(4) (table 7.06).

The sheets stack in a staggered motif along the *b*-axis and *a*-axis staggered by 6.192(5) Å with respect to each layer, this places the aromatic ring of the 1,2,4,5-benzenetetracarboxylate directly below the 4,4' net of the sheet above; shrinking the potential pore down the *c*-axis to 5.069(5) by 4.374(7) Å as shown in figure 71.6.

The sheets pack together up the *c*-axis held together by inter/intramolecular hydrogen bonds (figure 7.17) between the three coordinated water molecules and the uncoordinated molecules; O(6)-H(6B)⋯O(8F) 2.702(19) Å and O(7)-H(7B)⋯O(9G) 2.671(2) Å with the uncoordinated water molecules acting as the hydrogen bond acceptors. The uncoordinated water molecules O(8) and O(9) then form hydrogen bonds with the uncoordinated carboxylate oxygen atoms O(2) and O(4); O(8)-H(8A)⋯O(2) 2.815(19) Å, O(8)-H(8B)⋯O(4E) 2.803(2) Å and O(9)-H(9A)⋯O(3) 2.882(2) Å.

The thermostability of compound 24 was analysed using thermogravimetric analysis to investigate the potential of desolvating the compound to 'activate' the 4,4 nets for gas/vapour adsorption studies. The TGA plot produced shown in figure 7.18 shows dehydration begins immediately upon heating with excess solvent removed between 20-50°C. After the excess surface solvent is removed in stage 1 further desolvation occurs at stage 2 between 55-100°C resulting in a mass loss of 1.399 mg (30.61 %) comparable to the calculated water content in the single crystal data of 32.2 %. Compound 24 upon desolvation begins to collapse in stage 3 as the hydrogen bonds holding the structure together have been removed. The collapse occurs between 110-130°C during this temperature range there is a large uptake of thermal energy by compound 24 that cools the TGA column by 8°C, recognisable by the regression between 125-117°C in figure 7.18. After the thermal intake the compound reduces its rate of decomposition forming a slightly stable plateau between 130-190°C before the compounds fully degrades. The significant thermal uptake and subsequent stability of

compound 24 suggests the compound has undergone further chemical reaction upon heating and desolvation to form a new compound. The desolvated compound was analysed using powder X-ray diffraction that produced the powder diffraction pattern plotted in figure 7.19. The obtained powder diffraction data of the desolvated compound shows considerable differences from the predicted powder diffraction pattern of the single crystal data; with alterations in the 8-12 and 15-20 2-Theta regions.

The analysis of the bulk sample by elemental analysis after drying at 25°C for 24 hours produced the results C = 32.95 %, H = 4.13 % and N = 6.05 %. These values differ from the calculated values from the single crystal data; C = 21.533 %, H = 3.95 % and N = 0 %. The presence of nitrogen in the sample correlates with the use of pyridine in the reaction system, suggesting the sample needs to be heated to remove the residual pyridine; consistent with the TGA plot in figure 7.18.

A copper compound containing only the 1,2,4,5-benzenetetracarboxylate ligand and water is reported by Fernandes *et al.* (CSD Refcode: MOFJEW).<sup>1</sup> This compound forms linear chains of the five-coordinate square pyramidal copper nodes coordinated to two monodentate carboxylate and three cis water molecules similar to the copper node present in compound 24 (figure 7.14). The MOFJEW compound does not form sheets as a result of the partial deprotonation of the 1,2,4,5-benzenetetracarboxylate, that only coordinates through two of its four carboxylate groups. This coordination motif makes the MOFJEW compound a precursor to compound 24 forming comparable node geometries, water-water hydrogen bonds and metal-oxygen bond lengths.<sup>1</sup>

Compound 24 shows the progression of the reaction media used to synthesize compounds 22 and 23, with reducing the pyridine concentration to produce a fully deprotonated and coordinated 1,2,4,5-benzenetetracarboxylate framework without coordinating pyridine to the metal nodes. Compound 24 shows a retention of the 4,4' netted sheet; however it now does not stack in the similar motifs to that of compounds 22 and 23 relying on hydrogen bonding through an extensive network of coordinated and uncoordinated water ligands. This shifts the sheets into a staggered conformation partially closing the potential pores. The average metal-oxygen bond lengths of compounds 22, 23, 24 and MOFJEW<sup>1</sup> are compared in table 7.07.

**Table 7.05: Selected Bond Lengths [Å] and Angles [°] for Compound 24**

Cu–O(1)	2.0092(12)	Cu–O(3A)	1.9544(13)
Cu–O(5)	1.9491(14)	Cu–O(6)	1.9532(14)
Cu–O(7)	2.2374(14)	C(4)–O(1)	1.271(2)
C(4)–O(2)	1.249(2)	C(5)–O(3)	1.269(2)
C(5)–O(4)	1.243(2)		
O(1)–Cu–O(3A)	175.13(5)	O(1)–Cu–O(5)	93.72(6)
O(1)–Cu–O(6)	88.87(5)	O(1)–Cu–O(7)	86.41(5)
Cu–O(1)–C(4)	106.52(11)	Cu(C)–O(3)–C(5)	127.07(12)

Symmetry operations for equivalent atoms

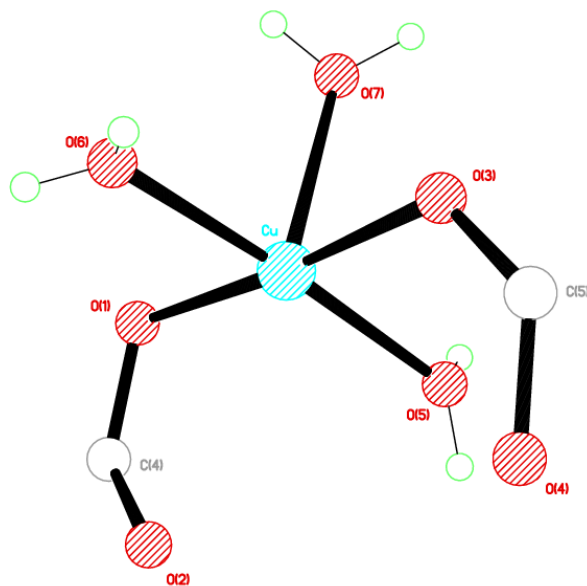
A  $-x+1/2, y+1/2, -z+3/2$ **Table 7.06: Selected Hydrogen bond Lengths [Å] and angles [°] for Compound 24**

D–H...A	d(D–H)	d(H...A)	d(D...A)	(DHA)
O(5)–H(5A)...O(7B)	0.734(14)	1.959(14)	2.6865(18)	171(3)
O(5)–H(5B)...O(1D)	0.756(14)	2.050(15)	2.8003(19)	172(2)
O(6)–H(6A)...O(4E)	0.759(14)	1.931(15)	2.6860(19)	172(2)
O(6)–H(6B)...O(8F)	0.751(14)	1.955(14)	2.7023(19)	173(3)
O(7)–H(7A)...O(2G)	0.755(13)	1.943(14)	2.6723(19)	162(2)
O(7)–H(7B)...O(9G)	0.762(14)	1.917(15)	2.671(2)	170(2)
O(8)–H(8A)...O(2)	0.86(2)	2.00(2)	2.8143(19)	159(2)
O(8)–H(8B)...O(4E)	0.770(15)	2.045(16)	2.803(2)	168(3)
O(9)–H(9A)...O(3)	0.751(15)	2.144(17)	2.882(2)	168(3)
O(9)–H(9B)...O(8H)	0.715(15)	2.64(2)	3.247(2)	144(3)

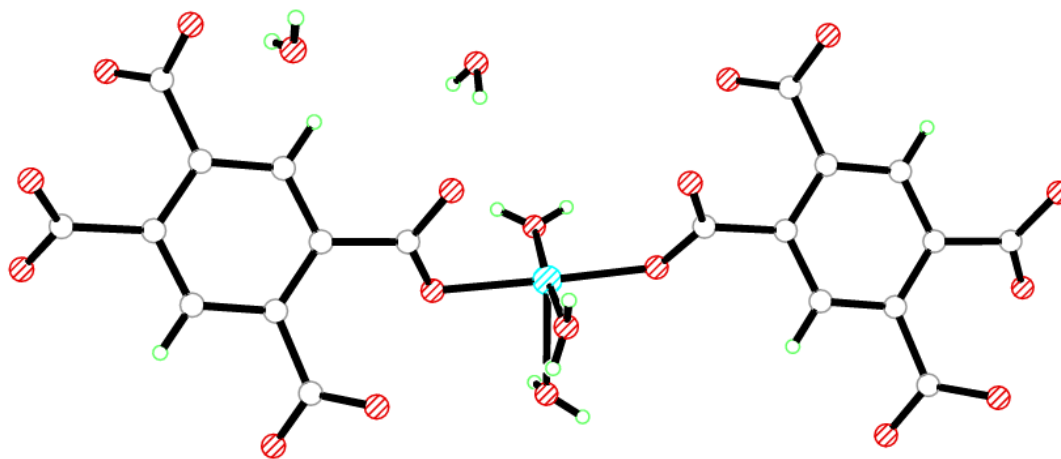
Symmetry operations for equivalent atoms

B  $-x, y, -z+3/2$  D  $x, -y+1, z-1/2$  E  $-x+1/2, -y+1/2, -z+2$ F  $-x+1, -y+1, -z+2$  G  $x, -y+1, z+1/2$  H  $-x+1/2, -y+1/2, -z+1$ **Table 7.07: Average bond length comparisons between Compound 24, Compound 22, Compound 23 and MOFJEW<sup>1</sup>**

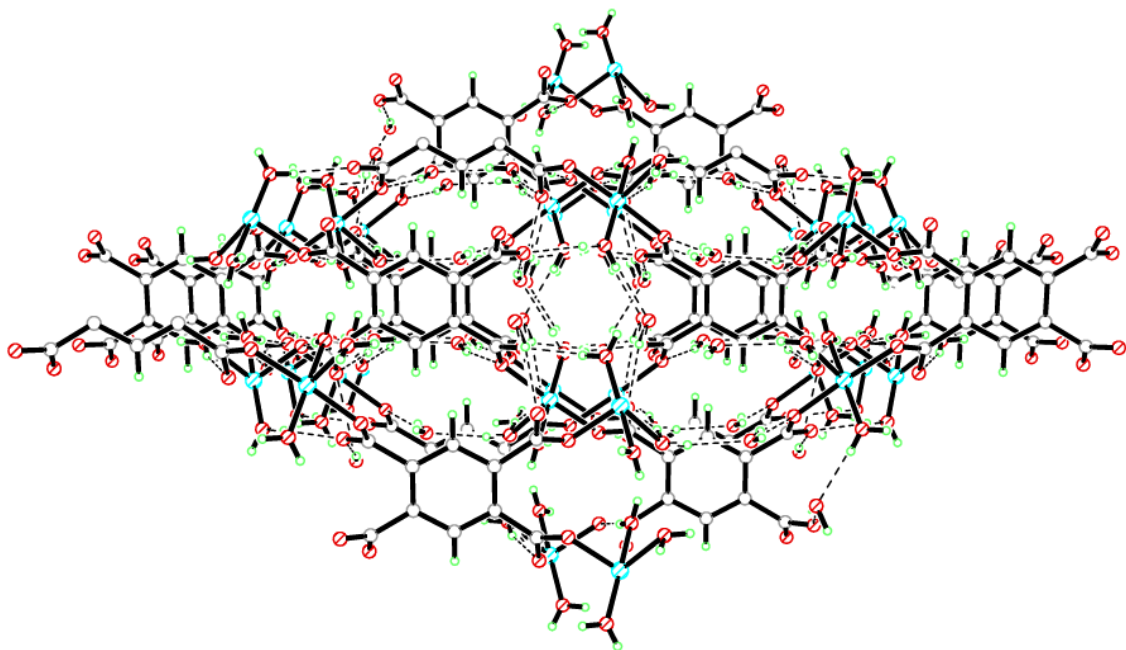
Compound	Bond	Average Bond Length (Å)
Compound 22	Co–O (carboxylate)	2.076
Compound 22	Co–O (methanol)	2.121
Compound 23	Cu–O (carboxylate)	1.965
Compound 23	Cu–O (methanol)	2.165
Compound 24	Cu–O (carboxylate)	1.975
Compound 24	Cu–O (water)	2.043
MOFJEW	Cu–O (carboxylate)	1.948
MOFJEW	Cu–O (water)	1.991



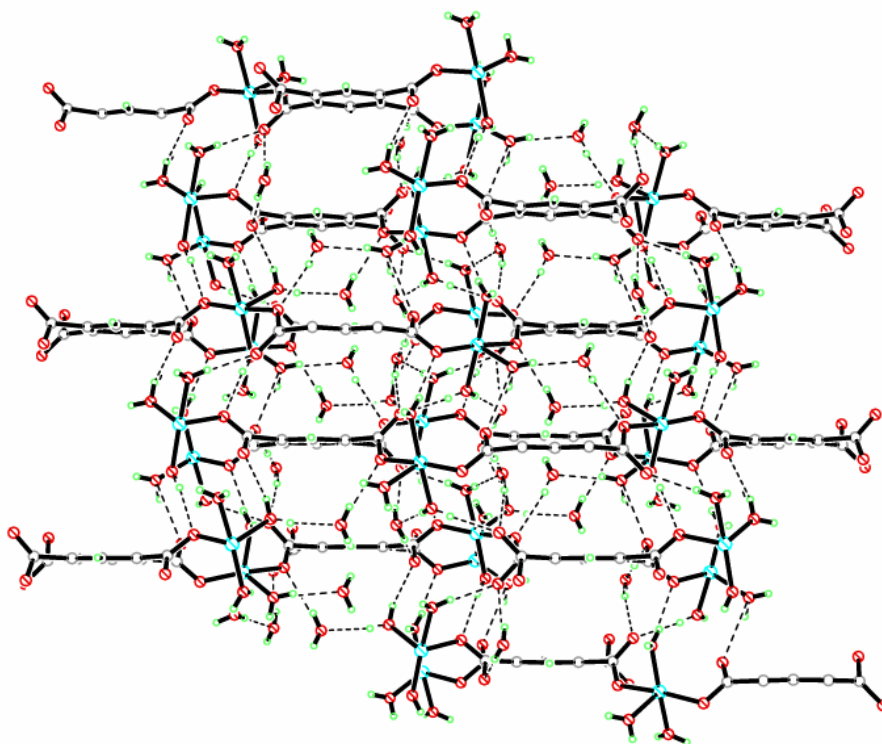
**Figure 7.14: Square pyramidal coordination environment of Cu(1) in compound 24**



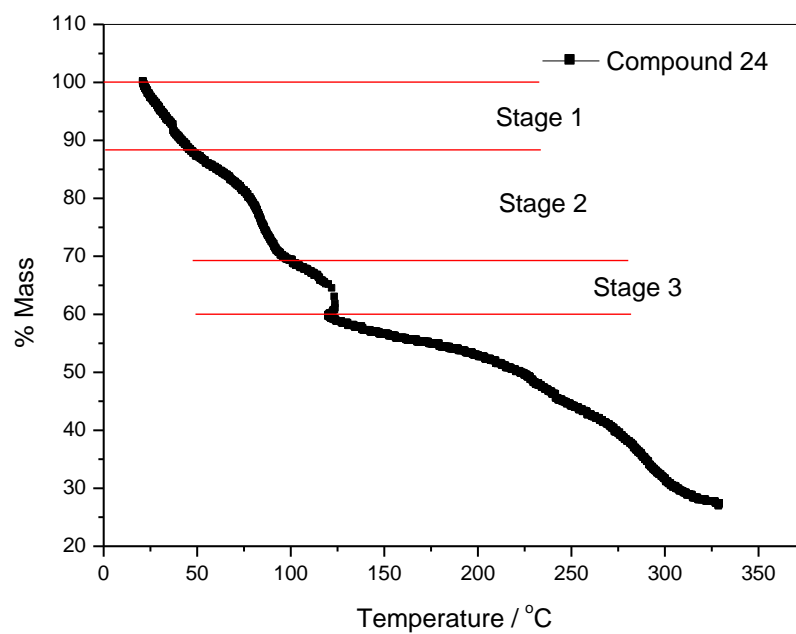
**Figure 7.15: Molecular building unit of Cu(1) in compound 24**



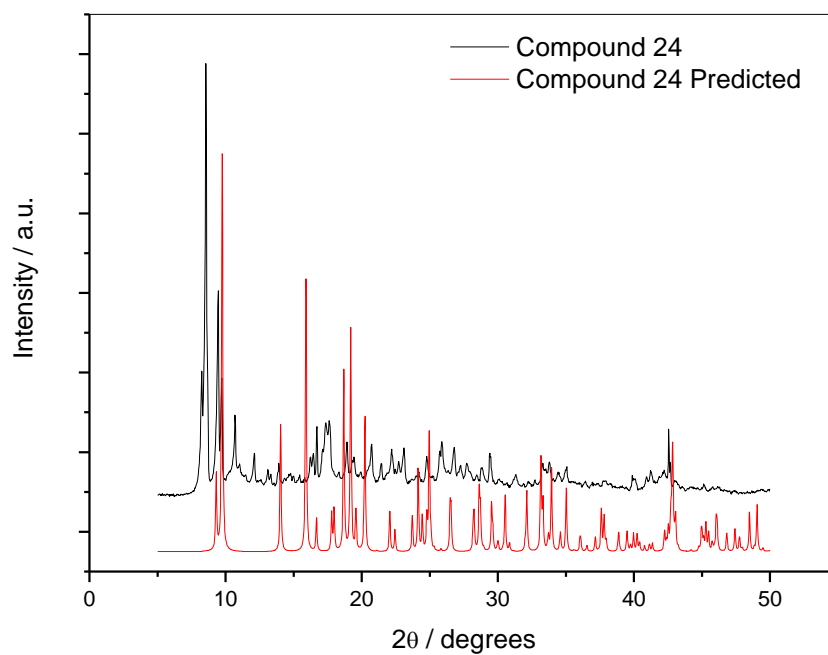
**Figure 7.16:** Two dimensional sheet of compound 24 viewed down the *c*-axis



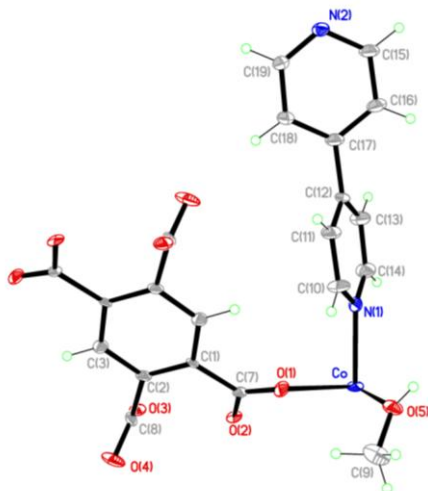
**Figure 7.17:** Three dimensional packing of the sheets via the extensive network of hydrogen bonds in compound 24 viewed down the *a*-axis



**Figure 7.18: Thermogravimetric analysis plot of compound 24**



**Figure 7.19: Powder X-ray diffraction pattern of Compound 24**

**Compound 25:**  $[\text{Co}_2(\text{C}_{10}\text{H}_2\text{O}_8)(\text{C}_{10}\text{H}_8\text{N}_2)_2(\text{CH}_4\text{O})_2]$ 

Chemical formula (total)	$\text{C}_{32}\text{H}_{26}\text{Co}_2\text{N}_4\text{O}_{10}$	
Formula weight	744.43	
Temperature	150(2) K	
Radiation, wavelength	MoK $\alpha$ , 0.71073 Å	
Crystal system, space group	triclinic, $P\bar{1}$	
Unit cell parameters	$a = 8.9313(6)$ Å	$\alpha = 62.303(8)^\circ$
	$b = 9.7415(9)$ Å	$\beta = 72.880(6)^\circ$
	$c = 10.1946(7)$ Å	$\gamma = 75.486(7)^\circ$
Cell volume	$743.73(10)$ Å <sup>3</sup>	
Z	1	
Crystal colour and size	pink, $0.10 \times 0.02 \times 0.02$ mm <sup>3</sup>	
Final $R$ indices [ $F^2 > 2\sigma$ ]	$R1 = 0.0824$	
$R$ indices (all data)	$wR2 = 0.2049$	
Largest diff. peak and hole	1.24 and $-0.87$ e Å <sup>-3</sup>	

**Figure 7.20:** Asymmetric Unit of Compound 25 all unique atoms labelled, additional atoms added to complete ligands

**Synthesis**

1 mL of a solution of  $\text{Co}(\text{NO}_3)_2 \cdot 6\text{H}_2\text{O}$  (0.08 g, 0.33 mmol) in methanol (10 mL) was syringed into one side of the H-Cell vessel, 1 mL of a solution of 1,2,4,5-benzenetetracarboxylic acid (0.043 g, 0.17 mmol) in methanol (10 mL) and 1 mL of a solution of 4,4'-bipyridine (0.027 g, 0.17 mmol) in methanol (10 mL) were then syringed into the other side of the H-Cell vessel. The independent solutions were bridged by 2 mL water that was carefully layered into the bridging tube. After nine weeks, pink spindle crystals formed.

## Structure Determination

The data were collected at 150 K using molybdenum radiation on an Oxford Diffraction Gemini A Ultra diffractometer. The structure was solved by direct methods. The semi-empirical absorption corrections were applied based on symmetry-equivalent and repeated data. The refinement gave a  $wR2$  of 0.0205 for all 2587 independent reflections and a conventional  $R1$  of 0.0824, for 1721 reflections with  $F^2 > 2\sigma$ . The residual electron density maximum and minimum were 1.24 and  $-0.87 \text{ e } \text{\AA}^{-3}$  respectively.

The hydrogen atoms were placed in geometrically calculated positions with  $U$  constrained to  $1.2 U_{\text{eq}}(\text{C})$  for aromatic hydrogen atoms and  $U$  constrained to  $1.5 U_{\text{eq}}(\text{C})$  for methyl hydrogen atoms. The ligands in the structure were disordered; with SIMU and DELU restraints being imposed for refinement. The full data of compound 25 can be found in Appendix 1.

## Structure Analysis

The asymmetric unit of compound 25 (figure 7.20) shows a half 1,2,4,5-benzenetetracarboxylate ligand completed by inversion symmetry around the centre of the aromatic ring, coordinated to one cobalt cation that is further coordinated to a 4,4'-bipyridine ligand and a terminal methanol. The cobalt cation forms a six-coordinate octahedron (figure 2.21) coordinating to the O(1) carboxylate oxygen of the O(1)-C(7)-O(2) carboxylate group forming the standard monodentate bond  $2.110(5) \text{ \AA}$ . The O(2) carboxylate oxygen coordinates to a symmetry equivalent cobalt cation Co(A) generated by an inversion centre  $2.375(4) \text{ \AA}$  away from the cobalt cation in the  $b$ -axis. The O(1)-C(7)-O(2) carboxylate group acts as a bidentate bridging group with the O(2) coordinating in the coplanar cis position to the symmetry equivalent O(1) oxygen; O(1)-Co-O(2A)  $91.73(19)^\circ$ . The remaining carboxylate group O(3)-C(8)-O(4) also coordinates to the symmetry equivalent cobalt cation cis to the Co-O(2) bond at O(2A)-Co(A)-O(3)  $85.00(2)^\circ$  and trans to the O(1) carboxylate group; this positions the cobalt cation between the two carboxylate groups. The methanol ligand completes the equatorial band of the carboxylates, coordinating cis to the O(1) oxygen and trans to the symmetry generated O(2A) oxygen effectively capping the node in the  $b$ -axis. The



remaining two axial coordination sites are occupied by a 4,4'-bipyridine ligand coordinating with the Co-N(1) 2.174(6) Å bond and its trans symmetry equivalent coordinates through the N(2) atom bridging two symmetry equivalent cobalt cations. The two pyridine aromatic rings are not coplanar, rotating by 59.00(7)° around the C(12)-C(17) single bond. This coordination motif forms the molecular building unit around the cobalt cation shown in figure 7.22. The inclusion of 4,4'-bipyridine in the reaction medium was intended to form connected columns between sheets of cobalt-1,2,4,5-benzenetetracarboxylates produced in compound 22. However the molecular building unit in figure 7.22 expands the structure into two dimensional sheets as the dinuclear cobalt units are capped by terminal methanol ligands, these are positioned on the same side of the building unit as the uncoordinated carboxylate oxygen O(4) preventing the connection of the sheets into three dimensions. In contrast the molecular building unit of compound 25 generates double layered sheets with the 4,4'-bipyridine expanding the sheet in the *c*-axis (figure 7.23).

The double layer 4,4'-bipyridines are linked by the 1,2,4,5-benzenetetracarboxylate ligands that form 'zigzag' chains that run along the *c*-axis and down the *a*-axis (figure 7.24). The sheets stack up the *b*-axis by forming hydrogen bonds between methanol OH and CH<sub>3</sub> groups with the O(3)-C(8)-O(4) carboxylate of an adjacent sheet; O(5)-H(5)⋯O(3E) 2.651(7) Å at 180° and C(9)-H(9A)⋯O(4E) 2.404(7) Å at 145.08(13)° (table 7.09). These hydrogen bonds form with the close proximity of the O(3)-C(8)-O(4) carboxylate group of the adjacent sheet that is stacked staggered with respect to the previous sheet due to the inversion symmetry (figure 7.25).

The regular columns of the 4,4'-bipyridine are joined at dinuclear nodes by chains of 1,2,4,5-benzenetetracarboxylate ligands forming a grid motif; however there are no available pores and no uncoordinated solvent molecules within compound 25. This occurs due to the coordination angles at the cobalt node, with the 1,2,4,5-benzenetetracarboxylate running almost parallel to the 4,4'-bipyridine ligands. This is further compounded by the close packing network of compound 25 that packs the sheets at an interplanar distance of 3.435(4) Å between the 4,4'-bipyridine ligands.

Further analysis of compound 25 was carried out using elemental analysis to determine the bulk purity of the compound, this produced the results C = 44.77 %, H =

3.59 % and N = 6.88 %. These are consistent with the calculated values from the single crystal data; C = 51.58 %, H = 3.49 % and N = 7.52 % showing that the synthesis route is producing a significantly pure compound.

Unfortunately the synthesis route using the H-Cell was not ideal as although adequate yields of compound 25 were produced the crystallisation times were in the region of 7-9 weeks, upon crystallisation the compound was extremely unstable, often degrading if removed from the original reaction medium preventing the acquisition of a powder X-ray diffraction pattern and thermostability profile. Compound 25 is one of only 14 transition metal, 4,4'-bipyridine and 1,2,4,5-benzenetetracarboxylate metal-organic frameworks reported in the database, with four compounds using cobalt as a cation (CSD Refcodes: ICAGID<sup>2</sup>, OGIHAO<sup>3</sup>, LASWEJ<sup>4</sup> and LASWIN<sup>4</sup>). Compounds ICAGID<sup>2</sup> and OGIHAO<sup>3</sup> form two dimensional sheets using octahedral cobalt cations. ICAGID<sup>2</sup> coordinates the 4,4'-bipyridine ligands cis to the partially deprotonated 1,2,4,5-benzenetetracarboxylate ligand with only two carboxylate groups coordinating to the cobalt cations. This forms a sheet structure capped by axial water ligands used to stack the sheets through hydrogen bonding as shown in figure 7.26.<sup>2</sup> The OGIHAO<sup>3</sup> compound forms double layer sheets with the 4,4-bipyridine coordinating cis to the bridging carboxylates of the 1,2,4,5-benzenetetracarboxylate ligand that coordinates two cobalt cations to form a dinuclear node similar to that presented in compound 25 (figure 7.27).<sup>3</sup> The sheets in OGIHAO<sup>3</sup> also stack in a staggered conformation with respect to the dinuclear cobalt nodes to allow the formation of hydrogen bonds between the axial water ligands and uncoordinated carboxylate oxygen atoms.<sup>3</sup> This packing motif is comparable to that of compound 25 that utilizes methanol ligands to hydrogen bond the sheets together, with bond lengths compared in table 7.10. The compounds LASWEJ and LASWIN<sup>4</sup> form three dimensional frameworks templated using DMF, compound LASWEJ<sup>4</sup> forms a structure with the double layer sheets of compound 25 and OGIHAO<sup>3</sup> (figure 7.27); combining them with additional 4,4'-bipyridine ligands to form the packing network observed in ICAGID<sup>2</sup> shown in figure 7.26.<sup>4</sup> These three dimensional open packing networks are the ideal target of these reactions, leading to a new phase of reactions that include DMF in the reaction media to aid the templating of the structure resulting in compound 26.

**Table 7.08: Selected Bond Lengths [Å] and Angles [°] for Compound 25**

Co–O(1)	2.110(5)	Co–O(2A)	2.055(5)
Co–O(3A)	2.138(5)	Co–O(5)	2.059(6)
Co–N(1)	2.174(6)	Co–N(2B)	2.171(6)
C(7)–O(2)	1.266(8)	C(7)–O(1)	1.239(9)
C(8)–O(4)	1.225(8)	C(8)–O(3)	1.293(9)
O(1)–Co–O(2A)	91.73(19)	O(1)–Co–O(3A)	171.21(18)
O(1)–Co–O(5)	89.6(2)	O(1)–Co–N(1)	85.6(2)
O(1)–Co–N(2B)	96.1(2)	Co–O(5)–C(9)	122.9(5)
Symmetry operations for equivalent atoms			
A $-x+1, -y+1, -z+1$ B $x-1, y, z+1$			

**Table 7.09: Selected Hydrogen bond Lengths [Å] and angles [°] for Compound 25**

D–H...A	d(D–H)	d(H...A)	d(D...A)	(DHA)
O(5)–H(5)...O(3E)	0.837(10)	1.814(13)	2.651(7)	180(10)
Symmetry operations for equivalent atoms				
E $x, y-1, z$				

**Table 7.10: Average bond length comparisons between Compound 25, ICAGID<sup>2</sup> and OGIHAO<sup>3</sup>**

Compound	Bond	Average Bond Length (Å)
Compound 25	Co–O (carboxylate)	2.079
Compound 25	Co–N (4,4-bipyridine)	2.172
ICAGID	Co–O (carboxylate)	2.077
ICAGID	Co–N (4,4-bipyridine)	2.168
OGIHAO	Co–O (carboxylate)	2.009
OGIHAO	Co–N (4,4-bipyridine)	2.149

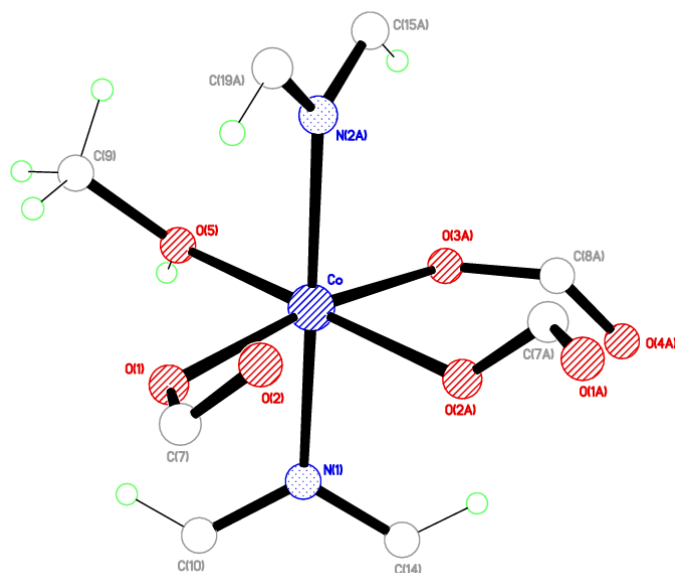


**Figure 7.21: Octahedral coordination environment of Co(1) in compound 25**

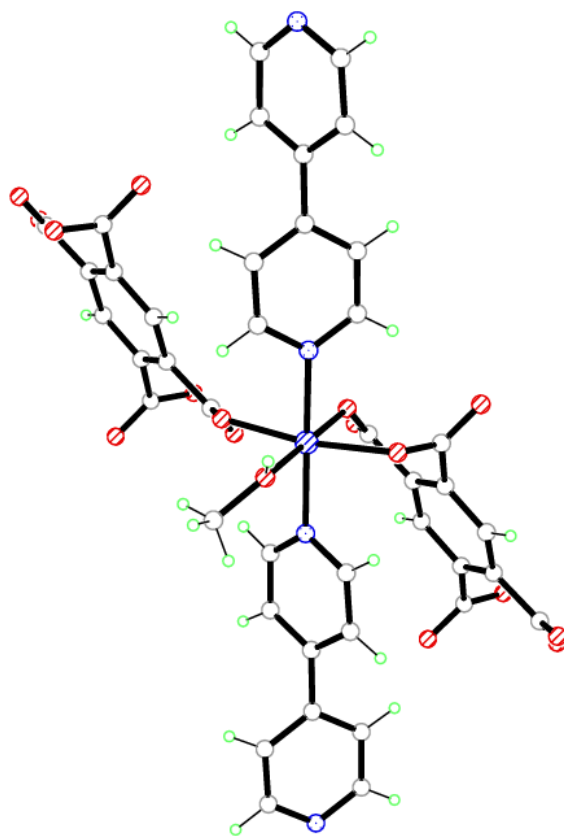


**Figure 7.22: Molecular building unit of Co(1) in compound 25**

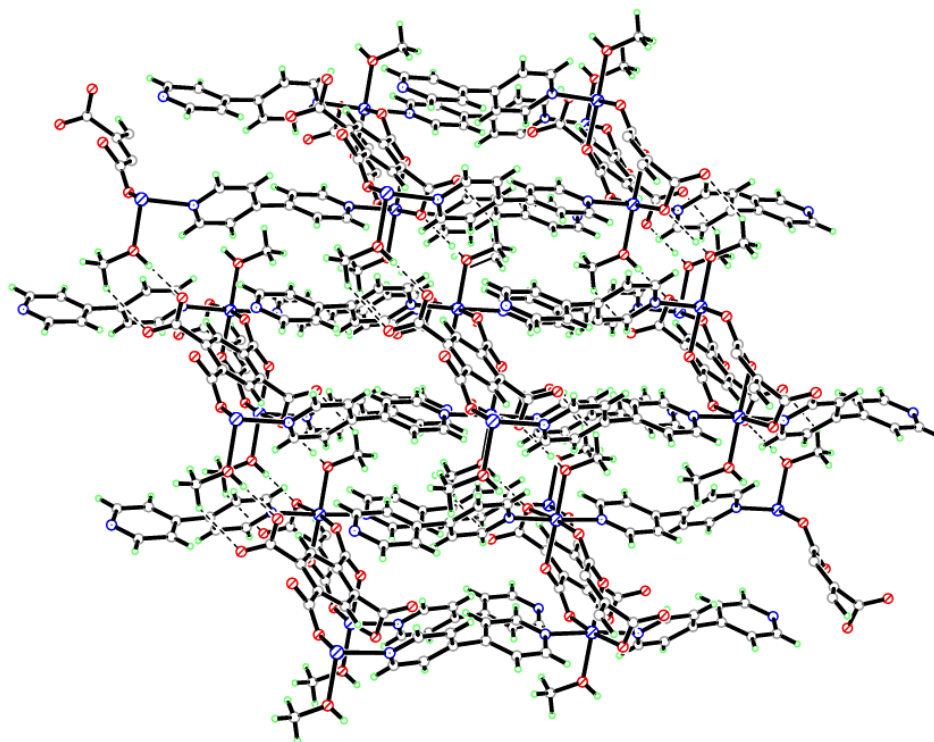


**Figure 7.23:** Two dimensional double layer sheet of compound 25 viewed down the *a*-axis

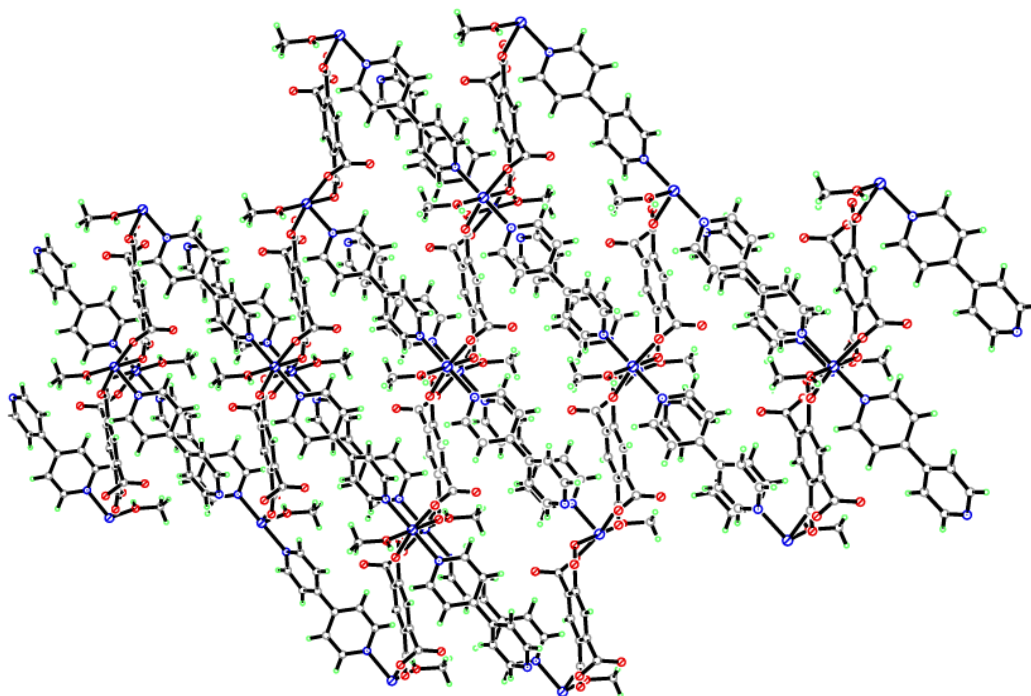


**Figure 7.24:** Two dimensional sheets connected by the 'zigzag' chains in compound 25 viewed down the *b*-axis

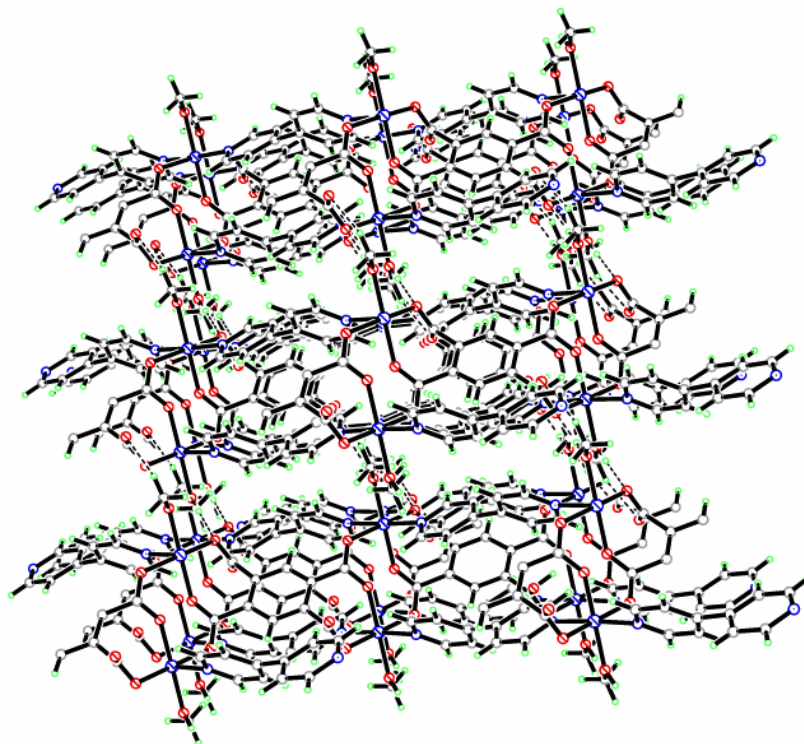


**Figure 7.25:** Three dimensional stacking of the double layer sheets of compound 25 viewed down the *c*-axis

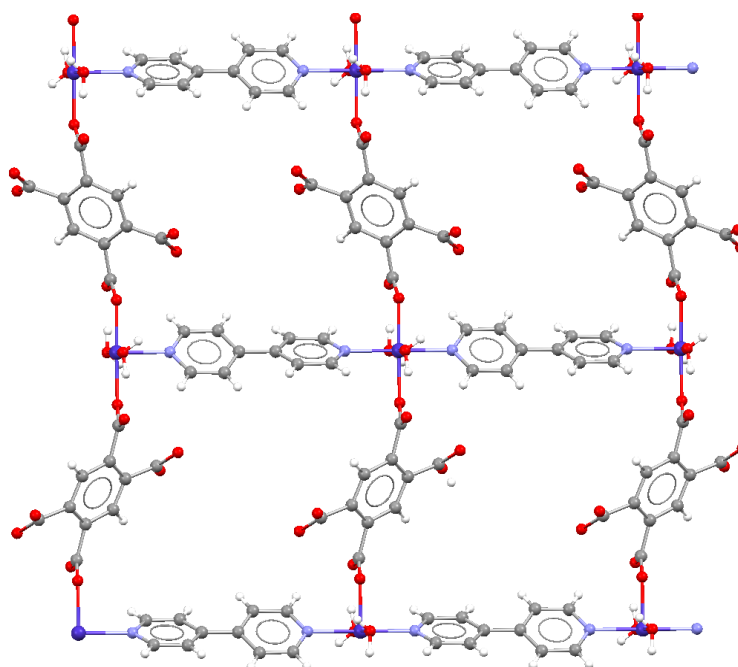


**Figure 7.26:** Two dimensional sheets of ICAGID viewed down the *a*-axis<sup>2</sup>

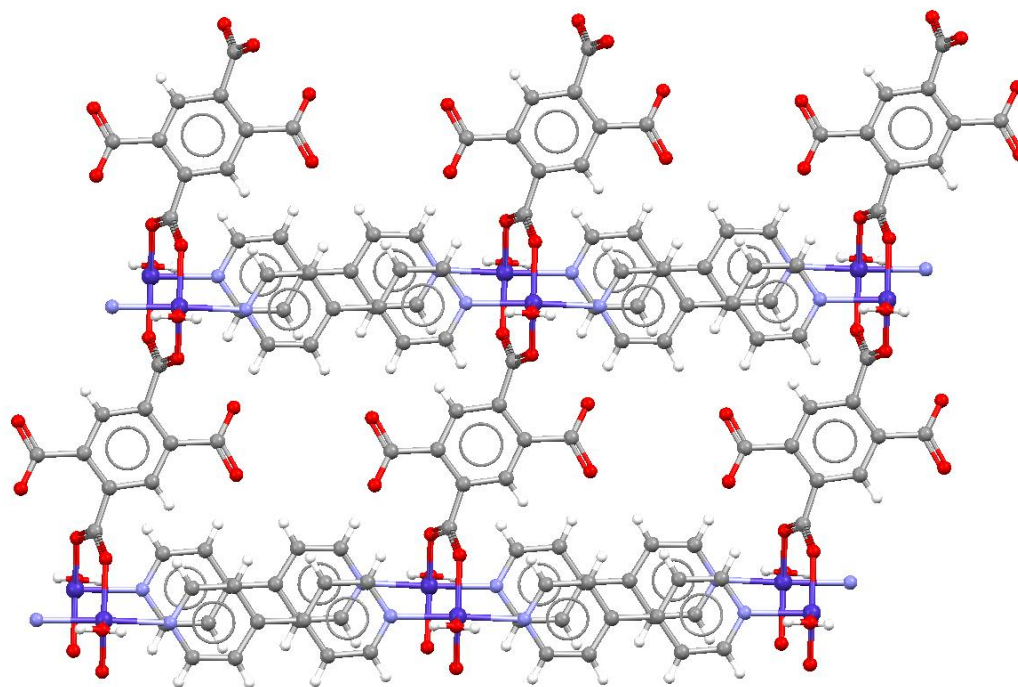


**Figure 7.27:** Two dimensional double layer sheets of OGIHAO viewed down the *b*-axis<sup>3</sup>

**Compound 26:**  $[\text{Ni}(\text{C}_{10}\text{H}_2\text{O}_8) (\text{C}_{10}\text{H}_8\text{N}_2)(\text{CH}_4\text{O})] \cdot \text{CH}_4\text{O} \cdot 2\text{C}_3\text{H}_7\text{NO}$



## Structure Determination

The data were collected at 150 K using molybdenum radiation on an Oxford Diffraction Gemini A Ultra diffractometer. The structure was solved by direct methods. The semi-empirical absorption corrections were applied based on symmetry-equivalent and repeated data. The refinement gave a  $wR2$  of 0.1163 for all 3249 independent reflections and a conventional  $R1$  of 0.0570, for 1723 reflections with  $F^2 > 2\sigma$ . The residual electron density maximum and minimum were 1.24 and  $-0.87 \text{ e } \text{\AA}^{-3}$  respectively, the high residual electron density is a result of the heavily disordered 4,4'-bipyridine ligands in compound 26, where it was not possible to model all the disorder.

The hydrogen atoms were placed in geometrically calculated positions with  $U$  constrained to  $1.2 U_{\text{eq}}(\text{C})$  for aromatic hydrogen atoms and  $U$  constrained to  $1.5 U_{\text{eq}}(\text{C})$  for methyl hydrogen atoms. The DMF and 4,4'-bipyridine ligands in the structure were disordered; with SIMU, DELU and FLAT restraints being imposed for refinement. The full data of compound 26 can be found in Appendix 1.

## Structure Analysis

The asymmetric unit of compound 26 (figure 7.28) shows a half 1,2,4,5-benzenetetracarboxylate ligand completed by inversion symmetry around the centre of the aromatic ring, coordinated to a nickel cation placed on a inversion symmetry centre further coordinated to half a 4,4'-bipyridine ligand that is completed by inversion symmetry. The nickel cation (Ni) forms a standard six-coordinate octahedral geometry (figure 7.29), coordinating to the O(1) carboxylate oxygen of the O(1)-C(7)-O(2) carboxylate group to form the monodentate bond Ni-O(1)  $2.061(2) \text{ \AA}$  with a symmetry equivalent coordinating in the trans coplanar position generated by inversion symmetry. The remaining coordination sites on the Ni cation are occupied by a terminal methanol and its coplanar trans symmetry equivalent coordinated in the cis position to the coplanar O(1)-C(7)-O(2) carboxylate group; forming a short intramolecular hydrogen bond to the uncoordinated O(2) carboxylate oxygen O(5)-H(5) $\cdots$ O(2A)  $2.560(4) \text{ \AA}$ . The last two coordination sites perpendicular to the carboxylate plane are filled by a half 4,4'-bipyridine ligand and its trans symmetry equivalent O(1)-Ni-N(1)  $90.84(11)^\circ$ . The

4,4'-bipyridine ligand is completed by inversion symmetry coordinating the aromatic rings through the C(12)-C(12A) bond to complete the molecular building unit shown in figure 7.30. The O(3)-C(8)-O(4) carboxylate group of the 1,2,4,5-benzenetetracarboxylate ligand is uncoordinated and consists of a carbon-oxygen double and single bond; C(8)-O(3) 1.327(5) Å and C(8)-O(4) 1.216(4) Å with O(3) protonated forming the O(3)-H(3) bond (table 7.11).

The lack of coordination from this carboxylate group to a nickel cation results in coplanar linear chains of Ni-1,2,4,5-benzenetetracarboxylate ligands forming down the *c*-axis. These are coordinated together by the 4,4'-bipyridine ligands in the *b*-axis to form sheets of 4,4' nets (figure 7.31) similar to those formed in compounds ICAGID<sup>2</sup> and LASWEJ<sup>4</sup>. The nets have dimensions 9.505(4) by 9.895(4) Å and contain two DMF molecules held in position by acting as hydrogen bond acceptors from the protonated carboxylate group; O(3)-H(3O)⋯O(6) 2.586(5) Å. The nets are also visible down the *b*-axis with a narrower entrance of 5.655(9) by 6.946(7) Å (figure 7.32).

The sheets stack parallel along the *a*-axis, however when compound 26 is viewed down the *c*-axis the sheets are staggered in the cell body diagonal by 4.553(2) Å with respect to the nickel cations (figure 7.33).

PLATON<sup>5</sup> confirms the presence of pores upon desolvation with a calculated pore volume 349.8 Å<sup>3</sup> per unit cell, corresponding to 44.4 %. These pores would be accessible down the crystallographic *a*-axis and *b*-axis of compound 26.

Thermogravimetric analysis of compound 26 was used to determine the thermostability upon desolvation of the compound producing the TGA plot shown in figure 7.34. The TGA stage 1 shows that desolvation of the compound begins at 75°C with the compound fully desolvated at 130°C with a mass loss of 2.15 mg (16.03 %) correlating to the calculated amount of DMF (16.83 %) in the single crystal structure of compound 26. The desolvated compound formed is semi-stable producing a plateau between 130-200°C with a significantly reduced rate of mass loss. The compound begins to fully degrade at 200°C when the terminal temperature of the metal-oxygen bonds is reached.

Elemental analysis was used to determine the bulk purity of compound 26 producing the results C = 46.82 %, H = 4.60 % and N = 7.96 %; these correlate with the

calculated values from the single crystal data of C = 49.6 %, H = 5.02 % and N = 8.27 % showing that the synthesis method is valid producing the pure compound.

Compound 26 shows how the reaction conditions can be tailored to produce structures templated around DMF, with slight alterations from the synthesis used for compound 25. The packing motif of the sheets is a 4,4' net that is indicative of the DMF template on the structural topology formation, present in all of LASWEJ, LASWIN<sup>4</sup> and compound 26. The potential applications of compound 26 resulted in several scale-up reactions, with little success in producing bulk samples of compound 26.

**Table 7.11: Selected Bond Lengths [ $\text{\AA}$ ] and Angles [ $^\circ$ ] for Compound 26**

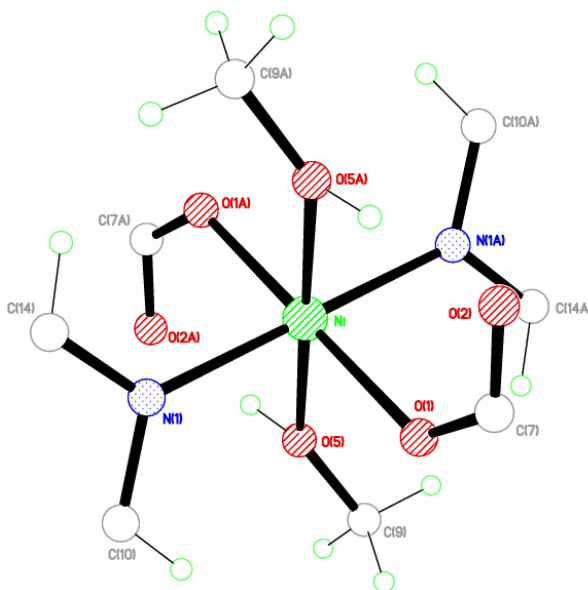
Ni–O(1)	2.061(2)	Ni–O(5)	2.088(3)
Ni–N(1)	2.082(3)	Co–O(5)	2.059(6)
Co–N(1)	2.174(6)	C(7)–O(1)	1.256(4)
C(7)–O(2)	1.246(5)	C(8)–O(3)	1.327(5)
C(8)–O(4)	1.216(4)		
O(1)–Ni–O(1A)	180.0	O(1)–Ni–O(5)	88.63(11)
O(1)–Ni–N(1)	90.84(11)	Ni–O(1)–C(7)	126.7(3)

Symmetry operations for equivalent atoms

A  $-x+1, -y+1, -z+1$ **Table 7.12: Selected Hydrogen bond Lengths [ $\text{\AA}$ ] and angles [ $^\circ$ ] for Compound 26**

D–H...A	d(D–H)	d(H...A)	d(D...A)	(DHA)
O(3)–H(3O)...O(6)	0.71(7)	1.88(7)	2.586(5)	171(8)
O(5)–H(5)...O(2A)	0.85(6)	1.72(6)	2.560(4)	173(6)

Symmetry operations for equivalent atoms

A  $-x+1, -y+1, -z+1$ **Figure 7.29: Octahedral coordination environment of Ni(1) in compound 26**

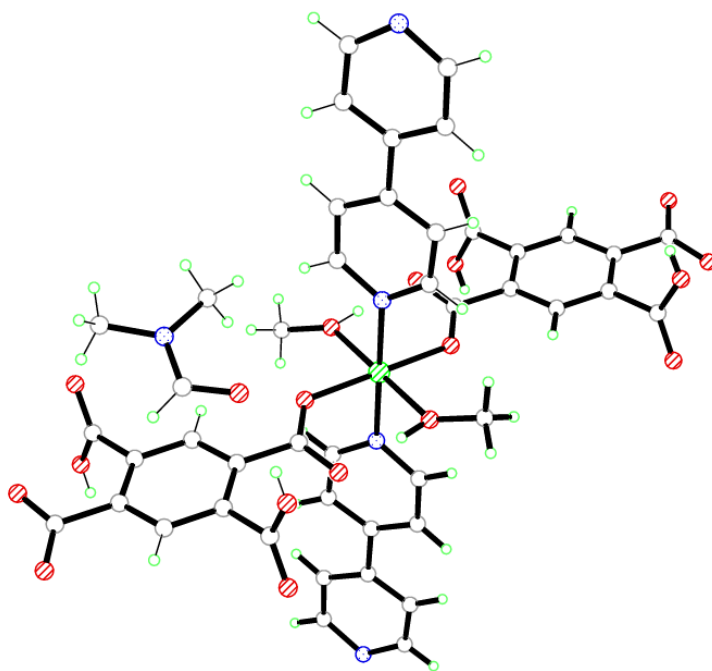


**Figure 7.30: Molecular building unit of Ni(1) in compound 26**

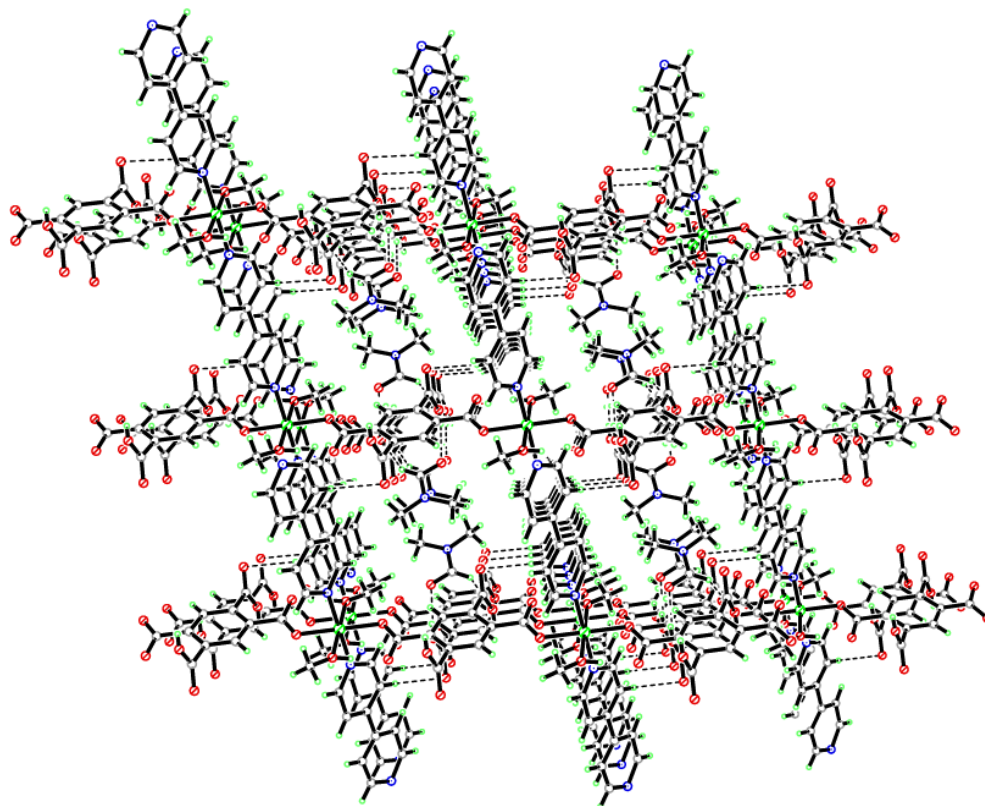


**Figure 7.31: Two dimensional 4,4' sheet in compound 26 viewed down the *a*-axis**

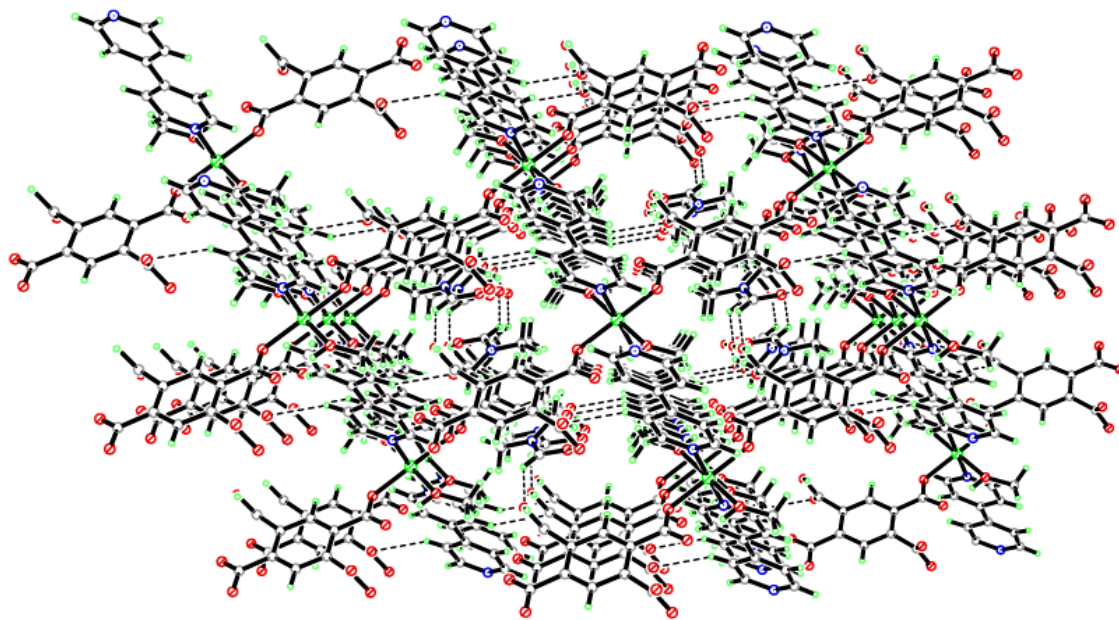


**Figure 7.32:** Two dimensional 4,4' sheet in compound 26 viewed down the *b*-axis

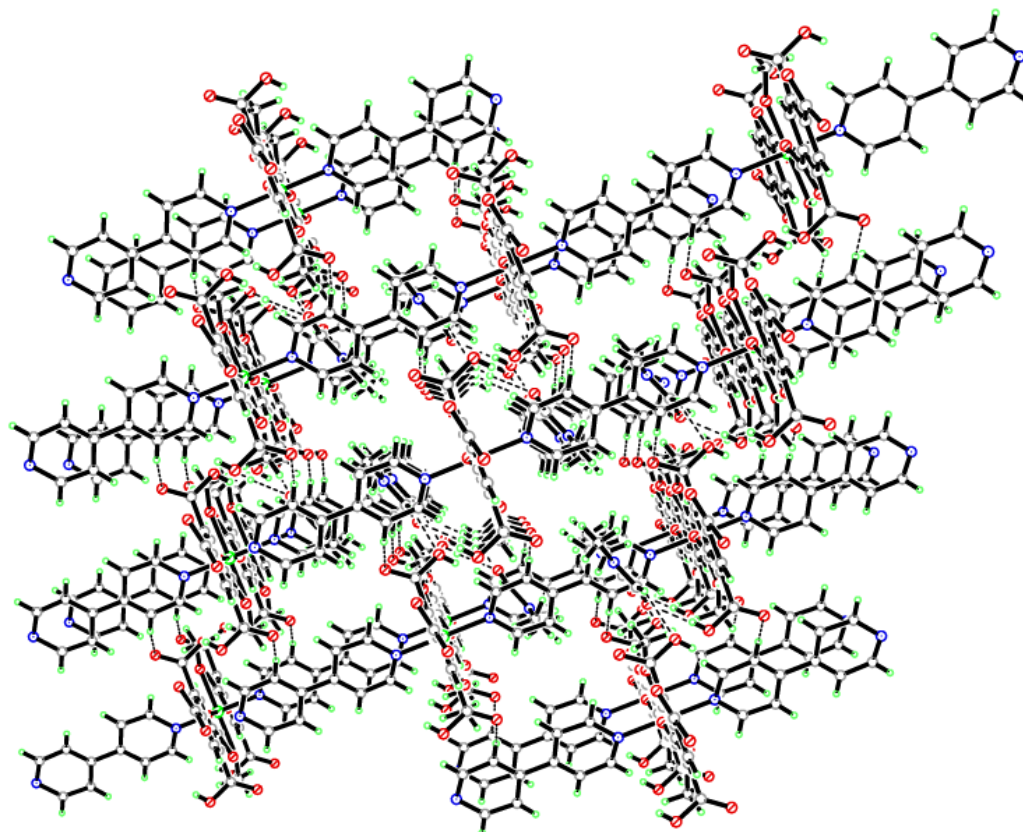


**Figure 7.33:** Three dimensional staggered stacking of the sheets of compound 26 viewed down the *c*-axis

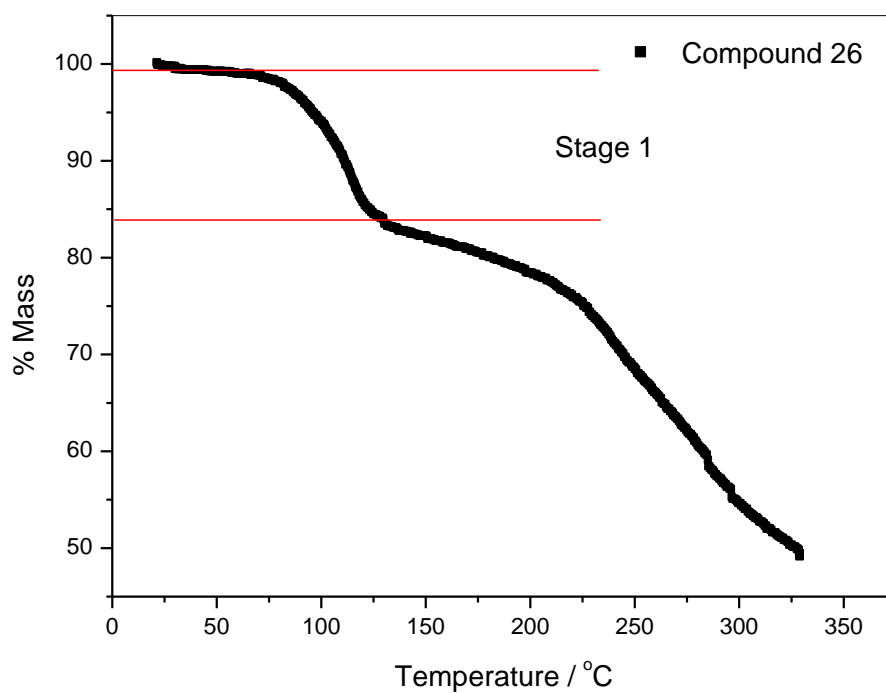
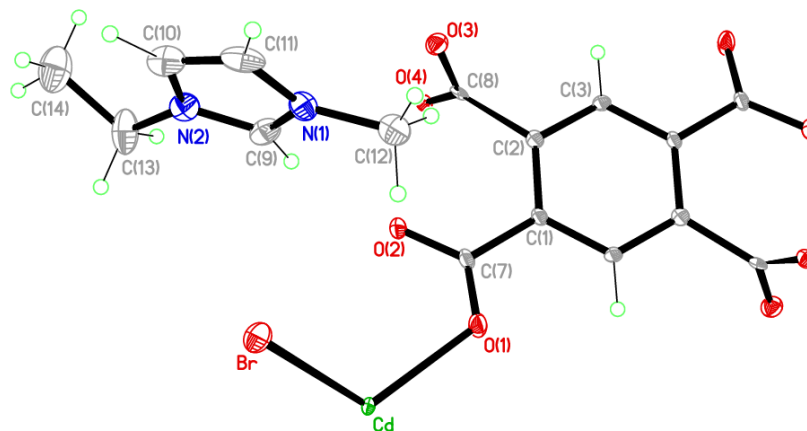


**Figure 7.34: Thermogravimetric analysis plot of compound 26**

**Compound 27:**  $[\text{Cd}_2(\text{C}_{10}\text{H}_2\text{O}_8)_2(\text{Br})_2]^{-2} \cdot 2\text{C}_6\text{H}_{11}\text{N}_2^+$



Chemical formula (total)	$\text{C}_{22}\text{H}_{24}\text{Br}_2\text{Cd}_2\text{N}_4\text{O}_8$	
Formula weight	857.07	
Temperature	150(2) K	
Radiation, wavelength	MoK $\alpha$ , 0.71073 Å	
Crystal system, space group	triclinic, $P\bar{1}$	
Unit cell parameters	$a = 7.4530(5)$ Å	$\alpha = 99.644(8)^\circ$
	$b = 9.5262(10)$ Å	$\beta = 98.632(6)^\circ$
	$c = 10.6307(9)$ Å	$\gamma = 112.789(8)^\circ$
Cell volume	$666.55(10)$ Å <sup>3</sup>	
Z	1	
Crystal colour and size	colourless, $0.22 \times 0.10 \times 0.01$ mm <sup>3</sup>	
Final $R$ indices [ $F^2 > 2\sigma$ ]	$R1 = 0.0312$	
$R$ indices (all data)	$wR2 = 0.0811$	
Largest diff. peak and hole	1.24 and $-0.73$ e Å <sup>-3</sup>	

**Figure 7.35: Asymmetric Unit of Compound 27 all unique atoms labelled, additional atoms added to complete ligands.**

### Synthesis

$\text{Cd}(\text{NO}_3)_2 \cdot 4\text{H}_2\text{O}$  (0.1 g, 0.33 mmol) and 1,2,4,5-benzenetetracarboxylic acid (0.043 g, 0.17 mmol) were added to a reaction mixture of 1-ethyl-3-methylimidazolium bromide (0.19 g, 1 mmol). This was placed into a 20mL Teflon-lined bomb and heated to 200°C for 7 days. The vessel was then cooled back down to room temperature at a rate of 0.1°C / min and allowed to stand for 2 hours before colourless plate crystals were retrieved from the vessel.



## Structure Determination

The data were collected at 150 K using molybdenum radiation on an Oxford Diffraction Gemini A Ultra diffractometer. The structure was solved by direct methods. The semi-empirical absorption corrections were applied based on symmetry-equivalent and repeated data. The refinement gave a  $wR2$  of 0.0811 for all 2354 independent reflections and a conventional  $R1$  of 0.0312, for 1859 reflections with  $F^2 > 2\sigma$ . The residual electron density maximum and minimum were 1.24 and  $-0.73 \text{ e } \text{\AA}^{-3}$  respectively.

The hydrogen atoms were placed in geometrically calculated positions with  $U$  constrained to  $1.2 U_{\text{eq}}(\text{C})$  for aromatic hydrogen atoms and  $U$  constrained to  $1.5 U_{\text{eq}}(\text{C})$  for the methyl hydrogen atoms. The 1,2,4,5-benzenetetracarboxylate ligand in the structure was slightly disordered and refined with SIMU and DELU restraints. The full data of compound 27 can be found in Appendix 1.

## Structure Analysis

The asymmetric unit of compound 27 (figure 7.35) shows a templated 1-ethyl-3-methylimidazolium cation along with half a 1,2,4,5-benzenetetracarboxylate ligand completed by inversion symmetry around the centre of its aromatic ring, coordinating to a six-coordinate distorted octahedral cadmium cation forming an anionic framework templated around an uncoordinated cation (figure 7.36).

The cadmium cation is coordinated by four carboxylate groups from a 1,2,4,5-benzenetetracarboxylate ligand and two symmetry equivalent ligands, with additional coordination to a bromide anion. The bromine anion coordinates to the Cd cation to form the elongated Cd-Br  $2.5452(8) \text{ \AA}$  bond. The large steric bulk of the bromine anion induces the distortion in the geometry of the cadmium cation with the O(1)-C(7)-O(2) carboxylate group coordinating at an angle O(1)-Cd-Br  $115.17(10)^\circ$ , significantly higher than an idealised  $90^\circ$  cis coordination in an octahedral node. The symmetry equivalent O(1A)-C(7A)-O(2A) carboxylate group coordinates providing a bridge between two symmetry equivalent cadmium cations with the O(2A) oxygen coordinating cis to the O(1) and Br atoms; O(1)-Cd-O(2A)  $90.15(14)^\circ$  and O(2A)-Cd-Br  $107.74(10)^\circ$ . The O(3A)-C(8A)-O(4A) carboxylate of the symmetry equivalent 1,2,4,5-

benzenetetracarboxylate also coordinates to the cadmium cation, bridging the cation between the two carboxylate groups with a bite angle of O(2A)-Cd-O(4A) 77.48°. The remaining two coordination sites are occupied by a bidentate O(3B)-C(8B)-O(4B) carboxylate group from a second symmetry equivalent 1,2,4,5-benzenetetracarboxylate that forms the slightly elongated bonds; Cd-O(3B) 2.440(4) Å and Cd-O(4B) 2.335(3) Å (table 7.13). These bridging symmetry equivalent ligands generate the molecular building unit shown in figure 7.37 that is templated around a 1-ethyl-3-methylimidazolium cation. The bridging motif of the carboxylate groups creates chains of dimeric cadmium cations that run down the *a*-axis with the bromine anions pointing out away from the chains at 128.65(13)° with respect to the aromatic plane of the bridging 1,2,4,5-benzenetetracarboxylate ligands. These carboxylate ligands also form chains that run parallel to the cadmium cations down the *a*-axis and link each chain along the *b*-axis creating a step-wise sheet (figure 7.38), with each coordinated chain raised by 1.275(2) Å in the *c*-axis as the sheet progresses down the *b*-axis.

The sheets stack along the *c*-axis with the bromine anions pointing out at 128.65(13)° from each 'step' in the sheet. The bromine anion is positioned between two coplanar 1-ethyl-3-methylimidazolium cations at a distance of 3.443(5) Å to each aromatic ring. Additional 1-ethyl-3-methylimidazolium cations are placed between these two coplanar symmetry equivalents, rotated by 180° in the *c*-axis to maximise hydrogen bonding between the bromine anion and the methyl hydrogens; C(10)-H(10)⋯Br 2.939(5) Å and C(12)-H(12A) ⋯Br 3.192(7) Å (figure 7.39).

The bulk of the sample of compound 27 was analysed using elemental analysis to determine the purity of the sample. The elemental analysis produced the results C = 28.09 %, H = 3.61 % and N = 8.67 % that correlate with the calculated values of C = 30.80 %, H = 2.80 % and N = 6.53 % from the single crystal data. There is a slight increase in the carbon and nitrogen quantities in the sample of compound 27 which can be attributed to residual 1-ethyl-3-methylimidazolium bromide that was used as the reaction medium and templating agent. The 1-ethyl-3-methylimidazolium bromide was difficult to remove from the compound, requiring several washes with water and ethyl acetate before the compound was then dried.

A similar compound to compound 27 was reported by Huang *et al.* (CSD Refcode: POLPIQ).<sup>6</sup> This compound has the same metal and ligand as compound 27 and is also templated around the 1-ethyl-3-methylimidazolium cations. POLPIQ<sup>6</sup> forms similar two dimensional sheets with dimeric cadmium cations packed together with a different orientation of the 1-ethyl-3-methylimidazolium cations.<sup>6</sup> Compound 27 and POLPIQ<sup>6</sup> have similar bond lengths with the cadmium-oxygen and cadmium-bromine bonds differing slightly (table 7.14).

The interesting nature of the ionic liquids to act as both solvent and template with possibilities of generating previously unobtainable anionic frameworks, resulted in further investigations to create structural analogues of compound 27. These reactions were designed to investigate the effect of alkyl chain length on packing motifs and topology formation due to the compression tension differences in the respective ionic liquids. This was coupled with the incorporation of mineralising agents to increase the yields of metal-organic frameworks and improve purity of the bulk sample with the sodium or potassium cations coordinating to excess bromine anions. Additional features of the mineralising agents that proved advantageous were observed in compounds 28 and 29; with the cations coordinating into the structures to add additional nodes with unusual geometries for coordination by linkers. The incorporation of mineralising agents into the ionothermal reactions resulted in the synthesis of compounds 30 and 31.

**Table 7.13: Selected Bond Lengths [Å] and Angles [°] for Compound 27**

Cd–Br	2.5452(8)	Cd–O(1)	2.255(4)
Cd–O(2A)	2.275(4)	Cd–O(3B)	2.440(4)
Cd–O(4B)	2.335(3)	Cd–O(4A)	2.488(3)
C(7)–O(1)	1.261(6)	C(7)–O(2)	1.268(6)
C(8)–O(3)	1.242(6)	C(8)–O(4)	1.274(6)
Br–Cd–O(1)	115.17(10)	Br–Cd–O(2A)	107.74(10)
Br–Cd–O(3B)	102.85(9)	Br–Cd–O(4B)	151.21(9)
O(1)–Cd–O(3B)	81.78(13)	O(1)–Cd–O(2A)	90.15(14)
O(1)–Cd–O(4B)	82.43(13)	O(1)–Cd–O(4A)	149.73(13)
Symmetry operations for equivalent atoms			
A $-x+1, -y+1, -z$ B $x-1, y, z$			

**Table 7.14: Bond length comparisons between Compound 27 and POLPIQ<sup>6</sup>**

Compound	Bond	Bond Length (Å)
Compound 27	Cd–Br	2.545(8)
Compound 27	Cd–O(1)	2.255(4)
Compound 27	Cd–O(2)	2.275(4)
Compound 27	Cd–O(3)	2.440(4)
Compound 27	Cd–O(4)	2.335(3)
POLPIQ	Cd–Br	2.544(6)
POLPIQ	Cd–O(1)	2.339(3)
POLPIQ	Cd–O(2)	2.452(4)
POLPIQ	Cd–O(3)	2.577(4)
POLPIQ	Cd–O(4)	2.540(3)



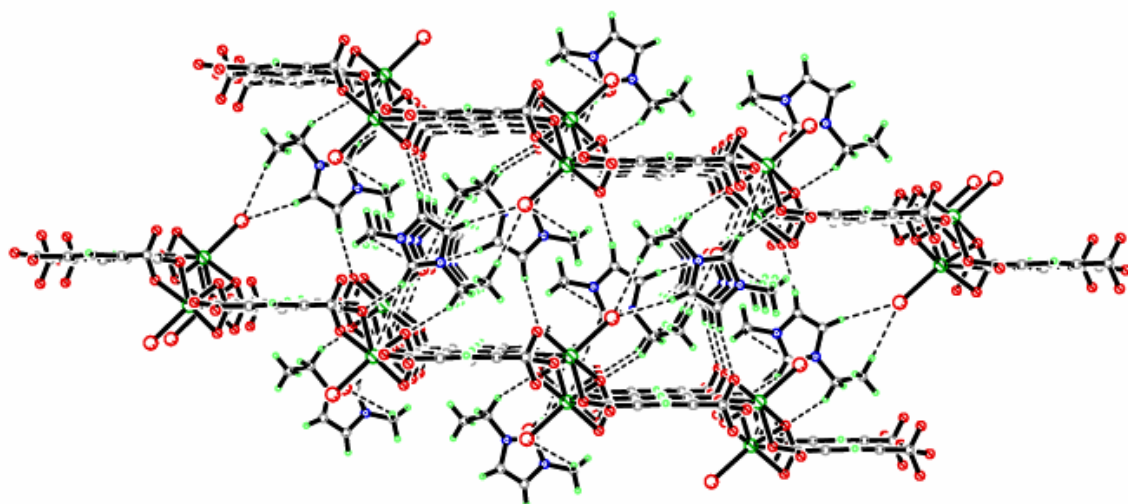


**Figure 7.38:** Packing of the two dimensional stepped sheet in compound 27 viewed down the *a*-axis

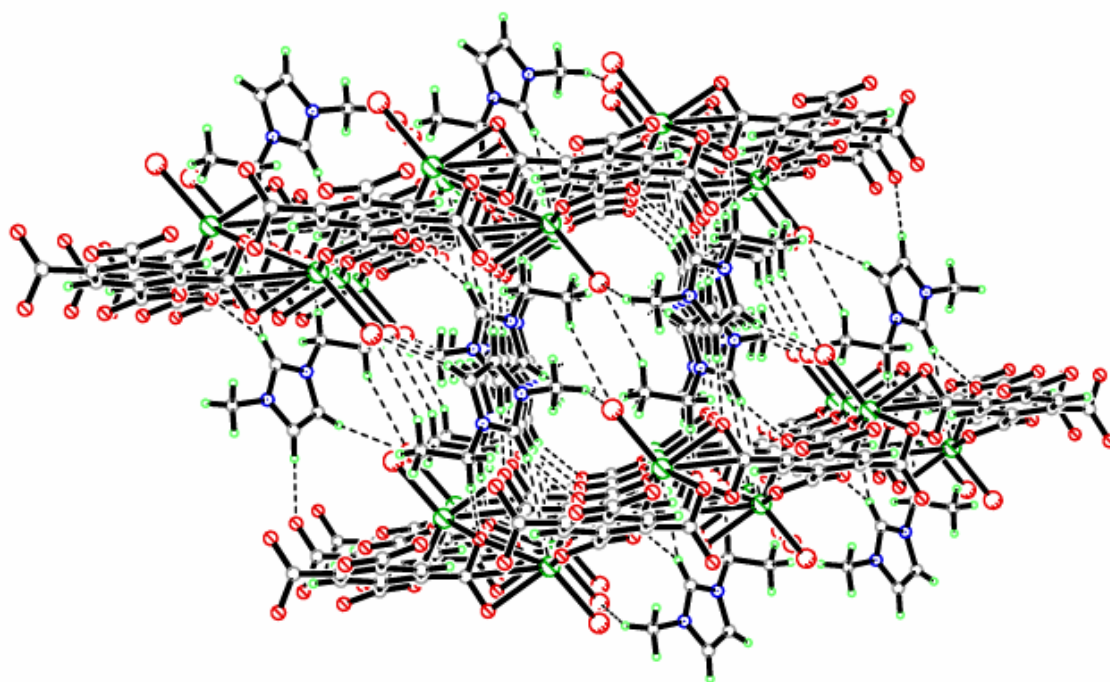
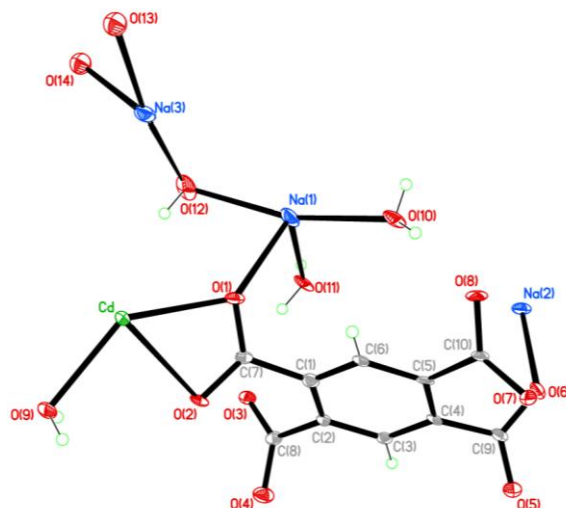


**Figure 7.39:** Two dimensional packing and hydrogen bonding of the 1-ethyl-3-methylimidazolium cations to the coordinated bromines of compound 27 viewed down the *b*-axis

**Compound 28:**  $[\text{CdNa}_2(\text{C}_{10}\text{H}_2\text{O}_8)(\text{H}_2\text{O})_5]$



Chemical formula (total)	$\text{C}_{10}\text{H}_{12}\text{CdNa}_2\text{O}_{13}$
Formula weight	498.58
Temperature	150(2) K
Radiation, wavelength	MoK $\alpha$ , 0.71073 Å
Crystal system, space group	monoclinic, $P2_1/c$
Unit cell parameters	$a = 6.3204(6)$ Å $b = 13.1566(15)$ Å $c = 18.349(3)$ Å $\beta = 93.103(11)^\circ$
Cell volume	$1523.6(3)$ Å <sup>3</sup>
Z	4
Crystal colour and size	colourless, $0.50 \times 0.05 \times 0.05$ mm <sup>3</sup>
Final $R$ indices [ $F^2 > 2\sigma$ ]	$R1 = 0.0415$
$R$ indices (all data)	$wR2 = 0.0801$
Largest diff. peak and hole	1.06 and $-0.73$ e Å <sup>-3</sup>

**Figure 7.40:** Asymmetric Unit of Compound 28 all unique atoms labelled, additional atoms added to complete ligands.

**Synthesis**

$\text{Cd}(\text{NO}_3)_2 \cdot 4\text{H}_2\text{O}$  (0.1 g, 0.33 mmol) in water (10 mL) and 0.5 mL of a solution of 1,2,4,5-benzenetetracarboxylic acid (0.043 g, 0.17 mmol) in water (10 mL) were placed on top of a 5 % tetramethoxysilane gel primed with sodium hydroxide (0.159 g, 4 mmol) instead a sample tube. The tube was covered and left until crystallisation was complete. After one week, colourless needle crystals formed.

## Structure Determination

The data were collected at 150 K using molybdenum radiation on an Oxford Diffraction Gemini A Ultra diffractometer. The structure was solved by direct methods. The semi-empirical absorption corrections were applied based on symmetry-equivalent and repeated data. The refinement gave a  $wR2$  of 0.0801 for all 2699 independent reflections and a conventional  $R1$  of 0.0415, for 1640 reflections with  $F^2 > 2\sigma$ . The residual electron density maximum and minimum were 1.06 and  $-0.73 \text{ e } \text{\AA}^{-3}$  respectively.

The hydrogen atoms were placed in geometrically calculated positions with  $U$  constrained to  $1.2 U_{\text{eq}}(\text{C})$  for aromatic hydrogen atoms and  $U$  constrained to  $1.5 U_{\text{eq}}(\text{C})$  for the methyl hydrogen atoms. The 1,2,4,5-benzenetetracarboxylate ligand in the structure was slightly disordered and refined with SIMU and DELU restraints. The full data of compound 28 can be found in Appendix 1.

## Structure Analysis

The asymmetric unit of compound 28 (figure 7.40) shows a complete 1,2,4,5-benzenetetracarboxylate ligand coordinating to one cadmium cation and three sodium cations in different coordination geometries in this polymeric compound. The cadmium forms a seven-coordinate pentagonal bipyramidal geometry, whilst the sodium Na(1) and Na(2) cations form six-coordinate distorted octahedral geometries with Na(2) positioned on a inversion centre and the remaining Na(3) cation forms a five-coordinate trigonal bipyramidal geometry.

The 1,2,4,5-benzenetetracarboxylate ligand is fully deprotonated with the delocalised carboxylate groups acting as multidentate coordination groups, coordinating through each carboxylate oxygen. The O(1)-C(7)-O(2) carboxylate coordinates to the cadmium cation through both oxygen atoms forming a bidentate coordination with a bite angle of O(1)-Cd-O(2)  $55.29(15)^\circ$ . The O(3)-C(8)-O(4) carboxylate group coordinates to a symmetry equivalent cadmium cation cis to the O(1) oxygen; O(1)-Cd-O(3A)  $79.39(14)^\circ$  with the shortest Cd-O bond in compound 28 of Cd-O(3A)  $2.290(14) \text{ \AA}$  (table 7.15). The O(5)-C(9)-O(6) carboxylate groups coordinates in a similar motif to the C(1)-C(7)-O(2) carboxylate with a bidentate coordination by the O(5) and O(6)



atoms forming the bite angle  $53.69(15)^\circ$  trans to the O(1)-C(7)-O(2) group. The remaining O(7)-C(10)-O(8) also coordinates to a symmetry equivalent cadmium cation through the monodentate Cd-O(7C) bond that coordinates in the cis position to the O(1) oxygen at  $81.87(15)^\circ$ . The cadmium cations coordination is completed by a terminal water molecule O(9) that coordinates cis to the O(1) and O(6) oxygens forming the coplanar Cd-O(9) 2.367(5) Å bond (figure 7.41).

The 1,2,4,5-benzenetetracarboxylate links the cadmium cations together to form a ‘zigzag’ sheet that runs down the *a*-axis and along the *c*-axis, the sheets are stacked in the *b*-axis with staggering between each sheet along the *a*-axis of 4.903(4) Å with respect to the cadmium cations. The carboxylates O(1)-C(7)-O(2) and O(5A)-C(9A)-O(6A) are coordinated coplanar; however the aromatic ring twists between each set of cadmium cations around the C(4)-C(9) bond by  $79.92(5)^\circ$  creating the ‘zigzag’ sheet motif. The sheets are coordinated together in the *b*-axis by chains of sodium cations that run  $[\text{Na}(1)\text{-Na}(3)\text{-Na}(3)\text{-Na}(1)\text{-Na}(2)\cdots]_n$  down the *c*-axis parallel to the 1,2,4,5-benzenetetracarboxylate sheets to form a three dimensional framework with the building unit shown in figure 7.42. The sodium cations are bridged together by the carboxylate groups of the 1,2,4,5-benzenetetracarboxylate ligands, with the O(1)-C(7)-O(2) group coordinating to two Na(1) cations with bite angles to the coordinated Cd cation of Cd-O(1)-Na(1)  $136.7(2)^\circ$  and Cd-O(2)-Na(1I)  $126.41(19)^\circ$ . The Na(1I) cation is further bridged by the O(3)-C(8)-O(4) carboxylate group that coordinates via the O(4) carboxylate oxygen forming the O(2)-Na(1I)-O(4) bridge at  $87.02(15)^\circ$ . The O(4) carboxylate oxygen also bridges to a Na(3) cation at Na(1)-O(4)-Na(3)  $94.38(2)^\circ$ . A second Na(3) cation generated by inversion symmetry is coordinated to its symmetry equivalent through the bridging water molecules O(13) and O(14). It is further coordinated to the O(5) oxygen of the O(5)-C(9)-O(6) carboxylate group forming a bite angle with the coordinated cadmium cation of Cd-O(5)-Na(3)  $129.4(2)^\circ$ . The O(6) carboxylate oxygen also bridges the cadmium cation to a Na(2) cation with the bite angle  $97.61(15)^\circ$ . The remaining O(7)-C(10)-O(8) carboxylate group also bridges a cadmium cation and the Na(2) cation forming a monodentate bond to the Cd cation, Cd-O(7) and a monodentate bond to the Na(2) cation Na(2)-O(8) to form a traditional carboxylate bridge. The combination of the bridged sodium cations and the sheets of

1,2,4,5-benzenetetracarboxylate-cadmium creates the three dimensional framework shown in figure 7.43.

The bulk sample of compound 28 was analysed using powder X-ray diffraction and elemental analysis after the sample was removed from the silica gel, washed then dried for 24 hours. The elemental analysis produced results of C = 3.17 %, H = 8.48 % and N = 0.028 %. These results are not consistent with the calculated values from the single crystal data of C = 24.06 %, H = 2.4 % and N = 0 %. The drastic difference in results is a consequence of the failure to remove all the silica gel from the sample which alters the mass calculations. A similar problem is encountered with the powder X-ray diffraction pattern (figure 7.44) that shows peaks at 10, 12.76, 16.72, 18.32, 19.31 and 21.43 2-Theta are consistent with the predicted powder diffraction pattern; however peaks present at 23-25 and 30-31 2 Theta are inconsistent indicating impurities are present in the sample. An underlying problem with compound 28 is the synthesis technique, although it provides an ideal platform for mineralising and deprotonating reactions, it produces impure and unusable products that cannot be separated fully from the silica gel.

There are similar structures in the CSD with nine structures containing transition metals, 1,2,4,5-benzenetetracarboxylate ligands and sodium cations. The compound BORLAW02 prepared by Niu *et al.*<sup>7</sup> shows a similar 'zigzag' sheet motif of cobalt cations of octahedral geometries connected by 1,2,4,5-benzenetetracarboxylate ligands. These are further coordinated by sodium cations that form chains down the *c*-axis connecting the sheets together. The octahedral geometry of the cobalt cations produces a different packing motif to that of compound 28; however both structures have comparable bond lengths (table 7.16).

**Table 7.15: Selected Bond Lengths [ $\text{\AA}$ ] and Angles [ $^\circ$ ] for Compound 28**

Cd–O(1)	2.383(4)	Cd–O(2)	2.392(4)
Cd–O(3A)	2.290(4)	Cd–O(5B)	2.533(5)
Cd–O(6B)	2.327(4)	Cd–O(7C)	2.305(4)
Cd–O(9)	2.367(5)	Na(1)–O(1)	2.385(5)
Na(1)–O(2D)	2.386(5)	Na(1)–O(4D)	2.748(5)
Na(1)–O(10)	2.394(5)	Na(1)–O(11)	2.416(5)
Na(1)–O(12)	2.443(6)	Na(2)–O(6)	2.356(4)
Na(2)–O(6E)	2.356(4)	Na(2)–O(8F)	2.246(4)
Na(2)–O(9H)	2.414(4)	Na(2)–O(9D)	2.414(4)
Na(3)–O(4D)	2.387(7)	Na(3)–O(5B)	2.298(7)
Na(3)–O(12)	2.231(7)	Na(3)–O(13)	2.347(12)
Na(3)–O(14)	2.460(11)	C(7)–O(1)	1.248(7)
C(7)–O(2)	1.273(7)	C(8)–O(3)	1.250(7)
C(8)–O(4)	1.272(8)	C(9)–O(5)	1.250(7)
C(9)–O(6)	1.265(8)	C(10)–O(7)	1.270(7)
C(10)–O(8)	1.238(7)		
O(1)–Cd–O(2)	55.29(15)	O(1)–Cd–O(3A)	79.39(14)
O(1)–Cd–O(5B)	93.06(14)	O(1)–Cd–O(6B)	144.41(15)
O(1)–Cd–O(7C)	81.87(15)	O(1)–Cd–O(9)	136.75(14)
Cd–O(1)–C(7)	91.2(4)	Cd–O(2)–C(7)	90.2(4)
Cd–O(3)–C(8)	133.2(4)	Cd–O(5)–C(9)	87.1(4)
Cd–O(7)–C(10)	116.8(4)	Cd–O(6)–C(9)	96.2(4)
Cd–O(1)–Na(1)	136.7(2)	Cd–O(2)–Na(1I)	126.41(19)
Na(1I)–O(4)–Na(3I)	94.8(2)	Cd–O(5)–Na(3H)	129.4(2)
Cd–O(6)–Na(2)	97.61(15)	Cd–O(9)–Na(2I)	94.99(16)

Symmetry operations for equivalent atoms

A  $x-1, y, z$  B  $x-1, -y+1/2, z-1/2$  C  $x, -y+1/2, z-1/2$ D  $-x+1, y+1/2, -z+1/2$  E  $-x+2, -y+1, -z+1$  F  $-x+1, -y+1, -z+1$ G  $x+1, y, z$  H  $x+1, -y+1/2, z+1/2$  I  $-x+1, y-1/2, -z+1/2$ **Table 7.16: Average bond length comparisons between Compound 28 and BORLAW02<sup>7</sup>**

Compound	Bond	Average bond Length ( $\text{\AA}$ )
Compound 28	Cd–O (carboxylate)	2.333
Compound 28	Na–O (carboxylate)	2.403
BORLAW02	Co–O (carboxylate)	2.118
BORLAW02	Na–O (carboxylate)	2.437

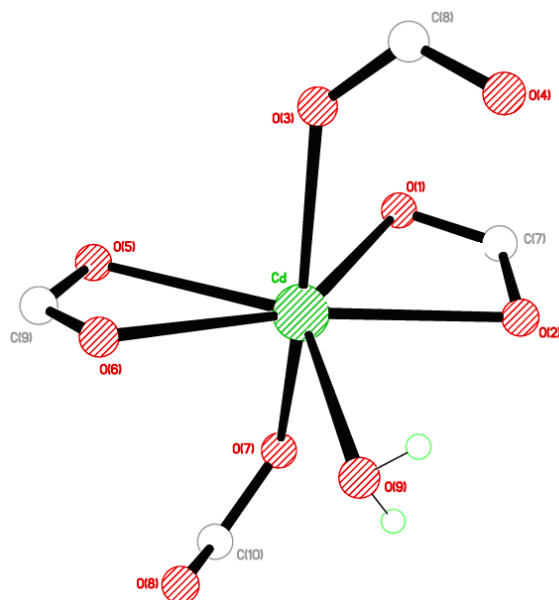


**Figure 7.41: Octahedral coordination environment of Cd(1) in compound 28**

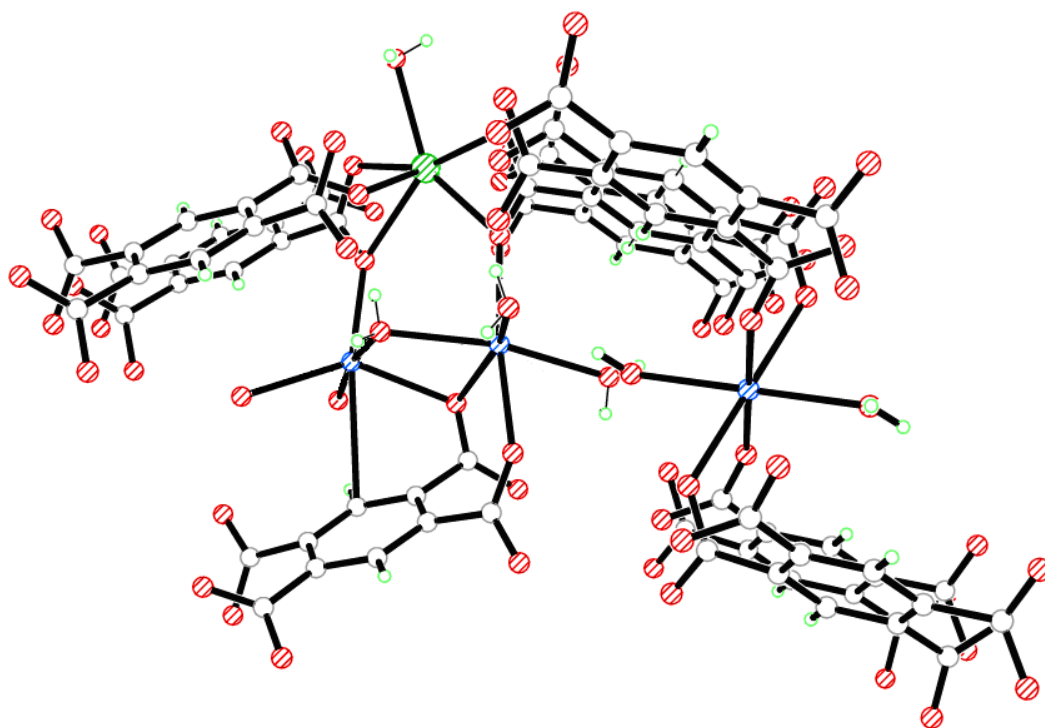


**Figure 7.42: Secondary building unit of Cd(1) and Na cations in compound 28**

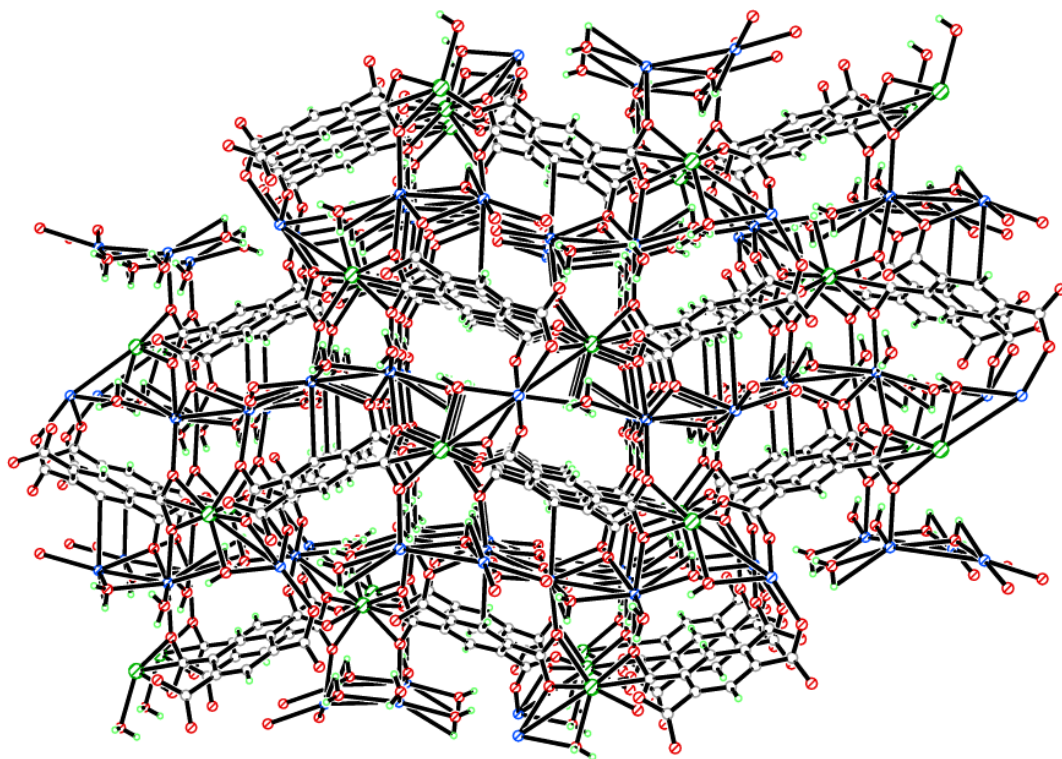


**Figure 7.43:** Three dimensional packing in compound 28 viewed down the *a*-axis

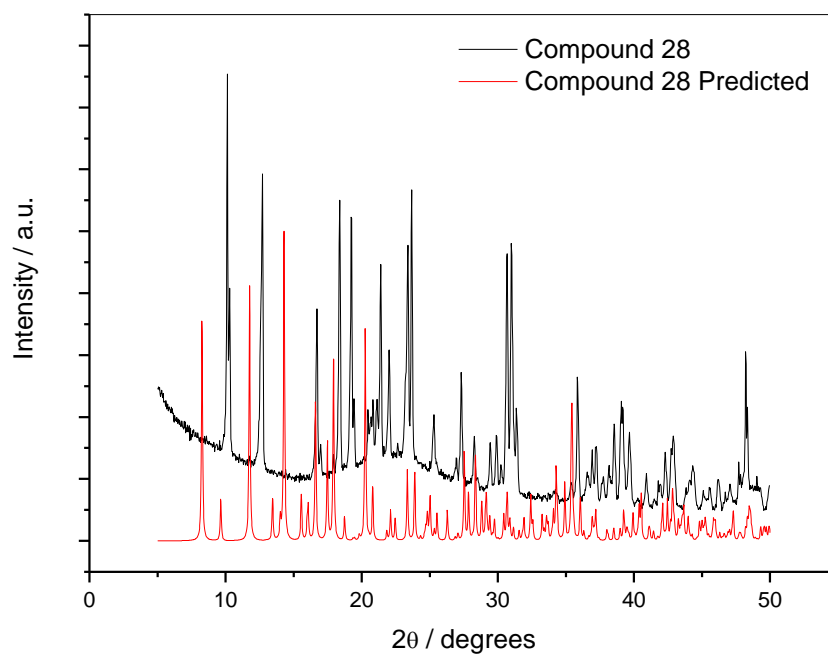
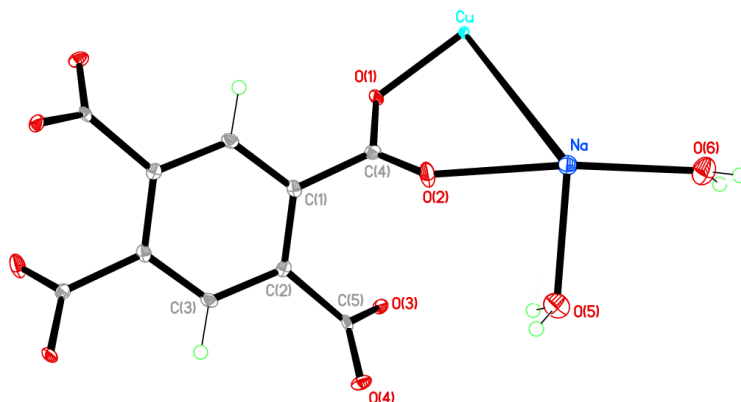


**Figure 7.44:** Powder X-ray diffraction pattern of Compound 28

**Compound 29:**  $[\text{CuNa}_2(\text{C}_{10}\text{H}_2\text{O}_8)(\text{H}_2\text{O})_4]$



Chemical formula (total)	$\text{C}_{10}\text{H}_{10}\text{CuNa}_2\text{O}_{12}$
Formula weight	431.70
Temperature	150(2) K
Radiation, wavelength	MoK $\alpha$ , 0.71073 Å
Crystal system, space group	monoclinic, $C2/c$
Unit cell parameters	$a = 6.9090(2)$ Å $b = 16.3710(6)$ Å $c = 12.9657(5)$ Å $\beta = 99.521(4)^\circ$
Cell volume	$1446.31(9)$ Å <sup>3</sup>
$Z$	4
Crystal colour and size	blue, $0.10 \times 0.07 \times 0.05$ mm <sup>3</sup>
Final $R$ indices [ $F^2 > 2\sigma$ ]	$R1 = 0.0225$
$R$ indices (all data)	$wR2 = 0.0608$
Largest diff. peak and hole	0.36 and $-0.37$ e Å <sup>-3</sup>

**Figure 7.45:** Asymmetric Unit of Compound 29 all unique atoms labelled, additional atoms added to complete ligands.

**Synthesis**

$\text{Cu}(\text{NO}_3)_2 \cdot 4\text{H}_2\text{O}$  (0.079 g, 0.33 mmol) in water (10 mL) and 0.5 mL of a solution of 1,2,4,5-benzenetetracarboxylic acid (0.043 g, 0.17 mmol) in water (10 mL) were placed on top of a 5 % tetramethoxysilane gel primed with sodium hydroxide (0.159 g, 4 mmol) instead a sample tube. The tube was covered and left until crystallisation was complete. After one week, blue needle crystals formed.

## Structure Determination

The data were collected at 150 K using molybdenum radiation on an Oxford Diffraction Gemini A Ultra diffractometer. The structure was solved by direct methods. The semi-empirical absorption corrections were applied based on symmetry-equivalent and repeated data. The refinement gave a  $wR2$  of 0.0608 for all 1282 independent reflections and a conventional  $R1$  of 0.0225, for 1238 reflections with  $F^2 > 2\sigma$ . The residual electron density maximum and minimum were 1.06 and  $-0.73 \text{ e } \text{\AA}^{-3}$  respectively.

The hydrogen atoms were refined freely within compound 29. The full data of compound 29 can be found in Appendix 1.

## Structure Analysis

The asymmetric unit of compound 29 (figure 7.45) shows a half 1,2,4,5-benzenetetracarboxylate ligand completed by inversion symmetry around the centre of the aromatic ring, coordinated to a square planar copper cation and an octahedral sodium cation. The four-coordinate square planar copper cation is positioned on a two-fold rotation axis with full coordination to carboxylate groups (figure 7.46). The O(1)-C(4)-O(2) carboxylate coordinates to the Cu cation with the monodentate Cu-O(1) 1.943(13) Å bond, a coplanar trans O(3)-C(5)-O(4) carboxylate group of a symmetry equivalent ligand coordinates forming the monodentate Cu-O(3) 1.959(13) Å bond at the angle O(1)-Cu-O(3B) 167.77(6)°. The remaining two coordination sites are occupied by the cis symmetry equivalent carboxylate groups generated by the two-fold rotation symmetry; O(1)-Cu-O(1A) 84.45(8)° with the carboxylate group rotated by 180° (figure 7.46). The O(1)-C(4)-O(2) carboxylate group further coordinates to a sodium cation forming a monodentate bond through the O(2) oxygen; Na-O(2) 2.352(16) Å with the carboxylate group forming a bridge between the sodium and copper cations placing them 3.432(9) Å apart. The sodium cation also coordinates to both the oxygens of the symmetry equivalent O(3)-C(5)-O(4) carboxylates, with the O(3) cation bridging the sodium and copper cations with a bite angle of Cu-O(3)-Na 100.54(6)°. The O(4) oxygen is bifurcated, chelating to two cis symmetry equivalent sodium cations with a bite angle of 94.85(5)°. The sodium cation completes its six-coordinate geometry by

coordinating to two terminal water molecules cis to one another; O(5)-Na-O(6) 91.66(6)° with similar bond lengths to the carboxylate groups (table 7.17).

The bridging 1,2,4,5-benzenetetracarboxylate is completed by the inversion symmetry at the centre of its aromatic ring, this expands the coordination of the copper and sodium cations to form the molecular building unit in figure 7.47. The molecular building unit expands the structure to form a fully coordinated three dimensional framework with columns of sodium and copper cations running down the *a*-axis connected by 1,2,4,5-benzenetetracarboxylate ligands along the *b*-axis (figure 7.48). These connecting ligands form chains that run along the *b*-axis and at a diagonal to the *a*-axis, each chain is related by the two-fold rotation axis that runs down the *b*-axis and results in the chains running in opposite directions with the diagonal direction flipped by 180° (figure 7.49). The chains are generated by inversion symmetry that generates two symmetry equivalent 1,2,4,5-benzenetetracarboxylate ligands 6.909(13) Å away from each other in the *a*-axis with respect to the aromatic rings. These ligands are then systematically staggered by the glide plane in the [101] axis that creates the diagonal running chain along the *b*-axis.

The coordinated water molecules create small pockets within the structure between the two aromatic rings of the 1,2,4,5-benzenetetracarboxylate ligands around the inversion centre mentioned previously. These form hydrogen bonds to adjacent carboxylate oxygens; O(5)-H(5A)···O(1C) 2.893(2) Å, O(5)-H(5B)···O(2D) 2.798(2) Å and O(6)-H(6A)···O(1G) 3.107(2) Å (table 7.18).

Compound 29 was synthesised using a 5 % gel, a large quantity of the compound formed as single crystals on the surface of the gel, allowing recovery of the compound without the gel. This prevented a repetition of the problems encountered by compound 28, enabling further analysis by powder X-ray diffraction and elemental analysis. The elemental analysis of compound 29 produced the results C = 25.36 %, H = 2.076 % and N = 0 %; these were consistent with the calculated values from the single crystal data of C = 27.79 %, H = 2.31 % and N = 0 %. The purity of the bulk sample was confirmed with the powder X-ray diffraction data (figure 7.50) that shows significant correlations in the diffraction pattern with peaks at 10.85, 14.08, 16.3 and 21.24 2 Theta present in both the obtained and predicted powder diffraction patterns.



Compound 29 is similar to compound 28 in chemical composition, with the switch from pentagonal bipyramidal cadmium cations to square planar copper cations altering the packing motif drastically. Compound 29 forms chains of 1,2,4,5-benzenetetracarboxylate connecting columns of sodium and copper cations in contrast to the ordered sheets of compound 28 connected by rows of sodium cations. Compound 29 is the only reported framework consisting of copper and sodium cations coordinated to 1,2,4,5-benzenetetracarboxylates in the database; however it shows consistency in bond lengths of transition metal-oxygen and sodium-oxygen bonds, with the sodium cations forming well defined octahedral geometries observed in previously reported structures such as WUPNIF<sup>8</sup>, KETZEP<sup>9</sup> and BORLAW02<sup>7</sup> (table 7.19).

**Table 7.17: Selected Bond Lengths [Å] and Angles [°] for Compound 29**

Cu–O(1)	1.9428(13)	Cu–O(3B)	1.9593(13)
Na–O(2)	2.3529(16)	Na–O(3C)	2.4819(15)
Na–O(4B)	2.4095(15)	Na–O(4D)	2.4227(15)
Na–O(5)	2.3539(18)	Na–O(6)	2.3668(18)
C(4)–O(1)	1.285(2)	C(4)–O(2)	1.231(2)
C(5)–O(3)	1.279(2)	C(5)–O(4)	1.240(2)
O(1)–Cu–O(1A)	84.95(8)	O(1)–Cu–O(3B)	167.77(6)
O(1)–Cu–O(3C)	92.66(6)	O(2)–Na–O(3C)	75.17(5)
O(2)–Na–O(4B)	95.23(6)	O(2)–Na–O(4D)	91.75(5)
O(2)–Na–O(5)	81.79(6)	O(2)–Na–O(6)	163.51(7)
Cu–O(3)–NaC	100.54(6)	NaF–O(4)–NaD	94.85(5)

Symmetry operations for equivalent atoms

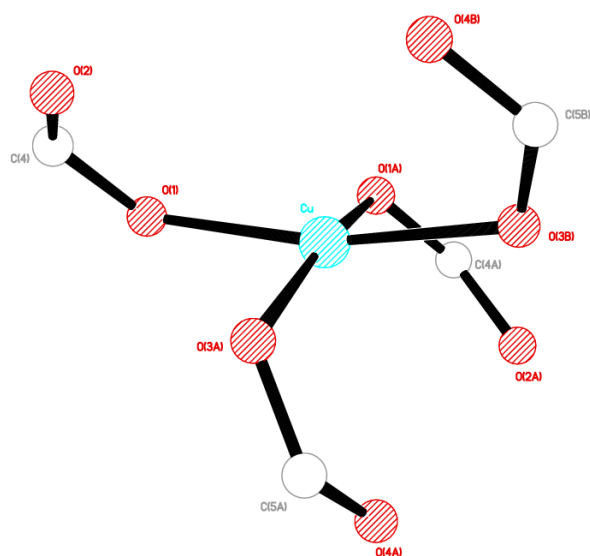
A  $-x+1, y, -z+3/2$  B  $x, -y+1, z+1/2$  C  $-x+1, -y+1, -z+1$ D  $-x+2, -y+1, -z+1$  F  $x, -y+1, z-1/2$ **Table 7.18: Selected Hydrogen bond Lengths [Å] and angles [°] for Compound 29**

D–H...A	d(D–H)	d(H...A)	d(D...A)	(DHA)
O(5)–H(5A)...O(1C)	0.75(3)	2.22(3)	2.893(2)	150(3)
O(5)–H(5B)...O(2D)	0.74(4)	2.07(4)	2.798(2)	170(3)
O(6)–H(6A)...O(1G)	0.73(4)	2.41(4)	3.107(2)	160(4)
O(6)–H(6B)...O(5H)	0.75(4)	2.26(4)	2.885(2)	142(3)

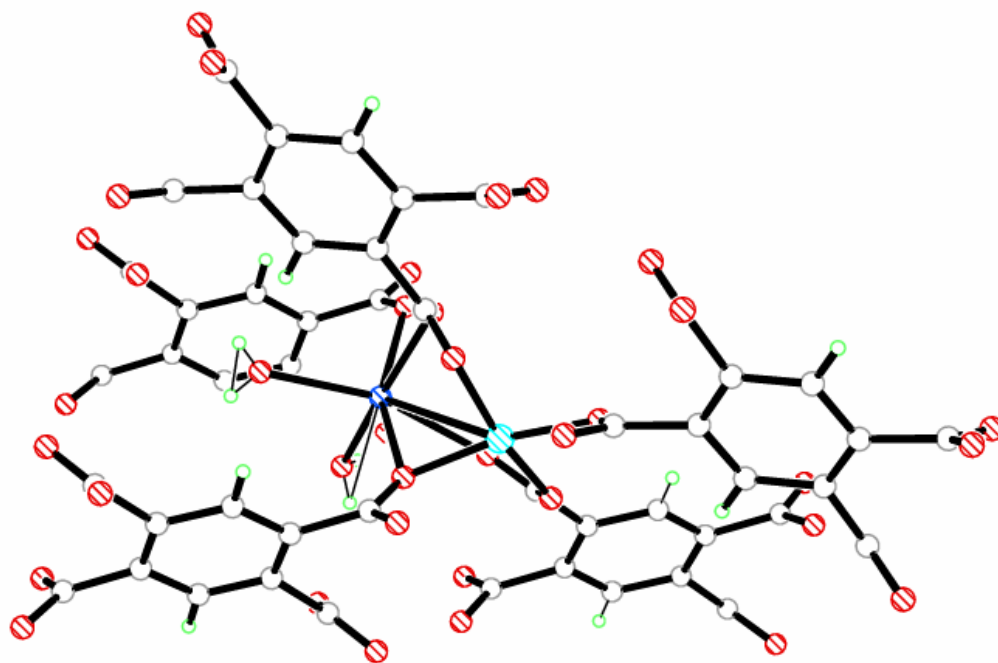
Symmetry operations for equivalent atoms

C  $-x+1, -y+1, -z+1$  D  $-x+2, -y+1, -z+1$  G  $x+1/2, y+1/2, z$ H  $-x+3/2, -y+3/2, -z+1$ **Table 7.19: Average bond length comparisons between Compound 29, Compound 28 WUPNIF<sup>8</sup>, KETZEP<sup>9</sup> and BORLAW02<sup>7</sup>**

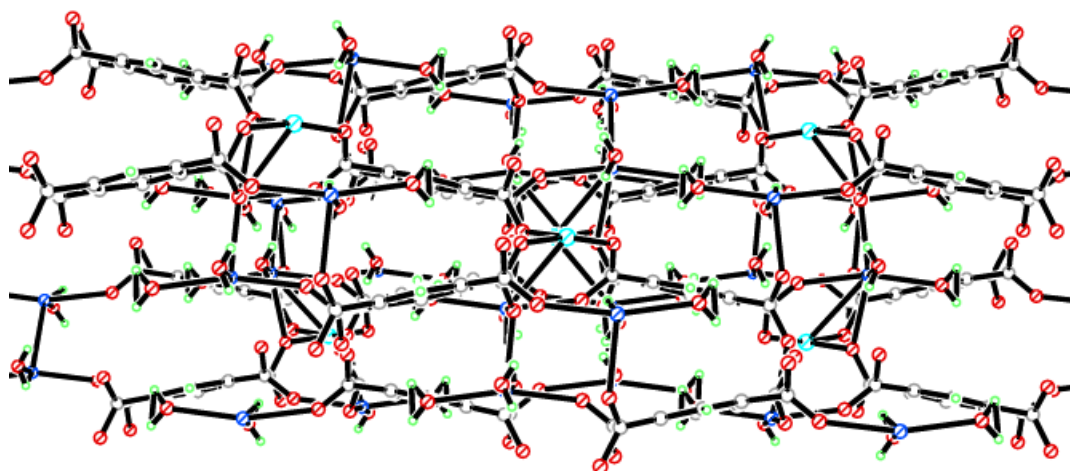
Compound	Bond	Average bond Length (Å)
Compound 28	Cd–O (carboxylate)	2.333
Compound 28	Na–O (carboxylate)	2.403
Compound 29	Cu–O (carboxylate)	1.948
Compound 29	Na–O (carboxylate)	2.394
BORLAW02	Co–O (carboxylate)	2.118
BORLAW02	Na–O (carboxylate)	2.437
WUPNIF	Zn–O (carboxylate)	1.968
WUPNIF	Na–O (carboxylate)	2.357
KETZEP	Ni–O (carboxylate)	2.076
KETZEP	Na–O (carboxylate)	2.434



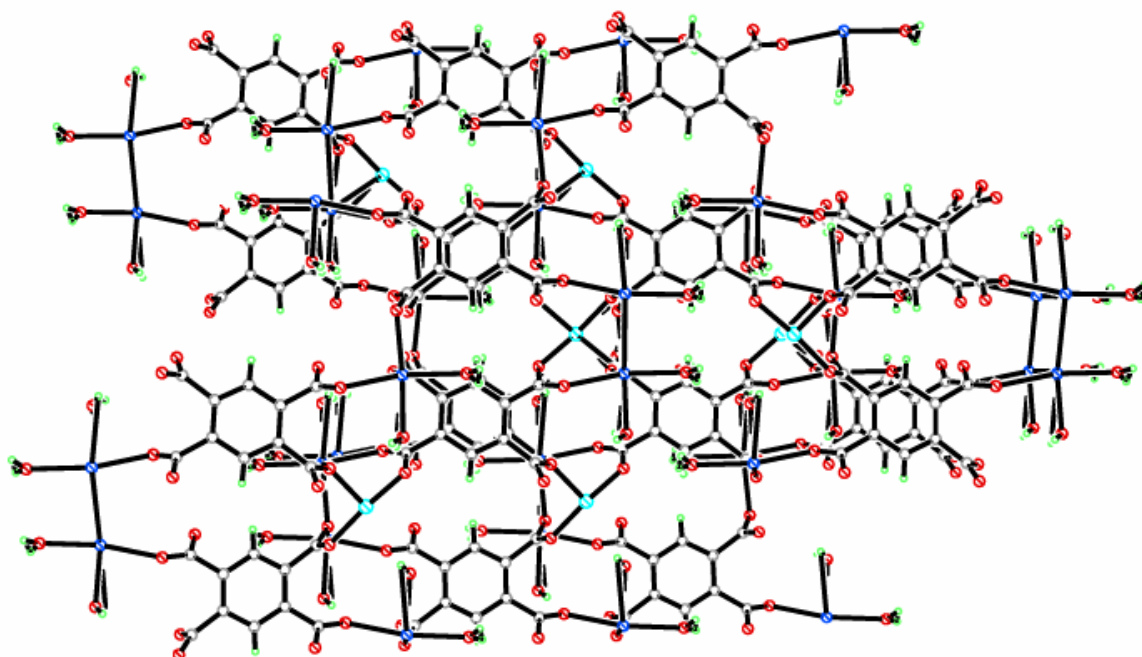
**Figure 7.46: Square planar coordination environment of Cu(1) in compound 29**



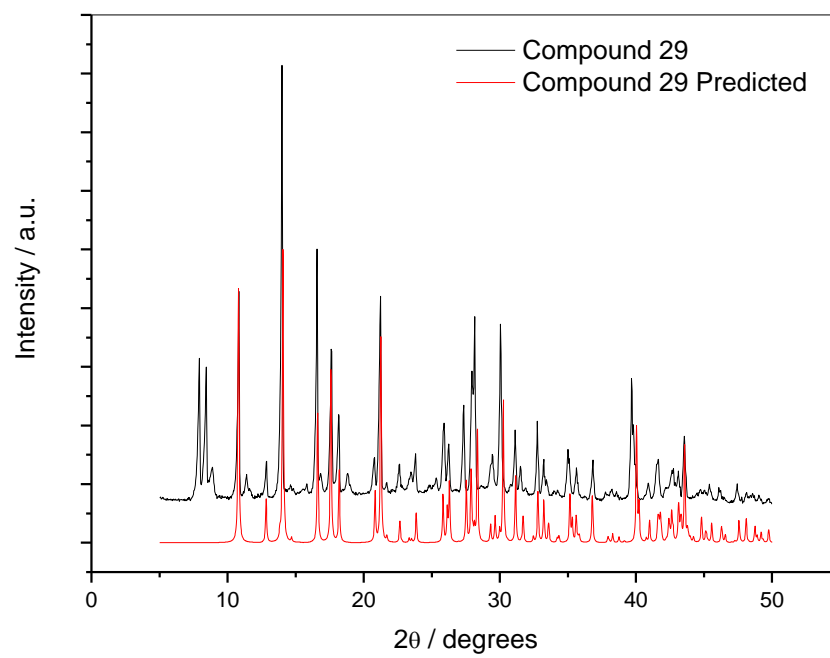
**Figure 7.47: Secondary building unit of Cu(1) and Na cations in compound 29**



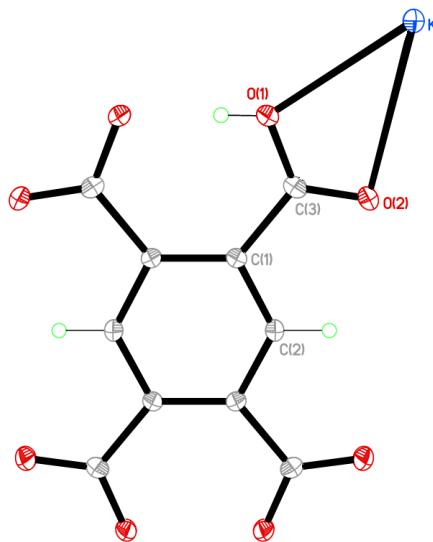
**Figure 7.48:** Three dimensional packing in compound 29 viewed down the *c*-axis



**Figure 7.49:** Three dimensional packing of the chains in compound 29 viewed down the *a*-axis



**Figure 7.50: Powder X-ray diffraction pattern of Compound 29**

**Compound 30:**  $[\text{K}_2(\text{C}_{10}\text{H}_4\text{O}_8)]$ 

Chemical formula (total)	$\text{C}_{10}\text{H}_4\text{K}_2\text{O}_8$	
Formula weight	330.33	
Temperature	150(2) K	
Radiation, wavelength	MoK $\alpha$ , 0.71073 Å	
Crystal system, space group	monoclinic, $C2/m$	
Unit cell parameters	$a = 7.5379(6)$ Å $b = 16.8380(9)$ Å $c = 4.6399(4)$ Å	$\beta = 113.023(10)^\circ$
Cell volume	$542.00(7)$ Å <sup>3</sup>	
$Z$	2	
Crystal colour and size	colourless, $0.10 \times 0.05 \times 0.05$ mm <sup>3</sup>	
Final $R$ indices [ $F^2 > 2\sigma$ ]	$R1 = 0.0308$	
$R$ indices (all data)	$wR2 = 0.0775$	
Largest diff. peak and hole	0.42 and $-0.27$ e Å <sup>-3</sup>	

**Figure 7.51:** Asymmetric Unit of Compound 30 all unique atoms labelled, additional atoms added to complete ligands.

**Synthesis**

$\text{Cd}(\text{NO}_3)_2 \cdot 4\text{H}_2\text{O}$  (0.308 g, 1 mmol) and 1,2,4,5-benzenetetracarboxylic acid (0.254 g, 1 mmol) were added to a reaction mixture of 1-ethyl-3-methylimidazolium bromide (0.38 g, 2 mmol) and potassium hydroxide (0.224 g, 4 mmol). This was placed into a 20mL Teflon-lined bomb and heated to 200°C for 7 days. The vessel was then cooled back down to room temperature at a rate of 0.1°C / min and allowed to stand for 2 hours before colourless needle crystals were retrieved from the vessel.

## Structure Determination

The data were collected at 150 K using molybdenum radiation on an Oxford Diffraction Gemini A Ultra diffractometer. The structure was solved by direct methods. The semi-empirical absorption corrections were applied based on symmetry-equivalent and repeated data. The refinement gave a  $wR2$  of 0.0775 for all 579 independent reflections and a conventional  $R1$  of 0.0308, for 496 reflections with  $F^2 > 2\sigma$ . The residual electron density maximum and minimum were 0.42 and  $-0.27 \text{ e } \text{\AA}^{-3}$  respectively.

The hydrogen atoms were refined freely in this compound. The full data of compound 30 can be found in Appendix 1.

## Structure Analysis

The asymmetric unit of compound 30 (figure 7.51) shows quarter of a 1,2,4,5-benzenetetracarboxylate ligand completed by a mirror plane in the  $[101]$  axis and a two-fold rotation axis the is parallel to the plane of the aromatic ring in the  $b$ -axis. The 1,2,4,5-benzenetetracarboxylate ligand coordinates to a potassium cation using the bidentate O(1)-C(3)-O(2) carboxylate group forming the elongated K-O(1) 2.754(15) Å and K-O(2) 2.911(14) Å bonds, which are consistent with similar structures in the crystallographic database.<sup>10</sup> The potassium cation is positioned on a two-fold rotation axis and is coordinated fully by symmetry equivalents of the O(1)-C(3)-O(2) carboxylate group to form a seven-coordinate distorted pentagonal bipyramidal geometry (figure 7.52). The symmetry equivalent bidentate carboxylate groups coordinate cis with an angle of  $67.14(6)^\circ$  between the coplanar groups, the O(2) carboxylate oxygen acts as a triply bridging unit linking three potassium cations with a bite angles of K-O(2)-K(B)  $89.10(4)^\circ$  and K-O(2)-K(F)  $100.51(3)^\circ$ . These additional symmetry equivalent monodentate bonds from O(2) chelate in the cis positions to the bidentate coordination of the O(1)-C(3)-O(2) carboxylate; O(1)-K-O(2C)  $135.57(5)^\circ$ , O(1)-K-O(2D)  $73.91(4)^\circ$  and O(1)-K-O(2E)  $73.91(4)^\circ$  (table 7.20).

The 1,2,4,5-benzenetetracarboxylate ligand in compound 30 exists as the  $[\text{C}_{10}\text{H}_4\text{O}_8]^{-2}$  anion with two  $\text{CO}_2^-$  and two  $\text{CO}_2\text{H}$  groups. In this anion a short

intramolecular hydrogen bond forms between a pair of adjacent CO<sub>2</sub><sup>-</sup> and CO<sub>2</sub>H groups; O(1)-H(1)⋯O(1G) 2.388(3) Å at 179(4)° (table 7.21). The partial delocalisation of the carboxylate groups in the ligand is observed with the protonation of the O(1) carboxylate oxygen and the presence of carbon-oxygen double and single bonds, with C(3)-O(2) 1.230(2) Å and C(3)-O(1) 1.281(2) Å respectively. The completion of the 1,2,4,5-benzenetetracarboxylate by the two-fold rotation and mirror symmetry with subsequent coordination to the potassium cation results in the molecular building unit shown in figure 7.53. The bridging motif of the carboxylate groups in this compound creates dual layer sheets of potassium cations that run down the *a*-axis and along the *c*-axis, these sheets are visible when compound 30 is viewed down the *b*-axis (figure 7.54). The sheets are staggered and run parallel with respect to one another in the *b*-axis connected by chains of 1,2,4,5-benzenetetracarboxylate ligands the *a*-axis and stack in the *c*-axis with a separation of 4.640(5) Å with respect to the aromatic rings. Each set of chains is staggered with respect to the adjacent chain in the *b*-axis by 4.993(7) Å as a result of the [101] glide plane (figure 7.55).

To investigate the difference in stability between transition metal-1,2,4,5-benzenetetracarboxylate frameworks and alkali metal-1,2,4,5-benzenetetracarboxylate frameworks, compound 30 was subjected to heating using the thermogravimetric analyser to obtain the temperature profile. Compound 30 upon heating begins to polymerise forming a new compound. The polymerisation and expansion of the compound resulted in the filling of the sample bucket on the TGA adhering it to the side of the furnace. The damage implications of the polymerisation prevented further thermal analysis of the compound; however in the initial TGA run a terminal temperature of the compound was recorded at 37.8°C indicating very low structural stability. The expansion of compound 30 may have been the result of impurities that upon heating coordinated into the framework. Previous compounds synthesized using ionothermal conditions have had residual 1-ethyl-3-methylimidazolium bromide within the bulk material, which melts upon heating and can act as a reaction medium and templating agent. Further analysis of the bulk material by powder X-ray diffraction and elemental analysis indicated impurities were present within the compound. The powder X-ray diffraction pattern in figure 7.56 shows peaks corresponding to compound 30 at 20.34,



23.63, 28.01, 29.01, 32-33 and 34.71 2-Theta, confirmed by the predicted powder diffraction pattern from the single crystal data; however anomalous peaks corresponding to the impurities were detected with high intensities between 10-20 2-Theta. The impurities were also confirmed with the results of the elemental analysis; C = 22.16 %, H = 2.03 % and N = 0.19% compared to the calculated values C = 36.33 %, H = 1.21 % and N = 0 %. The presence of nitrogen would indicate either nitrates or 1-ethyl-3-methylimidazolium bromide are present from the starting reagents.

Compound 30 was synthesised using ionothermal techniques, with the reaction used to form compound 27 seeded with potassium hydroxide to act as a mineralising agent. The previous compound 28 and 29 demonstrated how small concentrations of sodium cations introduced into the reaction have a profound effect on the three dimensional structure, compound 30 demonstrated how the concentration of alkali earth metal need to be low as higher concentrations result in potassium orientated structures. Expansion reactions of compound 30 yielded compound 31 when the potassium concentration was lowered to produce a dual metal complex.

Xaio *et al.* reported a similar structure to compound 30 [CSD Refcode: IWOKUA],<sup>10</sup> this compound contains only 1,2,4,5-benzenetetracarboxylate, potassium and water. The compound forms chains of potassium cations down the *c*-axis similar to those of compound 30. The 1,2,4,5-benzenetetracarboxylate are only partially deprotonated with carbon-oxygen double and single bonds present in each carboxylate group. The compound IWOKUA produces a different packing motif to compound 30, forming two dimensional sheets with the potassium cations capped by coordinated water molecules that hydrogen bond the structures together.<sup>10</sup> The bond lengths of compound 30 and IWOKUA<sup>10</sup> are compared in table 7.22 and show consistent values.

**Table 7.20: Selected Bond Lengths [Å] and Angles [°] for Compound 30**

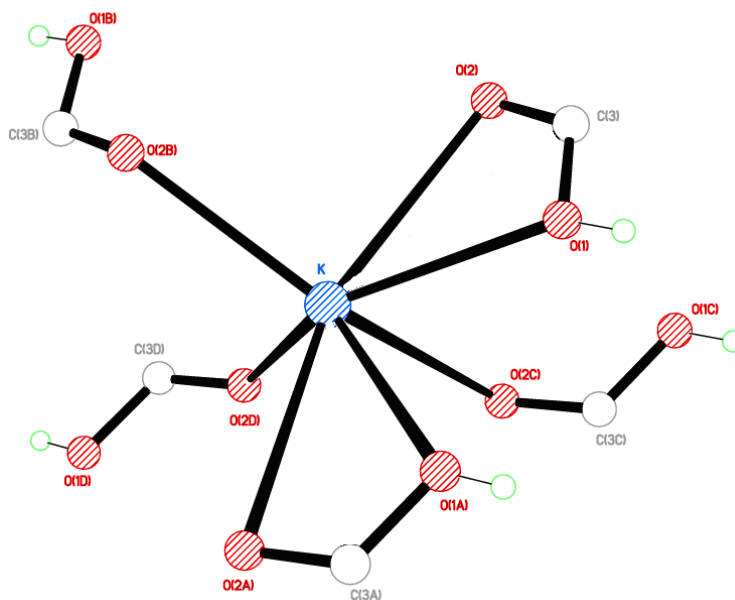
K–O(1)	2.7539(15)	K–O(2)	2.9907(14)
K–O(2B)	2.7566(16)	K–O(2D)	3.0435(18)
O(1)–C(3)	1.281(2)	O(2)–C(3)	1.230(2)
O(1)–K–O(1A)	67.14(6)	O(1)–K–O(2)	44.53(4)
O(1)–K–O(2B)	122.10(4)	O(1)–K–O(2C)	135.57(5)
O(1)–K–O(2A)	111.61(5)	K–O(1)–C(3)	102.19(12)
K–O(2)–KB	89.10(4)	KB–O(2)–KF	115.68(5)
K–O(2)–KF	100.51(5)	K–O(2)–C(3)	92.03(12)
KB–O(2)–C(3)	136.41(15)	KF–O(2)–C(3)	106.91(14)
Symmetry operations for equivalent atoms			
A	$-x, y, -z+2$	B	$-x+1/2, -y+3/2, -z+2$
C	$x-1/2, -y+3/2, z$		
D	$-x, y, -z+1$	F	$x, y, z-1$

**Table 7.21: Selected Hydrogen bond Lengths [Å] and angles [°] for Compound 30**

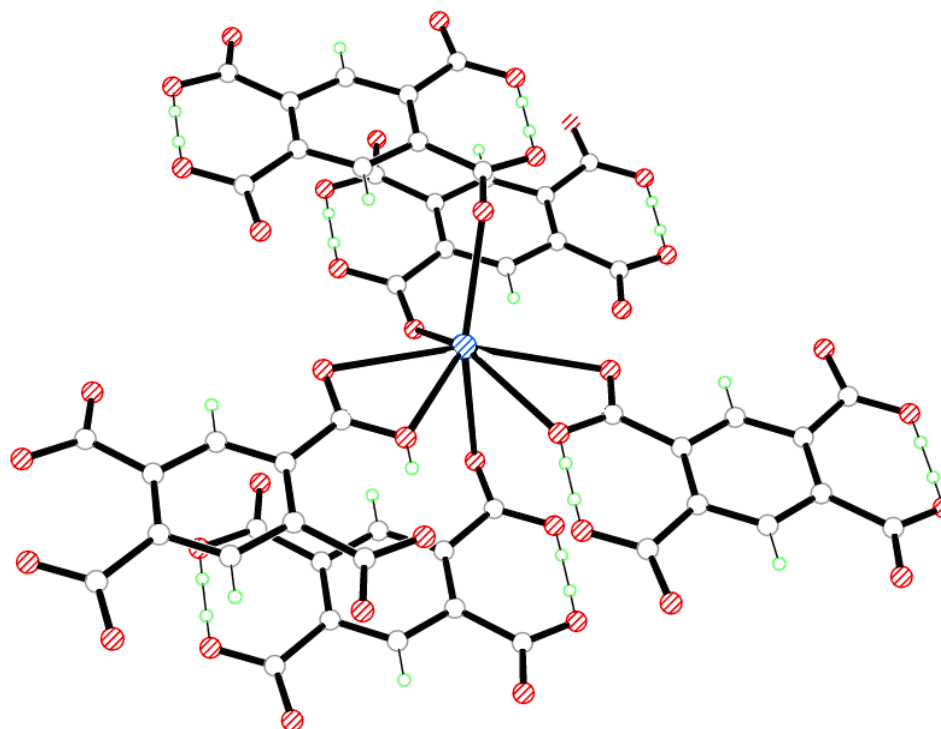
D–H...A	d(D–H)	d(H...A)	d(D...A)	(DHA)
O(1)–H(1)...O(1G)	0.75(4)	1.64(4)	2.388(3)	179(4)
Symmetry operations for equivalent atoms				
G	$x, -y+1, z$			

**Table 7.22: Bond length comparisons between Compound 30 and IWOKUA<sup>10</sup>**

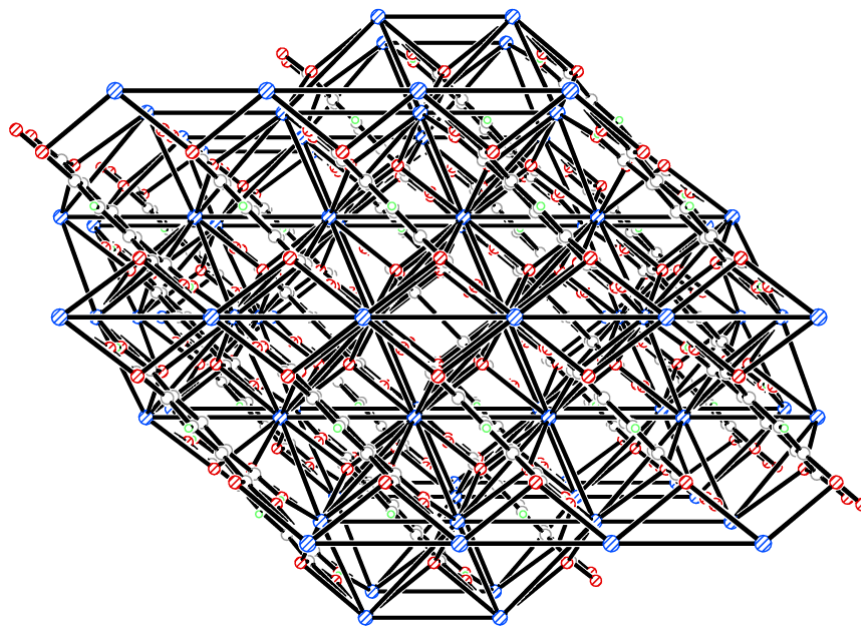
Compound	Bond	Bond Length (Å)
Compound 30	K–O(1) (carboxylate)	2.754(15)
Compound 30	K–O(2) (carboxylate)	2.991(14)
IWOKUA	K–O(7) (carboxylate)	2.717(2)
IWOKUA	K–O(6) (carboxylate)	2.695(1)
IWOKUA	K–O(3) (carboxylate)	2.872(1)
IWOKUA	K–O(1) (carboxylate)	2.831(1)



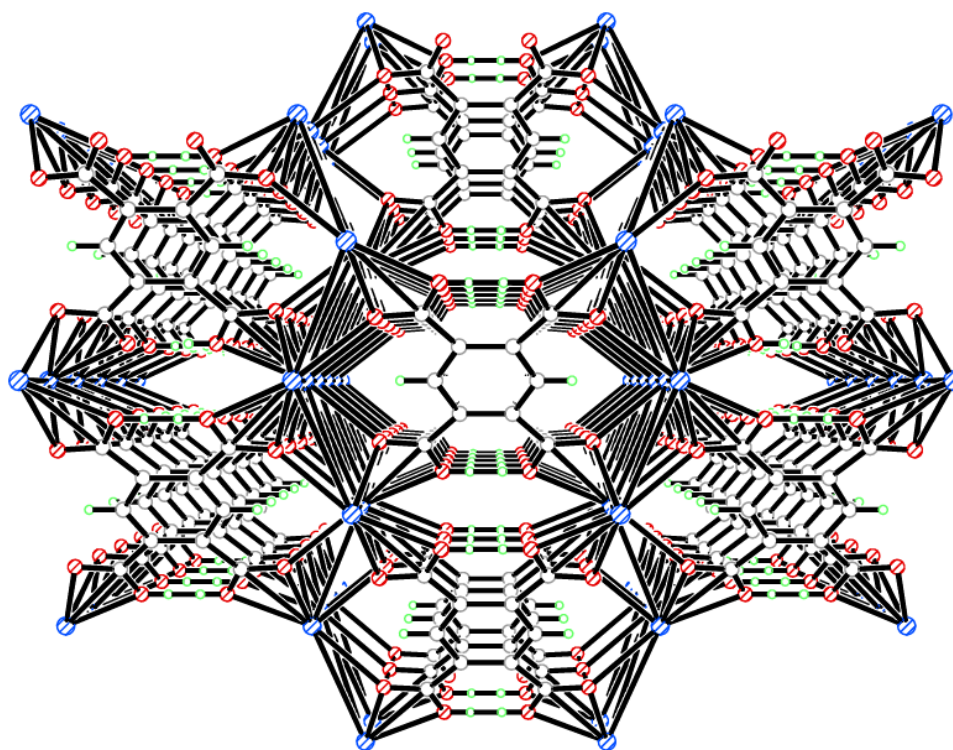
**Figure 7.52: Pentagonal bipyramidal coordination environment of K(1) in compound 30**



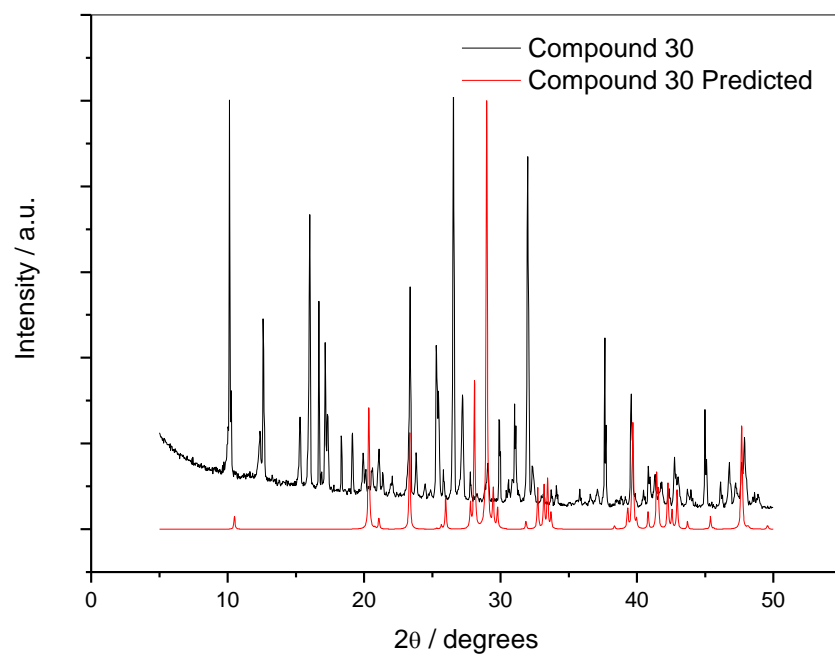
**Figure 7.53: Secondary building unit of K(1) in compound 30**



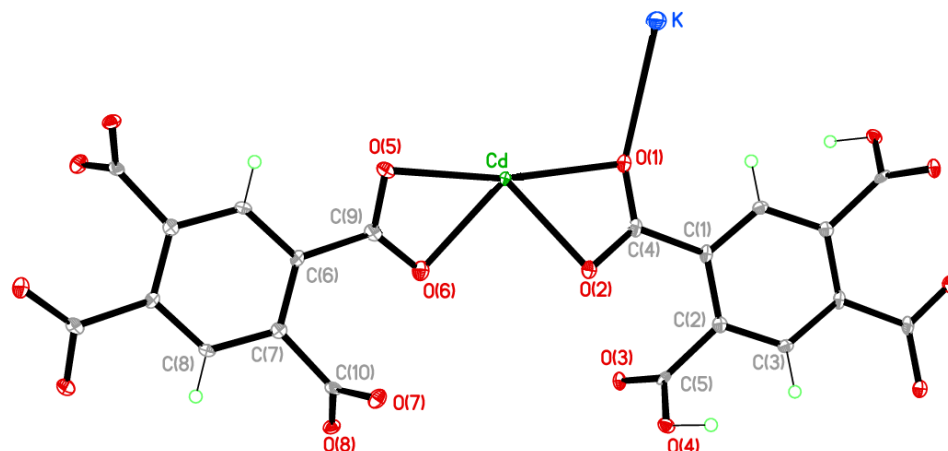
**Figure 7.54:** Three dimensional coordination motif of the dual layer potassium cations of compound 30 viewed down the *b*-axis



**Figure 7.55:** Coordination of the potassium layers by the staggered chains of 1,2,4,5-benzenetetracarboxylate ligands in compound 30 viewed down the *c*-axis



**Figure 7.56: Powder X-ray diffraction pattern of Compound 30**

**Compound 31:**  $[\text{Cd}_2\text{K}_2(\text{C}_{10}\text{H}_2\text{O}_8)(\text{C}_{10}\text{H}_4\text{O}_8)]$ 

Chemical formula (total)	$\text{C}_{20}\text{H}_6\text{Cd}_2\text{K}_2\text{O}_{16}$
Formula weight	805.25
Temperature	150(2) K
Radiation, wavelength	MoK $\alpha$ , 0.71073 Å
Crystal system, space group	triclinic, $P\bar{1}$
Unit cell parameters	$a = 7.6273(4)$ Å $b = 8.6788(6)$ Å $c = 8.7014(7)$ Å $\alpha = 76.950(7)^\circ$ $\beta = 67.825(7)^\circ$ $\gamma = 80.834(5)^\circ$
Cell volume	$517.86(6)$ Å <sup>3</sup>
Z	1
Crystal colour and size	colourless, $0.20 \times 0.18 \times 0.10$ mm <sup>3</sup>
Final $R$ indices [ $F^2 > 2\sigma$ ]	$R1 = 0.0201$
$R$ indices (all data)	$wR2 = 0.0422$
Largest diff. peak and hole	0.54 and $-0.48$ e Å <sup>-3</sup>

**Figure 7.57: Asymmetric Unit of Compound 31 all unique atoms labelled, additional atoms added to complete ligands.**

**Synthesis**

$\text{Cd}(\text{NO}_3)_2 \cdot 4\text{H}_2\text{O}$  (0.466 g, 1.5 mmol) and 1,2,4,5-benzenetetracarboxylic acid (0.254 g, 1 mmol) were added to a reaction mixture of 1-ethyl-3-methylimidazolium bromide (0.38 g, 2 mmol) and potassium hydroxide (0.042 g, 0.75 mmol). This was placed into a 20mL Teflon-lined bomb and heated to 200°C for 7 days. The vessel was then cooled back down to room temperature at a rate of 0.1°C / min and allowed to stand for 2 hours before colourless block crystals were retrieved from the vessel.

## Structure Determination

The data were collected at 150 K using molybdenum radiation on an Oxford Diffraction Gemini A Ultra diffractometer. The structure was solved by direct methods. The semi-empirical absorption corrections were applied based on symmetry-equivalent and repeated data. The refinement gave a  $wR2$  of 0.0422 for all 1802 independent reflections and a conventional  $R1$  of 0.0201, for 1580 reflections with  $F^2 > 2\sigma$ . The residual electron density maximum and minimum were 0.54 and  $-0.48 \text{ e } \text{\AA}^{-3}$  respectively.

The hydrogen atoms were refined freely in this compound. DELU and SIMU restraints were imposed on the 1,2,4,5-benzenetetracarboxylate ligands within compound 31 during refinement. The full data of compound 31 can be found in Appendix 1.

## Structure Analysis

The asymmetric unit of compound 31 (figure 7.57) shows two half 1,2,4,5-benzenetetracarboxylate ligands both completed by respective inversion centres at the centre of the aromatic rings, coordinated to a potassium cation and a cadmium cation. The cadmium cation forms a seven-coordinate pentagonal bipyramidal geometry (figure 7.58) coordinated fully by carboxylate groups of the 1,2,4,5-benzenetetracarboxylate ligands. The two 1,2,4,5-benzenetetracarboxylate ligands have different degrees of deprotonation, the C(1)-O(4) ligand is only partially deprotonated and forms a  $[\text{C}_{10}\text{H}_4\text{O}_8]^{-2}$  anion whilst the C(6)-O(8) ligand is fully deprotonated and delocalised carboxylates forming a  $[\text{C}_{10}\text{H}_4\text{O}_8]^{-4}$  anion (table 7.23).

The C(1)-O(4) ligand shows full deprotonation and delocalisation of the O(1)-C(4)-O(2) carboxylate group with comparable bond lengths (table 7.23), the O(3)-C(5)-O(6) carboxylate is protonated with carbon-oxygen double and single bonds; C(5)-O(3) 1.217(4) Å and C(5)-O(4) 1.309(3) Å respectively. The C(1)-O(4) ligand coordinates to both the potassium and cadmium cations through both carboxylate groups with the O(1)-C(4)-O(2) forming a bidentate bond to the cadmium cation with a bite angle of O(1)-Cd-O(2)  $55.21(7)^\circ$ , the carboxylate oxygens coordinate to three symmetry equivalent potassium cations generated through inversion symmetry in the  $a$ -axis. The O(1)

carboxylate oxygen is trifurcated, coordinating to the cadmium cation and two potassium cations with bite angles Cd-O(1)-K 105.69(8)°, Cd-O(1)-K(D) 100.18(7)° and K-O(1)-K(D) 103.82(6)°. The remaining O(2) oxygen coordinates to the cadmium cation and the potassium cation with a bite angle of 101.58(7)°, coordinating to the potassium cation at a distorted cis position to the symmetry equivalent O(1) carboxylate oxygens that are in coplanar cis positions; O(1)-K-O(2C) 154.08(7)° and O(1D)-K-O(2C) 93.48(6)°. The remaining carboxylate group O(3)-C(5)-O(4) although protonated still coordinates to the potassium cation forming a bidentate chelate with a bite angle of 42.04(5)°. The carboxylate also bridges the potassium cation and cadmium cations through the bifurcated O(3) oxygen that forms a second bond to the cadmium cation creating a bridge with a bite angle of 118.36(8)°. The O(3) carboxylate oxygen coordinates perpendicular to the O(1)-C(4)-O(2) group in the cis axial position at the angle O(1)-Cd-O(3A) 81.20(7)°.

The seven-coordinate geometry (figure 7.58) is completed by coordinating to three symmetry equivalent C(6)-O(8) [C<sub>10</sub>H<sub>4</sub>O<sub>8</sub>]<sup>4-</sup> anions. The C(6)-O(8) ligand chelates to the cadmium cation with the bidentate O(5)-C(9)-O(6) carboxylate group that forms a bite angle of 55.52(7)°, this group coordinates trans to the O(1)-C(4)-O(2) carboxylate groups at 167.86(7)° and is slightly twisted out of the plane of the aromatic ring by 62.06(8)°. The carboxylate oxygen atoms then coordinate to symmetry equivalent potassium cations to create bridging angles with the cadmium cation; Cd-O(5)-K(E) 105.53(8)° and Cd-O(6)-K(G) 103.15(8)° comparable to the Cd-O-K bridges of the C(1)-O(4) ligand (table 7.23). The O(7)-C(10)-O(8) carboxylate group forms a bidentate coordination to the potassium cation with the smallest bite angle in the compound of O(7C)-K-O(8C) 40.74(5)°. The O(7) and O(8) oxygens further coordinate to two symmetry equivalent cadmium cations with almost perpendicular bite angles to the potassium cations; Cd(5)-O(7)-K(G) 115.99(9)° and Cd(G)-O(8)-K(G) 90.99(6)°. The symmetry equivalent carboxylate oxygens coordinate to the cadmium in cis positions O(7B)-Cd-O(8C) 92.10(7)° completing the pentagonal bipyramidal geometry of the cadmium cation.

The multidentate nature of the carboxylate groups that bridge both the cadmium and potassium cations forms the molecular building unit in figure 7.59. This building



unit is comparable to the building unit of compound 30 (figure 7.53) that contains a seven-coordinate pentagonal bipyramidal metal node, coordinated to chains of coplanar parallel 1,2,4,5-benzenetetracarboxylate ligands. The molecular building unit of compound 31 (figure 7.59) expands the structure into three dimensions creating a fully coordinated framework consisting of bimetallic sheets of cadmium and potassium cations, coordinated together by bridging carboxylate groups that run down the *a*-axis and along the *b*-axis (figure 7.60). The sheets are stacked planar and run parallel to one another in the *b*-axis connected by chains of 1,2,4,5-benzenetetracarboxylate ligands that run along the *a*-axis; stacking in the *b*-axis with a  $\pi$ - $\pi$  separation of 4.180(7) Å. The chains are composed of symmetry equivalent ligands generated by inversion symmetry forming chains of C(1)-O(4) ligands alternating with chains of C(6)-O(8) ligands down the *b*-axis (figure 7.61).

Previous compounds containing alkali earth metals and compounds synthesised using ionothermal techniques have been restricted by the purity of the bulk sample such as compounds 27 and 30. Compound 31 was further analysed by powder X-ray diffraction and elemental analysis. The elemental analysis produced the results C= 26.85 %, H= 2.65 % and N = 6.44 %, these are not consistent with the calculated values from the single crystal data of C = 29.8 %, H = 0.75 % and N = O %. The powder X-ray diffraction data (figure 7.62) also indicates the presence of an impurity common to compound 30 (figure 7.56) with the anomalous peaks at 10-20 2-Theta. The impurity problems in compounds 27, 30 and 31 are a direct result of the synthesis protocol involving the ionic liquids such as 1-ethyl-3-methylimidazolium bromide leading to no further investigations involving ionic liquids as reaction media.

The ionic liquids provided a unique method of creating bimetallic structures with a step-wise progression from compound 27-30-31. Compounds 30 and 31 show significant similarities in their building units and packing motifs, with an almost direct substitution of the K-K dimeric unit to the Cd-K dimeric building unit. The difference in the packing motifs is due to compound 31 crystallising in the triclinic  $P\bar{1}$  space group and lacks the two-fold rotation and mirror symmetry used to form the packing motif of compound 30. The compounds 27, 30 and 31 show comparable bond lengths with very little divergence (table 7.24).

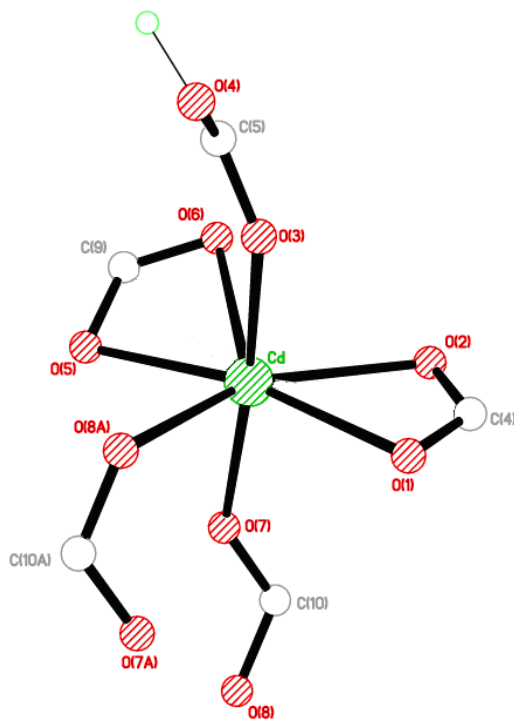
**Table 7.23: Selected Bond Lengths [Å] and Angles [°] for Compound 31**

Cd–O(1)	2.386(2)	Cd–O(2)	2.364(2)
Cd–O(3A)	2.3711(19)	Cd–O(5)	2.350(2)
Cd–O(6)	2.390(2)	Cd–O(7B)	2.282(2)
Cd–O(8C)	2.3322(18)	K–O(1)	2.808(2)
K–O(2C)	2.854(2)	K–O(3C)	2.801(2)
K–O(4C)	3.190(2)	K–O(5E)	2.965(2)
K–O(6C)	2.776(2)	K–O(7C)	2.721(2)
K–O(8C)	3.389(2)	C(4)–O(1)	1.259(3)
C(4)–O(2)	1.259(3)	C(5)–O(3)	1.217(4)
C(5)–O(4)	1.309(3)	C(9)–O(5)	1.261(3)
C(9)–O(6)	1.260(4)	C(10)–O(7)	1.245(4)
C(10)–O(8)	1.283(3)		
O(1)–Cd–O(2)	55.21(7)	O(1)–Cd–O(3A)	81.20(7)
O(1)–Cd–O(5)	167.86(7)	O(1)–Cd–O(6)	136.56(7)
O(1)–Cd–O(7B)	96.06(8)	O(1)–Cd–O(8C)	90.77(7)
O(1)–K–O(1D)	76.18(6)	O(1)–K–O(2C)	154.08(7)
O(1)–K–O(3C)	94.30(6)	O(1)–K–O(4C)	92.33(6)
O(1)–K–O(5E)	105.70(6)	O(1)–K–O(6C)	132.20(7)
O(1)–K–O(7C)	86.60(6)	O(1)–K–O(8C)	64.86(6)
Cd–O(1)–K	105.69(8)	Cd–O(1)–KD	100.18(7)
K–O(1)–KD	103.82(6)	Cd–O(2)–KG	101.58(7)
CdA–O(3)–KG	118.38(8)	Cd–O(5)–KE	105.53(8)
Cd–O(6)–KG	103.15(8)	CdB–O(7)–KG	115.99(9)
CdG–O(8)–KG	90.99(6)		

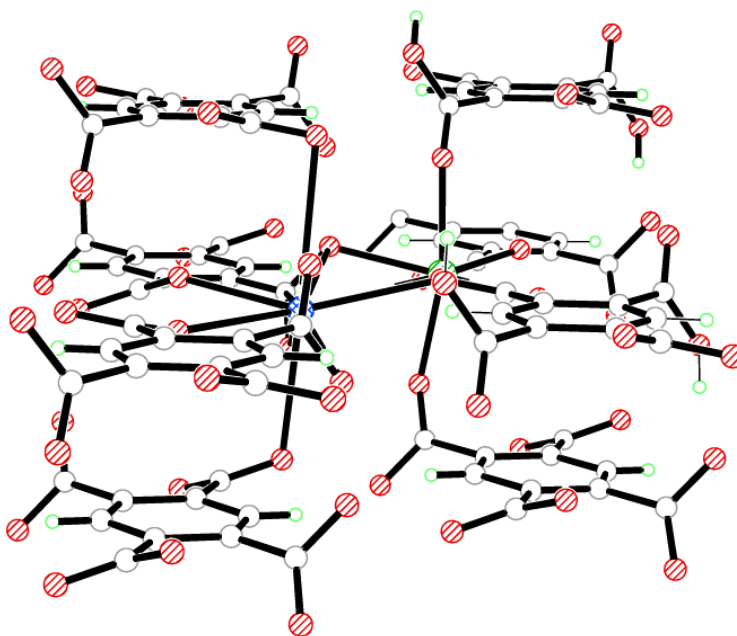
Symmetry operations for equivalent atoms

A  $-x+1, -y+1, -z+1$     B  $-x+1, -y+2, -z+1$     C  $x-1, y, z$ D  $-x, -y+1, -z+1$     E  $-x, -y+2, -z+1$     G  $x+1, y, z$ **Table 7.24: Average bond length comparisons between Compound 31, Compound 30 and Compound 27**

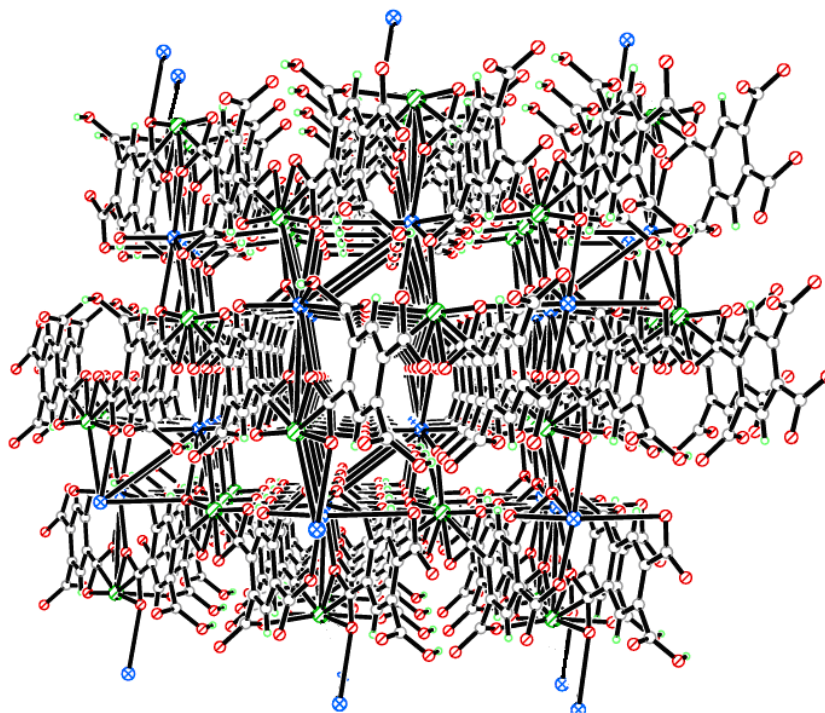
Compound	Bond	Average bond Length (Å)
Compound 27	Cd–O (carboxylate)	2.359
Compound 30	K–O (carboxylate)	2.873
Compound 31	Cd–O (carboxylate)	2.352
Compound 31	K–O (carboxylate)	2.984



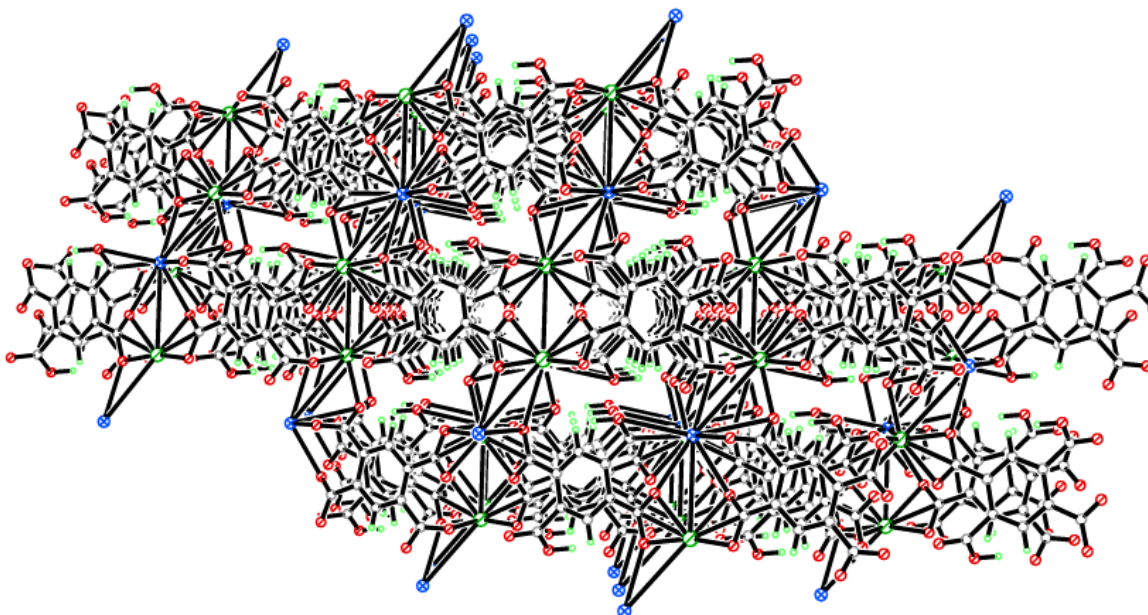
**Figure 7.58:** Pentagonal bipyramidal coordination environment of Cd(1) in compound 31



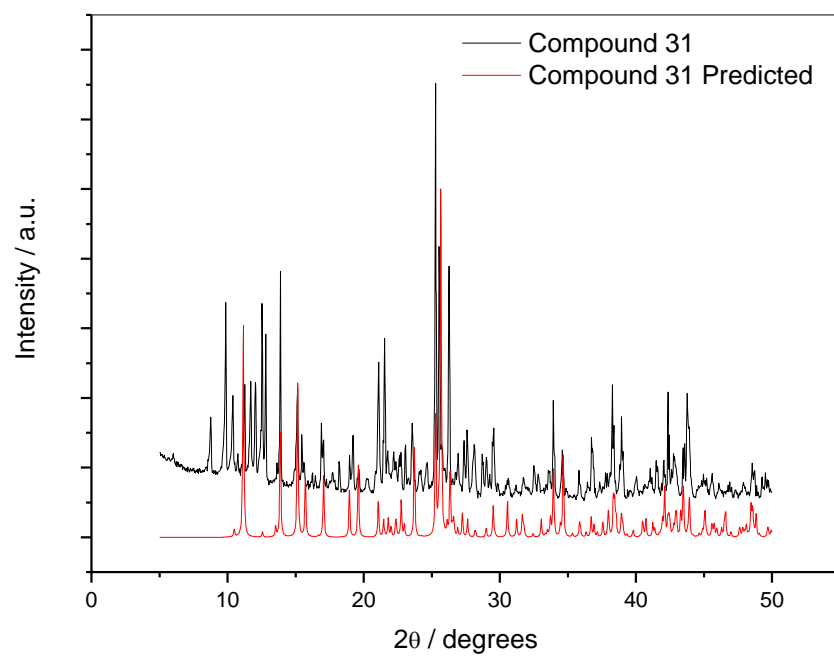
**Figure 7.59:** Secondary building unit of Cd(1) in compound 31



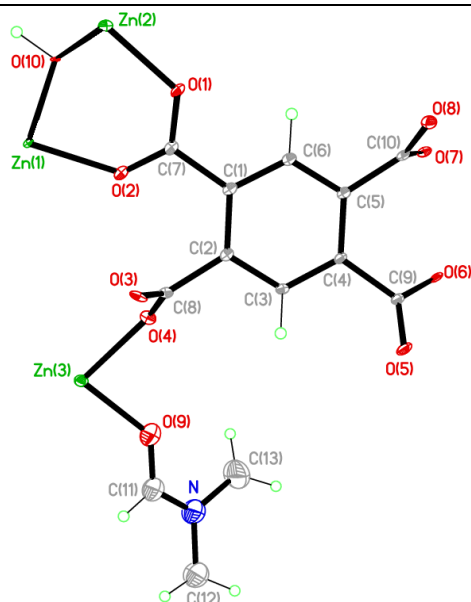
**Figure 7.60:** Three dimensional coordination motif of the bimetallic sheets potassium and cadmium cations of compound 31 viewed down the *c*-axis



**Figure 7.61:** Three dimensional coordination of compound 31 viewed down the *c*-axis



**Figure 7.62: Powder X-ray diffraction pattern of Compound 31**

**Compound 32:**  $[\text{Zn}_5(\text{C}_{10}\text{H}_2\text{O}_8)_2(\text{HO})_2(\text{C}_3\text{H}_7\text{NO})_2]$ 

Chemical formula (total)	$\text{C}_{26}\text{H}_{20}\text{N}_2\text{O}_{20}\text{Zn}_5$	
Formula weight	1007.29	
Temperature	150(2) K	
Radiation, wavelength	MoK $\alpha$ , 0.71073 Å	
Crystal system, space group	monoclinic, $P2_1/n$	
Unit cell parameters	$a = 7.1850(7)$ Å $b = 17.3170(18)$ Å $c = 13.1947(13)$ Å	$\beta = 97.076(10)^\circ$
Cell volume	$1629.2(3)$ Å <sup>3</sup>	
<i>Z</i>	2	
Crystal colour and size	colourless, $0.01 \times 0.01 \times 0.01$ mm <sup>3</sup>	
Final <i>R</i> indices [ $F^2 > 2\sigma$ ]	$R1 = 0.0543$	
<i>R</i> indices (all data)	$wR2 = 0.0954$	
Largest diff. peak and hole	0.93 and $-1.02$ e Å <sup>-3</sup>	

**Figure 7.63: Asymmetric Unit of Compound 32 all unique atoms labelled,****Synthesis**

$\text{Zn}(\text{NO}_3)_2 \cdot 6\text{H}_2\text{O}$  (0.09 g, 0.33 mmol) and 1,2,4,5-benzenetetracarboxylic acid (0.043 g, 0.17 mmol) were added to a reaction mixture of dimethylformamide (DMF) (4ml) ethanol (4mL) and water (3mL). This was placed into a 20mL Teflon-lined bomb and heated to 120°C for 24 hours. The vessel was then cooled back down to room temperature at a rate of 0.1°C / min and allowed to stand for 2 hours before colourless block crystals were retrieved from the vessel.

## Structure Determination

The data were collected at 150 K using molybdenum radiation on an Oxford Diffraction Gemini A Ultra diffractometer. The structure was solved by direct methods. The semi-empirical absorption corrections were applied based on symmetry-equivalent and repeated data. The refinement gave a  $wR2$  of 0.0954 for all 7585 independent reflections and a conventional  $R1$  of 0.0543, for 3721 reflections with  $F^2 > 2\sigma$ . The residual electron density maximum and minimum were 0.93 and  $-1.02 \text{ e } \text{\AA}^{-3}$  respectively.

The hydrogen atoms were placed in geometrically calculated positions with  $U$  constrained to  $1.2 U_{\text{eq}}(\text{C})$  for aromatic hydrogen atoms,  $1.5 U_{\text{eq}}(\text{C})$  for methyl hydrogen atoms and  $U$  constrained to  $1.5 U_{\text{eq}}(\text{O})$  for the hydroxyl hydrogen atoms. The ligands in the structure were slightly disordered and refined with SIMU and DELU restraints. The full data of compound 32 can be found in Appendix 1.

## Structure Analysis

The asymmetric unit of compound 32 (figure 7.63) shows a complete 1,2,4,5-benzenetetracarboxylate ligand, coordinating to the three zinc cations Zn(1), Zn(2) and Zn(3) that are in different coordination geometries within this polymeric compound. The Zn(1) (figure 7.64A) and Zn(3) (figure 7.64C) cations form six-coordinate octahedral geometries with the former positioned on an inversion centre. The Zn(2) cation (figure 7.64B) forms a distorted five-coordinate square pyramidal geometry.

The 1,2,4,5-benzenetetracarboxylate ligand is fully deprotonated with all four carboxylate groups delocalised, with each carboxylate oxygen coordinating to one or two (O(6), O(7)) zinc cations. The O(1)-C(7)-O(2) carboxylate coordinates to the zinc cations Zn(1) and Zn(2) through the monodentate bonds Zn(1)-O(2)  $2.031(6) \text{ \AA}$  and Zn(2)-O(1)  $1.974(6) \text{ \AA}$  forming a standard bidentate carboxylate bridge with a Zn(1)-Zn(2) distance of  $2.981(5) \text{ \AA}$ . The symmetry equivalent O(1A)-C(7A)-O(2A) is generated in the coplanar trans position by inversion symmetry around the Zn(1) cation. The Zn(1) and Zn(2) cations are further bridged by the carboxylate group O(5)-C(9)-O(6) that is a trifurcating coordination group. The O(5)-C(9)-O(6) coordinates to the Zn(1) cation forming the monodentate Zn(1)-O(6) bond and its coplanar trans symmetry

equivalent coordinates cis to the O(2) oxygen. The carboxylate group coordinates to the Zn(2) cation through the bidentate O(6) oxygen that forms a bite angle of Zn(1)-O(6)-Zn(2)  $87.1(2)^\circ$ , positioning the Zn(2) cation between the adjacent O(7)-C(10)-O(8) at an angle of O(6)-Zn(2)-O(7)  $81.6(2)^\circ$ . The O(5)-C(9)-O(6) carboxylate forms a standard bridge between Zn(1) and Zn(3) by coordinating to the Zn(3) cation through the O(5) carboxylate oxygen.

The five-coordinate Zn(2) cation is coordinated by four carboxylate groups of three symmetry equivalent carboxylate ligands, forming a bridge between Zn(1) and Zn(3). The bridging O(1)-C(7)-O(2) carboxylate group coordinates trans to the O(7)-C(8)-O(8) carboxylate of a symmetry equivalent ligand that also coordinates through the adjacent O(6)-C(9)-O(5) carboxylate as previously mentioned. The remaining chelating carboxylate is the O(3)-C(8)-O(4) group that coordinates to Zn(2) and Zn(3) cations forming the monodentate bonds Zn(2)-O(3) 2.001(6) Å and Zn(3)-O(4) 2.098(7) Å, forming a bridge between the two cations (table 7.25). The remaining O(7)-C(10)-O(8) carboxylate group also coordinates to both the Zn(2) cation and Zn(3) cation by forming a bidentate bond to the Zn(3) cation with the bite angle of O(7)-Zn(3)-O(8)  $53.1(2)^\circ$  (figure 7.64C). The Zn(3) cation also coordinates to a terminal DMF ligand cis to the trans carboxylates O(5) and O(4); O(4)-Zn(3)-O(9)  $86.5(3)^\circ$ ; the coordination geometries of the Zn(3), Zn(1) and Zn(2) cations in figure 7.64 are completed with coordination to the O(1) oxygen that forms a triply-bridged hydroxide group, linking all three coplanar zinc cations together to form the trinuclear cluster in figure 7.65. The expanded figure of 7.66 shows the full molecular building unit that expands the compound into a three dimensional coordinated framework. This forms a backbone of Zn(2)-Zn(1)-Zn(2) cations linked by the triply-bridged oxygen to Zn(3) that is also bridged by the O(3)-C(8)-O(4) and O(5)-C(9)-O(6) carboxylates to form a column of zinc cations that runs down the *a*-axis shown in figure 7.67. The columns have coordinated DMF molecules related by inversion symmetry pointing out away from the central Zn(1) cations; these point in towards the nanochannels created by the chains of 1,2,4,5-benzenetetracarboxylate ligands that link the columns of zinc cations together by creating planar pillars at  $76.68(5)^\circ$  to form the herringbone packing motif (figure 7.68). The nanochannels created by this packing motif are filled by the coordinated DMF



molecules with two pointing inwards from trans diagonals; if these coordinated ligands were removed from the structure by desolvation, nanochannels with dimensions 8.34(5) by 13.66(7) Å would be accessible for gas adsorption studies (figure 7.69). PLATON<sup>5</sup> calculates a pore volume of 612.7 Å<sup>3</sup> per unit cell corresponding to 37.3 %.

Thermogravimetric analysis was carried out on compound 32 to determine the thermostability after desolvation (figure 7.70). The TGA stage 1 shows the high thermostability of compound 32 with the compound remaining stable up to 270°C before mass loss occurs. Compound 32 undergoes a large mass loss of 2.16 mg during stage 2, compound stabilises briefly at 377°C after which it finally degrades during stage 3. The mass loss between 270-377°C equates to 16.6 % of the compound correlating to the calculated mass of DMF in the single crystal data of 14.49 %, suggesting desolvation occurs at 270°C. The desorption temperature is also close to the terminal temperature of the carboxylate metal-oxygen bonds at 330°C resulting in the framework decomposing upon desolvation.

Further analysis of the bulk sample of compound 32 was carried out using powder X-ray diffraction and elemental analysis. The powder diffraction data produced a clean diffraction pattern (figure 7.71) with peaks correlating to the predicted powder diffraction pattern from the single crystal data at 8.12 and 10.7 2-Theta. The purity of the compound was further confirmed with the elemental analysis results of C = 29.79 %, H = 1.63 % and N = 1.15 % that are consistent with the calculated values of C = 30.97 %, H = 1.98 % and N = 2.78 % from the single crystal data with small discrepancies in the nitrogen content of compound 32.

Compound 32 was synthesised using solvothermal techniques that included DMF to act as a deprotonating and templating agent. The packing motif of compound 32 around the DMF molecules and its potential porosity was of significant interest resulting in several new reactions to determine how the concentration of DMF affects of the packing orientation of the frameworks. The expanded reactions involved both increasing and decreasing the concentration of DMF; increasing the concentration produced compound 33 that shows an additional coordinated DMF that has a profound effect on the packing and availability of the nanopores. Protocols used to synthesize the analogue with no DMF coordinated in the framework proved unsuccessful producing amorphous

powders. However compounds published by Wen *et al.* (KAPHOZ)<sup>12</sup> and Zhang *et al.* (MUZHUL)<sup>13</sup> show that the packing motif with no DMF coordinated form standard grid networks with 4,4' nets of dimensions 9.554 by 9.554 Å and 7.356 by 7.356 Å respectively. The KAPHOZ<sup>12</sup> compound is templated around two potassium cations and contains eight water molecules per unit cell in the 4,4' nets, whilst MUZHUL<sup>13</sup> only contains two water molecules per unit cell.<sup>12,13</sup> Further comparisons of these compounds are carried out in conjunction with the analysis of compound 33.

**Table 6.25: Selected Bond Lengths [Å] and Angles [°] for Compound 32**

Zn(1)–O(2)	2.031(6)	Zn(1)–O(6B)	2.098(6)
Zn(1)–O(10)	2.055(5)	Zn(2)–O(1)	1.974(6)
Zn(2)–O(3D)	2.001(6)	Zn(2)–O(6B)	2.227(6)
Zn(2)–O(7B)	1.970(6)	Zn(2)–O(10)	1.999(6)
Zn(3)–O(4)	2.098(7)	Zn(3)–O(5E)	2.127(6)
Zn(3)–O(7C)	2.247(6)	Zn(3)–O(8C)	2.229(6)
Zn(3)–O(9)	1.995(7)	Zn(3)–O(10F)	2.023(5)
C(7)–O(1)	1.258(11)	C(7)–O(2)	1.243(11)
C(8)–O(3)	1.289(10)	C(8)–O(4)	1.214(10)
C(9)–O(5)	1.218(10)	C(9)–O(6)	1.272(10)
C(10)–O(7)	1.272(10)	C(10)–O(8)	1.231(10)
O(2)–Zn(1)–O(2A)	180.0(3)	O(2)–Zn(1)–O(6B)	90.5(3)
O(2)–Zn(1)–O(6C)	89.5(3)	O(2)–Zn(1)–O(10)	90.1(2)
O(2)–Zn(1)–O(10A)	89.9(2)	O(1)–Zn(2)–O(3D)	97.4(3)
O(1)–Zn(2)–O(6B)	88.7(2)	O(1)–Zn(2)–O(7B)	144.9(3)
O(1)–Zn(2)–O(10)	104.1(2)	O(4)–Zn(3)–O(5E)	169.7(2)
O(4)–Zn(3)–O(7C)	95.8(2)	O(4)–Zn(3)–O(8C)	87.6(2)
O(4)–Zn(3)–O(9)	86.5(3)	O(4)–Zn(3)–O(10F)	97.4(2)
Zn(2)–O(1)–C(7)	122.0(6)	Zn(1)–O(2)–C(7)	131.2(6)
Zn(2F)–O(3)–C(8)	124.8(6)	Zn(3)–O(4)–C(8)	137.4(6)
Zn(3G)–O(5)–C(9)	132.4(6)	Zn(1H)–O(6)–Zn(2I)	87.1(2)
Zn(1H)–O(6)–C(9)	135.2(6)	Zn(2I)–O(6)–C(9)	130.1(6)
Zn(2I)–O(7)–Zn(3H)	134.5(3)	Zn(2I)–O(7)–C(10)	130.0(6)
Zn(3H)–O(7)–C(10)	89.7(5)	Zn(3H)–O(8)–C(10)	91.6(6)
Zn(3)–O(9)–C(11)	132.3(8)	Zn(1)–O(10)–Zn(2)	94.6(2)
Zn(1)–O(10)–Zn(3D)	120.8(3)	Zn(2)–O(10)–Zn(3D)	116.5(3)
Symmetry operations for equivalent atoms			
A	$-x+1, -y+1, -z+1$	B	$x-1/2, -y+1/2, z-1/2$
C	$-x+3/2, y+1/2, -z+3/2$		
D	$x-1, y, z$	E	$-x+5/2, y+1/2, -z+3/2$
F	$x+1, y, z$		
G	$-x+5/2, y-1/2, -z+3/2$	H	$-x+3/2, y-1/2, -z+3/2$
I	$x+1/2, -y+1/2, z+1/2$		

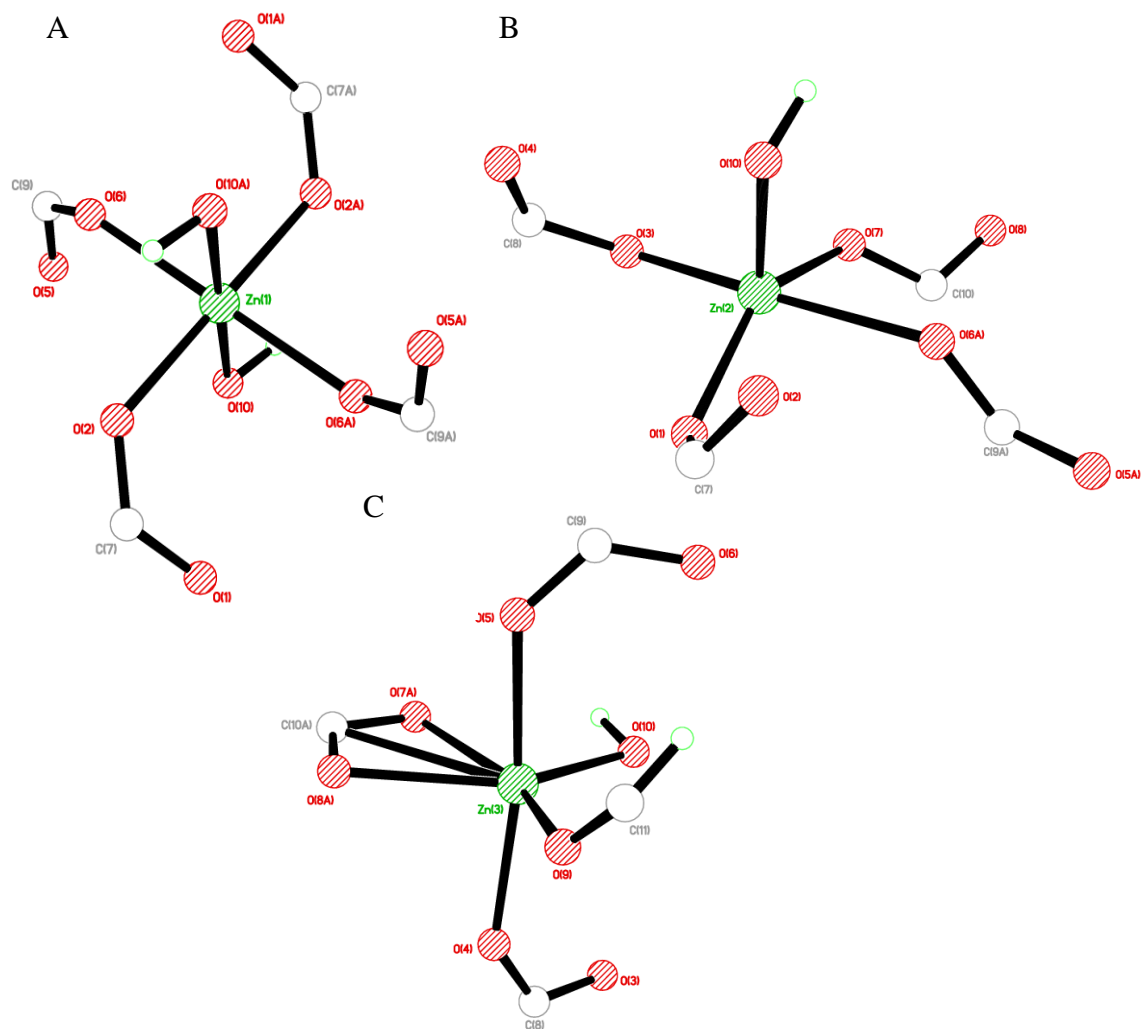


**Figure 7.64: A) Octahedral coordination environment of Zn(1), B) Square pyramidal coordination environment of Zn(2) and C) Octahedral coordination environment of Zn(3) in compound 32**

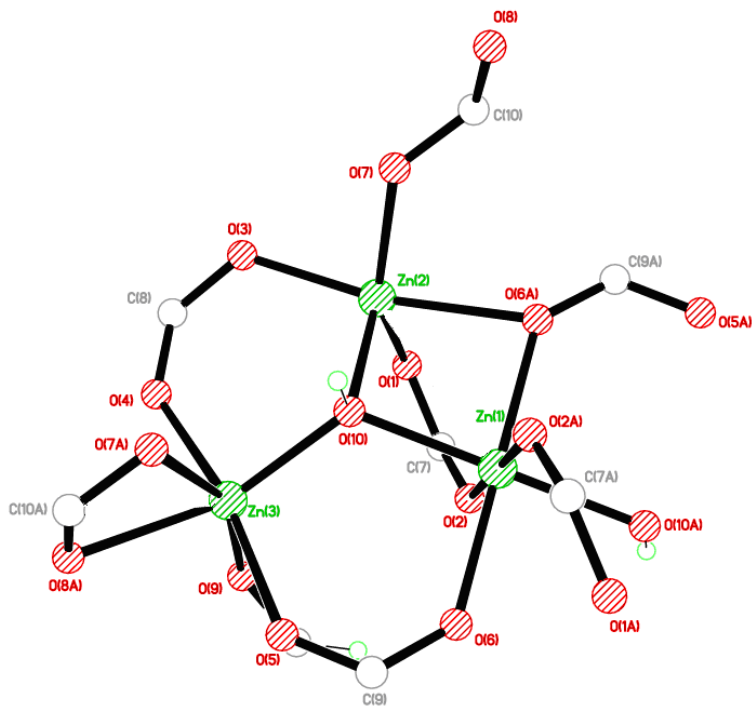


**Figure 7.65:** Trinuclear secondary building unit of Zn(1), Zn(2) and Zn(3) in compound 32 (only coordinating groups shown for clarity)

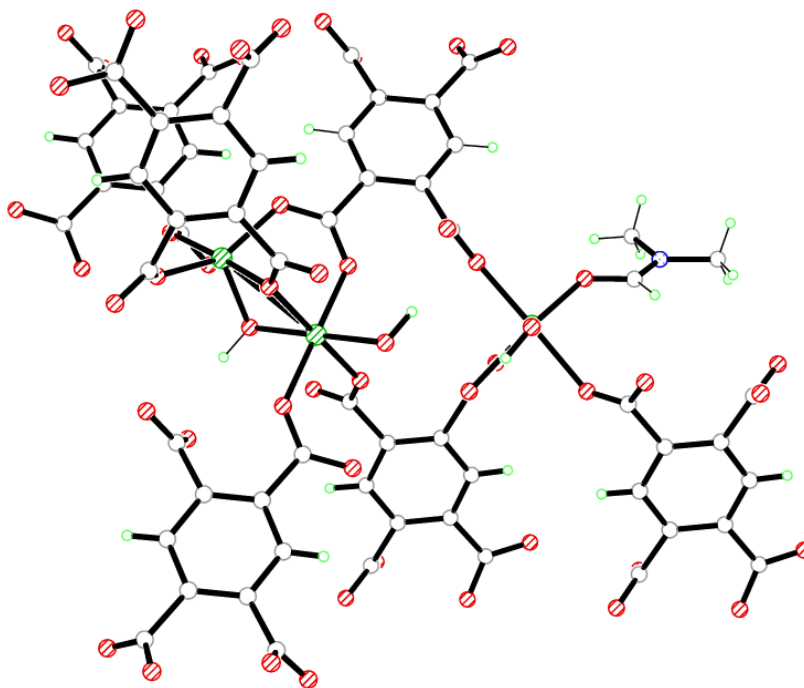


**Figure 7.66:** Trinuclear secondary building unit of Zn(1), Zn(2) and Zn(3) in compound 32

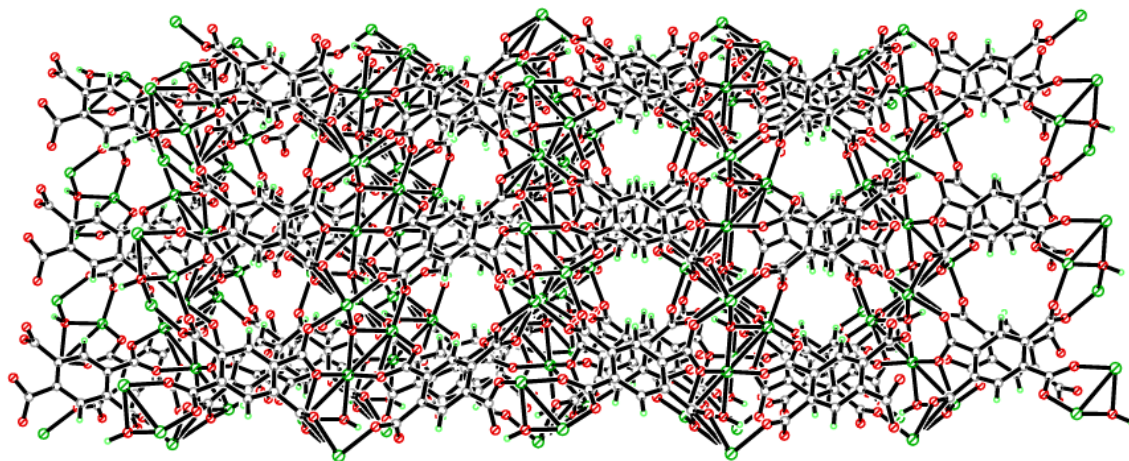


**Figure 7.67:** Three dimensional coordination of the columns in compound 32 viewed down the *b*-axis

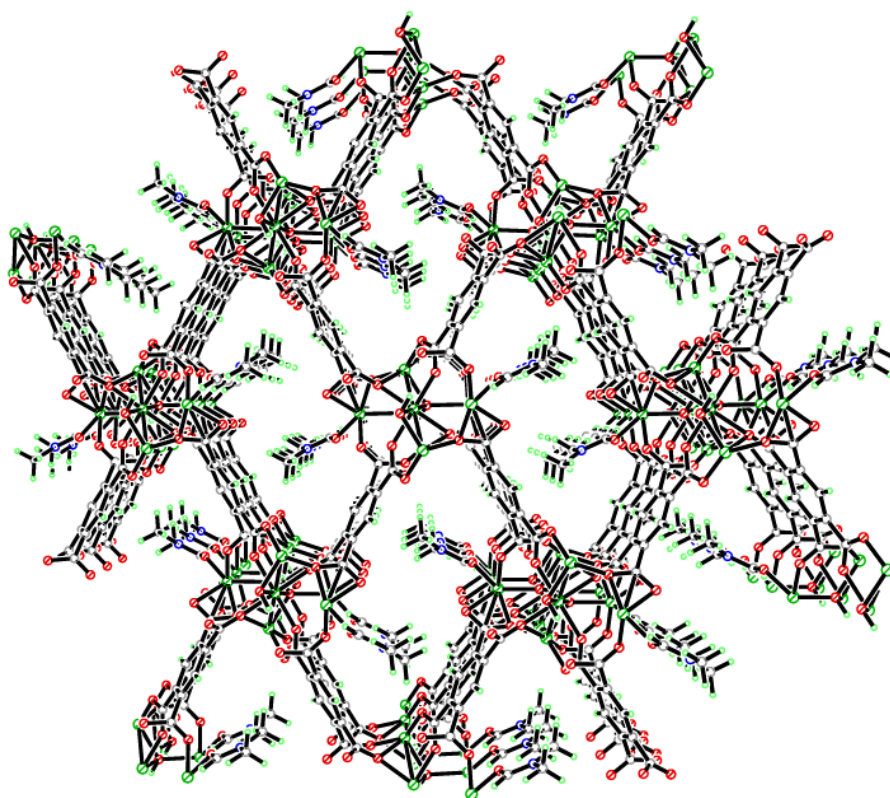


**Figure 7.68:** Three dimensional herringbone packing motif of compound 32 viewed down the *a*-axis

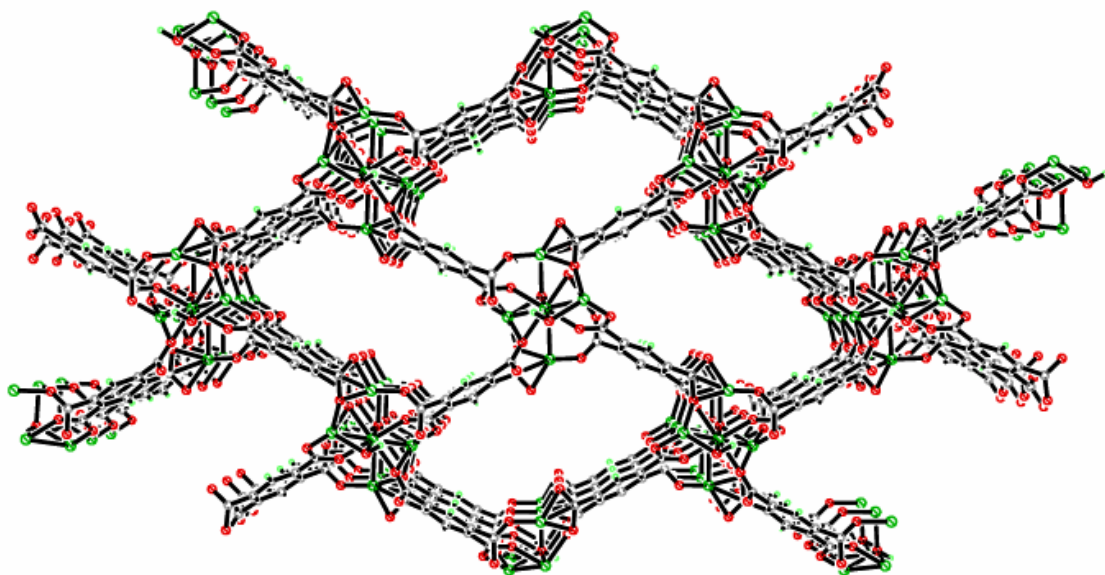


**Figure 7.69:** Three dimensional herringbone packing motif of compound 32 viewed down the *a*-axis (DMF molecules removed to display the ‘active’ pores)

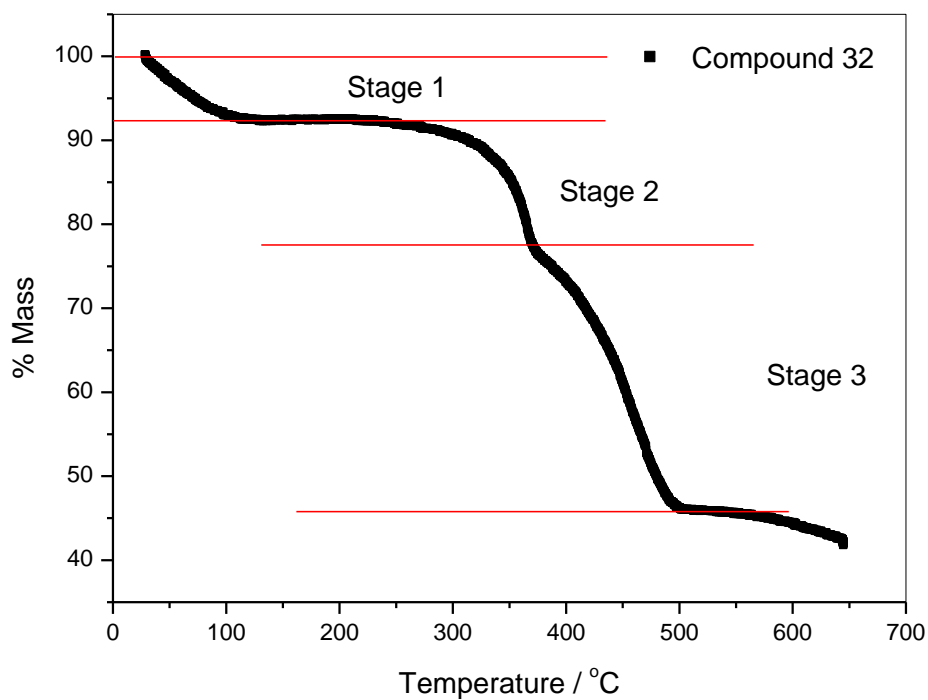


**Figure 7.70:** Thermogravimetric analysis plot of compound 32

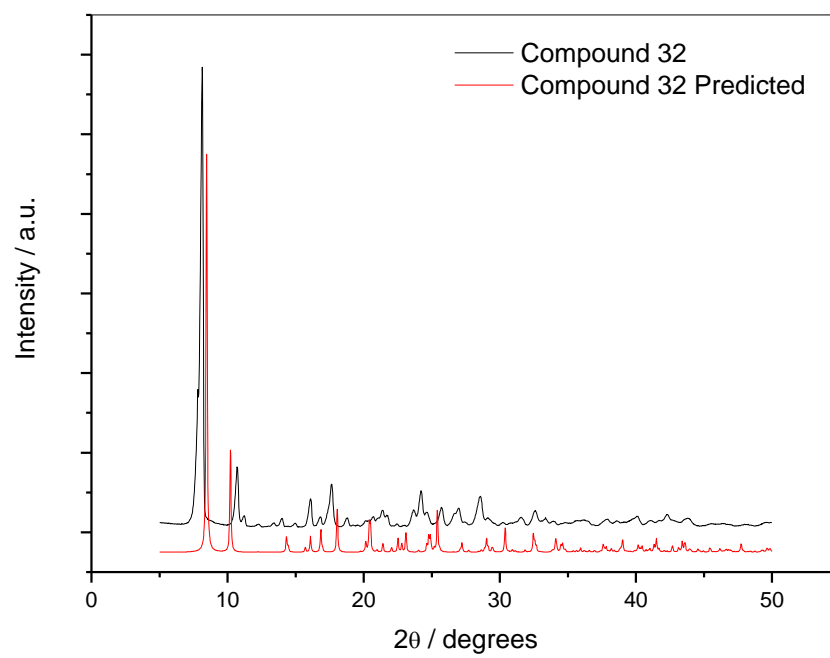
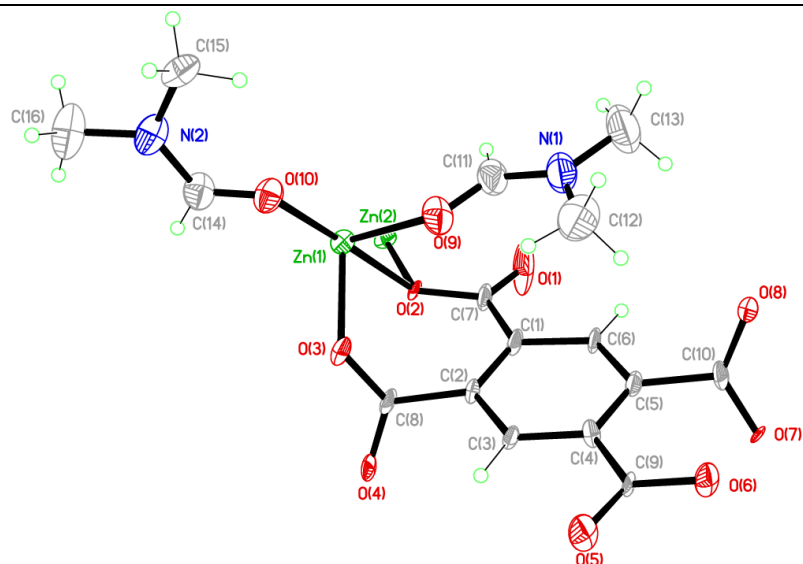


**Figure 7.71: Powder X-ray diffraction pattern of Compound 32**



**Compound 33:**  $[\text{Zn}_5(\text{C}_{10}\text{H}_2\text{O}_8)_2(\text{HO})_2(\text{C}_3\text{H}_7\text{NO})_2]$



Chemical formula (total)	$\text{C}_{16}\text{H}_{16}\text{N}_2\text{O}_{10}\text{Zn}_2$
Formula weight	527.05
Temperature	150(2) K
Radiation, wavelength	$\text{CuK}\alpha$ , 1.54178 Å
Crystal system, space group	tetragonal, $P4_2bc$
Unit cell parameters	$a = 18.72077(18)$ Å $b = 18.72077(18)$ Å $c = 11.8543(2)$ Å
Cell volume	$4154.54(9)$ Å <sup>3</sup>
Z	8
Crystal colour and size	colourless, $0.36 \times 0.06 \times 0.06$ mm <sup>3</sup>
Final $R$ indices [ $F^2 > 2\sigma$ ]	$R1 = 0.0901$
$R$ indices (all data)	$wR2 = 0.2410$
Largest diff. peak and hole	3.98 and $-0.98$ e Å <sup>-3</sup>

**Figure 7.72: Asymmetric Unit of Compound 33 all unique atoms labelled,**

**Synthesis**

$\text{Zn}(\text{NO}_3)_2 \cdot 6\text{H}_2\text{O}$  (0.09 g, 0.33 mmol) and 1,2,4,5-benzenetetracarboxylic acid (0.043 g, 0.17 mmol) were added to a reaction mixture of dimethylformamide (DMF) (4ml) and ethanol (4mL). This was placed into a 20mL Teflon-lined bomb and heated to 120°C for 24 hours. The vessel was then cooled back down to room temperature at a rate of 0.1°C / min and allowed to stand for 2 hours before colourless needle crystals were retrieved from the vessel.

## Structure Determination

The data were collected at 150 K using copper radiation on an Oxford Diffraction Gemini A Ultra diffractometer. The structure was solved by direct methods. The semi-empirical absorption corrections were applied based on symmetry-equivalent and repeated data. The refinement gave a  $wR2$  of 0.2410 for all 3661 independent reflections and a conventional  $R1$  of 0.0901, for 3609 reflections with  $F^2 > 2\sigma$ . The residual electron density maximum and minimum were 3.98 and  $-0.98 \text{ e } \text{\AA}^{-3}$  respectively; the high residual electron density in compound 33 is a result of disordered DMF molecules that although split into two parts not all the disorder could be modelled, along with the potential twinning of the structure that could not be assigned and modelled.

The hydrogen atoms were placed in geometrically calculated positions with  $U$  constrained to  $1.2 U_{eq}(\text{C})$  for aromatic hydrogen atoms. The ligands in the structure were slightly disordered and refined with SIMU, DELU and FLAT restraints. The full data of compound 33 can be found in Appendix 1.

## Structure Analysis

The asymmetric unit of compound 33 (figure 7.72) shows a complete 1,2,4,5-benzenetetracarboxylate ligand, coordinating to two zinc cations Zn(1) and Zn(2) that adopt different coordination geometries in this polymeric compound. The Zn(1) cation forms a six-coordinate octahedral geometry coordinating to four carboxylate groups from three symmetry equivalent 1,2,4,5-benzenetetracarboxylate ligands and two terminal DMF ligands (figure 7.73A). The Zn(2) cation forms a standard four-coordinate tetrahedral geometry coordinating to four symmetry equivalent 1,2,4,5-benzenetetracarboxylate ligands (figure 7.73B).

The Zn(1) cation is coordinated to the 1,2,4,5-benzenetetracarboxylate ligand by the monodentate bond to the O(2) oxygen of the O(1)-C(7)-O(2) carboxylate that forms the longest Zn-O bond of the complex at  $2.214(7) \text{ \AA}$ . The elongation of this bond occurs as the O(2) carboxylate oxygen also coordinates to the Zn(2) cation; Zn(2)-O(2)  $1.996(6) \text{ \AA}$  acting as a bidentate chelate to bridge both zinc cations with a bite angle of Zn(1)-O(2)-Zn(2)  $102.5(3)^\circ$ . The 1,2,4,5-benzenetetracarboxylate further coordinates to

the Zn(1) cation forming a monodentate bond Zn(1)-O(3) 2.030(7) Å that coordinates cis to the O(1)-C(7)-O(2) carboxylate holding the Zn(1) cation between the two carboxylate groups with a bite angle of O(2)-Zn(1)-O(3) 81.1(3)°. Symmetry equivalent 1,2,4,5-benzenetetracarboxylate ligands then coordinate to the Zn(1) cation through the monodentate bonds Zn(1)-O(5A) and Zn(1)-O(7B) in the trans and cis positions respectively to the O(3)-C(8)-O(4) carboxylate. The remaining two coordination sites on the octahedral zinc cation are occupied by terminal DMF molecules that coordinate in the cis and trans coplanar positions to the O(2) carboxylate oxygen; O(2)-Zn(1)-O(9) 91.4(3)° and O(2)-Zn(1)-O(10) 178.5(3)° (figure 7.73A)(table 7.26).

Symmetry equivalent Zn(2) cations are coordinated to each carboxylate group of the complete 1,2,4,5-benzenetetracarboxylate ligand in the asymmetric unit, allowing the carboxylates to form bridging units between the Zn(1) and Zn(2) cations producing the dinuclear pentacarboxylate building unit shown in figure 7.74. The Zn(2) cation is first bridged by the bidentate O(2) carboxylate oxygen with the O(1) oxygen remaining uncoordinated, the Zn(2) is then bridged to a symmetry equivalent Zn(1) cation by a standard carboxylate bridge with monodentate bonds from both carboxylate oxygens to the respective zinc cations to form the dinuclear building unit with a Zn(1)-Zn(2) distance of 3.267(5) Å. The O(5)-C(9)-O(6) and O(7)-C(10)-O(8) carboxylates act as the standard bridging carboxylates between the two zinc cations with O(6) and O(8) coordinating to the Zn(2) cation at an angle of O(6A)-Zn(2)-O(8B) 115.5(3)° within the tetrahedral geometry of the Zn(2) cation; with a respective coordination of O(5A)-Zn(1)-O(7B) 86.6(3)° to the Zn(1) cation. The bifurcated O(2) bridge completes the paddle-wheel of the dinuclear building unit, the building units are linked together by the O(3)-C(8)-O(4) carboxylate group that coordinates to Zn(1) and the to a Zn(2A) of a separate building unit at an angle of 90.94(10)°. This distorted paddle-wheel building unit creates columns of zinc cations that run down the *c*-axis connected by 1,2,4,5-benzenetetracarboxylates that run perpendicular to each other at 89.54(8)° intersecting at the paddle-wheel unit. This coordination motif forms nanochannels that run down the *c*-axis shown in figure 7.75, these channels are blocked by the coordinated cis DMF molecules on the Zn(1) cation that point away from each other at 89.7(3)°. This angle coupled with the positioning of the Zn(1) cation relative to the nanochannels, creates

nanochannels with two different coordination environments. The first nanochannel has the Zn(1) cations placed at the four corners of the square, with DMF molecules pointing inwards at an angle of  $67.55(4)^\circ$  to the adjacent aromatic ring of the 1,2,4,5-benzenetetracarboxylate ligand that forms the wall of the channel; the nanochannel is generated by a four-fold rotation axis at its centre that generates four DMF molecules inside the channel. The adjacent nanochannels are a result of the first channel with the second coordinated DMF of the Zn(1) cation pointing away from the first channel towards the adjacent nanochannel. The Zn(1) cation is positioned  $2.214(9) \text{ \AA}$  above the plane of the aromatic ring of the 1,2,4,5-benzenetetracarboxylate that forms the walls of the channels, this results in the second DMF only partially penetrating the second nanochannel threading through the  $9.225(8) \text{ \AA}$  gaps between the 1,2,4,5-benzenetetracarboxylates in the walls. As a result of this coordination a “chess-board” packing motif is formed with one open and one closed pore down the *c*-axis (figure 7.75). The open pore has a potential accessible pore before desolvation with dimensions  $4.566(9) \text{ by } 4.566(9) \text{ \AA}$  with a two-fold rotation axis at its centre. Prior to desolvation compound 33 could be useful as a nanoporous molecular sieve, with small selective pores similar to those in compound 17. After desolvation of the coordinated DMF a predicted grid motif shown in figure 7.76 would be formed with extensive pores of dimensions  $10.091(5) \text{ by } 10.091(5) \text{ \AA}$ ; these nanochannels are intersected by triangular channels running down the *a*-axis with dimensions  $8.056(10) \text{ by } 11.196(13) \text{ \AA}$  previously closed by DMF molecules before desolvation (figure 7.77).

PLATON<sup>5</sup> confirms the presence of pores upon desolvation with a calculated pore volume of  $2022.1 \text{ \AA}^3$  per unit cell, corresponding to 49 %.

Thermogravimetric analysis was carried out on compound 33 to determine the temperature profile indicating thermostability and desolvation temperatures (figure 7.78). The TGA stage 1 shows a rapid mass loss between  $20\text{--}50^\circ\text{C}$  resulting from excess surface solvent within the compound; stage 2 shows a mass loss of  $0.780 \text{ mg}$  is observed between  $75\text{--}95^\circ\text{C}$  before the compound stabilises up until  $135^\circ\text{C}$ , after which it begins to decompose in stage 3. The mass loss of  $0.780 \text{ mg}$  can be equated to 13.36 % of the mass loss of the dried compound, this is consistent to half the DMF calculated from the single crystal data of 27.70 % suggesting compound 33 can only be partially desolvated.

Further analysis of the bulk sample of compound 33 was carried out using powder X-ray diffraction and elemental analysis. The elemental analysis of compound 33 produced the results C = 37.01 %, H = 3.72 % and N = 3.84 % that correlate with the calculated values from the single crystal data; C = 36.42 %, H = 3.04 % and N = 5.31 % indicating the high purity of the bulk material. This is further confirmed with the powder X-ray diffraction data producing the diffraction pattern in figure 7.79 that is consistent with the predicted pattern calculated from the single crystal data; with major peaks at 9.27, 11.42, 24.53 and 30.31 2-Theta in both diffraction patterns.

Compound 33 was synthesised as an extension of compound 32 by removing water from the reaction media to increase the DMF concentration, this resulted in the double coordination of DMF to the zinc cation in compound 33 compared to that of the single axial DMF in compound 32. The double capped Zn(1) cation in compound 33 (figure 7.73A) prevents the structure from forming the triply bridged building unit observed in compound 32 (figure 7.65) and results in a geometrically standard packing motif with chains of 1,2,4,5-benzenetetracarboxylate ligands diverging perpendicular to one another forming the grid network motif observed in compound 33. The grid packing motif of compound 33 is indicative of the hydrated compounds KAPHOZ<sup>12</sup> and MUZHUL<sup>13</sup> with both structures composed of dimeric tetrahedral building units to form the regular arrays of perpendicular columns. The MUZHUL<sup>13</sup> compound also exhibits the intersecting triangular pores formed between the 1,2,4,5-benzenetetracarboxylate ligands that form the chains between the zinc building units and have the dimensions 4.650 by 8.162 Å. The bonding characterisation and potential pore sizes of compounds 32, 33, KAPHOZ and MUZHUL are compared in table 7.27 which shows the consistency throughout the compounds.

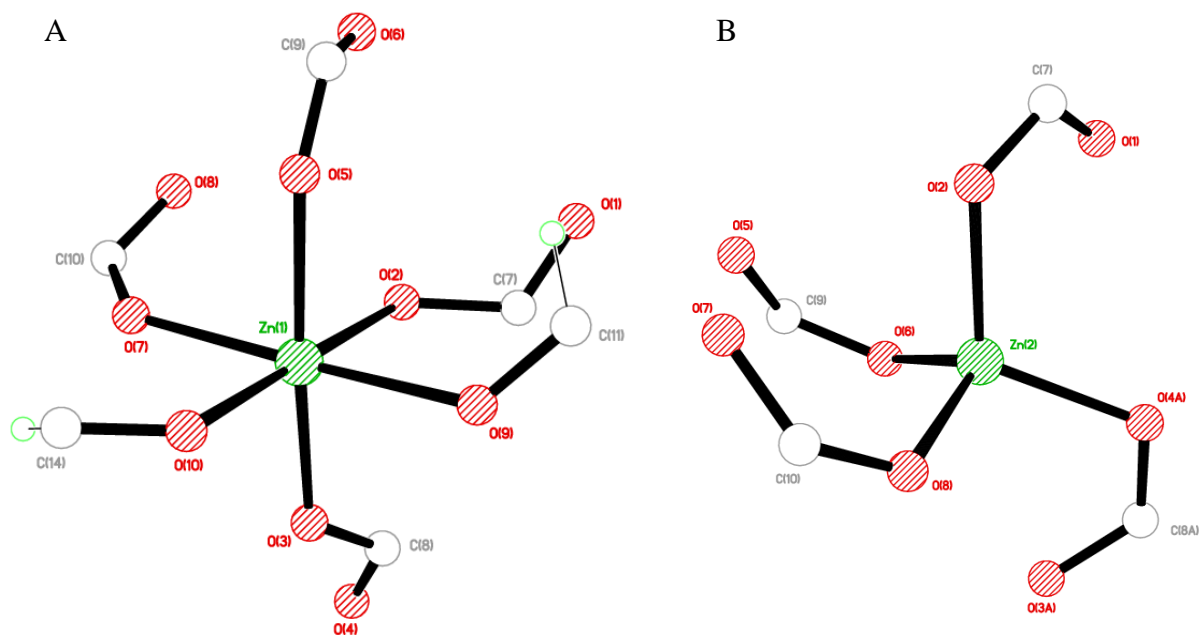
**Table 7.26: Selected Bond Lengths [ $\text{\AA}$ ] and Angles [ $^\circ$ ] for Compound 33**

Zn(1)–O(2)	2.214(7)	Zn(1)–O(3)	2.030(7)
Zn(1)–O(5A)	2.068(8)	Zn(1)–O(7B)	2.094(6)
Zn(1)–O(9)	2.104(8)	Zn(1)–O(10)	2.050(7)
Zn(2)–O(2)	1.996(6)	Zn(2)–O(4C)	1.958(7)
Zn(2)–O(6A)	1.934(7)	Zn(2)–O(8B)	1.980(7)
C(7)–O(1)	1.209(15)	C(7)–O(2)	1.320(12)
C(8)–O(3)	1.249(12)	C(8)–O(4)	1.242(12)
C(9)–O(5)	1.218(12)	C(9)–O(6)	1.258(12)
C(10)–O(7)	1.284(12)	C(10)–O(8)	1.246(12)
O(2)–Zn(1)–O(3)	81.1(3)	O(2)–Zn(1)–O(5A)	91.4(3)
O(2)–Zn(1)–O(7B)	92.6(3)	O(2)–Zn(1)–O(9)	91.0(3)
O(2)–Zn(1)–O(10)	178.5(3)	O(3)–Zn(1)–O(5A)	172.4(3)
O(3)–Zn(1)–O(7B)	93.0(3)	O(3)–Zn(1)–O(9)	91.2(3)
O(3)–Zn(1)–O(10)	97.5(3)	O(2)–Zn(2)–O(4C)	115.4(3)
O(2)–Zn(2)–O(6A)	108.3(3)	O(2)–Zn(2)–O(8B)	99.8(3)
Zn(1)–O(2)–Zn(2)	102.5(3)	Zn(1)–O(2)–C(7)	122.8(6)
Zn(2)–O(2)–C(7)	114.5(6)	Zn(1)–O(3)–C(8)	128.8(7)
Zn(2D)–O(4)–C(8)	113.9(6)	Zn(1E)–O(5)–C(9)	145.8(7)
Zn(2E)–O(6)–C(9)	119.7(6)	Zn(1F)–O(7)–C(10)	134.3(6)
Zn(2F)–O(8)–C(10)	125.3(6)		

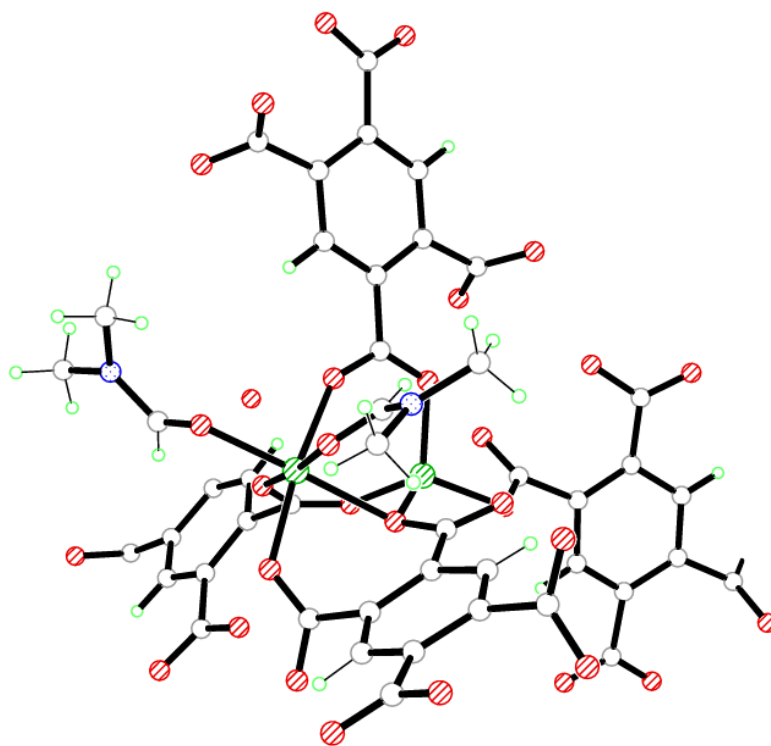
Symmetry operations for equivalent atoms

A  $y, -x, z-1/2$  B  $x+1/2, -y+1/2, z$  C  $-y+1/2, -x+1/2, z-1/2$ D  $-y+1/2, -x+1/2, z+1/2$  E  $-y, x, z+1/2$  F  $x-1/2, -y+1/2, z$ **Table 7.27: Average bond length and pore dimension comparisons between Compound 33, Compound 32, KAPHOZ<sup>12</sup> and MUZHUL<sup>13</sup>**

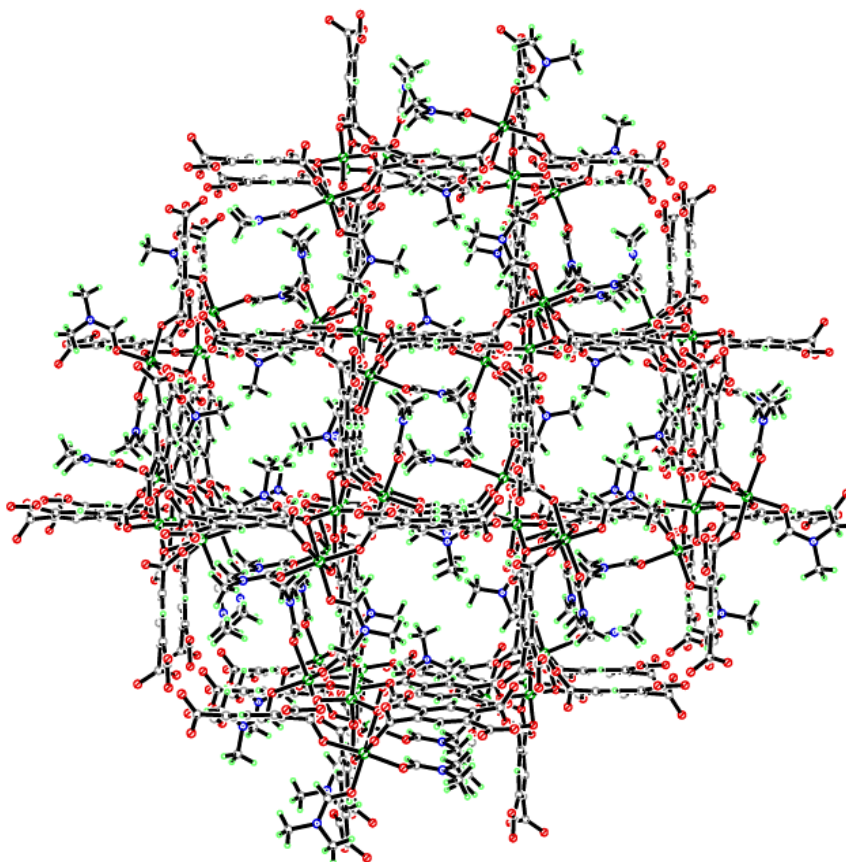
Compound	Bond	Average bond Length ( $\text{\AA}$ )	Pore dimensions ( $\text{\AA}$ )
Compound 32	Zn–O	2.098	8.34 by 13.66
Compound 33	Zn–O	2.023	10.09 by 10.09
KAPHOZ	Zn–O	1.977	9.554 by 9.554
MUZHUL	Zn–O	1.986	7.356 by 7.356



**Figure 7.73: A) Octahedral coordination environment of Zn(1) and B) Tetrahedral coordination environment of Zn(2) in compound 33**

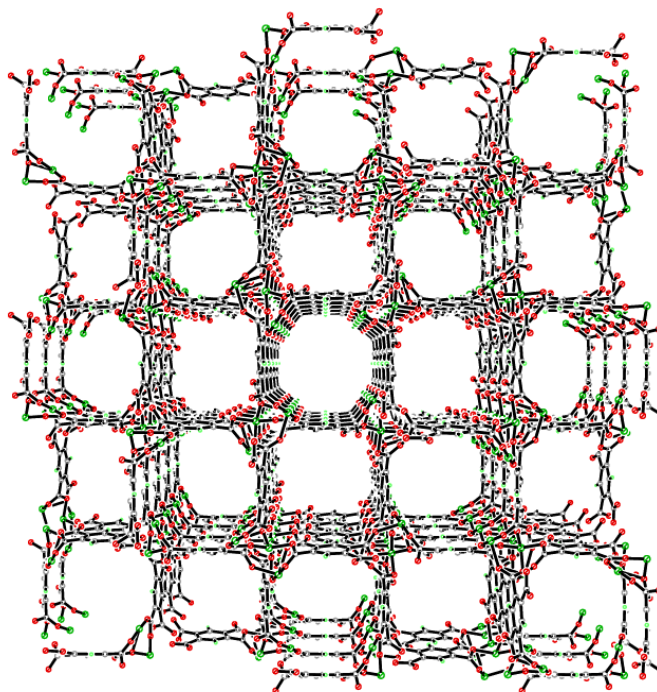


**Figure 7.74: Dinuclear paddle-wheel secondary building unit of Zn(1) and Zn(2) in compound 33**

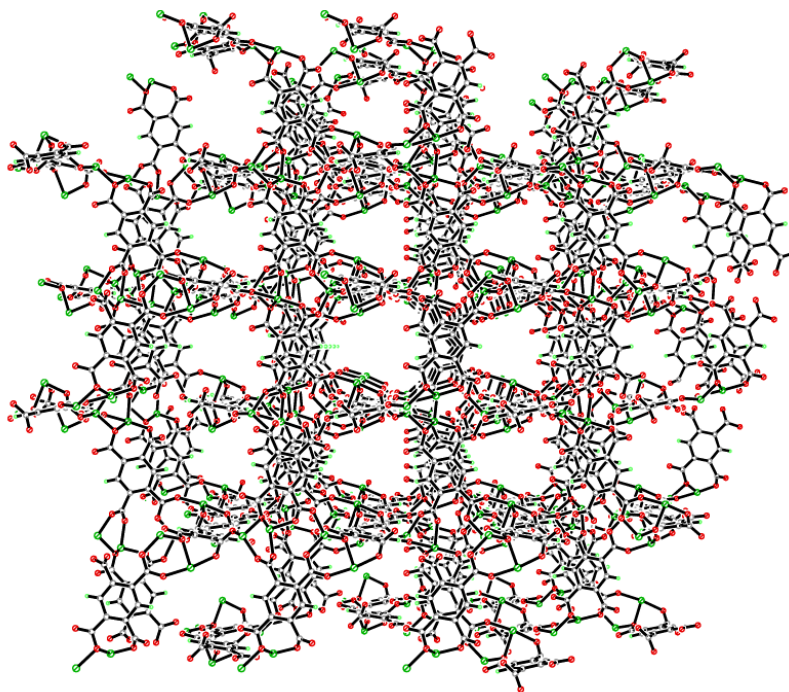


**Figure 7.75:** Three dimensional “chess board” packing in compound 33 viewed down the *c*-axis

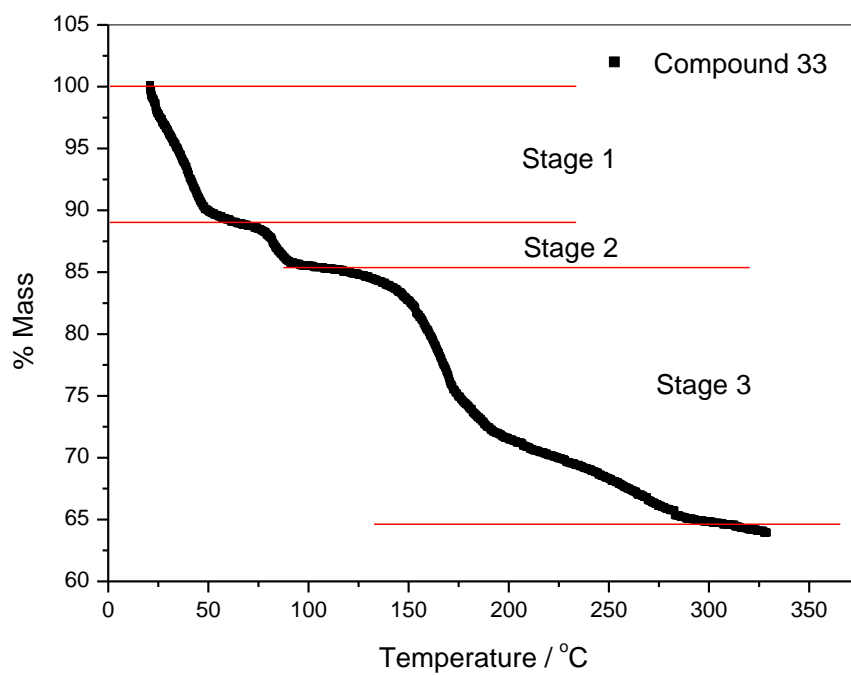




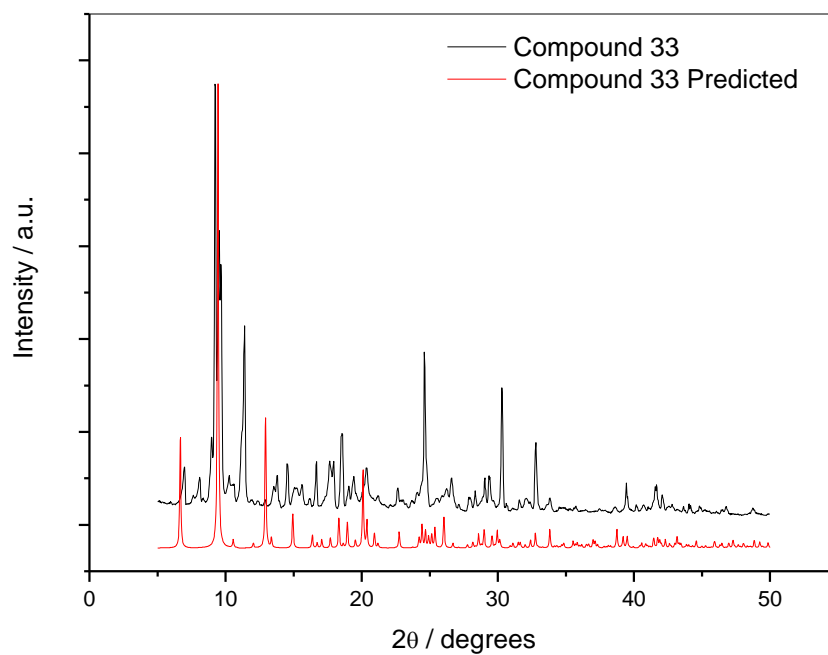
**Figure 7.76:** Predicted three dimensional “chess board” packing in compound 33 upon desolvation viewed down the *c*-axis



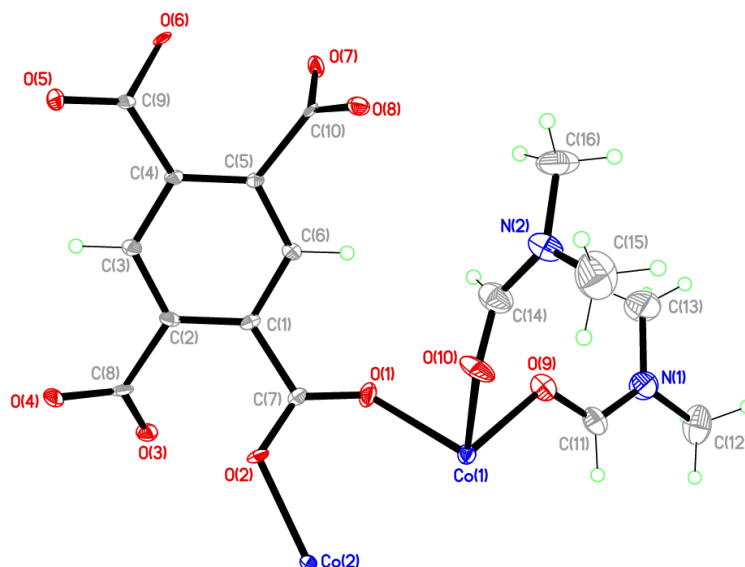
**Figure 7.77:** Three dimensional packing in compound 33 upon desolvation viewed down the *a*-axis



**Figure 7.78: Thermogravimetric analysis plot of compound 33**



**Figure 7.79: Powder X-ray diffraction pattern of Compound 33**

**Compound 34:**  $[\text{Co}_2(\text{C}_{10}\text{H}_2\text{O}_8)(\text{C}_3\text{H}_7\text{NO})_2]$ 

Chemical formula (total)	$\text{C}_{16}\text{H}_{16}\text{Co}_2\text{N}_2\text{O}_{10}$
Formula weight	514.17
Temperature	150(2) K
Radiation, wavelength	MoK $\alpha$ , 0.71073 Å
Crystal system, space group	monoclinic, <i>Cc</i>
Unit cell parameters	$a = 10.7225(6)$ Å $\beta = 90.545(5)^\circ$ $b = 15.4438(9)$ Å $c = 11.6936(6)$ Å
Cell volume	$1936.33(19)$ Å <sup>3</sup>
<i>Z</i>	4
Crystal colour and size	purple, $0.60 \times 0.05 \times 0.05$ mm <sup>3</sup>
Final <i>R</i> indices [ $F^2 > 2\sigma$ ]	$R1 = 0.0330$
<i>R</i> indices (all data)	$wR2 = 0.0458$
Largest diff. peak and hole	0.32 and $-0.35$ e Å <sup>-3</sup>
Absolute structure parameter	0.040(19)

**Figure 7.80: Asymmetric Unit of Compound 34 all unique atoms labelled,****Synthesis**

$\text{Co}(\text{NO}_3)_2 \cdot 6\text{H}_2\text{O}$  (0.09 g, 0.33 mmol) and 1,2,4,5-benzenetetracarboxylic acid (0.043 g, 0.17 mmol) were added to a reaction mixture of dimethylformamide (DMF) (4ml) and ethanol (4mL). This was placed into a 20mL Teflon-lined bomb and heated to 120°C for 24 hours. The vessel was then cooled back down to room temperature at a rate of 0.1°C / min and allowed to stand for 2 hours before colourless needle crystals were retrieved from the vessel.

## Structure Determination

The data were collected at 150 K using molybdenum radiation on an Oxford Diffraction Gemini A Ultra diffractometer. The structure was solved by direct methods. The semi-empirical absorption corrections were applied based on symmetry-equivalent and repeated data. The refinement gave a  $wR2$  of 0.0458 for all 2358 independent reflections and a conventional  $R1$  of 0.0330, for 1640 reflections with  $F^2 > 2\sigma$ . The residual electron density maximum and minimum were 0.32 and  $-0.35 \text{ e } \text{\AA}^{-3}$  respectively. Compound 34 crystallised in the non-centrosymmetric space group  $Cc$  and refined with a Flack parameter of 0.040 indicating the correct handedness has been selected.

The hydrogen atoms were placed in geometrically calculated positions with  $U$  constrained to  $1.2 U_{eq}(C)$  for aromatic hydrogen atoms and  $1.5 U_{eq}(C)$  for methyl hydrogen atoms. The ligands in the structure were slightly disordered and refined with SIMU, DELU restraints. The full data of compound 34 can be found in Appendix 1.

## Structure Analysis

The asymmetric unit of compound 34 (figure 7.80) shows a complete 1,2,4,5-benzenetetracarboxylate ligand, coordinating to two cobalt cations Co(1) and Co(2) that adopt different coordination geometries within this polymeric compound. The Co(1) cation forms a six-coordinate octahedral geometry coordinating to four carboxylate groups from three symmetry equivalent ligands and two terminal DMF ligands (figure 7.81A). The Co(2) cation forms a distorted four-coordinate tetrahedral geometry (figure 7.81B) coordinating to four carboxylate groups of symmetry equivalent 1,2,4,5-benzenetetracarboxylate ligands (table 7.28).

The Co(1) cation is coordinated to the 1,2,4,5-benzenetetracarboxylate by the monodentate bond to the O(1) of the O(1)-C(7)-O(2) carboxylate; Co(1)-O(1) 2.101(4) Å and by the monodentate O(3) from the O(3)-C(8)-O(4) carboxylate group from a symmetry equivalent ligand that coordinates in the cis position to the O(1) oxygen, O(1)-Co(1)-O(3A) 90.01(16)°. The remaining two carboxylate groups that coordinate to the Co(1) cation are provided by a third symmetry equivalent 1,2,4,5-benzenetetracarboxylate ligand that chelates through the O(6)-C(9)-O(5) and O(7)-

C(10)-O(8) carboxylates, bridging the Co(1) cation using the monodentate bonds Co(1)-O(6) and Co(1)-O(7) with a bite angle of  $80.59(15)^\circ$  that coordinates cis and trans to the O(1) carboxylate oxygen respectively. The Co(1) cations coordination geometry is completed by two terminal DMF ligands that coordinate cis to the O(1) oxygen and to one another; O(9)-Co(1)-O(10)  $87.51(17)^\circ$  and O(1)-Co(1)-O(9)  $95.15(17)^\circ$  forming the six-coordinate octahedral shown in figure 6.81A similar to the Zn(1) cation in compound 33 (figure 7.73A).

Symmetry equivalent Co(2) cations coordinate to each carboxylate group on the complete 1,2,4,5-benzenetetracarboxylate ligand allowing the carboxylates to act as bridging units between both Co(1) and Co(2) cations. The Co(2) cation is first bridged by the O(1)-C(7)-O(2) carboxylate that forms the monodentate bonds Co(2)-O(2)  $1.980(4) \text{ \AA}$  and Co(1)-O(1)  $2.101(4) \text{ \AA}$  forming a standard carboxylate bridge between Co(1) and Co(2). The two cations are further bridged by the O(3)-C(8)-O(4) carboxylate of a symmetry equivalent ligand that coordinates to Co(2) at an angle of O(2)-Co(2)-O(4A)  $126.89(18)^\circ$  with the monodentate bond Co(2)-O(4) and then to the Co(1) cation with the Co(1)-O(3) bond. The two cations are finally bridged by a bidentate carboxylate oxygen O(6) that bridges the Co(1) and Co(2) cations with a bridging angle of Co(1)-O(6)-Co(2)  $102.85(17)^\circ$ , completing the core of the paddle-wheel building unit with a Co(1)-Co(2) distance of  $3.229(5) \text{ \AA}$ . These dinuclear clusters are then linked together by the O(7)-C(10)-O(8) carboxylate group that coordinates to the Co(1) cation with the monodentate Co(1)-O(7) and then to the Co(2A) cation with the O(8) carboxylate that coordinates at an angle of O(2)-Co(2)-O(8A)  $118.16(16)^\circ$ . The bridges the two paddle-wheel building units at an angle of  $139.7(2)^\circ$  with an additional weak interaction forming between the Co(2A) and the O(7) carboxylate oxygen; Co(2A)-O(7)  $2.418(4) \text{ \AA}$ . This elongated interaction results in the distorted tetrahedral geometry of the Co(2) cation with bond angles listed in table 7.28.

The paddle-wheel building unit formed from the dinuclear cluster is shown in figure 7.82 with the Co(1) cation capped by the two DMF molecules. These units expand the structure to form a fully coordinated three dimensional framework consisting of 'zigzag' chains of dinuclear cobalt paddle-wheel units that run down the *c*-axis with each paddle-wheel positioned at  $139.7(2)^\circ$  with respect to next paddle-wheel,

creating the ‘zigzagging’ in the chain (figure 7.83). The paddle-wheel chains are connected by the axial and equatorial 1,2,4,5-benzenetetracarboxylate ligands that intersect at the paddle-wheel at an of  $119.4(6)^\circ$  with respect to the planes of the aromatic rings, these form the walls of the nanochannels that run down the *c*-axis forming the diamond net packing motif when viewed down the *c*-axis (figure 7.84). The nanochannels are blocked by two coordinated *cis* DMF molecules on the Co(1) cation that point away from each other into adjacent nanochannels, the positioning of the Co(1) cation with two symmetry equivalents at the corners of each nanochannel results in four DMF molecules pointing into each channel. This occurs as the Co(1) cation is positioned coplanar in the centre between the planar adjacent 1,2,4,5-benzenetetracarboxylate ligands that are separated by  $9.028(7) \text{ \AA}$  with the DMF ligands pointing away from each other at  $87.51(17)^\circ$ . These nanochannels if desolvated would form pores with dimensions  $9.041(5)$  by  $9.041(5) \text{ \AA}$  with the diamond packing shown in figure 7.85.

PLATON<sup>5</sup> confirms the presence of pores upon desolvation with a calculated pore volume of  $862.6 \text{ \AA}^3$  per unit cell corresponding to 44.6 %.

Thermogravimetric analysis of compound 34 produced the TGA plot in figure 7.86. The TGA shows that compound 34 begins to lose mass immediately upon heating in stage 1 and fully degrades between  $30\text{--}200^\circ\text{C}$ . The low thermal stability of compound 34 indicates that the material cannot be desolvated without structural collapse rendering the compound unusable for further applications.

The bulk sample of compound 34 was analysed further to determine the purity and validation of the synthesis method for further expansions. The elemental analysis showed satisfactory results of C = 35.61 %, H = 2.88 % and N = 4.73 %; which correspond to the calculated values from the single crystal data of C = 37.34 %, H = 3.12 % and N = 5.44 %. The powder X-ray diffraction data for compound 34 corresponds with the predicted diffraction pattern from the single crystal data, with significant peaks at 10 and 12 2-Theta with a slight shift in angle between the predicted and the calculated powder diffraction patterns (figure 7.87).

Compound 34 was synthesised as an expansion of compound 33 to investigate the templating effects of DMF on the structure of transition metal-1,2,4,5-

benzenetetracarboxylate frameworks. Compound 33 and 34 share similar building units with paddle-wheels directing the structure topology, with the formation of nanopores by cis coordinated DMF molecules on the octahedral nodes with bond lengths compared in table 7.29. Compound 34 forms a different pore packing to the regulated grids observed in compound 33 and MUZHUL<sup>13</sup> due to the glide plane symmetry that runs throughout the structure along with the lack of the four-fold and two-fold rotation symmetry that are present in compound 33. The structure of compound 34 has previously been reported by Ng *et al.* (OCACUR)<sup>14</sup> with very little structural and chemical analysis. A second compound published by Shi *et al.* (FITZUE)<sup>15</sup> shows how the packing motif is altered when the DMF molecules coordinate in the trans positions with respect to each other. The compound FITZUE forms two dimensional sheets comprising of 4,4' nets with dimensions 6.114 by 10.506 Å with a similar diamond shaped packing motif to compound 34 with the nets filled with four DMF molecules. The trans DMF molecules prevent the compound from expanding down the *b*-axis forcing the sheets to stack, held together by hydrogen bonds. This suggests that only the cis coordination of the DMF will result in a coordinated framework with a packing motif that contains diamond shaped nets. The synthesis of compound 34 and its structural similarities to compound 33 suggested that the possibility of producing compounds with less coordinated DMF including fully hydrated compound was possible. The synthesis that followed yielded compound 35, the fully hydrated analogue of compound 34.

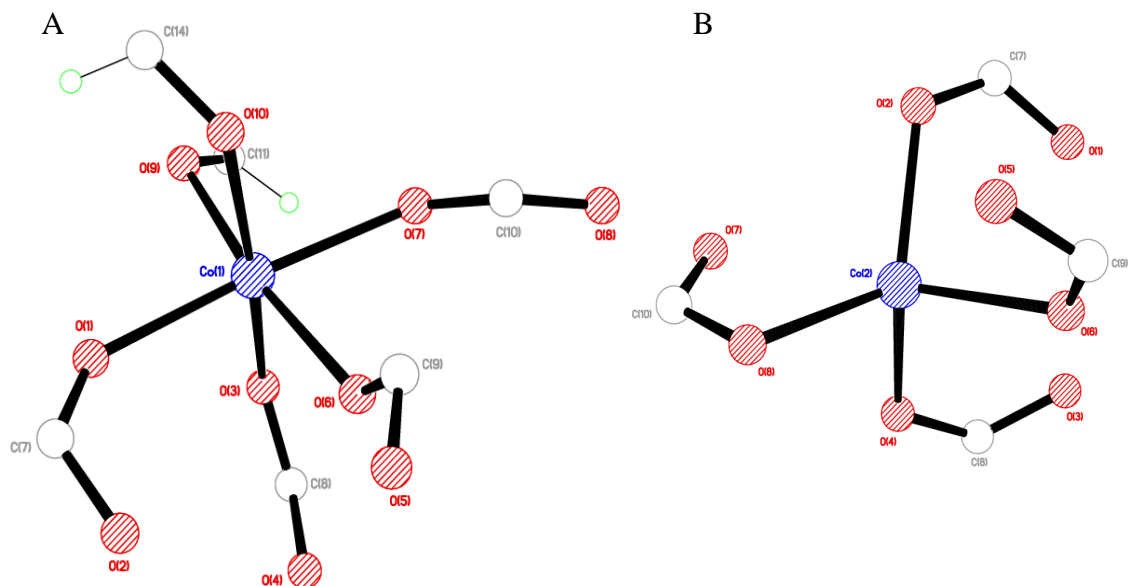
**Table 7.28: Selected Bond Lengths [ $\text{\AA}$ ] and Angles [ $^\circ$ ] for Compound 34**

Co(1)–O(1)	2.101(4)	Co(1)–O(3A)	2.055(4)
Co(1)–O(6B)	2.133(4)	Co(1)–O(7B)	2.096(4)
Co(1)–O(9)	2.066(5)	Co(1)–O(10)	2.056(4)
Co(2)–O(2)	1.980(4)	Co(2)–O(4A)	1.990(4)
Co(2)–O(6B)	1.995(4)	Co(2)–O(7C)	2.418(4)
Co(2)–O(8C)	1.999(4)	C(7)–O(1)	1.232(7)
C(7)–O(2)	1.261(7)	C(8)–O(3)	1.224(7)
C(8)–O(4)	1.289(8)	C(9)–O(5)	1.213(6)
C(9)–O(6)	1.306(7)	C(10)–O(7)	1.237(6)
O(1)–Co(1)–O(3A)	90.01(16)	O(1)–Co(1)–O(6B)	93.09(16)
O(1)–Co(1)–O(7B)	173.47(18)	O(1)–Co(1)–O(9)	95.15(17)
O(1)–Co(1)–O(10)	89.15(19)	O(2)–Co(2)–O(4A)	126.89(18)
O(2)–Co(2)–O(6B)	95.81(14)	O(2)–Co(2)–O(7C)	83.59(15)
O(2)–Co(2)–O(8C)	118.16(16)		
Symmetry operations for equivalent atoms			
A $x, -y+1, z+1/2$ B $x+1/2, -y+1/2, z+1/2$ C $x+1/2, y+1/2, z$			

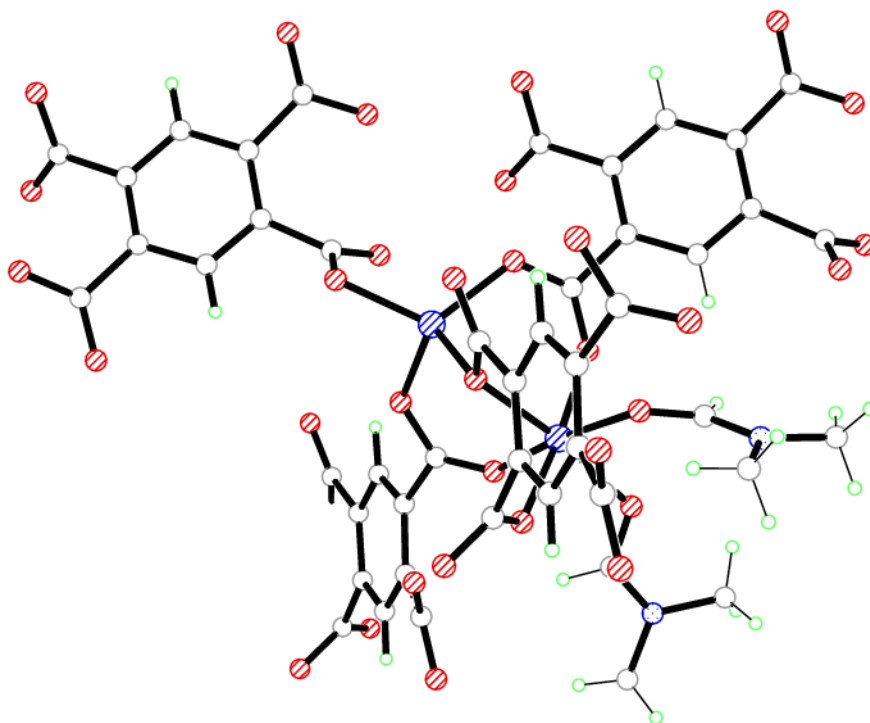
**Table 7.29: Average bond length and pore dimension comparisons between Compound 33, Compound 34 and FITZUE<sup>15</sup>**

Compound	Bond	Average bond Length ( $\text{\AA}$ )
Compound 33	Zn-O	2.023
Compound 34	Co-O	2.061
FITZUE	Co-O	2.049

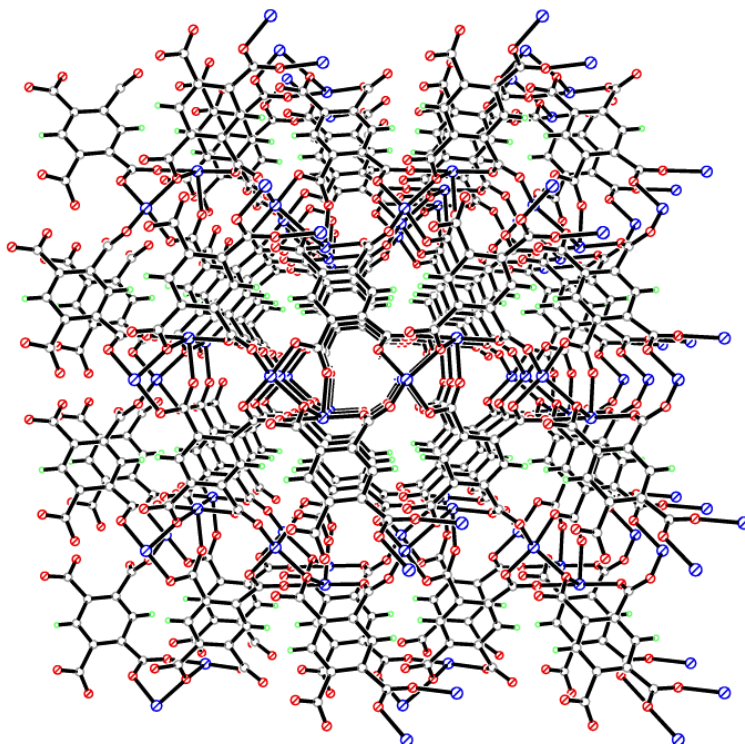




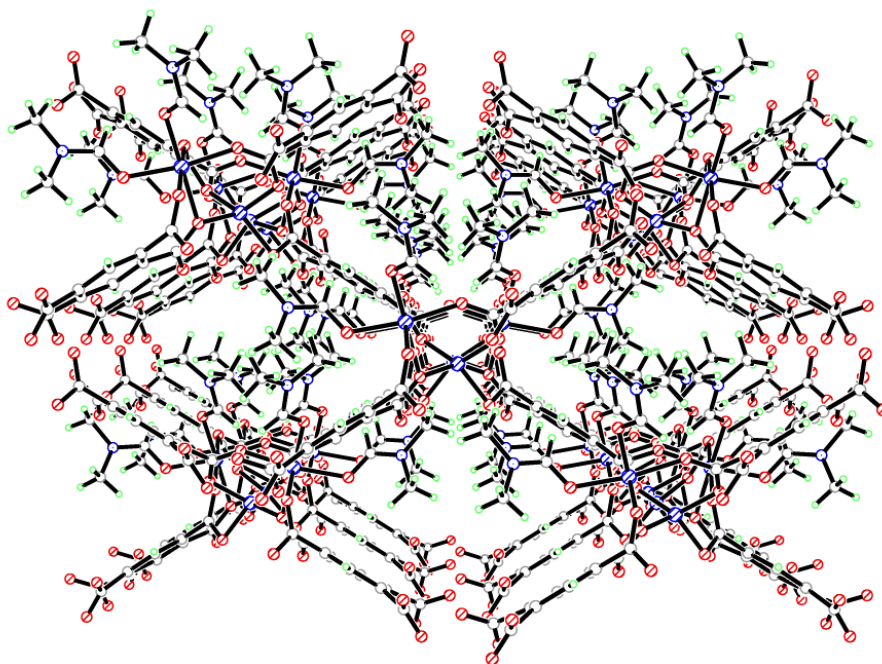
**Figure 7.81: A) Octahedral coordination environment of Co(1) and B) Tetrahedral coordination environment of Co(2) in compound 34**



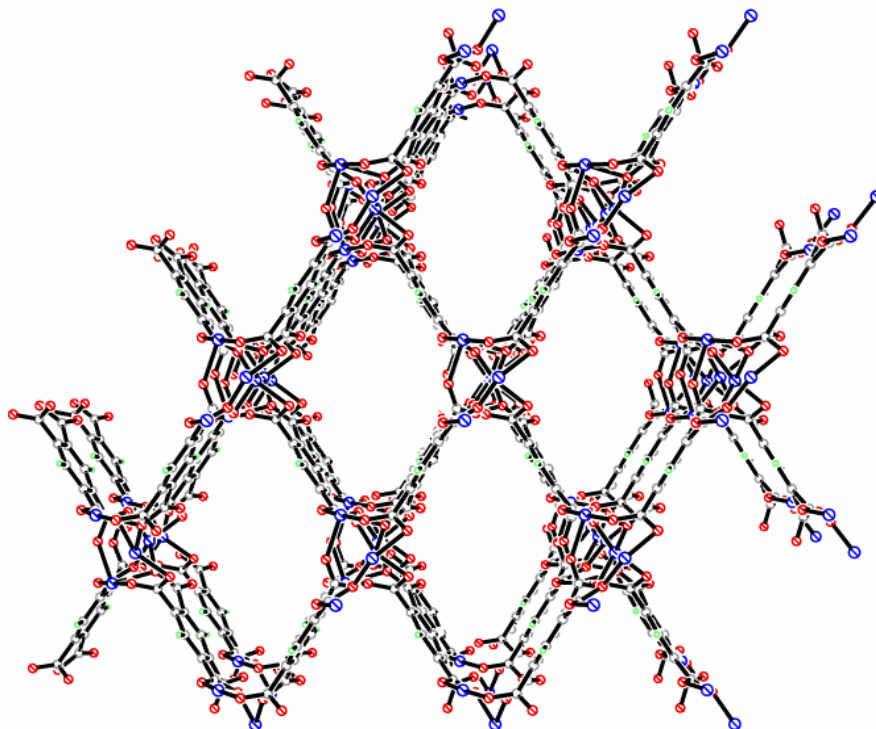
**Figure 7.82: Dinuclear paddle-wheel secondary building unit of Co(1) and Co(2) in compound 34**



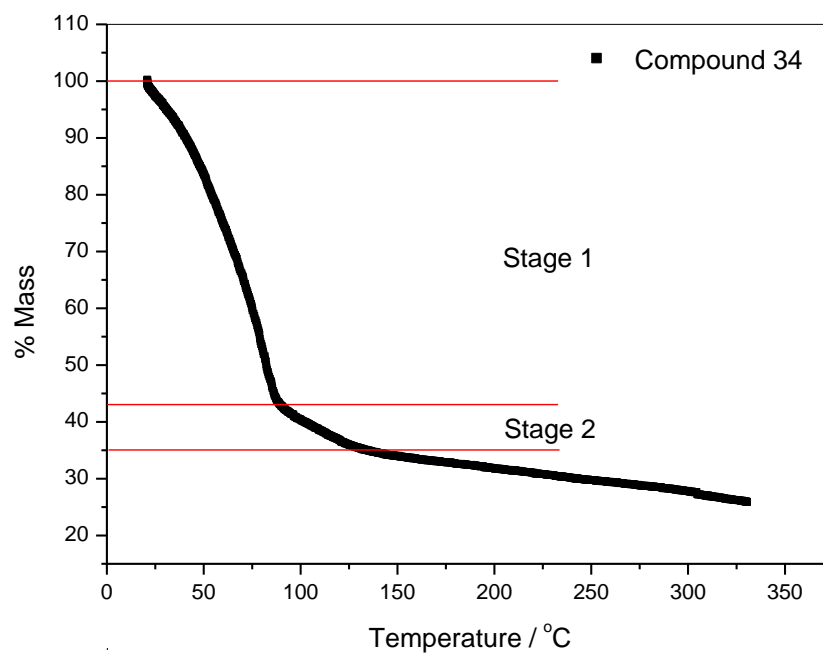
**Figure 7.83:** Three dimensional packing in compound 34 viewed down the *a*-axis



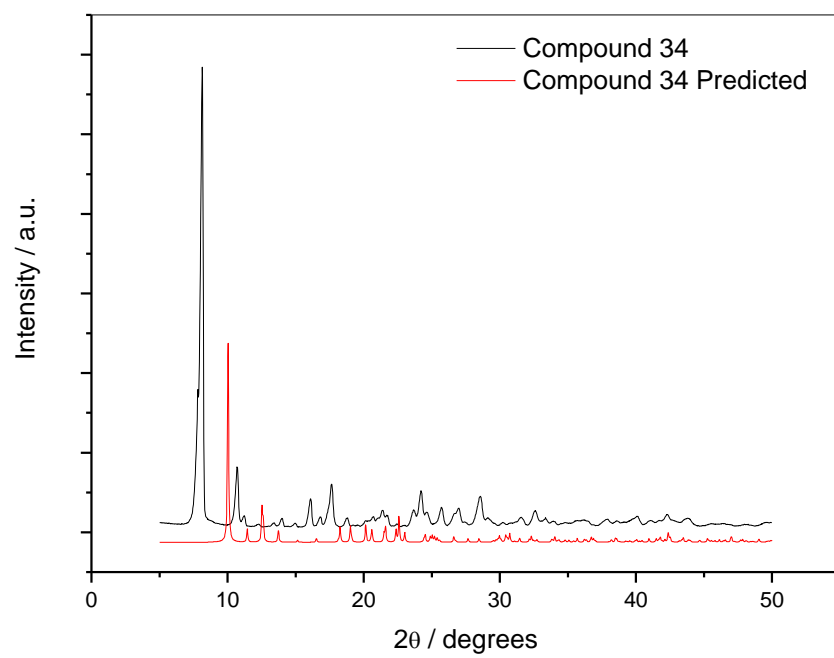
**Figure 7.84:** Three dimensional diamond packing in compound 34 viewed down the *c*-axis



**Figure 7.85:** Predicted three dimensional packing in compound 34 upon desolvation viewed down the *c*-axis



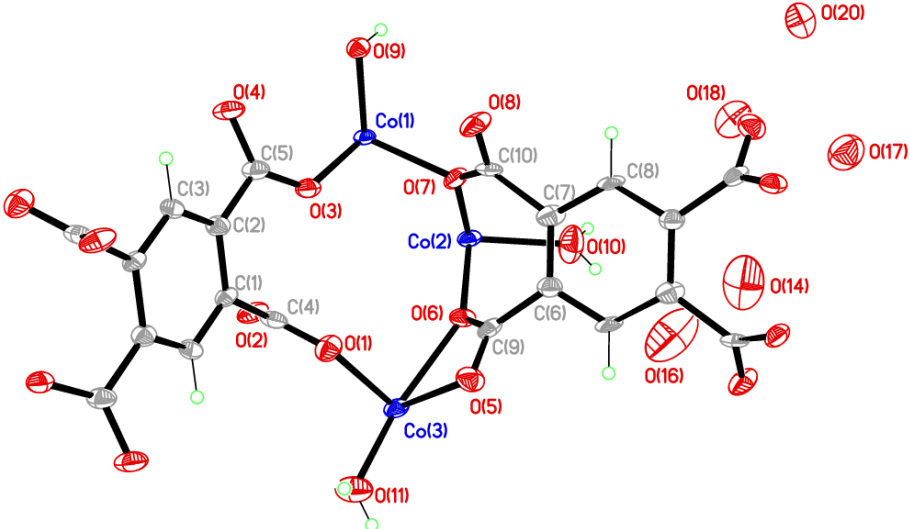
**Figure 7.86:** Thermogravimetric analysis plot of compound 34



**Figure 7.87: Powder X-ray diffraction pattern of Compound 34**

**Compound 35:**  $[\text{Co}_5(\text{C}_{10}\text{H}_2\text{O}_8)_2(\text{OH})_2(\text{H}_2\text{O})_4] \cdot 12\text{H}_2\text{O}$

---

	
Chemical formula (total)	$\text{C}_{20}\text{H}_{38.4}\text{Co}_5\text{O}_{34.2}$
Formula weight	1120.76
Temperature	150(2) K
Radiation, wavelength	CuK $\alpha$ , 1.54178 Å
Crystal system, space group	triclinic, $P\bar{1}$
Unit cell parameters	$a = 7.3542(7)$ Å $\alpha = 90.224(7)^\circ$ $b = 11.3815(11)$ Å $\beta = 103.941(7)^\circ$ $c = 11.7017(9)$ Å $\gamma = 104.896(9)^\circ$
Cell volume	$916.39(14)$ Å <sup>3</sup>
Z	1
Crystal colour and size	purple, $0.10 \times 0.10 \times 0.10$ mm <sup>3</sup>
Final <i>R</i> indices [ $F^2 > 2\sigma$ ]	$R1 = 0.0613$
<i>R</i> indices (all data)	$wR2 = 0.1603$
Largest diff. peak and hole	0.98 and $-0.83$ e Å <sup>-3</sup>

---

**Figure 7.88:** Asymmetric Unit of Compound 35 all unique atoms labelled, additional atoms added to complete ligands

**Synthesis**

1 mL of a solution of  $\text{Co}(\text{NO}_3)_2 \cdot 6\text{H}_2\text{O}$  (0.096 g, 0.33 mmol) in dimethylformamide (DMF) (10 mL) was syringed into one side of the H-Cell vessel, 1 mL of a solution of 1,2,4,5-benzenetetracarboxylic acid (0.043 g, 0.17 mmol) in DMF (10 mL) was then syringed into the other side of the H-Cell vessel. The independent solutions were bridged by 2 mL water that was carefully layered into the bridging tube. After ten weeks, purple block crystals formed.

## Structure Determination

The data were collected at 150 K using copper radiation on an Oxford Diffraction Gemini A Ultra diffractometer. The structure was solved by direct methods. The semi-empirical absorption corrections were applied based on symmetry-equivalent and repeated data. The refinement gave a  $wR2$  of 0.1603 for all 2829 independent reflections and a conventional  $R1$  of 0.0613, for 1846 reflections with  $F^2 > 2\sigma$ . The residual electron density maximum and minimum were 0.98 and  $-0.83 \text{ e } \text{\AA}^{-3}$  respectively.

The hydrogen atoms were placed in geometrically calculated positions with  $U$  constrained to  $1.2 U_{\text{eq}}(\text{C})$  for aromatic hydrogen atoms and  $U$  constrained to  $1.5 U_{\text{eq}}(\text{O})$  for hydroxyl hydrogen atoms. The water ligands in the structure were disordered; with SIMU and SADI restraints being imposed for refinement. The full data of compound 35 can be found in Appendix 1.

## Structure Analysis

The asymmetric unit of compound 35 (figure 7.88) shows two half 1,2,4,5-benzenetetracarboxylate ligands completed by inversion symmetry around the centre of the respective aromatic rings, coordinating to three cobalt cations Co(1), Co(2) and Co(3) that all form six-coordinate octahedral geometries (figure 7.89).

The Co(1) cation is positioned on an inversion centre and coordinates to both 1,2,4,5-benzenetetracarboxylate ligands, coordinating to the O(3)-C(5)-O(4) carboxylate through the monodentate Co(1)-O(3) 2.050(5) Å bond and then to the O(7)-C(10)-O(8) carboxylate with the monodentate Co(1)-O(7) 2.137(5) Å bond that coordinates cis to the O(3) oxygen at an angle of  $91.4(2)^\circ$ . The remaining coordination geometry is completed by a triply bridged hydroxide that links the Co(1), Co(2) and Co(3) cations together forming a trinuclear cluster through the O(9) oxygen; the remaining coordination sites are occupied by the trans coplanar symmetry equivalents of the coordinated ligands generated by the inversion symmetry at Co(1) (figure 7.89A).

The O(3)-C(5)-O(4) and O(7)-C(10)-O(8) carboxylates of the two respective 1,2,4,5-benzenetetracarboxylate ligands bridge the Co(1) and Co(2) cations; the O(3)-C(5)-O(4) carboxylate forms a standard carboxylate bridge with the monodentate bonds

Co(1)-O(3) and Co(2)-O(4) placing them coplanar with a Co(1)-Co(2) distance of 3.148(5) Å. This bridges the cations perpendicular to the O(9) triply bridged coordinating in the cis position on the respective cations. The O(7)-C(10)-O(8) carboxylate coordinates through the bidentate O(7) oxygen that forms a bite angle of Co(1)-O(7)-Co(2) 95.3(2)° coordinating cis to the O(9) triple bridge, in the coplanar position with a O(7)-O(9) distance 2.715(4) Å. The Co(2) cation is capped by a terminal water molecule trans to the triply bridged hydroxide O(9), the remaining two coordination sites are occupied by the remaining carboxylate on the 1,2,4,5-benzenetetracarboxylate ligand O(1)-C(4)-O(2) and O(5)-C(9)-O(6) that bridge the Co(2) and Co(3) cations. The O(1)-C(4)-O(2) carboxylate coordinates to the Co(2) cation in an axial position cis to the triply bridged O(9), the O(1) oxygen then coordinates to a Co(3) cation with the monodentate Co(3)-O(1) 2.062(5) Å bond that places the Co(3) cation planar to the Co(2) and Co(1) cations at a Co(2)-Co(3) distance of 3.516(5) Å. The Co(2) and Co(3) cations are further bridged by the O(5)-C(9)-O(6) carboxylate that bridges the cations using the bidentate O(6) carboxylate oxygen with a Co(2)-O(6)-Co(3) bite angle of 139.1(2)° (table 7.30). The O(5)-C(9)-O(6) carboxylate acts as a trifurcated chelate coordinating with a bidentate bond to the Co(3) cation with a bite angle of 58.39(19)°. This bidentate coordination introduces the distortion to the Co(3) cation octahedral geometry (figure 7.89C) coordinating cis to the trifurcated bridging carboxylate O(7)-C(10)-O(8) that connects all three cobalt cations and cis to the Co(2)-Co(3) bridging carboxylate O(1)-C(4)-O(2). The Co(3) cation completes its octahedral geometry coordinating to the triply bridged hydroxide O(9) that is coordinated slightly out the plane of the cobalt cations by 0.962(4) Å, this forms the trinuclear building unit shown in figure 7.90 and 7.91 that show the different orientations of the bridged cluster. The central trinuclear cluster in figure 7.90 is doubled by inversion symmetry through the Co(1) cation that becomes the central node of the columns consisting of cobalt cations that run down the *a*-axis, these are joined together by planar chains of 1,2,4,5-benzenetetracarboxylate ligands that are related by the inversion symmetry. The chains intersect at the columns coordinating perpendicular at an offset angle of 98.32(13)° forming the walls of the nanochannels that run down the *a*-axis (figure 7.92).

The nanochannels contain four coordinated water molecules that hydrogen bond to the twelve disordered uncoordinated water molecules in the channel related by inversion symmetry (table 7.31). If compound 35 was dehydrated it would create accessible pores with the dimensions 6.220(5) by 5.130(5) Å in a diamond packing motif (figure 7.93) that run down the *a*-axis. The channels can be viewed in the hydrated form down the *b*-axis (figure 7.94) that shows a cross section of the channels running parallel to the columns of cobalt cations. Smaller channels are also observed down the *b*-axis and *c*-axis that intersect the cross sections of the channels running down the *a*-axis when the compound is desolvated; these channels have dimensions 4.266(5) by 3.063(5) Å and are shown in figure 7.95.

PLATON<sup>5</sup> confirms the presence of an extensive porous network upon desolvation with a calculated pore volume of 401.8 Å<sup>3</sup> per unit cell corresponding to 44.3 %. To confirm the presence of the pores and their potential accessibility upon desolvation thermogravimetric analysis of compound 35 was carried out producing the TGA plot in figure 7.96. The TGA shows that compound 35 undergoes desolvation during stage 2 between 115-190°C with a mass loss of 1.26 mg corresponding to 23.59 % of the compound; this correlates with the calculated amount of water in the single crystal of 19.27 %. After desolvation the compound stabilises in stage 3 forming a plateau between 190-300°C before it reaches its terminal temperature and begins to degrade during stage 4 between 300-450°C. Further analysis of the thermostability of compound 35 was carried out using Hot-stage microscopy in an attempt to observe crystalline changes upon heating with the possibility of obtaining the desolvated crystal for structural analysis. The temperature profile for the Hot-stage followed that of the TGA with heating at slow increments of 5°C between 160-320°C before the temperature was held at 350°C for 24 hours to ensure desolvation before cooling to room temperature. During the Hot-stage process the crystals of compound 35 changed in colour from light pink to a deep purple/blue as the structure was desolvated (figure 97). After the heating and cooling phases the crystal was removed for further analysis; however upon removal the crystal shattered preventing the analysis of the desolvated compound by single crystal X-ray diffraction.



Additional analysis of the bulk material of compound 35 was carried out using elemental analysis to investigate the purity of the sample; this produced the results C = 19.87 %, H = 2.89 % and N = 0 % that are consistent with the calculated values from the single crystal data, C = 21.41 %, H = 3.43 % and N = 0 % indicating that the synthesis protocol has produced a significantly pure compound.

Compound 35 is the hydrated analogue of compound 34, both structures show similar packing motifs creating columns of cobalt cations connected by perpendicular chains of 1,2,4,5-benzenetetracarboxylate ligands that coordinate to the cations using multidentate carboxylate groups. The structures for the diamond packing motif creating nets with dimensions 6.22 by 5.13 Å and 9.04 by 9.04 Å respectively to form the diamond pores in figure 7.93 and 7.85. These packing motifs are achieved utilizing different coordination geometries of the respective cobalt cations. Compound 35 contains six-coordinate octahedral nodes bridged by a central hydroxide anion to form a trinuclear cluster, compound 34 is built around one octahedral and one tetrahedral node to form a dimeric paddle-wheel building unit. Although the two compounds utilize different building units they both involved the perpendicular coordination of the 1,2,4,5-benzenetetracarboxylate ligands with respect to each other, creating the walls of the nanochannels in the packing motif. The switch from DMF as a template in compound 34 to water in compound 35 reduces the gap between each adjacent 1,2,4,5-benzenetetracarboxylate ligand from 9.028(5) Å to 4.266(5) Å as the structure forms a close packing motif without the steric bulk of the interpenetrating DMF molecules. This results in the potential pore volume reducing from 44.6 % to 44.3 % as the intersecting pores are slightly narrower. The potential applications of compound 35 are hindered by the synthesis protocol used to prepare the compound, as the H-Cell has elongated crystallisation times and low reproducibility resulting in no further analysis of the compound; however new synthetic routes were beginning to prove successful with powder products produced from solvothermal reactions showing close matches to the predicted powder diffraction pattern of the single crystal data of compound 35.

**Table 7.30: Selected Bond Lengths [ $\text{\AA}$ ] and Angles [ $^\circ$ ] for Compound 35**

Co(1)–O(3)	2.050(5)	Co(1)–O(7)	2.137(5)
Co(1)–O(9)	2.090(5)	Co(2)–O(2B)	2.078(5)
Co(2)–O(4A)	2.045(5)	Co(2)–O(6)	2.085(5)
Co(2)–O(7)	2.122(5)	Co(2)–O(9A)	2.095(5)
Co(2)–O(10)	2.114(7)	Co(3)–O(1)	2.062(5)
Co(3)–O(5)	2.177(5)	Co(3)–O(6)	2.267(5)
Co(3)–O(8C)	2.092(6)	Co(3)–O(9C)	2.014(5)
Co(3)–O(11)	2.031(6)	C(4)–O(1)	1.249(9)
C(4)–O(2)	1.263(9)	C(5)–O(3)	1.245(9)
C(5)–O(4)	1.257(9)	C(9)–O(5)	1.264(9)
C(9)–O(6)	1.251(8)	C(10)–O(7)	1.285(9)
C(10)–O(8)	1.211(9)		
O(3)–Co(1)–O(3A)	180.0	O(3)–Co(1)–O(7)	91.4(2)
O(3)–Co(1)–O(9)	90.5(2)	O(2B)–Co(2)–O(4A)	94.7(2)
O(2B)–Co(2)–O(6)	90.0(2)	O(2B)–Co(2)–O(7)	172.1(2)
O(2B)–Co(2)–O(9A)	95.0(2)	O(2B)–Co(2)–O(10)	87.5(3)
O(1)–Co(3)–O(5)	84.8(2)	O(1)–Co(3)–O(6)	88.3(2)
O(1)–Co(3)–O(8C)	163.7(2)	O(1)–Co(3)–O(9C)	98.2(2)
O(1)–Co(3)–O(11)	86.1(2)	Co(1)–O(9)–Co(2A)	97.5(2)
Co(1)–O(9)–Co(3F)	116.1(2)	Co(2A)–O(9)–Co(3F)	117.6(2)
Symmetry operations for equivalent atoms			
A $-x+1, -y+1, -z+1$ B $-x, -y+1, -z+1$ C $x-1, y, z$ F $x+1, y, z$			

**Table 7.31: Selected Hydrogen bond Lengths [ $\text{\AA}$ ] and angles [ $^\circ$ ] for Compound 35**

D–H...A	d(D–H)	d(H...A)	d(D...A)	(DHA)
O(9)–H(9)...O(2A)	0.80(4)	2.56(5)	3.311(8)	158(8)
O(9)–H(9)...O(3A)	0.80(4)	2.43(8)	2.915(7)	120(7)
O(10)–H(10A)...O(13)	0.80(4)	1.96(5)	2.762(10)	177(12)
O(10)–H(10B)...O(16)	0.80(4)	2.08(7)	2.803(12)	150(10)
O(11)–H(11A)...O(13G)	0.80(4)	1.94(5)	2.737(9)	173(11)
O(11)–H(11B)...O(12)	0.80(4)	1.94(5)	2.717(9)	163(11)
Symmetry operations for equivalent atoms				
A $-x+1, -y+1, -z+1$ G $x, y+1, z$				



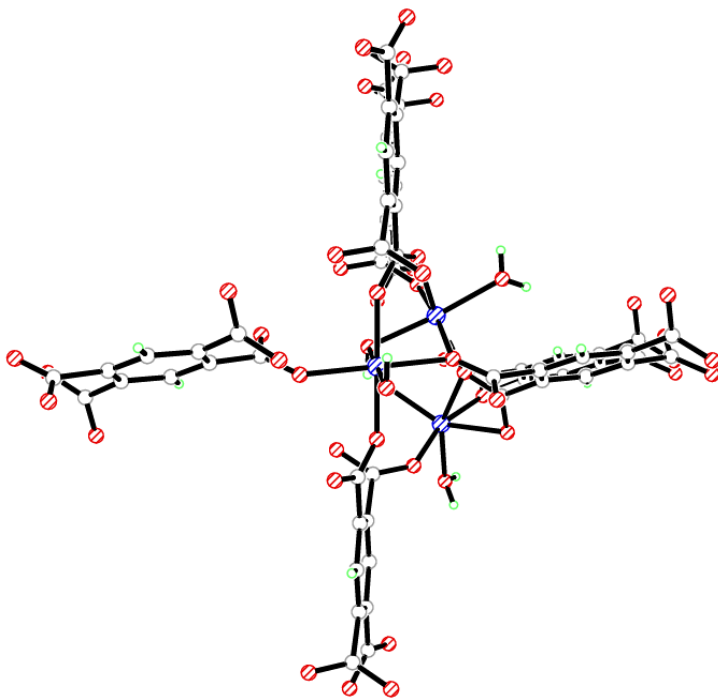


**Figure 7.90:** Trinuclear molecular building unit of the Co(1), Co(2) and Co(3) cations in compound 35

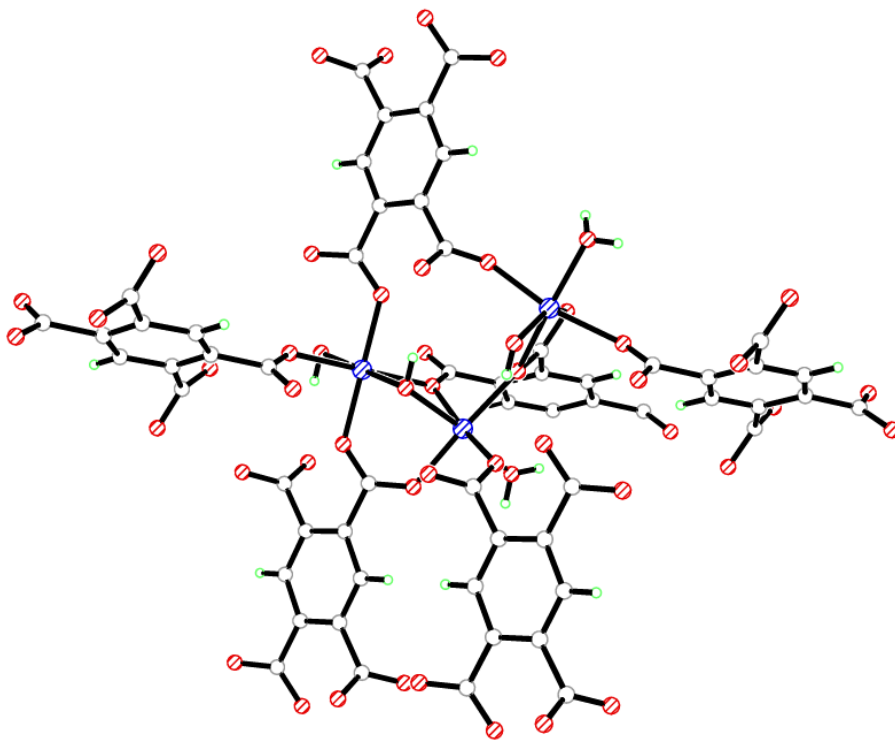


**Figure 7.91:** Trinuclear molecular building unit of the Co(1), Co(2) and Co(3) cations in compound 35

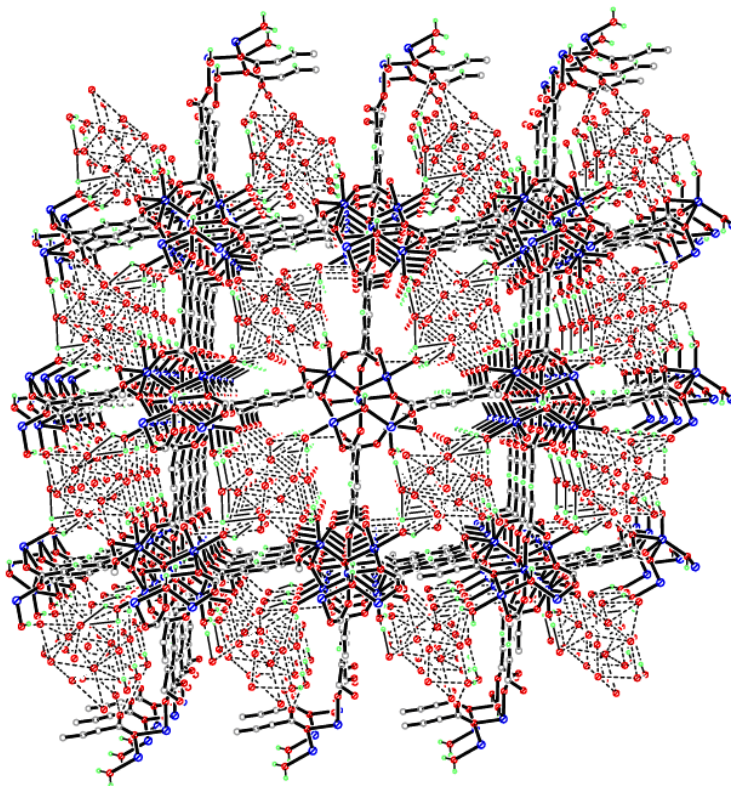


**Figure 7.92:** Three dimensional 4,4' net in compound 35 viewed down the *a*-axis

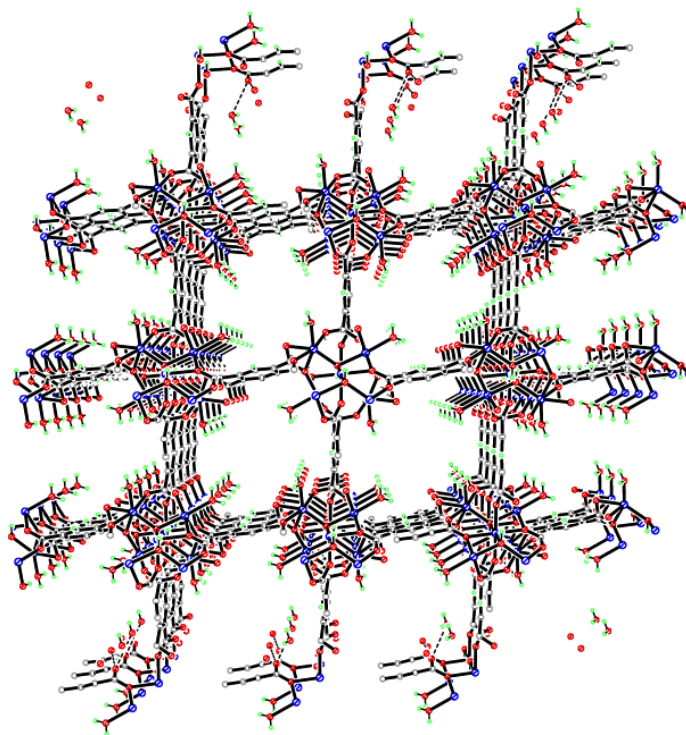


**Figure 7.93:** Three dimensional coordination and potential pores of compound 35 viewed down the *a*-axis

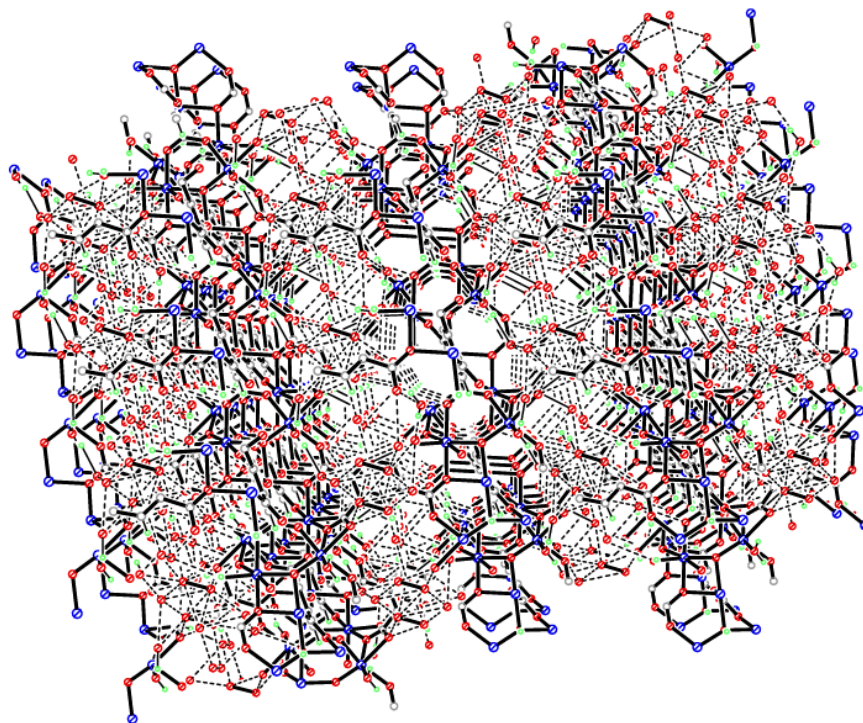


**Figure 7.94:** Three dimensional coordination in compound 35 viewed down the *b*-axis

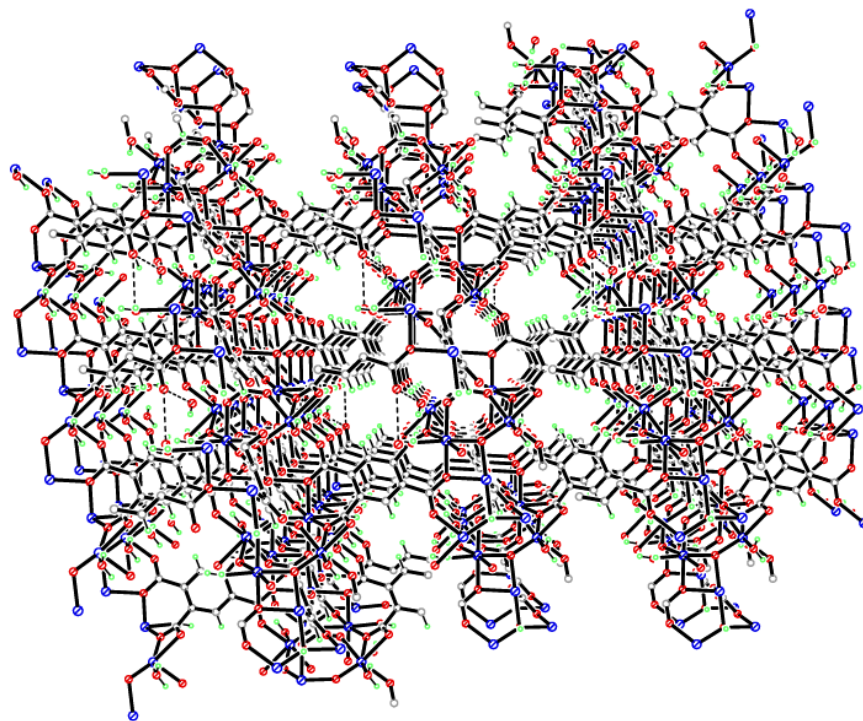


**Figure 7.95:** Three dimensional coordination of the predicted desolvated structure of compound 35 viewed down the *b*-axis



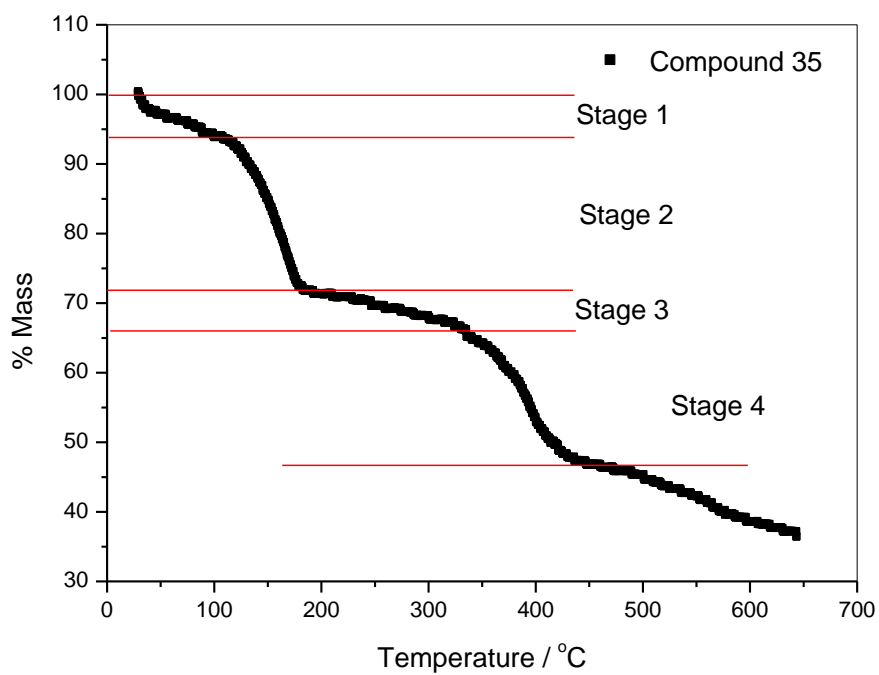


**Figure 7.96: Thermogravimetric analysis plot of compound 35**

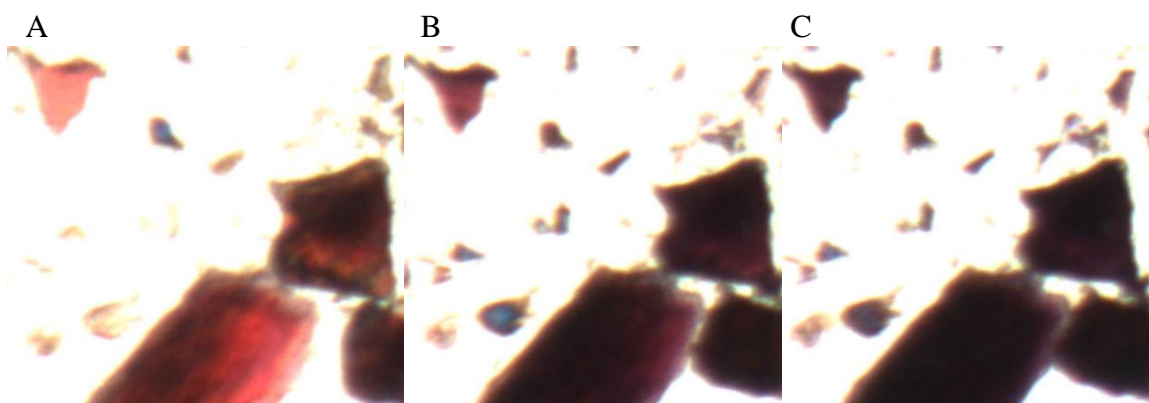
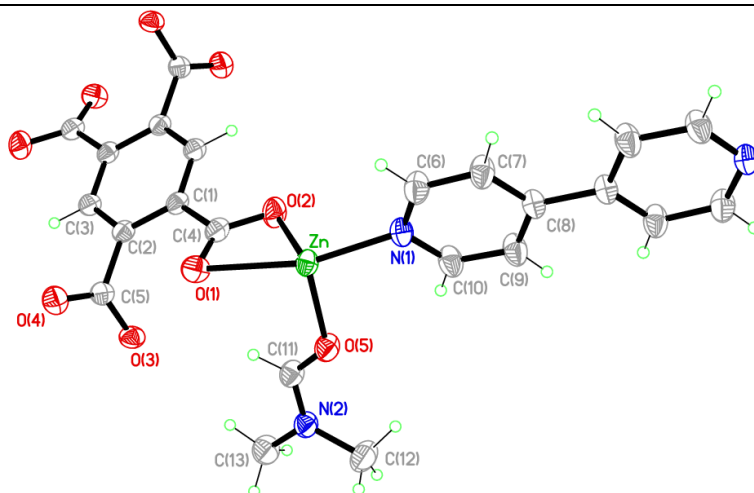


**Figure 7.97: Hot-stage images of compound 35 at temperatures A) 25°C, B) 150°C and C) 350°C**

**Compound 36:**  $[\text{Zn}_2(\text{C}_{10}\text{H}_2\text{O}_8)(\text{C}_{10}\text{H}_8\text{N}_2)(\text{C}_3\text{H}_7\text{NO})_2]$



Chemical formula (total)	$\text{C}_{20}\text{H}_{38.4}\text{O}_5\text{O}_{34.2}$
Formula weight	683.23
Temperature	150(2) K
Radiation, wavelength	synchrotron, 0.6889 Å
Crystal system, space group	Monoclinic, $P2_1/n$
Unit cell parameters	$a = 10.338(3)$ Å $\beta = 114.149(2)^\circ$ $b = 12.860(3)$ Å $c = 11.145(3)$ Å
Cell volume	$1352.0(6)$ Å <sup>3</sup>
Z	2
Crystal colour and size	colourless, $0.05 \times 0.02 \times 0.02$ mm <sup>3</sup>
Final $R$ indices [ $F^2 > 2\sigma$ ]	$R1 = 0.0321$
$R$ indices (all data)	$wR2 = 0.0873$
Largest diff. peak and hole	0.37 and $-0.40$ e Å <sup>-3</sup>

**Figure 7.98: Asymmetric Unit of Compound 36 all unique atoms labelled, additional atoms added to complete ligands**

**Synthesis**

1 mL of a solution of  $\text{Zn}(\text{NO}_3)_2 \cdot 6\text{H}_2\text{O}$  (0.098 g, 0.33 mmol) in dimethylformamide (DMF) (10 mL) was syringed into one side of the H-Cell vessel, 1 mL of a solution of 1,2,4,5-benzenetetracarboxylic acid (0.043 g, 0.17 mmol) in DMF (10 mL) and 1 mL of a solution of 4,4'-bipyridine (0.027 g, 0.17 mmol) in DMF (10 mL) were then syringed into the other side of the H-Cell vessel. The independent solutions were bridged by 2 mL water that was carefully layered into the bridging tube. After seven weeks, colourless needles crystals formed.



## Structure Determination

The data were collected at 150 K using synchrotron radiation on a Crystal Logic diffractometer and Rigaku Saturn 724+ CCD on beamline I19 at the Diamond Light Source facility. The structure was solved by direct methods. The semi-empirical absorption corrections were applied based on symmetry-equivalent and repeated data. The refinement gave a  $wR2$  of 0.0873 for all 3257 independent reflections and a conventional  $R1$  of 0.0321, for 2899 reflections with  $F^2 > 2\sigma$ . The residual electron density maximum and minimum were 0.37 and  $-0.40 \text{ e \AA}^{-3}$  respectively.

The hydrogen atoms were placed in geometrically calculated positions with  $U$  constrained to  $1.2 U_{eq}(C)$  for aromatic hydrogen atoms and  $U$  constrained to  $1.5 U_{eq}(C)$  for methyl hydrogen atoms. The full data of compound 36 can be found in Appendix 1.

## Structure Analysis

The asymmetric unit of compound 36 (figure 7.98) shows a half 1,2,4,5-benzenetetracarboxylate ligand completed by inversion symmetry around the centre of the aromatic ring, coordinating to a zinc cation further coordinated to half a 4,4'-bipyridine completed by inversion symmetry through an inversion centre between the C(8)-C(8A) bond. The zinc cation (Zn) forms a distorted five-coordinate square pyramidal geometry (figure 7.99) coordinating to the bidentate O(1)-C(4)-O(2) carboxylate group with a bite angle O(1)-Zn-O(2)  $58.47(6)^\circ$  and a symmetry equivalent 1,2,4,5-benzenetetracarboxylate, through the O(3)-C(5)-O(4) carboxylate coordinating with a monodentate bond to the O(3) carboxylate oxygen in the cis position at an angle of O(1)-Zn-O(3A)  $93.85(5)^\circ$  with distortion between the O(2)-Zn-O(3A) angle at  $144.85(6)^\circ$  (table 7.32). The remaining base coordination site is occupied by a 4,4'-bipyridine ligand that coordinates through the N(1) atom to form the Zn-N(1)  $2.068(16) \text{ \AA}$  bond cis to the O(2) carboxylate oxygen O(2)-Zn-N(1)  $106.08(6)^\circ$  expanding the structure down the  $c$ -axis by generating its second half through an inversion centre at the centre of the C(8)-C(8A) bond leading to the joining of two symmetry equivalent zinc cations. The square pyramidal geometry is completed with coordination to an axial DMF ligand that caps the node in the  $a$ -axis coordinating cis with respect to the other

ligands (figure 7.99), this forms the building unit shown in figure 7.100 that expands the structure into a three dimensional framework. The structure packs with planar 1,2,4,5-benzenetetracarboxylate ligands down the *c*-axis with a  $\pi$ - $\pi$  distance of 11.455(7) Å. They expand along the *a*-axis to form coplanar rows, each row is staggered with respect to the adjacent row in the *b*-axis by a distance of 5.169(6) Å between the aromatic rings; this is a result of the glide plane that runs along the [101] axis. The set of 1,2,4,5-benzenetetracarboxylates in this adjacent row are rotated by 180° in the *b*-axis due to a two-fold rotation axis, this forms a criss-crossing diamond net of 1,2,4,5-benzenetetracarboxylate ligands coordinating to the zinc cations. The 4,4'-bipyridine ligands then bridge the cations down the cell body diagonal interpenetrating the structure by forming 'zigzag' chains (figure 7.101). The adjacent 4,4'-bipyridine ligands are angled at 47.02(11)° and interpenetrate the 1,2,4,5-benzenetetracarboxylate net with the 4,4'-bipyridine ligand running perpendicular to the aromatic ring of the benzenecarboxylate ligand at a  $\pi$ - $\pi$  angle of 95.13(9)° at a distance of 3.772(4) Å (figure 7.102). This packing forms an intertwining and interpenetrating structure, as a result an interesting array of potential nanochannels are formed down the cell body diagonal with one coordinated DMF molecule pointing inwards to the pore (figure 7.103).

These nanochannels have dimensions 7.109(3) by 7.811(7) Å, the coordinated DMF ligands are separated by 6.104(5) Å and alternate in a staggered confirmation with a separation of 2.109(6) Å between the adjacent DMF ligands, the next collinear DMF is 11.697(13) Å. If the DMF ligands were removed from the structure an extensive porous network would be formed accessible down the cell body diagonal (figure 7.104). PLATON<sup>5</sup> confirms the presence of pores upon desolvation with a calculated pore volume 476.0 Å<sup>3</sup> per unit cell corresponding to 35.2 %.

Compound 36 was synthesised using the H-Cell apparatus, as a result only a few crystals were obtained with crystallisation times of 6-7 weeks preventing the large scale bulk preparation required for further analysis. There are relatively few examples of 4,4'-bipyridine-zinc-1,2,4,5-benzenetetracarboxylate frameworks in the literature; however a structure published by Huang *et al.* (TIFMOK)<sup>16</sup> shows some structural similarities. Compound 36 forms a distorted five-coordinate square pyramidal geometry not too different from that of the tetrahedral geometry of the zinc cation in TIFMOK with

similar coordination bond lengths (table 7.33). The lack of the fifth bond in TIFMOK prevents it coordinating into three dimensions; however it does form a similar packing motif of the 1,2,4,5-benzenetetracarboxylates with the formation of planar chains that are staggered to their adjacent equivalents. These are then interpenetrated by 4,4'-bipyridine ligands that cross the 1,2,4,5-benzenetetracarboxylates perpendicular at a distance of 4.005(3) Å similar to the interpenetrating distance in compound 36 of 3.772(4) Å.<sup>16</sup>

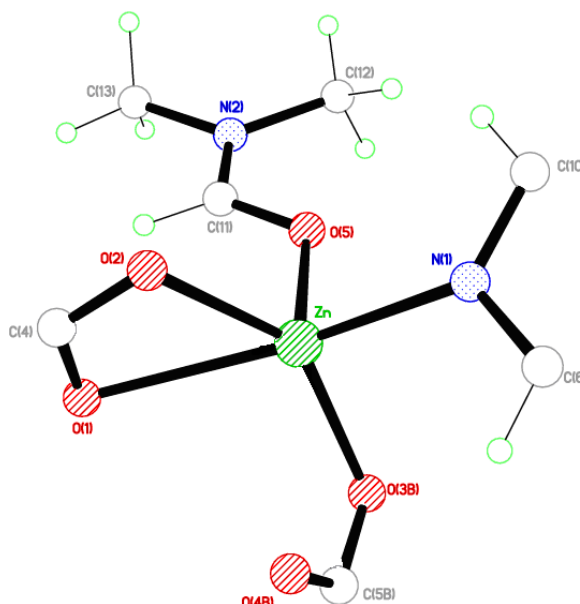
**Table 7.32: Selected Bond Lengths [ $\text{\AA}$ ] and Angles [ $^\circ$ ] for Compound 36**

Zn–O(1)	2.4428(15)	Zn–O(2)	1.9980(14)
Zn–O(3A)	1.9910(14)	Zn–N(1)	2.0683(16)
Zn–O(5)	2.0318(15)	C(4)–O(1)	1.239(3)
C(4)–O(2)	1.276(2)	C(5)–O(3)	1.276(2)
C(5)–O(4)	1.229(2)		
O(1)–Zn–O(2)	58.47(6)	O(1)–Zn–O(3A)	93.85(5)
O(1)–Zn–N(1)	163.54(6)	O(1)–Zn–O(5)	91.84(5)
Zn–O(1)–C(4)	79.90(11)	Zn–O(2)–C(4)	99.28(12)

Symmetry operations for equivalent atoms

A  $x-1/2, -y+3/2, z-1/2$ **Table 7.33: Average bond length comparisons between Compound 36, Compound 32 and TIFMOK<sup>16</sup>**

Compound	Bond	Average Bond Length ( $\text{\AA}$ )
Compound 32	Zn–O (carboxylate)	2.098
Compound 36	Zn–O (carboxylate)	2.154
Compound 36	Zn–N (4,4'-bipyridine)	2.068
TIFMOK	Zn–O (carboxylate)	1.995
TIFMOK	Zn–N (4,4'-bipyridine)	2.056

**Figure 7.99: A) Square pyramidal coordination environment of Zn(1) in compound 36**

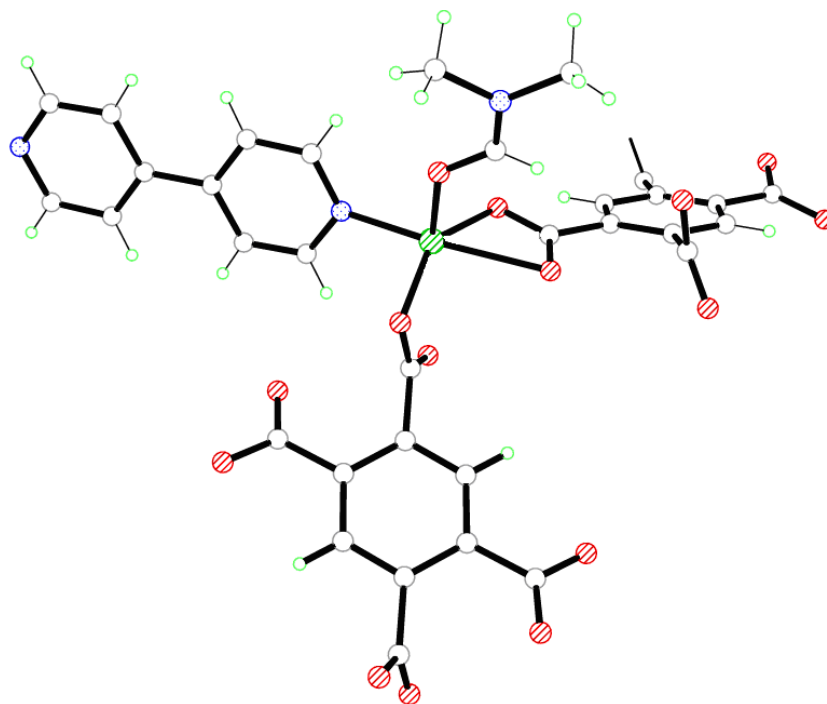


**Figure 7.100:** Molecular building unit of the Zn(1) in compound 36

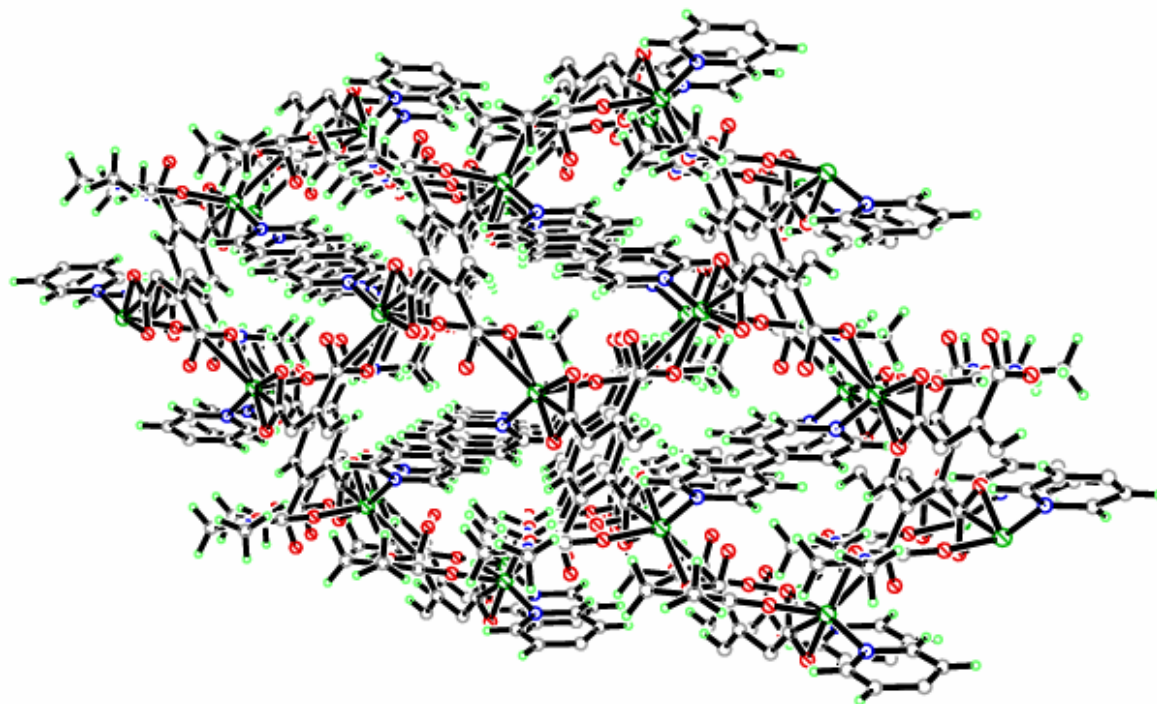


**Figure 7.101:** Three dimensional packing in compound 36 viewed down *c*-axis

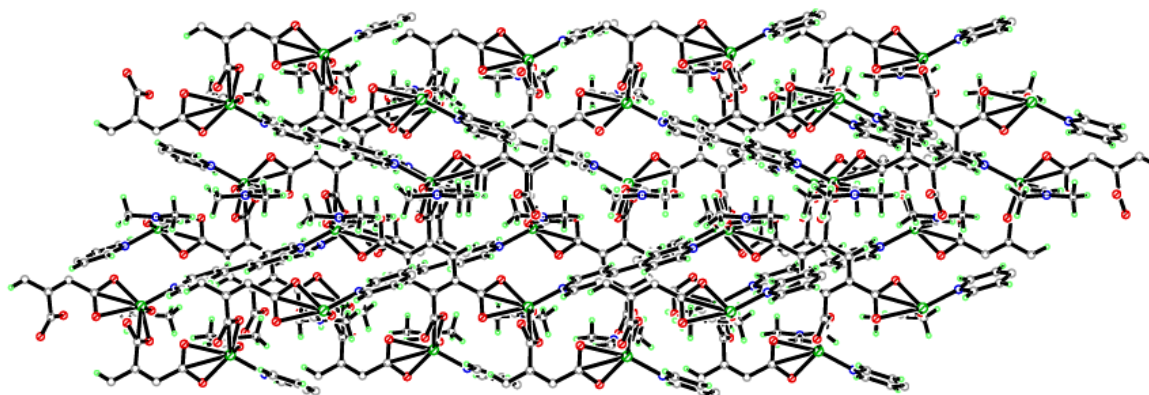


**Figure 7.102:** Three dimensional packing in compound 36 viewed down the *a*-axis

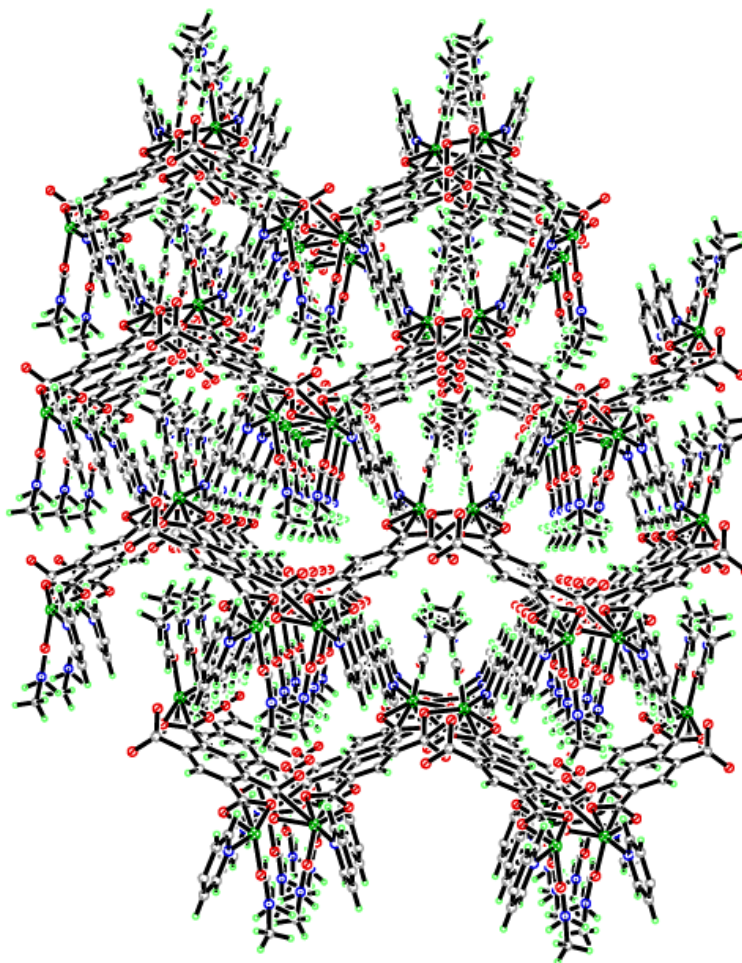


**Figure 7.103:** Three dimensional coordination and potential pores of compound 36 viewed down the cell body diagonal.

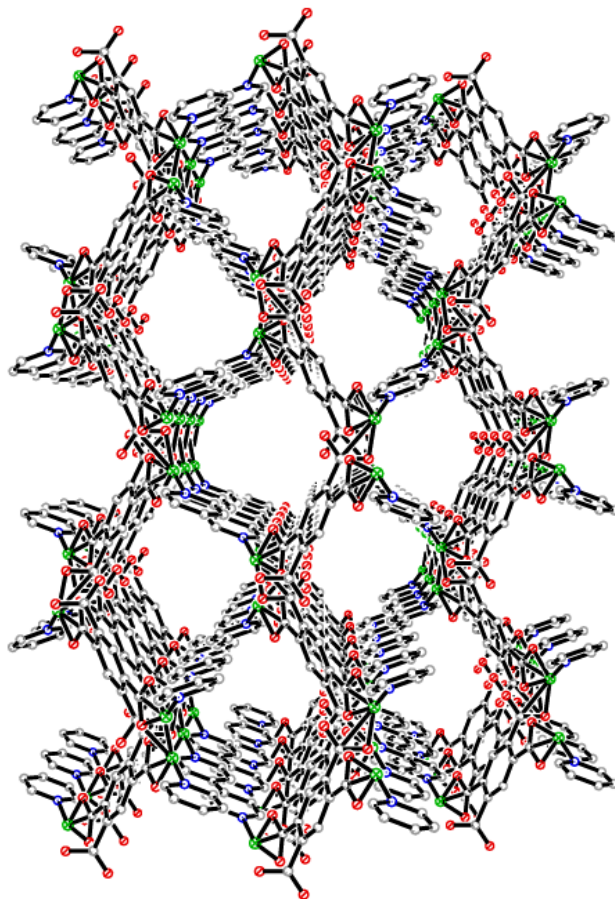


**Figure 7.104:** Three dimensional coordination and potential pores of the desolvated compound 36 viewed down the cell body diagonal.

## Conclusion

In this chapter fifteen compounds with 1,2,4,5-benzenetetracarboxylic acid were presented; three with zinc, four with cobalt, one with nickel, three with cadmium, three compounds with copper. These compounds were formed with a variety of solvents, mineralising agents and bases producing frameworks consisting of two dimensional sheets to three dimensional coordinated porous grids.

Compound 22 was synthesised using vapour diffusion of pyridine. This produced a two dimensional framework consisting of sheets of octahedral cobalt cations linked by 1,2,4,5-benzenetetracarboxylate ligands. The methanol ligands point inwards towards each other and fill the gaps between the four coplanar linkers with the pyridine ligands pointing axial to the sheets. The pyridine stack the sheets parallel with no offset between the respective sheets, this allows the pyridines to overlap with their counterparts on adjacent sheets creating strong  $\pi$ - $\pi$  stacking interactions that hold the framework together in three dimensions. This was synthesised as an expansion of the extensive vapour diffusion reactions investigating the templating effects of volatile bases on topology formation. This structure is comparable to compounds 23 and 24 with both compounds synthesised using similar reaction conditions. Compound 23 shows the effect of switching the cobalt cation for a copper cation and how the resulting coordination geometry change alters the packing motif of the pyridines. Compound 23 forms two dimensional sheets with a similar packing motif to that of compound 22. In contrast to the three methanol ligands pointing inwards to the potential pore as observed in compound 22, compound 23 has two pyridines and two methanols pointing inwards as a result of the square pyramidal geometry of the Cu cation. Compound 23 was synthesised as an analogue of compound 22; however upon substituting cobalt by copper, variations in the structure and packing motifs were able to form as a result of an extra square pyramidal Cu(1) cation in compound 23 that alters the coordination motif of the 1,2,4,5-benzenetetracarboxylate ligands. These cations show the preferential orientation of the carboxylate with respect to the pyridine and methanol ligands, indicating the coordinated monodentate carboxylate groups avoids the steric bulk of the pyridine. The structural directing nature of pyridine on these compounds was investigated further involving lower concentrations of pyridine in the reaction medium.



This was designed to develop products with similar motifs that do not pack around the pyridine ligands leading to the formation of compound 24. Compound 24 shows the progression of the reaction media used to synthesize compounds 22 and 23, with reducing the pyridine concentration to produce a fully deprotonated and coordinated 1,2,4,5-benzenetetracarboxylate framework without coordinating pyridine to the metal nodes. Compound 24 shows a retention of the 4,4' netted sheet; however it now does not stack in the similar motifs to that of compounds 22 and 23 relying on hydrogen bonding through an extensive network of coordinated and uncoordinated water ligands. This shifts the sheets into a staggered conformation partially closing the potential pores.

Alkali metal addition into the reactions resulted in the formation of compounds 27- 31 that show how the concentration of the alkali earth metal alters the topology of the frameworks. Compound 27 is synthesised using ionothermal techniques and shows templating to the ionic liquid that forms two dimensional sheets with partially capped cadmium cations coordinated to bromide anions. The incorporation of potassium and sodium salts was used to increase the yields of metal-organic frameworks and improve purity of the bulk sample with the sodium or potassium cations coordinating to excess bromide anions. Additional features of the alkali earth metals that proved advantageous were observed in compounds 28 and 29; with the cations coordinating into the structures to add additional nodes with unusual geometries for coordination by linkers, expanding two dimensional sheets into three dimensional coordinated frameworks through sodium cations. Compound 29 is similar to compound 28 in chemical composition, with the switch from pentagonal bipyramidal cadmium cations to square planar copper cations altering the packing motif drastically. Compound 29 forms chains of linkers connecting columns of sodium and copper cations in contrast to the sheets of compound 28 connected by rows of sodium cations. The incorporation of alkali metals into the ionothermal reactions resulted in the synthesis of compounds 30 and 31. Compound 30 was synthesised with a large concentration of potassium hydroxide, that coordinates over the cadmium cations to produce a thermally unstable framework of potassium and 1,2,4,5-benzenetetracarboxylate linkers. Investigations into lower concentrations of potassium hydroxide produced compound 31 that consists of both potassium cations and cadmium cations producing a coordinated three dimensional framework. Compounds 30

and 31 show significant similarities in their building units and packing motifs, with an almost direct substitution of the K-K dimeric unit to the Cd-K dimeric building unit. The difference in the packing motifs is due to compound 31 crystallising in the triclinic  $P\bar{1}$  space group and lacks the two-fold rotation and mirror symmetry used to form the packing motif of compound 30. The addition of potassium and sodium shows an effective method of producing three dimensional frameworks with the possibility of producing di-metallic compounds.

Solvent templating reactions investigated the templating effect of DMF on porous three dimensional frameworks, with the production of compounds 32-35. Compound 32 was synthesised using solvothermal techniques, with a solvent mixture of DMF, ethanol and water. This produced a framework with a backbone of triply bridged zinc cations that form a column. The columns have coordinated DMF molecules pointing out away from the center; these point in towards the nanochannels created by the chains of 1,2,4,5-benzenetetracarboxylate ligands that link the columns of zinc cations together by creating planar to form the herringbone packing motif. The nanochannels created by this packing motif are filled by the coordinated DMF molecules with two pointing inwards from trans diagonals; if these coordinated ligands were removed from the structure by desolvation, nanochannels with dimensions 8.34(5) by 13.66(7) Å. Compound 32 is thermally stable up to 270°C before the coordinated DMF molecules are removed and the compound degrades. The packing motif of compound 32 around the DMF molecules and its potential porosity was of significant interest resulting in several new reactions to determine how the concentration of DMF affects of the packing orientation of the frameworks. The expanded reactions involved both increasing and decreasing the concentration of DMF; increasing the concentration produced compound 33 that shows an additional coordinated DMF that has a profound effect on the packing and availability of the nanopores. Compound 33 forms a similar three dimensional grid network; however the zinc cations coordinate two cis DMF molecules that induce a change in the packing motif creating a tradition grid network instead of the herring-bone packing motif of compound 32. The nanochannels in compound 33 exhibit two different environments creating a chess board motif as the coordinated DMF molecules point fully and partially into two different pores, creating

one open pore and one closed pore. The open pore has a potential accessible pore before desolvation with dimensions 4.566(9) by 4.566(9) Å and pores of dimensions 10.091(5) by 10.091(5) Å after desolvation. This would create an highly porous material with 49 % porosity, the compound undergoes partial desolvation at 75°C and remains stable untill 135°C, making the compound suitable for gas adsorption studies in future research. Due to the success of compound 33, reactions were carried out to produce the cobalt analogues of both compound 33 and the fully hydrated compound, resulting in the formation of compound 34 and compound 35. Compound 34 is an analogue to compound 33 with the cobalt cations coordinating to two DMF molecules that point into the pores of the framework produced. The synthesis of compound 34 and its structural similarities to compound 33 suggested that the possibility of producing compounds with less coordinated DMF including the fully hydrated compound was possible. The synthesis that followed yielded compound 35, the fully hydrated analogue of compound 34. The structures show similar packing motifs creating columns of cobalt cations connected by perpendicular chains of 1,2,4,5-benzenetetracarboxylate ligands. The structures form the diamond packing motif creating nets with dimensions 6.22 by 5.13 Å and 9.04 by 9.04 Å. These packing motifs are achieved utilizing different coordination geometries of the respective cobalt cations. Compound 35 contains six-coordinate octahedral nodes bridged by a central hydroxide anion to form a trinuclear cluster, compound 34 is built around one octahedral and one tetrahedral node to form a dimeric paddle-wheel building unit. Although the two compounds utilize different building units they both involved the perpendicular coordination of the 1,2,4,5-benzenetetracarboxylate ligands with respect to each other, creating the walls of the nanochannels in the packing motif. The switch from DMF as a template in compound 34 to water in compound 35 reduces the space group volume with a change from *Cc* (1936 Å<sup>3</sup>) to *P* $\bar{1}$  (916 Å<sup>3</sup>) resulting in the gap between each adjacent 1,2,4,5-benzenetetracarboxylate ligand from 9.028(5) Å to 4.266(5) Å as the structure forms a close packing motif without the steric bulk of the interpenetrating DMF molecules. The progression of compounds 32-35 shows the significance of DMF within the reaction system, and how the H-Cell can crystallise new products away from certain solvents.

## References:

- 1 R. Diniz, H. A. de Abreu, W. B. der Almeda, M. T. C. Sansiviero, N. G. Fernandes, *Eur. J. Inorg. Chem.*, **2002**, 1115.
- 2 C. R. Perez, P. L. Luis, M. Hernandez-Molina, M. M. Laz, F. S. Delgado, P. Gili, M. Julve, *Eur. J. Inorg. Chem.*, **2004**, 3873.
- 3 O. Fabelo, J. Pasan, L. C. Delgado, F. S. Delgado, C. Yuste, F. Lloret, M. Julve, C. R. Perez, *Cryst. Eng. Commun.*, **2009**, 11, 2169.
- 4 P. Sing, B. Liu, Y. Li, J. Yang, Z. Wang, X. Li, *Cryst. Eng. Commun.*, **2012**, 14, 2296.
- 5 A. J. Spek, *J. Appl. Crystallogr.*, **2003**, 36, 7.
- 6 Z. L. Xie, M. L. Feng, J. R. Li, X. Y. Huang, *Inorg. Chem. Commun.*, **2008**, 11, 1143.
- 7 Z. F. Shi, J. Jin, L. Li, Y. Xing, S. Y. Niu, *Acta. Phys. Chim. Sin.*, **2009**, 25, 2011.
- 8 Y. B. Chen, Y. Kang, J. Zhang, *Chem. Commun.*, **2010**, 46, 3182.
- 9 L. P. Sun, S. Y. Niu, J. Jin, G. Yang, L. Ye, *Eur. J. Inorg. Chem.*, 2006, 5130.
- 10 C. Wang, X. Chen, C. Huang, H. Zhang, Z. Lian, G. Xiao, *Acta. Crystallogr. Sect. E.*, **2004**, 60, 641.
- 11 M. Eddaoudi, H. Li, O. M. Yaghi, *J. Am. Chem. Soc.*, **2000**, 122, 1391.
- 12 K. L. Lu, Y. F. Chen, Y. W. Cheng, R. T. Liao, Y. H. Liu, Y. S. Wen, *Cryst. Growth Des.*, **2005**, 5, 403.
- 13 D. Feng, S. Liu, W. Zheng, P. Sun, F. Ma, C. Zhang, *Z. Anorg. Allg. Chem.*, **2009**, 636, 1133.
- 14 Y. L. Fu, J. L. Ren, S. W. Ng, *Acta. Crstyallogr. Sect. E. Struct. Rep. Online*, **2004**, 60, 1400.
- 15 W. D. Liu, J. M. Shi, *Pol. J. Chem.*, **2004**, 78, 997.
- 16 C. D. Wu, C. Z. Lu, D. M. Wu, H. H. Zhuang, J. S. Huang, *Inorg. Chem. Commun.*, **2001**, 4, 561.

## **Chapter Eight – Crystal Structures of Transition Metal and 1,2,3,4,5,6-benzenehexacarboxylic acid Compounds**

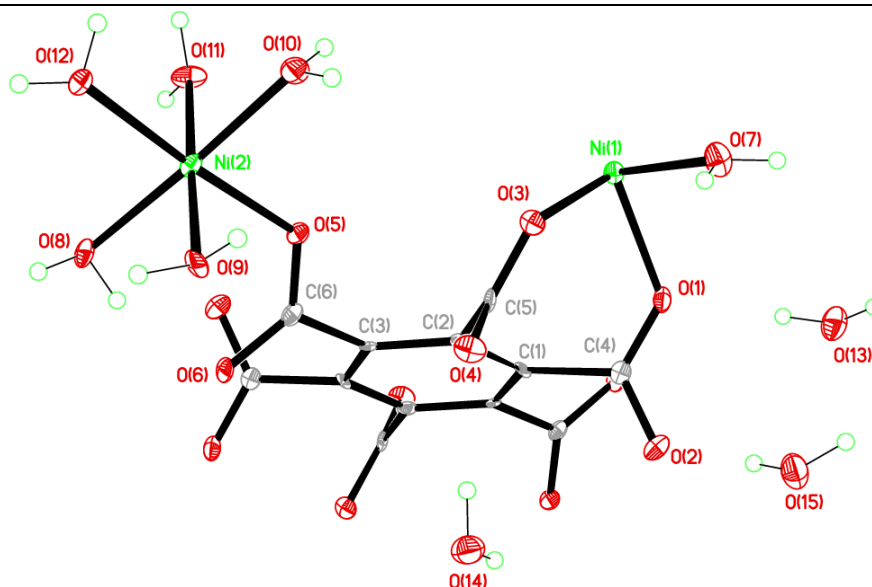
### **Introduction**

The following chapter presents compounds produced using the transition metals; cobalt, nickel, copper and cadmium. These metals were reacted with 1,2,3,4,5,6-benzenehexacarboxylic acid in a range of reaction conditions to investigate the templating effects of different solvents, bases, alkali earth metals and additional ligands such 4,4'-bipyridine on topology formation.

The eight compounds presented in this chapter include one dimensional chains (compound 37), two dimensional sheets (compounds 39, 41, 42) and three dimensional coordinated frameworks (compounds 38, 40, 43, 44). Compounds 37-41 presented in this chapter show the templating effects of the alkali metals sodium and potassium. Compounds 42-43 highlight templating effect of pyridine on topology formation with the further expansion of the lattice using 4,4'-bipyridine in compound 44.

The compounds present in this chapter were analysed further with elemental analysis, powder X-ray diffraction and thermogravimetric analysis, where possible, to determine the purity of the bulk material and the thermostability properties of the compounds.

**Compound 37:**  $[\text{Ni}_3(\text{C}_{12}\text{O}_{12})(\text{H}_2\text{O})_{12}]\cdot 6\text{H}_2\text{O}$



Chemical formula (total)	$\text{C}_{12}\text{H}_{36}\text{Ni}_3\text{O}_{30}$
Formula weight	836.54
Temperature	150(2) K
Radiation, wavelength	MoK $\alpha$ , 0.71073 Å
Crystal system, space group	orthorhombic, <i>Pbca</i>
Unit cell parameters	$a = 16.9667(9)$ Å $b = 8.4375(4)$ Å $c = 19.9676(9)$ Å
Cell volume	$2858.5(2)$ Å <sup>3</sup>
<i>Z</i>	4
Crystal colour and size	green, $0.30 \times 0.15 \times 0.10$ mm <sup>3</sup>
Final <i>R</i> indices [ $F^2 > 2\sigma$ ]	$R1 = 0.0329$
<i>R</i> indices (all data)	$wR2 = 0.0402$
Largest diff. peak and hole	0.43 and $-0.53$ e Å <sup>-3</sup>

**Figure 8.01: Asymmetric Unit of Compound 37 all unique atoms labelled, additional atoms added to complete ligands.**

**Synthesis**

2 mL of a solution of  $\text{Ni}(\text{NO}_3)_2 \cdot 6\text{H}_2\text{O}$  (0.09 g, 0.33 mmol) in water (10 mL) was layered over 2 mL of a solution of benzenhexacarboxylic acid (0.058 g, 0.17 mmol) in water (10 mL) in small sample vial. The vial was covered and left until crystallisation was complete. After four weeks, green block crystals formed.

## Structure Determination

The data were collected at 150 K using molybdenum radiation on an Oxford Diffraction Gemini A Ultra diffractometer. The structure was solved by direct methods. The semi-empirical absorption corrections were applied based on symmetry-equivalent and repeated data. The refinement gave a  $wR2$  of 0.0402 for all 2513 independent reflections and a conventional  $R1$  of 0.0329, for 1361 reflections with  $F^2 > 2\sigma$ . The residual electron density maximum and minimum were 0.43 and  $-0.53 \text{ e } \text{\AA}^{-3}$  respectively.

The hydrogen atoms were freely refined within this compound, DELU and SIMU restraints were imposed on the ligands in compound 37 with further SADI restraints on the water molecules. The full data of compound 37 can be found in Appendix 1.

## Structure Analysis

The asymmetric unit of compound 37 (figure 8.01) shows half a benzenehexacarboxylate ligand completed by inversion symmetry through the centre of the aromatic ring, coordinating to two six-coordinate octahedral nickel cations; Ni(1) and Ni(2) with the former positioned on an inversion centre (figure 8.02).

The six coordinate Ni(1) cation (figure 8.02A) coordinates to both carboxylate groups O(1)-C(4)-O(2) and O(3)-C(5)-O(4) of the benzenehexacarboxylate ligand through the monodentate bonds; Ni(1)-O(1) 2.055(2) Å and Ni(1)-O(3) 2.053(2) Å. These coordinate in the coplanar cis positions bridging the Ni(1) cation with a bite angle of O(1)-Ni(1)-O(3) 89.45(9)°, the carboxylates are rotated out of the planes of the aromatic rings by 118.8(4)° and 118.6(3)° respectively placing the nickel cation above the plane of the aromatic ring by 2.938(4) Å. The axial position of the Ni(1) cation is capped by a coordinated water molecule, this coordinates cis to the carboxylate groups at an angle O(1)-Ni(1)-O(7) 86.36(11)°. The six-coordinate geometry is completed by the inversion symmetry at the centre of the Ni(1) cation that generates the three coplanar trans symmetry equivalent ligands (figure 8.02A) (table 8.01).

The remaining carboxylate group of the benzenehexacarboxylate O(5)-C(6)-O(6) forms a monodentate coordination to the Ni(2) cation forming the Ni(2)-O(5) 2.040(2)

Å bond. The Ni(2) cation forms a terminal node completing the six-coordinate geometry with coordination to five terminal water molecules; O(8), O(9), O(10), O(11) and O(12) that coordinate with standard bond angles and lengths listed in table 8.01 (figure 8.02B).

The completion of the half benzenhexacarboxylate through the inversion symmetry forms the molecular building unit shown in figure 8.03, this expands the compound forming one dimensional chains in a 'stepped' motif due to the rotation of the O(1)-C(4)-O(2) and O(3)-C(5)-O(4) carboxylate groups out of the aromatic ring plane (figure 8.04). The chains run down the *b*-axis and are stacked in the *a*-axis by hydrogen bonding between the capped Ni(2) nodes and the uncoordinated carboxylate oxygens O(2) and O(4) of an adjacent chain. This forms an extensive hydrogen bonding network using uncoordinated water molecules to bridge the chains; O(11)-H(11A)···O(13F) 2.733(4) Å, O(13)-H(13B)···O(2C) 3.239(4) Å and O(13)-H(13A)···O(1) 2.725(4) Å all hydrogen bonds listed in table 8.02 (figure 8.05). The chains are hydrogen bonded in the *c*-axis using the coordinated water molecules and carboxylate oxygens O(3) and O(6) with the primary hydrogen bond donor, the O(9) water molecule positioned between both these carboxylate groups forming the hydrogen bonds; O(9)-H(9A)···O(3E) 2.708(4) Å at 173(4)° and O(9)-H(9B)···O(6D) 2.698(4) Å at 176(4)° (figure 8.06).

To maximise hydrogen bonding interactions the chains stack running in opposite directions rotated by a two-fold rotation axis between the adjacent layers of collinear chains in the *a*-axis, tipping the Ni(2) cations of each layer towards each other. The chains stack parallel *c*-axis and run parallel up the *b*-axis forming sheets of chains that overlap by 2.040(4) Å with respect to symmetry equivalent Ni(2) cations; this allows the formation of the hydrogen bonds between the O(9) water and the adjacent O(6) and O(4) carboxylates shown in figure 8.06, expanding the structure into three dimensions.

Further analysis of compound 37 was carried out on the bulk sample to determine overall purity using powder X-ray diffraction and elemental analysis. The powder X-ray diffraction data produced the diffraction pattern shown in figure 8.07; this shows strong correlation with the predicted powder diffraction pattern from the single crystal data, with the presence of significant peaks at 10.35, 13.67, 15.49, 17.21 and 22.5-23 2-Theta. The elemental analysis produced the results C = 17.21 %, H= 4.49 % and N =0.16 %; these are consistent with the values calculated from the single crystal



data of C = 17.21 %, H = 4.31 % and N = 0 %. These techniques indicate that the bulk material of compound 37 is consistent with the structure determined by the single crystal X-ray diffractometry.

Compound 37 is a structural analogue of the compound  $[\text{Co}_3(\text{C}_{12}\text{O}_{12})(\text{H}_2\text{O})_{12}] \cdot 6\text{H}_2\text{O}$  reported by Hentschel et al. (JIYNOU)<sup>1</sup> displaying identical packing motifs with both compounds crystallised in the *Pbca* space group. Compound 37 is the nickel analogue and displays slightly shorter bond lengths between the carboxylate oxygens and the nickel cations than the cobalt derivative JIYNOU (table 8.03).<sup>1</sup> The compounds utilize the six-coordinate octahedral geometry creating the ‘stepped’ chain packing motif.

**Table 8.01: Selected Bond Lengths [Å] and Angles [°] for Compound 37**

Ni(1)–O(1)	2.055(2)	Ni(1)–O(3)	2.053(2)
Ni(1)–O(7)	2.066(3)	Ni(2)–O(5)	2.040(2)
Ni(2)–O(9)	2.070(3)	Ni(2)–O(10)	2.047(2)
Ni(2)–O(11)	2.054(3)	Ni(2)–O(12)	2.054(3)
C(4)–O(1)	1.261(4)	C(4)–O(2)	1.245(4)
C(5)–O(3)	1.256(4)	C(5)–O(4)	1.257(4)
C(6)–O(5)	1.250(4)	C(6)–O(6)	1.261(4)
O(1)–Ni(1)–O(1A)	180.0	O(1)–Ni(1)–O(3)	89.45(9)
O(1)–Ni(1)–O(7)	86.36(11)	O(5)–Ni(2)–O(8)	93.26(10)
O(5)–Ni(2)–O(9)	93.06(11)	O(5)–Ni(2)–O(10)	89.03(10)
O(5)–Ni(2)–O(11)	85.73(11)	O(5)–Ni(2)–O(12)	176.14(11)
Ni(1)–O(1)–C(4)	129.5(2)	Ni(1)–O(3)–C(5)	128.8(2)
Ni(2)–O(5)–C(6)	124.4(2)		
Symmetry operations for equivalent atoms			
A $-x+1, -y+2, -z+1$ B $-x+1, -y+1, -z+1$			

**Table 8.02: Selected Hydrogen bond Lengths [Å] and angles [°] for Compound 37**

D–H...A	d(D–H)	d(H...A)	d(D...A)	(DHA)
O(7)–H(7A)...O(15C)	0.837(15)	2.03(2)	2.833(4)	161(3)
O(7)–H(7B)...O(12D)	0.835(15)	2.036(19)	2.840(4)	161(3)
O(8)–H(8A)...O(4E)	0.837(15)	1.865(18)	2.674(3)	162(3)
O(8)–H(8B)...O(6)	0.829(15)	1.833(19)	2.612(3)	156(3)
O(9)–H(9A)...O(3E)	0.835(15)	1.878(16)	2.708(3)	173(4)
O(9)–H(9B)...O(6D)	0.845(15)	1.853(16)	2.698(4)	176(4)
O(10)–H(10A)...O(6D)	0.830(15)	2.24(2)	2.915(4)	138(3)
O(10)–H(10A)...O(9D)	0.830(15)	2.50(3)	3.067(4)	127(3)
O(10)–H(10B)...O(13A)	0.802(15)	1.934(15)	2.728(4)	170(3)
O(11)–H(11A)...O(13F)	0.823(16)	1.93(2)	2.733(4)	166(4)
O(11)–H(11B)...O(8G)	0.826(16)	1.996(18)	2.818(4)	173(4)
O(12)–H(12A)...O(14D)	0.837(15)	1.891(16)	2.722(4)	172(4)
O(12)–H(12B)...O(14H)	0.822(16)	1.92(2)	2.702(4)	159(4)
O(13)–H(13A)...O(1)	0.829(15)	1.897(16)	2.725(4)	178(4)
O(13)–H(13B)...O(11A)	0.822(16)	2.47(3)	2.919(4)	116(3)
O(13)–H(13B)...O(2C)	0.822(16)	2.56(4)	3.239(4)	141(5)
O(14)–H(14A)...O(4)	0.831(16)	1.948(17)	2.776(4)	175(4)
O(14)–H(14B)...O(15I)	0.825(15)	1.929(18)	2.743(4)	169(4)
O(15)–H(15A)...O(2C)	0.842(16)	2.01(2)	2.833(4)	164(4)
O(15)–H(15B)...O(2)	0.79(4)	1.97(4)	2.760(4)	178(6)
Symmetry operations for equivalent atoms				
A $-x+1, -y+2, -z+1$ C $-x+3/2, y+1/2, z$ D $-x+1, y+1/2, -z+3/2$				
E $-x+1, y-1/2, -z+3/2$ F $x-1/2, -y+3/2, -z+1$ G $-x+1/2, y+1/2, z$				
H $x-1/2, y, -z+3/2$ I $-x+3/2, y-1/2, z$				

**Table 8.03: Average bond length comparisons between Compound 37 and JIYNOU<sup>1</sup>**

Compound	Bond	Average Bond Length (Å)
Compound 37	Ni-O (carboxylate)	2.056
JIYNOU	Co-O (carboxylate)	2.129

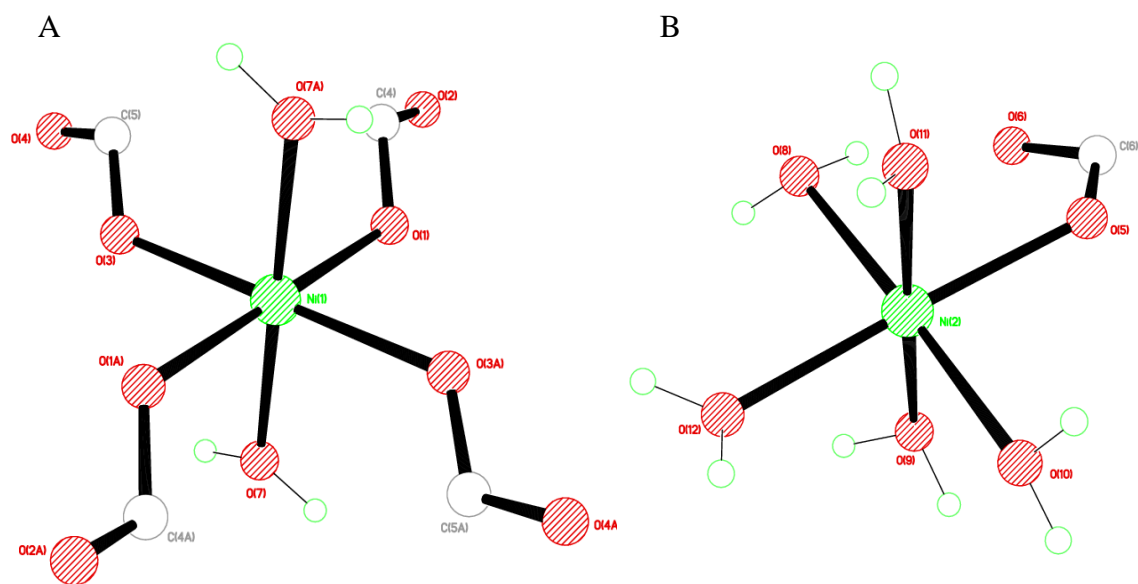


**Figure 8.02: A) Octahedral coordination environment of Ni(1) and B) Octahedral coordination environment of Ni(2) in compound 37**

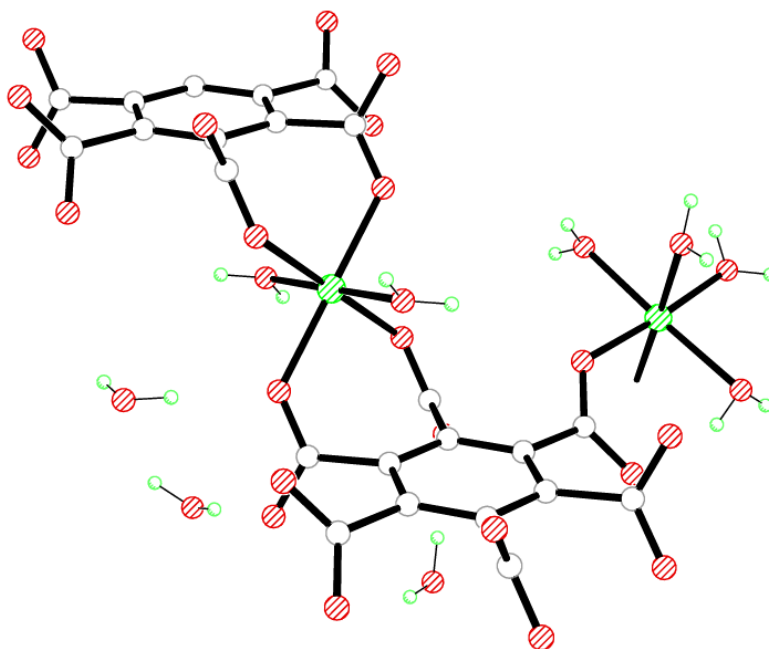


Figure 8.03: Secondary building unit of Ni(1) and Ni(2) in compound 37

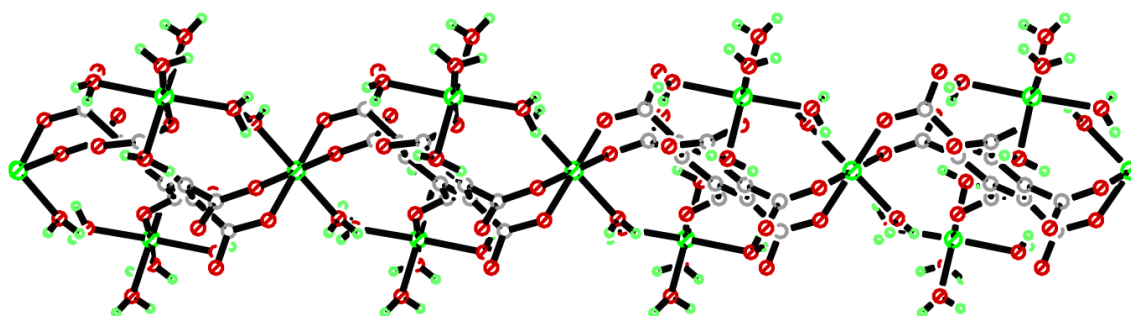
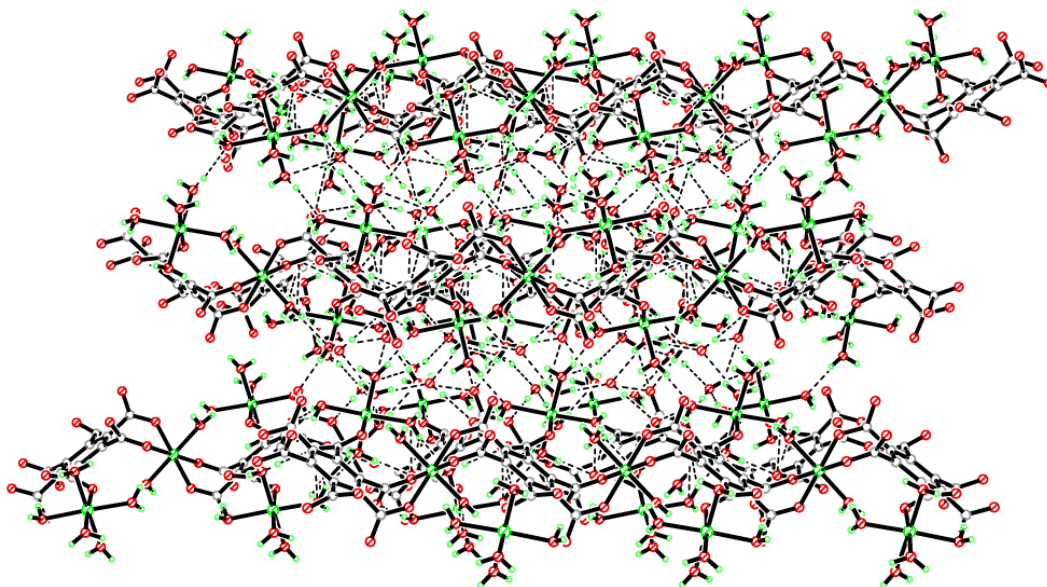
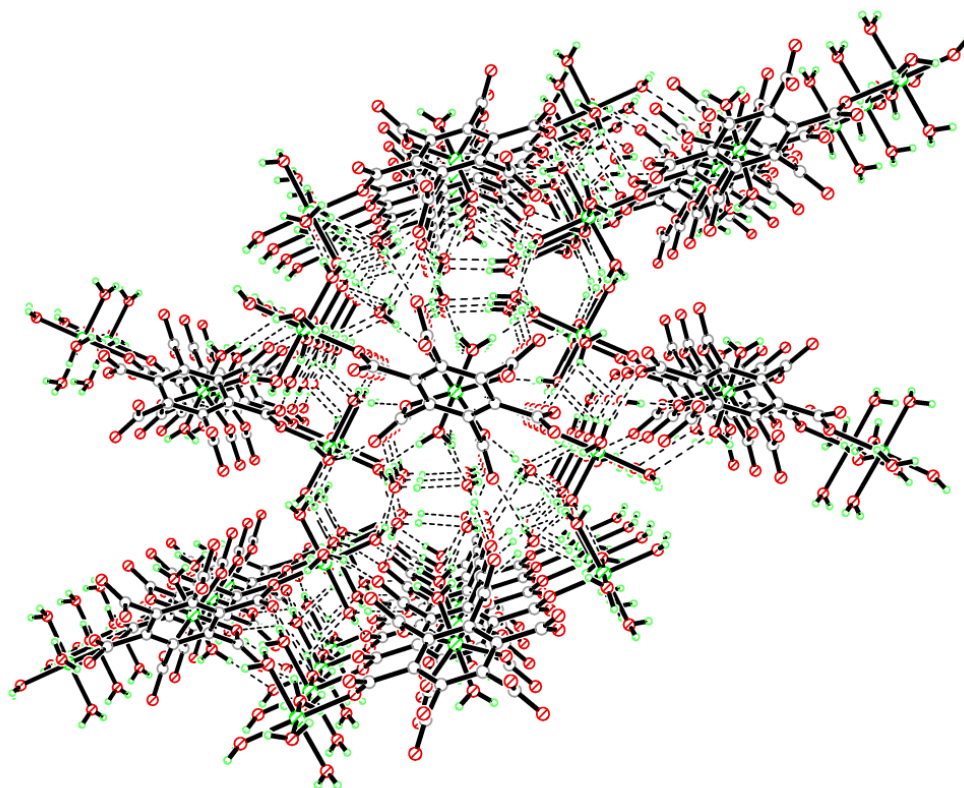


Figure 8.04: One dimensional chains in compound 37 viewed down the *c*-axis



**Figure 8.05:** Two dimensional stacking of the chains in the *a*-axis of compound 37 using hydrogen bonds, viewed down the *c*-axis



**Figure 8.06:** Two dimensional stacking of the chains in the *c*-axis of compound 37 using hydrogen bonds, viewed down the *b*-axis

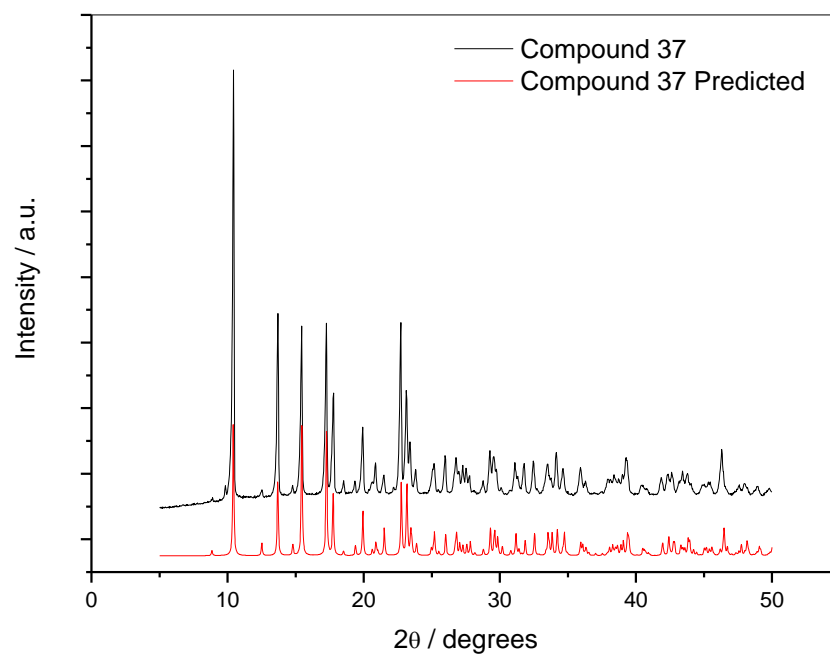
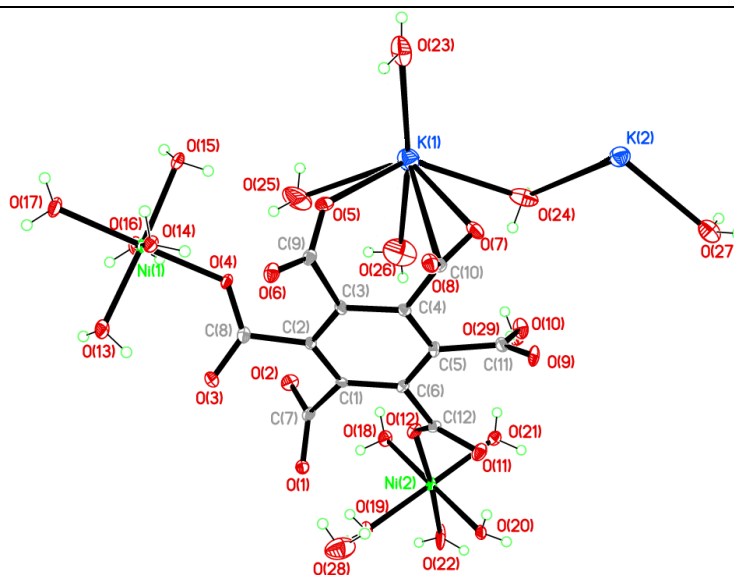


**Figure 8.07: Powder X-ray diffraction pattern of Compound 37**

**Compound 38:**  $[\text{Ni}_2\text{K}_2(\text{C}_{12}\text{O}_{12})(\text{H}_2\text{O})_{15}]\cdot 2\text{H}_2\text{O}$



Chemical formula (total)	$\text{C}_{12}\text{H}_{34}\text{K}_2\text{Ni}_2\text{O}_{29}$
Formula weight	838.01
Temperature	150(2) K
Radiation, wavelength	MoK $\alpha$ , 0.71073 Å
Crystal system, space group	monoclinic, $P2_1/c$
Unit cell parameters	$a = 6.7014(2)$ Å $b = 19.2147(6)$ Å $c = 23.0383(6)$ Å $\beta = 92.119(3)^\circ$
Cell volume	$2964.51(15)$ Å <sup>3</sup>
Z	4
Crystal colour and size	green, $0.20 \times 0.20 \times 0.10$ mm <sup>3</sup>
Final $R$ indices [ $F^2 > 2\sigma$ ]	$R1 = 0.0524$
$R$ indices (all data)	$wR2 = 0.1263$
Largest diff. peak and hole	1.65 and $-0.96$ e Å <sup>-3</sup>

**Figure 8.08:** Asymmetric Unit of Compound 38 all unique atoms labelled, additional atoms added to complete ligands.

### Synthesis

2 mL of a solution of  $\text{Ni}(\text{NO}_3)_2 \cdot 6\text{H}_2\text{O}$  (0.09 g, 0.33 mmol) in water (10 mL) was layered over 2 mL of a solution of benzenhexacarboxylic acid (0.058 g, 0.17 mmol) in water (10 mL) with potassium hydroxide (0.336 g, 6 mmol) in small sample vial. The vial was covered and left until crystallisation was complete. After two weeks, green block crystals formed.

## Structure Determination

The data were collected at 150 K using molybdenum radiation on an Oxford Diffraction Gemini A Ultra diffractometer. The structure was solved by direct methods. The semi-empirical absorption corrections were applied based on symmetry-equivalent and repeated data. The refinement gave a  $wR2$  of 0.1263 for all 6679 independent reflections and a conventional  $R1$  of 0.0524, for 3912 reflections with  $F^2 > 2\sigma$ . The residual electron density maximum and minimum were 1.65 and  $-0.96 \text{ e } \text{\AA}^{-3}$  respectively, the high residual electron density is a result of unmodelled disorder generated by the twinning of the structure.

The hydrogen atoms were freely refined within this compound, DELU and SIMU restraints were imposed on the ligands in compound 38 with further SADI restraints on the water molecules. The full data of compound 38 can be found in Appendix 1.

## Structure Analysis

The asymmetric unit of compound 38 (figure 8.08) shows a complete benzenehexacarboxylate ligand coordinating two nickel cations Ni(1) and Ni(2), and two potassium cations K(1) and K(2). The nickel cations Ni(1) and Ni(2) are situated on general positions forming six-coordinate regular octahedra (figure 8.09) (table 8.04), whilst the potassium cations K(1) and K(2) generate irregular geometries forming the seven-coordinate distorted capped trigonal prismatic geometry.

The benzenehexacarboxylate ligand coordinates to the Ni(1) cation through the monodentate carboxylate O(3)-C(8)-O(4) carboxylate forming the Ni(1)-O(4) 2.055(3) Å bond, the carboxylate group coordinates coplanar to the cis water molecule O(13) allowing the formation of a hydrogen bond between the uncoordinated O(3) carboxylate oxygen and the coordinated water molecule; O(13)-H(13A)···O(3) 2.739(4) Å (table 8.05). The Ni(1) cation completes its six-coordinate octahedral geometry coordinating to a total of five terminal water ligands; O(13), O(14), O(15) and O(16) forming the equatorial coplanar belt cis to the O(3)-C(8)-O(4) carboxylate whilst O(17) occupies the trans coordination site O(4)-Ni(1)-O(17) 177.68(14)° (figure 8.09A).



The Ni(2) cation is coordinated in a similar motif to the Ni(1) cation forming the node in figure 8.09B, with coordination to the benzenhexacarboxylate ligand through the monodentate bond with the O(12) carboxylate oxygen. The carboxylate group coordinates coplanar to the cis O(20) coordinated water molecule forming a strong hydrogen bond O(20)-H(20A)···O(11) 2.676(3) Å at an angle of 174(5)° (table 8.05). The Ni(2) cation completes its six-coordinate geometry with coordination to five water ligands; O(18), O(19), O(20) and O(21) cis to the carboxylate and O(22) trans at O(12)-Ni(2)-O(22) 174.85(12)° (figure 8.09B) (table 8.04). The Ni(2) cation does not form a fully capped node with further coordination to symmetry equivalent K(2) cations. This coordination occurs through the coordinated water molecules that form bidentate bridges between the Ni(2) and K(2) cations. The water molecules O(18) and O(21) around the equatorial belt of the Ni(2) cation coordinate to the K(2) cation at an angle of 61.00(10)° with respect to each other. The O(19) and O(20) water molecules coordinate to a symmetry equivalent K(2) cation with the angle of 60.38(9)° with respect to each other and at angles of O(18E)-K(2)-O(19F) 82.71(10)° and O(18E)-K(2)-O(20F) 112.20(11)° to the symmetry equivalent water molecules. The K(2) cation further coordinates to the water molecule O(22) completing the bridges between the K(2) cation and the Ni(2) cation that have comparable bridging bite angles; Ni(2)-O(18)-K(2B) 98.79(12)°, Ni(2)-O(19)-K(2C) 94.72(11)°, Ni(2)-O(20)-K(2C) 103.13(12)°, Ni(2)-O(21)-K(2B) 94.92(12)° and Ni(2)-O(22)-K(2B) 81.51(14)°. The completion of the K(2) cation coordination geometry occurs with coordination to a terminal water molecule O(27) and a bridging water molecule O(24), forming the bridge between the K(2) and K(1) cations with a bite angle of K(1)-O(24)-K(2) 116.30(14)°. The K(2) cation is coordinated in the framework completely independent of the benzenhexacarboxylate ligand and acts as a crucial bridging node expanding the structure into two dimensions.

The benzenhexacarboxylate completes its coordination forming bonds to symmetry equivalent K(1) cations through the O(5)-C(9)-O(6) and O(7)-C(10)-O(8) carboxylate groups. These carboxylates bridge the K(1) cations through the monodentate bonds; K(1)-O(5) 2.863(4) Å and K(1)-O(7) 2.777(4) Å creating a bite angle of O(5)-K(1)-O(7) 72.46(10)° which is the smallest bite angle in the compound. The O(7)-C(10)-O(8) further coordinates to a symmetry equivalent K(1) cation with the

K(1)-O(8A) 2.751(3) Å bond trans to the symmetry equivalent O(7) oxygen; O(7)-K(1)-O(8A) 123.64(10)°. This coordination results in the carboxylates coordinating in the trans positions of the trigonal prismatic geometry, with the equatorial positions cis to these groups occupied by four coordinated water molecules including the bridging O(24) water that is coordinated at a distorted angle of 73.91(10)° to the cis O(8) carboxylate oxygen.

The remaining two carboxylate groups of the benzenhexacarboxylate ligand O(1)-C(7)-O(2) and O(9)-C(11)-O(10) are uncoordinated, showing full deprotonation and delocalisation with comparable bond lengths through out all the carboxylates in this compound (table 8.04). These uncoordinated carboxylates act as hydrogen acceptors for hydrogen bonds from the coordinated water molecules on adjacent coordinated water molecules on Ni(1) and Ni(2) cations (table 8.05).

The coordination of the benzenhexacarboxylate to the nickel and potassium cations in conjunction with the bridging waters and K(2) cation form the molecular building unit shown in figure 8.10. This molecular building unit expands the structure into a coordinated three dimensional framework, composed of sheets of nickel-benzenhexacarboxylates that expand along the *b*-axis and down the *c*-axis. These sheets are composed of discrete units of [Ni(1)-benzenetetracarboxylate-Ni(2)] with the nickel cations capped by coordinated water molecules. The discrete units pack together in a chequered motif with each unit related by inversion symmetry with staggering due to a glide plane running down the (101) plane; the benzenhexacarboxylates are rotated by 180° as they pack up the *c*-axis as a result of a two-fold rotation axis. The discrete units are then linked by out of plane potassium cations forming the sheet shown in figure 8.11 when compound 38 is viewed down the *a*-axis. The potassium cations are out of plane to the sheets in the *a*-axis coordinating the individual discrete units as well as further coordination between the sheets creating columns that run down the *b*-axis and stack in the *c*-axis due to the terminal water molecules on the K(1) cations (figure 8.12).

Further analysis of compound 38 was carried out to determine the purity of the bulk sample using powder X-ray diffraction and elemental analysis. The powder X-ray diffraction data shows a strong correlation between the obtained powder diffraction pattern (figure 8.13) and the predicted powder diffraction pattern calculated from the

single crystal data; with the major peaks present in both at 13.17, 27.09 and 32.94 2-Theta. Purity of the compound was confirmed by elemental analysis that provided results C = 17.73 %, H = 3.77 % and N = 0 % consistent with the calculated values of C = 17.18 %, H = 4.05 % and N = 0 % from the single crystal data.

Compound 38 was synthesised as an expansion of compound 37 by using potassium hydroxide to fully deprotonate the benzenhexacarboxylate ligand and act as a templating agent forming further coordination. Compound 38 and compound 37 both show structures containing two six-coordinate nickel cations that are capped by coordinated water molecules. The molecular building units of both compounds show consistent features with compound 37 forming a stepped chain with bidentate coordination to the Ni(1) cation with a capped Ni(2) cation coordinated by the adjacent carboxylate (figure 8.03); the molecular unit of compound 38 (figure 8.10) forms the connected planar sheets using a bidentate potassium cation that links the two benzenhexacarboxylates with a capped Ni(1) cation coordinated to the adjacent carboxylate. The structures differ as the bidentate potassium is located in a general position and not on an inversion centre such as the Ni(1) in compound 37, this results in the K(1) cation coordinating to a benzenhexacarboxylate positioned directly underneath the previous creating columns of collinear carboxylate ligands rather than the stepped chain motif.

The success of expanding compound 37 into three dimensions resulted in additional reactions with alternative transition metals in order to produce structural analogues of JIYNOU<sup>1</sup> and compound 37, leading to the production of compounds 39, 40 and 41.

**Table 8.04: Selected Bond Lengths [Å] and Angles [°] for Compound 38**

O(4)–Ni(1)	2.055(3)	O(5)–K(1)	2.863(4)
O(6)–K(1A)	3.403(4)	O(7)–K(1)	2.777(4)
O(8)–K(1A)	2.751(3)	O(12)–Ni(2)	2.020(3)
O(14)–Ni(1)	2.021(4)	O(15)–Ni(1)	2.065(4)
O(16)–Ni(1)	2.019(4)	O(17)–Ni(1)	2.089(3)
O(18)–Ni(2)	2.049(3)	O(18)–K(2B)	2.721(4)
O(19)–Ni(2)	2.052(3)	O(19)–K(2C)	2.920(4)
O(20)–Ni(2)	2.030(3)	O(20)–K(2C)	2.672(3)
O(21)–Ni(2)	2.069(3)	O(21)–K(2B)	2.832(4)
O(22)–Ni(2)	2.097(4)	O(22)–K(2B)	3.310(5)
O(23)–K(1)	2.866(5)	O(24)–K(1)	2.905(5)
O(24)–K(2)	2.707(4)	O(25)–K(1)	3.009(5)
O(26)–K(1)	2.815(5)	O(27)–K(2)	2.709(4)
C(7)–O(1)	1.247(6)	C(7)–O(2)	1.262(6)
C(8)–O(3)	1.253(5)	C(8)–O(4)	1.261(6)
C(9)–O(5)	1.236(6)	C(9)–O(6)	1.273(6)
C(10)–O(7)	1.255(5)	C(10)–O(8)	1.260(6)
C(11)–O(9)	1.267(6)	C(11)–O(10)	1.231(6)
C(12)–O(11)	1.268(5)	C(12)–O(12)	1.255(5)
O(4)–Ni(1)–O(13)	92.82(13)	O(4)–Ni(1)–O(14)	87.65(13)
O(4)–Ni(1)–O(15)	89.87(13)	O(4)–Ni(1)–O(16)	91.60(13)
O(4)–Ni(1)–O(17)	177.68(14)	O(12)–Ni(2)–O(18)	88.65(14)
O(12)–Ni(2)–O(19)	86.87(13)	O(12)–Ni(2)–O(20)	91.89(14)
O(12)–Ni(2)–O(21)	92.37(13)	O(12)–Ni(2)–O(22)	174.88(12)
O(5)–K(1)–O(6D)	97.42(9)	O(5)–K(1)–O(7)	72.46(10)
O(5)–K(1)–O(8D)	151.16(11)	O(5)–K(1)–O(23)	80.76(10)
O(5)–K(1)–O(24)	131.39(11)	O(5)–K(1)–O(25)	67.81(11)
O(5)–K(1)–O(26)	97.05(13)	O(18E)–K(2)–O(19F)	82.72(10)
O(18E)–K(2)–O(20F)	112.20(11)	O(18E)–K(2)–O(21E)	61.00(10)
O(18E)–K(2)–O(22E)	56.19(10)	O(18E)–K(2)–O(24)	129.31(12)
O(18E)–K(2)–O(27)	97.00(11)	Ni(2)–O(18)–K(2B)	98.79(12)
Ni(2)–O(19)–K(2C)	94.72(11)	Ni(2)–O(20)–K(2C)	103.13(12)
Ni(2)–O(21)–K(2B)	94.92(12)	Ni(2)–O(22)–K(2B)	81.51(14)
K(1)–O(24)–K(2)	116.30(14)		
Symmetry operations for equivalent atoms			
A	x–1,y,z	B	–x+2,y–1/2,–z+3/2
C	–x+1,y–1/2,–z+3/2		
D	x+1,y,z	E	–x+2,y+1/2,–z+3/2
F	–x+1,y+1/2,–z+3/2		

**Table 8.05: Selected Hydrogen bond Lengths [Å] and angles [°] for Compound 38**

D–H...A	d(D–H)	d(H...A)	d(D...A)	(DHA)
O(13)–H(13A)...O(3)	0.739(16)	2.08(3)	2.739(4)	150(6)
O(13)–H(13B)...O(9G)	0.739(16)	1.974(19)	2.709(4)	173(5)
O(14)–H(14A)...O(6)	0.739(16)	1.97(2)	2.705(4)	171(6)
O(14)–H(14B)...O(5H)	0.743(16)	1.827(19)	2.559(5)	169(6)
O(15)–H(15A)...O(23I)	0.749(17)	2.07(2)	2.757(5)	153(5)
O(15)–H(15B)...O(25)	0.740(16)	2.53(2)	3.246(6)	165(4)
O(15)–H(15B)...O(4)	0.740(16)	2.54(5)	2.910(5)	113(5)
O(16)–H(16A)...O(27G)	0.747(16)	2.080(18)	2.820(5)	171(5)
O(16)–H(16B)...O(10G)	0.741(16)	1.99(2)	2.691(4)	158(5)
O(17)–H(17A)...O(8H)	0.748(17)	2.17(2)	2.899(5)	166(6)
O(17)–H(17B)...O(11G)	0.740(16)	2.221(18)	2.958(5)	174(6)
O(18)–H(18A)...O(1J)	0.739(16)	2.008(17)	2.747(4)	178(6)
O(18)–H(18B)...O(28D)	0.735(17)	1.999(17)	2.730(5)	174(5)
O(19)–H(19A)...O(1)	0.741(16)	2.069(17)	2.810(4)	179(6)
O(19)–H(19B)...O(2J)	0.746(16)	1.886(18)	2.626(4)	171(5)
O(20)–H(20A)...O(11)	0.734(16)	1.97(2)	2.676(5)	161(5)
O(20)–H(20B)...O(7C)	0.727(16)	1.838(17)	2.562(5)	173(5)
O(21)–H(21A)...O(29)	0.738(17)	2.03(2)	2.763(5)	170(6)
O(21)–H(21B)...O(8C)	0.736(16)	2.028(19)	2.757(4)	171(6)
O(22)–H(22A)...O(9C)	0.743(17)	2.06(2)	2.789(5)	167(7)
O(22)–H(22B)...O(3J)	0.747(17)	2.21(2)	2.942(5)	166(6)
O(23)–H(23A)...O(29E)	0.753(17)	2.51(7)	2.824(6)	107(6)
O(23)–H(23B)...O(14H)	0.740(17)	2.15(4)	2.814(5)	151(7)
O(24)–H(24A)...O(9D)	0.743(17)	2.03(2)	2.755(5)	164(6)
O(24)–H(24B)...O(10)	0.745(17)	2.34(3)	3.035(5)	155(7)
O(25)–H(25A)...O(4)	0.750(17)	2.28(3)	2.989(5)	157(8)
O(25)–H(25B)...O(6D)	0.750(17)	2.21(5)	2.820(6)	139(8)
O(26)–H(26A)...O(28D)	0.752(17)	2.39(4)	3.084(6)	154(8)
O(26)–H(26B)...O(25)	0.758(17)	2.13(4)	2.785(8)	145(8)
O(27)–H(27A)...O(2K)	0.741(17)	2.24(3)	2.887(5)	147(5)
O(27)–H(27B)...O(3L)	0.750(17)	2.22(2)	2.944(5)	164(6)
O(28)–H(28A)...O(26A)	0.745(17)	2.52(5)	3.084(6)	134(7)
O(28)–H(28B)...O(1)	0.746(17)	2.04(4)	2.741(5)	156(8)
O(29)–H(29A)...O(11D)	0.743(17)	2.24(3)	2.905(5)	150(5)
O(29)–H(29B)...O(10)	0.743(17)	2.12(2)	2.848(5)	166(6)

Symmetry operations for equivalent atoms

A  $x-1, y, z$  C  $-x+1, y-1/2, -z+3/2$  D  $x+1, y, z$ E  $-x+2, y+1/2, -z+3/2$  G  $x, -y+1/2, z-1/2$  H  $-x+1, -y+1, -z+1$ I  $-x+2, -y+1, -z+1$  J  $-x+1, -y, -z+1$  K  $x, -y+1/2, z+1/2$ L  $x+1, -y+1/2, z+1/2$

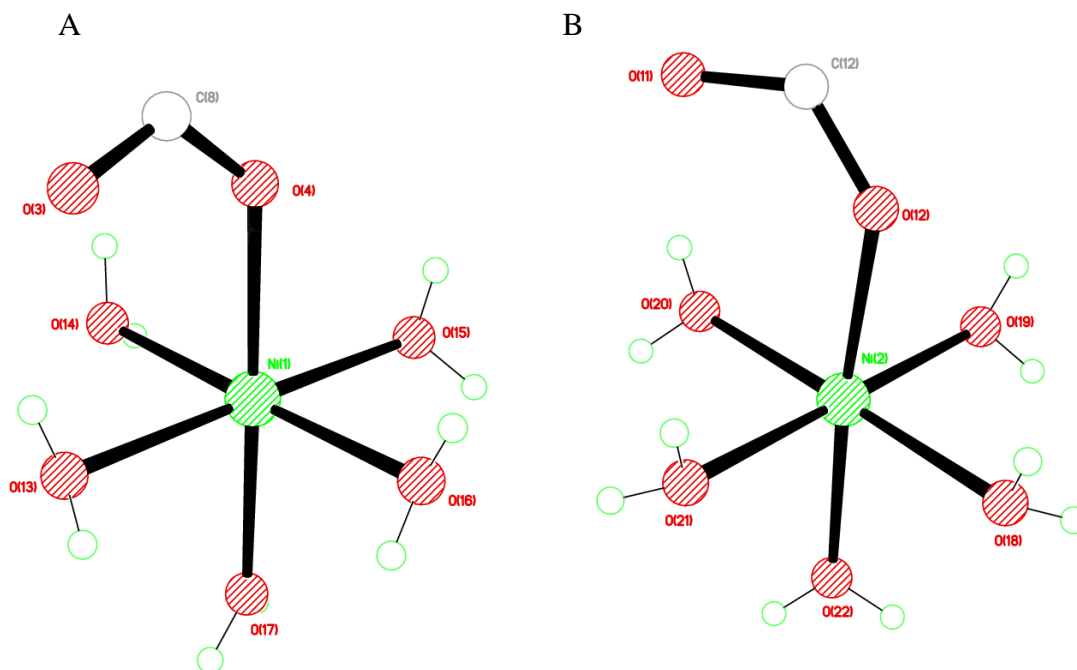


**Figure 8.09: A) Octahedral coordination environment of Ni(1) and B) Octahedral coordination environment of Ni(2) in compound 38**

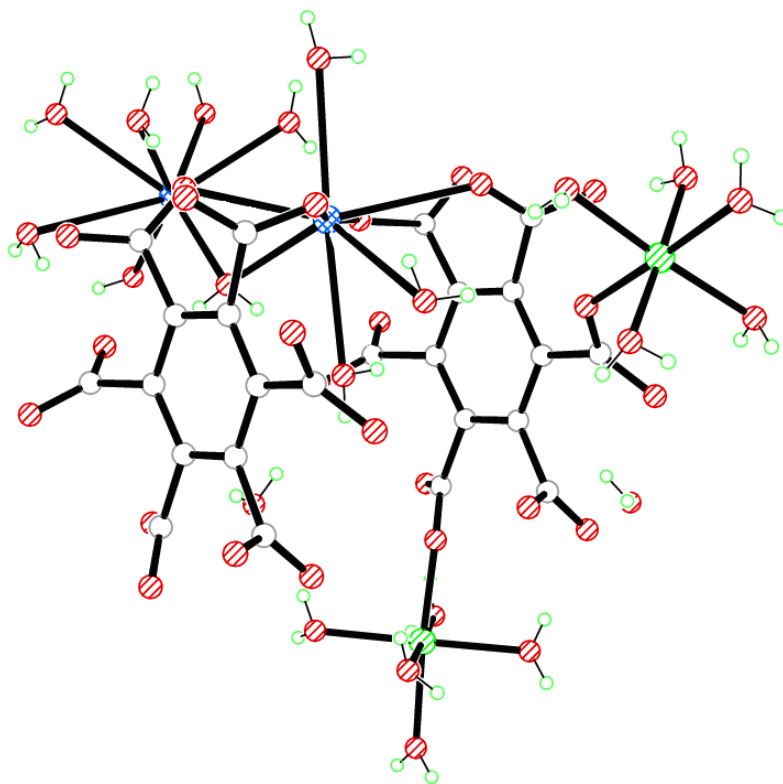


**Figure 8.10: Secondary building unit in compound 38**

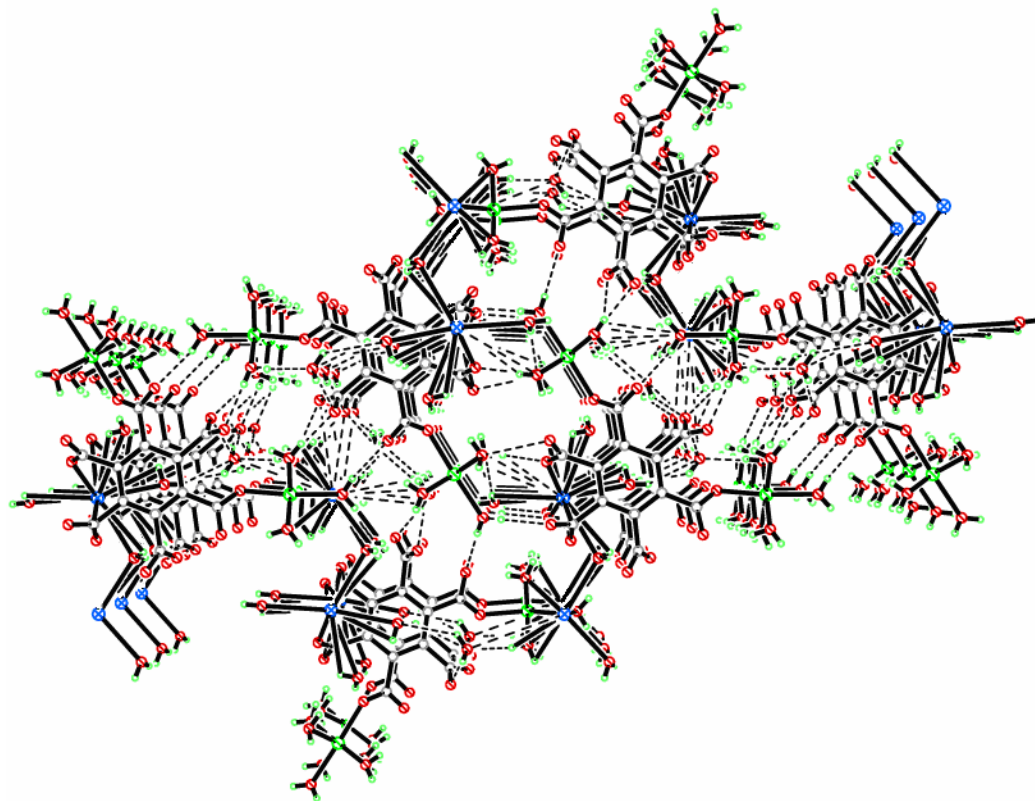


**Figure 8.11:** Two dimensional sheet of the discrete units compound 38 viewed down the *a*-axis

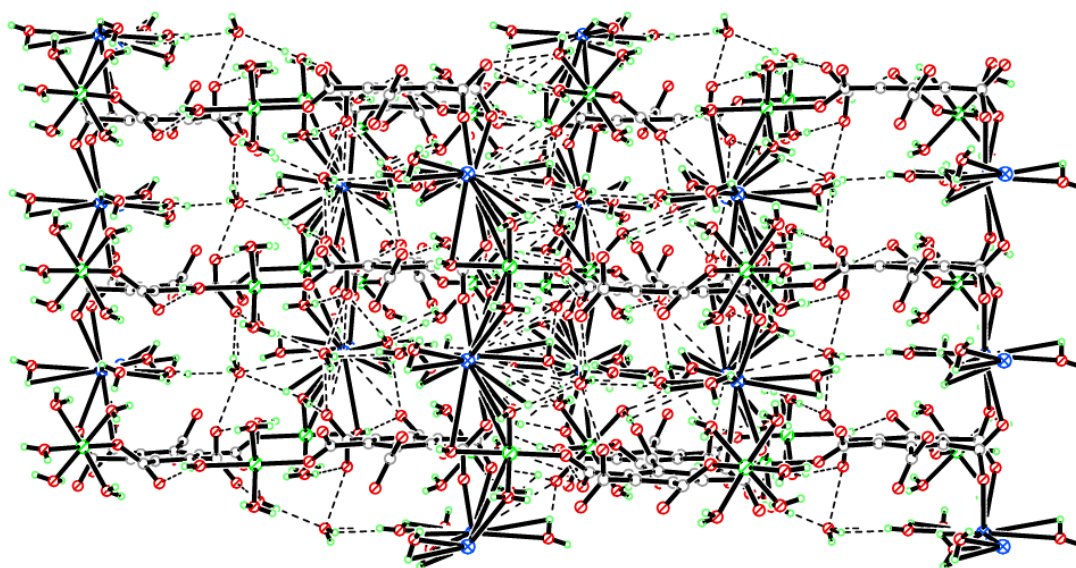


**Figure 8.12:** Two dimensional columns of the potassium and nickel cations of compound 38 connecting the sheets viewed down the *c*-axis

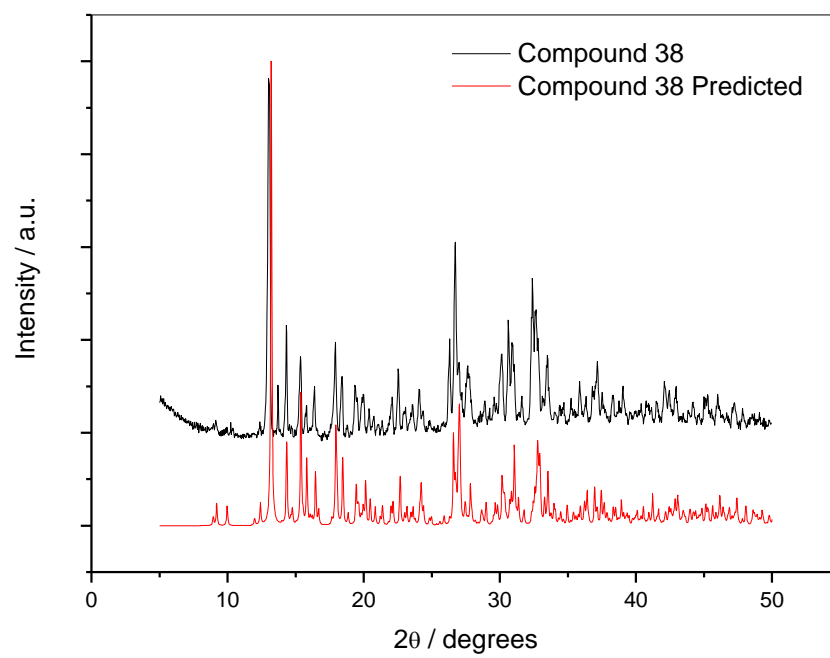
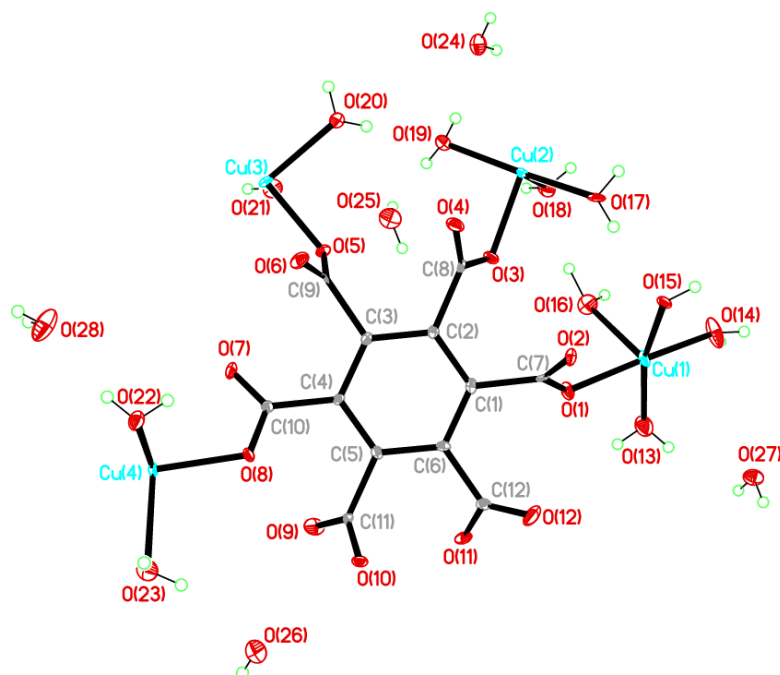


**Figure 8.13: Powder X-ray diffraction pattern of Compound 38**



**Compound 39:**  $[\text{Cu}_7(\text{C}_{12}\text{O}_{12})_2(\text{HO})_2(\text{H}_2\text{O})_{18}] \cdot 10\text{H}_2\text{O}$



Chemical formula (total)	$\text{C}_{24}\text{H}_{58}\text{Cu}_7\text{O}_{54}$
Formula weight	1655.48
Temperature	150(2) K
Radiation, wavelength	MoK $\alpha$ , 0.71073 Å
Crystal system, space group	orthorhombic, <i>Iba</i> 2
Unit cell parameters	$a = 19.2600(4)$ Å $b = 21.0541(3)$ Å $c = 12.8450(2)$ Å
Cell volume	$5208.67(15)$ Å <sup>3</sup>
<i>Z</i>	4
Crystal colour and size	blue, $0.30 \times 0.10 \times 0.05$ mm <sup>3</sup>
Final <i>R</i> indices [ $F^2 > 2\sigma$ ]	$R1 = 0.0229$
<i>R</i> indices (all data)	$wR2 = 0.0488$
Largest diff. peak and hole	0.78 and $-0.39$ e Å <sup>-3</sup>
Absolute structure parameter	0.026(8)

**Figure 8.14: Asymmetric Unit of Compound 39 all unique atoms labelled,**

### Synthesis

2 mL of a solution of  $\text{Cu}(\text{NO}_3)_2 \cdot 4\text{H}_2\text{O}$  (0.079 g, 0.33 mmol) in water (10 mL) was layered over 2 mL of a solution of benzenehexacarboxylic acid (0.058 g, 0.17 mmol) in water (10 mL) in small sample vial. The vial was covered and left until crystallisation was complete. After three weeks, blue plate crystals formed.

## Structure Determination

The data were collected at 150 K using molybdenum radiation on an Oxford Diffraction Gemini A Ultra diffractometer. The structure was solved by direct methods. The semi-empirical absorption corrections were applied based on symmetry-equivalent and repeated data. The refinement gave a  $wR2$  of 0.0488 for all 4891 independent reflections and a conventional  $R1$  of 0.0229, for 4472 reflections with  $F^2 > 2\sigma$ . The residual electron density maximum and minimum were 0.78 and  $-0.39 \text{ e } \text{\AA}^{-3}$  respectively. Compound 39 crystallised in the non-centrosymmetric space group *Iba2* and refined with a Flack parameter of 0.026 indicating the correct handedness has been selected.

The hydrogen atoms were refined within this compound, with SADI restraints imposed on the water molecules during refinement. The full data of compound 39 can be found in Appendix 1.

## Structure Analysis

The asymmetric unit of compound 39 (figure 8.14) shows a complete benzenehexacarboxylate ligand coordinating four copper cations; Cu(1), Cu(2), Cu(3) and Cu(4). The copper cations in compound 39 adopt the five-coordinate square pyramidal geometry shown in figure 8.15 and 8.16 with regular bond angles listed in table 8.06.

The benzenehexacarboxylate coordinates to both Cu(1) and Cu(4) cations creating a standard carboxylate bridge through the bidentate O(1)-C(7)-O(2) carboxylate that forms the monodentate bonds; Cu(1)-O(1) 1.991(19) Å and Cu(4)-O(2) 1.992(19) Å. The carboxylate group rotates by  $115.5(2)^\circ$  out of the plane of the aromatic ring holding the cations above and below the plane of the aromatic ring. The Cu(1) and Cu(4) cations are further bridged by a bidentate hydroxide O(15) with a bite angle of Cu(1)-O(15)-Cu(4)  $107.26(10)^\circ$ , the Cu(1) cation completes its five-coordinate geometry with coordination to three terminal water molecules (figure 8.15A). The Cu(4) cation further coordinates to the benzenehexacarboxylate ligand through a symmetry equivalent O(7)-C(10)-O(8) carboxylate group that coordinates through the monodentate Cu(4)-O(8) 1.975(18) Å bond in the trans coplanar position to the O(1)-C(7)-O(2)

carboxylate; O(2)-Cu(4)-O(8A) 165.68(8)° with the O(7)-C(10)-O(8) carboxylate rotated out of the plane of the aromatic ring by 114.4(2)°. The Cu(4) cation completes its coordination geometry coordinating to two water molecules O(22) trans to the bridging hydroxide and O(23) in the coplanar cis position to the carboxylate groups, shown in figure 8.16B.

The benzenehexacarboxylate coordinates to the Cu(2) and Cu(3) cations that bridge between symmetry equivalents of the ligand. The O(3)-C(8)-O(4) carboxylate coordinates to the Cu(2) cation through the Cu(2)-O(3) 1.945(19) Å bond, a trans symmetry equivalent ligand coordinates through the Cu(2)-O(11) monodentate bond from the coplanar O(11)-C(12)-O(12) carboxylate. The remaining coordination sites perpendicular to the plane of the carboxylates are occupied by terminal water ligands O(17) and O(19) trans to one another, with the final axial coordination site occupied by the O(18) water molecule (figure 8.15B).

The remaining Cu(3) cation is coordinated by a monodentate bond from the O(5)-C(9)-O(6) carboxylate group, Cu(3)-O(5) 1.925(19) Å. The Cu(3) cation is positioned on a two-fold rotation axis that runs up the *c*-axis through the O(21) coordinated water molecule perpendicular to the carboxylate group and the O(20) water molecule that is in the coplanar cis position to O(5). The two-fold rotation axis generates the coplanar trans symmetry equivalent ligands of the carboxylate and O(2) water molecule completing the five-coordinate geometry shown in figure 8.16A.

The benzenehexacarboxylate coordinates through all the available carboxylate groups except the O(9)-C(11)-O(10), this uncoordinated carboxylate contains comparable bond lengths to the fully deprotonated and delocalised carboxylates of the benzenehexacarboxylate ligand (table 8.06). The benzenehexacarboxylate expands the structure through the linking nodes Cu(2), Cu(3) and Cu(4) to form the molecular building unit shown in figure 8.17.

The molecular building unit expands the structure into a two dimensional sheet along the *a*-axis and down the *b*-axis (figure 8.18). The sheets stack together in the *c*-axis forming hydrogen bonding between the coordinated water molecules that protrude perpendicular from the layers (figure 8.19). The layers stack in a staggered conformation along the *b*-axis by 4.723(4) Å with each layer rotated by 180° in the plane of the

aromatic ring through a two-fold rotation axis running up the *c*-axis. This staggering maximises hydrogen bond interactions by placing the coordinated waters on Cu(1) and Cu(2) in close proximity of the uncoordinated carboxylate oxygens of the adjacent layer; whilst bring water molecules on Cu(3) into ideal positions to form hydrogen bonds as donors to uncoordinated water molecules within the compound (table 8.06).

Compound 39 was analysed further using elemental analysis producing the results C = 29.16 %, H = 4.11 % and N = 4.31 %; these are inconsistent with the values calculated from the single crystal data of C = 17.39 %, H = 3.51 % and N = 0 % showing significant impurities are present in the bulk material. Additional analysis using powder X-ray diffraction provided the powder diffraction pattern shown in figure 8.20, the data is consistent with the predicted powder diffraction pattern generated from the single crystal data with the high intensity peaks 9.39, 11.73, 18.78, 20.19 and 28.9-31.05 2-Theta accounted for in both data sets. However peaks in the 15.99-17.71 2-Theta range suggest that impurities are present compound 39.

Compound 39 was previously reported by Mori et. al. (VAPLED)<sup>2</sup> and is reported here due to the difference in synthesis protocol and its presence as a precursor to compound 40 a structural analogue with a metal substitution.

**Table 8.06: Selected Bond Lengths [Å] and Angles [°] for Compound 39**

Cu(1)–O(1)	1.9905(19)	Cu(1)–O(13)	1.939(3)
Cu(1)–O(14)	1.950(2)	Cu(1)–O(15)	1.934(2)
Cu(1)–O(16)	2.201(3)	Cu(2)–O(3)	1.9455(19)
Cu(2)–O(11A)	1.9253(19)	Cu(2)–O(17)	1.949(2)
Cu(2)–O(18)	2.377(3)	Cu(2)–O(19)	2.003(2)
Cu(3)–O(5)	1.9245(19)	Cu(3)–O(20)	2.037(2)
Cu(3)–O(21)	2.139(3)	Cu(4)–O(2C)	1.9922(19)
Cu(4)–O(8)	1.9753(18)	Cu(4)–O(15C)	1.923(2)
Cu(4)–O(22)	1.946(2)	Cu(4)–O(23)	2.375(3)
C(7)–O(1)	1.256(4)	C(7)–O(2)	1.266(4)
C(8)–O(3)	1.291(4)	C(8)–O(4)	1.230(3)
C(9)–O(5)	1.280(4)	C(9)–O(6)	1.214(4)
C(10)–O(7)	1.227(3)	C(10)–O(8)	1.294(4)
C(11)–O(9)	1.244(4)	C(11)–O(10)	1.262(4)
C(12)–O(11)	1.273(4)	C(12)–O(12)	1.225(4)
O(1)–Cu(1)–O(13)	90.76(10)	O(1)–Cu(1)–O(14)	175.38(11)
O(1)–Cu(1)–O(15)	93.46(9)	O(1)–Cu(1)–O(16)	89.07(9)
O(3)–Cu(2)–O(11A)	175.20(9)	O(3)–Cu(2)–O(17)	88.25(10)
O(3)–Cu(2)–O(18)	92.10(9)	O(3)–Cu(2)–O(19)	93.17(9)
O(5)–Cu(3)–O(5B)	175.25(13)	O(5)–Cu(3)–O(20)	90.20(9)
O(5)–Cu(3)–O(21)	87.63(7)	O(2C)–Cu(4)–O(8)	165.68(8)
O(2C)–Cu(4)–O(15C)	88.93(8)	O(2C)–Cu(4)–O(22)	90.76(9)
O(2C)–Cu(4)–O(23)	98.65(8)	Cu(1)–O(15)–Cu(4D)	107.26(10)

Symmetry operations for equivalent atoms

A  $x-1/2, -y+3/2, z$     B  $-x+1, -y+1, z$     C  $-x+3/2, y-1/2, z$ D  $-x+3/2, y+1/2, z$

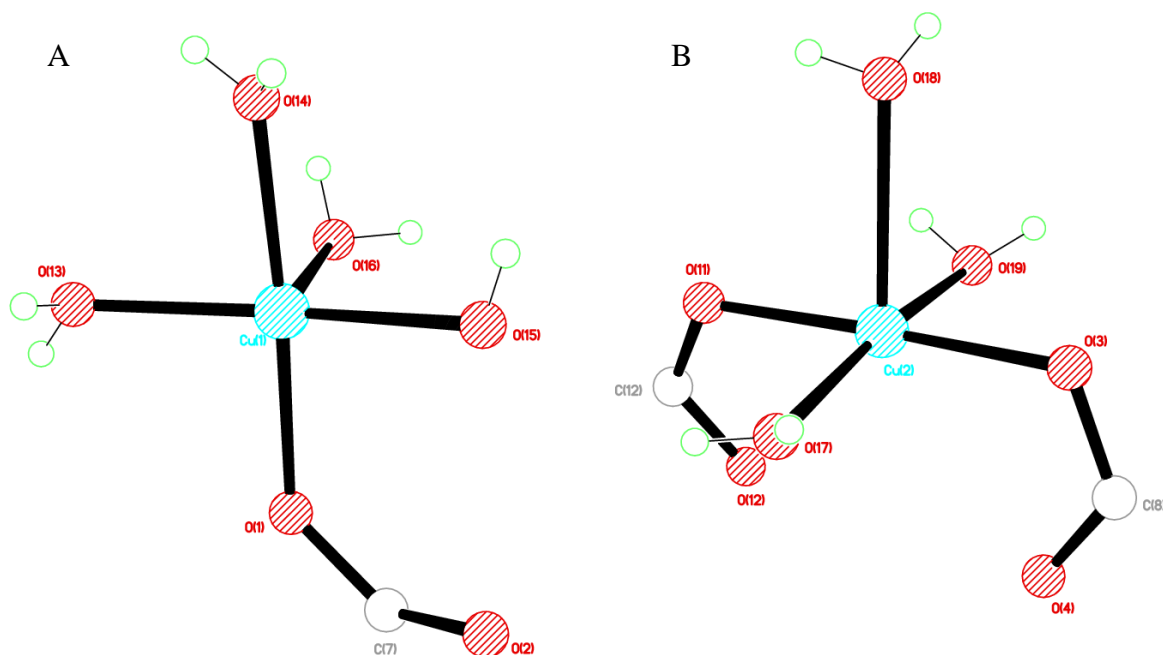


**Figure 8.15: A) Square pyramidal coordination environment of Cu(1) and B) Square pyramidal coordination environment of Cu(2) in compound 39**

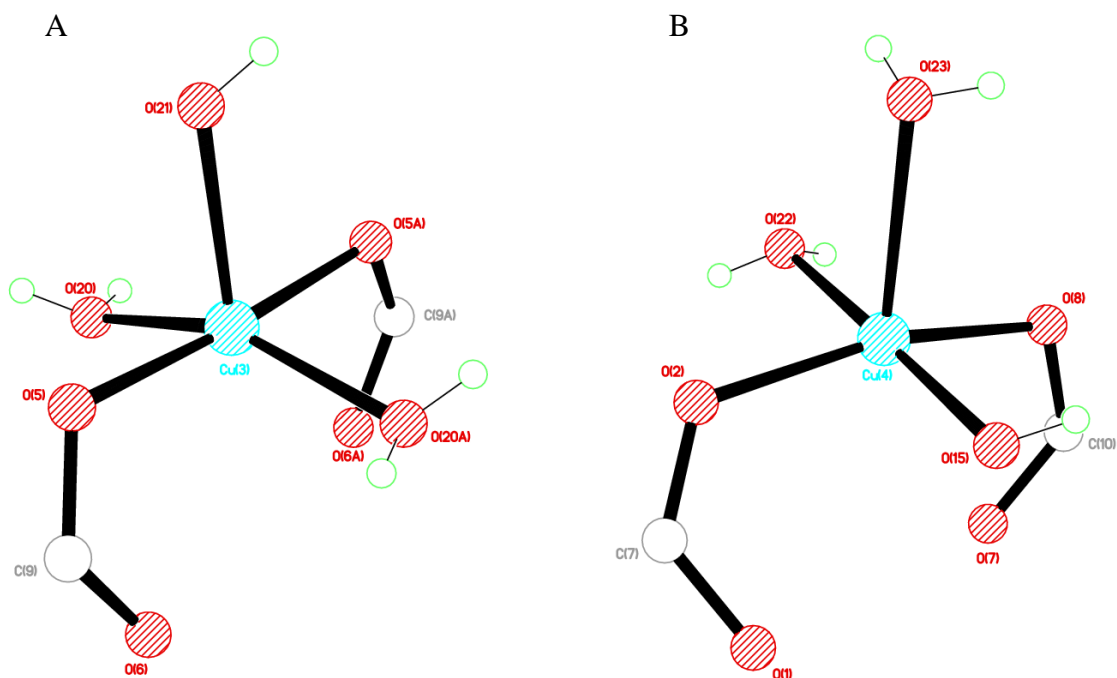


**Figure 8.16: A) Square pyramidal coordination environment of Cu(3) and B) Square pyramidal coordination environment of Cu(4) in compound 39**

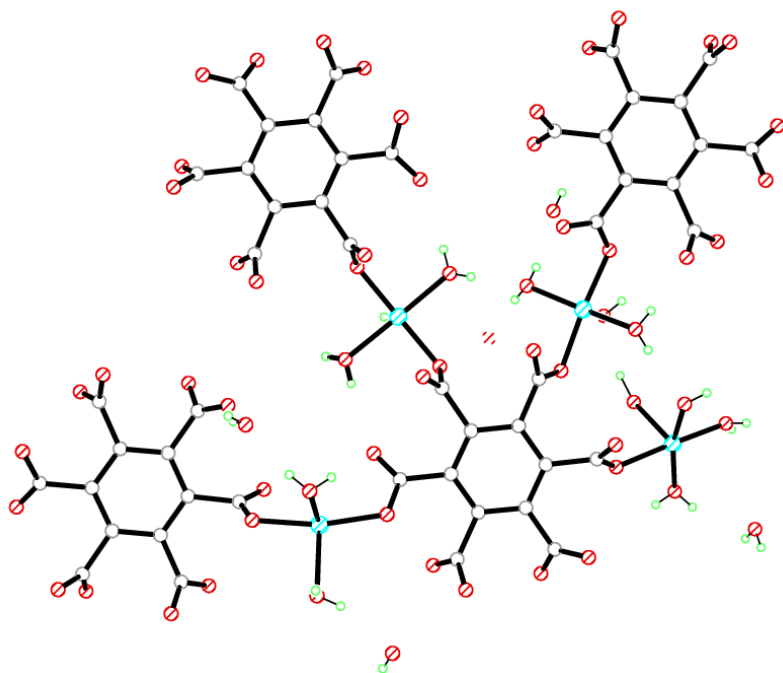


**Figure 8.17: Molecular building unit of compound 39**

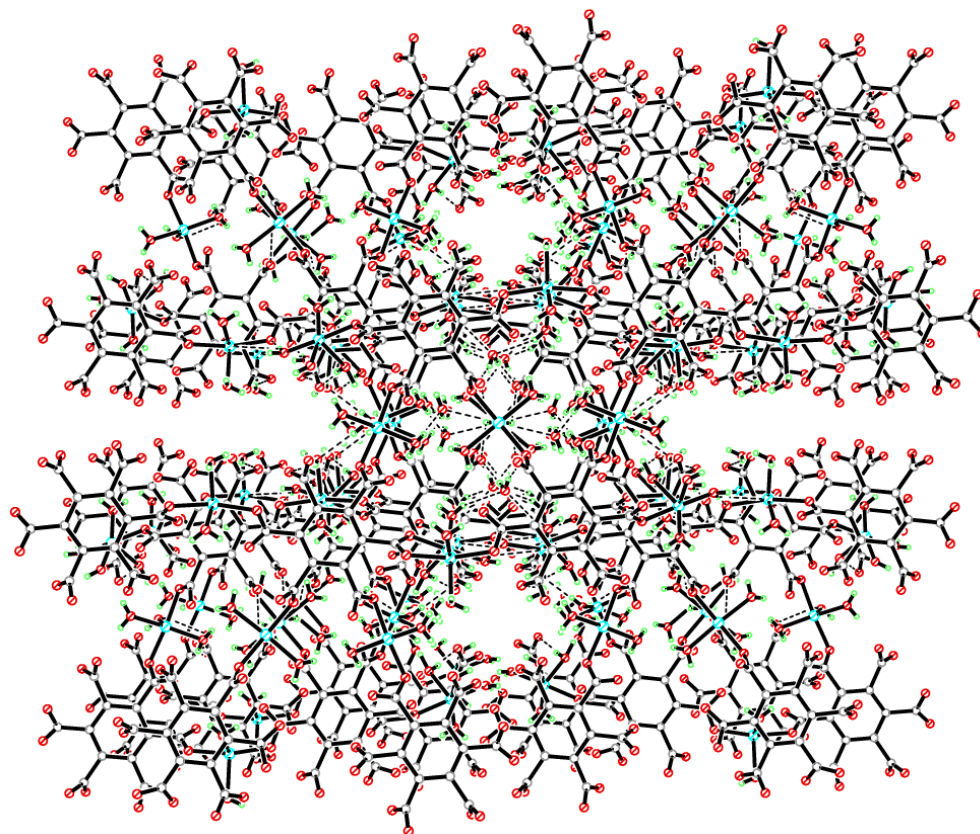


**Figure 8.18: Two dimensional sheets of compound 39 viewed down the *c*-axis**

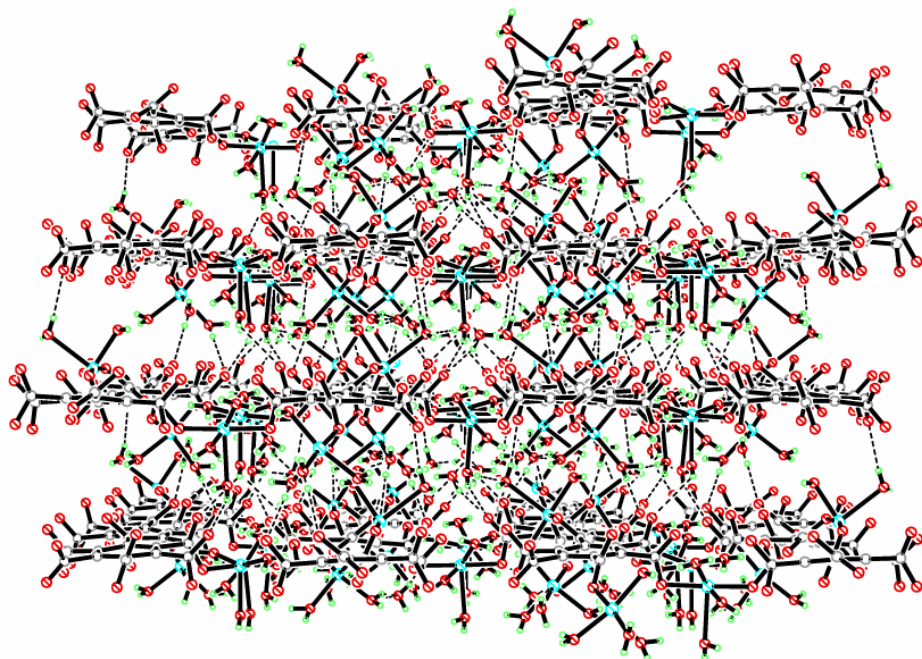


**Figure 8.19:** Two dimensional packing of the sheets in compound 39 viewed down the *b*-axis

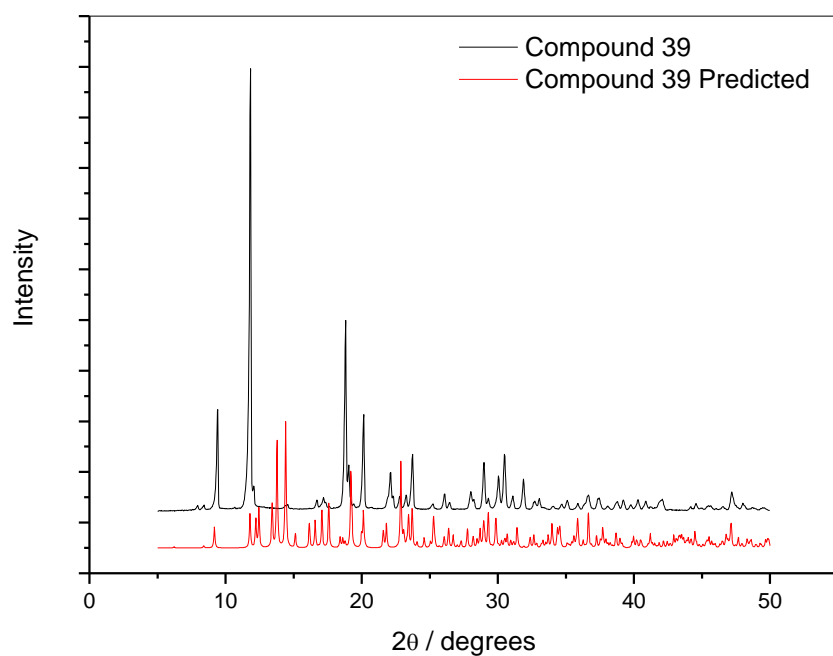
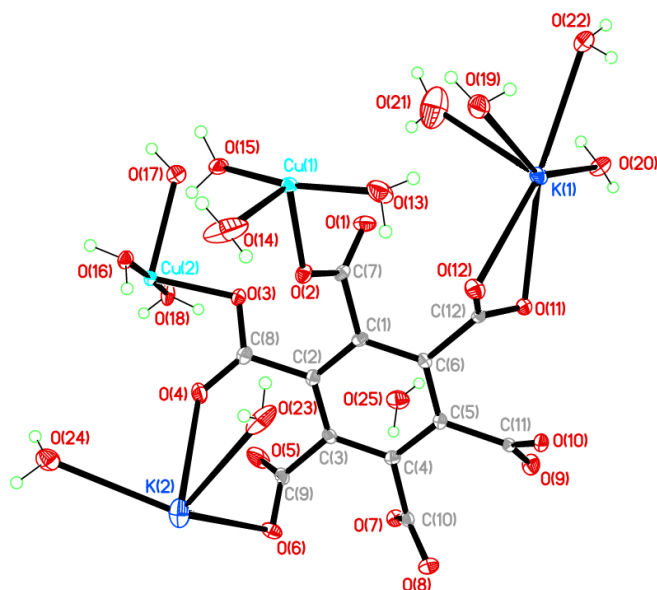


**Figure 8.20:** Powder X-ray diffraction pattern of Compound 39



**Compound 40:**  $[\text{Cu}_2\text{K}_2(\text{C}_{12}\text{O}_{12})(\text{H}_2\text{O})_{13}]$



Chemical formula (total)	$\text{C}_{12}\text{H}_{26}\text{Cu}_2\text{K}_2\text{O}_{25}$
Formula weight	775.61
Temperature	150(2) K
Radiation, wavelength	synchrotron, 0.6889 Å
Crystal system, space group	orthorhombic, <i>Pbca</i>
Unit cell parameters	$a = 19.4561(10)$ Å $b = 12.5110(6)$ Å $c = 21.4202(11)$ Å
Cell volume	$5214.0(5)$ Å <sup>3</sup>
Z	8
Crystal colour and size	blue, $0.12 \times 0.04 \times 0.03$ mm <sup>3</sup>
Final <i>R</i> indices [ $F^2 > 2\sigma$ ]	$R1 = 0.0347$
<i>R</i> indices (all data)	$wR2 = 0.0962$
Largest diff. peak and hole	0.73 and $-0.67$ e Å <sup>-3</sup>

**Figure 8.21:** Asymmetric Unit of Compound 40 all unique atoms labelled,

**Synthesis**

2 mL of a solution of  $\text{Cu}(\text{NO}_3)_2 \cdot 4\text{H}_2\text{O}$  (0.079 g, 0.33 mmol) in water (10 mL) was layered over 2 mL of a solution of benzenehexacarboxylic acid (0.058 g, 0.17 mmol) in water (10 mL) with potassium hydroxide (0.336 g, 6 mmol) in small sample vial. The vial was covered and left until crystallisation was complete. After two weeks, blue needle crystals formed.

## Structure Determination

The data were collected at 150 K using synchrotron radiation on a Crystal Logic diffractometer and Rigaku Saturn 724+ CCD on beamline I19 at the Diamond Light Source facility. The structure was solved by direct methods. The semi-empirical absorption corrections were applied based on symmetry-equivalent and repeated data. The refinement gave a  $wR2$  of 0.0962 for all 6453 independent reflections and a conventional  $R1$  of 0.0347, for 5626 reflections with  $F^2 > 2\sigma$ . The residual electron density maximum and minimum were 0.73 and  $-0.67 \text{ e } \text{\AA}^{-3}$  respectively.

The hydrogen atoms were refined within this compound, with SADI restraints imposed on the water molecules during refinement. The full data of compound 40 can be found in Appendix 1.

## Structure Analysis

The asymmetric unit of compound 40 (figure 8.21) shows a complete benzenehexacarboxylate ligand coordinating to two copper cations and two potassium cations in general positions. The copper cations Cu(1) and Cu(2) are both five-coordinate square pyramids with regular bond lengths and angles (figure 8.22) (table 8.07). The potassium cations form two different geometries in this polymeric compound; K(1) forms an eight coordinate distorted square antiprismatic geometry with disorder over two sites and the K(2) cation forms the seven-coordinate capped trigonal prismatic geometry (table 8.07).

The benzenehexacarboxylate coordinates to the Cu(1), K(1) and K(2) cations through the trifurcated O(1)-C(7)-O(2) carboxylate; it coordinates to the Cu(1) cation forming the monodentate bond Cu(1)-O(2)  $1.944(16) \text{ \AA}$  whilst the O(1) carboxylate forms a bidentate coordination to the K(1) and K(2) cations with a bridging angle of  $105.84(8)^\circ$  with both cations placed below the plane of the aromatic ring. The Cu(1) cation coordinates to a symmetry equivalent benzenehexacarboxylate ligand through the O(5)-C(9)-O(6) carboxylate that coordinates in the trans coplanar position to the O(1)-C(7)-O(2) carboxylate; O(2)-Cu(1)-O(6A)  $178.76(7)^\circ$ . The O(5)-C(9)-O(6) carboxylate also coordinates to a K(2) cation that is further bridged by a coordinated water molecule

on the Cu(1) cation that coordinates in the coplanar cis position to the carboxylates, this creates a bite angle of O(6)-K(2)-O(13) 58.68(5)°. The Cu(1) cation completes its five-coordinate geometry with coordination to two additional terminal water ligands; O(15) that coordinates trans to the bridging O(13) water and O(14) that coordinates in the apical position perpendicular to the carboxylates, O(2)-Cu(1)-O(14) 93.03(7) Å (figure 8.22). The potassium cations K(1) and K(2) bridged by the bidentate O(1) carboxylate oxygen further coordinate to the benzenhexacarboxylate ligand through adjacent carboxylate groups. The K(1) cation is coordinated to the bidentate O(11)-C(12)-O(12) carboxylate with the smallest bite angle of the compound; O(11)-K(1)-O(12) 46.09(4)°. This group coordinates cis to the O(1) oxygen at 53.21(4)° and shows the significantly shorter bonds; K(1)-O(11) 2.782(4) Å and K(1)-O(12) 2.962(18) Å compared to the K(1)-O(1) 3.360(6) Å. The K(1) cation completes its coordination geometry with four terminal water molecules O(19), O(20), O(21) and O(22) (table 8.07).

The bridged K(2) cation is also held between two carboxylates with additional coordination to the O(3) carboxylate oxygen forming a bridging angle of O(1)-K(2)-O(3A) 66.6(5)°. The O(3)-C(8)-O(4) carboxylate is twisted out of the plane of the benzene ring by 41.98(18)° and coordinates to a symmetry equivalent K(2) cation 7.233(4) Å above its symmetry equivalent in the *b*-axis. This creates a bite angle of O(3)-K(2)-O(4H) 135.39(5)° between the two carboxylate groups, this additional symmetry equivalent K(2) cation is bridged further by the O(5)-C(9)-O(6) carboxylate with a bite angle of O(4)-K(2)-O(6) 72.60(5)°. The benzenhexacarboxylate finally coordinates to the Cu(2) cation through the monodentate bond Cu(2)-O(3) 1.950(16) Å and the trans coplanar carboxylate group O(9)-C(11)-O(10) that coordinates through the Cu-O(10) 1.951(13) Å bond. The Cu(2) cation completes its coordination geometry by coordinating to the terminal water molecules O(16) and O(18) coplanar to the carboxylates in the cis positions along with O(17) in the apical position perpendicular to the carboxylates (figure 8.22B) (table 8.07). This bridging motif creates a chain consisting of [Cu(1)-O(6)-K(2)-O(4)-Cu(2)-O(3)-K(2)-O(1)-K(1)-O(8)···]<sub>n</sub> that forms the molecular building unit with the linking benzenhexacarboxylates shown in figure 8.23. The molecular building unit expands the structure into a two dimensional sheet along the *a*-axis and down the *c*-axis shown in figure 8.24 when the compound is

viewed down the *b*-axis. The sheets stack together in the *b*-axis linked by bridging potassium cations that form layers that run parallel to the [Cu-benzenehexacarboxylate] layers (figure 8.25). The layers of benzenehexacarboxylates are staggered along the *c*-axis by 4.728(4) Å with respect to the aromatic rings, with each layer rotated by 180° around the plane of the aromatic ring through a two-fold rotation axis that runs up the *b*-axis. This staggering allows the potassium cations to coordinate in between the layers avoiding the steric bulk of the hydrated copper cations that point in between the layers, the coordinated cations then hold the layers apart at a distance of 6.420(5) Å with respect to the plane of the benzene rings. The packing motif of compound 40 is almost identical to compound 39 and VAPLED,<sup>2</sup> with all three structures forming sheets of [Cu-benzenehexacarboxylate] with linking via five-coordinate square pyramidal nodes with coplanar trans carboxylates and capped water molecules (figure 8.22) (figure 8.15). The comparison of the asymmetric units of the compounds, shows that the Cu(1) and Cu(4) cations in compound 39 have been substituted for the K(1) and K(2) cations in compound 40. The K(1) and K(2) cations coordinated out of the plane of the benzene ring creating a three dimensional coordinated framework in compound 40 compared to the hydrogen bonded two dimensional sheets of compound 39. Although the replacement of Cu(1) and Cu(4) leads to the fully coordinated structure, the layers are still staggered with respect to one another with similar distances; compound 40 4.728(4) Å and compound 39 4.723(4) Å with the interplanar distances of 6.420(5) Å to 6.962(5) Å respectively. The compounds show consistency in the bond lengths with compounds 40, 39 and the potassium-oxygen bond lengths of compound 38 compared in table 8.09.

The synthesis of compound 40, the potassium substituted analogue of compound 39, is consistent with the expansion of compound 37 to compound 38 using potassium hydroxide. Compound 37 is an analogue of the known compound JIYNOU<sup>1</sup>, leading to a set of reactions to produce the potassium analogue of the cobalt compound; these produced compound 41.

**Table 8.07: Selected Bond Lengths [ $\text{\AA}$ ] and Angles [ $^\circ$ ] for Compound 40**

Cu(1)–O(2)	1.943(16)	Cu(1)–O(6A)	1.958(16)
Cu(1)–O(13)	1.992(18)	Cu(1)–O(14)	2.247(19)
Cu(1)–O(15)	1.966(16)	Cu(2)–O(3)	1.950(15)
Cu(2)–O(10B)	1.951(15)	Cu(2)–O(16)	2.003(16)
Cu(2)–O(17)	2.328(17)	Cu(2)–O(18)	1.951(16)
C(7)–O(1)	1.239(3)	C(7)–O(2)	1.283(2)
C(8)–O(3)	1.280(3)	C(8)–O(4)	1.234(3)
C(9)–O(5)	1.236(3)	C(9)–O(6)	1.278(3)
C(10)–O(7)	1.273(2)	C(10)–O(8)	1.247(3)
C(11)–O(9)	1.233(3)	C(11)–O(10)	1.289(2)
C(12)–O(11)	1.272(3)	C(12)–O(12)	1.252(3)
O(1)–K(1A)	3.360(6)	O(1)–K(2C)	2.967(17)
O(3)–K(2C)	2.952(16)	O(4)–K(2)	2.802(18)
O(6)–K(2)	2.850(16)	O(8)–K(1E)	2.695(3)
O(8)–K(1AE)	3.060(7)	O(11)–K(1)	2.752(18)
O(12)–K(1)	2.962(18)	O(13)–K(2A)	2.866(2)
O(19)–K(1)	2.803(2)	O(20)–K(1)	2.763(19)
O(21)–K(1)	2.668(5)	O(22)–K(1)	2.858(19)
O(23)–K(2)	2.940(2)	O(24)–K(2)	2.838(19)
O(2)–Cu(1)–O(6A)	178.76(7)	O(2)–Cu(1)–O(13)	90.84(7)
O(2)–Cu(1)–O(14)	93.03(7)	O(2)–Cu(1)–O(15)	90.47(7)
O(3)–Cu(2)–O(10B)	174.75(7)	O(3)–Cu(2)–O(16)	93.27(6)
O(3)–Cu(2)–O(17)	90.82(6)	O(3)–Cu(2)–O(18)	89.50(6)
K(1A)–O(1)–K(2C)	105.84(8)	Cu(1D)–O(6)–K(2)	102.02(6)
Cu(1)–O(13)–K(2A)	100.60(8)	O(8G)–K(1)–O(11)	116.92(10)
O(8G)–K(1)–O(12)	110.60(9)	O(8G)–K(1)–O(19)	82.23(7)
O(8G)–K(1)–O(20)	87.74(7)	O(8G)–K(1)–O(21)	129.81(11)
O(8G)–K(1)–O(22)	58.18(6)	O(1H)–K(2)–O(3H)	66.60(5)
O(1H)–K(2)–O(4)	158.01(5)	O(1H)–K(2)–O(6)	106.18(5)
O(1H)–K(2)–O(13D)	74.60(5)	O(1H)–K(2)–O(23)	131.61(5)
O(1H)–K(2)–O(24)	87.89(5)		

Symmetry operations for equivalent atoms

A  $x-1/2, y, -z+1/2$    B  $x, -y+1/2, z+1/2$    C  $-x+1, y-1/2, -z+1/2$ D  $x+1/2, y, -z+1/2$    E  $x+1/2, -y+1/2, -z$    F  $x, -y+1/2, z-1/2$ G  $x-1/2, -y+1/2, -z$    H  $-x+1, y+1/2, -z+1/2$

**Table 8.08: Selected Hydrogen bond Lengths [Å] and angles [°] for Compound 40**

D–H...A	d(D–H)	d(H...A)	d(D...A)	(DHA)
O(13)–H(13A)...O(19)	0.786(15)	1.963(18)	2.690(3)	154(3)
O(13)–H(13B)...O(21I)	0.760(15)	1.931(17)	2.641(4)	155(3)
O(14)–H(14A)...O(17I)	0.767(15)	2.127(16)	2.881(3)	168(4)
O(14)–H(14B)...O(21I)	0.754(15)	2.57(3)	3.132(5)	133(4)
O(14)–H(14B)...O(1I)	0.754(15)	2.61(3)	3.207(3)	138(4)
O(15)–H(15A)...O(7A)	0.770(14)	1.979(15)	2.736(2)	167(3)
O(15)–H(15B)...O(16)	0.761(14)	1.980(14)	2.740(2)	178(3)
O(16)–H(16A)...O(11B)	0.766(14)	1.954(15)	2.715(2)	172(3)
O(16)–H(16B)...O(25H)	0.768(14)	1.861(16)	2.616(2)	168(3)
O(17)–H(17A)...O(20J)	0.784(14)	1.945(15)	2.726(2)	174(3)
O(17)–H(17B)...O(8C)	0.778(14)	2.26(2)	2.956(2)	149(3)
O(18)–H(18A)...O(23C)	0.770(14)	1.917(15)	2.684(2)	174(3)
O(18)–H(18B)...O(22D)	0.768(14)	1.878(16)	2.620(2)	162(3)
O(19)–H(19A)...O(4A)	0.777(14)	2.43(3)	2.980(3)	130(3)
O(19)–H(19A)...O(5A)	0.777(14)	2.467(18)	3.145(3)	147(3)
O(19)–H(19B)...O(9G)	0.771(14)	2.049(14)	2.818(2)	175(3)
O(20)–H(20A)...O(12K)	0.783(14)	1.949(15)	2.711(2)	164(3)
O(20)–H(20B)...O(7L)	0.791(14)	1.987(15)	2.773(2)	172(3)
O(21)–H(21A)...O(23K)	0.799(16)	2.52(3)	3.286(5)	160(6)
O(21)–H(21A)...O(2K)	0.799(16)	2.57(5)	3.073(4)	123(5)
O(21)–H(21B)...O(1)	0.805(16)	2.20(4)	2.838(5)	136(6)
O(22)–H(22A)...O(8G)	0.792(14)	1.971(18)	2.704(2)	154(3)
O(22)–H(22B)...O(10K)	0.790(14)	1.953(14)	2.742(2)	175(3)
O(23)–H(23A)...O(5H)	0.790(14)	1.906(16)	2.681(3)	167(4)
O(23)–H(23B)...O(2)	0.770(14)	2.316(18)	3.060(3)	163(4)
O(24)–H(24A)...O(11H)	0.786(14)	2.086(16)	2.855(2)	166(3)
O(24)–H(24B)...O(9B)	0.776(14)	2.084(15)	2.832(2)	162(3)
O(25)–H(25A)...O(7)	0.763(14)	2.128(17)	2.877(2)	167(3)
O(25)–H(25B)...O(24C)	0.757(14)	2.090(16)	2.814(3)	160(3)

Symmetry operations for equivalent atoms

A  $x-1/2, y, -z+1/2$     B  $x, -y+1/2, z+1/2$     C  $-x+1, y-1/2, -z+1/2$   
D  $x+1/2, y, -z+1/2$     G  $x-1/2, -y+1/2, -z$     H  $-x+1, y+1/2, -z+1/2$   
I  $-x+1/2, y+1/2, z$     J  $-x+1/2, -y, z+1/2$     K  $-x+1/2, y-1/2, z$   
L  $-x+1, -y, -z$

**Table 8.09: Average bond length comparisons between Compound 40, Compound 39 and Compound 38**

Compound	Bond	Average Bond Length (Å)
Compound 38	K–O (carboxylate)	2.797
Compound 39	Cu–O (carboxylate)	1.992
Compound 40	Cu–O (carboxylate)	2.018
Compound 40	K–O (carboxylate)	2.887

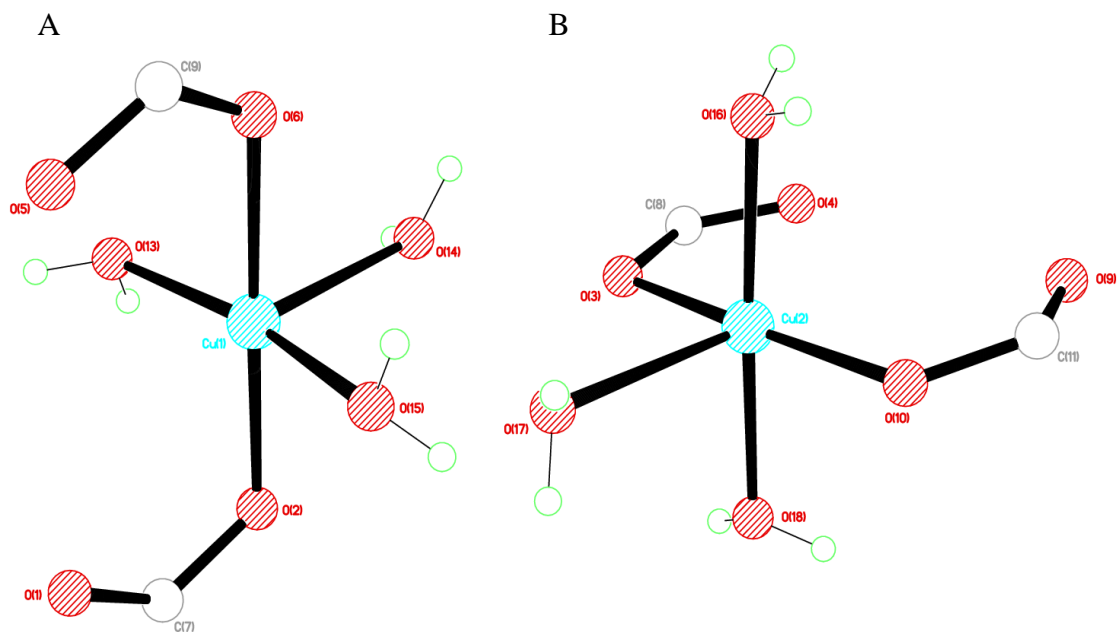


**Figure 8.22: A) Square pyramidal coordination environment of Cu(1) and B) Square pyramidal coordination environment of Cu(2) in compound 40**

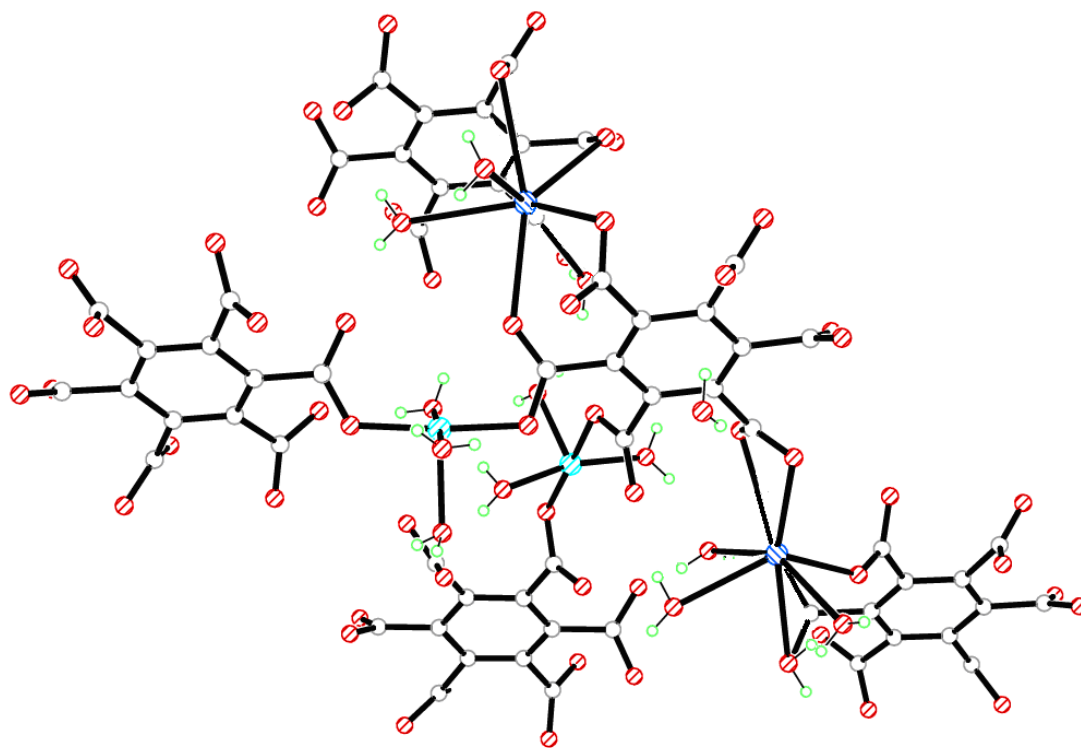


**Figure 8.23: Molecular building unit of compound 40**

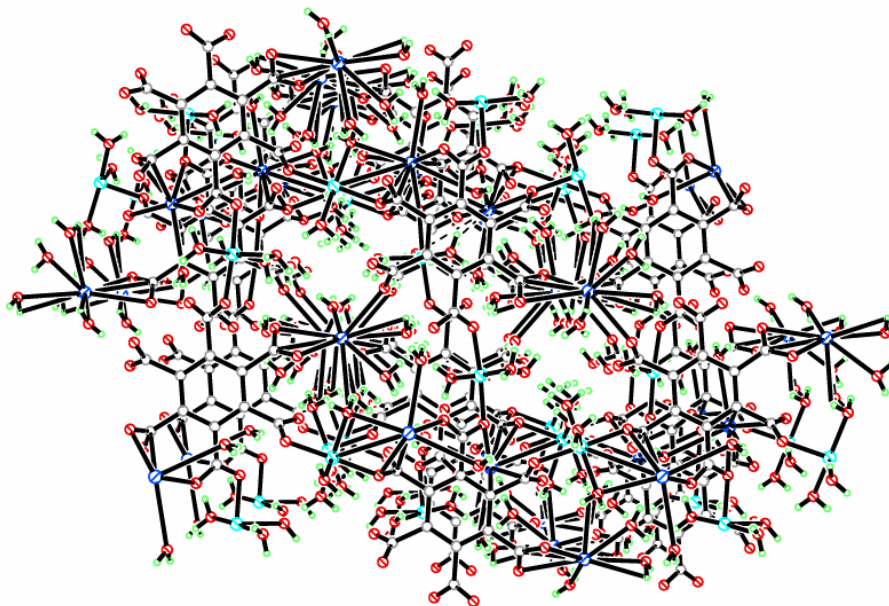


**Figure 8.24:** Two dimensional sheets of compound 40 viewed down the *b*-axis

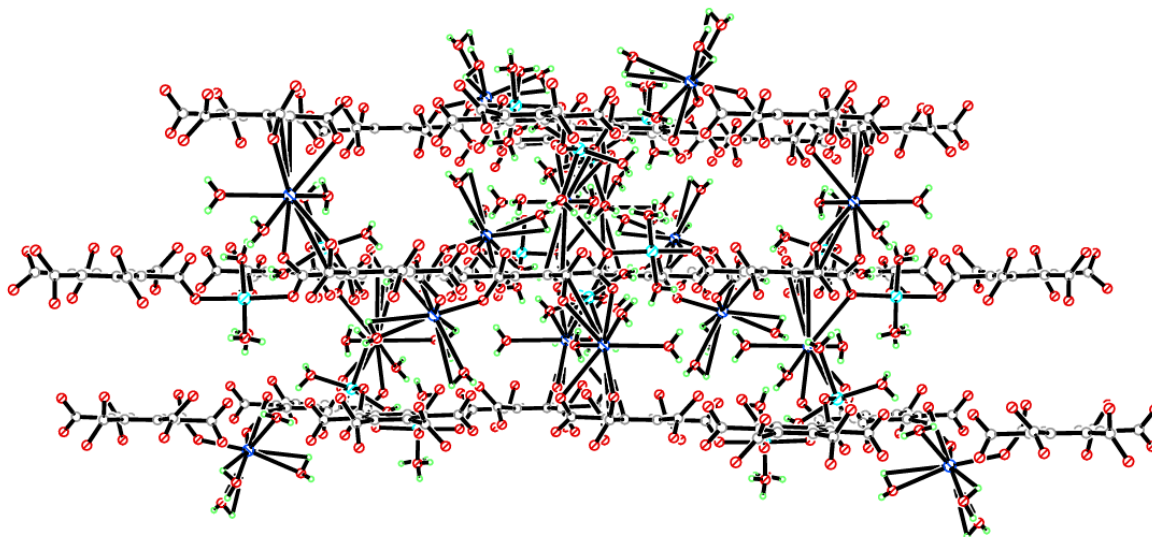
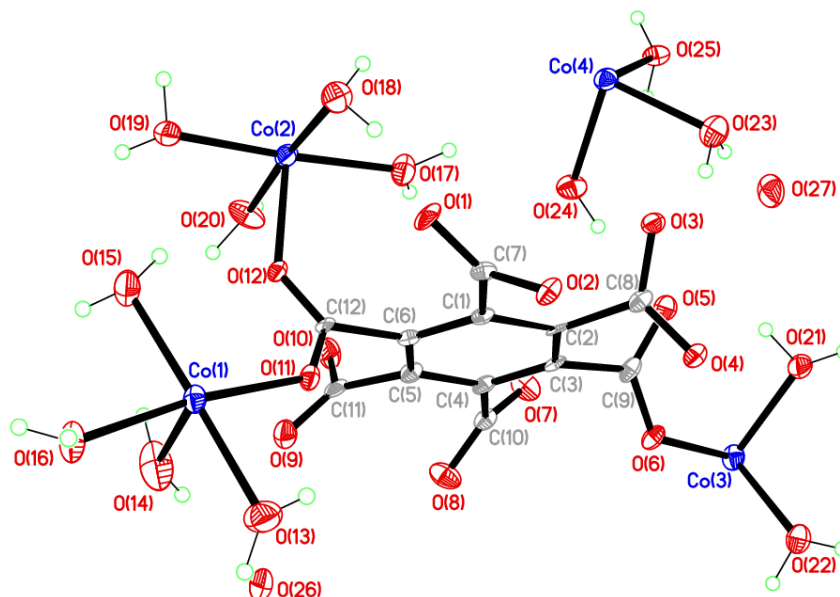


**Figure 8.25:** Three dimensional coordination of the sheets in compound 40 viewed down the *a*-axis



**Compound 41:**  $[\text{Co}_5(\text{C}_{12}\text{O}_{12})_2(\text{H}_2\text{O})_{20}] \cdot \text{Co}(\text{H}_2\text{O})_6 \cdot 4\text{H}_2\text{O}$



Chemical formula (total)	$\text{C}_{12}\text{H}_{30}\text{Co}_3\text{O}_{27}$
Formula weight	783.15
Temperature	150(2) K
Radiation, wavelength	$\text{CuK}\alpha$ , 1.54184 Å
Crystal system, space group	triclinic, $P\bar{1}$
Unit cell parameters	$a = 8.7373(7)$ Å $b = 9.7058(6)$ Å $c = 15.3909(14)$ Å $\alpha = 84.254(6)^\circ$ $\beta = 81.361(7)^\circ$ $\gamma = 78.367(6)^\circ$
Cell volume	$1260.58(17)$ Å <sup>3</sup>
Z	2
Crystal colour and size	pink, $0.50 \times 0.50 \times 0.05$ mm <sup>3</sup>
Final R indices [ $F^2 > 2\sigma$ ]	$R1 = 0.0503$
R indices (all data)	$wR2 = 0.1309$
Largest diff. peak and hole	0.96 and $-0.61$ e Å <sup>-3</sup>

**Figure 8.26:** Asymmetric Unit of Compound 41 all unique atoms labelled,

### Synthesis

2 mL of a solution of  $\text{Co}(\text{NO}_3)_2 \cdot 6\text{H}_2\text{O}$  (0.096 g, 0.33 mmol) in water (10 mL) was layered over 2 mL of a solution of benzenehexacarboxylic acid (0.058 g, 0.17 mmol) in water (10 mL) with potassium hydroxide (0.336 g, 6 mmol) in small sample vial. The vial was covered and left until crystallisation was complete. After two weeks, pink plate crystals formed.

## Structure Determination

The data were collected at 150 K using copper radiation on an Oxford Diffraction Gemini A Ultra diffractometer. The structure was solved by direct methods. The semi-empirical absorption corrections were applied based on symmetry-equivalent and repeated data. The refinement gave a  $wR2$  of 0.1309 for all 3862 independent reflections and a conventional  $R1$  of 0.0503, for 2667 reflections with  $F^2 > 2\sigma$ . The residual electron density maximum and minimum were 0.96 and  $-0.61 \text{ e } \text{\AA}^{-3}$  respectively.

The hydrogen atoms were refined within this compound, with SIMU and DELU restraints imposed upon the ligands with further SADI restraints imposed on the water molecules during refinement. The full data of compound 41 can be found in Appendix 1.

## Structure Analysis

The asymmetric unit of compound 41 (figure 8.26) shows a complete benzenhexacarboxylate ligand coordinating to three cobalt cations Co(1), Co(2) and Co(3) with a forth uncoordinated hexaaquacobalt Co(4) cation present within the structure. The cobalt cations all adopt the six-coordinate octahedral geometry with standard bond angles listed in table 8.10.

The Co(1) cation coordinates to the benzenhexacarboxylate through the Co(1)-O(2) 2.098(4) Å monodentate bond to the O(1)-C(7)-O(2) carboxylate, the cation is further coordinated by a symmetry equivalent O(11)-C(12)-O(12) carboxylate that coordinates cis to the O(1)-C(7)-O(2) carboxylate forming a bridging angle of  $93.90(13)^\circ$ . The Co(1) cation completes its six coordinate geometry coordinating to four terminal water molecules O(13), O(14), O(15) and O(16) forming the octahedron shown in figure 8.27A.

The Co(2) cation is bridged to the Co(1) cation via coordination to the O(11)-C(12)-O(12) carboxylate with the monodentate Co(2)-O(12) 2.135(4) Å bond, this coordination places the cobalt cations 5.316(6) Å away from each other at an angle of  $109.03(15)^\circ$  with the Co(1) cation above the plane of the aromatic ring and Co(2) below the plane in the  $a$ -axis. The Co(2) cation acts as a linking node between two symmetry equivalent benzenhexacarboxylate ligands with the O(3)-C(8)-O(4) carboxylate

coordinating in the trans position with respect to the O(11)-C(12)-O(12) carboxylate; O(4)-Co(2)-O(12) 172.83(15)°. The Co(2) cation further coordinates to four water molecules that are perpendicular to the carboxylate oxygens O(4) and O(12), completing the equatorial belt of the octahedral geometry (figure 8.27B).

The benzenehexacarboxylate coordinates to the Co(3) cation through the O(5)-C(9)-O(6) carboxylate forming the monodentate Co(3)-O(6) 2.067(4) Å bond; the Co(3) cation then bridges to a symmetry equivalent ligand with the generation of the trans coplanar O(5A)-C(9A)-O(6A) carboxylate group through the inversion centre at the Co(3) cation. The Co(3) cation coordinates to two additional cis water molecules O(21) and O(22) at angles O(6)-Co(3)-O(21) 92.41(16)° and O(6)-Co(3)-O(22) 89.55(15)°, with the respective trans symmetry equivalents generated through the inversion symmetry to complete the six coordinate geometry (figure 8.28A).

The Co(4) cation is not coordinated to the benzenehexacarboxylate ligand and coordinates to three terminal water molecules; O(23), O(24) and O(25) that coordinate cis with respect to one another. The six coordinate geometry is completed with the generation of the trans symmetry equivalents through inversion symmetry at the centre of the Co(4) cation (figure 8.28B). The Co(4) cation is positioned 3.761(4) Å away from the O(3) carboxylate oxygen in the *c*-axis and 4.056(8) Å away from the O(5) carboxylate oxygen positioning it almost midway between the two adjacent carboxylates with a angle of 48.57(8)°. This positioning allows the formation of the hydrogen bonds O(23)-H(23B)⋯O(3) 2.787(6) Å and O(24)-H(24B)⋯O(5) 2.697(6) Å, with additional hydrogen bonds to the uncoordinated O(8) carboxylate oxygen through the hydrogen bond donor O(25)-H(25B)⋯O(8I) 2.667(5) Å (table 8.11).

The coordinated Co(1), Co(2) and Co(3) cations act as bridging nodes between symmetry equivalent benzenehexacarboxylates coordinating in the 1, 2, 3 and 6 positions of the benzenehexacarboxylate. This expands the structure along the *a*-axis and *c*-axis forming the molecular building unit shown in figure 8.29; the O(7)-C(10)-O(8) and O(9)-C(11)-O(10) carboxylates are uncoordinated showing full deprotonation and delocalisation, with no evidence of carbon-oxygen double and single bonds (table 8.10). These uncoordinated carboxylate groups prevent the molecular building unit expanding into three dimensions along the *b*-axis, as a result the compound forms dual

layer columns that interlock around the Co(1) cations and adjacent Co(2) cations shown in figure 8.30. This interlocking forms several hydrogen bonds between the coordinated water molecules of Co(1) and the carboxylate attached to the adjacent Co(2) cation and vice versa shown in table 8.11 with the respective cations positioned at a distance of 6.804(4) Å.

The columns are composed of collinear chains of benzenhexacarboxylate ligands that run parallel with respect to one another, these are related by the inversion symmetry at the centre of the Co(3) cation that connects the two chains together. The uncoordinated O(7)-C(10)-O(8) and O(9)-C(11)-O(10) carboxylates point inwards, sticking out of the aromatic rings plane forming hydrogen bonds between the uncoordinated Co(4) hexahydrate node and then to adjacent columns (figure 8.31). The side view of the double layer column shows the positioning of two respective columns with the interlocked Co(1) and Co(2) cations including the uncoordinated Co(4) out of plane and the bridging Co(3) cations (figure 8.32).

Further analysis of the bulk sample of compound 41 was carried out using elemental analysis that provided the results C = 18.51 %, H = 4.19 % and N = 0.06 % correlating to the calculated values of C = 18.38 %, H = 3.83 % and N = 0 % from the single crystal data.

The thermostability of the benzenhexacarboxylate framework was investigated using thermogravimetric analysis that produced the TGA plot shown in figure 8.33. Compound 41 shows low thermostability with the structure immediately decomposing upon heating between 25-125°C due to the hydrogen bonding three dimensional coordination of this framework.

Compound 41 was synthesised as an attempt to continue the series of compounds by producing the potassium doped JIYNOU<sup>1</sup> structure with the addition of potassium hydroxide to the original reaction medium; however although the full deprotonation of the benzenhexacarboxylate occurs the potassium fails to coordinate into the structure forming an alternative new two dimensional product.

**Table 8.10: Selected Bond Lengths [Å] and Angles [°] for Compound 41**

Co(1)–O(2A)	2.098(4)	Co(1)–O(11)	2.047(4)
Co(1)–O(13)	2.112(5)	Co(1)–O(14)	2.136(4)
Co(1)–O(15)	2.123(4)	Co(1)–O(16)	2.063(4)
Co(2)–O(4B)	2.095(4)	Co(2)–O(12)	2.135(4)
Co(2)–O(17)	2.092(4)	Co(2)–O(18)	2.087(4)
Co(2)–O(19)	2.089(4)	Co(2)–O(20)	2.065(4)
Co(3)–O(6)	2.067(4)	Co(3)–O(21)	2.064(4)
Co(3)–O(22)	2.215(4)	Co(4)–O(23)	2.145(4)
Co(4)–O(24)	2.035(4)	Co(4)–O(25)	2.128(4)
O(1)–C(7)	1.220(6)	O(2)–C(7)	1.281(6)
O(3)–C(8)	1.254(6)	O(4)–C(8)	1.259(7)
O(5)–C(9)	1.250(7)	O(6)–C(9)	1.275(6)
O(7)–C(10)	1.247(7)	O(8)–C(10)	1.247(7)
O(9)–C(11)	1.254(7)	O(10)–C(11)	1.262(7)
O(11)–C(12)	1.270(6)	O(12)–C(12)	1.238(6)
O(2A)–Co(1)–O(11)	93.90(15)	O(2A)–Co(1)–O(13)	91.52(17)
O(2A)–Co(1)–O(14)	178.25(19)	O(2A)–Co(1)–O(15)	90.53(16)
O(2A)–Co(1)–O(16)	92.48(16)	O(4B)–Co(2)–O(12)	172.83(15)
O(4B)–Co(2)–O(17)	88.14(17)	O(4B)–Co(2)–O(18)	84.97(16)
O(4B)–Co(2)–O(19)	90.21(16)	O(4B)–Co(2)–O(20)	97.89(17)
O(6)–Co(3)–O(21)	92.41(16)	O(6)–Co(3)–O(22)	89.55(15)
O(23)–Co(4)–O(24)	87.82(17)	O(23)–Co(4)–O(25)	91.50(17)

Symmetry operations for equivalent atoms

A  $-x+1, -y+1, -z$     B  $x+1, y, z$

**Table 8.11: Selected Hydrogen bond Lengths [ $\text{\AA}$ ] and angles [ $^\circ$ ] for Compound 41**

D–H...A	d(D–H)	d(H...A)	d(D...A)	(DHA)
O(13)–H(13A)...O(8F)	0.878(14)	1.90(3)	2.704(6)	151(6)
O(13)–H(13B)...O(1A)	0.878(14)	1.90(3)	2.714(6)	153(6)
O(14)–H(14A)...O(15)	0.878(14)	2.38(6)	2.952(7)	124(5)
O(14)–H(14B)...O(26)	0.876(14)	1.99(4)	2.768(6)	147(6)
O(15)–H(15A)...O(9G)	0.880(14)	1.850(17)	2.727(5)	174(7)
O(15)–H(15B)...O(12)	0.877(14)	2.15(5)	2.846(6)	136(6)
O(15)–H(15B)...O(19)	0.877(14)	2.36(4)	3.127(6)	146(6)
O(16)–H(16A)...O(3A)	0.875(14)	1.92(2)	2.774(5)	166(6)
O(16)–H(16B)...O(10G)	0.876(14)	1.91(2)	2.750(5)	159(5)
O(17)–H(17A)...O(25D)	0.878(14)	2.012(16)	2.884(6)	172(5)
O(17)–H(17B)...O(22B)	0.877(14)	2.155(16)	3.030(6)	175(6)
O(18)–H(18A)...O(1)	0.878(14)	1.81(2)	2.665(6)	164(5)
O(18)–H(18B)...O(4B)	0.876(14)	2.37(5)	2.825(6)	113(4)
O(18)–H(18B)...O(27D)	0.876(14)	2.433(18)	3.301(6)	172(6)
O(19)–H(19A)...O(2B)	0.876(14)	1.91(2)	2.757(5)	163(5)
O(19)–H(19B)...O(26G)	0.878(14)	1.892(18)	2.764(6)	172(6)
O(20)–H(20A)...O(6B)	0.876(14)	1.86(3)	2.661(6)	150(5)
O(20)–H(20B)...O(14G)	0.877(14)	1.90(2)	2.753(7)	164(6)
O(21)–H(21A)...O(5)	0.880(14)	2.01(4)	2.732(6)	138(6)
O(21)–H(21A)...O(27)	0.880(14)	2.51(4)	3.176(6)	133(5)
O(21)–H(21B)...O(23H)	0.880(14)	2.06(4)	2.839(6)	146(6)
O(22)–H(22A)...O(7C)	0.880(14)	2.10(2)	2.936(6)	160(5)
O(22)–H(22B)...O(10E)	0.881(14)	1.99(3)	2.811(6)	154(6)
O(23)–H(23A)...O(27)	0.880(14)	1.83(2)	2.686(6)	165(7)
O(23)–H(23B)...O(3)	0.880(14)	1.97(3)	2.787(6)	154(5)
O(24)–H(24A)...O(7I)	0.878(14)	1.75(2)	2.589(5)	159(5)
O(24)–H(24B)...O(5)	0.879(14)	1.84(2)	2.697(6)	166(5)
O(25)–H(25A)...O(3D)	0.879(14)	1.86(3)	2.689(5)	156(6)
O(25)–H(25B)...O(8I)	0.879(14)	1.84(3)	2.667(5)	157(5)

Symmetry operations for equivalent atoms

A  $-x+1, -y+1, -z$  B  $x+1, y, z$  C  $-x, -y, -z+1$ D  $-x+1, -y+1, -z+1$  E  $x-1, y, z$  F  $-x+1, -y, -z$ G  $-x+2, -y, -z$  H  $-x, -y+1, -z+1$  I  $-x+1, -y, -z+1$

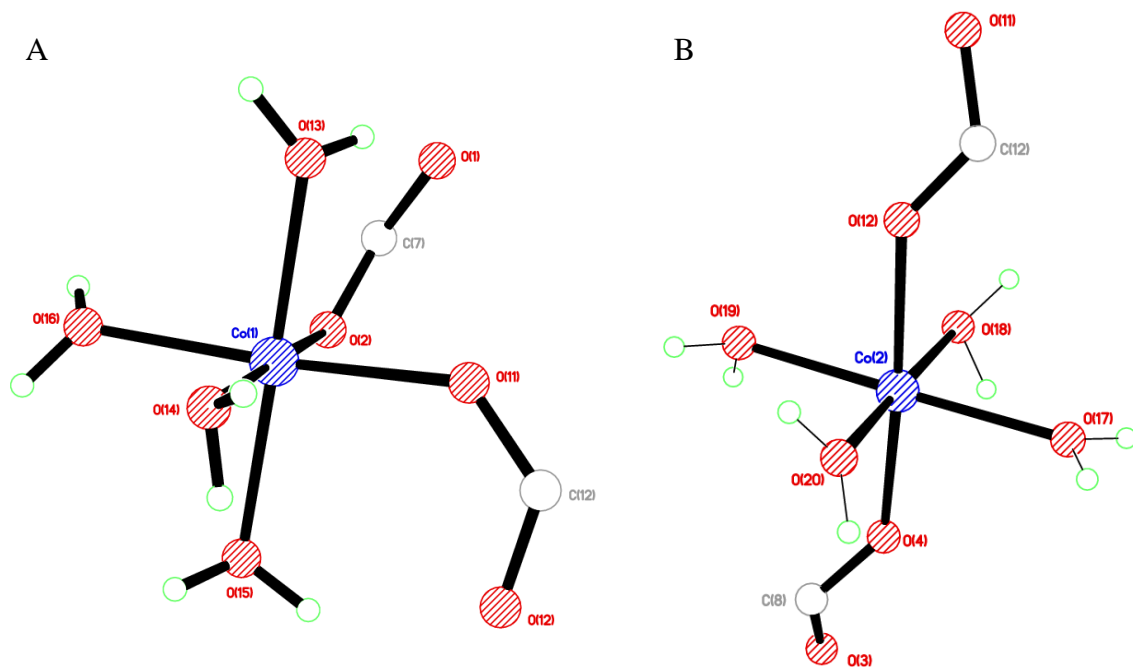


**Figure 8.27: A) Octahedral coordination environment of Co(1) and B) Octahedral coordination environment of Co(2) in compound 41**

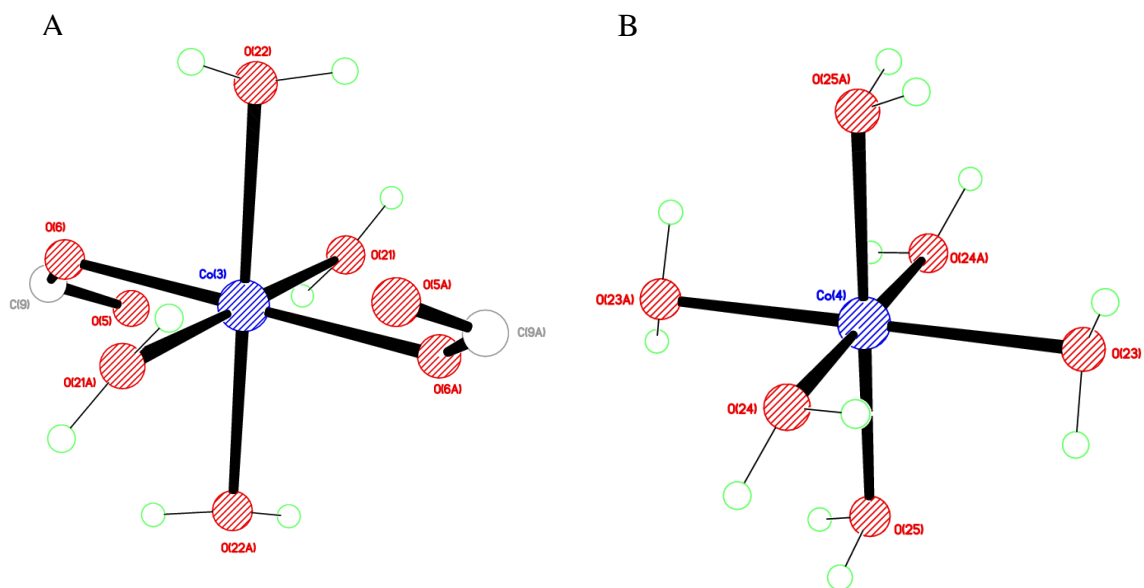


**Figure 8.28: A) Octahedral coordination environment of Co(3) and B) Octahedral coordination environment of Co(4) in compound 41**

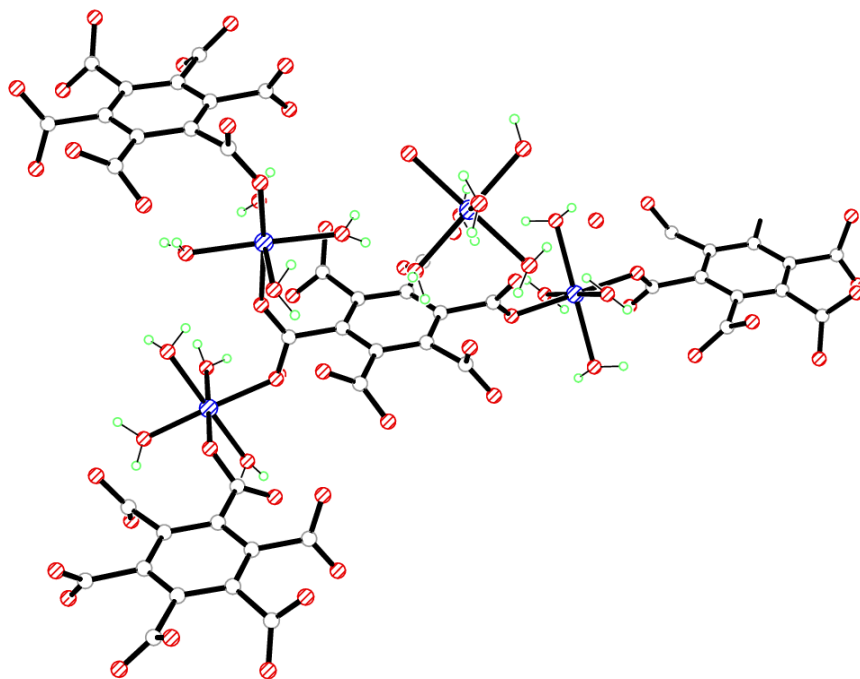


**Figure 8.29: Molecular building unit of compound 41**

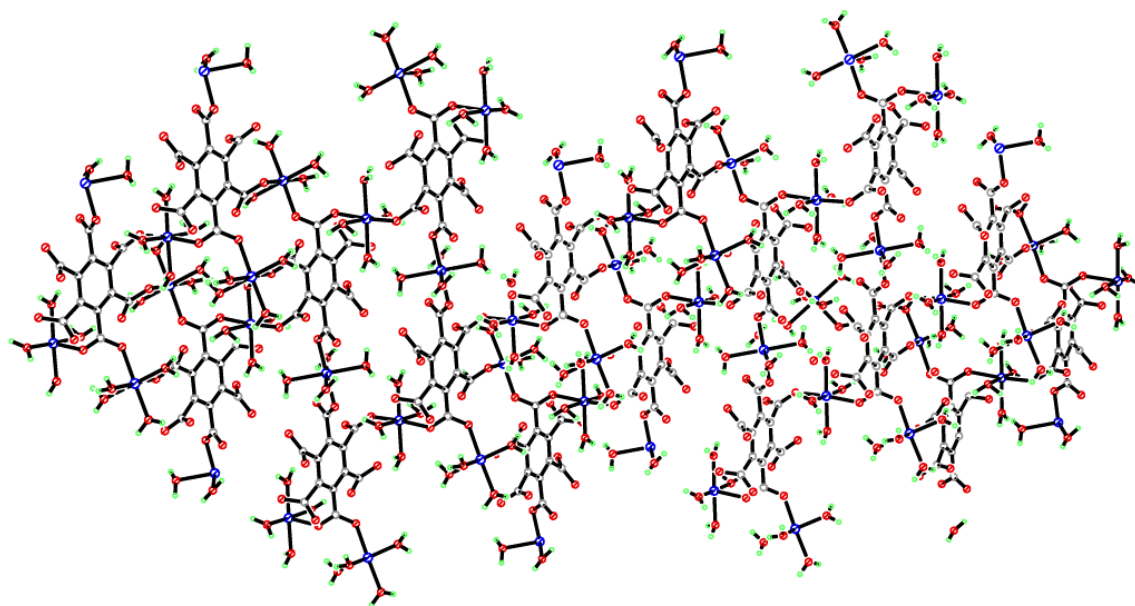


**Figure 8.30: Two dimensional packing of the columns in compound 41 viewed down the *b*-axis**



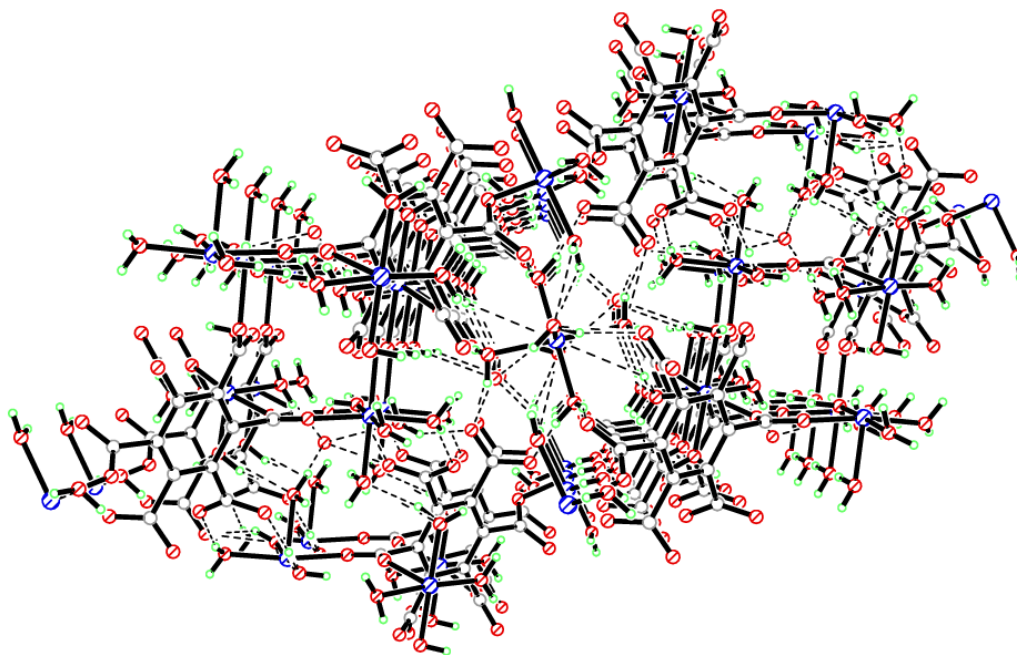


**Figure 8.31:** Three dimensional packing of the columns in compound 41 viewed down the *a*-axis

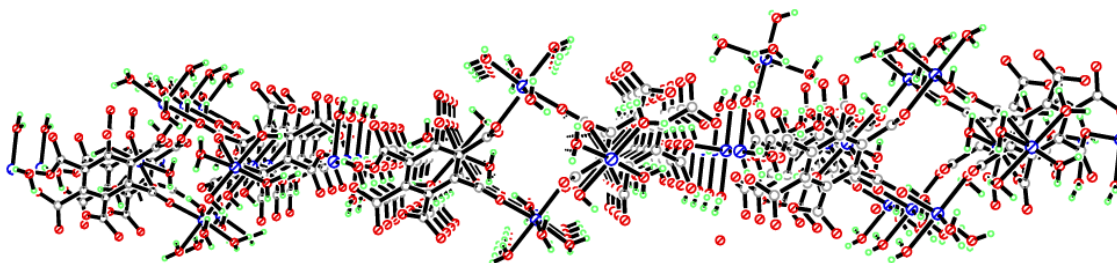


**Figure 8.32:** Double layer column in compound 41 viewed down the *a*-axis

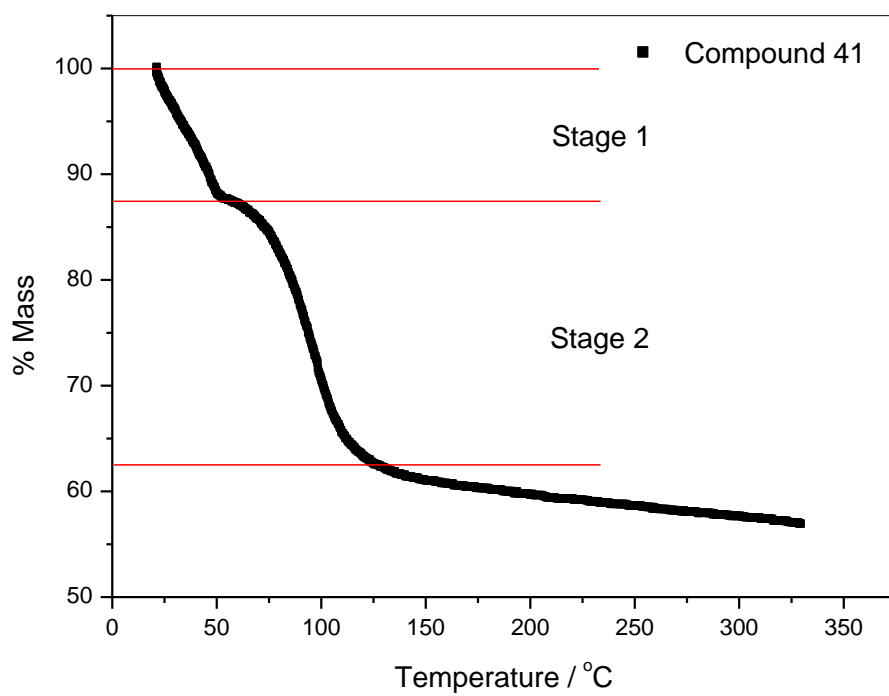
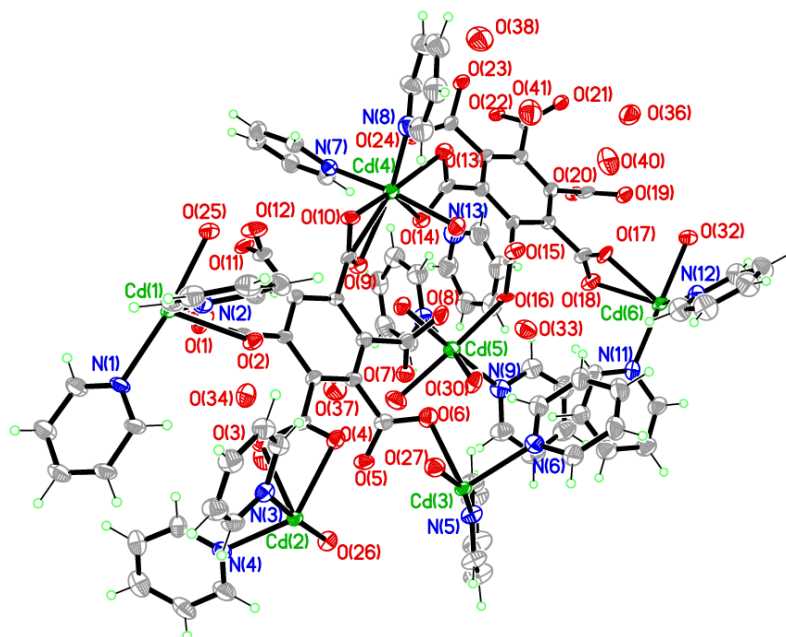


**Figure 8.33: Thermogravimetric analysis plot of compound 41**

**Compound 42:**  $[\text{Cd}_6(\text{C}_{12}\text{O}_{12})_2(\text{C}_5\text{H}_5\text{N})_{17}(\text{H}_2\text{O})_9] \cdot 8\text{H}_2\text{O}$

---



Chemical formula (total)	$\text{C}_{89}\text{H}_{99}\text{Cd}_6\text{N}_{13}\text{O}_{41}$	
Formula weight	2681.21	
Temperature	150(2) K	
Radiation, wavelength	synchrotron, 0.6889 Å	
Crystal system, space group	triclinic, $P\bar{1}$	
Unit cell parameters	$a = 13.789(3)$ Å	$\alpha = 77.006(2)^\circ$
	$b = 13.969(3)$ Å	$\beta = 77.643(2)^\circ$
	$c = 28.232(6)$ Å	$\gamma = 78.231(3)^\circ$
Cell volume	$5106.1(19)$ Å <sup>3</sup>	
<i>Z</i>	2	
Crystal colour and size	colourless, $0.04 \times 0.03 \times 0.01$ mm <sup>3</sup>	
Final <i>R</i> indices [ $F^2 > 2\sigma$ ]	$R1 = 0.0832$	
<i>R</i> indices (all data)	$wR2 = 0.2433$	
Largest diff. peak and hole	4.83 and $-1.56$ e Å <sup>-3</sup>	

---

**Figure 8.34:** Asymmetric Unit of Compound 42 all unique atoms labelled

### Synthesis

1 mL of a solution of  $\text{Cd}(\text{NO}_3)_2 \cdot 4\text{H}_2\text{O}$  (0.1 g, 0.33 mmol) in water (10 mL) and 1 mL of a solution of benzenhexacarboxylic acid (0.058 g, 0.17 mmol) in water (10 mL) were placed into a small sample vial. This was covered with Whatman Laboratory Sealing Film and placed inside a larger sample vial. In the larger sample vial pyridine (0.05 mL,

0.22 mmol) was added before it was covered and left until crystallisation was complete. After five weeks, colourless spindle crystals formed.

### Structure Determination

The data were collected at 150 K using synchrotron radiation on a Crystal Logic diffractometer and Rigaku Saturn 724+ CCD on beamline I19 at the Diamond Light Source facility. The structure was solved by direct methods. The semi-empirical absorption corrections were applied based on symmetry-equivalent and repeated data. The refinement gave a  $wR2$  of 0.2433 for all 17595 independent reflections and a conventional  $R1$  of 0.0832, for 11468 reflections with  $F^2 > 2\sigma$ . The residual electron density maximum and minimum were 4.83 and  $-1.56 \text{ e } \text{\AA}^{-3}$  respectively, the high residual electron density is a result of imperfect adsorption corrections for the high number of cadmium atoms within the asymmetric unit as compound 42 was collected using synchrotron radiation. The hydrogen atoms were placed in geometrically calculated positions with  $U$  constrained to  $1.2 U_{\text{eq}}(\text{C})$  for aromatic hydrogen atoms, with SIMU and DELU restraints imposed on the ligands during refinement. The full data of compound 42 can be found in Appendix 1.

### Structure Analysis

The asymmetric unit of compound 42 (figure 8.34) shows two complete benzenhexacarboxylate ligands coordinating six cadmium cations that further coordinate to two terminal pyridine ligands each. The cadmium cations in this polymeric compound are composed of two different coordination geometries with Cd(5) forming a six-coordinate octahedron, whilst the remaining cations form similar seven-coordinate distorted pentagonal bipyramidal geometries shown in the figures 8.35 and 8.36.

The benzenhexacarboxylate ligands C(1)-O(12) and C(13)-O(24) have fully deprotonated and delocalised carboxylates, with all but one carboxylate; O(7)-C(10)-O(8) coordinating to a cadmium cation (table 8.12). The C(1)-O(12) benzenhexacarboxylate ligand coordinates to the Cd(1) cation through the bidentate O(1)-C(7)-O(2) carboxylate forming the Cd(1)-O(1) 2.412(8)  $\text{\AA}$  and Cd(1)-O(2) 2.409(8)  $\text{\AA}$  bonds. The ligand further coordinates to a symmetry equivalent Cd(1) cation

generated by inversion symmetry, this coordination occurs through the bidentate O(11)-C(12)-O(12) carboxylate adjacent to the O(1)-C(7)-O(2) carboxylate on the benzene ring. The Cd(1)-O(11) and Cd(1)-O(12) bonds coordinate in the trans coplanar position to the symmetry equivalent O(1)-C(7)-O(2) carboxylate creating a bridge between two symmetry equivalent C(1)-O(12) benzenhexacarboxylate ligands at a angle of  $129.9(3)^\circ$ . The Cd(1) cation completes its coordination geometry with two cis pyridine ligands C(25)-N(1) and C(30)-N(2) that coordinate at an angle of  $N(1)-Cd(1)-N(2)$   $102.1(4)^\circ$ , with the final axial coordination site occupied by a water molecule O(15) trans to the C(25)-N(1) pyridine (figure 8.35A). This bridging motif of adjacent bidentate carboxylates of symmetry equivalent benzenhexacarboxylates generated by inversion symmetry creates a dinuclear capped paddle-wheel building unit shown in figure 8.37. The carboxylate groups in the building unit are rotated out of the plane by  $59.74(11)^\circ$  (O(1)-C(7)-O(2)) and  $58.74(11)^\circ$  (O(11)-C(12)-O(12)), and coordinate the Cd(1) cations in the plane of the benzene ring with a Cd(1)-Cd(1A) distance of 5.166(5) Å. The coordinated pyridines that cap the paddle-wheel point out away from the building unit at  $47.91(8)^\circ$  (C(25)-N(1)) and  $62.54(8)^\circ$  (C(30)-N(2)) with respect to the plane of the benzene ring. This dinuclear paddle-wheel building unit that links two benzenhexacarboxylate ligands is observed in the coordination of Cd(2) and Cd(3) along with an almost identical building unit between Cd(6) and Cd(6A).

The C(1)-O(12) benzenhexacarboxylate coordinates to the Cd(2) cation through the O(3)-C(8)-O(4) carboxylate that forms a bidentate bond with a bite angle of  $53.1(3)^\circ$ , the Cd(2) cation then coordinates to the C(13)-O(24) benzenhexacarboxylate through the bidentate O(23)-C(24)-O(24) carboxylate in the trans coplanar position making the Cd(2) cation a bridging node between two unique benzenhexacarboxylate ligands. The Cd(2) cation coordinates to three terminal ligands; two cis pyridines C(35)-N(3) perpendicular to the carboxylate groups and the cis C(40)-N(4) pyridine with the remaining axial position of the pentagonal bipyramid occupied by the water molecule O(26) (figure 8.35B) (table 8.12). The adjacent carboxylate group O(5)-C(9)-O(6) coordinated in the '3' position on the benzene ring of the C(1)-O(12) ligand forms a bidentate bond to the Cd(3) cation with a bite angle of  $47.45(3)^\circ$  with an elongated Cd(3)-O(5) 3.043(9) Å bond and the shortest cadmium-oxygen bond in the compound

Cd(3)-O(6) 2.243(9) Å. The Cd(3) cation then coordinates to a trans coplanar O(21)-C(23)-O(22) carboxylate of the C(13)-O(24) benzenhexacarboxylate ligand, this carboxylate is in the '5' position next to the O(23)-C(24)-O(24) carboxylate in the '6' position on the benzene ring. The coordination of the adjacent carboxylates on the respective ligands to the Cd(2) and Cd(3) cations creates the dinuclear building unit observed for the Cd(1) cations shown in figure 8.37. The pyridine ligands that coordinate cis with respect to one another on the Cd(3) cation point out of the plane of the benzene rings at a angle of 65.33(5)° (C(45)-N(5)) and 35.11(4)° (C(50)-N(6)); these angles are consistent to those of the pyridines coordinated to the Cd(2) in the molecular building unit of 39.96(5)° (C(35)-N(3)) and 63.19(5)° (C(40)-N(4)). The Cd(2) and Cd(3) cations are placed at a distance of 5.096(4) Å to one another, similar to the distance of the Cd(1)-Cd(1A) cations in this compound.

The C(1)-O(12) and C(13)-O(24) ligands are further bridged by the Cd(4) cation that forms a single bridge through two coplanar carboxylate groups that coordinate bidentate to the cation through the O(9)-C(11)-O(10) and O(13)-C(19)-O(14) carboxylates at an angle of O(9)-Cd(4)-O(13) 140.0(3)°. The Cd(4) cation is coordinated slightly below the plane of the benzene rings as the carboxylate groups twist out of plane by 46.75(4)°. The cation forms a similar node to the Cd(1), Cd(2) and Cd(3) cations with coordination to two cis pyridines C(55)-N(7) and C(6)-N(8) with an additional axial water molecule O(28) trans to the C(55)-N(7) pyridine (figure 8.36A).

The C(13)-O(24) benzenhexacarboxylate completes its coordination with bonds to the Cd(5) and Cd(6) cations; the O(15)-C(20)-O(16) carboxylate group coordinates to the Cd(5) cation with a monodentate bond from the O(16) carboxylate oxygen, positioning the Cd(5) cation below the plane of the benzene ring. The Cd(5) cation would have the capability to expand the structure into three dimensions due to its proximity to the adjacent plane of benzenhexacarboxylate ligands; however it is capped by five terminal ligands to form the octahedral geometry shown in figure 8.36B. The adjacent O(17)-C(21)-O(18) carboxylate in the '3' position on the C(13)-O(24) ligand forms a bidentate bond to the Cd(6) cation through the Cd(6)-O(17) 2.361(8) Å and Cd(6)-O(18) 2.550(19) Å bonds. The ligand further coordinates to a symmetry equivalent Cd(6) cation generated by inversion symmetry; this coordination is formed

through the bidentate O(19)-C(22)-O(20) carboxylate in the '4' position adjacent to the O(17)-C(21)-O(18) carboxylate. The Cd(6)-O(19) and Cd(6)-O(20) bonds are coplanar and trans to the symmetry equivalent O(17)-C(21)-O(18) carboxylate creating a bridge between the two symmetry equivalent C(13)-O(24) benzenehexacarboxylate ligands. The Cd(6) cation completes its coordination geometry with two cis pyridine ligands C(75)-N(11) and C(80)-N(12) that coordinate at a N(11)-Cd(6)-N(12) angle of  $89.0(4)^\circ$  with the final axial coordination site occupied by a water molecule O(32) trans to the C(75)-N(11) pyridine (figure 8.36C). The bridging motif of adjacent carboxylate groups of symmetry equivalent ligands generated by inversion symmetry creates a dinuclear capped paddle-wheel building unit almost identical to the Cd(1)-Cd(1A) unit shown in figure 8.37. The carboxylate groups of the Cd(6)-Cd(6A) building unit are twisted out of the benzene ring plane by  $63.34(13)^\circ$  (O(17)-C(21)-O(18)) and  $55.51(14)^\circ$  (O(19)-C(22)-O(20)) placing the Cd(6) cations out of plane with respect to the benzene rings, with a Cd(6)-Cd(6A) distance of  $5.286(4) \text{ \AA}$ . The coordinated pyridines that cap the paddle-wheel point out from the building unit at angles  $39.94(15)^\circ$  (C(75)-N(11)) and  $55.05(10)^\circ$  (C(80)-N(12)) from the plane of the benzene rings comparable to those in the Cd(1)-Cd(1A) and Cd(2)-Cd(3) bridging units. The dinuclear bridging units expand the structure into a two dimensional sheet that forms hexagonal nets as shown in figure 8.38 when the coordinated pyridines are removed. The two dimensional sheets run along the cell body diagonal and are composed of planar benzenehexacarboxylate ligands. The sheets stack with the pyridine ligands pointing above and below the plane of the benzene rings forming  $\pi$ - $\pi$  stacking interactions between adjacent C(65)-N(13) and C(70)-N(10) pyridines and symmetry equivalents of the C(80)-N(12) pyridines with  $\pi$ - $\pi$  distances of  $3.659(7) \text{ \AA}$  and  $4.014(5) \text{ \AA}$  respectively. Additional  $\sigma$ - $\pi$  interactions are formed between the C(30)-N(2) and the C(70)-N(10) pyridines at a distance of  $2.892(4) \text{ \AA}$  (figure 8.39). The sheets stack with an interplanar distance of  $9.383(7) \text{ \AA}$  with staggering of the sheets along the *a*-axis. Compound 42 was synthesised to investigate the templating effects of pyridine upon the benzenehexacarboxylate frameworks, this compound shows a high level of coordination to the templating agent preventing the paddle-wheel dimeric building units from expanding the structure into three dimensions. Further reactions with lowered concentrations of pyridine resulted in compound 43.

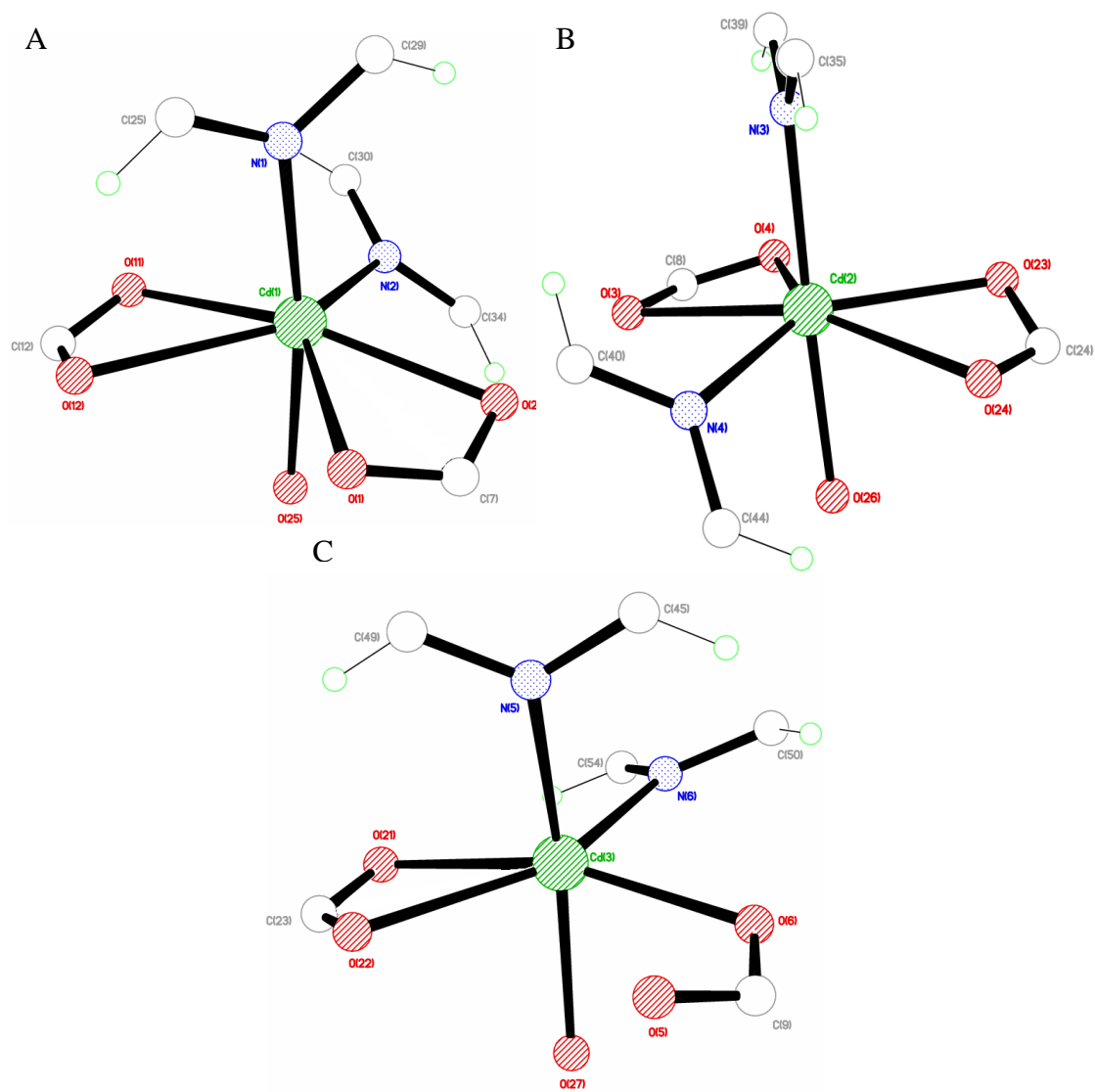
**Table 8.12: Selected Bond Lengths [Å] and Angles [°] for Compound 42**

Cd(1)–O(1)	2.412(8)	Cd(1)–O(2)	2.409(8)
Cd(1)–O(11A)	2.365(8)	Cd(1)–O(12A)	2.615(10)
Cd(1)–N(1)	2.321(10)	Cd(1)–N(2)	2.329(11)
Cd(1)–O(25)	2.353(8)	Cd(2)–O(3)	2.536(8)
Cd(2)–O(4)	2.386(9)	Cd(2)–O(23B)	2.460(8)
Cd(2)–O(24B)	2.458(9)	Cd(2)–N(3)	2.312(10)
Cd(2)–N(4)	2.309(10)	Cd(2)–O(26)	2.323(8)
Cd(3)–O(6)	2.243(9)	Cd(3)–O(21B)	2.411(9)
Cd(3)–O(22B)	2.400(8)	Cd(3)–N(5)	2.300(11)
Cd(3)–N(6)	2.313(11)	Cd(3)–O(27)	2.338(9)
Cd(4)–O(9)	2.375(9)	Cd(4)–O(10)	2.461(9)
Cd(4)–O(13)	2.518(9)	Cd(4)–O(14)	2.428(9)
Cd(4)–N(7)	2.314(10)	Cd(4)–N(8)	2.278(12)
Cd(4)–O(28)	2.320(8)	Cd(5)–O(16)	2.286(8)
Cd(5)–N(9)	2.305(11)	Cd(5)–N(10)	2.275(12)
Cd(5)–O(29)	2.308(8)	Cd(5)–O(30)	2.274(9)
Cd(5)–O(31)	2.298(9)	Cd(6)–O(17)	2.361(8)
Cd(6)–O(18)	2.550(9)	Cd(6)–O(19C)	2.563(9)
Cd(6)–O(20C)	2.386(8)	Cd(6)–N(11)	2.291(12)
Cd(6)–N(12)	2.351(11)	Cd(6)–O(32)	2.318(9)
O(1)–C(7)	1.255(14)	O(2)–C(7)	1.238(15)
O(3)–C(8)	1.248(14)	O(4)–C(8)	1.249(14)
O(5)–C(9)	1.276(15)	O(6)–C(9)	1.265(15)
O(7)–C(10)	1.264(14)	O(8)–C(10)	1.245(15)
O(9)–C(11)	1.264(15)	O(10)–C(11)	1.230(14)
O(11)–C(12)	1.239(16)	O(12)–C(12)	1.241(16)
O(1)–Cd(1)–O(2)	54.3(3)	O(1)–Cd(1)–O(11A)	129.9(3)
O(1)–Cd(1)–O(12A)	79.9(3)	O(1)–Cd(1)–N(1)	95.5(3)
O(1)–Cd(1)–N(2)	138.6(3)	O(1)–Cd(1)–O(25)	84.5(3)
O(3)–Cd(2)–O(4)	53.1(3)	O(3)–Cd(2)–O(23B)	137.1(3)
O(3)–Cd(2)–O(24B)	161.0(3)	O(3)–Cd(2)–N(3)	93.5(3)
O(3)–Cd(2)–N(4)	79.4(3)	O(3)–Cd(2)–O(26)	86.6(3)
O(6)–Cd(3)–O(21B)	160.1(3)	O(6)–Cd(3)–O(22B)	126.8(3)
O(6)–Cd(3)–N(5)	97.9(4)	O(6)–Cd(3)–N(6)	84.6(4)
O(6)–Cd(3)–O(27)	80.3(3)	O(9)–Cd(4)–O(10)	54.1(3)
O(9)–Cd(4)–O(13)	140.1(3)	O(9)–Cd(4)–O(14)	87.5(3)
O(9)–Cd(4)–N(7)	92.5(3)	O(9)–Cd(4)–N(8)	138.2(4)
O(9)–Cd(4)–O(28)	82.8(3)	O(16)–Cd(5)–N(9)	89.2(3)
O(16)–Cd(5)–N(10)	95.4(4)	O(16)–Cd(5)–O(29)	89.3(3)
O(16)–Cd(5)–O(30)	88.2(3)	O(16)–Cd(5)–O(31)	173.1(3)
O(17)–Cd(6)–O(18)	52.5(3)	O(17)–Cd(6)–O(19C)	126.8(3)
O(17)–Cd(6)–O(20C)	161.2(3)	O(17)–Cd(6)–N(11)	101.5(3)
O(17)–Cd(6)–N(12)	88.4(3)	O(17)–Cd(6)–O(32)	78.3(3)

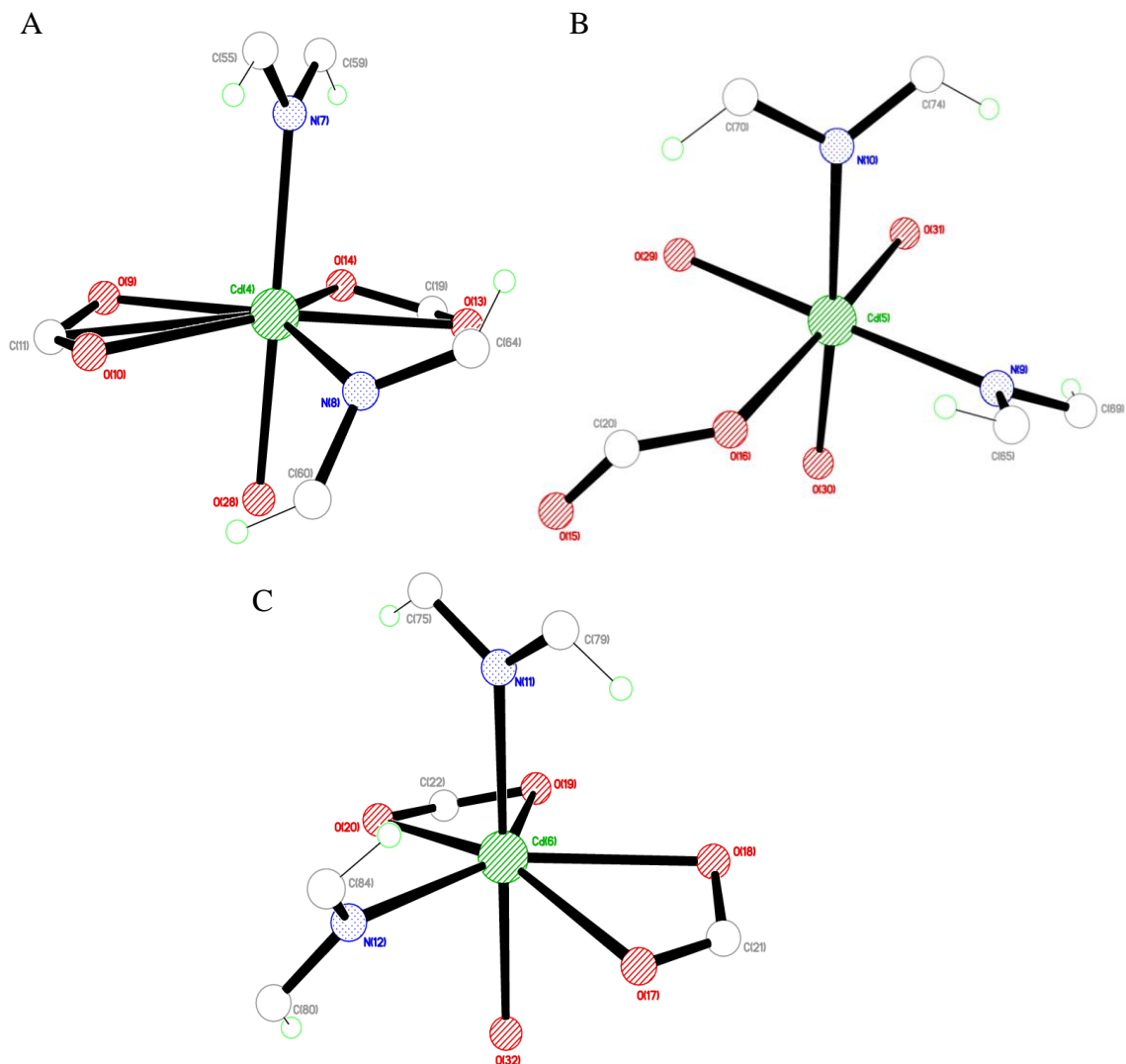
Symmetry operations for equivalent atoms

A  $-x+1, -y+2, -z$     B  $x-1, y+1, z$     C  $-x+1, -y, -z+1$

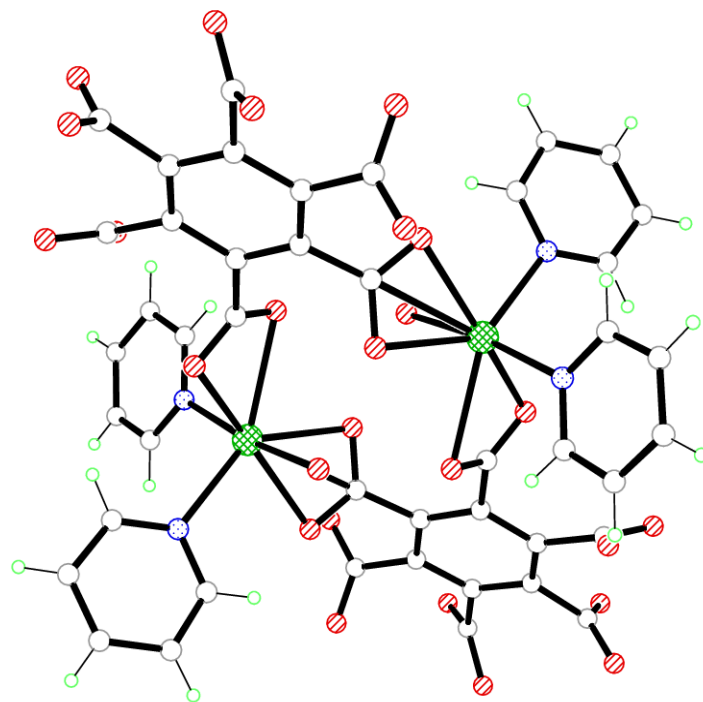




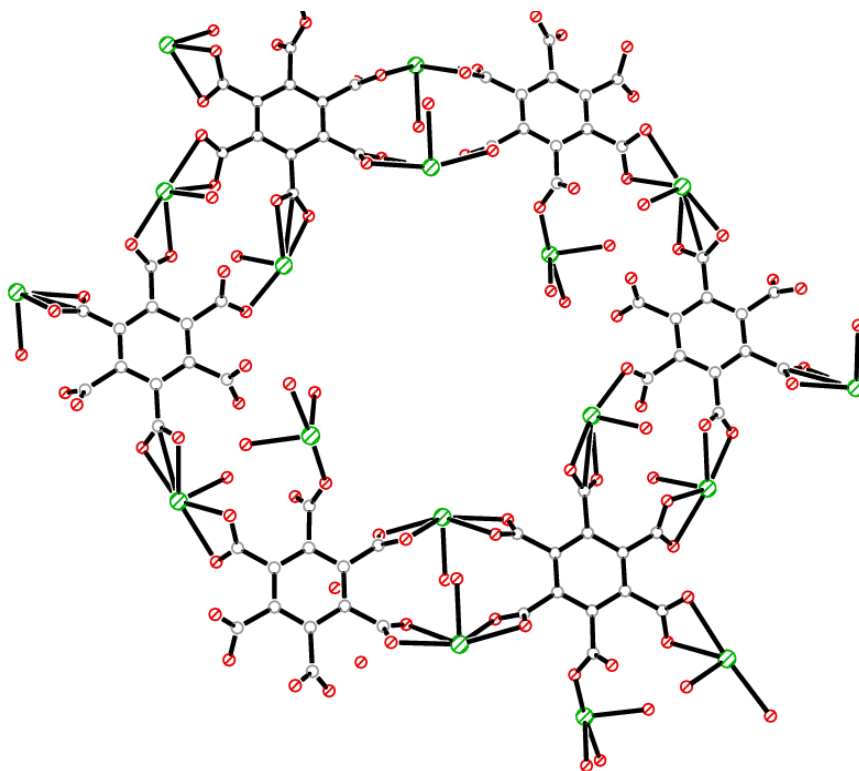
**Figure 8.35: Pentagonal bipyramidal coordination environments of A) Cd(1), B) Cd(2) and C) Cd(3) in compound 42 (all unique atoms labeled)**



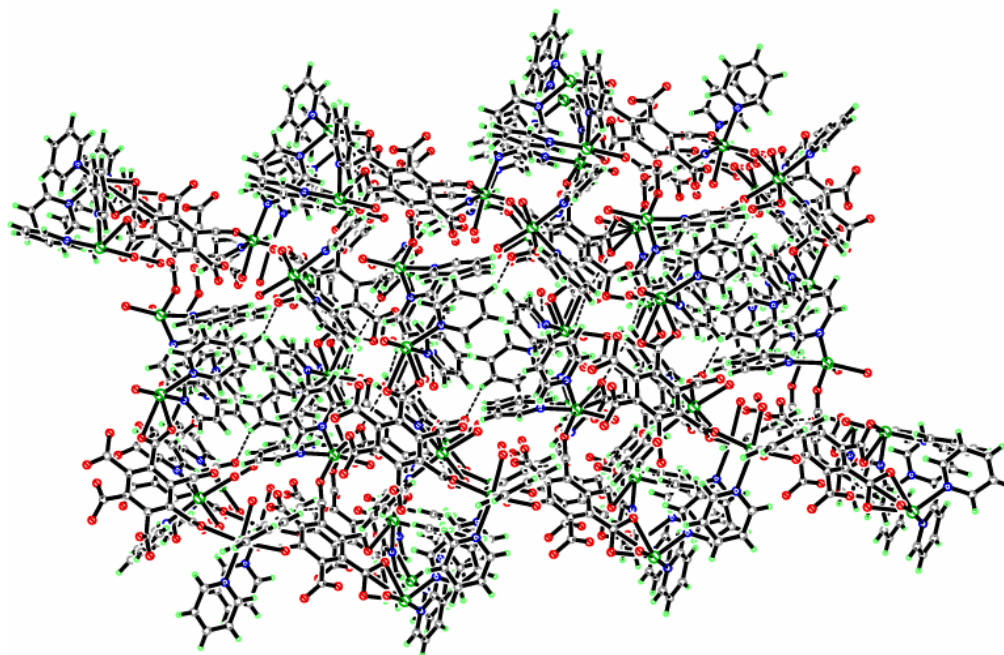
**Figure 8.36: A) Pentagonal bipyramidal coordination environment of Cd(4), B) Octahedral coordination environment of Cd(5) and C) Pentagonal bipyramidal coordination environment of Cd(6) in compound 42 (all unique atoms labeled)**



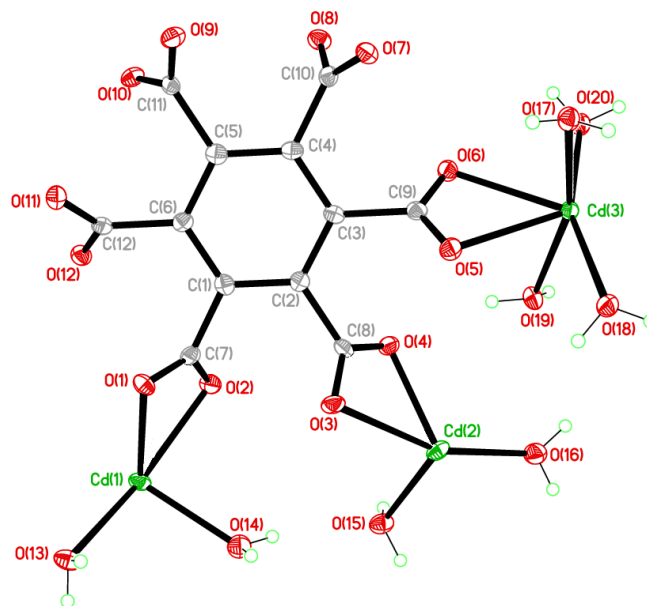
**Figure 8.37: Dinuclear paddle-wheel molecular building unit in compound 42**



**Figure 8.38: Two dimensional sheet of hexagonal nets in compound 42**



**Figure 8.39:** Three dimensional overlapping packing of the sheets in compound 42 viewed down the  $a$ -axis

**Compound 43:**  $[\text{Cd}_3(\text{C}_{12}\text{O}_{12})(\text{H}_2\text{O})_8]$ 

Chemical formula (total)	$\text{C}_{12}\text{H}_{16}\text{Cd}_3\text{O}_{20}$
Formula weight	817.45
Temperature	120(2) K
Radiation, wavelength	synchrotron, 0.6889 Å
Crystal system, space group	Orthorhombic, <i>Pbca</i>
Unit cell parameters	$a = 13.320(4)$ Å $b = 13.258(3)$ Å $c = 22.758(6)$ Å
Cell volume	$4019.0(18)$ Å <sup>3</sup>
<i>Z</i>	8
Crystal colour and size	colourless, $0.05 \times 0.002 \times 0.002$ mm <sup>3</sup>
Final <i>R</i> indices [ $F^2 > 2\sigma$ ]	$R1 = 0.0241$
<i>R</i> indices (all data)	$wR2 = 0.0603$
Largest diff. peak and hole	0.80 and $-0.62$ e Å <sup>-3</sup>

**Figure 8.40: Asymmetric Unit of Compound 43 all unique atoms labelled****Synthesis**

1 mL of a solution of  $\text{Cd}(\text{NO}_3)_2 \cdot 4\text{H}_2\text{O}$  (0.1 g, 0.33 mmol) in water (10 mL) and 1 mL of a solution of benzenhexacarboxylic acid (0.058 g, 0.17 mmol) in water (10 mL) were placed into a small sample vial. This was covered with Whatman Laboratory Sealing Film and placed inside a larger sample vial. In the larger sample vial pyridine (0.02 mL, 0.11 mmol) was added before it was covered and left until crystallisation was complete. After five weeks, colourless spindle crystals formed.

## Structure Determination

The data were collected at 120 K using synchrotron radiation on a Crystal Logic diffractometer and Rigaku Saturn 724+ CCD on beamline I19 at the Diamond Light Source facility. The structure was solved by direct methods. The semi-empirical absorption corrections were applied based on symmetry-equivalent and repeated data. The refinement gave a  $wR2$  of 0.0603 for all 4074 independent reflections and a conventional  $R1$  of 0.0241, for 3262 reflections with  $F^2 > 2\sigma$ . The residual electron density maximum and minimum were 0.80 and  $-0.62 \text{ e } \text{\AA}^{-3}$  respectively.

The hydrogen atoms were refined with SADI restraints imposed on the water molecules during refinement. The full data of compound 43 can be found in Appendix 1.

## Structure Analysis

The asymmetric unit of compound 43 (figure 8.40) shows a complete benzenhexacarboxylate ligand coordinating to three cadmium cations Cd(1), Cd(2) and Cd(3) in general positions. The cadmium cations form two different geometries in this polymeric compound, Cd(1) and Cd(2) form distorted six-coordinate octahedra with Cd(3) forming an eight-coordinate trans bicapped octahedral geometry (figure 8.41).

The benzenhexacarboxylate ligand is fully deprotonated with delocalised carboxylate groups that all act as bidentate ligands to cadmium cations. The O(1)-C(7)-O(2) carboxylate group forms a bidentate bond to the Cd(1) cation with the bonds Cd(1)-O(1) 2.341(3) Å and Cd(1)-O(2) 2.312(2) Å that coordinate with a bite angle of  $56.73(8)^\circ$ . The O(1)-C(7)-O(2) carboxylate group is rotated out of the plane of the benzene ring by  $63.35(8)^\circ$  and coordinates the Cd(1) cation coplanar to the benzene ring. The Cd(1) cation is further coordinated by a symmetry equivalent of the benzenhexacarboxylate ligand with the bidentate O(9)-C(11)-O(10) carboxylate group coordinating with a bite angle of  $55.68(8)^\circ$ , this group coordinates in the distorted cis position perpendicular to the O(1)-C(7)-O(2) carboxylate with an O(1)-Cd(1)-O(9A) angle of  $83.94(8)^\circ$ . The O(9)-C(11)-O(10) carboxylate group is twisted out of the plane of the benzene ring by  $57.19(7)^\circ$ , this places the aromatic rings of the equivalent ligands perpendicular to the *b*-axis at a angle of  $102.67(13)^\circ$  running collinear down the *c*-axis.

The Cd(1) cation completes its coordination geometry coordinating to two terminal water molecules that point away from the carboxylates in the cis position to the O(1) carboxylate oxygen (figure 8.41A).

The Cd(2) cation is coordinated to the benzenhexacarboxylate by the O(3)-C(8)-O(4) carboxylate that forms the Cd(2)-O(3) 2.518(3) Å and Cd(2)-O(4) 2.214(2) Å bonds with a bite angle of 55.51(8)°. A symmetry equivalent benzenhexacarboxylate coordinates to the Cd(2) cation through the O(7)-C(10)-O(8) bidentate carboxylate, coordinating with a bite angle of 56.80(8)° in the cis position to the O(3)-C(8)-O(4) carboxylate at a angle of O(3)-Cd(2)-O(7) 87.70(8)°. The O(7)-C(10)-O(8) carboxylate is rotated out of the plane of the benzene ring by 65.51(8)° placing the symmetry equivalent ligand perpendicular with respect to the aromatic rings of the benzenhexacarboxylate ligands. The Cd(2) cation completes its six-coordinate distorted octahedral geometry with coordination to two terminal water molecules O(15) and O(16) that coordinate cis to the O(4) carboxylate oxygen; O(4)-Cd(2)-O(15) 108.67(9)° and O(4)-Cd(2)-O(16) 161.61(9)° (figure 8.41B) (table 8.13).

The benzenhexacarboxylate completes its coordination forming bonds to the Cd(3) cation through the O(5)-C(9)-O(6) and O(11)-C(12)-O(12) carboxylates. The Cd(3) cation forms a eight-coordinate trans bicapped octahedral geometry with both carboxylates coordinating in the trans axial positions with four cis water molecules coordinating to form the equatorial belt (figure 8.41C). Although the carboxylates coordinate trans they are rotated by 90° to one another and out of the planes of the respective aromatic rings by 54.31(13)° O(5)-C(9)-O(6) and 56.09(8)° for the O(11)-C(12)-O(12) placing the coordinated symmetry equivalent benzenhexacarboxylate ligands perpendicular to one another running down the *c*-axis.

The array of bridging cadmium cations that flip adjacent benzenhexacarboxylates by approximately 90° with respect to the plane of the benzene rings, forms chains that run along the *c*-axis with alternating benzenhexacarboxylate ligands (figure 8.42). These coordinate to four sets of cadmium cation chains that are collinear running down the *c*-axis parallel to the benzenhexacarboxylates creating a microporous grid network (figure 8.43). The nanochannels have dimensions 5.946(7) by

8.410(7) Å upon desolvation of coordinated water molecules that point inwards towards them (figure 8.44).

PLATON<sup>3</sup> confirms the presence of pores upon desolvation with a calculated pore volume of 1033.9 Å<sup>3</sup> per unit cell, corresponding to 25.7 %. Thermogravimetric analysis was carried out on compound 43 to determine the temperature profile, indicating the thermostability and desolvation temperature of the compound (figure 8.45). The TGA plot show that the compound is stable up to 110°C, after this point desolvation occurs resulting in the framework collapsing between 110-250°C. The TGA plot indicates the low thermal stability of the compound suggesting it would be unsuitable for further analysis.

Compound 43 was synthesised to investigate how the concentration of pyridine affects its role as a templating agent, by lowering the concentration by 50 % a structural motif was formed devoid of any pyridine templating agent. As a consequence the cadmium nodes in compound 43 are not sterically hindered by the pyridine ligands that induce a coplanar trans coordination of the carboxylate ligands observed in compound 42. In contrast compound 43 adopts the cis coordination geometry, creating the alternating chains of benzenhexacarboxylate ligands that form the walls of the nanochannels with close packing to adjacent chains. Previous experiments containing the 1,4-benzenedicarboxylate and 1,2,4,5-benzenetetracarboxylate ligands showed the ability to modify the frameworks templated with pyridine by replacing it with 4,4'-bipyridine to produce the new compounds 25, 26 and 36; by extending this modification to the benzenhexacarboxylate series compound 44 was produced.



**Table 8.13: Selected Bond Lengths [ $\text{\AA}$ ] and Angles [ $^\circ$ ] for Compound 43**

Cd(1)–O(1)	2.341(3)	Cd(1)–O(2)	2.312(2)
Cd(1)–O(9A)	2.492(3)	Cd(1)–O(10A)	2.234(2)
Cd(1)–O(13)	2.227(3)	Cd(1)–O(14)	2.252(3)
Cd(2)–O(3)	2.518(3)	Cd(2)–O(4)	2.214(2)
Cd(2)–O(7B)	2.308(3)	Cd(2)–O(8B)	2.349(3)
Cd(2)–O(15)	2.218(3)	Cd(2)–O(16)	2.251(3)
Cd(3)–O(5)	2.457(3)	Cd(3)–O(6)	2.446(3)
Cd(3)–O(11C)	2.369(2)	Cd(3)–O(12C)	2.552(3)
Cd(3)–O(17)	2.362(3)	Cd(3)–O(18)	2.428(3)
Cd(3)–O(19)	2.345(3)	Cd(3)–O(20)	2.320(3)
O(1)–C(7)	1.249(4)	O(2)–C(7)	1.266(4)
O(3)–C(8)	1.251(4)	O(4)–C(8)	1.271(4)
O(5)–C(9)	1.249(5)	O(6)–C(9)	1.247(5)
O(7)–C(10)	1.263(4)	O(8)–C(10)	1.257(4)
O(9)–C(11)	1.250(4)	O(10)–C(11)	1.268(4)
O(11)–C(12)	1.262(4)	O(12)–C(12)	1.254(4)
O(1)–Cd(1)–O(2)	56.73(8)	O(1)–Cd(1)–O(9A)	83.94(8)
O(1)–Cd(1)–O(10A)	136.70(9)	O(1)–Cd(1)–O(13)	98.53(9)
O(1)–Cd(1)–O(14)	106.37(10)	O(2)–Cd(1)–O(9A)	86.81(9)
O(2)–Cd(1)–O(10A)	101.77(9)	O(2)–Cd(1)–O(13)	154.43(10)
O(2)–Cd(1)–O(14)	88.74(9)	O(3)–Cd(2)–O(4)	55.51(8)
O(3)–Cd(2)–O(7B)	87.70(8)	O(3)–Cd(2)–O(8B)	84.91(9)
O(3)–Cd(2)–O(15)	99.69(9)	O(3)–Cd(2)–O(16)	161.61(9)
O(5)–Cd(3)–O(6)	53.24(8)	O(5)–Cd(3)–O(11C)	143.64(9)
O(5)–Cd(3)–O(12C)	142.74(8)	O(5)–Cd(3)–O(17)	81.05(8)
O(5)–Cd(3)–O(18)	75.00(9)	O(5)–Cd(3)–O(19)	80.57(9)
O(5)–Cd(3)–O(20)	125.64(9)	Cd(1)–O(1)–C(7)	89.7(2)
Cd(1)–O(2)–C(7)	90.6(2)	Cd(2)–O(3)–C(8)	83.7(2)
Cd(2)–O(4)–C(8)	97.1(2)	Cd(3)–O(5)–C(9)	91.4(2)
Cd(3)–O(6)–C(9)	91.9(2)	Cd(2D)–O(7)–C(10)	90.9(2)
Cd(2D)–O(8)–C(10)	89.1(2)	Cd(1E)–O(9)–C(11)	84.4(2)
Cd(1E)–O(10)–C(11)	95.8(2)	Cd(3F)–O(11)–C(12)	96.7(2)
Cd(3F)–O(12)–C(12)	88.4(2)		
Symmetry operations for equivalent atoms			
A $-x+1, y+1/2, -z+1/2$	B $x+1/2, -y+1/2, -z+1$	C $x, -y+1/2, z+1/2$	
D $x-1/2, -y+1/2, -z+1$	E $-x+1, y-1/2, -z+1/2$	F $x, -y+1/2, z-1/2$	

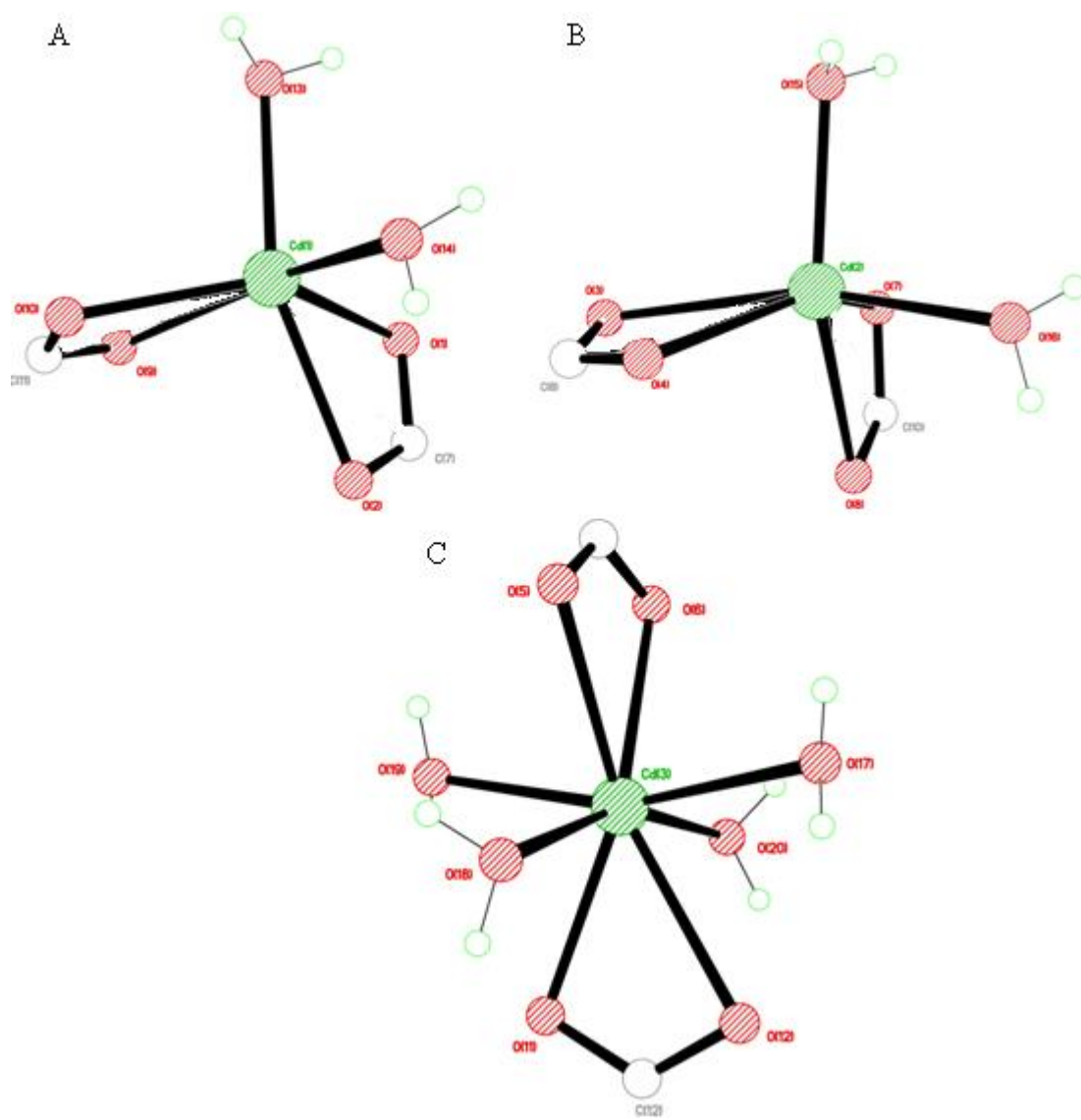


**Figure 8.41: Distorted octahedral coordination environments of A) Cd(1), B) Cd(2) and C) Trans bicapped octahedral Cd(3) in compound 43 (all unique atoms labelled)**

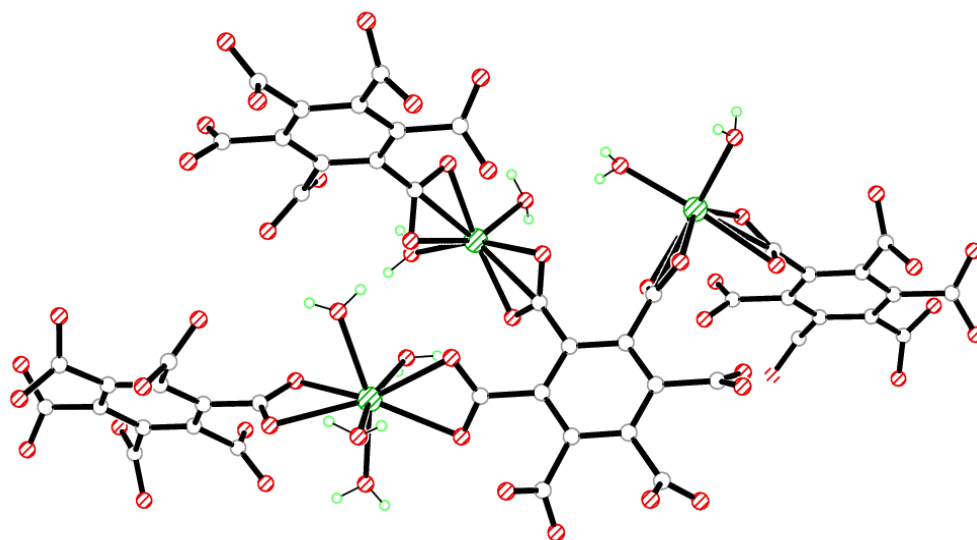


**Figure 8.42: Molecular building unit in compound 43**

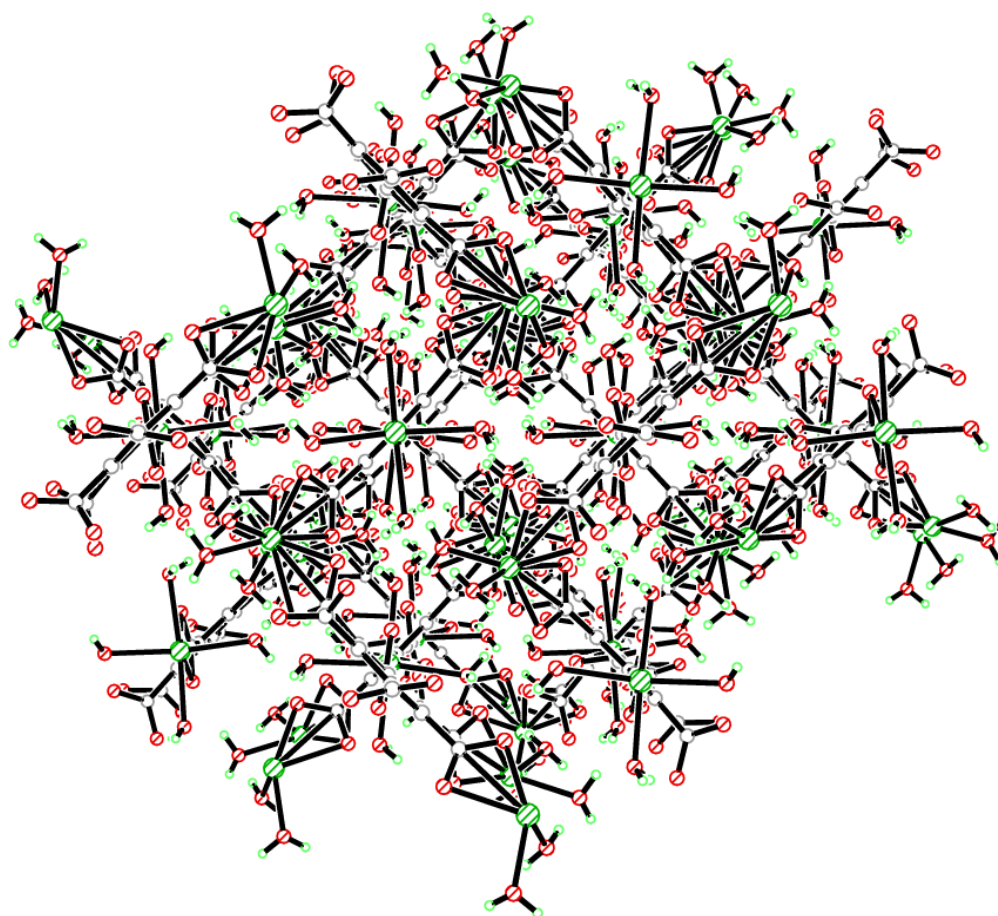


**Figure 8.43: Three dimensional coordination in compound 43 viewed down the *c*-axis**

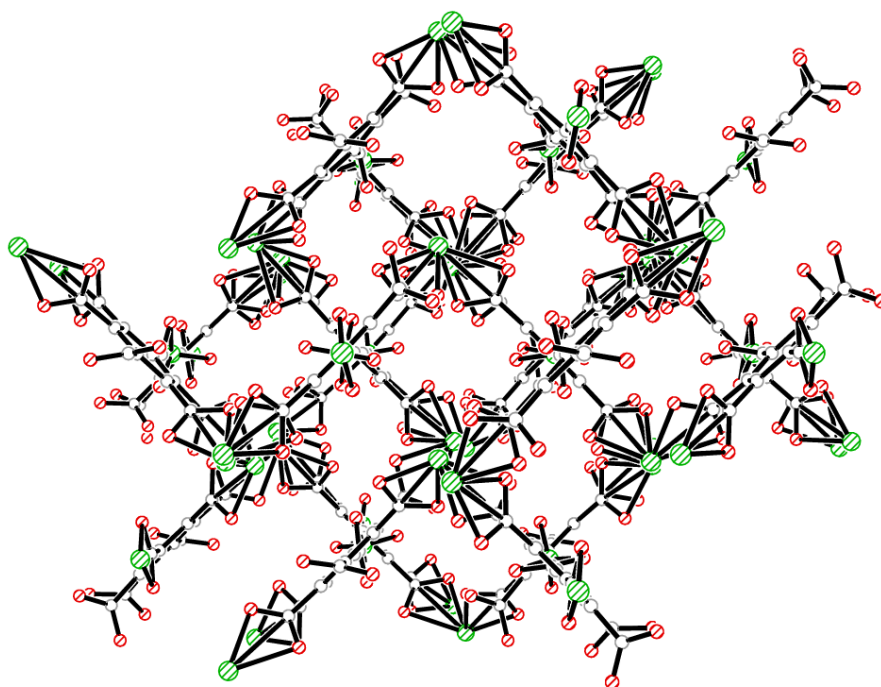


**Figure 8.44:** Three dimensional coordination in compound 43 showing the desolvated grid network viewed down the *c*-axis

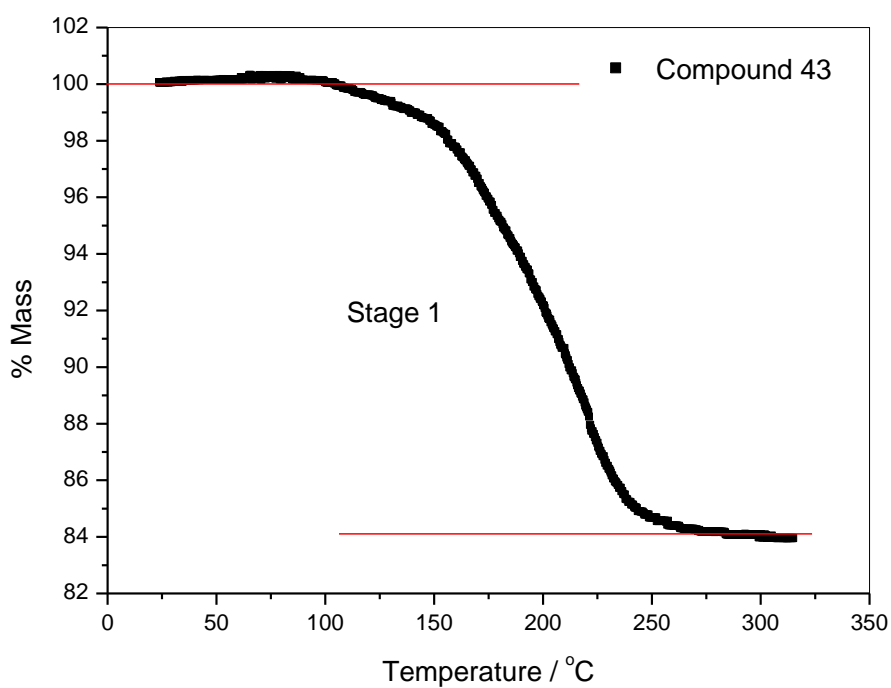
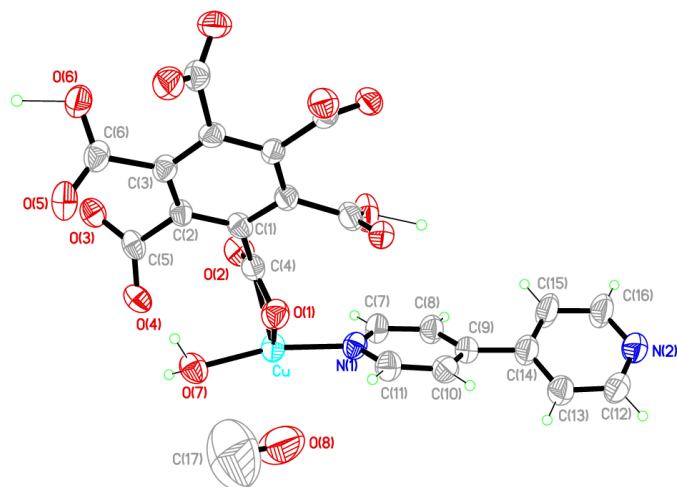


**Figure 8.45:** Thermogravimetric analysis plot of compound 43

**Compound 44:**  $[\text{Cu}_2(\text{C}_{12}\text{H}_2\text{O}_{12})(\text{C}_{10}\text{H}_8\text{N}_2)_2(\text{H}_2\text{O})_2] \cdot 2\text{CH}_4\text{O}$



Chemical formula (total)	$\text{C}_{33}\text{H}_{26}\text{Cu}_2\text{N}_4\text{O}_{15}$
Formula weight	845.66
Temperature	150(2) K
Radiation, wavelength	synchrotron, 0.6889 Å
Crystal system, space group	trigonal, $P3_221$
Unit cell parameters	$a = 10.136(3)$ Å $c = 26.725(7)$ Å
Cell volume	$2377.8(12)$ Å <sup>3</sup>
Z	3
Crystal colour and size	blue, $0.03 \times 0.03 \times 0.02$ mm <sup>3</sup>
Final $R$ indices [ $F^2 > 2\sigma$ ]	$R1 = 0.0492$
$R$ indices (all data)	$wR2 = 0.1449$
Largest diff. peak and hole	0.64 and $-0.49$ e Å <sup>-3</sup>
Absolute structure parameter	0.05(2)

**Figure 8.46: Asymmetric Unit of Compound 44 all unique atoms labelled, additional atoms added to complete ligands**

### Synthesis

1 mL of a solution of  $\text{Cu}(\text{NO}_3)_2 \cdot 4\text{H}_2\text{O}$  (0.08 g, 0.33 mmol) in methanol (10 mL) was syringed into one side of the H-Cell vessel, 1 mL of a solution of benzenehexacarboxylic acid (0.058 g, 0.17 mmol) in methanol (10 mL) and 1 mL of a solution of 4,4'-bipyridine (0.027 g, 0.17 mmol) in methanol (10 mL) were then syringed into the other side of the H-Cell vessel. The independent solutions were bridged by 2 mL water that was carefully layered into the bridging tube. After four weeks, blue spindle crystals formed.

## Structure Determination

The data were collected at 150 K using synchrotron radiation on a Crystal Logic diffractometer and Rigaku Saturn 724+ CCD on beamline I19 at the Diamond Light Source facility. The structure was solved by direct methods. The semi-empirical absorption corrections were applied based on symmetry-equivalent and repeated data. The refinement gave a  $wR2$  of 0.1449 for all 3901 independent reflections and a conventional  $R1$  of 0.0492, for 3307 reflections with  $F^2 > 2\sigma$ . The residual electron density maximum and minimum were 0.64 and  $-0.49 \text{ e } \text{\AA}^{-3}$  respectively. Compound 44 crystallised in the chiral space group  $P3_121$  and refined with a Flack parameter of 0.05 indicating the correct handedness has been selected.

The hydrogen atoms were placed in geometrically calculated positions with  $U$  constrained to  $1.2 U_{\text{eq}}(\text{C})$  for aromatic hydrogen atoms. The water molecules in the structure had SADI restraints imposed for refinement. The full data of compound 44 can be found in Appendix 1.

## Structure Analysis

The asymmetric unit of compound 44 (figure 8.46) shows a half benzenhexacarboxylate completed by two-fold rotation symmetry through the centre of the aromatic ring, coordinating to a copper cation that is singly coordinated by a 4,4'-bipyridine ligand.

The copper cation is a four-coordinate square planar node (figure 8.47) coordinating to the O(1)-C(4)-O(2) carboxylate with the Cu-O(1)  $1.986(3) \text{ \AA}$  and a trans symmetry equivalent ligand coordinates through a monodentate bond from the adjacent O(3)-C(5)-O(4) carboxylate forming the Cu-O(3)  $1.941(3) \text{ \AA}$  bond in the trans coplanar position; O(1)-Cu-O(3)  $176.58(12)^\circ$  (figure 8.47). The copper cation also coordinates to a 4,4'-bipyridine ligand through the Cu-N(1) bond that coordinates cis to the O(1)-C(4)-O(2) carboxylate group; O(1)-Cu-N(1)  $91.50(13)^\circ$  forming the molecular building unit in figure 8.48. The bridging copper cation links symmetry equivalent benzenhexacarboxylate ligands with the carboxylate groups rotating out of the plane by  $58.67(4)^\circ$ . The 4,4'-bipyridine ligand coordinates perpendicular to the plane of the

benzene ring rotated by 90° around the Cu-N(1) bond. The copper cation forms a long range interaction with a methanol molecule Cu-O(8) 2.792(4) Å, this bridges two symmetry equivalent building units with the angle Cu-O(8)-Cu(A) 132.4(3)°. The molecular building unit expands the structure into a three dimensional framework that forms planar sheets that run along the *b*-axis and down the *a*-axis stacked together in the *c*-axis. The sheets are then coordinated together by columns of collinear benzenhexacarboxylate ligands that run up the *c*-axis perpendicular to the sheets (figure 8.49). The 4,4'-bipyridine ligands coordinate to the copper cation through the N(1) atom and point down the *a*-axis bridging across the layers to form a hydrogen bond to the protonated O(5)-C(5)-O(6)-H(6) carboxylate of the adjacent sheet; O(6)-H(6)···N(2F) 2.553(5) Å at 179(8)°. The hydrogen atom lies part way between the two atoms with a O(6)-H(6) distance of 1.31(5) Å and a N(2)-H(6D) distance of 1.24(5) Å (table 8.15) (figure 8.50). The bridging of the 4,4'-bipyridine ligand is observed down the *c*-axis where they bridge across multiple layers partially filling the hexagonal nets (figure 8.52) forming nanochannels with dimensions 10.136(8) by 10.136(8) Å that run down the *c*-axis of compound 44.

Compound 44 is one of only two known frameworks that contain transition metals, benzenhexacarboxylate ligands and 4,4'-bipyridine ligands, the second compound is a structure reported by Yao et al. (RAHMAP).<sup>4</sup> The RAHMAP<sup>4</sup> compound forms two independent polymers with helical substructures that interweave into a three dimensional framework that hosts one dimensional  $[\text{Cu}(\text{C}_{10}\text{H}_8\text{N}_2)(\text{H}_2\text{O})_4]^{2+}_n$  chains.<sup>4</sup> This is in stark contrast to the fully coordinated three dimensional packing of compound 44 that coordinates to square planar nodes compared to the octahedral nodes in RAHMAP<sup>4</sup>. The two structures do however show comparable bond lengths to the respective ligands shown in table 8.16.

**Table 8.14: Selected Bond Lengths [Å] and Angles [°] for Compound 44**

Cu–O(1)	1.986(3)	Cu–O(3A)	1.941(3)
Cu–N(1)	1.995(3)	Cu–O(7)	1.989(3)
Cu–O(8)	2.792(4)	C(4)–O(1)	1.233(5)
C(4)–O(2)	1.233(5)	C(5)–O(3)	1.276(5)
C(5)–O(4)	1.240(5)	C(6)–O(5)	1.242(6)
C(6)–O(6)	1.260(6)	O(6)–H(6)	1.31(5)
N(2)–H(6D)	1.24(5)		
O(1)–Cu–O(3A)	176.58(12)	O(1)–Cu–N(1)	91.50(13)
O(1)–Cu–O(7)	90.10(13)	O(1)–Cu–O(8)	76.85(13)
Symmetry operations for equivalent atoms			
A $x-y+1, -y+1, -z+5/3$ D $x+1, y-1, z$			

**Table 8.15: Selected Hydrogen bond Lengths [Å] and angles [°] for Compound 44**

D–H...A	d(D–H)	d(H...A)	d(D...A)	(DHA)
O(6)–H(6)...N(2F)	1.31(5)	1.24(5)	2.553(5)	179(8)
O(7)–H(7A)...O(5A)	0.93(4)	1.92(5)	2.768(4)	152(5)
O(7)–H(7B)...O(4)	0.94(5)	1.91(6)	2.788(4)	156(10)
Symmetry operations for equivalent atoms				
A $x-y+1, -y+1, -z+5/3$ F $x-1, y+1, z$				

**Table 8.16: Average bond length comparisons between Compound 44 and RAHMAP<sup>4</sup>**

Compound	Bond	Average Bond Length (Å)
Compound 44	Cu–O (carboxylate)	1.963
Compound 44	Cu–N (4,4-bipyridine)	1.995
RAHMAP	Cu–O (carboxylate)	1.956
RAHMAP	Cu–N (4,4-bipyridine)	2.003



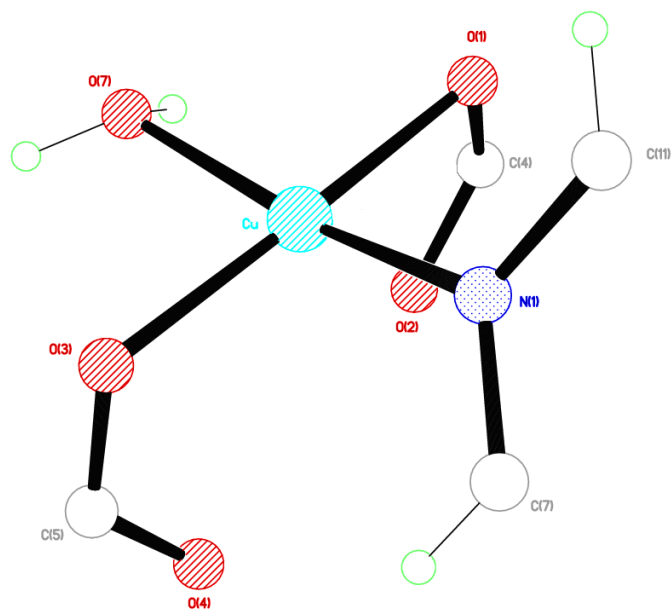


**Figure 8.47: Square planar coordination environment of Cu(1) in compound 44**

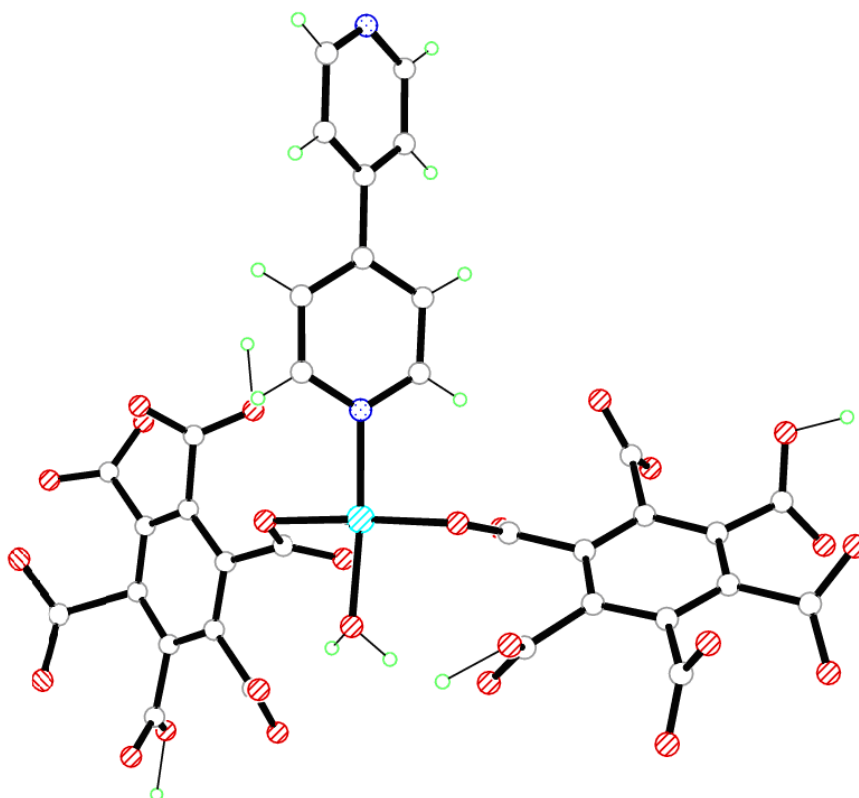


**Figure 8.48: Molecular building unit of Cu(1) in compound 44**

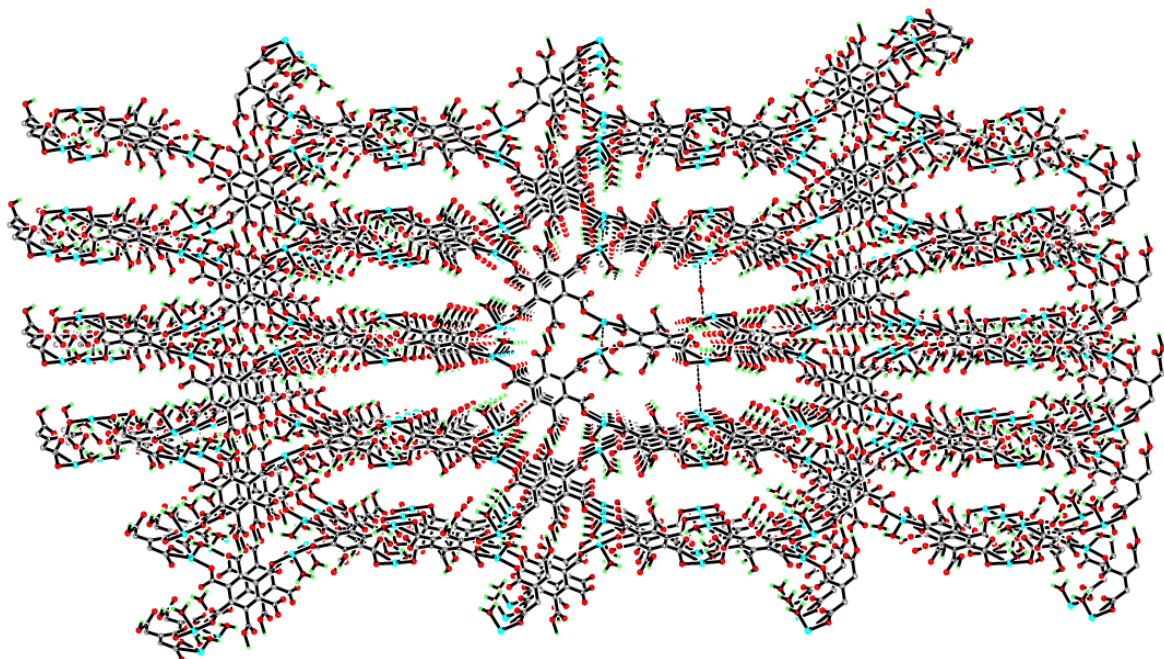


**Figure 8.49:** Three dimensional coordination of compound 44 viewed down the *a*-axis (4,4'-bipyridine removed for clarity)

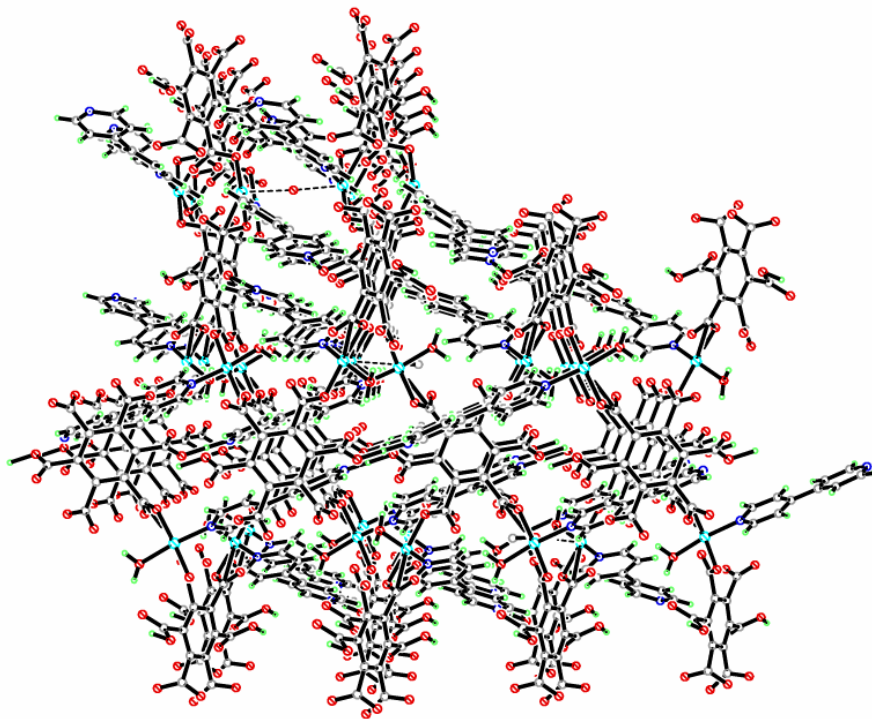


**Figure 8.50:** Three dimensional coordination of compound 44 viewed down the *a*-axis

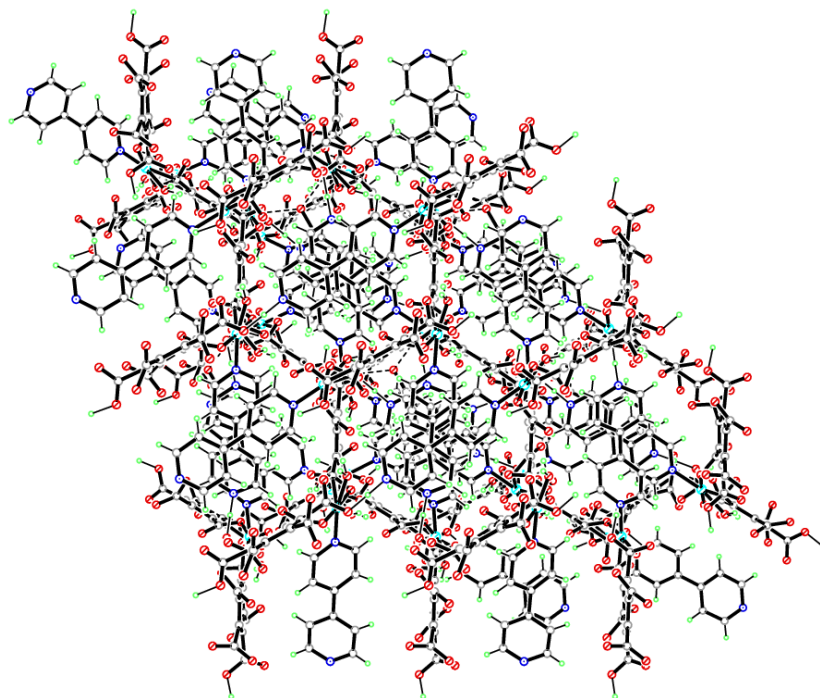


**Figure 8.51: Three dimensional coordination of compound 44 viewed down the *c*-axis**

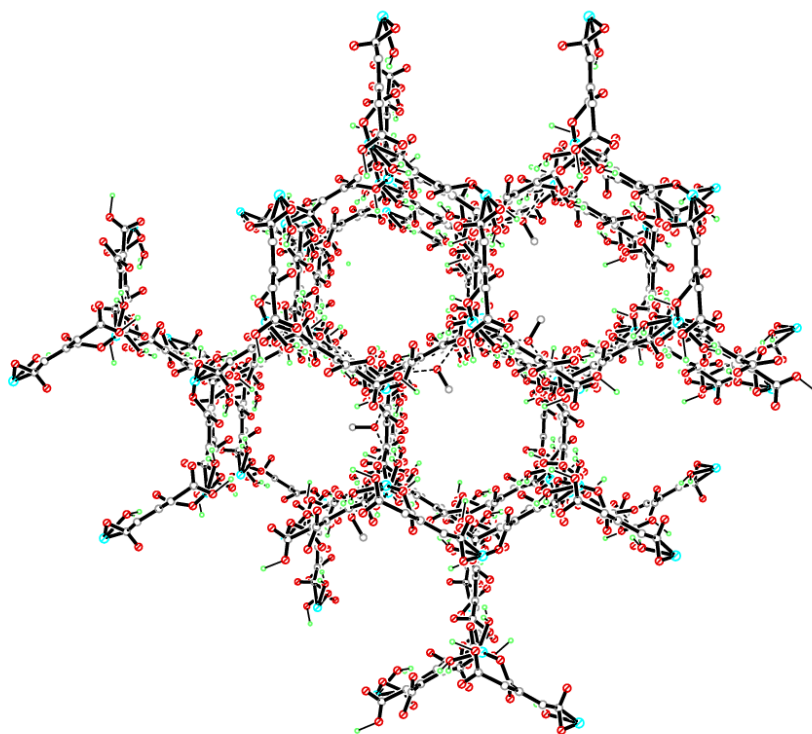


**Figure 8.52: Three dimensional coordination and hexagonal net motif of compound 44 viewed down the *c*-axis (4,4'-bipyridine removed for clarity)**

## Conclusion

In this chapter eight compounds with 1,2,3,4,5,6-benzenehexacarboxylic acid were presented; one with cobalt, two with nickel, two with cadmium, three compounds with copper. These compounds were formed with a variety of solvents and bases producing frameworks consisting of one dimensional chains to three dimensional coordinated porous grids.

Direct addition reactions were used to investigate the effect of potassium hydroxide on topology formation, this resulted in compound 37-41. Compound 37 was synthesised from nickel nitrate and benzenehexacarboxylic acid in water. This produced a one dimensional framework, consisting of stepped chains hydrogen bonded together. It was theorised that the structure could be expanded by the inclusion of potassium cations in the form of potassium hydroxide. This expansion created compound 38 with coordination of the benzenehexacarboxylate to the nickel and potassium cations in conjunction with the bridging waters and K(2) cation to produce a coordinated three dimensional framework; composed of sheets of nickel-benzenehexacarboxylates. These sheets are composed of discrete units of [Ni(1)-benzenetetracarboxylate-Ni(2)] with the nickel cations capped by coordinated water molecules. The discrete units pack together in a chequered motif with each unit related by inversion symmetry, the potassium cations are out of plane to the sheets in the *a*-axis and coordinate the individual discrete units as well as further coordination between the sheets creating columns. Compound 38 and compound 37 both show structures containing two six-coordinate nickel cations that are capped by coordinated water molecules. The molecular building units of both compounds show consistent features with compound 37 forming a stepped chain with bidentate coordination to the Ni(1) cation with a capped Ni(2) cation; molecular unit of compound 38 forms the connected planar sheets using a bidentate potassium cation that links the two benzenehexacarboxylates with a capped Ni(1) cation coordinated to the adjacent carboxylate. The structures differ as the bidentate potassium is located in a general position and not on a inversion centre resulting in the K(1) cation coordinating to a benzenehexacarboxylate positioned directly underneath the previous creating columns of collinear carboxylate ligands rather than the stepped chain motif. The success of expanding compound 37 into three dimensions resulted in additional

reactions with alternative transition metals in order to produce structural analogues of JIYN<sup>1</sup> and compound 37, leading to the production of compounds 39, 40 and 41. Compound 39 was synthesised using similar reaction conditions to compound 37 producing into a two dimensional sheets that stack together forming hydrogen bonding between the coordinated water molecules that protrude perpendicular from the layers. The layers stack in a staggered conformation with each layer rotated by 180° in the plane of the aromatic, this staggering maximises hydrogen bond interactions. This is a precursor to the potassium substituted analogue; compound 40. Compound 39 was expanded using the reaction conditions of compound 38 to form compound 40. Compound forms two dimensional sheets linked by bridging potassium cations that form layers that run parallel to the [Cu-benzenehexacarboxylate] layers. The layers of benzenehexacarboxylates are staggered with respect to the aromatic rings, this staggering allows the potassium cations to coordinate in between the layers avoiding the steric bulk of the hydrated copper cations. The packing motif of compound 40 is almost identical to compound 39 with both structures forming sheets of [Cu-benzenehexacarboxylate] with linking via five-coordinate square pyramidal nodes with coplanar trans carboxylates and capped water molecules. The comparison of the space groups shows the change from *Iba2* to *Pbca*, that have similar volumes. Comparison of the asymmetric units of the compounds, shows that the Cu(1) and Cu(4) cations in compound 39 have been substituted for the K(1) and K(2) cations in compound 40. The K(1) and K(2) cations coordinated out of the plane of the benzene ring creating a three dimensional coordinated framework in compound 40 compared to the hydrogen bonded two dimensional sheets of compound 39. The synthesis of compound 40, the potassium substituted analogue of compound 39, is consistent with the expansion of compound 37 to compound 38 using potassium hydroxide. Compound 37 is an analogue of the known compound JIYN<sup>1</sup>, leading to a set of reactions to produce the potassium analogue of the cobalt compound; these produced compound 41. Compound 41 forms dual layer columns composed of collinear chains of benzenehexacarboxylate ligands that run parallel with respect to one another, that interlock around the Co(1) cations and adjacent Co(2) cations. Compound 41 was synthesised as an attempt to continue the series of compounds by producing the potassium doped JIYN<sup>1</sup> structure with the addition of

potassium hydroxide to the original reaction medium; however although the full deprotonation of the benzenhexacarboxylate occurs the potassium fails to coordinate into the structure forming an alternative new two dimensional product.

Compound 42 was synthesised to investigate the templating effects of pyridine upon the benzenhexacarboxylate frameworks, this compound shows a high level of coordination to the templating agent preventing the paddle-wheel dimeric building units from expanding the structure into three dimensions; forming two dimensional sheet with hexagonal net motif. Further reactions with lowered concentrations of pyridine resulted in compound 43. Compound 43 was synthesised by lowering the concentration of pyridine by 50 %; a structural motif was formed devoid of any pyridine templating agent. As a consequence the cadmium nodes in compound 43 are not sterically hindered by the pyridine ligands that induce a coplanar trans coordination of the carboxylate ligands observed in compound 42. In contrast compound 43 adopts the cis coordination geometry, creating the alternating chains of benzenhexacarboxylate ligands that form the walls of the nanochannels with close packing to adjacent chains. The nanochannels have dimensions 5.946(7) by 8.410(7) Å upon desolvation of coordinated water molecules that point inwards towards them, generating a pore volume of 25.7 %. Unfortunately the framework is not stable upon desolvation with degradation beginning at 110°C. The formation of compound 43 highlights the templating effects of pyridine and its prevention of the formation of porous frameworks when concentrations are slightly too high, further work on these structures can be carried out to form analogues of the compounds creating a complete series of frameworks, to investigate the implications on metal node geometries.

Previous experiments containing the 1,4-benzenedicarboxylate and 1,2,4,5-benzenetetracarboxylate ligands showed the ability to modify the frameworks templated with pyridine by replacing it with 4,4'-bipyridine to produce the new compounds 25, 26 and 36; by extending this modification to the benzenhexacarboxylate series compound 44 was produced.

Compound 44 is one of only two known frameworks that contain transition metals, benzenhexacarboxylate ligands and 4,4'-bipyridine ligands, and was synthesised using the H-Cell apparatus. The molecular building unit of compound 44

expands the structure into a three dimensional framework that forms planar sheets. The sheets are then coordinated together by columns of collinear benzenhexacarboxylate ligands that run perpendicular to the sheets. The bridging of the 4,4'-bpyridine across multiple layers partially fills the hexagonal nets forming nanochannels with dimensions 10.136(8) by 10.136(8) Å. Additional reactions were still crystallising at the end of this research with promising reactions involving nickel and cobalt, further work involving these transition metals can be carried out to produce potentially porous frameworks similar to those observed for the 1,4-benzenedicarboxylate and 1,2,4,5-benzenetetracarboxylate ligands. These compounds would form a platform for benzenhexacarboxylate frameworks with potential applications in gas adsorption studies, an area of MOF chemistry yet to be ventured into.

## References:

- 1 C. Robl, S. Hentschel, Z. Naturforsch, *B: Chem. Sci.*, **1991**, 46, 1188.
- 2 H. Tamura, K. Ogawa, W. Mori, *J. Cryst. Spec. Res.*, **1989**, 19, 203.
- 3 A. J. Spek, *J. Appl. Crystallograp*, **2003**, 36, 7.
- 4 E. Yang, J. Zhang, Z. J. Li, S. Gao, Y. Kang, Y. B. Chen, Y. H. Wen, Y. G. Yao, *Inorg. Chem.*, **2004**, 4B, 6525.



## Chapter Nine – Suggestions for Future Work

### Future Objectives

Selections of the compounds presented in this thesis have potentially interesting thermal and adsorption properties; however the lack of bulk material prevents their further investigation. These materials include compounds synthesised in conjunction with 4,4'-bipyridine using the H-Cell apparatus, such as; the 1,4-benzenedicarboxylate compound 7, the 1,3,5-benzenetricarboxylate framework compound 10, the 1,2,4,5-benzenetetracarboxylate frameworks compounds 26 and 36 and the benzenhexacarboxylate framework compound 44. These materials are of significant interest due to the flexibility of the 4,4'-bipyridine ligands that can have positive affects on gas adsorption, with current focus of MOFs with potential applications in fuel cells, molecular sieving and biomedical applications with activated release properties orientating around flexible MOFs.

The first phase of future investigations would be to develop rapid synthesis protocols using either direct addition or solvothermal conditions with consistent reagent concentrations. Any powder products would need to be compared to the predicted powder diffraction patterns obtained from the single crystal data of the aforementioned compounds, before further bulk scale reactions are implemented. A second phase of investigations would orientate around the thermal properties of the compounds; if desirable desolvation temperatures and thermal stability are achieved further characterisation of the porous nature of the material can be carried out to determine potential applications. Considerable investigations into the expansion and further characterisation of the benzenhexacarboxylate framework compound 44 could be carried out, as the area of porous benzenhexacarboxylate frameworks is relatively unexplored, with the desirable predicted high thermal stabilities of the fully coordinated ligands to cadmium cations; presents a potential framework that could open up new applications for MOFs in harsh condition reactions in catalysis, an area still dominated by zeolites.

Compounds 18, 19 and 35 were also synthesised using the H-Cell methodology, these compounds show interesting packing motifs that would be of further interest in thermal stability studies with potential applications of the desolvated structures. These compounds would need to be developed in a similar phase based protocol as the previous set of compounds, with the aim of obtaining pure bulk samples. Compound 19 is a 1,3,5-benzenetricarboxylate framework that exhibits similar herring-bone pores to the series of 1,2,4,5-benzenetetracarboxylate frameworks; compounds 32-35 that were investigated to identify the effect of DMF concentration on topology formation. The similarities would indicate that if a bulk synthesis of compound is achieved, then a similar series of compounds could be produced using the 1,3,5-benzenetricarboxylate ligand. Additional reactions of the synthesis protocols of compounds 32-35 could also be investigated for alternative transition metals such as copper, to develop compounds with potential open metal sites for catalysis applications utilising the open and closed pore packing of compound 33 that shows high thermostability upon desolvation.

Compound 17 the zinc-HKUST-1 analogue, shows interesting post synthetic rearrangement around the dinuclear paddle-wheel building units to create a nanoporous framework upon desolvation. The crystal structure of the desolvated state is required to identify further potential applications and synthesis routes to analogues, current methods involving capillary tubes and Hot-stage microscopy have failed to produce the desolvated crystal structure. Further initial reactions utilizing gas cells at a synchrotron source may provide a method to obtain a desolvated crystal structure. Current adsorption studies on compound 17 have been successful with carbon dioxide, with initial nitrogen adsorption isotherms showing the potential of the compound in kinetic molecular sieving; further adsorption research is required to conclusively determine the application properties of this compound.